AGARDograph Number
One Hundred and Twentyeight

Inertial Component Testing: Philosophy and Methods

The Advisory Group for
Aerospace Research and
Development, NATO

Editor

W. G. DENHARD
Associate Director
Charles Stark Draper Laboratory, Massachusetts Institute of Technology

(Until January 1970, the C. S. Draper Laboratory was known, and is referred to throughout this volume, as the Instrumentation Laboratory.)

Printed and published by

Technivision Services
Slough, England

A Division of Engelhard Hanovia International Ltd.

International Standard Book No. 0 85102 021 6
Library of Congress Catalog Card No. 70 - 82414

Contents

1

Introduction: the Testing of Sensors for Inertial Quantities

C.S. DRAPER
Director of Instrumentation Laboratory, MIT, Cambridge, Massachusetts, USA

Vehicle space, established by structural members, and some external space chosen as the reference in describing desired paths of motion are two essential entities that always appear in systems for control, navigation and guidance. Equipment to provide these functions must include computing and readout subsystems to calculate desired geometrical relationships between the two spaces on the basis of sensed information with indications of vehicle orientation, location, velocity, direction, deviations, etc., as outputs. Computations and indications require complex electro-mechanical and electronic arrangements, but under the circumstances of today's advanced technology do not impose fundamental limits in either performance or reliability. Even less troublesome are vehicle coordinates which become available through the simple alignment and mounting of components to convenient structural members. Reference space, from which orientations and locations of vehicle coordinates may be accurately represented in terms of signals suitable as computing system inputs, may be realized in many ways but requires especially careful design and construction if it is to be achieved by means of self-contained mechanizations. As a matter of experience with well-engineered equipment, the problems associated with these mechanizations are usually the factors that determine performance and reliabilty for present-day control, navigation and guidance systems.

External space to which orientation and location of vehicle space may be related is easily available when good visual, radio, radar or other electro-magnetic radiation contacts exist with landmarks on the earth. In situations of this kind the earth's surface itself serves as the reference space so it is a simple matter to choose coordinates especially convenient for any given set of circumstances. When lines of sight to heavenly bodies are available, the celestial sphere is available for use as an auxiliary reference space for paths either on the earth, in orbit or among celestial bodies.

Reference spaces external to guided vehicles become usable only when radiation contact signals of some sort are available. Signals of this kind are not well adapted for use in establishing orientational references of high accuracy and locational information contains 'noise' components that must be averaged out over considerable time periods if the good results are to be achieved. When effective radiation contact with all external spaces is lost in flight because of bad weather, passage over regions either hostile or without cooperative radio stations, in submarines at depth or in space vehicles maneuvering through regions blacked out for radiation contacts with earth, control, navigation and guidance by on-board, self-contained equipment becomes necessary if results of good accuracy are desired.

Subsystems that may be combined to give satisfactory performance present engineering problems rather than limiting factors as far as vehicle space, computation and indication are concerned. The greatest difficulty resides in the essential subsystems that must provide accurate, always available, and reliable on-board geometrical references from which variations in vehicle orientation and changes in linear motion may be measured. Because the inertial principles described by Newton's Laws of Motion make it possible to realize subsytems of this kind, equipments using such references are commonly called inertial systems.

Indicators based on gyroscopic elements adapted to the purposes of providing reference coordinates for the control of orientation in aircraft, marine vessels and space vehicles have been universally accepted routine instruments during the past fifty years. The indications from these conventional devices are usually not better than a few degrees of angle or at best a few arc minutes. Subsystems providing orientational reference accuracies several orders of magnitude better than these levels are needed for the purposes of navigation and guidance. In combination with such references, devices designed to sense specific force (the vector resultant of gravitational force and inertia reaction force) and to produce signals representing the integral of this input can provide the basic signals for completely realizing self-contained geometrical references.

Briefly stated, two basic functions are involved in all self-contained geometrical reference subsystems: (a) the sensing of angular deviations from instrumentally adjustable reference orientations and (b) the sensing of specific force with the generation of signals that accurately represent this input over a wide range of operations. Angular deviation sensors for which reference orientations are indicated by signals and which have the ability to hold initial settings of these references for acceptably long periods of time make it possible to use servo-controlled, mechanical members arranged for complete angular freedom with respect to supporting bases to serve as physically accessible reference space. Signals from a set of specific force receivers having fixed and known orientations to selected coordinates fixed in this space may, starting from arbitary initial settings, be integrated twice, modified on the basis of recorded field pattern data to compensate for gravitational effects and used as the essential inputs for computers to generate the desired output indications from systems for control, navigation and guidance.

Today, the technology of such systems has reached a state in which overall performance and life limitations are commonly set by the capabilities of available mechanizations in the two fundamental types of inertial quantity sensors. Of these types, angular deviation sensors must respond with clear output signals to small changes in orientation with determinable, or preferably insignificant, drift (undesired changes of instrumental reference orientations) components during periods of self-contained operation. The second type, specific force sensors, must reliably respond to both low and high input levels with output signals accurately related by determinable relationships to the corresponding input changes over the range of operation. It is obvious that inertial quantity sensors of both kinds must continue to operate without significant impairment of their functions under any environmental conditions that may be associated with operation.

Testing, as this term applies to sensors for inertial quantities, is the complex of activities directed toward the determination of sensor capabilities for receiving angular deviation and specific force with output signals that accurately represent these inputs over the ranges encountered in operation and under the full span of expected environmental conditions. In practice, the input levels involved span so many orders of magnitude and the spectrum of environmental conditions is so wide that any adequate coverage of sensor performance by direct measurements

made at a sequence of points with adequately close spacing is clearly beyond the realm of possibility. For example, the testing of specific force sensors working over the not extraordinary range of 10^{-5} gravity to 10 gravities on the basis of discrete measurements would require many thousands of separate observations. To force this situation toward manageable proportions it is universal practice to calibrate: that is, to establish information describing relationships of outputs to corresponding inputs-in terms of mathematical equations covering the full range of operating levels after a limited number of parameters have been determined by properly designed test procedures. The forms usually applied for representing calibration data on inertial sensors are power series expansions combining a constant term, first power terms and second power terms. After experimental confirmation that a chosen equation is valid, the measurement of a few constants makes it possible to predict performance for the full range of operation. Calibration equations can be derived from the engineering features used in particular designs or they can be assumed on the basis of the general principle that continuous physical relationships may be represented by means of power series expansions. It is, of course, possible to apply many other mathematical relationships for representing sensor performance but in all cases it is always necessary to demonstrate that any chosen form does actually predict results in accord with engineering theory and with all the data from controlled experiments.

Testing of sensors involves the conception and realization of experiments in which accurately known inputs are applied and corresponding output signals recorded under carefully controlled environmental conditions. Attention is generally directed toward the determination of parameters for assumed Calibration Equations and demonstrations that these equations truly represent sensor behavior over the widest range of levels for which accurately known inputs are available. When inputs of test quality are not available over the full spectrum of levels expected in operation, special attention must be devoted to the calibration equation and proof of its validity over ranges within which all mechanism components operate without malfunctions. In many cases, environmental effects may become indistinguishable from actuating inputs unless special care and refined procedures are applied in testing. An example of this kind appears when high performance angular deviation sensors are test mounted on platforms subjected to natural and man-made tremors of the earth. Special servo-driven members isolated from surface motions can be applied to greatly improve this situation. It is to be expected that test equipment will require more and more refinements as engineering developments result in sensors of higher and higher quality.

Testing may be grouped into various categories identified by the objectives involved. For the purposes of discussion these categories may be considered as: (a) research tests, (b) engineering subsystem tests, (c) engineering tests, (d) calibration type tests, (e) screening tests, (f) calibration tests and (g) inspection tests.

Testing of inertial quantity sensors always involves four basic phases: first, the establishment of suitable and known environments; second, the application of actuating inputs carefully controlled and accurately known in orientation and magnitude; third, means for indicating and recording the output responses of the devices under test; and, fourth, the evaluation of results in terms of these experimentally determined output-to-input relationships. It is the objective to be fulfilled by knowledge of these relationships that determines the equipment used, the data-collecting procedures and the forms employed for describing results.

Research tests are concerned with basic information on the reactions among natural principles that may be applied in various possible mechanizations for realizing devices to perform the functions necessary in the sensing of inertial quantities.

For example, research tests on signal generators and torque generators are needed in the development of devices with behavior that may be combined with actions provided by other components to result in useful subsystems.

Engineering subsystem tests are directed toward determining the contributions that groups of components, integrated into subsystems, can provide toward building up high-quality performance from complete sensors. An illustration of this kind of activity is the testing of rotors spinning on their special bearings within gimbal structures, which is an essential part of the engineering for gyroscopic instruments of all kinds. Exhaustive engineering tests of subsystems are fundamentally important for the design of angular deviation receivers.

After complete instruments have been built up with subsystems of known performance, engineering tests covering the full range of inputs, outputs and environmental variations are needed to determine in quantitative terms the functional capabilities of complete sensors based on the natural principles and the features applied in particular designs. A typical illustration is the case of a specific force receiver subjected to input levels both lower and higher than those of design goals for the purpose of determining the operational performance margins to be expected in practice.

Calibration type tests go beyond the verification of functions associated with engineering tests and concentrate on the careful and extensive measurements necessary to accurately determine the output-to-input relationships needed to describe the overall performance of typical sensors built to a particular design. In general, these results depend upon the collection of enough data to establish specific values for parameters of the accepted calibration equation and to demonstrate the validity of this equation over specified ranges of operation.

Once calibration type tests have shown that representative instruments of a given design are capable of meeting given performance specifications, the next level of testing is applied to the identification of production line instruments that are without significant flaws from the standpoint of satisfactory performance under service conditions. Screening tests of this kind are necessary for the rejection of defective units before more than minimum amount of effort is uselessly expended in attempts toward calibration.

Calibration tests are standard procedures applied to sensors not eliminated by screening tests. Their purpose is to establish numerical values for calibration equation parameters to describe the essential behaviour of particular instruments. In practice, for situations involving the routine use of inertial quantity sensors, a considerable part of all the effort involved is often associated with calibration tests.

Inspection tests have the nature of abbreviated calibration tests with the objective of determining whether or not particular instruments meet a limited number of critical performance criteria. Tests of this kind and the equipment used for taking the essential data are generally designed to involve a minimum of effort and expense, as they are applied to insure that systems using accepted sensors will have satisfactory performance in service.

Testing across the broad spectrum from research to inspection for inertial sensors is a major activity associated with the realization of operational systems for control, navigation and guidance. The equipment required in these activities includes means for applying accurately measurable angular deviations, gravitational components and linear accelerations as inputs under known environments. The earth itself as it rotates with respect to inertial space serves as an excellent turntable with a rate of fifteen degrees per hour with respect to inertial space.

Specific force inputs are available in nature from the earth's gravitational field while centrifuges are available for levels higher than one gravity, and linear vibrators offer a range of dynamic conditions. Algebraic signs and various input magnitudes may be adjusted by changing orientations of sensor input axes with respect to input vectors. Many possibilities for generating inputs exist and are being exploited in a wide variety of test arrangements. Signals representing input states and the corresponding output responses are usually recorded by standard or special purpose equipment. Interpretation of these recorded data either by human operators or automatic arrangements leads to verification of acceptable sensor performance and the determination of values for calibration parameters.

With the development of inertial systems from small beginnings some thirty years ago until the rapidly spreading service applications of today, so much activity has been devoted to testing associated with inertial sensors that meetings extending over several days are hardly sufficient to cover even the fundamentals involved.

However simple or complex the equipment, methods and interpretation of data applied in this testing may be, the fundamental process of determining and representing input-output relationships established by the instrument under test remains basically identical for all cases. Starting from this fundamental situation there is a very wide spectrum of possibilities in the choice of ways to write specifications, in the selection of mathematical calibration equations, in the mechanization of test equipment, in test procedures, in patterns of representing results in methods for describing performance capabilities of instrument types and of particular units. Many creative people have been drawn together in this conference by their common interest in the testing of inertial sensors. With broadly varying backgrounds of motivation, support and working situations it is not surprising that a variety of approaches to testing and a considerable range of conclusions are reported in the papers that make up this volume. The Guidance and Control Panel of AGARD who suggested the theme, Mr. William G. Denhard from the MIT Instrumentation Laboratory, who served as Lecture Series Director, and Mr. Rolland A. Willaume, AGARD Director of Plans and Programmes, who implemented this project are to be congratulated on the imagination and effort they have applied to the organization of a conference that has been very rewarding for those who attended its meetings. The international team of speakers has been excellent and deserve particular thanks for the information they have presented so well in their papers.

Although the writer did not attend he has received reports that the round table summary was inspiring and served to improve understanding of questions that were not clear to all listeners during initial discussions. The pattern of discussion was effective and added to the luster of AGARD as an agent for the transfer of technological information among nations.

almost simultaneously, although a replacement for and an improvement on the magnetic compass, was not yet of itself the basis of navigation by our definition.

The gyrocompass was, however, one of the first real-life applications of the gyro. As such, the gyrocompass is due a large measure of respect for furthering the engineering state-of-the-art of gyros.

It required many years after 1914 and indeed after 1923, when Dr Schuler published his article (1) in the Journal of Physics entitled 'The Disturbance of Pendulum and Gyroscopic Apparatus by the Acceleration of the Vehicle', for engineers to develop a working and practicable application of all inertial navigation using Dr Schuler's theory. At Massachusetts Institute of Technology, we give credit for this application to the SPIRE Systems developed in 1953. Yet we must acknowledge the work of the German scientists in the early 1940's in guidance.

Accelerometer development has paralleled gyro development. Performance improvement of both types of instruments required extreme reduction of output-axis friction. The lessons of the one instrument were applied to the other.

It might be said that both instruments developed along two major lines: for the gyro, single-degree-of-freedom and two-degree-of-freedom; for the accelerometer, the pendulous accelerometer and the pendulous integrating gyro. There are additional variations of each which are not fully accounted for here since it is the intent to expound not the instruments themselves but rather the testing of them.

The overall lecture series will discuss testing for several specific varieties of today's instruments. This historical chapter will concentrate on the transition of testing methods and equipment carried through from early fire-control instruments to the considerably more precise gyros and accelerometers in use today for navigation and guidance. However, based upon the author's background, it must concentrate upon the single-degree-of-freedom floated integrating gyro and both the more simple floated pendulous accelerometer and the more complex pendulous integrating gyro accelerometer.

At the time of early development of the gyrocompass, testing could be quite simple. Compared to a known north line, how well did the gyrocompass indicate north, and was its accuracy too severely impaired by real or simulated ships' motion? The shipboard gyrocompass had considerable angular momentum with which to overcome precession-axis friction. Today, we do not think of large-angular-momentum gyros. Therefore, neither do we think today in terms of gyros which can accept significant precession-axis friction. The gyro refinement of today is for infinitesimal precession-axis friction and an acceptable life-time of reliable performance. To capitalize on these factors, other elements of the gyro besides precession-axis friction - e.g. bias torques, mass instabilities, etc. - have had to be refined simultaneously, in keeping with overall performance and reliability.

The story of the accelerometer is not very different. Again, output-axis friction, whether for the pivot of the simple pendulum or for the sleeve bearing or spring of the force-displacement accelerometer or for the precession axis of the pendulous gyro accelerometer, has had to be reduced to an infinitesimal value. Similarly, as for the gyro, the other physical and electrical elements of the instrument have had to be refined.

The testing of these instruments in terms of techniques, equipment, and data processing has had to keep in step with the accuracy of the instruments to be tested, and in large measure has had to lead the way. If we now quickly review the evolution of the last twenty years of testing, first of gyros and then of accelero-

meters, we shall observe not only a change in degree or level of observation, but also a change in what is observed and what data is recorded.

The Gyroscope

Examination of figure 2-1 will help to clarify definitions and nomenclature, thereby avoiding a misunderstanding in identifying elements of the gyro.

In the earlier unfloated gyros for gyrocompassing, the need for reducing friction of the precession-axis bearings made some amount of gyro wheel unbalance useful in providing small amplitude vibrations called 'dither'. In the considerably more precise floated instruments of today, such gyro wheeel unbalance produces only unwanted noise. In the early stages of development of the single-degree-of-freedom floated integrating gyro, wheel unbalance caused destruction of the precession-axis bearings which were then sapphire jewels with thrust plates supporting the pivots. The unbalance had to be eliminated (2). In contrast, rather than use of an unbalance in the gyro wheel, more recent work with unfloated gyros included a forced oscillation of a pair of three-race pivot bearings to reduce precession-axis friction.

The data for these early floated gyros always included a measure representing precession-axis friction. Figure 2-2 is a plot of such data. The performance ratio of angular-velocity output to angular-velocity input has been plotted in such a manner that lines of constant slope represent the various friction levels in dyne-cm (3). Note that the precession-axis friction uncertainty shown has an average value of five dyne-cm for 19 gyros and a value of 0.5 dyne-cm (ten times better than average) for the best gyro. Today we expect such uncertainties to be small compared to 0.1 dyne-cm.

Some twenty years ago, much of the original work on development and testing of floated gyros was being done for applications in fire-control systems. Like the unfloated gyros they were meant to improve upon, the early floated gyros were single-degree-of-freedom and intended for intermittent use only. Such a thing as a life test was either not done or was satisfied by 100 to 200 hours of operation. The desired output information was a measure of slew-rate or angular-velocity input and not position, and was therefore obtained under rather forced input conditions, as exemplified by figure 2-2. The principle of testing for both unfloated and floated gyros was to apply a rate input to the gyro and determine that it would respond to a lower level commensurate with desired tracking rates, and have a linear response, or at least one that could be calibrated, up to the highest rate desired. Through a closed feedback loop from the gyro signal generator, the torquer of the gyro was energized in proportion to the gyro output angle about the precession axis so as to limit or restrain this gyro output angle. The circuit was called a rate feedback loop or a torque-restraint loop and had a current level proportional to slew rate or angular-velocity input to the gyro. Such a gyro in the unfloated form is shown in figure 2-3, and as a floated gyro is shown in figure 2-5 and 2-6. In service with a torque-restraint loop for feedback, the integrating factor of the gyro was not used, but the damping did smooth the response.

The test equipment for determining performance, besides that for electrical excitation, consisted primarily of a reversible rate table with a set of gear changes to allow variation in the drive rate. By today's standards, the equipment was crude; electrical stability was of the order of five percent and drive rate was fairly good through use of a synchronous motor, but quite noisy owing to the gear train. However, accuracies from the overall system of the order of ten to twenty-five percent in rate measurement and lower levels of rate sensing of one mrad/sec or 200 seconds of arc/second (nearly 14 earth rates) were all that was required.

Therefore, gyro and test equipment sufficed. A typical test setup is shown in figure 2-4.

Evolution of floated-gyroscope development beyond fire-control requirements to navigation requirements produced two approaches to testing. The first carried over directly from the fire-control application and consisted primarily of improved methods of studying gyro response to rather high rates of the order of one earth rate or greater. The second started with a simple manually operated electrical torque-to -balance measurement of the precession torque due to horizontal and vertical components of earth rate at various compass headings. This second technique later evolved further into one utilizing certain feedback loops. One feedback loop was to continue to utilize torque-restraint loops (similar in principle to fire-control restraint loops) while another utilized space-stabilized dynamic servo loops.

For that test technique, which was an evolution of testing for fire-control purposes, the single-degree-of-freedom gyro was turntable mounted with the output or precession axis horizontal and the gyro input or angular-rate-sensitive axis and the turntable axis vertical. The gyro signal-generator output was coupled through a dynamic servo feedback loop to the drive system of the vertical turntable axis. Through the sum of inputs to the gyro – i.e. vertical component of earth rate, mass-gravity pendulosity torque, and mechanical and electrical bias torques – the gyro float rotated about the precession axis, thereby generating an electrical output signal. The amplified signal energized the servo loop and drive of the turntable. For the test, the table was then allowed to rotate from two or three degrees on one side of a reference mark to a similar angle on the other side of the reference mark (Fig. 2-7), and the time per degree of rotation was recorded.

The angles on each side of the reference mark were established with a precision of 5 to 10 seconds of arc at best. This accuracy did not impair results since the overall test included many repeated sweeps through the same total angle. To accomplish this, after each data run the turntable was forced to rotate back to the starting point by manually or automatically exciting the gyro torque generator so as to 'torque' the turntable back via the gyro torque and the servo loop. From this technique and the relation to an old cog wheel, the test was called a cogging test. The repeat tests were compared as to average time and the bandwidth or one sigma value about the mean. Wild data could be rejected and frequently were as will be discussed later.

The cogging test was undoubtedly representative of a fire-control application in that operation was intermittent with frequent caging of the gyro (in this case, resetting to the starting angle). However, it was not representative of stabilized platform operation of the type required for navigation for today's more accurate requirements and therefore has fallen into disuse.

In the handling of the data from a cogging test, improvement of the data numbers was effected by rejecting data points that did not fit the overall data pattern and also by taking a large number of data points so as to improve the significance of the mean value. However, evidence appeared that the identical gyro tested under varying gravity positions and/or on a long-term test on a space stabilization servo could look considerably poorer in performance than it did in the cogging test. This brings to mind the story that certain gyros, tested and accepted with the cogging test by the manufacturer for autopilot service, were completely rejected by the customer who used the more advanced testing techniques. The result was that the supplier and the customer had considerable added expense but the shipping agency gained considerable business from the flow of gyros back and forth. The problem was resolved when the manufacturer adopted the more advanced testing

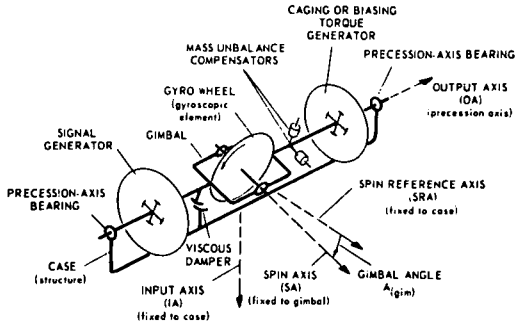

Fig. 2-1 Line schematic of the MIT single-degree-of-freedom integrating gyro

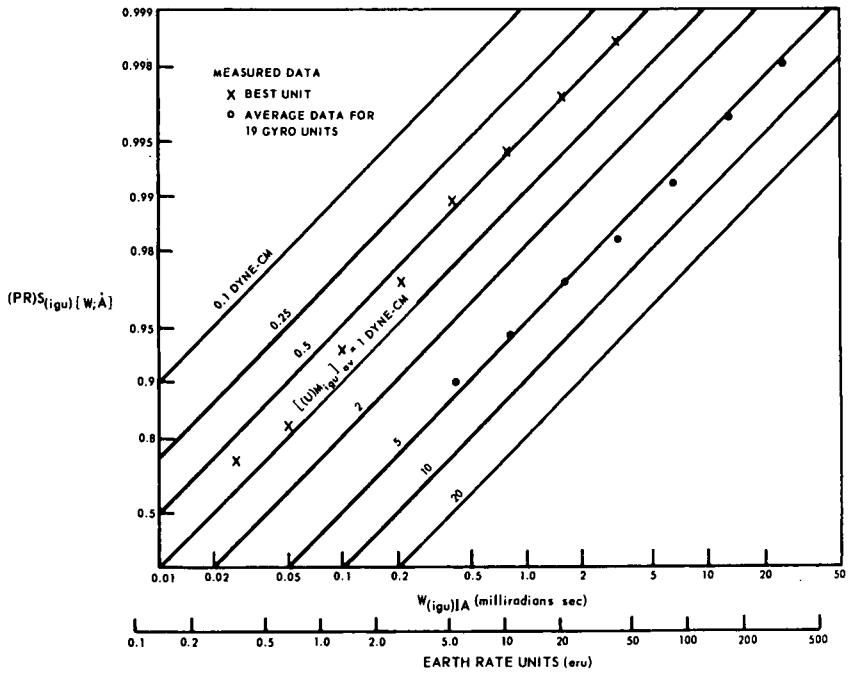

$$(PR)S_{(igu)\{W;\dot{A}\}} = \frac{S_{(igu)\{W;A\}}}{S_{(igu)\{W;\dot{A}\}_{ref}}} = 1 - \frac{[(U)M_{igu}]}{H_g W} \qquad H_g = 10^5 \frac{\text{gm-cm}^2}{\text{sec}}$$

$$(PR)_{(igu)\{W;\dot{A}\}} = \frac{\dfrac{\dot{A}_{out}}{W_{(igu)IA}}}{\left[\dfrac{\dot{A}_{out}}{W_{(igu)IA}}\right]_{ref}} = \frac{\dfrac{(D)A_{out}}{(D)A_{in}}}{\left[\dfrac{(D)A_{out}}{(D)A_{in}}\right]_{ref}} \qquad W_{(igu)IA} = \dot{A}_{in}$$

$$S_{(igu)\{W;\dot{A}\}} = 1$$

Fig. 2-2 Precession-axis friction data

b*

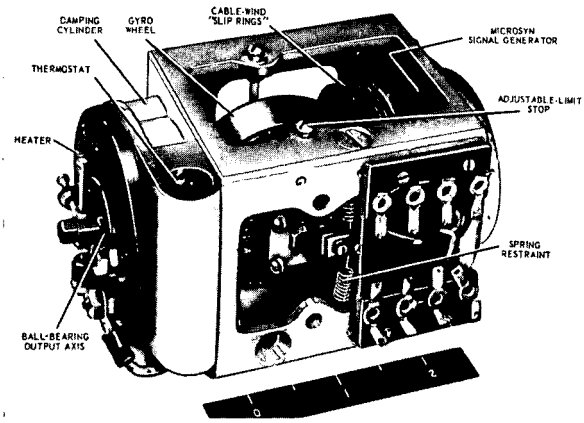

Fig. 2-3 Nonfloated airborne-fire-control rate gyro

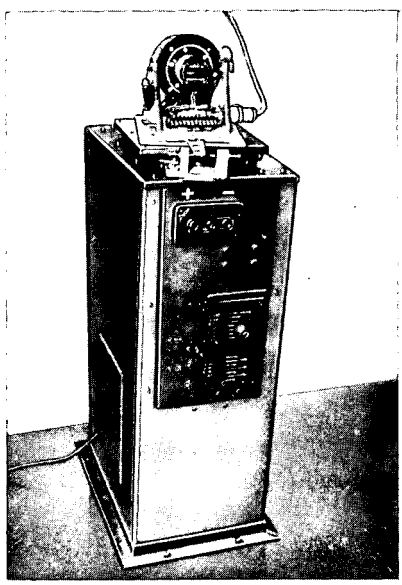

Fig. 2-4 Gear-drive rate table

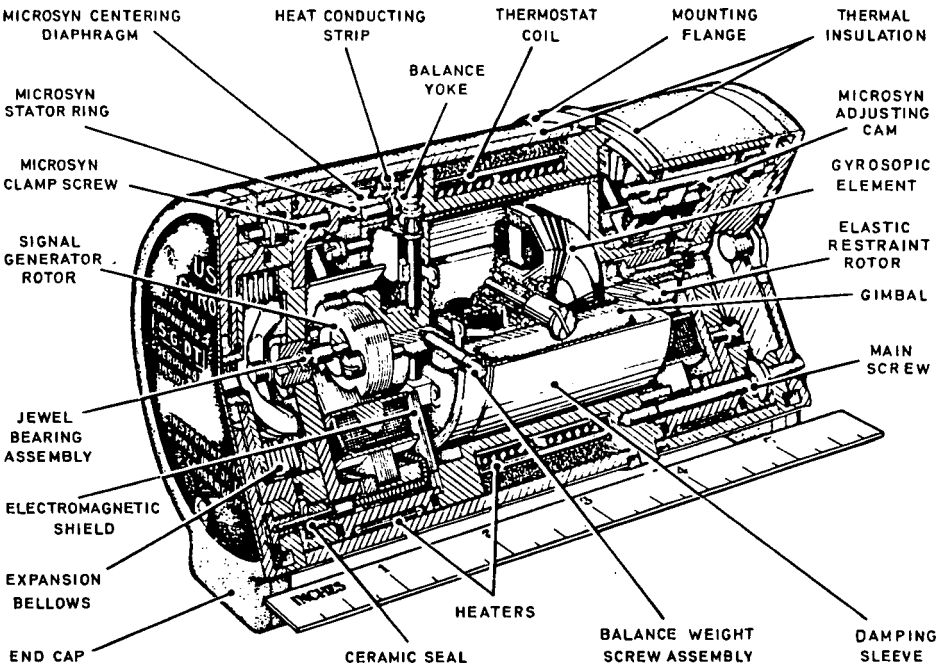

Fig. 2-5 Pictorial cutaway view of the type H rate gyro unit

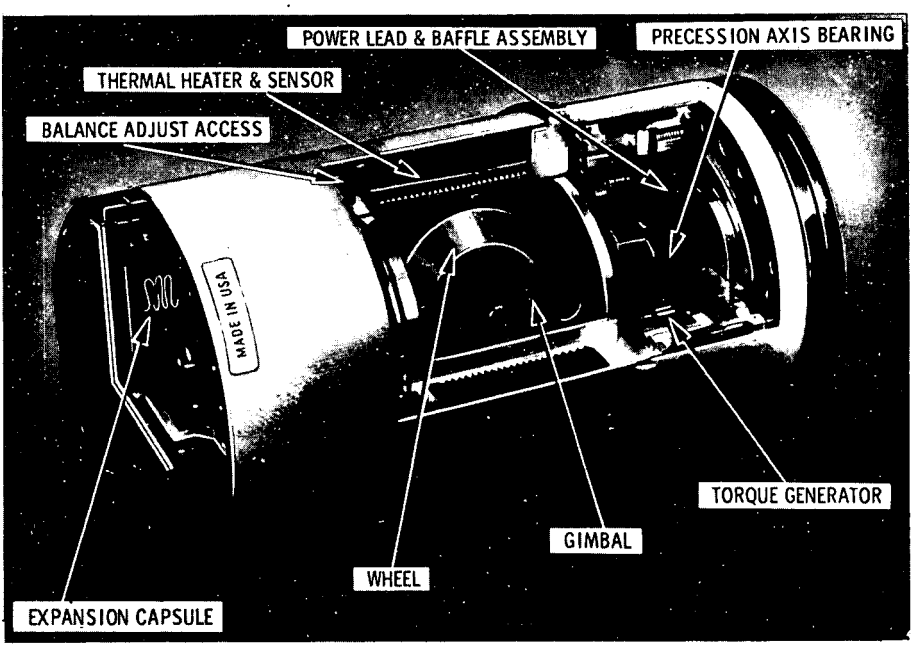

Fig. 2-6 Type H rate gyro unit (Photo courtesy of Honeywell, Inc.)

methods. From these he discovered that his product needed improved manufacturing techniques in order to pass the new tests. In studying the evolution of techniques for testing, we thus see the direct translation of test results from a more advanced technique into a more reliable product.

As more consideration was given to testing of gyros for application to space stabilization platforms, new methods of testing evolved representative of the second approach referred to earlier (4). It was felt that gyros must now detect a small part of earth rate - one-hundredth or even one-thousandth of earth rate (0.15 to 0.015 degree/hour). Cogging tests had indicated the repeatability of behavior at approximately one earth rate without searching for the threshold of rate detection.

What better way could there be to determine the threshold of small rate detection than to measure the precession torque resulting from components of earth rotation itself? To this end, the single-degree-of-freedom gyro was mounted with its output or precession axis vertical and its input axis in the horizontal plane. When mounted on a fixture which was rotatable about the vertical axis, the gyro input axis could then be aligned parallel to the peak horizontal component of the earth's rotation vector, i.e. north or south, or parallel to the zero component, i.e. east or west. Points in between would follow a sine curve. Figure 2-8 shows such a test setup.

The precession torque due to a component of earth rate in the horizontal plane was determined by manually adjusting the excitation to the gyro torque generator until the applied torque just equalled the combination of precession torque due to the component of earth rate parallel to the gyro input axis plus any electrical or mechanical bias torques acting about the gyro precession axis. Data were manually recorded for the torque proportional to the torquer excitation current(s). Reversing the direction of rotation of the gyro wheel then reversed the precession torque without affecting the bias torques. In practice, use of this technique generally disregarded the fact that the bias torque from the excitation of the torque generator was different for each torque level applied. Solution of a pair of simultaneous equations resulted in values for the precession torque and for the assumed constant bias torque.

If data were taken for a full circle sweep of IA in the horizontal plane, the effect of bias torque was to shift the zeros of the sine curve from the true east and west point of the inertial compass. This effect is shown in data form in figure 2-9, as is a second curve showing the result of reversing the gyro wheel-spin direction.

It is worth commenting here that, at the time this test technique was widely used, gyro performance was more often than not a considerable step better than that required for fire-control applications - more in accord with auto-pilot applications today - but was, at that, only capable of consistently detecting a threshold torque of about one-fourth to two dyne-cms; this meant of the order of one percent of earth rate at the time. Furthermore, such performance was determined for output axis vertical and did not tackle the problem of spin-axis stability.

As a parenthetical note, the determination of the best gyro uncertainty at the level near one dyne-cm at this time led to an attempt to overcome this assumed coulomb-friction problem by use of larger-angular-momentum gyros. Advancing technology later showed this not only to be unnecessary but also to be an incorrect approach since the problem was not coulomb friction in the floated gyro.

Since the first of the larger-angular-momentum gyros did indeed exhibit a lower threshold of sensitivity to components of earth's rotation (although not a lower

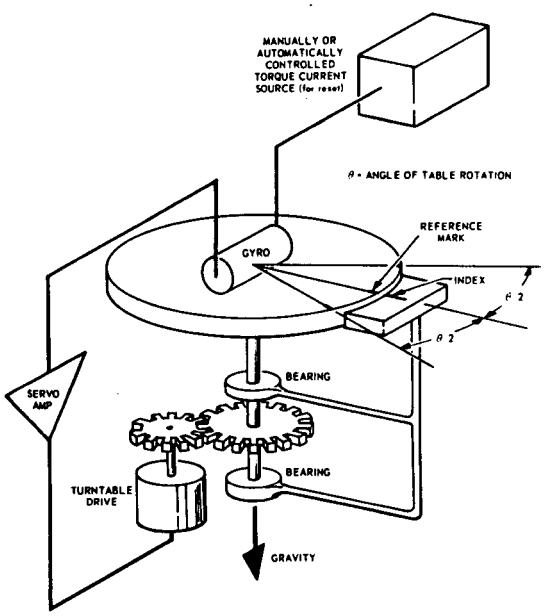

Fig. 2-7 Pictorial diagram of cogging test

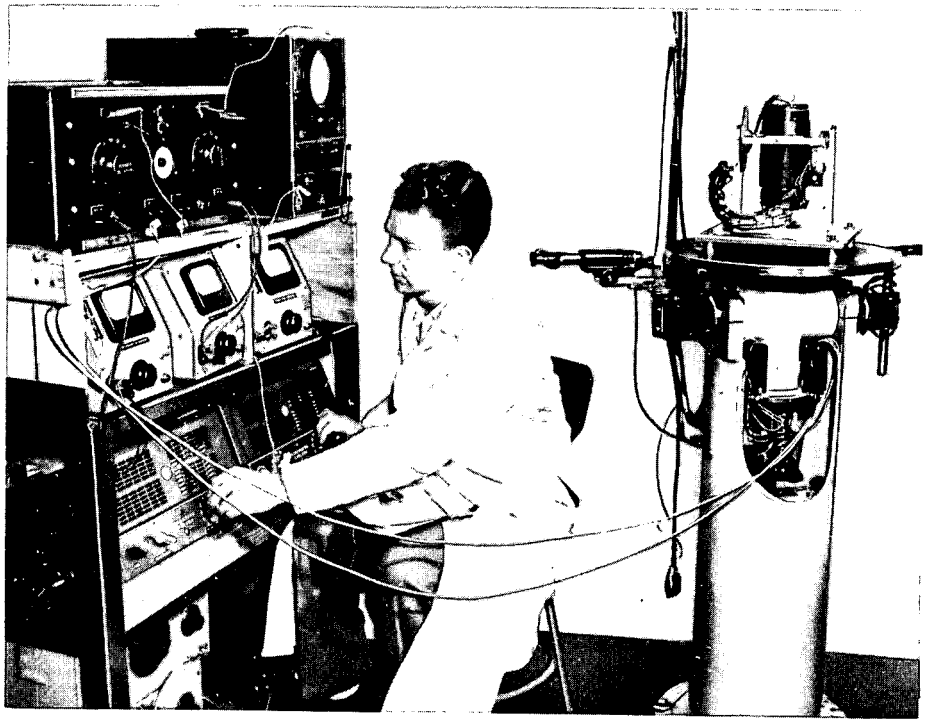

Fig. 2-8 OA-vertical test

uncertainty in dyne-cm), a more critical test was instituted. This was the dynamically stabilized single-axis servo turntable test. For this test, the gyro sensed the vertical component of earth's rotation and servo-controlled the vertical turntable axis as shown in figure 2-10. The test was called the Input-Axis Vertical Servo Test or the IA Vertical Servo Test, or just IA-V.

Performance was judged in several ways. Initially, the idea was to clock the table over a small sector of about 40 degrees of successive one-degree intervals. This was done manually, as shown in figure 2-10, using an optical sight for reading an azimuth circle and a stopwatch for timing. Consistency of one-degree time intervals provided a basis of judgment. Later, with some of the problems in the new gyro designs resolved, the table was modified to allow automatic data recording. This was accomplished through a series of trip pins at ten-degree intervals of the azimuth circle. A switch tripped by these pins actuated a continuously running recording timer, thereby giving data in the form of time per ten degrees of table rotation. Throughout the history of gyro testing on servo runs, these timers have proven irreplaceable for backup data behind far more complex timing devices. Performance was determined by consistency of ten-degree time intervals and comparison of total turntable angle to earth's vertical component rotation angle in that elapsed-time period. Each revolution of the turntable required 36 hours. This was modified by gyro unbalance, of course, and first steps to correct this unbalance by torquer excitation were initiated. For a stable current source, a wet-cell automobile battery was used.

For a more severe test of the gyro, the test table together with the gyro was reoriented so that the table shaft and the gyro input axis were parallel to the earth's rotation axis (Fig. 2-11). This tumbled the gyro in the earth's gravity field, tending to exaggerate deficiencies of construction or of flotation-fluid cleanliness. Instead of requiring 36 hours per revolution of the turntable based on the vertical component of earth's rotation at MIT (5), it now required 24 hours per revolution and as previously noted, provided a more stringent test for the gyro. Performance for the so-called Input Axis Parallel to Earth's Axis Test (IA || EA) could be judged in several ways. Mass-pendulosity torques and others varied as a function of gravity and therefore table rotation position, making the time intervals sinusoidally vary with table rotation angle. Again gyro error corrections through excitation of the gyro torquer were applied using an automatic torque supply unit. This unit was a constant current supply with a 36-point stepping relay used to insert 36 adjustable resistive elements in the stabilizing feedback loop as the turntable rotated to each 10-degree interval.

Performance could also be judged by comparing total turntable angle of rotation (when gyro corrections were used) in a given period of time with earth's angular rotation in the same time period. This resulted in a plot of the error angle of the turntable compared to earth angle.

Interestingly, data for the IA || EA test could also be handled solely on the basis of rate by comparing turntable incremental rotation rate for each one-degree or ten-degree interval data point, as desired, to earth's rotation rate. From this evolved the practice of expressing the difference between gyro controlled turntable rate and earth's rate as so many one-thousandth parts of earth's rotation rate; thus,

$$\text{Turntable deviation angular velocity} = \left(\frac{\text{Turntable Rate - Earth Rate}}{\text{Earth Rate}} \right) 10^3$$

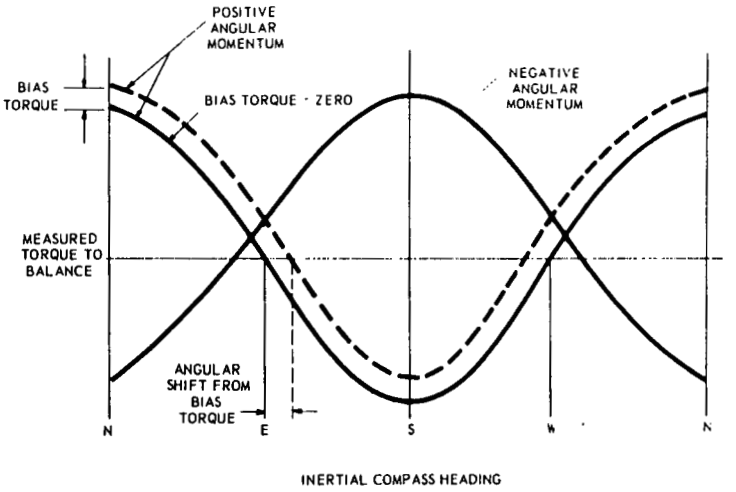

Fig. 2-9 Measured torque-to-balance versus gyro input-axis heading in horizontal plane

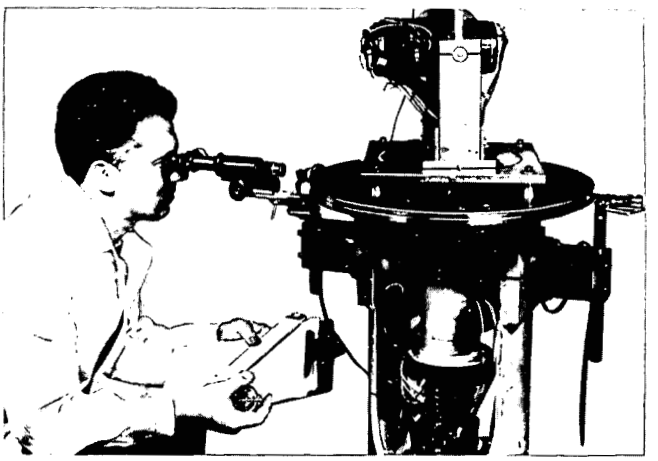

Fig. 2-10 IA-vertical servo test

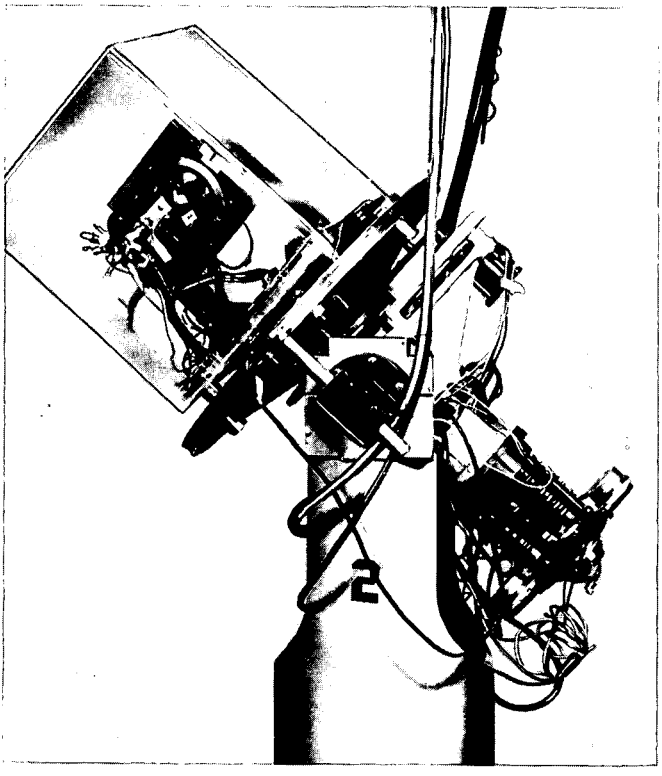

Fig. 2-11 IA parallel EA servo test

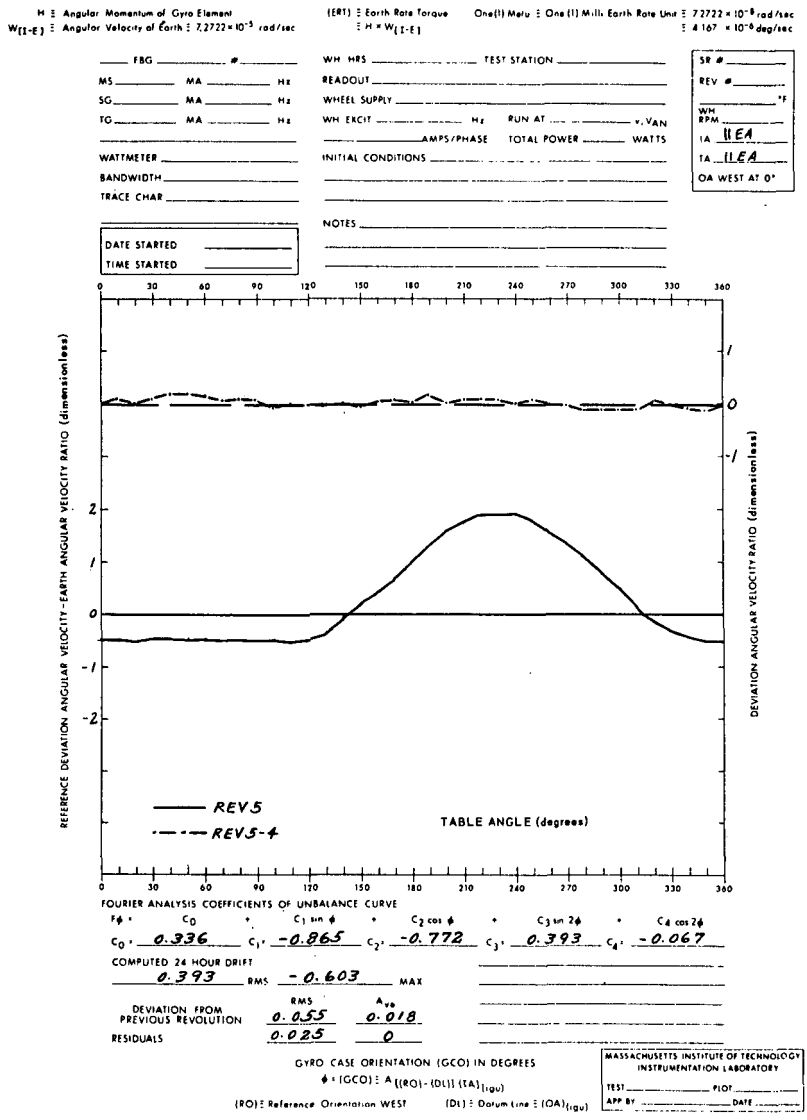

Fig. 2-12 Gyro drift data

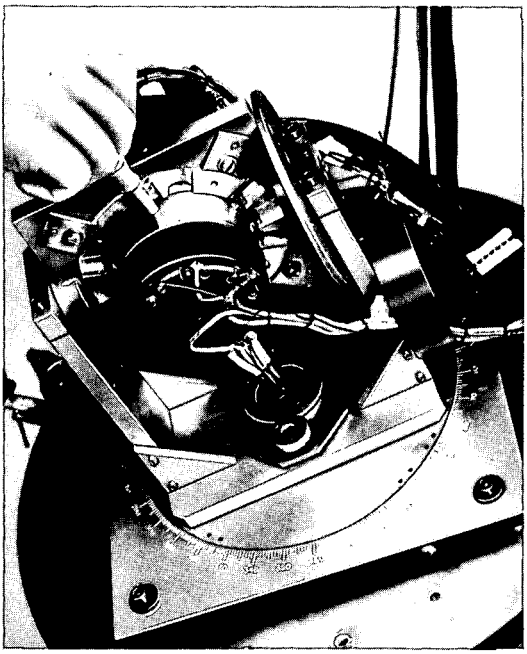

Fig. 2-13 Balance adjustment

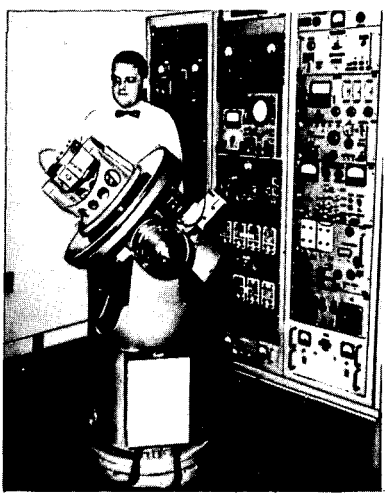

Fig. 2-14 Tumbling test, OA parallel

The unit resulting was called a milli earth rate unit, or meru, and gyro performance is regularly expressed in meru. One meru equals 0.015 degree/hour or, in navigation terms, very nearly one minute of arc/hour (subtended at the earth's center). By computing the rotation error rate of the table in meru for each unit angular interval data point (ten degrees or one degree as desired) for at least two revolutions and making the following assumptions and computations, gyro performance in meru as a measure of gyro nonrepeatability could be judged without the need of applying torque compensation. On the assumption of perfect compensation of the gyro for the second revolution by a hypothetical computer controlling the current input to the gyro torquer, the data from the first revolution were subtracted from that of the second revolution on a point-by-point basis. The root-mean-square values of the point-by-point differences gave a very reasonable interpretation of gyro performance in meru, on the basis that the point-by-point differences represent lack of repeatability of the gyro from second to first revolutions of the turntable. Such data is shown in figure 2-12.

These point-by-point differences can also be converted by integration (summation) to angular units to represent turntable angular error compared to earth's rotation on the same assumption. For such a test, it behooves the gyro manufacturer to insure that the test equipment does not add to the errors attributed to the gyro. This is accomplished by utilizing very stable test equipment or by accounting for its errors.

An explanatory note regarding general gyro performance and adjustments may be in order. Fifteen to twenty years ago (as today), gyros were not perfectly adjusted and balanced prior to delivery to test. That is, there were and generally are today mass-pendulosity adjustments to be made in order to reduce the response of the gyro to acceleration and earth's gravity field. Also, in prior years, adjustment of the signal-generator and torque-generator stator mechanical radial positions was required. These adjustments in early units presented many difficulties since they involved physical entrance of a tool into the fluid of the gyro to make the balance adjustment (Fig. 2-13) and loosening of several seals to adjust the signal- and torque-generator stators. After all this handling, the gyros often would not perform with a repeatability much better than one earth rate, but every once in a while the shining example of one-tenth to one-hundredth of earth rate in repeatability would appear. More spasmodically and much more briefly, one-thousandth of earth rate would show up and then fade away. Those years were truly the triumph of hope over experience. The transition to the performance of today, generally categorized as one meru or better, is vindication of that faith and was achieved by attention to the most minute details without benefit of any major breakthrough. Almost needless to say, slip-joint seals and interlocking tines for mass-pendulosity adjustments replaced the open-port and wrench method as a part of the improvement.

With use of servo-turntable testing fully established for determining the performance of gyros in terms of repeatability, attention now turned to a better definition of gyro response to acceleration. This led to the initial introduction of the so-called tumbling test. This test required the use of the rate-feedback (torque-restraint) loop referred to earlier, with considerably higher gain and automatic recording of torque versus gravity orientation. While connected in this feedback loop, the gyro on the turntable was rotated by the turntable clock drive through a systematic and sinusoidal variation of attitude in the earth's gravity field. As shown in figure 2-14, the gyro is positioned on the turntable with its output or precession axis parallel to the table axis and being a single-degree-of-freedom gyro is not directly sensitive to turntable rotation. For testing with the gyro wheel operating, the turntable axis is parallel to the earth's axis. Evolution of this tumbling test has led to Fourier and least-squares analysis of gyro response to acceleration (using gravity as the input variable) to the zero, first, and second

powers (i.e., a^0, a^1 and a^2). The zero-power term represents the fixed-bias or acceleration-insensitive coefficient of the gyro. The first power term represents the fixed pendulous mass or so-called unbalance coefficient(s), and the second power term represents the anisoelastic coefficients of the gyro.

As the performance of the gyro is examined ever more closely and the gyro model equation (6) expanded to incorporate what once were insignificant and second-order effects, the old tumbling test, the servo test, and the processing of the data therefrom are going through further evolutionary development, as will be brought out in the following chapters.

Special tests on the gyro, conducted to study cleanliness of assembly and coefficient stability, have been and are today carried out using modified servo or tumbling tests. These tests were used to focus attention on the problem of mass stability along the spin axis as it influences gyro behavior. This work has been adopted for today's Apollo program and reported by that project as a great help in quality control of gyros. Again, test techniques have been translated into a more reliable product (7, 8).

The study of mass stability along the spin axis led in turn to series of projects to improve the life and performance qualities of the spin-axis bearings. These projects have led to accomplished lifetimes of tens of thousands of hours in superior-quality gyros. At each step in the series of bearing research and improvement projects, bearing tests and gyro tests were utilized to evaluate the results. Figure 2-16 indicates the testing and research programs carried out.

It must be understood that a gyro can be no better than its spin-axis bearings (and indeed the same can be said for a myriad of other details of the gyro) either in terms of life or performance. Therefore, a complete test program is always concerned with bearing tests (9). Start, stop, slew capability, running- and starting-torque stability, and dynamic stability are a few of the particulars to be monitored during gyro buildup and acceptance testing. Figure 2-15 is a flow chart for bearing evaluation. As gyro engineers, we advocate the intermittent monitoring of most of these during gyro end use also.

The reader must allow for the fact that although this synopsis of the history of precision single-degree-of freedom floated integrating gyro testing does not introduce totally new tests beyond the servo test and the tumbling test for one-g testing, the state-of-the-art has not stood still. In detail, these tests are still undergoing change. The more pronounced recent advances have been in better test equipment and in newer methods of gyro torquing and data handling. For example, the old five-percent stability electrical a.c. supplies for gyro excitation have improved to 0.01 percent in commercial equipment. The torque-restraint loops frequently are based on digital techniques today and much of the data is processed through digital computers. These allow the processing of a considerably greater data volume with resultant finer bits or closer resolution in establishing gyro performance. Figure 2-20 in the section on restrained pendulous accelerometers describes a block diagram for a pendulous accelerometer which is applicable for gyro torquing as well. For the gyro, the pulse has a value in meru-second which is equivalent to an incremental angle.

Simultaneously with the improvement of test equipment and the attendant improvement in gyro performance, increased attention has been focused in the test laboratory upon the influence of the environment (including the test equipment) upon the gyro and its performance. Whereas twenty years ago the manually recorded data consisted only of the proportional gyro torquer current response to various slew rates or the time per cogging cycle, today automatically recorded data may

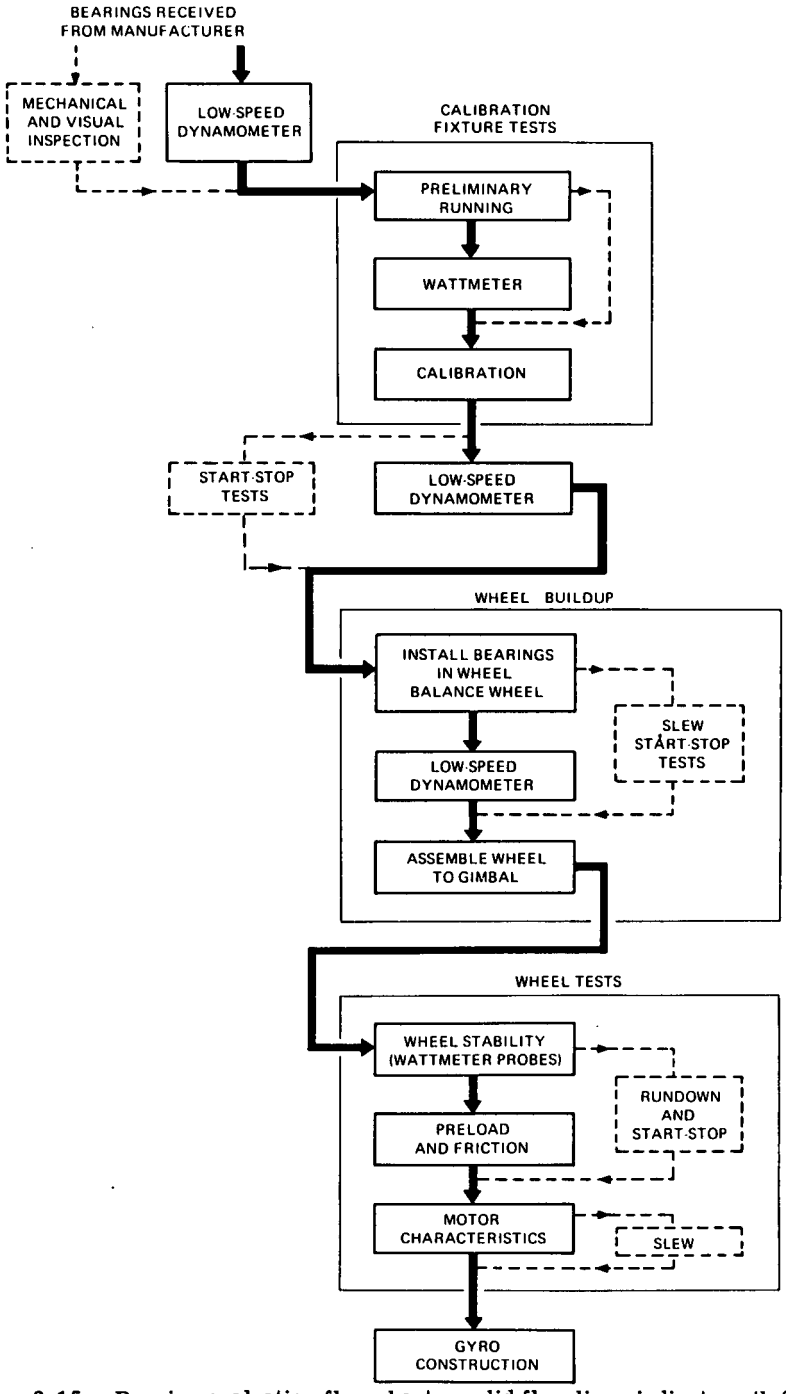

Fig. 2-15 Bearing evaluation flow chart; solid flow lines indicate path for ball bearings; dashed flow lines indicate revised path for gas bearings.

include all the supply excitation voltages and/or currents, room ambient temperature, gyro temperature, sub-voltages on the electromagnetic elements within the gyro, and even floor-leveling errors. These environmental factors will be discussed in more depth in other chapters.

The last element of gyro-testing evolution is in the area of environmental testing. For such testing, rather than just record the environment and minimize its influence on the data, the engineer is interested in varying the environment purposefully to note the effect upon the gyro. Frequently this goes to the extreme of determining survivability under high-acceleration loads from vibratory sources or from linear sources. Since this is an area of much current activity, the major discussion is left to other contributors.

Twenty years ago floated gyros intended for navigation purposes were kept at operating temperaure continuously, since cooling caused air leakage into the gyro and fluid leakage out. On the other hand, fire-control gyros had such a loose performance requirement that air-leakage problems were barely detectable and the reduced precession-axis friction gained from use of flotation made them far superior to the unfloated type. Therefore, fire-control gyros were usually cooled off between duty cycles.

With today's design improvements eliminating leakage problems, navigation gyros are coolable between duty cycles also. Depending upon performance requirements and/or the feasability of recalibrating for each duty cycle, the gyro may or may not be cooled. Tests carried out to measure the effect of cooling of gyros have made use of both the tumbling test and the IA || EA servo test before and after cooling. These tests are able to show whether gyro performance has changed as determined by Fourier coefficient stability from revolution to revolution of the turntable in either test method or by the root-mean-square point-by-point repeatability of the servo test referred to earlier. Comparison of Fourier coefficients between data taken before and after the cooling cycles determines calibration stability, and performance requirements in turn indicate whether the need for recalibration following cooling exists.

Beyond thermal cycling, environmental testing has involved use of voice coil and linear shake tables and centrifuges. When direct data are being taken during the test, the torque-restraint loop with up-to-date digital techniques is now used, having outgrown the analog approach a few years back. More critical judgement of the influence of such tests on gyro performance is again determined by tumbling and servo tests made before and after the shake or centrifuge tests.

The Pendulous Accelerometer

Turning attention to the accelerometer, initial efforts at developing instruments of suitable caliber for application in feedback damped Schuler-tuned systems were concentrated on reducing output-axis friction. At MIT this effort was directed toward a floated-type pendulous accelerometer. Twenty years ago, when this work was in the early stages, the pendulous-accelerometer design had much in common with the gyro design. The pendulous accelerometer could be tested using the same excitation sources required for the gyro, including those for using analog torquing of the pendulous floated element in the accelerometer.

To clarify definitions and nomenclature, a schematic of the pendulous accelerometer is given in figure 2-17. Testing of early pendulous accelerometers consisted primarily of tests designed to ascertain the presence of any so-called stiction or uncertainty in the output-axis bearings. These bearings, as in the gyros of that day, were of the pivot-and-jewel type (2). The test data were presented as in figure 2-18, and indicated uncertainty in indicating the vertical. The float, and therefore the pendulous element, was torqued off null and allowed to return

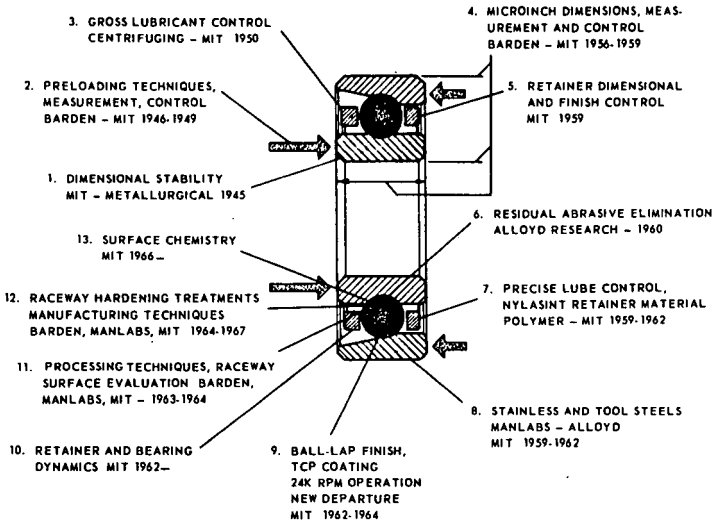

Fig. 2-16 Past and pending efforts on ball bearing improvement

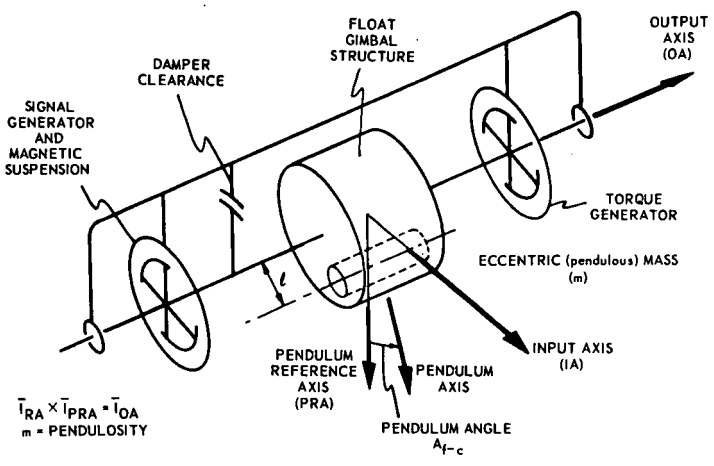

Fig. 2-17 Line schematic of a floated pendulum unit

INSTRUMENTATION LABORATORY
MASSACHUSETTS INSTITUTE OF TECHNOLOGY
CAMBRIDGE, MASS.

PREPARED BY:

DATE: 60 FP 2 # 166

UNCERTAINTY ANGLE DATA

Initial float displacement = ±6000 mv = ±100 mr.

SG OUTPUT VOLTAGE (mv) AFTER:		(3) UNCERTAINTY Angle - mv = $\frac{(1)-(2)}{2}$	(4) DEVIATION FROM AVERAGE VALUE
POSITIVE ANGULAR DISPLACEMENT (1)	NEGATIVE ANGULAR DISPLACEMENT (2)		
+15.2	−2.75	8.98	0.12
+19.2	1.5	8.85	0.01
+24.5	7.0	8.75	0.11
	Sum =	26.58	0.24
	$(U)_e$ Average =	8.86	0.08
	max. value =	8.98	0.12

1.11

$(U)_M = \left[(3)_{(av)} \pm (4)_{(av)} \right] \left[S_{(pu)} [e; M] \right] = 9.83 \pm 0.09$ dyne cm

$(U)_A = \left[(3)_{(av)} \pm (4)_{(av)} \right] \left[S_{(pu)} [e; A] \right] = 31.45 \pm 0.28$ sec arc

9.55

Fig. 2-18 Uncertainty angle test data

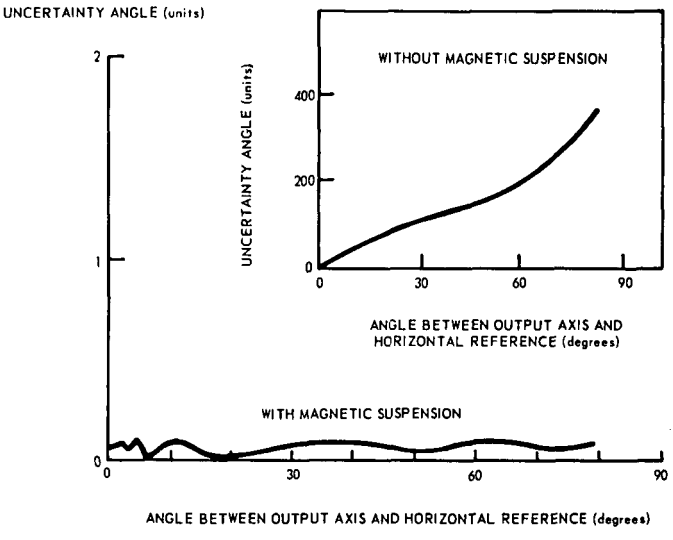

Fig. 2-19 Uncertainty angle as a function of output-axis deviation from the horizontal for the floated pendulum

under action of gravity after the torquer was turned off. The repeatability of such tests in returning to null from clockwise and counterclockwise off-null positions was the measure of performance and was expressed in seconds of arc of uncertainty.

The data shown represent a poorer level of uncertainty. More accurate (5 seconds of arc) indication of the vertical was a prerequisite for the Schuler-tuned platform application to prevent oscillations generated by any step changes in apparent acceleration caused by the pendulum sticking and releasing in the output-axis bearings. Such action would initate a Schuler period oscillation.

The pendulous accelerometers were used without restraint torque in the early inertial-navigation systems, and it was expected that rates of change in acceleration would be in keeping with use of Schuler tuning. In fact, because of the free pendulums, these systems had to be 'latched in' after the airplane was airborne - using a preplanned azimuth and constant velocity. Studies were made on the pendulous accelerometers for linearity to allow for flight paths that deviated from the planned great circle. These linearity studies consisted of aligning the pendulum IA to precise angles off horizontal and reading the signal-generator output. A series of angles over 100 or more milliradians gave a measure of signal versus angle linearity. This was usually plotted in terms of the deviation from linearity.

Because of the compound leverage in a pendulum due to its pendulosity, as shown in figure 2-17, any cross-axis acceleration along its output axis places a torsional load on the pair of output-axis bearings. Under combined input-axis and output-axis loading, the uncertainty of the pendulum increased markedly. Introduction of the magnetic-suspension system (10) to instrument design, to supplement flotation and eliminate pivot-to-jewel contact, virtually eliminated this problem as shown in figure 2-19. The magnetic suspension did much to improve gyro performance also.

Tests today, although of different data format, are still aimed at detection of uncertainty in floated pendulums but, in addition, involve electrical torque restraint of the pendulum to allow for use in other than local vertical system application and at higher accelerations. For example, the Apollo guidance system uses a clock-synchronized pulse torqued restraint loop to keep the pendulum output angle small and,through summing or integration of these pulses in the computer, measures the velocity of the vehicle in each of three coordinate directions (one associated with each pendulum). The block diagram for such a test is shown in figure 2-20.

The pendulous accelerometer of twenty years ago was tested repeatedly for reassurance of low uncertainty and the ability to indicate vertical. The pendulous accelerometer of today will be so tested and also by repeated measurements of full gravity and components thereof using a torque-restraint loop to cage the pendulum float at the null position. The difference between former and present tests can be defined by the position of the pendulous accelerometer when tested. Twenty years ago, with the output axis horizontal, the input axis of the accelerometer was aligned horizontal. After torquing the pendulous element off null, the return of the pendulous element to the vertical after each test was the measure of performance. Today, the output axis and pendulum axis together with the pendulous element are initially aligned horizontal and the caging torque is measured for repeatability and linearity of scale factor as the alignment of the input axis is adjusted in something like ten-degree steps back to the horizontal position. Under this condition, the linearity of pendulum signal-generator output versus angle is not needed or utilized.

Further testing for higher acceleration levels is done on a centrifuge utilizing the digital pulse torque-restraint loop. Again, torquing linearity is studied. In

c*

all these tests, use of the torque-restraint loop allows integration over extended periods of time for finer data definition and extended studies of performance. Other one-g tests with cross-axis loading-i.e., output axis off horizontal- are carried out to insure suitable operation under such conditions.

As in the development of testing of the gyro, that for the pendulous accelerometer has turned to more thorough examination of what used to be considered insignificant or secondary factors. A large part of the test effort, if not the greater part, now is directed toward calibration of bias torques. This includes measurement of the changes in bias caused by excitation changes and radial and axial position of the floated element inside the housing (caused by cross accelerations, imperfect flotation, etc.). The tests for establishing torquer scale factor and linearity have previously been discussed.

Add to the foregoing tests those for changes in bias or torquer scale factor and linearity from cooling and storage below operating temperatures. Many repeat tests are made to observe changes due to intermittent use while kept at operation temperature.

The Pendulous Integrating Gyro Accelerometer (PIGA)

In discussing testing of the floated pendulous integrating gyro accelerometer, the discussion cannot go back twenty years for MIT experience but only to approximately 1953. However, German activity in early designs of pendulous gyro accelerometers is known to have occurred in the early 1940's. Figure 2-21 is a schematic drawing of the floated PIGA with definitions and nomenclature.

As initially developed, the floated pendulous integrating gyro accelerometer did not include the magnetic suspension. However, the pendulous gyro, like the simple pendulum, was subject to loading of the output-axis bearings by cross-axis acceleration. Use of the magnetic suspension has been of great value in insuring acceptable operation of the PIGA with cross-axis loading.

A distinction between the floated integrating gyro discussed previously and the floated pendulous integrating gyro accelerometer should be made. The 'integrating gyro' term derives from the high internal damping of the gyro to motion about the precession axis, thus enabling self-contained integration of rates applied about the gyro input axis. The output voltage of the signal generator is proportional to the integrated angle of rotation about the input axis, and the gyro becomes ideal for a space stabilized servo application. On the other hand, the integration taking place in the pendulous integrating gyro accelerometer is represented by the total angle of rotation of the drive shaft on which the floated pendulous gyro is mounted. This total angle represents the integration of linear acceleration, i.e. linear velocity. The internal integrating property of the pendulous gyro itself is not a direct output but serves to smooth and integrate data. Any roughness due to lag in the servo drive for the output shaft would be smoothed by the gyro integration property.

Initial testing for the PIGA is done on the gyro or pendulous integrating gyro (PIG) assembly by installing in the driveshaft assembly. The PIG is tested for wheel operation, 'clean' assembly, and for unbalance or pendulosity value.

The PIGA instruments have always been tested by a series of multiple-position tests (plus and minus full gravity along the accelerometer input axis) to determine scale factor (output shaft radians/second per unit acceleration) and bias (apparent measured acceleration with no acceleration input). The evolution of testing has, like that of the gyro, been in terms of more precise test equipment and data recording to keep pace with instrument improvements. Stability of scale factor and bias are studied over much longer periods of time and determined in units of parts per

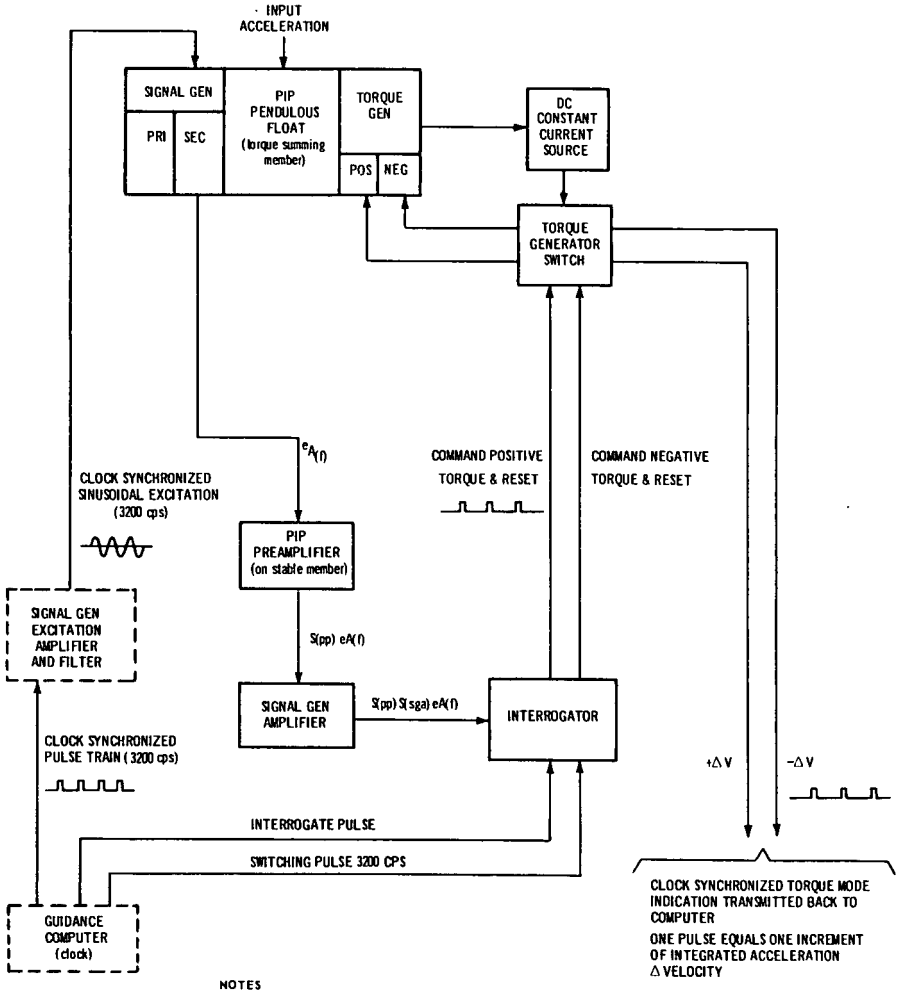

Fig. 2-20 PIP accelerometer block diagram

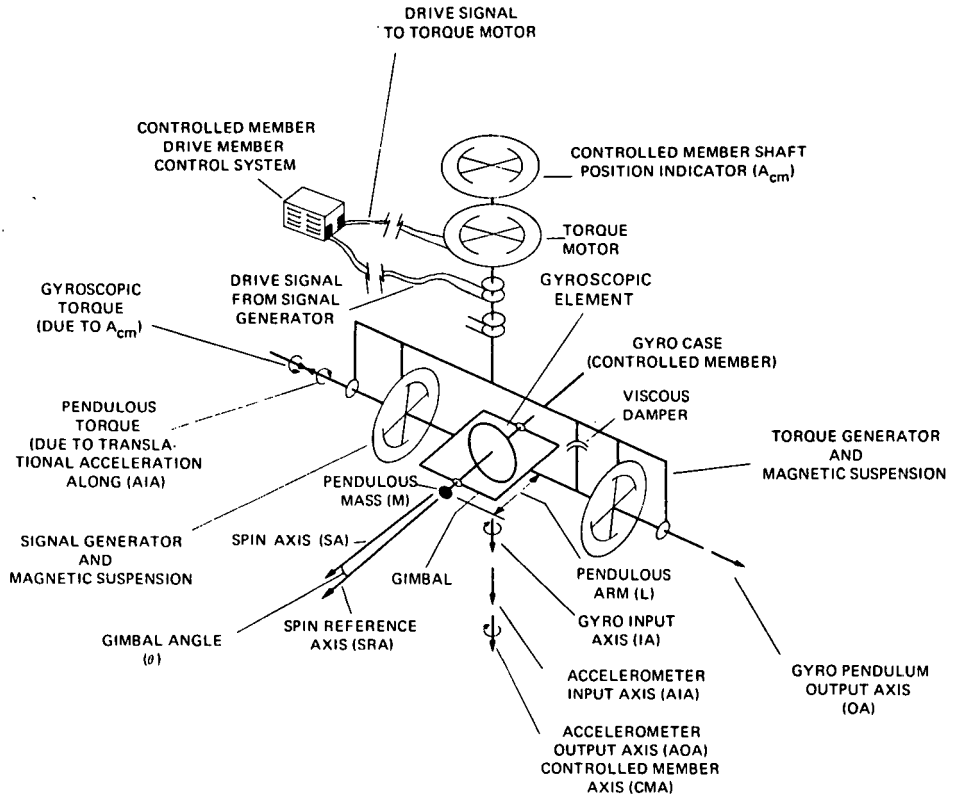

Fig. 2-21 Line schematic of pendulous gyro accelerometer

million of scale-factor variation and micro g's of bias variation. In addition, the influence of environment (including temperature cycling and high acceleration) on these properties is studied.

One of the critical aspects required of the PIGA is the alignment of the PIGA input axis to the driveshaft assembly. This is checked and corrected as needed.

Because of the inherent integrating property of the floated pendulous integrating gyro accelerometer, performance can be studied over extended periods of time at either a fixed acceleration input or a programmed variation in acceleration input. Such tests on automatic equipment are conducted today and the data are processed through a digital computer for studies of scale factor and bias stability. Data are presented as a plot of bias and scale-factor deviation versus time.

A principal application of the pendulous integrating gyro accelerometer has been for acceleration levels greater than one g, as in missiles. For this reason, considerable testing is done on such devices as centrifuges to determine linearity of sensitivity to acceleration. Tests under shock and vibration to insure instrument survival are made, with tests of bias and scale factor made before and after.

Considerably more information on the testing of PIGA's will be given in later chapters.

References

(1) Schuler, M., 'The Disturbance of Pendulum and Gyroscopic Apparatus by Accelerating the Vehicle', Journal of Physics, Vol XXIV, Kiel, Germany, July 1923.

(2) **Denhard, W.G. and Freeman, A.P.**, 'Inertial Gyro Pivot-and-Jewel Suspension', GL-211, Inertial Gyro Group, Instrumentation Laboratory, MIT, Cambridge, Mass. Sept. 1956.

(3) **Whitman, H., Langdon Wales, R. and Andersen, J.P.**, 'The Type H Gyro, Computing and Accelerometer Units', R-17, Instrumentation Laboratory, MIT, Cambridge, Mass. Sept. 1953 (Reprinted April 1954).

(4) **Denhard, W.G.**, 'Laboratory Testing of a Floated Single-Degree-of-Freedom, Integrating Inertial Gyro', R-105, Instrumentation Laboratory, MIT, Cambridge, Mass. Sept. 1956.

(5) Ibid., Appendix 11, GT-16.

(6) **Palmer, P.J.**, 'Gyro Torque Coefficients', E-1601, Instrumentation Laboratory, MIT, Cambridge, Mass. Revised Jan. 1966.

(7) **Hall, E.J.**, 'Gyro Reliability Achieved through Proper Design and Effective Performance Monitoring', R-568, Instrumentation Laboratory, MIT, Cambridge, Mass. March 1967.

(8) **Ragan, R.R., Mayo, G.W, and Feldman, J.**, 'Apollo Guidance and Navigation Flight System Reliability,' R-569, Instrumentation Laboratory, MIT, Cambridge, Mass. March 1967.

(9) **Freeman, A. P.**, 'Gyro Ball Bearings — Technology Today', Feb. 1968, Prepared for presentation at the Sixth AGARD Guidance and Control Meeting, 'Inertial Navigation Components', at Braunschweig, Germany, May 1968.

(10) **Gilinson, P. J., Jr., Denhard, W. G., and Frazier, R. H.,** ' A Magnetic Support for Floated Inertial Instruments', Report R-277, Instrumentation Laboratory, MIT, Cambridge, Mass., 1960.

Bibliography

'Air, Space and Instruments' (Draper Anniversary Volume), ed. by S. Lees, McGraw-Hill, New York, 1963.

'Space Navigation Guidance and Control', AGARDograph 105, Technivision Ltd., Maidenhead, England, 1966.

Barry, J., 'Development of PIGA Functional Block Diagram and Preliminary Study of 11 PIGA Dynamic Performance', MCR-65, Miniature Components Group, Instrumentation Laboratory, MIT, Cambridge, Mass. June 1965.

Colman, G., 'Generation of Calibrating Signals for Ultra-Sensitive Accelerometers', Thesis No. T-437, Instrumentation Laboratory, MIT, Cambridge, Mass. Sept. 1965.

Draper, C. S., Wrigley, W. W. and **Hovorka, J.,** 'Inertial Guidance', Pergamon Press, New York, 1960.

Mueller, R. K., 'Microsyn Electromagnetic Components', E-224, Instrumentation Laboratory, MIT, Cambridge, Mass. 1953.

Mueller, R. K., 'Proposed Method for Producing a Lead Performance Function in Integrating Gyros', E-38, Instrumentation Laboratory, MIT, Cambridge, Mass. March 1951.

Savet, P. H., 'Gyroscopes, Theory and Design', McGraw-Hill, New York, 1961.

Schnee, L., 'Accelerometer Performance Parameters and Tests in One-Gravity Field', Session 17, Inertial Navigation Equipment Evaluation Techniques, Vol II, Notes for Summer 1963 Program 16, 39S, Department of Aeronautics and Astronautics, MIT, Cambridge, Mass.

Slater, J. M., 'Inertial Guidance Sensors', Reinhold, London, England, 1964.

Weinstock, H., 'Laboratory Test Equations for a Pendulous Integrating Gyroscope and the Linear Integrating Accelerometer', E-1400, Instrumentation Laboratory, MIT, Cambridge, Mass. Aug. 1963.

3

The Economic Justification for Gyro Testing

W. G. DENHARD
Associate Director, Instrumentation Laboratory, Massachusetts Institute of Technology, Cambridge, Massachusetts, USA

Summary

The chapter concerns itself with a discussion of the determination of the Reliable Performance Life of gyroscopes through a testing program adequate in duration and content. The development of this topic leads to a comparison of overall costs of purchase and use versus Reliable Performance Life. It is shown that increased testing, although raising purchase price, can result in a lower Cost per Use Hour via a longer Reliable Performance Life by rejecting deficient gyros.

Two possible series of tests for limited times of approximately 50 and 100 hours are presented as are recommendations for sampling tests of longer duration for a higher assurance level of test validity.

Corollaries between gyroscopes and other types of equipment allowing application of the viewpoints expressed should be possible.

Introduction

'Cost Effectiveness' is an American expression currently very much in vogue which relates to government procurement. Its meaning is the accomplishment of any spending of government funds effectively. So far all is noble and good. But now - just what does spending government funds effectively mean? To different people it can mean many different things:

(a) To the purchasing agent, it calls for minimum unit cost; and for repeat orders, less unit cost for each subsequent order.

(b) To the supply depot, it signifies not only minimum unit cost but also fast delivery.

(c) To the Air Force or Navy pilot, it represents whatever cost is necessary to insure his safe return after completion of a mission.

The contrast to be found in these different meanings for spending government funds effectively is readily developed. In the first example, the interpretation is based upon an immediately measurable value - unit cost. The judgement seems more nearly tied to budgetary requirements than other values. In the second example, another criteria is added - that of delivery. The maintaining of a numerically adequate stock level acquired within budgetary bounds is used for judgement. In the third example, which leaps over a number of intermediate viewpoints, the basic judgement of survival is applied and budgetary funding requirements are made secondary. Implied also is delivery on a schedule that places the equipment in the airplane for the mission.

Ultimately, all these viewpoints should be compatible. The basic thesis of this chapter is that such compatibility must ultimately have as its basis the pilot's viewpoint with budgetary goals set to accomplish his needs at least-total-cost. (It sometimes happens that budgetary needs are met first and fixes then applied to work in the pilot's requirements. This path is not always less expensive than a proper initial approach.)

Because this chapter is focused upon gyros, and more specifically upon the testing of gyros, the interpretation of Cost Effectiveness will be applied to establish some criteria for predicting the Reliable Performance Life and the Cost per Use Hour associated with that life. These two factors are considered significant to the pilot's viewpoint (i.e. predicting replacement cycles to insure reliability), and to the effective spending of government funds (i.e. reducing unit cost not in terms of piece cost but in terms of an amortizing cost per hour of use).

In developing the thesis of this chapter, utilizing gyro testing as the path of approach, a question to be answered is: What is Cost Effectiveness in terms of the amount of testing and the specifications required? The answer to this is not straightforward. In fact, the chapter will not give an explicit answer, but will provide material for some new looks at current practices and a forceful look at true total costs, Cost per Use Hour, and Reliable Performance Life.

The procurement of precision gyros is used as an example to indicate the value of testing in terms of Cost Effectiveness. For the purposes of this chapter precision gyros are considered to be the type used in highly accurate inertial-navigation systems and should be differentiated from crude gyros such as are used in short-range air missiles for example, although the principles expounded here hold for all.

Low-price versus High-price Gyros

The first step is to determine whether, in a functional sense, there is more than one kind of gyro. If there is, then the question of Cost Effectiveness should be answered separately for each. In deciding this several factors can be studied:

(a) Purpose - A gyro responds to angular position or rotation, depending on the nature of its support. Depending upon internal characteristics and external equipment, the gyro, through sensing angular velocity, measures rate, change of rate, angle of rotation, or deviation from intended position. The gyro may serve to sense unwanted rotations and, through gimbals and servos, stabilize a platform.

(b) Basic Gyro Components - A gyro comprises the following components:

  (i) A gyro wheel, which must spin rapidly to create the angular-momentum vector and which must keep spinning for the life of the gyro.

  (ii) Precession-axis bearings, which must be near frictionless, certainly have low friction, to allow gyro precession: or for a two-degree-of-freedom gyro, to allow stabilization of the angular-momentum vector.

  (iii) A pick-off or signal generator, which may be visual, electrical, or perhaps mechanical, and which must not interfere with the gyro's sensing and responding to angular-velocity inputs.

  (iv) A caging or biasing torquer, which, although not used in all gyros, is a must in many applications for gyro erection, correction of gyro errors, and for external correction and/or modification of servo-system position.

(v) An overall structure, which carries the gyro components and physically adapts the assembly to the end-use item, i.e., servo platform, autopilot, panel board, etc.

(c) Significance to Mission - Depending on the application and redundancy, the gyro may well be totally critical to mission performance and to the safety of the vehicle and crew.

In line with the foregoing, and using a single-degree-of-freedom floated integrating gyro as an example, a line schematic diagram of the gyro might be as depicted in figure 3-1.

The most interesting factor relative to the preceding discussion and to figure 3-1 is that no mention is made of performance, reliability, life, or price in order to describe a gyro in these general terms. In other words, a description of gyro purpose, basic components and significance to mission is not influenced by desired performance, reliability, life, or price. In a functional sense there is only one kind of gyro, though the detailed implementations may vary - e.g., floated or not, single- or two-degree-of-freedom, ball or gas spin-axis bearings, etc.

It is an extremely vital point that gyro description is independent of desired performance, reliability, life, or price since specifications that reduce or limit performance, reliability, life, and price cannot do so by changing gyro purpose or basic components. In addition, only by redundancy or willingness to abort a mission can the significance to mission success be reduced.

The point is that a low-price gyro is describable in the same terms as a high-price gyro. One could take the attitude - why buy a high-price gyro if nothing is added? The point of the chapter is that something should be added by higher price. That something is assurance of performance, reliability, and life. Turning the phrase around, a higher price should mean increased Reliable Performance Life. The following sections present the arguments supporting this statement.

Length of Testing versus Probable Life

When a gyro is purchased, the manufacturer does a certain amount of testing before delivery. This testing is intended to assure some level of performance and provide a basis for an expected reliable lifetime. This chapter now presents the argument that testing time represents from 5 to 15 percent of the expected total operating life of the gyro. Furthermore, the lower in price the gyro, the more likely it is that the test time represents a higher percentage of expected operating life. MTBF (mean time between failures) is purposely not used since the representation of life as here used is absolute - i.e., individual gyro life until failure, either in performance or operation.

From the foregoing figure 3-2 is derived for the conditions where test time represents 5, 10 and 15 percent of expected operating life. In the expectation that the economics involved will prove advantageous, it appears worthwhile to seek specifications, test conditions, etc., to assure that testing represents only 5 percent of expected operating life. It has already been stated that higher-price gyros should have greater reliable performance and life. The lower-price gyros work against this in that test time represents a greater percentage of total operating life.

In an attempt to be realistic, it is worth adding here that some 5 to 20 percent of the units passing a given test program may have performance or operating deficiencies such as to limit total operating life to one half to one tenth of that expected. Again, lower-price gyros with more limited testing are more likely to suffer and

are more likely to encounter a catastrophic type of failure although specific design and environmental factors can influence catastrophic failures.

The section on 'Maximum effectiveness of 50 - to 100-hour tests' (p. 52) suggests a test program that can be stipulated to maximize successful initial testing - i. e., to weed out inferior gyros.

Cost per Use Hour

Testing time is not only valuable in determining the quality of the gyro bought, but also, because of its influence on gyro operating life, can be economically profitable to the purchaser. This latter statement will be shown to be true even though increased testing adds to the purchase price.

The basis of the argument is as follows. Assume that a lot of 500 gyros is ordered so that a reasonable quantity for a production run is involved and pricing is based accordingly. The gyro involved is further assumed to be a model that has been built before. Therefore, all tooling and drawings exist and no development effort is needed. The variable in the purchaser's control is taken as the amount of testing called for in the request for quotation and in the ultimate purchase order.

A comment should be inserted here that the full amount of testing to be done and the results to be achieved should be specified both in the initial request for quotation and in the resultant purchase order to avoid work scope and cost changes. Such testing, required results, and electrical and physical interface specifications will not only serve as sufficient to define the gyro but also will serve to eliminate ineligible bidders if the contract is made either fixed price or shared-cost with a limitation on the purchaser's total cash outlay. The basis for this statement is that the quantity of gyros involved (500) is indicative of a real buy and not a trial procurement on which the contractor can take a present loss to obtain a preferred position for a later big buy. Therefore, the unit selling price per gyro, with its potential for profit or loss by the contractor, must be multiplied by 500 to determine the gross profit or loss. Any contractor wanting to 'buy in' would have to be prepared for a very large buy-in price.

A certain level of performance should not be contracted for unless adequate testing to prove that performance is also contracted for. The same is true in contracting for a Reliable Performance Life. Testing time representing a percentage of total expected operating life must be contracted for and applied fully. At the least, the test results should indicate the worth of committing the gyro to field service.

Using this example, the concept is now developed of Cost per Use Hour as a function of the amount of testing required by the purchaser and of the resultant price per gyro.

The original assumption was a purchase order for 500 gyros of a model ready for, or actually in, production. To this assumption is added that of testing time representing 10 percent of expected operating life and, as a starting point, a minimum price per gyro of $2000 which covers 50 hours of test time. This basis is expanded to develop the data listed in table 3-1 and plotted in figure 3-3.

In stating the hours for total testing time in table 3-1, certain assumptions based on experience are involved. For gyros priced at $4000 and less, a sufficient amount of testing to certify the condition of the spin-axis bearings and gyro precession-axis uncertainty is not usually carried out. Costs dictate this situation. However, as the gyro price rises, more significant testing for the condition of the spin-axis bearings and for the precession-axis uncertainty is added to the test program.

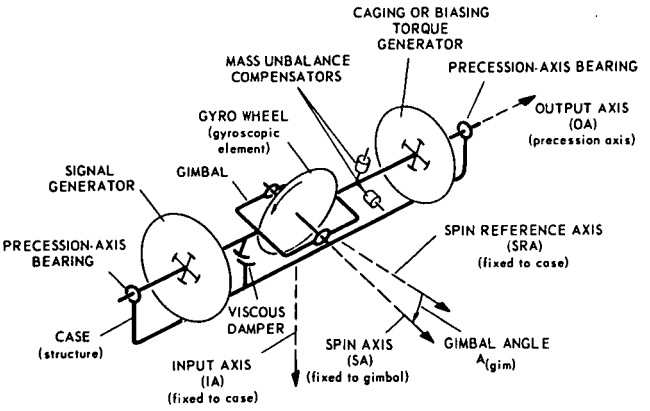

Fig. 3-1 Line schematic of the single-degree-of-freedom floated integrating gyro unit

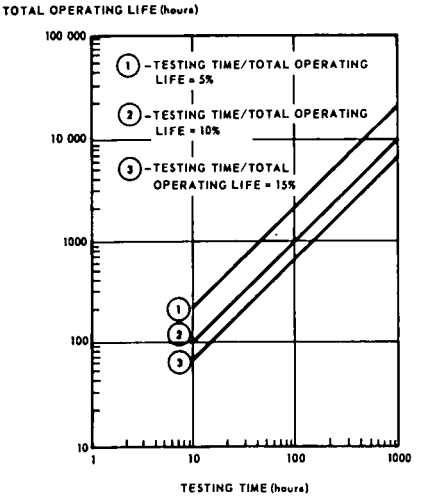

Fig. 3-2 Total operating life as a function of testing time

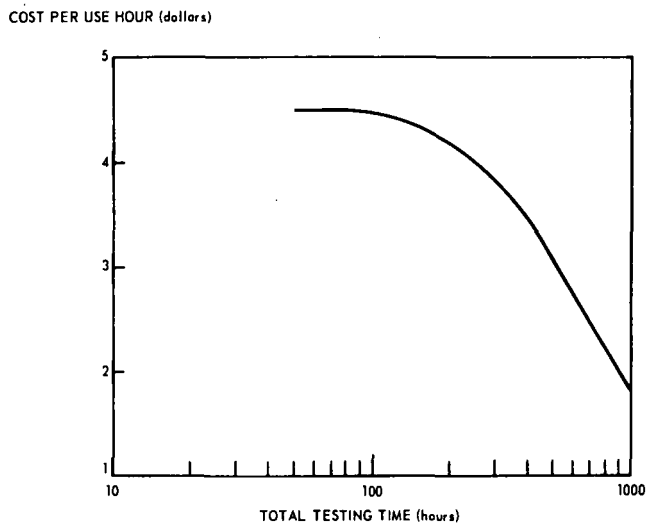

Fig. 3-3 Cost per Use Hour as a function of total testing time (from table 3-1)

Table 3-1 **Cost per Use Hour as a function of total testing time and total expected operating life**

	Total testing time (hours)	Purchase price (dollars)	Total expected operating life (hours)	Cost per Use Hour (dollars)
Basic Unit	50	2000	500	4.50
	100	4000	1000	4.50
	150	6000	1500	4.50
	250	9000	2500	4.00
	450	12 000	4500	3.00
	750	15 000	7500	2.20
	1000	17 000	10 000	1.90

$$\text{Cost per Use Hour} = \frac{\text{Purchase price}}{\text{Useful life}}$$

Useful life = Total expected operating life minus total testing time

Testing of the spin-axis bearings for the lower-price gyros consists primarily of ascertaining that the wheel will start at a required voltage and that for some minimal number of running hours (48 hours or less) this starting requirement is met. Similarly, the number of starts is limited to probably less than 20. These limitations assure that the data will be insignificant for ascertaining life exceeding 1000 hours and, indeed, may preclude ascertaining as much as 1000 hours of life. Remember, though, that this situation is dictated by price and not by negligence or by evil intent.

As a higher price for the gyro is allowed, more significant testing of the spin-axis bearings can be carried out. This leads to use of higher-caliber equipment. For ball bearings, the low-speed dynamometer (1) is brought into use as is the milliwattmeter-dynamometer (2), preload control, longer running, and assessment of friction and windage versus running time and preload versus running time. For gas bearings, the milliwattmeter-dynamometer is brought into use and assessment of run-up time versus running hours, slew tests, and multiple start tests are introduced.

In precession-axis-bearing uncertainty tests, the very fact that longer total testing time allows these to be made over a longer span of real time adds to the assurance of reliability. This is definitely related to the fact that the gyro is in use over the increased testing time undergoing handling, dynamic operation, numerous wheel starts, and intentional or accidental precession through relatively large angles. Temperature cycling should also be included.

Variations in Cost per Use Hour

It is interesting to study the Cost per Use Hour information in table 3-1 and figure 3-3 to determine the necessary price for gyros with 500- or 1000-hour expected total operating life if the stipulation of Cost per Use Hour equal to the $1.90 per hour of the $17 000 gyro is applied. This turns out to be a purchase price of $850 for the 500-hour gyro and $1700 for the 1000-hour gyro. If the reader is able to purchase a gyro for $1700 or less with Reliable Performance Life of 900 hours (1000 total less 100 test hours), with assurance of success, he is in an excellent position. This is providing, of course, that the gyro will meet his performance and environmental specifications in the first place over that life.

Cost per Use Hour as developed in this chapter is strictly an amortization cost for the purchase price of the gyro. It does not allow for installation or removal costs. Obviously, shorter-life gyros incur these costs more often; and although such a gyro may be replaced or repaired at lower cost than a more expensive gyro, the installation and removal costs also represent real costs associated with the gyro. Add to this the expected increased hazard of failure and mission or equipment loss incurred with the lower-price gyro, and a new meaning of Cost Effectiveness begins to appear.

To bring this last point out more fully, consider figure 3-4, which shows that total equipment effectiveness and perhaps utility and safety can be depicted as being supported critically by the gyro. Should the gyro fail, the inverted pyramid may crumble to scrap.

The Real Cost of Increased Total Testing Time

Examination of table 3-1 appears to indicate that testing alone adds considerably to instrument cost: this is true since some types of testing can involve both expensive equipment and several technical personnel. However, more important is the fact that the requirement for added testing (and more-indicative test results) places a much greater responsibility for reliability and performance on the manufacturer.

For a gyro required to have a total operating life, or Reliable Performance Life, of 4500 hours, a test program of 450 hours is required assuming the 10-percent factor. Based on the data in table 3-1, this means that the manufacturer would be testing the $2000 gyro to extinction and the $4000 gyro to half life. Presumably his in-house failure rates in both cases would be prohibitive and he would have to put more gyro assemblies in the production line to meet the delivery requirements by selectivity or else basically improve the quality of his instrument. Either way his building costs, apart from his testing costs, would markedly increase, and he would no longer be marketing a gyro priceable at $2000 or $4000.

The Maintenance Factor in Cost

The approach to testing is most often dictated by the approach to cost. If the approach to cost is for low initial outlay, testing will be severely limited. Sometimes foresight will allow maintenance costs of a reasonable amount to be associated with low initial cost. If the low initial cost yields enough reliability to keep maintenance costs within bounds, this is a reasonable approach. However, subsequent discussion argues against this possibility being a reality.

Most often the low-initial-cost approach takes it for granted that the only thing sacrificed by this cost limitation is performance-from something better than specifications down to specification level. Reasonably long reliable life is still expected. Do the reader's own experiences justify this? The writer is sure that over 50 percent of readers cannot verify this expectation from experience.

Too often the cost factors of installation and removal of the gyro for maintenance are overlooked. These costs may involve removing large assemblies just to get access to the gyro. They certainly should be considered to involve an 'out-of-service' charge for equipment-e.g., an airplane in a nonoperative state while removal and installation work is going on.

Figure 3-5, although nondimensional, shows that gross maintenance costs can be considered to increase with increasing Cost per Use Hour. This follows from table 3-1 and figure 3-3 which indicate that lower Cost per Use Hour is effected through longer-total-operating-life gyros. Less maintenance activity is associated with a gyro that needs replacement less often. Table 3-1 and figure 3-3 are in turn based on knowledge indicating that the lower Cost per Use Hour gyro is the result of higher purchase price and more testing allowing adequate screening.

Failure - What is it?

Failure of a gyro can take the form of any one or more of several modes. Some of these modes are catastrophic and some are relative failures. At the time of acceptance by the purchaser it is feasible to reject on the basis of either type of failure. When the gyro is required for service in an aircraft or other vehicle which critically depends in a go/no-go manner on the gyro for mission success or safe return to its base, it is worth carefully viewing the types of failure causing initial delivery rejects. A significant number of catastrophic failures (examples are open circuits, spin-bearing lockup, or precession-axis bearing failure) would perhaps indicate a higher risk than desirable in the application.

A critical dependence could occur in control of vehicle dynamics, navigating with a closely figured fuel load, single-pass flight plan, etc. A pathfinder assignment could multiply the critical nature of the application.

Thus, the types of failure which occur may have significance and influence beyond mere percentages. Furthmore, the types of failure are indicative of strong and

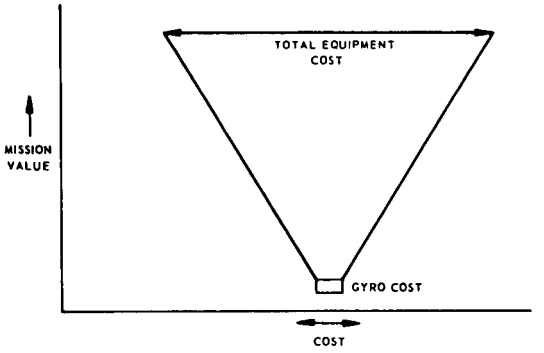

Fig. 3-4 The inverted pyramid of mission value versus cost

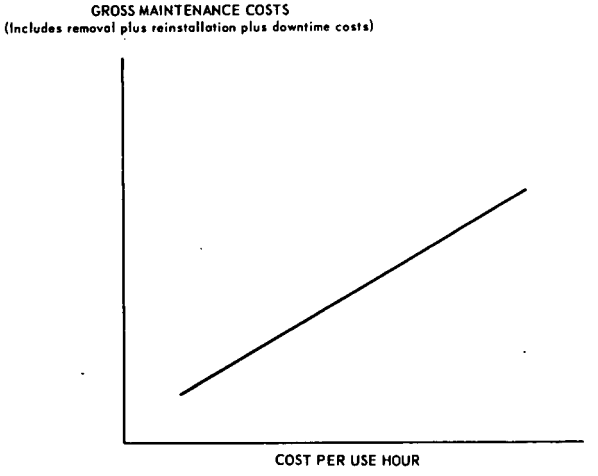

Fig. 3-5 Maintenance cost (gross) per Cost per Use Hour

weak points of design and/or of contractor capability. Absolute judgements cannot be made within the scope of this chapter.

MTBF - Fact or Fancy?

It is not unusual to cite the worth of a gyro (or system or bearing) on an MTBF (Mean Time Between Failures) basis. This, however, can be misleading due to several factors.

During a period of expansion in application of vehicles, systems, gyros, etc., new units are being installed in operation and the number of units in service is increasing rapidly. All the gyros, though having few operating hours, are adding to the sum of operating hours. At this time an MTBF number may look very good but be very misleading because no gyro really has a significant number of operating hours.

Another factor leading to an unrealistically high MTBF is that which occurs when systems (or vehicles, etc.) containing gyros are cycled to a depot for model changes of the gyros or other parts, or for repair of a nongyro element. This provides an opportunity to install new gyros without affecting the MTBF figure.

Those taking heart in a good MTBF number should investigate the conditions involved and either perpetuate these conditions to insure a stable MTBF or prepare for a later change in MTBF.

The writer contends that absolute-life figures of individual gyros would be more useful than MTBF figures in evaluating field performance and true costs per operating field-hour. After all, a design change is of itself indicative of a need for improvement.

Maximum Effectiveness of 50- to 100-Hour Tests

As already indicated, the amount of testing to be carried out before instrument delivery is most often dictated by allowable price. Any time that gyros or other instruments are bought on a low-initial-cost basis, the first items to be cut to meet the cost goal are test items.

Thinking only in short-range immediate-cost terms, this is logical. Testing may involve (depending on the gyro-performance caliber) anywhere from $6000 to $150 000 worth of equipment and from part-time use of a technician to full-time use of an engineer, one or more technicians, and a data processor. Taking average costs per man (including overhead) as $10 per hour, one hundred hours of test involving an engineer, one technician, and a data processor will cost $3000. Of course, these costs could be worked to one-half or one-third of this value by judicious use of multiple test stations. In addition, certain mechanizations or automation of the test equipment could save considerable labor cost for the most simple tests and for many of the long-time tests. But even so, there is no denying the fact that testing, when viewed alone and out of context, is expensive.

It is within our experience to observe that limited testing - 50 to 100 hours - unless done with extreme care, i.e. good engineering participation, will give very low assurance of reliability and long life. This was indicated also in discussing Cost per Use Hour. The manufacturer himself cannot know the Reliable Performance Life of his instrument to any certainty by only limited testing.

Assume that a high-quality gyro is desired with a Reliable Performance Life of 1000 hours or more, and yet with funding such as to limit the amount available for testing to a 50- or 100-hour test program. The following are some thoughts on testing attuned to that situation.

(a) Require 90-percent acceptance on instrument test before any repeat tests are allowed on failed gyros.

(b) Require every 4th, 6th or 8th gyro (depending on the quantity in the purchase order) to be tested an additional 100 to 200 hours, and stipulate that 90 percent of such gyros must pass this test. If 90-percent acceptance on this test is not achieved, perform this double testing on all gyros until reliability is restored.

The background leading to the preceding two statements is as follows:

(a) For limited testing of 50 to 100 hours, the span of time and the amount of testing are insufficient to get a true spread (a so-called bell curve) of performance and reliability of a good gyro. The time should be sufficient for a poor gyro. Therefore, any spread of performance or reliability determined in this limited testing has to be more indicative of a poor gyro, which is assumed to be undesirable. By demanding a very high acceptance rate (90 percent or greater) during the first run-through testing of each gyro, the manufacturer is forced to insure reliability and performance more commensurate with a good gyro. Repeat tests should be more stringent than initial tests; this forces the manufacturer to make the choice between rebuild costs and heavy test costs, which perhaps will be a waste of time if the gyro fails again. Except for specifically defined cases, agreed upon between purchaser and manufacturer, no more than one repeat test should be allowed. However, at the option of the manufacturer this one repeat test could be delayed a considerable time after the initial test.

(b) The requirement for additional testing to insure nonmarginal gyros is useful in giving the purchaser a look at extended testing for reassurance of quality. It is also useful in giving the manufacturer a quality-control check on his production quality. The requirement for a high acceptance level here (90 percent or greater) is again in line with desire for ultimate receipt by the purchaser of higher-quality gyros with Reliable Performance Life exceeding 1000 hours.

For a limited testing program, emphasis must be placed on precession-axis uncertainty and spin-axis-bearing reliability. A suggested 50-hour gyro test program is outlined in table 3-2. A suggested 100-hour gyro test program incorporates the 50-hour program of table 3-2 and adds a servo test, as outlined in table 3-3. The testing details and performance specifications associated with the test programs are covered in the referenced documents, particularly in reference (6).

Note that the recommended tests do not invalidate the previously stipulated extra tests on every 4th, 6th, or 8th gyro.

Conclusions

Low-price gyros and high-price gyros are virtually indistinguishable in terms of purpose, functional description, and significance to mission, but a higher-price gyro should mean increased reliable performance and life.

Total gyro testing time represents a roughly definable percentage (5 to 15 percent) of total gyro operating life. Cost per Use Hour actually decreases with increased

d*

gyro price. However, much of the increased gyro price goes into the manufacture of reliability into the instrument rather than into the testing effort itself. Maintenance costs are higher with lower-price gyros, which have a higher Cost per Use Hour.

Gyro (or other critical equipment) life should be defined in terms of absolute life rather than MTBF.

A set of tests is suggested for limited gyro testing (50 to 100 hours) in order to obtain the most effective screening. Fully effective testing of 500 to 1000 hours can best be described and discussed in another chapter or by other authors.

The principles expressed should be applicable to other types of equipment for which realistic testing can be indicative of an expected Reliable Performance Life.

References

(1) 'R4 Ball Bearing Acceptance Tests', GA-189, Inertial Gyro Group, Instrumentation Laboratory, MIT, Cambridge, Mass. Feb. 1963.

(2) **Denhard, W.G.**, 'A Recording Milliwattmeter-Dynamometer - A Research and Production Tool for High-Performance Gyroscopes', R-175, Instrumentation Laboratory, MIT, Cambridge, Mass, April 1958.

(3) 'Uncertainty Investigation', GT-326, Inertial Gyro Group, Instrumentation Laboratory, MIT, Cambridge, Mass, Oct 1960.

(4) 'Gyro Motor and Bearing Evaluation', GT-327E, Inertial Gyro Group, Instrumentation Laboratory, MIT, Cambridge, Mass, March 1966.

(5) 'Six-Point Analysis of Static Unbalances', GT-325, Inertial Gyro Group, Instrumentation Laboratory, MIT, Cambridge, Mass, Aug 1964.

(6) **Denhard, W.G.**, 'Laboratory Testing of a Floated, Single-Degree-of-Freedom, Integrating, Inertial Gyroscope', R-105, Vol I and II, Instrumentation Laboratory, MIT, Cambridge, Mass, Sept 1956.

Table 3-2 Suggested 50-hour gyro test program

	Test	Hours
1.	Circuitry check	1
2.	Precession-axis uncertainty (3)	$1\frac{1}{2}$
3.	Spin-axis-bearing characteristics (1, 2, 4) (Milliwattmeter-dynamometer, rundown, touchdown, breakaway) For a gas-bearing gyro, 30 starts and stops should precede the above.	$2\frac{1}{2}$
4.	Rough measurement of g sensitive terms (5)	2
5.	Mechanical compensation of g sensitive terms and check of results	5
6.	Repeat of test 2	$1\frac{1}{2}$
7.	Electrically caged gyro tests on drive table (tumbling tests) (6)	15
8.	Repeat of test 3	$2\frac{1}{2}$
9.	Repeat of test 2	$1\frac{1}{2}$
10.	Temperature cycling	6
11.	Shortened repeat of test 7	6
12.	Repeat of test 5 (optional, depending on data from test 11)	[5]
13.	Repeat of test 2	$1\frac{1}{2}$
14.	Repeat of test 3	$2\frac{1}{2}$
15.	Physical and electrical examination and preparation for shipment	$1\frac{1}{2}$
	Total Hours required:	50 to 55

Table 3-3 Suggested 100-hour test program

	Test	Hours
1-14.	Same as table 3-2 for a 50-hour test program	$48\frac{1}{2}$ to $53\frac{1}{2}$
15.	Servo Test (6)	48
16.	Repeat of test 2	$1\frac{1}{2}$
17.	Physical and electrical examination and preparation for shipment	$1\frac{1}{2}$
	Total Hours required:	$99\frac{1}{2}$ to $104\frac{1}{2}$

4

Gyro Test Instrumentation

D. F. KEANEY and R. L. KING
Instrumentation Laboratory, Massachusetts Institute of Technology, Cambridge, Massachusetts, USA

Summary

The performance of today's precision inertial gyro places stringent requirements on the test instrumentation used for its evaluation. In many instances, technology has already been pushed to a boundary or accuracy limitation.

Test instrumentation at the MIT Instrumentation Laboratory has evolved over the years from individual items of equipment to today's concept that the gyro and its test instrumentation constitute a complete system. No single component of this system can be thought of as an entity unto itself; its interface with other components must be considered in detail.

As gyro performance has improved over the years, interfering inputs once considered negligible have become significant. This is illustrated by tracing the evolution of gyro testing stations at MIT.

Current philosophy in the areas of environment control such as base-motion isolation and temperature control, environment simulators such as vibrators and centrifuges, and minimization of error sources both electrical and mechanical is described in considerable detail. Examples of existing one-g and linear vibration high-g test stations follow to show the application of this philosophy to practice. Certain aspects of the test station are focused upon to illustrate the trade-offs necessary to arrive at a technically sound, economically justifiable test station.

Test stations for tomorrow's gyros may be of the conventional type using either a single-axis or a two-axis test table on a carefully chosen and prepared site. Alternatively, it may be necessary to utilize the inertial-guidance system itself to satisfactorily evaluate high-performance gyros. Advantages and disadvantages of each method are presented from both the technical and the cost viewpoints.

Orders of magnitude improvement in gyro performance have necessitated similar orders of magnitude improvement in the test instrumentation, with costs increasing proportionally. The test equipment designer must carefully weigh the economic aspects of his design along with the technical aspects if he is to provide the optimum equipment for the particular task at hand.

1. Introduction

The performance of today's precision inertial gyro places stringent requirements on the test instrumentation used for its evaluation. This chapter describes the test instrumentation in current use for this purpose at the Instrumentation Laboratory of the Massachusetts Institute of Technology (MIT).

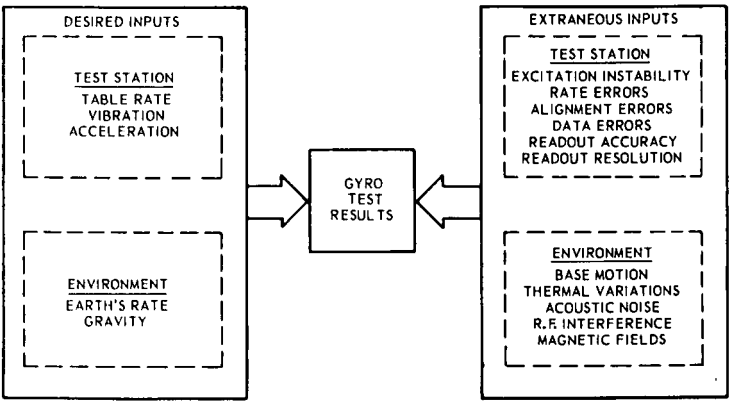

Fig. 4-1 Simplified block diagram of error and uncertainty sources in gyro testing

Test Instrumentation Philosophy

Gyro testing is performed basically to determine the degree of compliance of the gyro's performance with a set of specifications or design goals. The actual evaluation may range from a very limited set of tests designed to ascertain specific items of performance to a comprehensive examination of all aspects of the gyro's performance as required for future development work. The various purposes of gyro testing are covered in chapter 5; but, irrespective of the purpose, the results obtained are compared with a previously defined mathematical error model of the gyro. Thus, the test instrumentation utilized in the testing is the means by which the test engineer or gyro designer is able to determine the magnitude of the terms in the error equation. The accuracy to which this determination may be made is the concern of the test-instrumentation engineer.

The collection of individual pieces of instrumentation used in the testing or evaluation of a gyro is referred to at MIT as a gyro test station. The term 'test station' will be used in this context for the remainder of this paper.

Basically, a gyro test station is composed of a test platform and associated electronic equipment. The test platform may be any mechanical holding device such as a turntable and related fixtures, or it may be an environment-simulation device such as a centrifuge or electromechanical vibrator. The electronic equipment associated with a test station is that equipment used to control the test platform, to provide electrical excitation and control of the gyro under test, and to monitor instrument performance.

With the exception of certain diagnostic information, the sum total of information about gyro performance is contained in one electrical signal, the output-axis-pick-off or signal-generator output signal. (Reference is made here and throughout the chapter to the MIT single-degree-of-freedom integrating gyro—see chapter 5). Since the gyro is a precisely balanced angular-rate-sensing device, testing is accomplished by subjecting it to known rates about its input axis in various orientations with respect to gravity and observing the results. The input rate may be zero, some multiple of earth's rate, or a varying quantity depending upon the particular test being conducted. Meaningful decoding or interpretation of the signal-generator output signal can only be accomplished when adequate information about the influence of extraneous inputs on the content of this signal is available. In the case of vibration or centrifuge tests, other known inputs in addition to angular rate may be applied; however, the data-collection process is the same. As may be seen in figure 4-1, these extraneous inputs may be divided into two categories: those that are the result of laboratory environmental conditions, and those that are produced by the test station itself.

The instrumentation engineer must carefully evaluate each component of the test station with respect to each of the categories of extraneous inputs. The errors and uncertainty of each component whether self-generated or generated as a result of extraneous environmental inputs must be weighed against the error budget for the overall test station. This required an intelligent blending of analytical and practical effort. The analytical aspect of the effort is, of course, based on the best possible assumptions at the time. Realizing that most of the useful theories utilized in analytical work have been proven by practical experiments, it is then obvious that whatever new test equipment may be devised must be subjected to empirical testing itself to substantiate that it fulfills its function. If the equipment is not fully tested, it may have uncertainties which will compromise the data obtained by using it.

Test equipment should fulfil a specific need, and the need must be adequately

defined. Once the need has been adequately defined, then the simplest, stablest, most direct device and/or technique should be devised:

(a) to produce test results of an adequate signal-to-noise ratio,

(b) to provide sufficient operational flexibility for obtaining all or most of the test information needed,

(c) to allow referencing to some fixed datum or at least provide the ability for direct comparison with another similar device.

In any field of endeavor, it is best to strive for the ideal even though it is known that in reality the ideal can never be achieved. This is equally true in the case of test instrumentation where certain ideal characteristics can be listed despite the fact that compromises must be made in the real-life situation to allow progress. An ideal set of test instrumentation would exhibit the following characteristics: (a) simplicity, (b) versatility, (c) reliability, (d) repeatability, (e) stability, (f) low cost.

The first characteristic, simplicity, will aid in achieving the other characteristics. This point is more important today than ever before because the temptation to complicate test instrumentation and equipment with highly sophisticated sensors and their support equipment is greater today than ever before. Sound progress is made only with proven calibrated instrumentation. This does not in any way imply a disregard for better instrumentation, only that a new device, like any standard instrumentation, should not be relied upon until all of its operating characteristics are thoroughly understood and calibrated.

Versatility may be relatively unimportant in a large production facility, but it is especially important in the case of a research and development organization such as the Instrumentation Laboratory. A versatile test station permits conducting a great many different types of tests in various testing modes. In addition, various gyros of the same family can be tested without major equipment changes because of adjustable excitations and varied interconnecting possibilities.

Reliability simply means that the equipment will continue to perform to its specified level for a given period of time. This does not mean that specifying or defining realistic reliability criteria is a simple task, since this can be a long and tedious empirical effort.

Repeatability aids the user in developing confidence in the predictability of the instrumentation, which in turn may lead to successful computer programming of test sequences. Computer direction of repetitive operations is in existence in operational systems now; and in some production test facilities, programmed testing has been in operation for a number of years. However, these tests have had a relatively wide band of acceptance criteria. The computer-controlled test station would aid the test engineer to test and evaluate the gyro almost simultaneously. This would permit the observation and investigation of any inconsistencies before the parameters causing them had an opportunity to change - thus, the test engineer would have more of an opportunity to observe and detect the cause of transient conditions.

Stability relates to the level at which the equipment will operate during its life. Highest accuracy requires a nimimum bandwidth of variation from a specified operating level, or greater stability. This in turn means higher cost since more effort must be expended on the equipment to make it capable of the specified performance, and more testing must be done to certify the equipment's ability to perform as specified. In addition, stability means inherent low response to changes in environment such as temperature variations, power variations, vibration, or shock.

Cost is a relative matter, which in the case of instrumentation, as in the case of gyros, should probably be stated in cost per use hour (see chapter 3). As gyro testing requirements become more stringent in terms of both performance and duration, the requirements on the test equipment obviously must keep pace. For example, a power supply that is expected to have a reliable operating life of ten years must itself be tested by its manufacturer for a longer period of time than a supply with an expected reliable life of only one year. Obviously, this adds to the initial price of the supply, but the cost per use hour of the more expensive supply may be less.

The performance of today's and the expected performance of tomorrow's inertial gyros are the major factors in the cost of test equipment. For example, consider figure 4-2, which is taken from various unclassified sources. That figure shows that published gyro performance today is of the order of 0.001 degree per hour random drift. Test-station-induced drift should therefore be less than 10 percent of the gyro drift or 0.0001 degree per hour random drift. Figure 4-3 is an extrapolated curve of test station cost as a function of station-induced drift, which shows that a test station introducing less than 0.0001 degree per hour would cost of the order of $ 100,000. Meeting the best performance levels shown on figure 4-2 requires test stations stable to 0.00001 degree per hour, or 0.036 second of arc per hour. Such a station would cost in the vicinity of a quarter of a million dollars.

Cost is determined by many other factors in addition to the level of performance required. Some of these are: (a) the number of test stations required, (b) funding available, (c) time available, (d) ingenuity, (e) inventiveness, (f) current technological advances in allied fields, (g) techniques employed. However, the major factor remains the level of precision required.

The interdependence of all the individual parts of a test station is now so evident that the test station and gyro are being treated as a system in itself. Knowledge of the expected performance of the individual parts such as the gyro to be tested, the gyro and table electronics, the test turntable and the gyro holding fixture enable the instrumentation engineer to evaluate the total performance of the system.

When the test station is treated as a complete system and the gyro holding fixture is attached to or is part of the test table, alignment corrections may be made at the gyro interface. This can compensate for limited machining capability elsewhere in the turntable assembly. If sufficient data is accumulated in the performance of a test station, it is further possible to program compensating events or phenomena which will correct any periodic misbehavior of the test station. It is even possible that future test stations will have a programmed monitor that will correct the test station's environment whenever necessary. This effort is already underway in the form of servo-controlled platforms that stabilize the axis of the test equipment with respect to local gravity and the earth's axis. Efforts to reduce the effects of equipment-generated errors and uncertainty are evident in simultaneous multiple-gyro testing where one gyro, in effect, monitors the others and in gyro testing directly in a stabilized-inertial-system configuration.

Test-instrumentation philosophy can probably best be summarized as follows. The test equipment should be the simplest system possible that will enable the gyro test engineer to subject the gyro to the proper desired inputs while at the same time minimizing the effect of extraneous inputs. Thus, the test results will be obtained in the most economic manner with a minimum of uncertainty.

Objective of this Chapter

The objective of this chapter is to describe methods and techniques of implementing the philosophy just stated. After briefly reviewing the history of gyro test

instrumentation at MIT, section 2 describes today's typical one-gravity (one-g) test station and predicts the changes that will occur in tomorrow's test station. Section 3 covers modes of testing: table-tracking microsyn (or sectosyn) tests to check out the station, and the basic gyro test modes - servo-turntable and rate-feedback. Environmental-simulation test stations are covered in section 4. These include angular- and linear-vibration stations and a centrifuge station. Error sources and their minimization are covered in the next two sections, test-station generated in section 5 and environment generated in section 6. The overall instrumentation effort is summarized in section 7.

2. One-Gravity Test Stations

Gyro testing in the one-g environment has always been the mainstay of gyro evaluation efforts. Even with today's emphasis on missile guidance with its accompanying high-g levels, the one-g test station is still the major gyro-evaluation tool.

The one-g test station is utilized in virtually all phases of gyro evaluation at MIT. These include not only tests on complete gyros but also tests performed during instrument design and assembly. An example of the latter category is testing performed on a viscous integrator (the gyro unit without an angular-momentum generator) to evaluate the performance of the signal- and torque-generator components. Examples of the former category are a specialized set of acceptance tests for a specific application or a comprehensive set of engineering evaluation tests to indicate the direction of future design efforts. Diagnostic testing performed to identify specific gyro anomalies is a further example of this category. In the case of test programs which include environmental testing at higher g levels, i.e. centrifuge testing and/or vibration testing, the one-g test station is normally utilized to obtain performance data from a set of control tests performed immediately before and after the environmental exposure.

To satisfactorily complete all the functions just described, the one-g test station must possess all of the characteristics described in the previous section. A high degree of versatility and flexibility is required, especially in the case of a research and development organization, so that many different tests on various models may be conducted at one installation. High reliability is required to achieve consistency and repeatability among tests and to permit the accomplishment of long-term (thirty days or greater) performance runs. Efficient processing or accomplishment of tests coupled with the minimization of human error dictates that simplicity of design and operation be heavily considered.

Design and construction of gyro test stations is a highly specialized art as is evidenced by the fact that there are currently only three major manufacturers of complete test-station complexes in the entire United States. These three organizations have acquired familiarity with the problems confronting the gyro-testing organization through the demands for tighter tolerances, lower-friction bearings, higher-precision electronics and more reliable long-term performance.

This section describes the evolution of today's typical one-g test station at the Instrumentation Laboratory and indicates possible future approaches to test-station design. Although the test station and gyro are, in reality, designed as a complete system, for ease of presentation the test-station history is broken up into its three basic components - the test turntable, the gyro holding fixture and the electronics. Evolution of the current state-of-the-art in each of these areas is described in the following three subsections and is followed by a description of possible next-generation test stations. Specific modes of testing and the particular instrumentation required for these modes are covered in section 3.

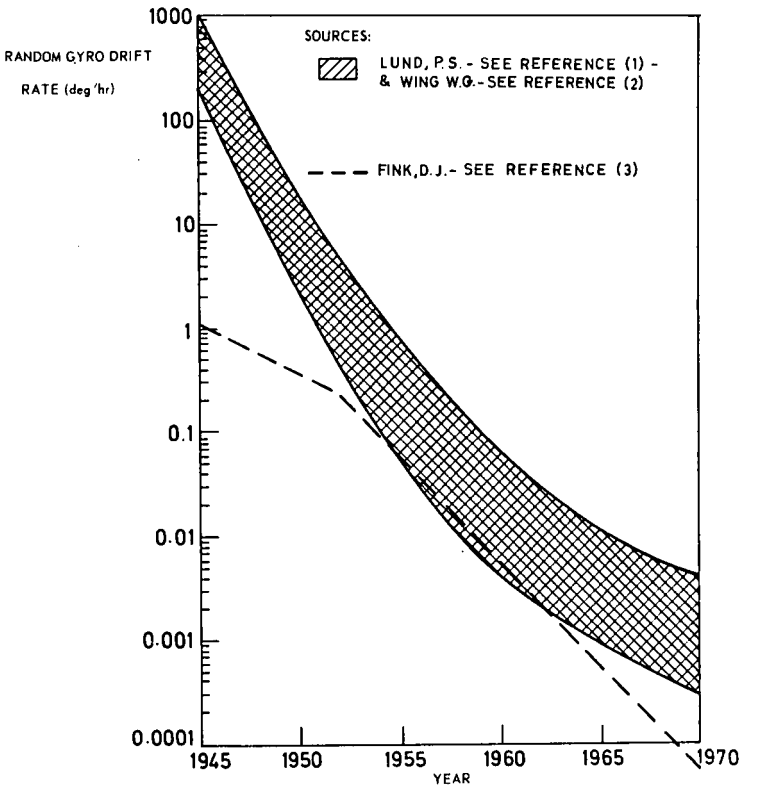

Fig. 4-2 Predicted gyro performance

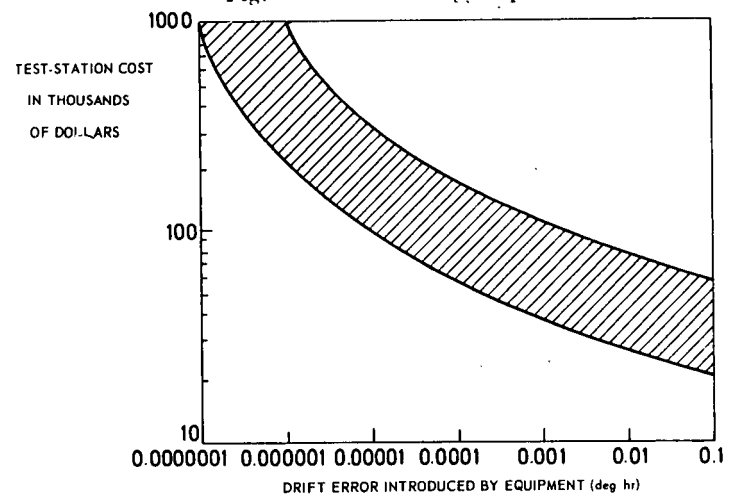

Fig. 4-3 Test-station cost as a function of station-induced drift error

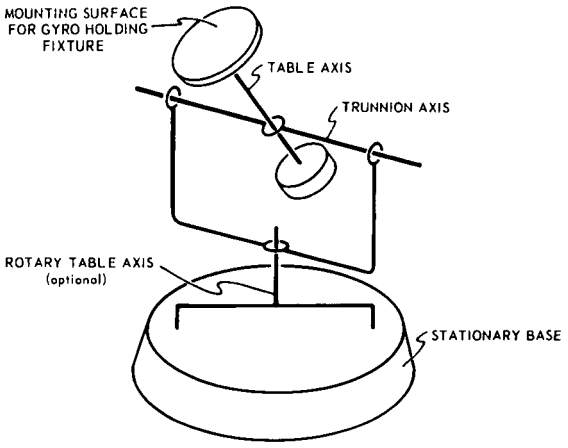

Fig. 4-4 Line schematic of a gyro test turntable

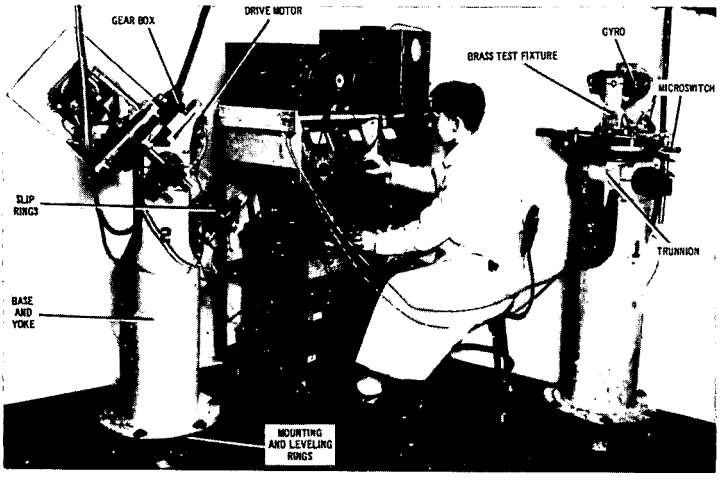

Fig. 4-5 Model B test turntables

Turntables

The basic functions of the gyro test turntable are to provide an axis about which angular velocity may be imposed or compensated for and to provide for orientation of this axis with respect to the earth's axis and the local gravity vector. To accomplish these functions the gyro test turntable must have certain basic features as indicated in figure 4-4. There must be a mounting surface, or table top, to which the gyro and its holding fixture can be secured. The table top must be capable of rotation through 360 degrees about the table axis. Another axis, perpendicular to the table axis, called the trunnion axis must be capable of rotation through at least 180 degrees for various orientations with respect to gravity. A third axis parallel to the local gravity vector, about which the entire turntable can be rotated, the rotary table axis, is optional. The precision with which these axes are located with respect to one another is a function of the accuracy of the gyro to be tested and of course, of the capability of the fabricator. In addition to the bare essentials indicated in the figure, the turntable must include rate and servo drives for the table axis, a table-angle indicating device, slip rings, an incremental angle readout or drive sensor (a table-tracking microsyn or sectosyn), associated wiring, etc.

Early MIT Tables. The earliest predecessor to the gyro test turntable as it is known today was constructed about 1945. Typical machining tolerances on this table, which was designated as Model A, were in the range of 0.001 to 0.0001 inch. The table axis was supported by conventional ball bearings and was driven by a direct-drive alternating-current torque motor. Use of this motor was in advance of the state-of-the-art, and difficulties due to eccentricities resulting from machining limitations were experienced. A major problem was heating of the motor due to internal power dissipation and subsequent expansion problems, which eventually caused the table to bind. Another problem was found to be angular drift of the trunnion axis during positioning and lockdown of about five-to-six seconds of arc.

Angular-position readout on the Model A table was accomplished by means of a microswitch and small balls imbedded on the circumference of the table top at ten-degree intervals. The position resolution was of the order of minutes of arc.

The next table to be developed was the Model B, two of which are shown in figure 4-5. The Model B tables were first operational about 1950 and, like the C tables to follow, were basically a modification of the Model A.

The major difference between the Model A and Model B tables was the replacement of the direct-drive a.c. torque motor with a precision gear train. Servo-turntable testing, where the servo loop is closed to the gyro through rotation of the test-table top, was accomplished by means of a small a.c. torque motor which drove the precision gear train. During rate-feedback testing where the table is driven at some multiple of earth's rate, a synchronous motor was used to drive the gear train. Accuracy of the gear train was a few minutes of arc.

A photoreflective technique of angle readout was tried on the Model B tables for a short period. This technique could probably be developed to a useful level in the light of today's technology, but it proved to be unsatisfactory at the time.

The Model C table, which was put into service about 1953, featured refinements to the gear drive of the Model B tables. The gears were fitted and lapped, but gear-tooth errors were still evident.

The Model D Family. Most of the test turntables currently in use in the United States can trace their lineage back to the test tables developed at the Instrumentation Laboratory and in particular to the Model shown in figure 4-6. The Model D, which became operational about 1954, represented a complete upgrading in turntable design (4).

The Model D tables used precision tapered roller bearings to support the table axis. The bearings were matched pairs with a total indicated runout (TIR) that did not exceed fifty microinches. The bearings were located $9\frac{1}{2}$ inches center-to-center on the shaft; this geometry permitted a maximum coning of only two seconds of arc, a factor of three improvement over the earlier tables. The bearing inner races were a tight fit to the table shaft, and the outer races were press-fitted into the trunnion. In that manner, relative motion of these major contributors to coning error was kept to a minimum. As noted, machining tolerances were held to fifty microinches as opposed to 100 microinches on the Model B and Model C tables.

The ball-and-microswitch table-position indicator on earlier tables was replaced on the Model D table with an electro-optical pickoff system (5). The optical system was associated with a photocell scanning device that generated a pair of peaking signals each time the ruled lines of a precision circular scale passed over a light source at the index point. The pair of peaking signals were generated by a set of splitter prisms and a shutter mechanism in the path of light to the photocell. With proper electrical circuitry, the change in phase of the pair of peaking signals tripped a relay, thereby recording (through auxiliary equipment) the instant of time at which the peaking signal reversed phase. This elapsed-time record was obtained for each of the ruled lines on the circular scale. (The record of time required for angular increments of table rotation is used to evaluate the gyro on test.)

Experience on the earlier tables using servo motors to drive the table through a large-ratio gear train had shown that improved dynamic performance as well as reduced maintenance could be achieved by eliminating the gears. As a result, the Model D table was designed for direct d.c. torque-motor drive.

In 1959, preliminary development was started on a fluid-bearing test turntable. The purpose of the fluid bearing was both to reduce the instantaneous changes in friction in the tapered roller bearings and to provide a reduction in shaft coning error. This effort culminated in the so-called Model D prototype fluid-bearing table, which was basically a test bed to prove the noncontact liquid-seal techniques and to indicate feasibility of such a table. Figure 4-7 is a photograph of the completed table.

Bearing friction was significantly reduced in the Model D prototype table. Friction torque in the Model D tables was approximately 1.25 foot-pounds; in the Model D fluid prototype, it was 0.16 foot-pounds. This factor, of course, contributed significantly to the reduction of friction perturbations during testing. In fact, the Model D prototype table was so successful that all of the remaining D tables at MIT were converted to fluid-bearing tables. This conversion, along with other updating, resulted in the Model D fluid-conversion table, of which a cutaway view and a photograph are shown in figure 4-8.

Table-shaft runout (coning) in the Model D fluid conversion tables is 0.2 second of arc as opposed to five seconds of arc in the Model D tables. Orthogonality of the table axes is on the order of ± 1 second of arc on the D fluid conversion tables, whereas it was ± 5 seconds of arc on the D tables. Bearing radial stiffness is virtually identical for both tables: 15×10^6 pounds per inch for the fluid bearing versus 15.4×10^6 pounds per inch for the tapered roller bearings.

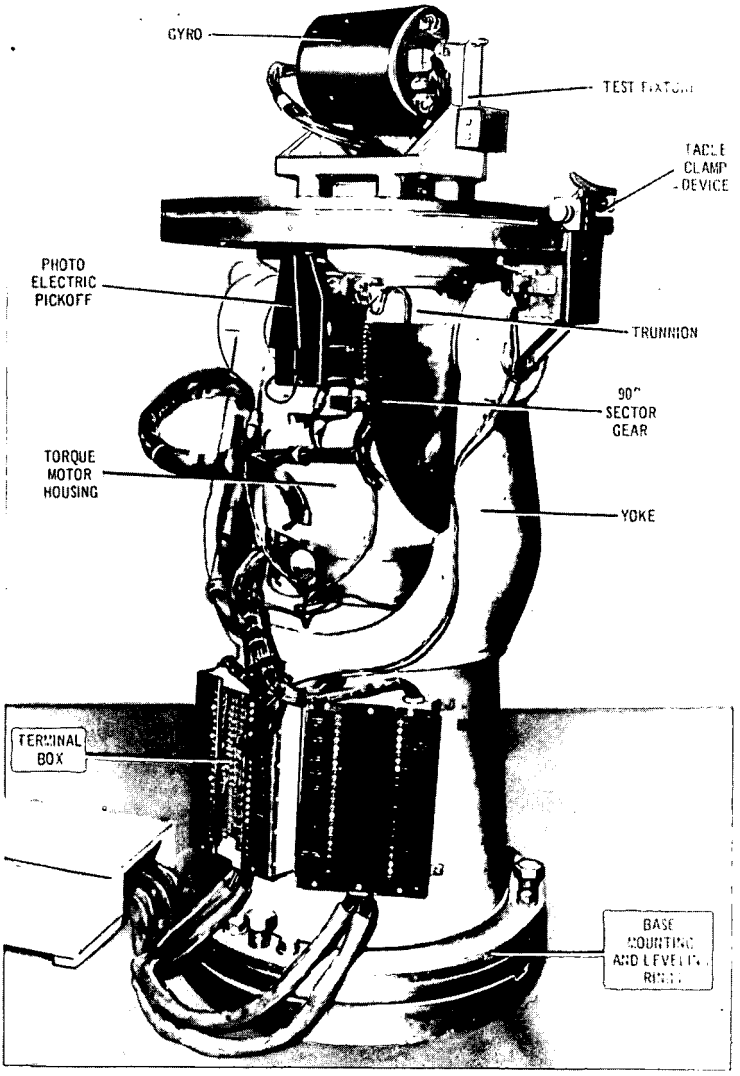

Fig. 4-6 Model D test turntable

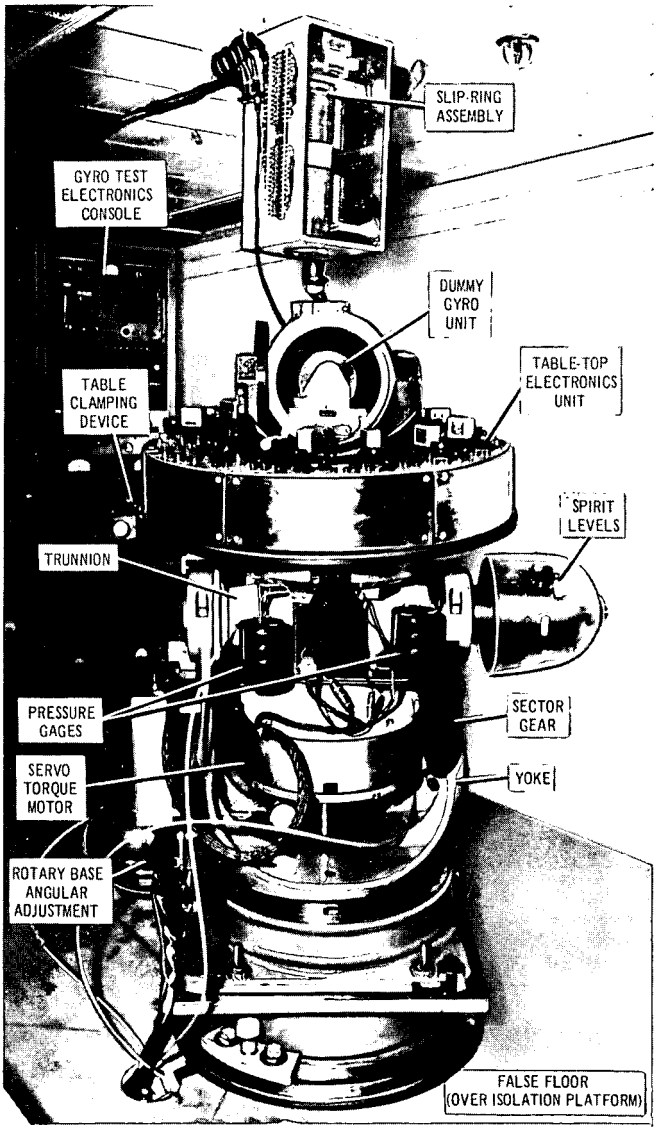

Fig. 4-7 D prototype fluid bearing table

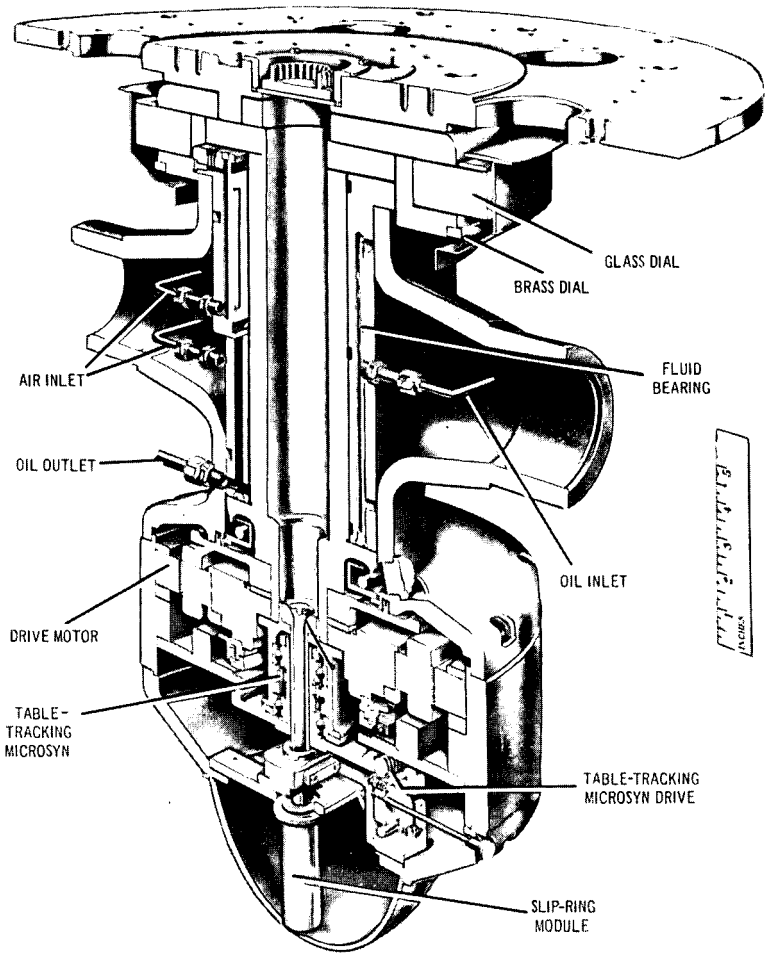

Fig. 4-8 Model D turntable fluid conversion

e*

Model E Table. Design and construction of a completely new gyro test turntable was the next step in the evolutionary process. The design goals were:

(a) elimination of magnetic materials in the table structure

(b) tighter orthorgonality requirements on the table axis (i.e., trunnion to table shaft, table yoke to trunnion) to the limit of manufacturing capability

(c) the stiffest table-shaft bearing consistent with lowest operating friction

(d) an advanced table-angle readout device

(e) integration of the test electronics into the table structure wherever possible

The culmination of the effort was the Model E turntable, which represents the state-of-the-art in operational tables today. Figures 4-9 and 4-10 are cutaway views and photographs of the Model E table.

Some of the major characteristics of the Model E gyro test turntable are tabulated below. A more complete description follows the tabulation.

(a) The foundation is a large steel base ring which bolts in place by means of six lag screws.

(b) A stationary base bolts to the base ring in six places and has three leveling bolts which rest on the three load-leveling pads, 120 degrees apart from each other, on the base ring.

(c) A rotary base, bolted to the stationary base on each of its four corners, permits adjustment of the turntable yoke about the vertical with an accuracy of ±3 seconds of arc.

(d) Pressure-compensated axial and radial fluid bearings are used on the turntable shaft. Three radial fluid bearings have a total stiffness of 25×10^6 lb/in. Two thrust bearings have a combined stiffness of 50×10^6 lb/in.

(e) A glass dial is mounted beneath the table top and is scribed around the top of its circumferential edge with graduations that are one degree apart and shorter graduations that are six minutes of arc apart. The scribed graduations are accurate with ±2 seconds of arc. The glass dial is mounted so that the graduations are concentric with the axis of rotation of the turntable shaft within three seconds of arc.

(f) An optical readout system, a dual photoelectric scale reader, is used to define the rate of rotation of the turntable by relating the angular position of the table top to recorded time. The accuracy of this system is not limited by the accuracy of the glass dial but only by its own stability.

(g) A magnetic table-tracking device, a sectosyn, is used to track the angular position of the turntable top with respect to a sidereal reference with an accuracy of ±2 seconds of arc.

(h) Pressure-compensated air bearings are used on both ends of the trunnion axis.

(i) An optical readout system accurate to within ±1 second of arc is used to determine the trunnion tilt angle with respect to the vertical. This system eliminates eccentric errors by simultaneously indicating opposite sides of a graduated six-inch dial. Movement of a deviating prism moves the lines of right- and left-hand scales into coincidence and a micrometer scale indicates the true gimbal angle.

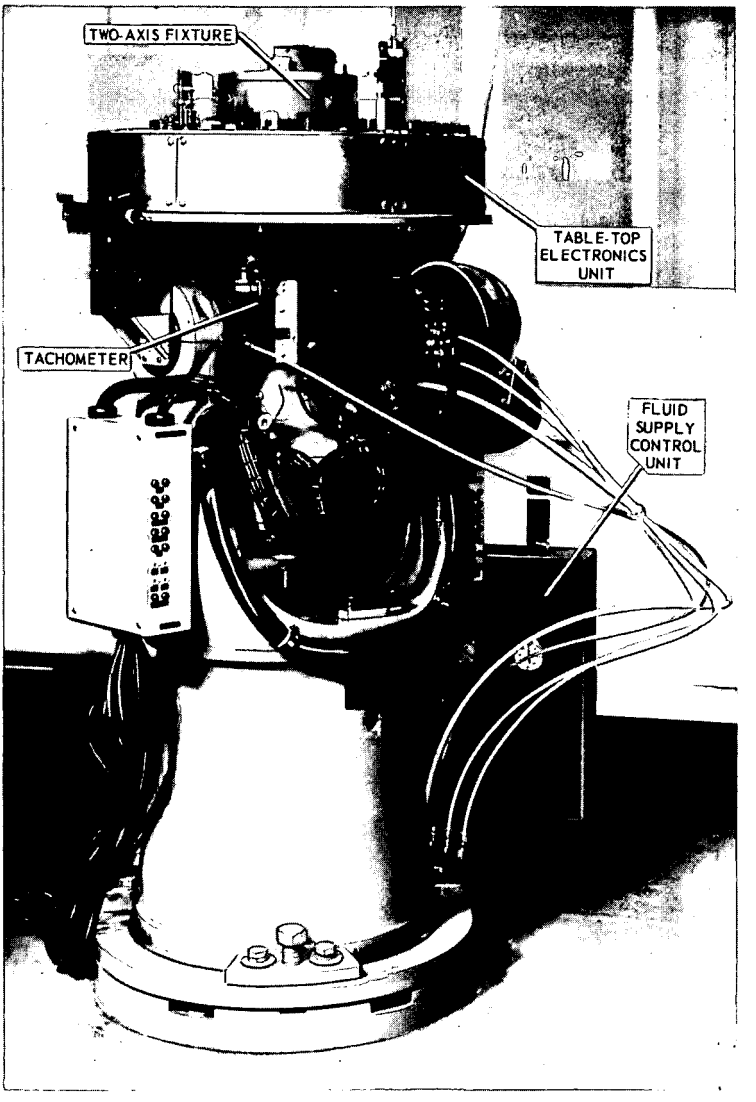

Fig. 4-8 continued

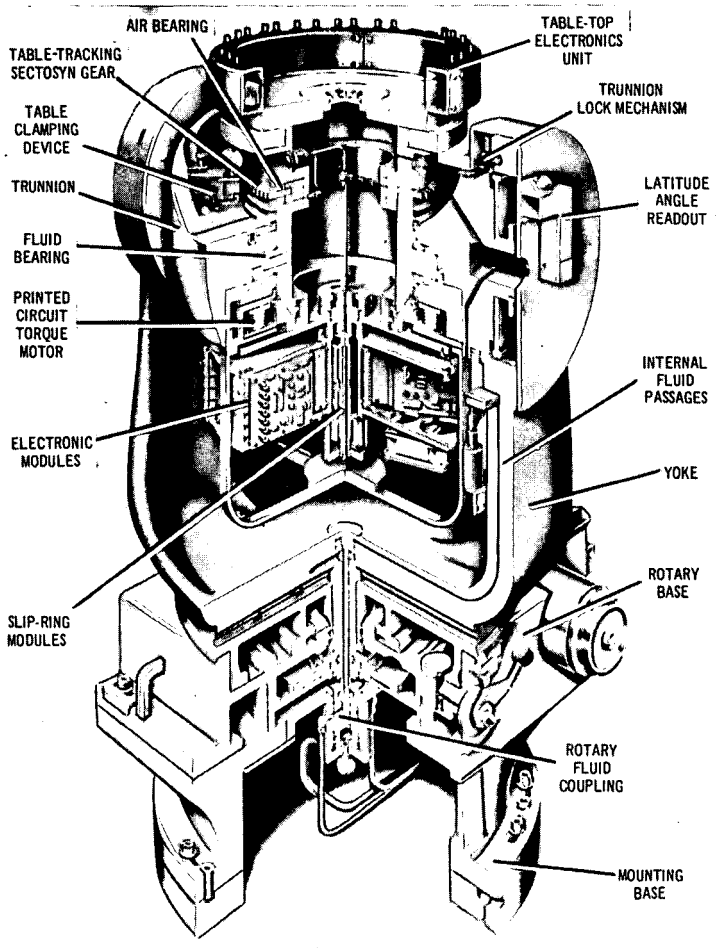

Fig. 4-9 Cutaway views of Model E test turntable

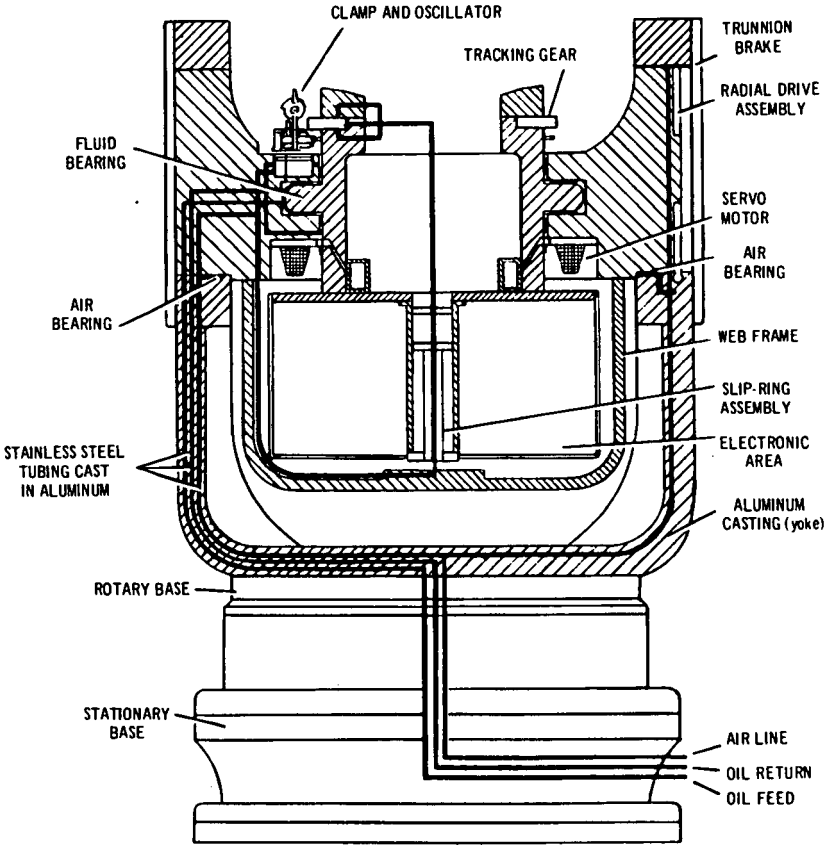

ARRANGEMENT OF AIR AND OIL LINES

Fig. 4-9 continued

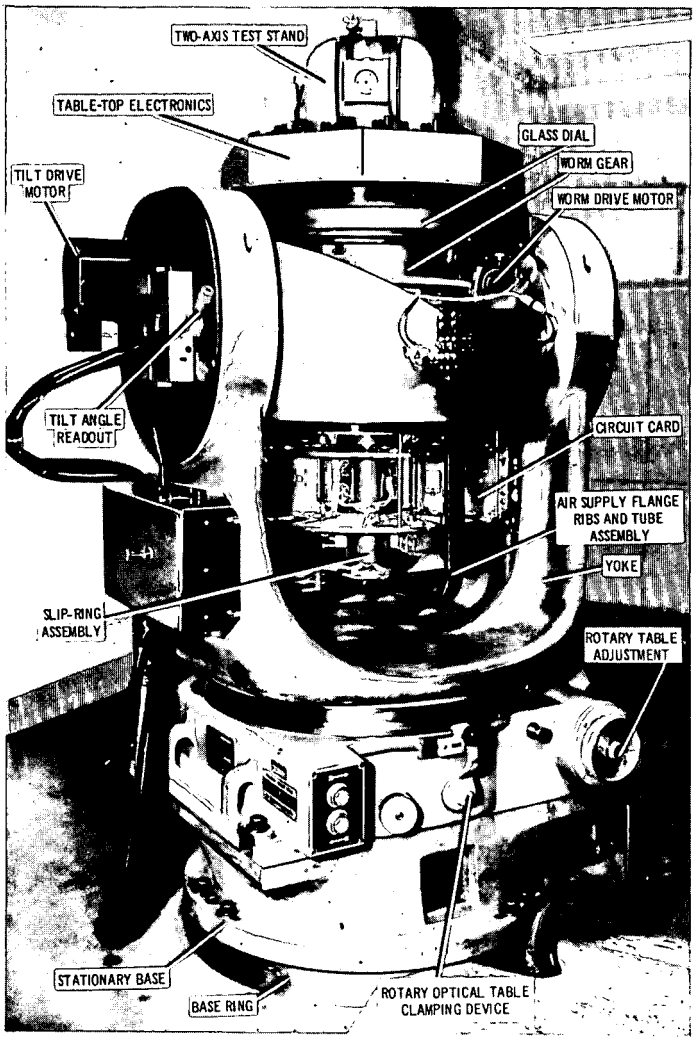

Fig. 4-10 Model E test turntable

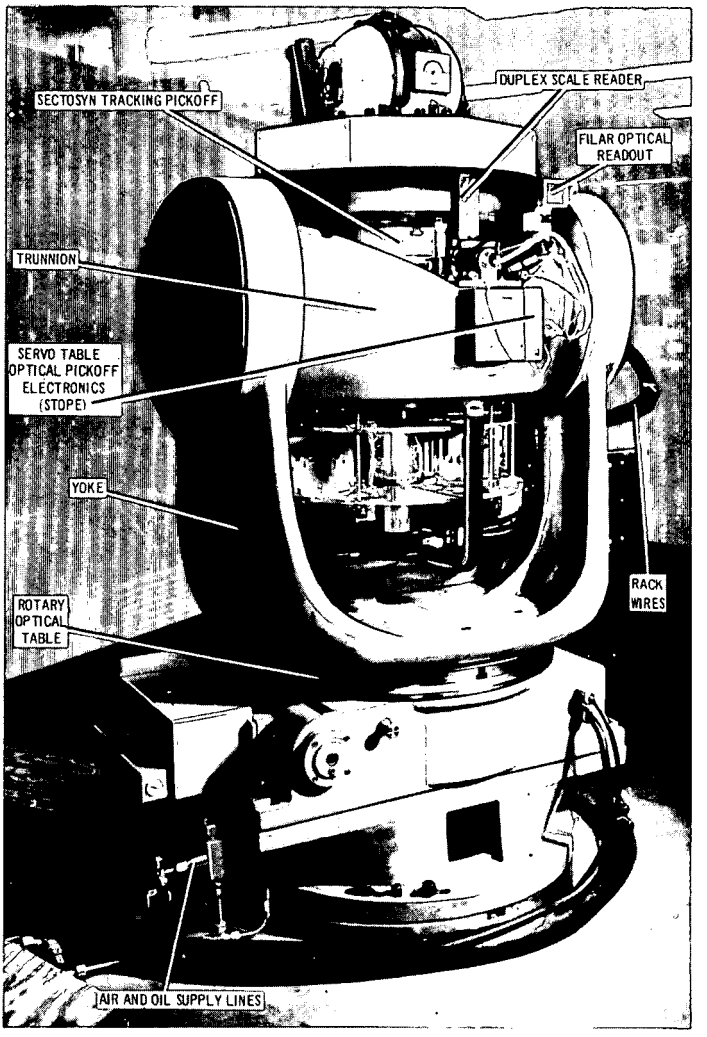

Fig. 4-10 continued

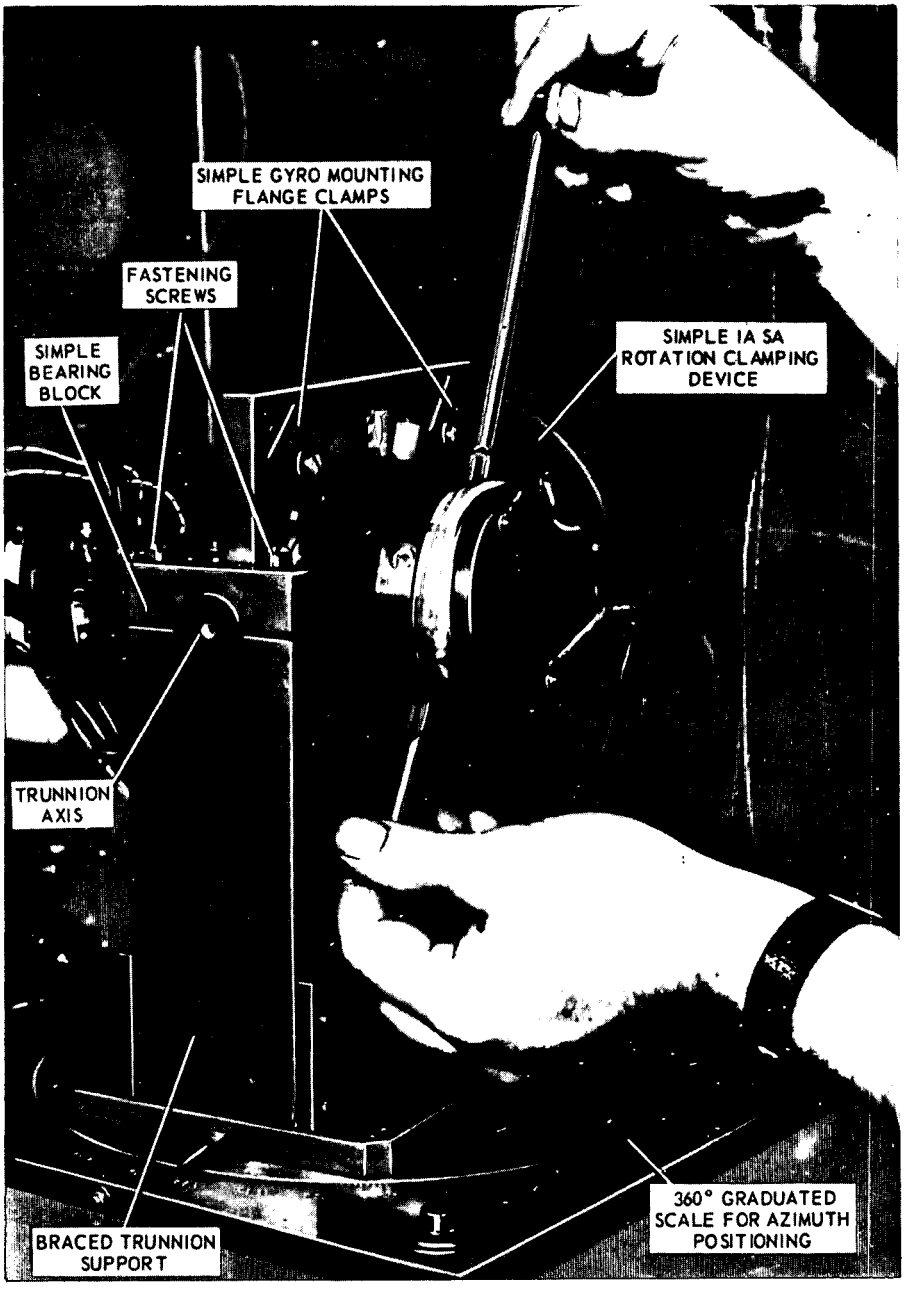

Fig. 4-11 Early gyro test stand

(j) An optical readout system, a filar reading system, is used to project a magnified image of a one-degree segment of the glass dial on a screen and permits adjustment of a calibrated indicator to determine the angular position of the table top within ±5 seconds of arc.

(k) Two slip-ring assemblies provide eighty-four rings and brushes to permit the transfer of energy between the stationary and rotating components of the test table. The slip-ring assemblies have a friction torque of 1.97 oz-in.

The basic structural material of the Model E turntable is type 356 aluminum because it is nonmagnetic, easily cast, easily machined, of proven stability, and compatible with the casting technique used to contain the various fluid lines within the table structure. The need for 360-degree rotation about all table axes suggested that fluid transfer be accomplished at a minimum radius from each axis to keep coupling friction torques as low as possible.

The various stainless-steel-tubing fluid conductors were assembled and silver soldered prior to placement in the mold. Type 304 stainless steel was used for the fluid conductors to meet the nonmagnetic-material requirements and to approximate the 356 aluminum's coefficient of expansion sufficiently to reduce separation of the casting from the stainless steel. One problem that did occur was distortion of the yoke arms, which upon further calculation was found to be caused by the stainless-steel conductors in the arms. The problem was corrected by the application of strain and heat to the yoke in a compensating direction with a final stress-relief program. Appropriate stress-relieving programs were performed at points of gross material removal in an attempt to reduce residual strain to a minimum.

The table-axis bearings in the Model E table are pressure-compensated fluid bearings. The fluid used is a grade of aviation instrument oil. The fluid flow was designed small to keep the support equipment (pumps, reservoirs, etc.) of a reasonable size for the operating pressures used. The bearing operates on a pressure of 200 lb/in. Flow restrictors are jeweled orifices. The bearing surfaces are hard coated (aluminum oxide), ground and lapped. As already noted, radial bearing stiffness is 25×10^6 lb/in and thrust bearing stiffness is 50×10^6 lb/in. The bearing total indicated runout is less than 10 microinches.

The table-tracking worm wheel is a fifteen-inch-diameter aluminum gear, hard coated for abrasion resistance, with 1440 teeth machined and lapped to the mating worm gear. The worm gear, spring loaded to compensate for worm-wheel irregularities, has provisions to be driven by any of a series of geared speeds of a synchronized motor.

The tracking gear is supported by air flowing through jeweled-orifice flow restrictors. Operating pressure is 30 lb/in^2 and air flow is approximately 0.34 standard cubic feet per minute. The radial and thrust gaps are less than 0.0002 inch. All bearing surfaces are hard coated, ground and lapped. The tracking gear is equipped with an E-type transformer array which enables the test engineer to track table position as a function of null-signal variation. This process is similar to the table-tracking microsyn on the Model D tables except that the null sensitivity has been increased ten times by an appropriate increase in radius from the axis of rotation to the transformer pole faces. The gear may also be used to drive the turntable when its air support bearing is deactivated on one side, thereby locking the gear to the table shaft.

Design of the dual-head optical pickoff was initiated as part of the Model E table design along with its accompanying servo table optical pickoff electronics. The basic principle of the design is the observation and recording of successive single scribe marks on a precision glass dial as the scribe marks traverse two indices separated by a calibrated distance.

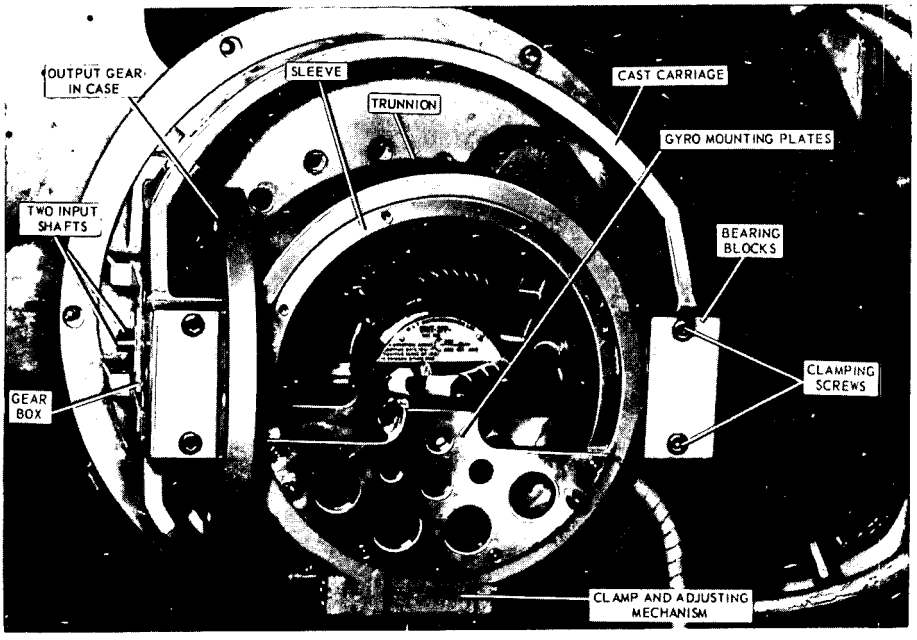

Fig. 4-12 First two-axis gyro test stand

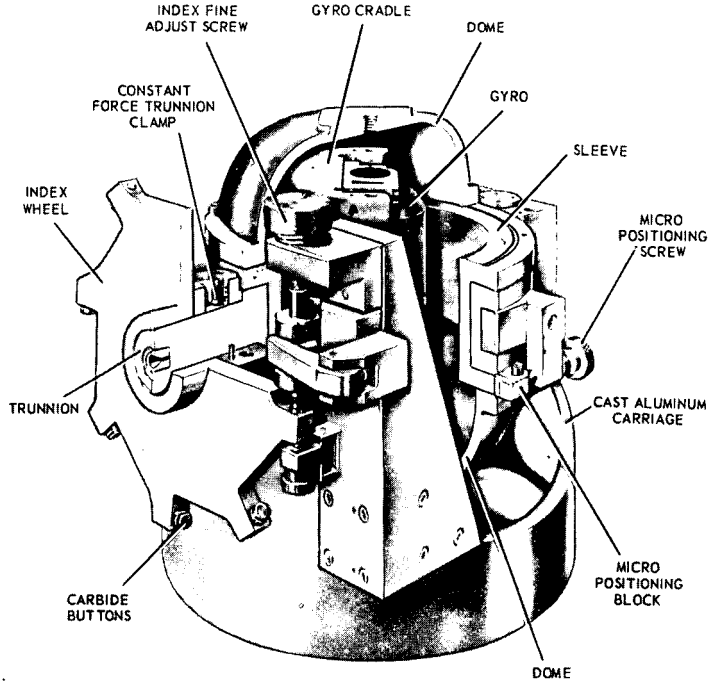

Fig. 4-13 Current two-axis gyro test stand

The tilt axis of the table is supported for rotation with 180-degree air bearing, pressure compensated with jeweled-orifice restrictors. The bearing areas are hard coated, ground and lapped. The bearings are activated by a switch-and-solenoid-valve pair arrangement with an electrical interlock to prevent the tilt-drive motor from operating if the air should fail or not be switched on. The tilt drive is variable speed with a manual option for fine positioning. An air-actuated brake band holds the tilt position when the bearings are deactivated.

The rotary table supplies the test engineer with another degree of freedom about the vertical axis. This enables the table axis to be positioned to any azimuth within the accuracy of the optical readout of the rotary base, which is defined by the supplier as within three seconds of arc.

The gyro-test-fixture interface surface on the test-turntable top is square to the table axis with 4.85×10^{-6} radians. An optical check was made of the squareness and orthogonality after two years and no appreciable change was found.

Gyro Holding Fixtures

The gyro holding fixture is the interface device that mates the gyro on test to the test turntable. The fixture may be as simple a device as a pair of angle brackets or as complex as a completely enclosed pressure- and temperature-controlled stand that can be accurately rotated about two orthogonal axes. As with any piece of test equipment, the requirements of the particular task dictate the ultimate design.

Standard machine or tool parts would be perhaps the simplest, least-expensive gyro holding fixture. For example, angle brackets used singularly or compounded can provide multiple-orientation testing with respect to a fixed surface by merely re-positioning the bracket, or brackets. Two simple brackets with a precision spindle between them can provide even more flexibility. In general, however, flexibility and simplicity work against one another in test-fixture design. The currently used two-axis test fixture is an attempt to provide almost unlimited flexibility to the test engineer while simultaneously providing the technician with as simple a device as possible commensurate with the ultimate in technical precision.

Early Types. Figure 4-11 is a photograph of a gyro test fixture used at MIT in the 1945-1950 era. It was developed to provide the least-complicated device that permitted orientation of the gyro on test about each of its three axes with some degree of precision. The fixture material was brass, which had sufficient mechanical strength and stability and was easily machinable. Machining tolerances were of the order of 0.001 inch.

Positioning the gyro output axis (the longitudinal axis of the cylindrical gyro shown in the photograph) about the gyro input or spin axis (IA or SA, perpendicular to each other and to the output axis, OA) could be very tedious since the torque applied to the fastening screws on the trunnion axis caused a torque moment about the trunnion axis. Depending on the accuracy required, this torque moment could excessively prolong alignment time. Thus, the major inadequacy of this fixture was the limited alignment accuracy that could be obtained in a reasonable time. This illustrates one extremely important point in test-instrumentation design - namely that an artisan can achieve the ultimate in accuracy with fairly crude equipment and that a trade-off generally must be made between built-in accuracy and cost.

Figure 4-12 shows the first of the so-called two-axis test stands. This particular version was in use from 1953 to 1960, and incorporated the modifications that were found necessary to increase testing accuracy, repeatability and rapidity. The braced trunnion support of the older fixture was replaced with a symmetrical stiff aluminum casting of type 356 aluminum stress-relieved for long-term stability.

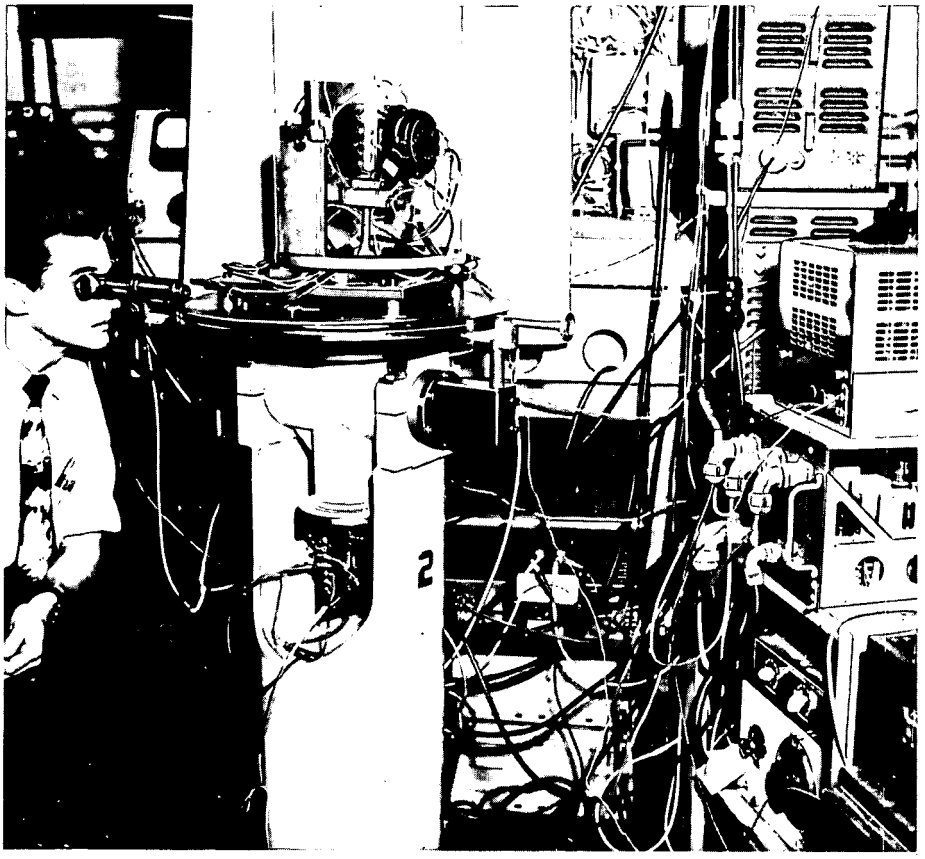

Fig. 4-14 Gyro test station-circa 1950

The bearings caps, which clamp the trunnion shaft to the carriage, were enlarged in proportion to the overall fixture and a through-boring operation was performed on the carriage to place the trunnion bore parallel with the fixture base within 0.0005 inch in 10 inches, or 10 seconds of arc. A two-stage gear box was added to facilitate positioning the gyro about its input or spin axis and additionally to provide sufficient torque capability to hold and position the gimbal accurately as the clamping screws were torqued down on the bearing caps. Technicians still found difficulty, however, aligning the gyro in this fixture. The difficulties were attributed to the clamping screws which would apply a torquing moment to the trunnion shaft as the technican attempted to simultaneously force the trunnion gimbal into position and fasten it firmly in place with the clamping screws. This problem was not finally resolved until the next generation of fixture.

The wide gimbal frame of the two-axis stand had a twofold purpose. One was to provide a larger area for more accurate alignment of the sleeve in the gimbal frame to provide orthogonalities of approximately 50 seconds of arc. The other was to provide support for the larger sleeves necessitated by the fact that the gyros to be tested were mounted by their end bosses, which required a mating mounting plate at the gyro's extremes.

Up to this time, fixture modifications were basically to stiffen and ruggedize the structure. These were not done because of enviromental conditions but rather to increase the repeatability characteristics of the fixture from one gyro to another.

Two-Axis Universal Fixture. Figure 4-13 shows the fixture used at the Instrumentation Laboratory for gyro testing since 1963(6). As the figure shows, the carriage was only slightly modified; but the size of the carriage, and of the overall fixture, was predicated on the expected size of the gyros for the next ten years and the size of the turntable mounting surface. The bearing caps were modified to provide a constant spring force applied to a friction disc. This in turn applied a force to the trunnion shaft sufficient to hold the trunnion gimbal at any attitude with respect to the fixture base with any gyro that would fit the fixture without assistance from a holding device. This modification permitted the combining of two operations into one, which is usually a good justification for making a change.

A positioning device was added to the trunnion axis which facilitated positioning the gyro about its input or spin axis to discrete 45-degree intervals. These intervals are accurate to ±2 seconds of arc and are repeatable to 12 seconds of arc.

The sleeve and trunnion gimbals were redesigned to provide a friction holding force between them. In addition, a micropositioning block-and-screw device was added to permit accurate positioning of the gyro input axis about the output axis.

The gyro cradle was designed to provide a common mode of mounting for any style gyro. Its basic concept utilizes three strong mounting flanges which mate with three precision inserts affixed to, and final machined on, the trunnion gimbal.

Domes were included in the redesign of the sleeve to provide an integral pressure, vacuum, and temperature-control facility. Thus, the gyro on test is isolated from possible changes in the laboratory ambient.

At about the time the current two-axis fixture was developed, the gyro-test-station complex was just beginning to take on the aspects of a complete system in itself. As a result, one two-axis fixture was assigned to each gyro test turntable and was aligned specifically to that table. The procedure was performed using level vials accurate to two seconds of arc to transfer the reference axis from the test turntable to the fixture mounting surface. This technique circumvents to some extent the buildup of tolerances.

Fig. 4-15 Model D test station circa 1954

Electronics

The electronics portion of gyro test instrumentation has gone through much the same evolutionary process as the test turntable and gyro holding fixture. As will be shown, a sharp contrast exists between early attempts at electronic test-station instrumentation and what exists today.

The basic functions of the test-station electronics, i.e. excitation, control and monitoring, were required in the early stations and are still required in the present-day stations. These include electrical excitation of the gyro wheel; signal-generator, torque-generator and suspension circuitry; positional control of the gyro float and unit orientation, in other words, the rate-feedback and servo-turntable loops (see section 3); and data acquisition and monitoring of the signal-generator output and other gyro parameters. Although the electronics performs the same basic functions, the scope, degree of sophistication and means of implementation have changed drastically.

History. Figure 4-14 depicts a gyro test station about 1950. The various items of electronics equipment are general-purpose readily available devices; little specifically designed equipment was required. Accuracy was of the order of 10 percent. The test engineer is manually clocking the table rate during a servo-turntable run by observing a graduated scale on the table and using a stop watch.

Inertial-navigation systems at this time were used primarily for aircraft navigation over relatively short periods of time (a few hours) and were calibrated prior to each flight. Thus no long-term gyro performance tests were required, and long-term equipment reliability and stability were unimportant. Even short-term equipment errors were relatively insignificant with respect to the level of gyro performance at the time.

As gyro design progressed and more refined instruments for the navigational application emerged, the need for more accurate performance data and the dependence of the performance data on the test equipment became clearly evident. The development of the gyro mathematical model and progress in instrument design proceeded hand in hand. Model terms were postulated and then experimentally evaluated. There were times when the ability of the test equipment to truly measure gyro performance uncovered and made possible the rectification of design defects. There were other times when gyro performance exceeded the ability of the test equipment. As the model developed, more and more emphasis was placed on the accuracy and quality of the test equipment.

Figure 4-15 depicts the electronic test equipment in use with one of the early Model D turntables about 1954. That figure illustrates one of the first attempts to provide specific permanent electronic test instrumentation. The console on the left was a wheel-power distribution source housing three-phase wheel-supply control panels for several test stations. The power source for the gyro-wheel excitation was a remotely located rotating motor-generator set. The right-hand console contained the gyro microsyn excitation sources, i.e. oscillator and amplifiers, rudimentary monitoring equipment and the table servo-loop electronics. The accuracy and short-term stability of this equipment was a few percent.

The steady decrease in the rate-detection threshold of the gyro unit and increasing emphasis on long-term testing made the consideration of errors in the performance data produced by the electronic test equipment mandatory. Accurate determination of gyro performance now involved more subtle effects such as microsyn reaction torques, wheel-power sensitivity and disturbances caused by small temperature variations. The effects of time, temperature excursions, line-voltage fluctuations and electrical loading conditions all had assumed increased importance. In order

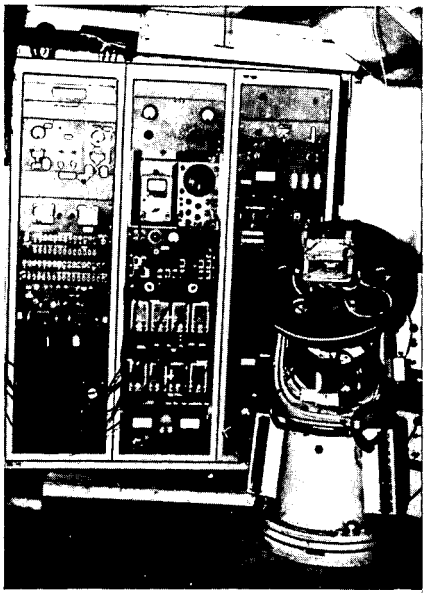

Fig. 4-16 Gyro test station-circa 1958

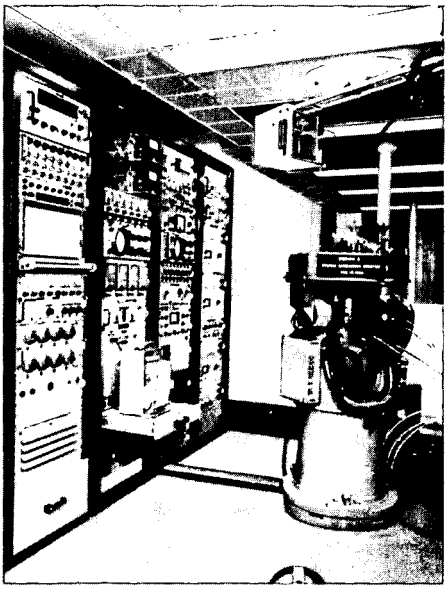

Fig. 4-17 Gyro test station-circa 1965

that extraneous effects could be removed from the data of a completed test, it became common practice to continuously monitor variables other than those directly related to instrument performance, i.e. torque-to-balance in the rate-feedback mode or table rate in the servo-turntable mode. Among these additional parameters were such things as ambient temperature, microsyn-excitation voltages, gyro-wheel-excitation voltage and a.c. line voltage.

The test station depicted in figure 4-16 can be considered the forerunner of present-day gyro test stations. Major improvements in the electronic test equipment included a more precise self-contained wheel-excitation source and fork-controlled oscillator for microsyn excitation. These sources had accuracy and long-term stability (one or two days) of better than one percent. The station was equipped with an improved servo amplifier utilizing a motor-generator set to drive the table d.c. torque motor in the servo mode, and an automatic electro-optical system was installed for determining table rate. The gyro, shown mounted on the turntable, utilized a magnetic-suspension technique for controlling translational movement of the gyro float, and the electronics console provided means by which this suspension circuitry could be adjusted and monitored. Mobile strip-chart recorders were moved to within close proximity of the station to provide the necessary recording capability.

Current Practice. Experience with early generations of test stations coupled with steadily improving gyro performance characteristics dictated the philosophy of rigidly controlling all inputs (electrical and otherwise) to the gyro undergoing tests. To accomplish this objective, which would result in the determination of true gyro performance free of equipment-induced errors, a number of factors had to be evaluated. Among these were:

(a) The ability of the equipment to perform the test. This required definition of the anticipated level of performance of the gyros to be tested and a corresponding equipment-error level to be decided upon. In other words, an error budget had to be established.

(b) The performance level of each individual component of the electronics system. The errors of each component had to be determined and their relationship and effect on the other components evaluated.

(c) Monitoring capability. Provisions had to be made for monitoring many test variables to assure adherence to the specified equipment operational levels.

(d) Flexibility and cost. These factors had to be considered together since the high cost of gyro test equipment generally dictated that it be used for as many tests as possible and for as long a time as possible to reduce the cost per use hour.

(e) Reliability. Longer-term tests were required as gyro operational time between calibrations was extended from hours to months. Interrupted tests and repeated tests as a result of equipment break-downs not only would delay gyro programs but also would be more costly.

(f) Consistency between stations. This factor was necessary if data taken on different test stations was to be compared. In addition, it eased the problem of operator training.

(g) Thorough test-station evaluation and check-out capability (reference (7) gives a complete test-station check-out procedure). Test stations were by now sufficiently complex to warrant meticulous examination of all operating functions before being declared acceptable for gyro testing. Although this increased the initial cost, it decreased cost per use hour of the test station by increasing test-station reliable operating life.

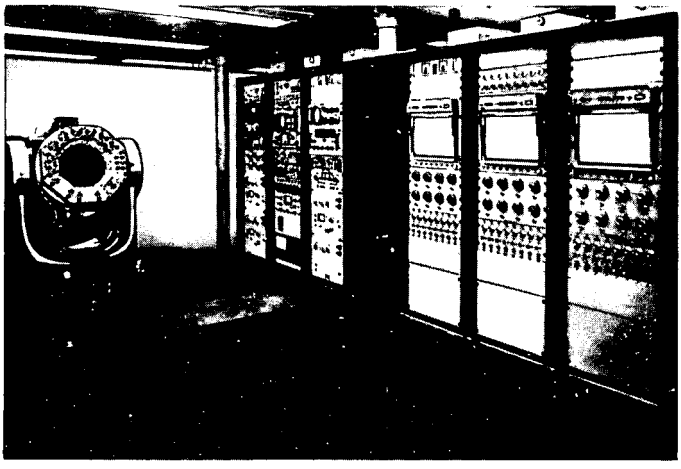

TEST TABLE AND MAIN ELECTRONICS CONSOLE

RATE FEEDBACK MODE

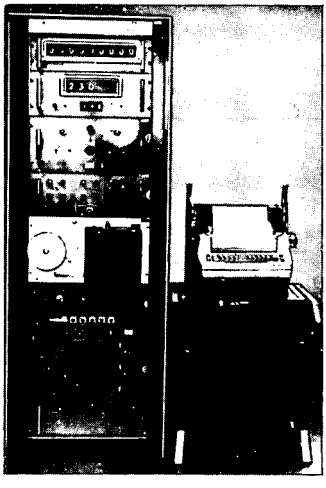

SERVO TURNTABLE MODE

DIGITAL DATA CHANNELS

Fig. 4-18 Present-day test station

One of the first test stations exemplifying the above characteristics is shown in figure 4-17. Two of the more obvious changes in this test station from the electronics point of view are the increased monitoring capability, illustrated by the eight-channel recorder in the left-hand rack, and the electronics mounted on the top of the gyro test table. The table-top electronics were necessary to locate particularly sensitive circuitry in as close proximity to the gyro as possible. Included in the table-top unit is the magnetic-suspension circuitry, which must be close to the gyro to eliminate the effects of lead capacitance. In addition, the signal-generator-output and temperature-controller preamplifiers are located in the table-top unit to eliminate the need of passing low-level signals through slip rings and long cables. This alleviated noise and interference problems.

One means of eliminating connector and slip-ring resistance problems at high-current levels would be to mount all of the various precision a. c. power supplies required for gyro excitation on the test-turntable top. However, size and weight considerations rule out that approach. This problem has been solved by the use of remote-sensing low-current leads at the gyro connector to result in highly stable excitations at the gyro - rather than at the power-supply output.

Figure 4-18 is a photograph of a present-day test station. The most obvious differences between this test station and its predecessors are its digital as well as analog data-recording capability and increased analog monitoring capability. A not-so-obvious difference is the fact that the main electronics console itself is air conditioned with the inside temperature maintained at 75 ±5°F with a stability of ±0.5° F over a seven-day period. Commercial equipment using solid-state circuitry was selected to improve performance and reliability and to reduce weight, size, and heat generation. In-house-designed equipment includes extensive use of transistors for the same reasons.

Figure 4-19 illustrates the arrangement of the electronics equipment in the test station. Weight of equipment and ease of meter, oscilloscope and recorder readings were prime considerations in the arrangement. Units containing test points and controls are located conveniently for operating personnel. The table-mounted electronics are divided into two groups: those mounted on the rotating table top and those mounted on nonrotating parts of the table.

Not all of the electronics are used simultaneously since these include components used during test-station-check-out runs, rate-feedback tests, earth-reference servo-turntable tests, and inertial-reference servo-turntable tests. The various modes of testing are described in section 3.

The following paragraphs give brief descriptions and some of the more pertinent parameters of the various items of electronics.

Main Console - Rack 1

The 400-Hz Power Supply is a flexible a. c. power supply used as the excitation source for the temperature controller. It can be externally driven by a 20-volt rms signal and furnishes 400-Hz single-phase power. It features separate plug-in external-signal drive units and plug-in oscillators, which are available in both fixed and variable frequencies from 45 to 5000 Hz.

The Magnetic Amplifier Temperature Controller maintains the temperature within the two-axis test stand to a preset narrow range. Temperature stability is ±0.1°F/24 hours at 125°F.

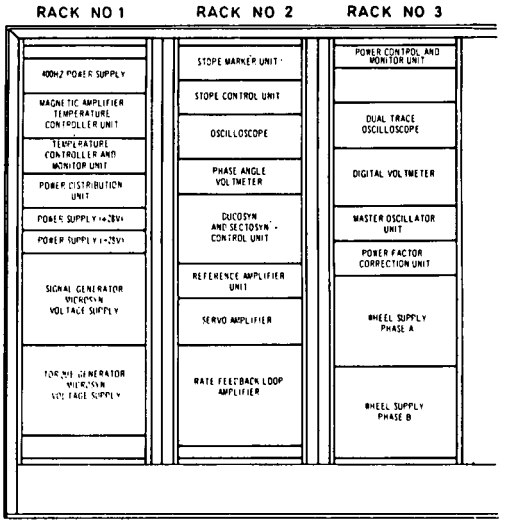

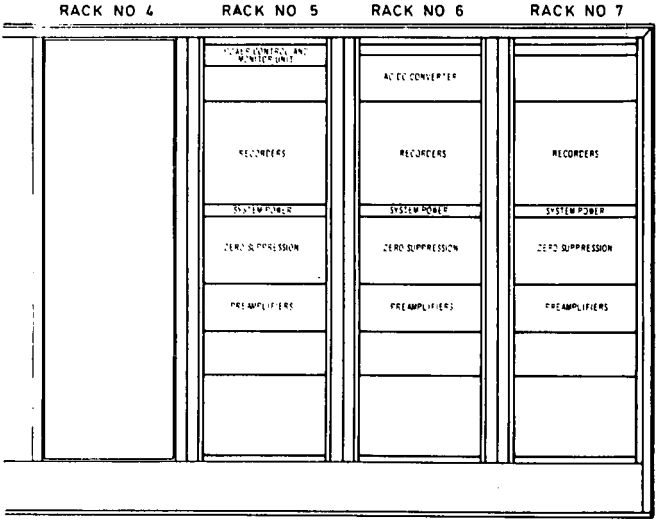

MAIN CONSOLE

Fig. 4-19 (a) Location of electronics in present-day test station

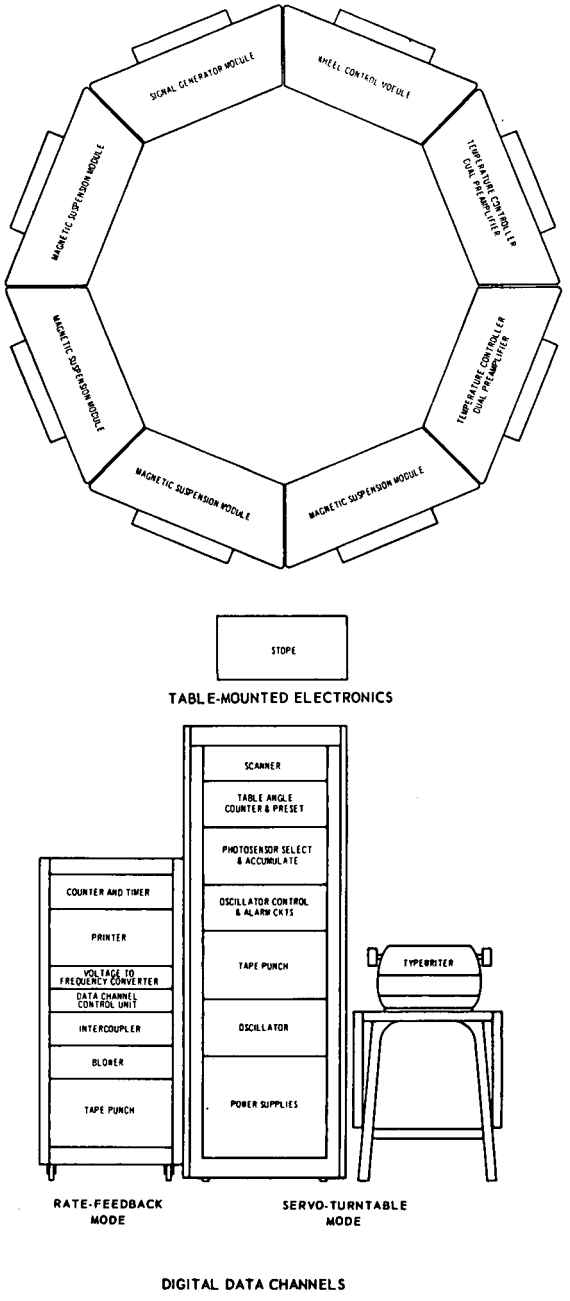

Fig. 4-19(b) Location of electronics in present-day test station

The Temperature Controller and Monitor Unit (with two identical table-mounted dual preamplifier units) controls the gyro temperature to a narrow preset range at the gyro flotation temperature. Stability is better than 0.01° F per day at 125°F. The preamplifier units on the test table contain the control and monitor bridges in addition to associated preamplifiers. The temperature control and monitor unit in the console contains the power supply and power amplifiers for the gyro heaters and the power supply required for the temperature-controller dual preamplifier unit.

For both channels, the error signal from the control bridge and the error signal from the monitor bridge are received in the temperature control and monitor unit. The control-bridge error signal is fed to the temperature-controller power amplifer and thence to the gyro heater. The monitor-bridge error signal is routed to the station recording system.

Meters are provided to monitor the heater voltage and current as well as the outputs of the two d. c. power supplies +40 volts and +100 volts, respectively.

The Power Distribution Unit distributes power to the various console and table units. It also contains safety circuits and the central grounding point for the test station.

The D. C. Power Supplies (+28 volts and -28 volts) are commercial units modified by replacing the control potentiometer with a fixed resistor to provide fixed voltage outputs. The essential regulating circuitry employed is a closed-loop d. c. servo system providing voltage regulation of 0.01 percent. The following units are supplied power by these supplies:

(a) reference amplifier

(b) master oscillator

(c) signal-generator-preamplifier module

(d) buffer-amplifier (auxiliary magnetic-suspension unit and torque-generator voltage-supply phase adjust)

(e) rate-feedback-loop amplifier

The Microsyn Voltage Supplies are two a. c. sine-wave power supplies, one for signal-generator and one for torque-generator excitation. These units are completely transistorized, have an output voltage range from 1 to 121 volts rms continuously adjustable, and will provide 20 voltamperes or $1\frac{1}{2}$ amperes. Stability is 50 ppm for a period of one week after suitable warm-up. Voltage regulation is by means of the remote-sensing technique previously described to eliminate the effects of slip rings and line drops.

Main Console - Rack 2

The STOPE (Servo Table Optical Pickoff Electronics) Marker Unit is used when the gyro is operated in the rate-feedback mode. While the table is being driven at ten times earth's rate or some multiple, the marker unit produces a signal at every ten degrees, usually 0°, 10°, 20°, etc. of table rotation. This signal is used to operate marking pens on the strip-chart recorders.

The STOPE Control Unit consists of two 28-volt power supplies and associated circuitry for controlling the power to the table-mounted STOPE. Other components included in the unit are a meter for monitoring ± 28-volt power supplies and an adapter for coupling the signal to the elapsed-time recorder. A variable 60-Hz voltage source is used to provide the light source. The 115-volt 60-Hz shutter-motor supply is also controlled by this unit.

The Oscilloscope in Rack 2 is intended for the general-purpose display of selected console signals. Identical X and Y amplifiers are provided thereby permitting phase measurements.

The Phase-Angle Voltmeter is a multifunctional instrument designed for precise measurements of complex a.c. signals at any of the three fixed frequencies. It is intended to measure magnitude and phase angle of a signal; however, it can function as a vacuum-tube voltmeter, phase-angle meter, in-phase and quadrature signal meter, phase-sensitive null detector, impedance meter, and power-factor meter. This unit is included in the console for monitoring the signal-generator output signal, checking the phase relationship between signal and reference of the gyro-float radial and axial signals, adjusting input versus reference of the servo amplifier, and checking phase relationship of wheel-supply phases A and B and the wheel current versus voltage. It is also used for any troubleshooting problems that may arise.

The Ducosyn and Sectosyn Control Unit controls the excitation for the gyro microsyns and for the table-mounted sectosyn. It includes provision for open-loop torquing of the gyro as well as for routing appropriate signals for the servo and rate-feedback loops. The output of the signal-generator voltage supply is routed through this unit and fed to the gyro signal-generator primary and magnetic-suspension windings. The output of the torque-generator voltage supply is phase adjusted in this unit and fed to the gyro torque-generator primary. The unit also has provision for controlling the sectosyn excitation voltage and for routing of the sectosyn output signal.

The Reference Amplifier Unit consists of eight individual amplifiers of identical design. Separate control is thereby provided for any a.c. reference signals such as signal-generator excitation, torque-generator excitation, or gyro float radial and axial signals. The signals can be phase shifted through 360 degrees and are used as references for oscilloscopes, phase-sensitive demodulators, and other signal-monitoring devices.

The Servo Amplifier accepts an a.c. error signal from either the gyro or an angle-to-voltage transducer and supplies d.c. power to the torque motor of the table to control table position. The low-level circuitry of the unit is constructed on five plug-in, printed-circuit cards. These include an a.c. amplifier/demodulator, a d.c. amplifier, an a.c. feedback amplifier, a phase-shift amplifier, and an overcurrent protection circuit. The demodulator receives its reference voltage from the signal-generator voltage supply.

To prevent table runaway, rate-trip circuitry disconnects the torque motor when the table rate exceeds a preset level. The trip level can be adjusted from 0.1 rad/sec to a point where the rate trip becomes inoperative.

The Rate-Feedback-Loop Amplifier may be any one of three circuits - a d.c. tumbling loop, an a.c. tumbling loop and product resolver, or a pulse-torquing loop. Basically all three provide a current (d.c., a.c., or pulses) to the gyro torque generator to cancel the gyro float unbalance during a rate-feedback, or tumbling, test. The input to the loop is the gyro signal-generator output signal, which is coupled through the table-top-electronics preamplifier. A high-current, low-sensitivity tumbling loop is required for a gyro with high unbalances whereas a low-current, high-sensitivity tumbling loop is used with a low-unbalance gyro.

The recording of current to the gyro torque generator can be calibrated in torque units and thus is a record of the torque to balance the gyro. With the d.c. tumbling loop, the current can be recorded directly on a strip-chart recorder. With a.c. tumbling loop, the torque-generator primary and secondary excitation currents are

fed to the X and Y coils of a product resolver, the output of which is a d.c. current that can be recorded on a strip-chart recorder. With the pulse-torquing loop, a pulse count can be fed directly into the digital data channels.

Main Console - Rack 3

The Power Control and Monitor Unit controls and monitors the 115-volt, 60-Hz line power to the console. A voltmeter and ammeter monitor the voltage and current supplied to the line-voltage regulator, and a main power switch to this unit controls the power to the line-voltage regulator. (Each component in the console also has individual on-off switches).

The Dual-Trace Oscilloscope provides dual-trace capabilities by utilizing twin vertical amplifiers for simultaneous comparison of signals such as signal-generator-end and torque-generator-end radial and axial signals, and STOPE and STOPE marker wave shapes.

The Digital Voltmeter is a five-digit transistorized multimeter capable of measuring d.c. volts, d.c. ratios, a.c. volts and resistance. Decimal-point placement and d.c. signal polarity are determined automatically and are displayed along with the digital value of the input signal on a three-position tilting readout.

The Master Oscillator Unit generates all frequencies required by the test station except the sidereal-time frequency. Its primary uses are microsyn-voltage-supply excitation, suspension-voltage-supply excitation, and wheel-supply excitation. All frequencies are provided time locked or in phase synchronism with each other. Frequency stability is 5 parts in 10^7 per month.

The Power-Factor Correction Unit is designed to correct the lagging phase angle caused by the inductive gyro load. Decade capacitors connected in parallel with each phase of the power supply are arranged so that panel adjustments can correct the lagging power factor.

The Wheel Supply provides the excitation for the gyro wheel. The unit is completely transistorized, has an output voltage range from 1 to 121 volts rms continuously adjustable, and will provide 20 voltamperes or $1\frac{1}{2}$ amperes. Stability is 50 ppm for one week after suitable warm-up. Voltage regulation is by means of the remote-sensing technique previously described to eliminate the effects of slip rings and line drops.

Main Console - Rack 4

This rack, which has no controls on the front panel, houses voltage regulators and encloses one of the building columns in the test laboratory, where clear floor space is greatly limited.

Main Console - Racks 5, 6, 7

The remaining three racks of the main console each contain an eight-channel strip-chart recorder, thus giving a total analog recording capability of 24 channels. The eight-channel recorders are direct-writing devices capable of accepting either a.c. or d.c. signals. Signals to be recorded are processed by input circuitry called signal conditioners. In the case of d.c. signal, the signal conditioner is a d.c. amplifier. In the case of an a.c. signal, it is either a rectifier or a phase-sensitive demodulator depending on the nature of the a.c. signal to be monitored. The signal conditioners impart the necessary gain or attenuation to the signal so that the necessary recording sensitivity may be obtained on the chart. The recorder includes a precision highly stable (20 ppm) d.c. zero-suppression source.

The output of this source is used to buck out or cancel the major unchanging portion of the input signal, thereby allowing significant scale expansion and monitoring of the residual or varying portion of the signal. These recorders are capable of monitoring incremental changes in the test variables to a resolution of 0.01 percent over periods as long as a week. Parameters recorded are the gyro signal-generator excitation and output signal, torque-generator excitations, float radial and axial signals, wheel-excitation voltage and current, gyro temperature, ambient temperature, console temperature, power-supply outputs, etc.

Table-Mounted Electronics

The test-turntable-mounted electronics comprise basically two major items: the table-top unit which rotates as the table rotates and the servo-table-optical-pickoff electronics (STOPE) unit, which is mounted on the nonrotating part of the table.

The Table-Top Electronics Unit, which is shown close-up in figure 4-20, comprises those items that must be mounted as close to the gyro as possible. These include:

(a) Signal-generator preamplifier. This module also contains reaction-torque and elastic-restraint-compensation circuitry.

(b) Magnetic-suspension modules. These four modules contain the gyro magnetic-suspension external circuitry and gyro float radial and axial position-monitoring circuitry.

(c) Temperature-controller dual preamplifiers. These two modules each contain a dual preamplifier for zone temperature control of the gyro.

(d) Wheel-control module, which contains wheel-rundown- and excitation-monitoring circuitry.

The STOPE Unit and optics are mounted on the nonrotating part of the table. The position of the table is optically determined by photocell-optical methods. At preselected positions an accurately coordinated pulse is electronically generated for actuation of timers or other devices. The STOPE accepts the photocell-circuitry output, which is a 120-Hz suppressed-carrier signal. This signal is then amplified and demodulated. The null of the demodulated signal actuates a Schmitt trigger which provides a negative impulse of approximately 1-microsecond duration. This 1-microsecond impulse can be used to trigger an electronic timer or a -28-volt pulse which in turn actuates a relay controlling an elapsed-time recorder. The STOPE also contains a duplexer circuit which, if a duplex optical system is used, switches the input alternately from one photocell to the other. The duplexer circuit simultaneously switches the output to the proper channel.

Digital Data Channel - Rate-Feedback Tests

Conventional analog-data acquisition and reduction techniques required that the torque to balance the gyro float be continuously monitored and recorded on a strip-chart recorder during a rate-feedback test. The magnitude of this quantity was manually transcribed from the chart as a function of turntable angle, and the data were then subjected to Fourier analysis and other data-reduction routines. One major drawback to that procedure was lack of resolution due to a relatively wide bandwidth of noise present in the data and corresponding difficulty in interpreting the trace on the paper chart. Eyeball averaging was a common tool in data processing.

The advantages of digital-data acquisition and reduction, i.e. consistent automatic interpretation of data coupled with rapid mathematical manipulation by computer, are solutions to the limitations of the analog loop previously described.

For digital-data processing to be used with the analog loop, the performance data must be converted to digital form. The d. c. output voltage from the product resolver or from the d. c. tumbling loop is applied to the input of a voltage-to-frequency converter, which functions as an analog-to-digital converter. The frequency of the sinusoidal output of this converter (0 to 150 kHz) varies directly with the magnitude of the d. c. input voltage. Hence variations in frequency are directly related to torque variations. As the input voltage is bipolar (+ or - for CW or CCW torque), the converter contains a built-in offset voltage that causes the output frequency to be 50 kHz with no input present. Negative voltage inputs cause output frequencies below 50 kHz; positive inputs cause frequencies above 50 kHz. The computer program is structured to accept inputs corresponding to 50 kHz as zero torque.

The pulse train is received by a preset counter and timer unit. As the name implies, the unit has two functions. The preset counter may be set to any desired integer value (N) and will generate a start pulse on receipt of the first pulse in the train and a stop pulse on receipt of the Nth pulse. These pulses are used to control the timer circuitry. The timer measures the elapsed time between start and stop pulses by counting the frequency of a precision internal 1-MHz oscillator and displays this time in microseconds. Since the number of pulses (N) and the time required to accumulate them are the required information for computing torque, all necessary data has been obtained. The counter and timer operate in a continuous mode in the sense that they are designed to measure consecutive time intervals of N pulses with no loss of information. In addition to visual display, the elapsed time is coded in binary coded digit (BCD) form, fed to a printer and tape, and appears as hard copy on printed tape. The intercoupler receives the parallel-form BCD output of the counter-timer and converts it to serial information for punching on tape. A data-channel control panel is provided to allow individual control of the various units and to contain circuitry for manually entering identification data on the punched tape.

This readout is also used as the acquisition equipment with the pulsed torque loop. In this case, the information is already in digital form and the analog-to-digital conversion is not required. The pulse train is fed directly to the counter-timer, and the operation is then the same as for the analog loop.

Digital Data Channel - Servo-Turntable Tests

The gyro-drift-data monitor is a precision electronic timer utilized as a means of measuring and recording turntable rate during servo-turntable tests. This rate may then be compared with earth's rate and the gyro drift rate determined. The gyro-drift-data monitor accepts electrical pulses generated by the photoelectric scale readers mounted on the test turntables. Two such readers are in use and are mounted nearly 180 degrees apart on the periphery of the glass scale. Each reader generates a pulse every one degree of table rotation, and the drift-data monitor computes the elapsed time between successive pulses by counting the frequency of a precision crystal-controlled oscillator. The stability of this oscillator is 1 ppm per 100 days. With both scale readers in operation, the drift-data monitor measures the elapsed time between pulses from each scale reader and computes the mathematical average. This averaging technique corrects for the errors introduced into the data by eccentricities in the glass dial. The output information from the monitor consists of two variables of quantities. The first is the time interval or table-rate information, and the second is the total accumulated turntable angle. This output is presented in three ways: (a) as a visual digital display on the instrument front panel, (b) as copy on an electric typewriter, (c) coded and punched on paper tape. In addition, the typewriter may be used to enter test identification on the punched tape if desired.

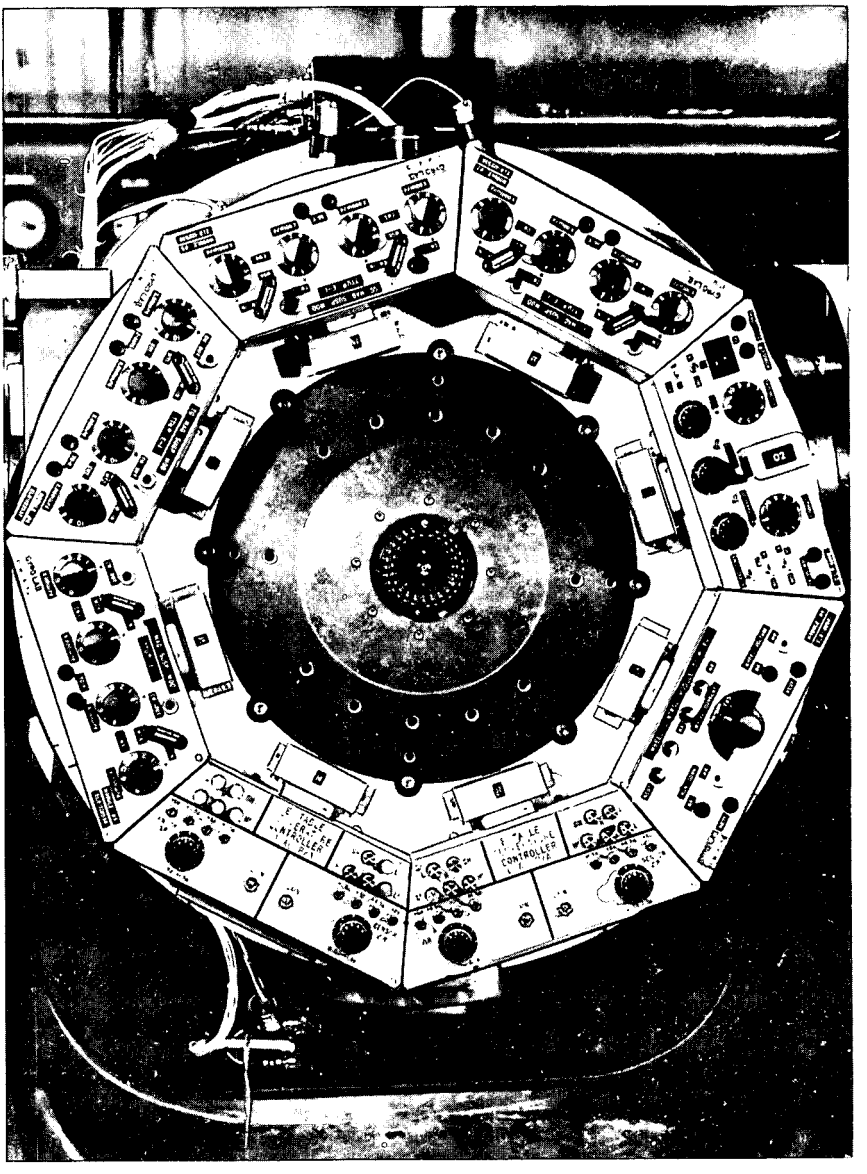

Fig. 4-20 Close-up of table-top electronics unit

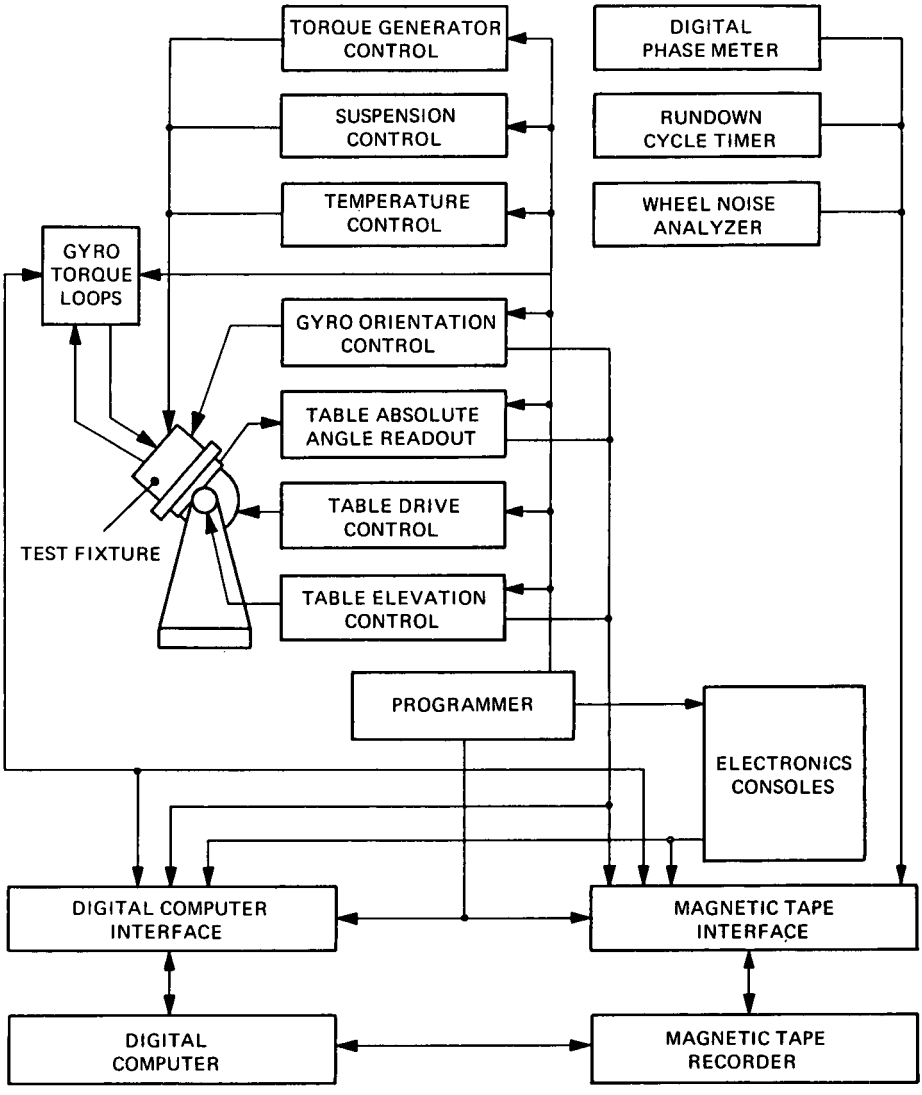

Fig. 4-21 Block diagram of proposed computer-controlled automated gyro test station

Future Test Stations

Future test stations may be of diverse types ranging from more simple test stands than today's to complete inertial-navigation systems at the two extremes with a next generation of the current test station somewhere in between. Each divergent approach has advantages and disadvantages that must be weighed against the particular factors pertinent to the design at the time.

Added precision can be achieved if flexibility is sacrificed. This would mean simple test stands each at a fixed orientation parallel or perpendicular to the earth's axis, vertical, or horizontal. Each stand could have a singular high-precision fluid bearing or merely provide a mounting surface for a high-precision test fixture. Devices capable of sensing local vertical could be affixed directly to each stand in order to monitor and maintain orientation of the gyro mounting surface.

Another approach to a gyro test station is to test the gyro in an inertial-system configuration. This has the advantage of testing the gyro with the hardware with which it is to be used, but it has the disadvantage of decreased flexibility plus the increased cost of tying up expensive system hardware to test components.

Future steps in the design of a next-generation test station at the Instrumentation Laboratory where flexibility is one of the prime considerations will involve continuing improvement in many of the areas previously described. Emphasis will continue to be given to the development of electronic equipment with enhanced precision, flexibility, and long-term stability and reliability. Test-fixture and turntable design will focus on the use of new materials and new methods of achieving even tighter mechanical tolerances. The goal of this effort is a one-g test station having the basic functional characteristics of present-day test stations but possessing increased versatility coupled with the ability to further insulate the gyro from extraneous perturbations generated either by the test station itself or by its environment. Base-motion isolation, azimuth determination with continuous astronomical reference, and instrument-temperature-control capability are the salient areas for future development effort.

The next generation of test station will undoubtedly provide for simultaneous multiple-gyro testing in the rate-feedback mode unless a major breakthrough is achieved in the state-of-the-art of environmental control (see section 6). With more than one gyro on the test table, anomalies appearing simultaneously in the data from all gyros can be dismissed as enviroment or equipment induced. In other words, the gyros on test are the only devices known today with the precision capable of monitoring themselves (see chapter 5).

Until recently, the techniques and metrology utilized in gyro test instrumentation have been largely analog in nature. Experience has already shown that certain gyro performance parameters may be more accurately and efficiently determined using digital-data acquisition and reduction techniques. The speed, capacity and precision of digital techniques have already been proven compatible with the performance levels of today's gyros and the expected performance levels of tomorrow's. This greatly expanded use of digital technology will also be an integral part of tomorrow's test station.

Computer-control will probably be another feature of tomorrow's test station. For example, consider the following problems that exist in present-day test stations and the effect of computer control on these problem areas:

(a) The need to monitor and record additional test parameters concurrently with performance data. With the aid of a multiplexer, virtually any number

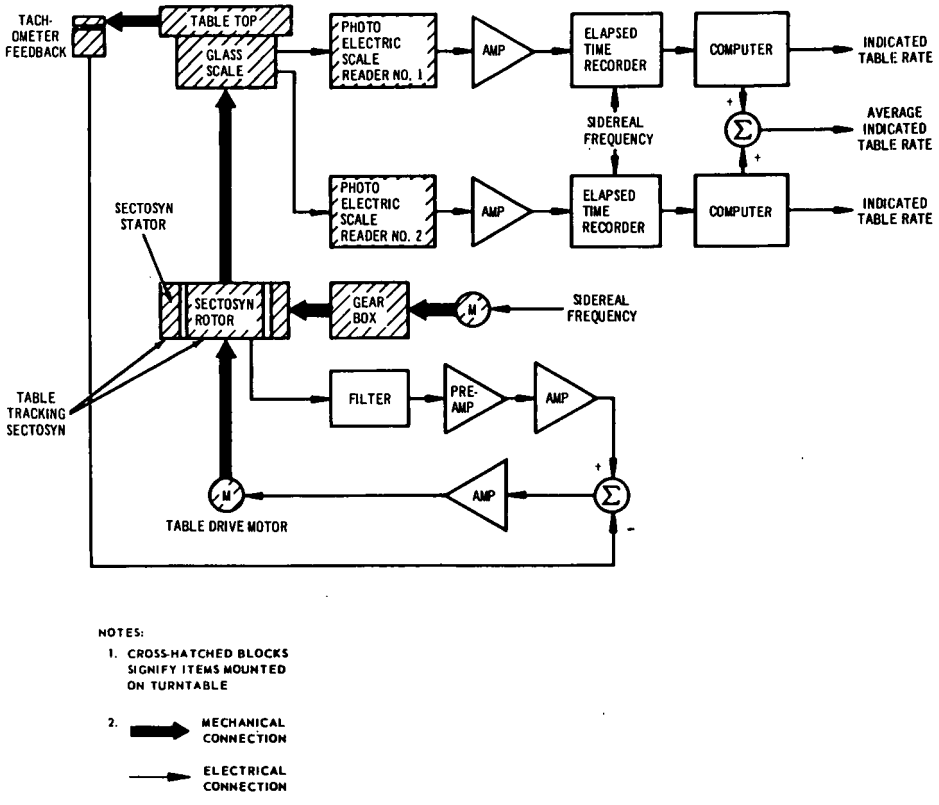

Fig. 4-22 Operating-mode block diagram - table-tracking-sectosyn test

of parameters could be recorded in digital form and stored on magnetic tape for easy retrieval. Preset limits on parameters could be programmed into the computer and an alarm circuit activated if these limits were exceeded.

(b) Inefficient methods of correlating auxilary information with performance data and inefficient storage mechanisms. Paper analog recorder charts are currently folded and filed away, but only eight channels of data are available on any one chart. Correlation of data is difficult because of varying time bases and because of the literally miles of paper tape that are accumulated. Data storage on magnetic tape would alleviate these problems.

(c) Inconsistency and lack of repeatability in performing tests. Whenever a human operator is involved, the possibility of error exists. Computer-controlled sequenced testing would eliminate this possibility and would also eliminate transients in the data caused by personnel activity in close proximity to the test station.

(d) Time lag between data acquisition and data reduction for evaluation. A computer operating in real time at the test station could analyse the test data as it was taken and thus reduce data turn-around time.

Thus, a completely automated multiple-gyro test station controlled by a digital computer that will guide the station through the test sequences appears to be next step in one-g test-station evolution at the Instrumentation Laboratory. Type of test, table orientation, table rate, fixture positioning, excitation-voltage levels, excitation frequencies, and all other test variables will be predefined and under control of the computer. Human intervention or assistance will not be required during the normal course of a test sequence. This will result in two major benefits: increased consistency and decreased disturbances from personnel activity near the station. All of the variables that can influence gyro performance will be monitored and recorded on magnetic tape. Although the majority of this data may not be used, it is necessary that it be available for future reference or correlation studies. A block diagram of such a test station is shown in figure 4-21 (8).

3. Modes of Testing

The one-g test station is the most versatile tool available to the gyro test engineer. The many types of tests that are conducted on such a station are described in chapter 5; for the purposes of this chapter, it is sufficient to describe the various modes of testing.

All of the tests conducted on a one-g test station fall into one of four basic modes; (a) open-loop tests, (b) table-tracking-sectosyn tests, (c) rate-feedback tests, (d) servo-turntable tests.

Open-loop tests are self-explanatory and therefore will not be discussed further. Table-tracking-sectosyn tests are the final check-out test on the test station itself. They are closed-loop servo tests, but no gyro is in the test loop. Rate-feedback and servo-turntable are the basic closed-loop gyro-test configurations.

Table-Tracking Sectosyn Tests

The complexity of today's gyro test station is such that a complete check-out of the station itself must be conducted before a gyro is ever mounted on the table (7). The final performance run of this check-out is the table-tracking-sectosyn test.

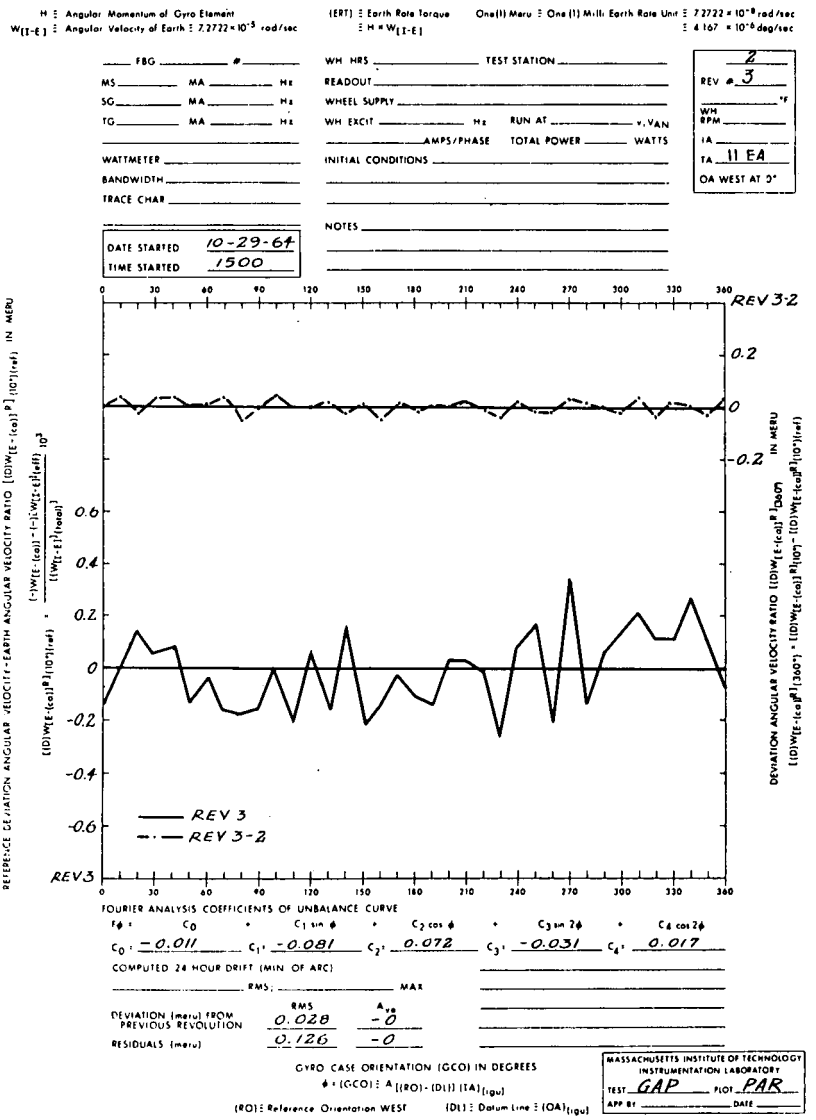

Fig. 4-23(a) Table-tracking-sectosyn test data

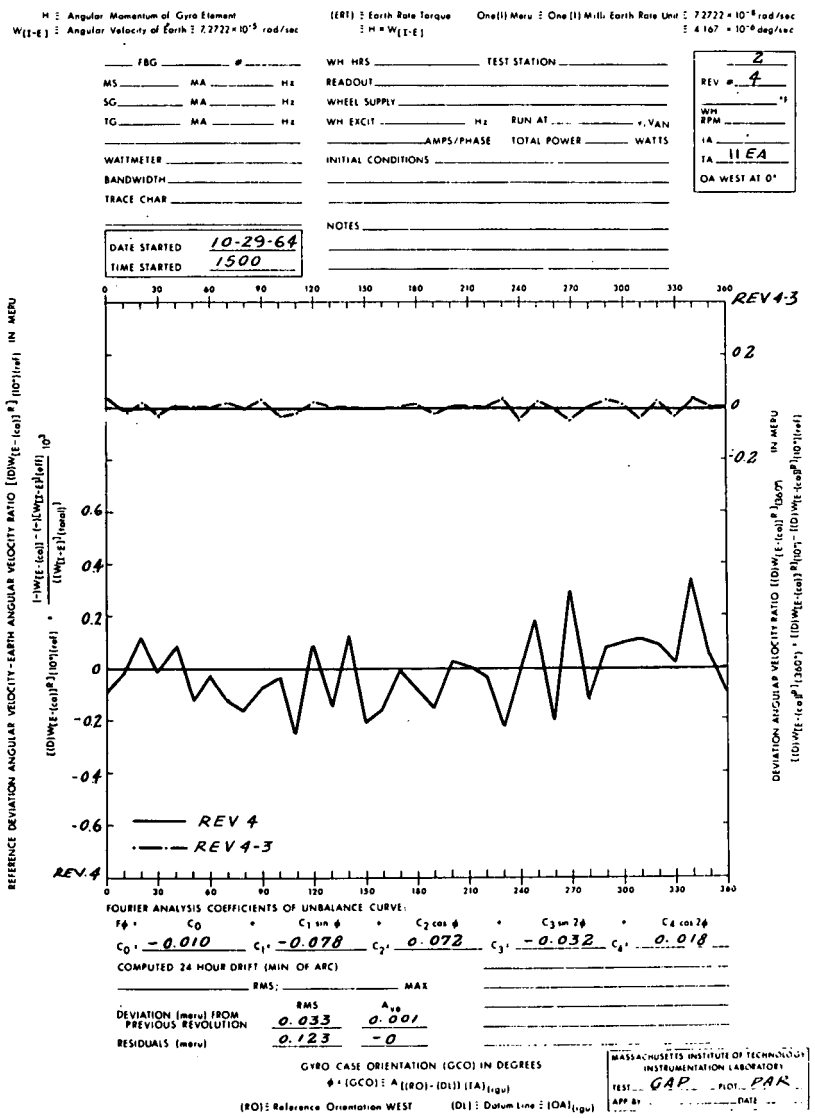

Fig. 4-23(b) Table-tracking-sectosyn test data

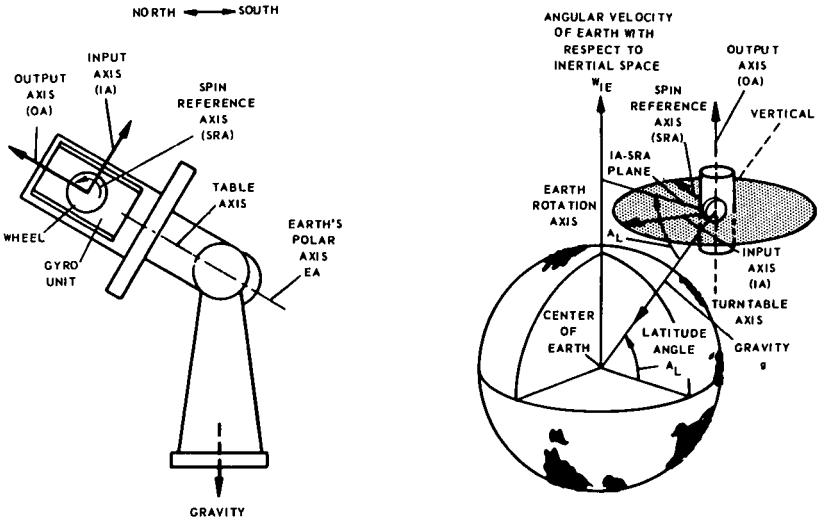

Fig. 4-24 Typical gyro orientation for rate-feedback testing

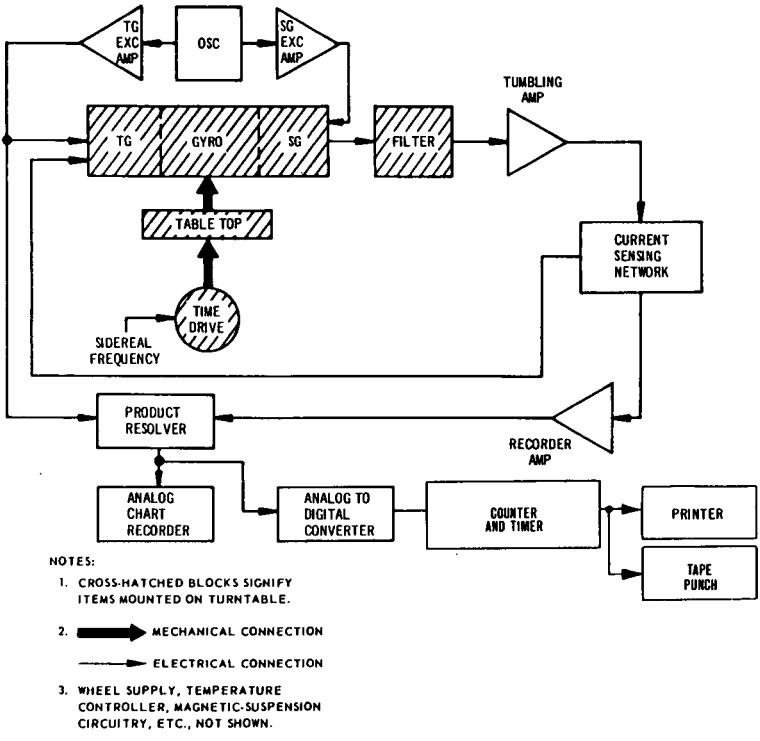

Fig. 4-25 Operating-mode block diagram — a. c. analog rate-feedback test with both analog and digital readout

Figure 4-22 illustrates the basic circuitry employed in a table-tracking-sectosyn test. The sectosyn is excited and connected in the servo loop. The sectosyn rotor is driven at earth's rate, thereby creating an error signal to the servo loop, which in turn drives the servo motor to null the sectosyn. The table rate is measured and treated as if it were actual gyro data. The run is normally of the same duration as the currently specified duration of gyro servo runs. Rate data is measured every degree of table rotation and is averaged over ten-degree increments, which results in thirty-six data points per revolution. These are plotted and subjected to Fourier analysis. Also plotted is a point-to-point deviation curve comparing each revolution to the previous revolution. Figure 4-23 represents two of the five revolutions of test data obtained on a test station at the Instrumentation Laboratory. The lower curve indicates the basic inaccuracy of the station, while the upper curve represents the point-by-point deviation of that revolution from the previous revolution, in other words, the station uncertainty. The Fourier coefficients of the basic curve and an rms of the deviation are recorded at the bottom of each sheet. The sharp peaks of the basic curve from each revolution are caused by micro-imperfections inherent in the gear and worm mechanisms used to drive the sectosyn. Translational motions of the gear with respect to the table shaft produce the complex waveform of the curve which may be analyzed into Fourier coefficients C_1 through C_4.

Large discontinuities in the basic curve accompanied by poor deviations are indicative of high and/or varying friction in the table bearing. The cause can be further correlated by comparing these curves to the sectosyn output signal, which is recorded during the run. The output signal should remain relatively small (about 0.5 mv) and should be constant throughout the run. If the table-bearing friction is high, a large signal will be generated to produce a torque to overcome this friction at which time the table will usually drive through the sectosyn null and stop until enough signal is again built up to drive the table.

As well as using the average of the two photoelectric readouts, one can be used separately to trigger a clock. This data should be very similar to the averaged readout data unless one of the photoelectric readouts is not functioning correctly due to misalignment, loose components, etc. A comparison of the two recordings will indicate which of the photoelectric readouts is at fault.

Rate-Feedback Tests

The total torque appearing about the output axis of a gyro in an inertial-system application is composed of precession torque resulting from angular rates about the gyro input axis, command torque generated by the gyro torque generator, error torques and uncertainty torques: 'error' is defined as the predictable component of inaccuracy, which can be measured and compensated; 'uncertainty' is the random component of inaccuracy, which is only predictable statistically (9). The error torques include mass unbalances, compliances, bias torque, etc. (see chapter 5). As mentioned previously, gyro testing at MIT is directed toward determining a set of torque coefficients for the gyro error model. Accurate knowledge of the magnitude and time stability of these coefficients is necessary if the system computer is to be programmed to compensate for the error torques.

The rate-feedback mode of testing is the primary method used at MIT for obtaining the data from which the torque coefficients are computed. Testing is normally performed with the test turntable rotating at some multiple of earth's rate with the gyro oriented such that its sensitive axis, the input axis, remains perpendicular to both the table rate and earth's rate. One such orientation is depicted in figure 4-24. The signal-generator output signal is amplified and applied as a correction current to the gyro torque generator to keep the gyro float at its zero-angle position, i.e. at the signal-generator null. With the sensitivity of the torque generator known,

a record of the current to the torque generator yields the error torque of the gyro float about the output axis as a function of the turntable angle with respect to a given reference. Analysis of the data from tests in various orientations yields the gyro error coefficients (see chapter 5).

Until recently, testing in the rate-feedback mode was accomplished using analog restraint loops. Early analog restraint loops utilized direct-current circuity with the gyro torque generator. However, this required a d.c. reference current to the torque-generator primary, which resulted in a reaction torque that did not exist when the d.c. current was removed, i.e., when the gyro was not in the d.c. rate-feedback mode. In addition the d.c. current magnetized the torque generator which introduced hysteresis-type torques that could be eliminated only by frequent demagnetization. To circumvent these problems, an a.c. restraint loop was devised, and the d.c. loop is currently used only with gyros that incorporate permanent-magnet-type torque generators. In these units, the polarity of the developed torque is dependent on the direction of current flow in the torque-generator windings, and a bipolar d.c. loop is used.

Limitations in the torque-resolution capability of analog loops and the dissimilarity with the system torquing circuitry (which are normally digital in nature) have fostered the development of digital pulsed-torque restraint loops for use in the test laboratory. All these types of loops - a.c., d.c. and pulsed - are described in the following subsections.

A.C. Analog Rate-Feedback Mode. The total torque about the output axis of the gyro under test is determined by measuring the required torque supplied by the instrument's torque generator to balance the gyro float. This torque may be expressed as:

$$M_{(tg)} = I_{(ref)} I_{(tg)} K_{(tg)} \cos\theta \qquad \text{(Eq. 4-1)}$$

where

$M_{(tg)}$ = total applied torque in dyne-cm
$I_{(ref)}$ = torque-generator primary reference current in ma
$I_{(tg)}$ = torque-generator control current in ma
$K_{(tg)}$ = torque-generator sensitivity in dyne-cm/ma^2
θ = angle between $I_{(ref)}$ and $I_{(tg)}$ in radians

The quantities $I_{(ref)}$, $K_{(tg)}$, and cos θ are either known for a particular instrument or are fixed in value for a particular test. Hence, all that is required for the determination of $M_{(tg)}$ is a knowledge of the control current, $I_{(tg)}$. The function of the rate-feedback loop is to hold the gyro float at or near null by applying a feedback current, $I_{(tg)}$, to the gyro torque generator to cancel the torque causing the float to leave null.

Figure 4-25 is a functional block diagram of the a.c. analog rate-feedback loop incorporating both analog and digital readout. The loop is closed to the gyro through the filter, tumbling amplifier, and current-sensing network. The filter removes unwanted electrical noise from the signal-generator output voltage. The tumbling amplifier is a variable-gain a.c. amplifier utilized as a current source for the torque-generator control winding. The current-sensing network develops a voltage proportional to $I_{(tg)}$, which serves as the input signal to the recording circuitry. The torque-generator primary current, $I_{(ref)}$, is supplied by a frequency source and the torque-generator-excitation amplifier (similar circuitry is used to develop the signal-generator primary excitation current). The two inputs to the product

resolver are the torque-generator primary current, $I_{(ref)}$ and the recorder-amplifier output current. The recorder amplifier is required because the output of the current-sensing network is normally a low-level signal. The product resolver is an electronic multiplier which produces d.c. output voltage proportional to the dot product of the two input currents. Since these currents are $I_{(ref)}$ and a current directly proportional to $I_{(tg)}$, equation 4-1 has been mechanized. The d.c. output voltage of the product resolver is directly proportional to the torque required to balance the gyro float.

Since the developed torque is proportional to the product of $I_{(ref)}$ and $I_{(tg)}$, variations in either will produce torque changes. The product resolver takes into account changes in $I_{(tg)}$, caused by small variations in $I_{(ref)}$ due to equipment instabilities. The d.c. output of the product resolver may be directly recorded on an analog strip-chart recorder and the data reduced manually, or the digital read-out equipment described in section 2 may be used.

Figure 4-26 is a mathematical block diagram of the analog loop. In that diagram

M_d = gyro drift torque in dyne-cm

$M_{(tg)}$ = torque to balance in dyne-cm

$N_{W(IA)}$ = ambient input noise in dyne-cm

$c_{(CF)O}$ = gyro damping coefficient in dyne-cm/sec

p = Laplace transform variable

τ = gyro first-order characteristic time in sec

A_g = float (gimbal) angle in radians

$S_{(sg)}$ = signal-generator sensitivity in mv/mr

N_e = electrical noise in volts

$S_{(t\ell)}$ = rate-feedback (tumbling) loop sensitivity in ma/mv

$I_{(tg)}$ = torque-generator control current in ma

$S_{(tg)}$ = torque-generator sensitivity in dyne-cm/ma

$= I_{(ref)}K_{(tg)}$

With no input to the system other than the drift torque, M_d, the system transfer function is

$$\frac{I_{(tg)}}{M_d} = \frac{\dfrac{S_{(sg)}S_{(t\ell)}}{c_{(CF)O}}}{\dfrac{S_{(sg)}S_{(t\ell)}S_{(tg)}}{c_{(CF)O}} + p(\tau p + 1)} \qquad \text{(Eq. 4-2)}$$

Substituting $j\omega$ for p, the amplitude ratio in the steady-state case is

$$\left|\frac{I_{(tg)}}{M_d}(\omega)\right| = \frac{\dfrac{S_{(sg)}S_{(t\ell)}}{c_{(CF)O}}}{\sqrt{\omega^2 + \left(\dfrac{S_{(sg)}S_{(t\ell)}S_{(tg)}}{c_{(CF)O}} - \tau\omega^2\right)^2}} \qquad \text{(Eq. 4-3)}$$

At $\omega = 0$, equation 4-3 may be solved for $I_{(tg)}$ yielding

$$I_{(tg)}(0) = \frac{M_d(0)}{S_{(tg)}} \qquad \text{(Eq. 4-4)}$$

which is independent of the amplifier gain, $S_{(t\ell)}$. As a result, the feedback current, $I_{(tg)}$, is a direct measure of constant drift torques, i.e. at $\omega = 0$.

If the conditions $0 < \omega < \sqrt{S_{(sg)}S_{(t\ell)}S_{(tg)}/c_{(CF)o}}$ and $\tau < 1$ are applied to equation 4-3,

$$|I_{(tg)}(\omega)| \approx \frac{|M_d(\omega)|}{S_{(tg)}} \qquad \text{(Eq. 4-5)}$$

as a good approximation. Hence, in this frequency range, the feedback current $I_{(tg)}$ is again a direct measure of sinusoidal drift torque of constant amplitude independent of the amplifier gain, $S_{(t\ell)}$.

However, in the system described by the transfer function of equation 4-2, amplifier gain, $S_{(t\ell)}$, has a direct effect on the gyro float-to-case angle, A_g, at all frequencies. The expression relating float angle and drift torque is (from Fig. 4-26),

$$\frac{A_g}{M_d} = \frac{\dfrac{1}{c_{(CF)o}}}{\dfrac{S_{(sg)}S_{(t\ell)}S_{(tg)}}{c_{(CF)o}} + p(\tau p + 1)} \qquad \text{(Eq. 4-6)}$$

Applying the same frequency conditions as before, at $\omega = 0$ and $p = j\omega$

$$A_g(0) = \frac{M_d(0)}{S_{(sg)}S_{(t\ell)}S_{(tg)}} \qquad \text{(Eq. 4-7}$$

and at $0 < \omega < \sqrt{S_{(sg)}S_{(t\ell)}S_{(tg)}/c_{(CF)o}}$ with $\tau < 1$

$$|A_g(\omega)| \approx \frac{|M_d(\omega)|}{S_{(sg)}S_{(t\ell)}S_{(tg)}} \qquad \text{(Eq. 4-8)}$$

As equation 4-8 shows, the gyro float-to-case angle is inversely proportional to amplifier gain, $S_{(t\ell)}$. This offset angle results in microsyn reaction torques and cross coupling between the gyro input and spin axes.

To summarize the foregoing, the feedback current resulting from constant amplitude torques ($\omega = 0$) is an instantaneous direct measure of the unbalance drift torque and is independent of the loop-amplifier gain. At frequencies other than $\omega = 0$, the amplitude of the feedback current is a direct measure of the unbalance drift torque, but there is a time delay between the instantaneous value of the gyro drift torque and the feedback torque (which is related to the phase angle of the transfer function, equation 4-2). This time delay depends on the value of the loop-amplifier gain and is inversely proportional to it. This latter consideration is depicted in figure 4-27 where the time lag is represented by t_d.

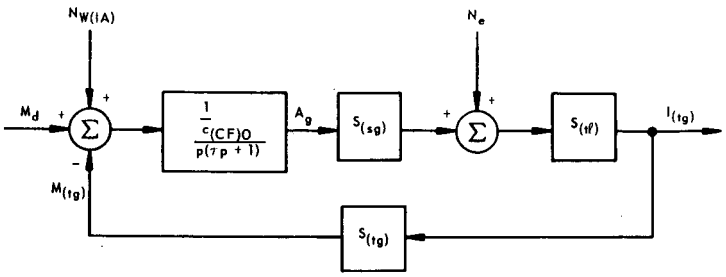

Fig. 4-26 Mathematical block diagram of the analog rate-feedback loop

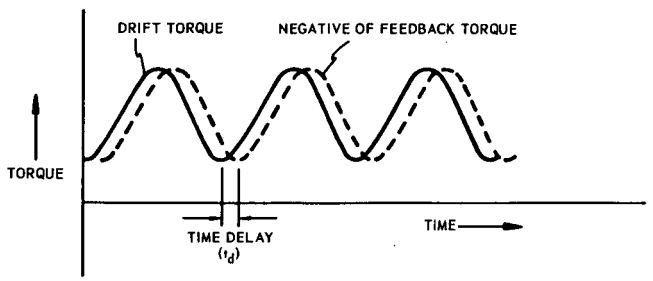

Fig. 4-27 Steady-state torque with $\omega > 0$

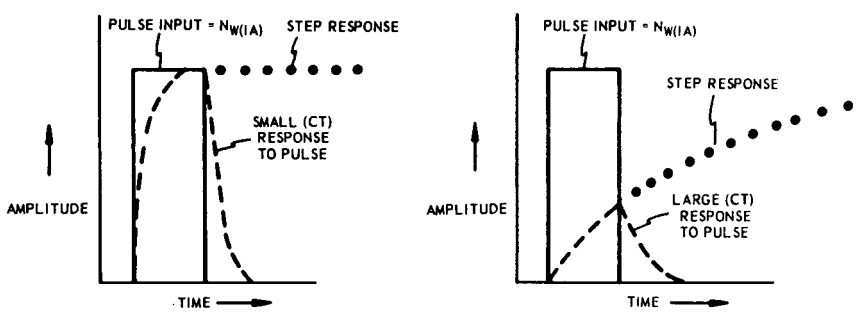

Fig. 4-28 Effect of CT on transient response

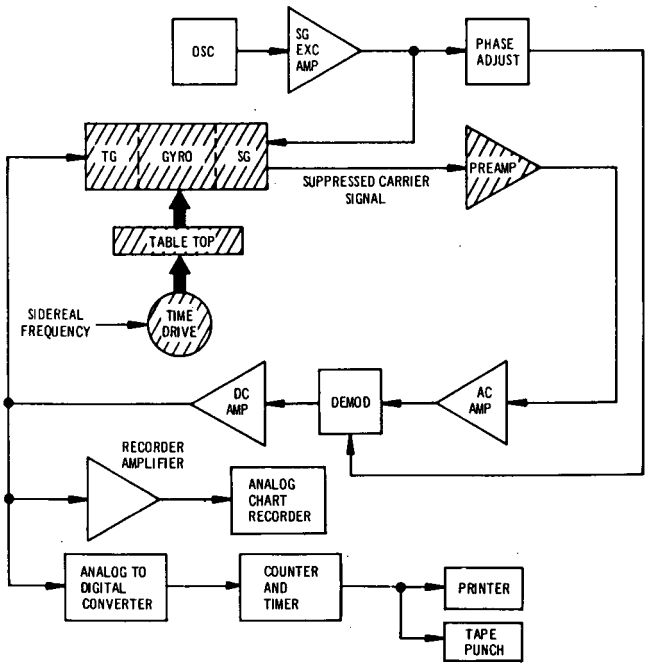

NOTES:

1. CROSS-HATCHED BLOCKS SIGNIFY ITEMS MOUNTED ON TURNTABLE.
2. ➡ MECHANICAL CONNECTION
   → ELECTRICAL CONNECTION
3. WHEEL SUPPLY, TEMPERATURE CONTROLLER, MAGNETIC-SUSPENSION CIRCUITRY, ETC., NOT SHOWN.

Fig. 4-29 Operating-mode block diagram - d.c. analog rate-feedback test with both analog and digital readout

The time delay is the equivalent of a phase angle between the gyro drift torque and the lagging feedback torque. This angle is referred to as the dynamic response angle (DRA) and should be kept small if the assumption that the instantaneous value of the feedback torque is equivalent to the gyro drift torque is to be valid. A high value of loop-amplifier gain is consistent with a small DRA and also results in a short characteristic time (CT) - 'characteristic time' is the time required after a step input for the output to reach 63 percent of its final value starting at the initial value. A relatively long CT is desired in order that the loop act as a filter to high-frequency interfering inputs about the gyro input axis. This effect is exhibited in figure 4-28 in which the response to a pulse input is described for both a long and a short characteristic time. The choice of loop-amplifier gain, $S_{(t\ell)}$, and therefore characteristic time, must be a compromise between the long CT desired for adequate filtering and the short CT consistent with a small DRA and minimum elastic-restraint torque.

D.C. Analog Rate-Feedback Mode. The d.c. analog rate-feedback mose is used today only with gyros incorporating permanent-magnet-type torque generators. This torque generator consists of a stable multipole permanent-magnet rotor mounted on the gyro float and an air-core stator mounted on the end housing. Impedance is independent of the angular displacement of the rotor with respect to the stator, and the time constant is low, which is important in pulse-torquing applications. The torque on the rotor is proportional to the magnitude of the torquing current, and its direction depends on the polarity of the current.

Figure 4-29 is a functional block diagram of the d.c. loop, which is essentially the same as the a.c. loop previously described. A 4800-Hz carrier is supplied to the gyro signal generator and as a reference to the phase-sensitive synchronous demodulator. The suppressed-carrier signal from the signal generator is amplified and then demodulated, amplified in a d.c. amplifier, and applied to the torque generator as a d.c. current. A d.c. voltage directly proportional to this current is fed to the recorder amplifier for the analog readout or to the analog-to-digital converter in the case of digital readout.

The mathematics of the d.c. rate-feedback-loop operation are identical to those of the a.c. loop.

Digital Rate-Feedback Mode. As the performance level of inertial gyros has steadily improved, the requirements on accuracy and resolution in the determination of the gyro torque coefficients have become increasingly stringent. With the analog restraint loop, factors that could be overlooked when the requirement for unbalance-torque determination was on the order of one part in a thousand become limitations when greater resolution is required. Characteristics such as gain instability, linearity, and phase-shift variations in the recording circuitry are directly related to the ability to accurately measure torque and serve to degrade the quality of measurement. In addition, the product resolver used with the a.c. restraint loop is an electromechanical device employing a pivot-and-jewel mechanism, the friction of which contributes further uncertainty to the torque measurement. These factors coupled with susceptibility to physical and electrical noise inputs dictate that an improved means of measuring unbalance torque be utilized.

Digital methods in which the torque is applied to the float in discrete pulses are in general use in inertial-guidance systems. A digital torque loop for use in the test laboratory offers the required torque-resolution capability and is relatively free of the disturbances previously described. This subsection describes a digital restraint loop currently in use at the Instrumentation Laboratory and examines its limitations.

In the analog loop, the torque to balance the gyro float (or feedback torque) is a continuous quantity equal and opposite to the gyro drift torque under constant torque conditions, and equal and opposite to the gyro drift torque under varying torque conditions except for a dynamic lag angle which is kept to a minimum. In a digital restraint loop, the feedback torque, $M_{(tg)}$, is not a continuous quantity but comprises a series of torque pulses of constant magnitude and fixed time duration. The pulses are applied to the torque generator in such a manner as to cause either positive or negative torque (CW or CCW) as required by the float position. As each pulse has a specific torque weight, determination of the gyro drift torque is made from a knowledge of the number and polarity of torque pulses applied over an interval of time. Hence, the information derived is the average torque over a time interval rather than the instantaneous value of torque as in the case of the analog restraint loop.

Figure 4-30 is a block diagram of the digital rate-feedback loop in the binary mode. ('Binary' is defined as existing in two states, in this case as either positive or negative pulses. In ternary pulsing, three states exist: positive, negative, and zero). If the gyro float is subjected to a torque, the resulting rotation about the output axis is sensed by the signal generator. The signal-generator signal is amplified and sampled by the interrogator, which transmits a torque command to the switch calling for a torque polarity that will drive the float towards null. The interrogator receives clock pulses from an external source at intervals of T_s seconds. The interrogator is constrained such that the torque commands from the interrogator to the switch can only change on the negative-going slope of the clock pulse. The action of the interrogator is depicted in figure 4-31. Depending on the command signal, the output of the torque switch will be a current pulse to the torque-generator primary of constant amplitude and of duration NT_s (where N is the number of clock pulses received by the interrogator between changes in state of its output).

Since the loop operates in the binary mode, it must be in either of the two available states, i.e. applying positive or negative torque current pulses to the torque generator. Hence with no gyro drift torque, M_d, present, the gyro float is still subjected to torque pulses, the average of which must equal zero over a period of time.

With the gyro float on one side of null, restoring torque pulses will be applied to it until it is driven through null and out the other side. The float will not receive a restoring torque pulse of opposite polarity immediately after it crosses null but only on the next clock pulse when a torque-polarity reversal can take place. After the torque-polarity reversal occurs, the float is subjected to a number of pulses of the new polarity until it is once more driven through null, where the process is repeated. The float thus alternately receives an equal number of positive and negative restoring-torque pulses, and as a result oscillates about null, i.e. limit cycles, the limit cycle being described by the mode. Thus, if the float alternately receives two or three restoring-torque pulses, the limit cycle is termed as the 2:2 or 3:3 mode, etc. Ideally the 1:1 limit cycle mode will correspond to the zero-gyro-drift condition. This is shown in figure 4-32 (10).

With a gyro drift torque, M_d, present, the float will be subjected to a feedback torque, $M_{(tg)}$, such that it will be constrained around null. The difference in this case, as opposed to the case with zero M_d, is that the limit cycle is now unbalanced - for example, a 5:2 mode might be typical - and the resulting difference between the number of positive and the number of negative pulses is proportional to the applied feedback torque. This situation is illustrated in figure 4-33a. Since the feedback torque must occur in integer numbers of discrete pulses, the

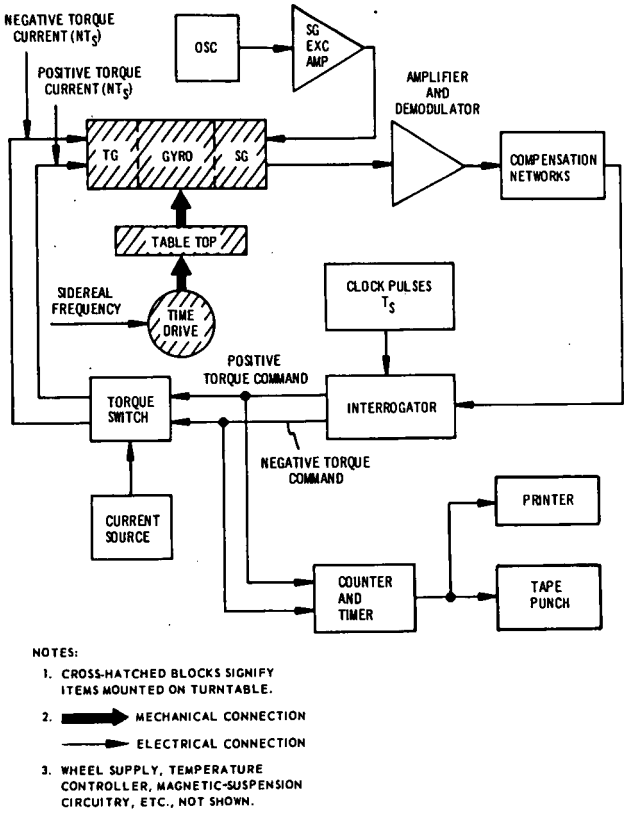

NOTES:

1. CROSS-HATCHED BLOCKS SIGNIFY ITEMS MOUNTED ON TURNTABLE.
2. ➡ MECHANICAL CONNECTION
   → ELECTRICAL CONNECTION
3. WHEEL SUPPLY, TEMPERATURE CONTROLLER, MAGNETIC-SUSPENSION CIRCUITRY, ETC., NOT SHOWN.

Fig. 4-30 Operating-mode block diagram - digital rate-feedback test

feedback torque alternately leads and lags the gyro drift torque with the resulting float-angle condition described in figure 4-33b. This condition may result in a torque readout error if the time over which the net difference in torque pulses is accumulated does not coincide with the zero-angle crossover points. As shown in figure 4-33c, at T_1 the average angle is zero corresponding to exact cancellation of M_d; therefore, there is no readout error. Over time T_2, the average angle is not zero, M_d has not been exactly compensated, and a readout error exists. This effect and other error sources are treated in detail in reference 10. As may be seen, the magnitude of this error is dependent on the limit-cycle mode: i.e. the higher the moding, the larger the error. To reduce this error to acceptable limits, it is necessary to reduce the limit-cycle mode by increasing the frequency at which the loop will oscillate.

In the binary torque loop, the upper limit of this frequency is controlled by the interrogator which may only change states coincident with a clock pulse. Hence the upper frequency limit for oscillation is $f = (1/2)T_s$ or the 1:1 limit-cycle mode. This result may be achieved by applying lead compensation as described in reference 11. Table 4-1 displays the maximum lag angles associated with the possible limit-cycle modes and the frequency of oscillation in terms of the clock frequency and the corresponding lag angles.

Table 4-1 Limit-cycle mode and maximum phase lag for various frequencies of oscillation

Frequency	Limit Cycle Mode	Maximum Phase Lag
$\omega_s/2$	1:1	180°
$\omega_s/4$	2:2	90°
$\omega_s/6$	3:3	60°
$\omega_s/8$	4:4	45°
$\omega_s/10$	5:5	36°

The mathematical block diagram for the system is shown in figure 4-34. In that diagram

$M_{(int)}$ = interfering torque

$\frac{K_1}{p(\tau p + 1)}$ = gyro transfer function

p = Laplace transform variable

K_2 = amplifier and demodulator gain

$G_{fc}(p)$ = compensation-network transfer function

$N(E)$ = describing function for the nonlinear elements (interrogator, switch, and current source)

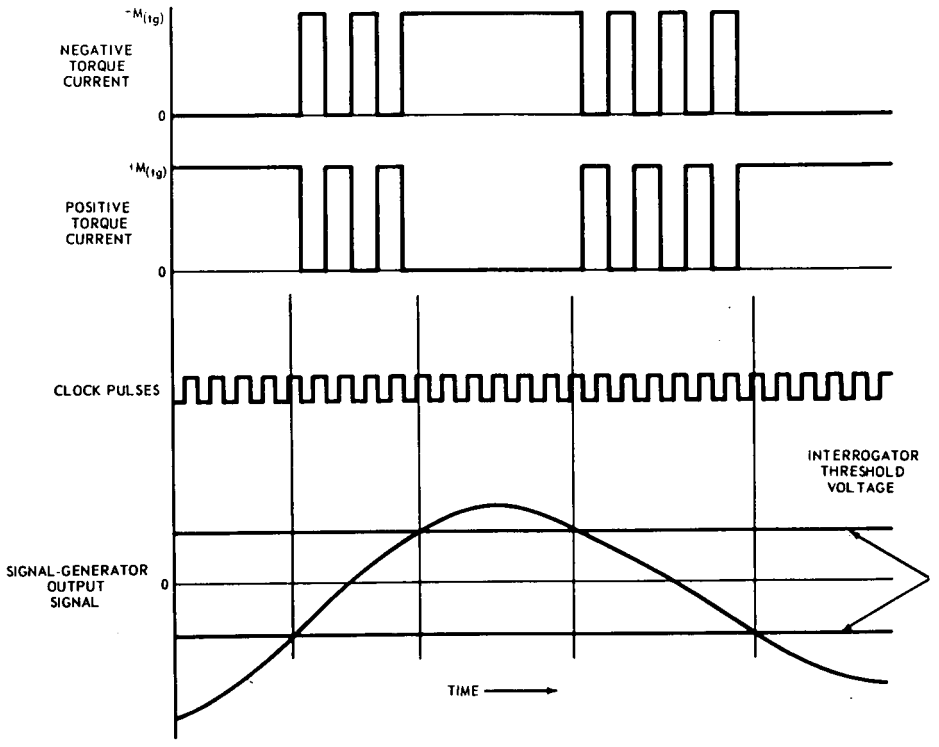

Fig. 4-31 Relationship between torque current pulses and signal-generator output signal

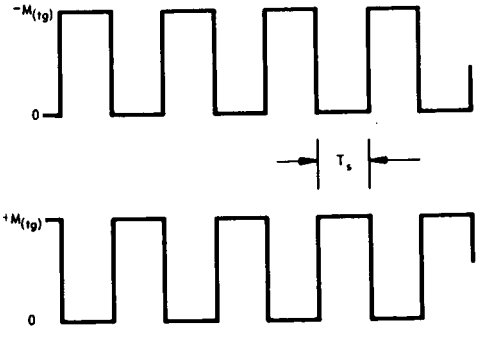

Fig. 4-32 Output of torque switch in 1:1 mode with zero input to interrogator

The corresponding system transfer function is

$$\frac{M_{(tg)}}{M_d} = \frac{\dfrac{K_1K_2}{p(\tau p+1)} G_{fc}(p)N(E)}{1+\dfrac{K_1K_2}{p(\tau p+1)}G_{fc}(p)N(E)} \qquad \text{(Eq. 4-9)}$$

Defining

$$G_1(p) = \frac{K_1K_2}{p(\tau p+1)} G_{fc}(p) \qquad \text{(Eq. 4-10)}$$

we have

$$\frac{M_{(tg)}}{M_d} = \frac{G_1(p)N(E)}{1+G_1(p)N(E)} \qquad \text{(Eq. 4-11)}$$

where

$G_1(p)$ = transfer function of linear elements in the loop

$N(E)$ = transfer function of nonlinear elements in the loop

The poles of equation 4-11 are found by setting

$$1 + G_1(j\omega)N(E) = 0 \qquad \text{(Eq. 4-12)}$$

or

$$G_1(j\omega) = -\frac{1}{N(E)} \qquad \text{(Eq. 4-13)}$$

In order to determine if a limit cycle can occur, the functions $G_1(j\omega)$ and $-(1/N(E))$ are plotted on a Nyquist diagram or Nichol's chart. At each possible frequency of oscillation, the maximum phase-lag angle from table 4-1 is added to the transfer function of the linear elements. If an intersection with $-(1/N(E))$ loci occurs, the loop may oscillate at that frequency. Compensation consists of adding sufficient lead to cancel the phase lag associated with the frequency of oscillation.

Figure 4-35 is a Nichol's chart of the uncompensated system. These plots show that the system can sustain limit cycles at the following frequencies.

Limit cycle mode	Frequency
1:1	$\omega_s/2$
2:2	$\omega_s/4$
3:3	$\omega_s/6$

Figure 4-36 is a Nichol's chart of a compensated system. The compensation used has the following transfer function

$$\frac{(8\tau_s p+1)(\tau p+1)}{(\tau_s p+1)}$$

where

$$\tau_s = \frac{1}{2\pi f_s}$$

That figure shows that the compensated system will sustain only the 1:1 limit cycle.

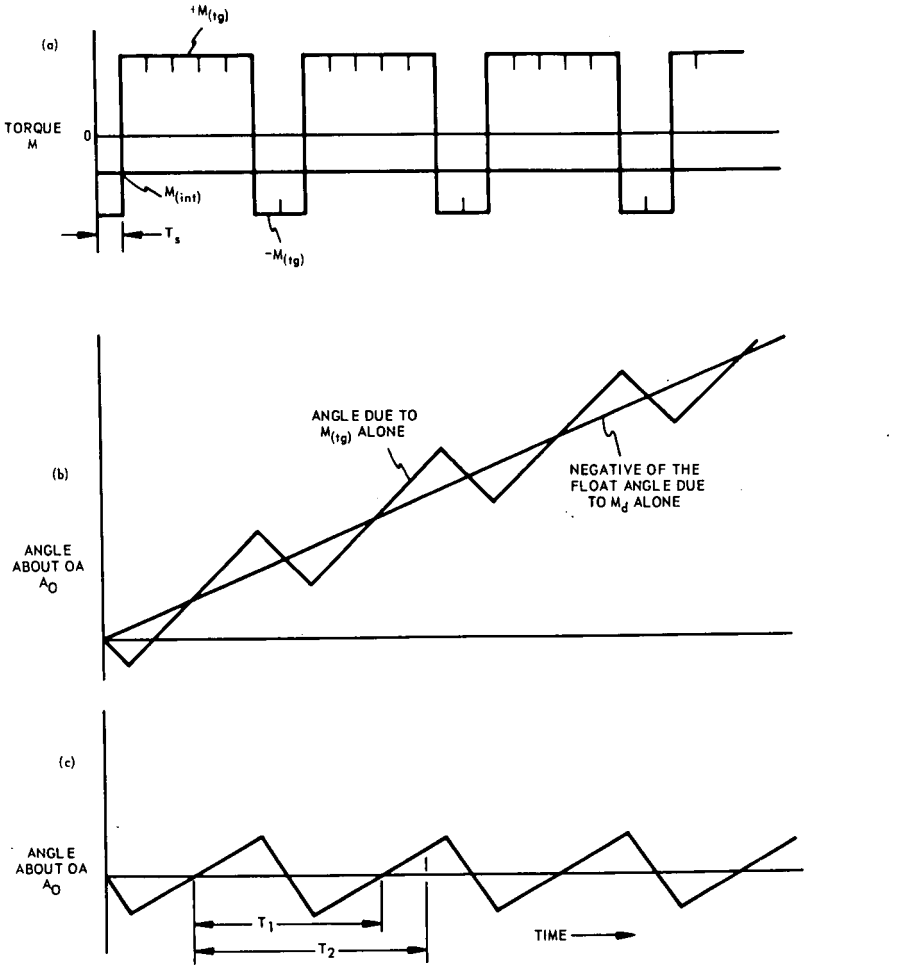

Fig. 4-33 Relationship between indicated and actual gyro interference torque in a binary-mode digital rate-feedback loop

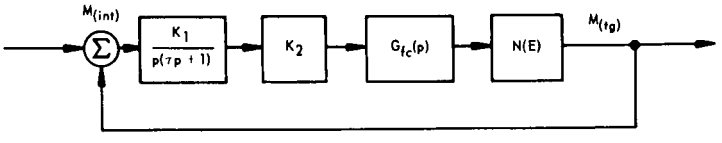

Fig. 4-34 Mathematical block diagram of the digital rate-feedback loop

In addition to frequency compensation discussed above, the digital torquing loop has a number of design parameters that limit the accuracy and resolution of the measurement of unbalance torques. They are:

(a) signal-generator null sensitivity

(b) torque-generator current magnitude

(c) torque-generator current stability

(d) sampling frequency

(e) sampling-frequency stability

The signal-generator null sensitivity affects the accuracy and resolution of measurement because the gyro is an integrating device; that is, the signal-generator output is proportional to the integral of the net torque applied to the torque-summing member. For a typical gyro, this relationship can be expressed by the equation

$$E_o = KT \ \frac{\text{microvolts}}{\text{meru}} \qquad \text{(Eq. 4-14)}$$

where

E_o = signal-generator output

T = time

K = a constant proportional to gyro response time

If E_o is considered the noise threshold or null sensitivity of the gyro, the time required to move through various noise thresholds as a function of net torque can be calculated.

In order to maximize system performance, the resolution of the digital torquing should be equal to or greater than the resolution capability of the gyro signal generator. The digital torquing resolution as a function of time is given by

$$\text{Resolution} = M_{(tg)} \ \frac{T_s}{T} \qquad \text{(Eq. 4-15)}$$

where

$M_{(tg)}$ = restraint torque magnitude

T_s = torque pulse width in seconds

T = data accumulation time

The digital torquing resolution is a function of the pulse weight (pulse height times pulse width).

For a compatible system, the resolution of the torque generator is equated to the resolution of the signal generator. Figure 4-37 shows plots of gyro resolution

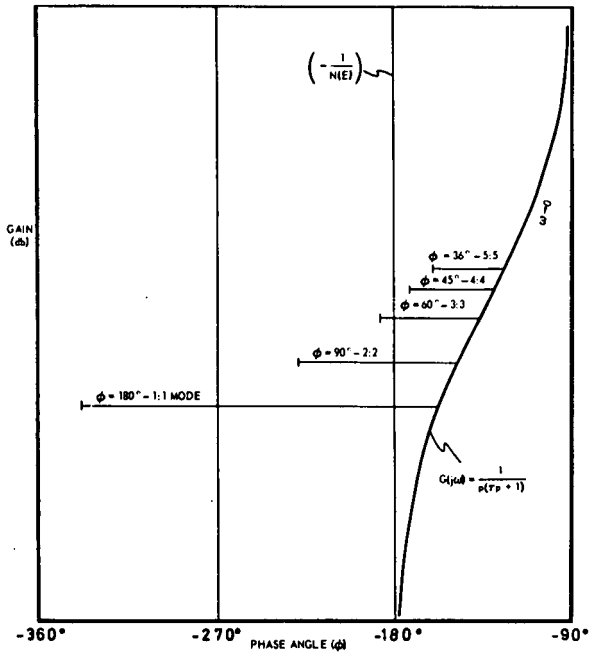

Fig. 4-35

Nichols chart of uncompensated digital torquing loop

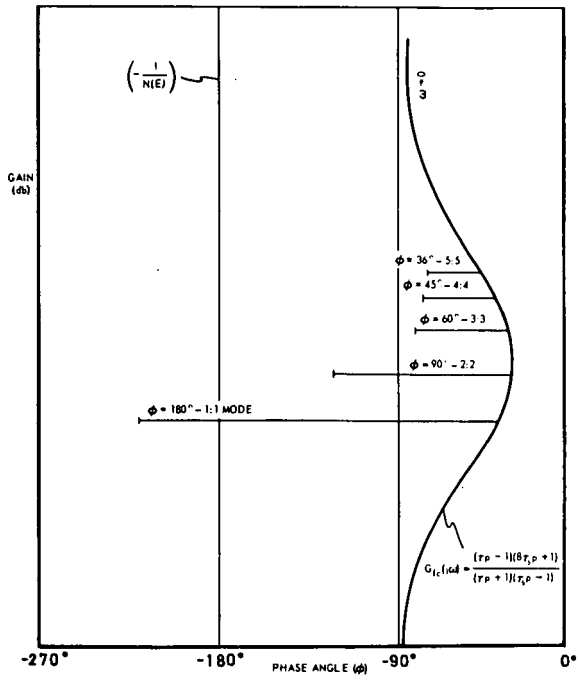

Fig. 4-36

Nichols chart of compensated digital torquing loop

as a function of time for various realizable signal-generator noise thresholds and associated pulse weights. These curves show that a digital torquing loop can easily provide a torquing resolution equal to the sensing resolution of the gyro signal generator while simultaneously nulling out large values of interference torques.

The error introduced by torque-generator current instability is directly related to the magnitude of interference torque, $M_{(int)}$, for which the torque generator must compensate. For the error contribution due to current instability to be equivalent to the weight of one pulse, the following relationship holds.

$$\frac{\Delta I}{I_{(tg)}} = \frac{M_{(tg)}}{M_{(int)}} \cdot \frac{T_s}{T} \qquad \text{(Eq. 4-16)}$$

Figure 4-38 gives plots of the torque-generator current stability required to measure gyro drift as a function of gyro bias torque. These curves show that high resolution cannot be achieved if the torque generator must compensate very large unbalance torques.

The error due to frequency instability would be the same as that due to current instability. However, this can be made negligible by the use of the very stable crystal oscillators available today. Long-term stabilities of one part in 10^7 per 100 days are easily attainable.

Servo-Turntable Tests

The servo-turntable test is useful in gyro evaluation because it is the only test in which the gyro is operated in the manner in which it is used in the system. In both, the loop is closed to the gyro through motion of the base upon which the gyro is mounted, and the loop dynamics are similar. Unlike the rate-feedback test whose basic purpose is to measure the gyro error coefficients, the basic purpose of the servo-turntable test is to measure the long-term performance of the gyro.

One typical gyro orientation used in servo-turntable testing is depicted in figure 4-39. In that figure, the gyro is mounted with its sensitive axis, the input axis, parallel to both the test-table axis and the earth's axis. The gyro senses full earth's rate, and the resulting precession of the gyro float drives it away from its null position with respect to the case. As indicated in figure 4-40, the output signal from the gyro signal generator is amplified and fed to a servo motor that drives the test turntable in the proper direction to compensate for the earth's rate input. Thus, the gyro stabilizes the turntable with respect to inertial space, and the turntable rotates at nearly one revolution per sidereal day in the direction opposite to the earth's rotation. If the turntable rate is measured as a function of turntable angle with respect to the earth and if the earth's-rate input is subtracted, the remaining rate is due to error and uncertainty torques in the gyro and to errors and uncertainty in the test equipment. This rate can be converted to equivalent torque units. The result is the unbalance torque about the gyro output axis as a function of turntable angle.

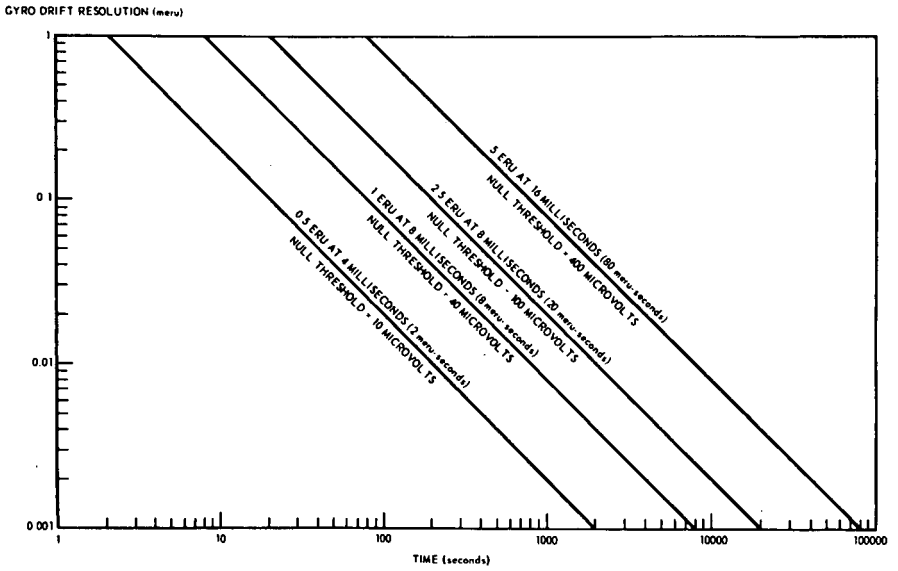

Fig. 4-37 Time required to resolve gyro drift as a function of torque-generator pulse weight and signal-generator null threshold

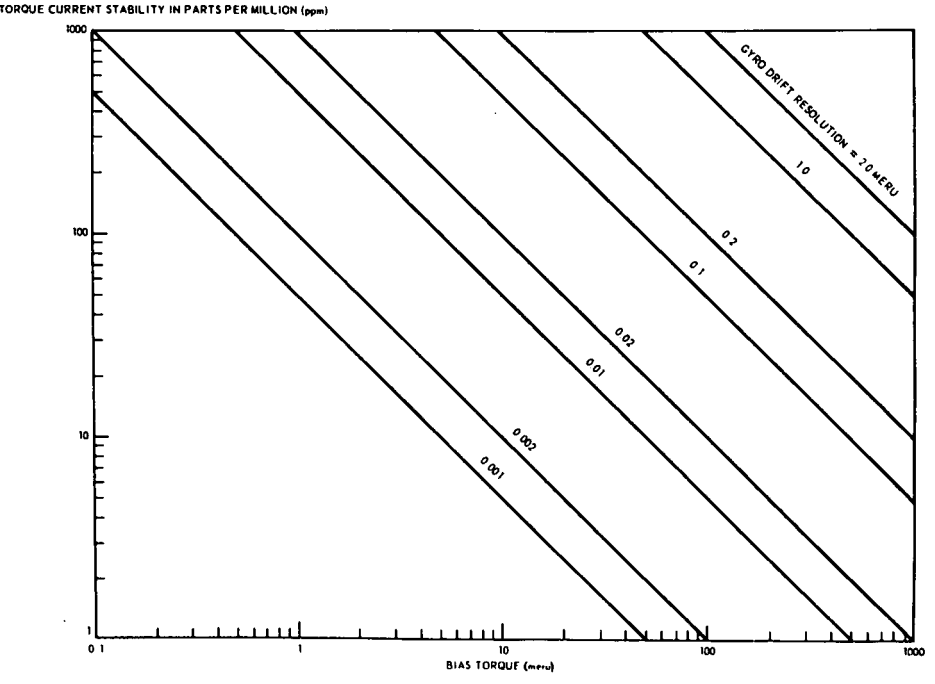

Fig. 4-38 Torque-generator current stability required to measure gyro drift as a function of gyro bias torque

A Fourier analysis of servo data will yield some of the gyro torque coefficients, but no one servo test will yield all of the coefficients. However, as previously noted, servo tests are used more as a measure of long-term gyro performance than as a means of determining individual torque coefficients. For example, in a multi-revolution test, the first revolution can be considered a calibration run. Data from this revolution can then be applied to the gyro float as correction torques from the gyro torque generator during succeeding revolutions or can be computed from the data obtained during succeeding revolutions. The results, then, are an indication of the nonrepeatable errors, or uncertainty, of the gyro and test setup.

Another common servo test is the OA-vertical, IA east (or west) test where the gyro senses no earth's rate. In the ideal case in this test, the turntable would remain stationary with respect to the earth. Any rotation of the turntable top as indicated by the table-tracking sectosyn is therefore a measure of the error and uncertainty torques within the gyro and the errors and uncertainty of the test setup.

The servo system should be a high-gain loop in order that the maximum torque stiffness be obtained. High stiffness is desirable to attenuate as much as possible all unwanted loop disturbances. The servo loop used at MIT has a forward gain of approximately 1.5×10^6, which makes synchronization a difficult problem because the resulting conditionally stable system when cascade compensation is used becomes unstable when the forward loop amplifier saturates, i.e. on turning on the system. ('Synchronization' is the ability of the loop to drive to null during turn-on procedures when some of the loop components may be saturated. By 'conditionally stable' is meant a situation where a large enough increase or decrease in gain will result in instability). This nonlinear saturated system is easily stabilized and forced into the linear region of operation by the use of tachometer feedback, but introduction of the tachometer results in an unwanted base-motion interference. This can be visualized by noting that if the table top is stabilized with respect to inertial space and the tachometer is mounted on the base (since it cannot be mounted in inertial space), then any relative motion between base and table results in a signal that is not referred to inertial space and is thus an interfering input. In a well-designed servo loop, however, the tachometer-feedback-caused base-motion interference is smaller than the error resulting from base-motion acting as a direct error source. Thus, the tachometer can be left in the loop to serve as a stabilizing network even in the linear region of operation, which considerably simplifies the loop design and construction.

Figure 4-41 is a mathematical block diagram of the servo-turntable loop. In that diagram

U_W = gyro drift to be measured

p = Laplace transform variable

$= \sigma + j\omega$

$Y_g(p) = \dfrac{H/c_{(CF)O} S_{(sg)} K_1}{\tau p + 1}$

H = gyro-wheel angular momentum

$c_{(CF)O}$ = gyro damping coefficient

$S_{(sg)}$ = gyro-signal-generator sensitivity

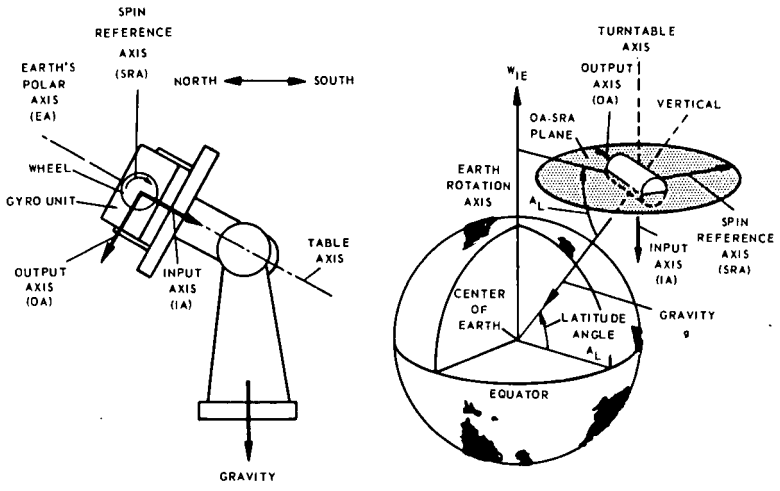

Fig. 4-39 Typical gyro orientation for servo-turntable testing

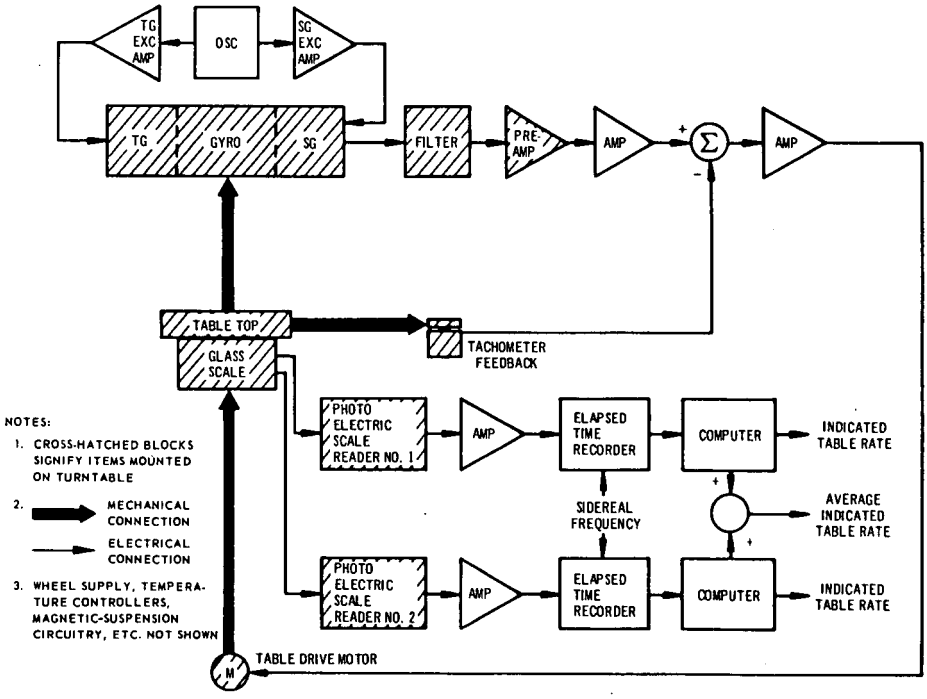

Fig. 4-40 Operating-mode block diagram - servo-turntable test

K_1 = equivalent servo gain in cascade with gyro output

τ = gyro first-order characteristic time

$Y_f(p)$ = cascade compensation transfer function, having neither poles nor zeros at p = 0

$Y_b(p)$ = tachometer-feedback transfer function, having neither poles nor zeros at p = 0

$Y_m(p)$ = motor transfer function = $\dfrac{K_T/R}{(1+p/R/L)}$

K_T = motor torque constant

R = motor resistance

L = motor inductance

$M_{(int)}$ interfering torque

J = moment of inertia of the table

W_{IT} = angular velocity of the table relative to inertial space

K_e = motor back-emf constant

W_{IB} = angular velocity of the table base relative to inertial space

W_{BT} = angular velocity of the table relative to its base

int = interfering

The transfer function for this system, neglecting interfering inputs is

$$\frac{W_{IT}}{U_W} = \frac{Y_f Y_m Y_g}{p^2(j + Y_b Y_f Y_m) + pY_m K_e + Y_f Y_m Y_g} = (PF)_{c\ell} \qquad \text{(Eq. 4-17)}$$

where

$(PF)_{c\ell}$ = closed-loop performance function

This relationship considers the motion of the turntable with respect to inertial space as the system output and the interfering inputs $M_{(int)}$ and $W_{(IB)int}$ equal to zero.

In actual practice, the output quantity which is measured is the turntable rate with respect to the base, W_{BT}. This quantity necessarily includes the base motion of the table structure with respect to inertial space, and this interfering input is designated $W_{(IB)int}$ in figure 4-41. The remaining interfering input, $M_{(int)}$, is due to table friction, table-mass unbalance, gyro reaction torque and motor-ripple torque.

The dependent of the monitored table rate, W_{BT}, on the closed-loop performance function and the interfering inputs is

$$W_{BT} = (PF)_{c\ell}\left[U_W + \frac{pM_{(int)}}{Y_f Y_m Y_g} + \left(\frac{p^2 Y_b}{Y_g} + \frac{pK_e}{Y_f Y_g} - \frac{1}{(PF)_{c\ell}}\right) W_{(IB)int}\right] \qquad \text{(Eq. 4-18)}$$

where

$W_{IB} = W_{IE} + W_{EB}$

W_{IE} = angular velocity of the earth relative to inertial space

W_{EB} = angular velocity of the base relative to the earth

Since the earth's rate, W_{IE}, is a constant, equation 4-18 may be rewritten as

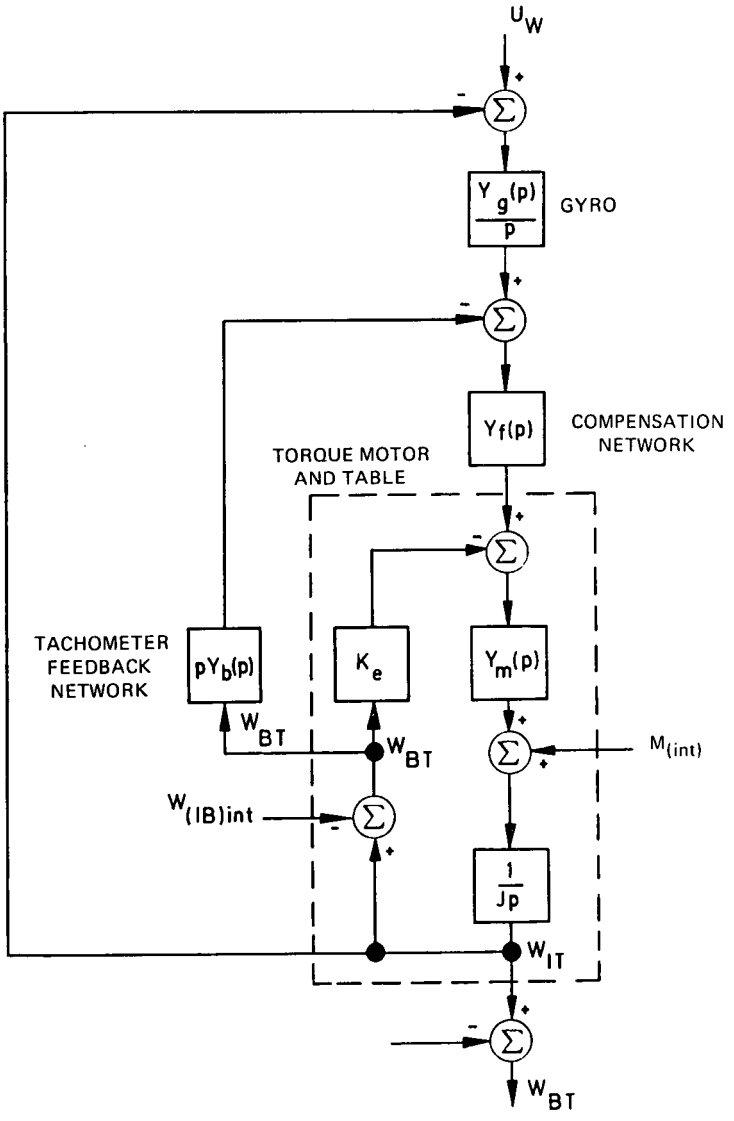

Fig. 4-41 Mathematical block diagram of the servo-turntable loop

$$W_d = (PF)_{c\ell} \left[U_W + \frac{pM_{(int)}}{Y_f Y_m Y_g} + \left(\frac{p^2 Y_b}{Y_g} + \frac{pK_e}{Y_f Y_g} + \frac{1}{(PF)_{c\ell}} \right) W_{EB} \right] \qquad \text{(Eq. 4-19)}$$

where

W_d = table drift rate with W_{IE} neglected

Examination of equation 4-19 reveals that the drift velocity, W_d, is dependent on the gyro drift to be measured, U_W, and on four error terms induced by the interfering inputs, three of which result from base motion, W_{EB}.

The effect of the interfering input, $M_{(int)}$, on the drift velocity is

$$W_d \Big|_{\text{due to } M_{(int)}} = \frac{(PF)_{c\ell}\, pM_{(int)}}{Y_f Y_m Y_g} \qquad \text{(Eq. 4-20)}$$

where

$Y_f Y_m Y_g$ = torque stiffness M_s

$$Y_f(p)\, Y_m(p)\, Y_g(p) \propto M_s \qquad \text{(Eq. 4-21)}$$

Hence, the error contributed to $M_{(int)}$ is reduced by increasing the torque stiffness, M_s.

Similarly the error terms

$$W_d \Big|_{\text{due to tach}} = (PF)_{c\ell} \frac{p^2 Y_b}{Y_g} W_{EB} \qquad \text{(Eq. 4-22)}$$

and

$$W_d \Big|_{\text{due to motor back emf}} = (PF)_{c\ell} \frac{pK_e}{Y_f Y_g} W_{EB} \qquad \text{(Eq. 4-23)}$$

contributed by the tachometer and table torque motor which are the result of base motion are reduced by high values of Y_g and $Y_f Y_g$, respectively. Both of these conditions are compatible with high torque stiffness.

The remaining error term

$$W_d \Big|_{\text{due to base motion}} = -W_{EB} \qquad \text{(Eq. 4-24)}$$

is due directly to base motion and is falsely interpreted as motion of the table with respect to the base. No provision for minimizing this error source may be made in the servo-system design, but other methods such as base-motion isolation (see section 6) may be used.

4. Environment-Simulation Equipment

Environment-simulation equipment runs the gamut from extremely complex devices of such a size that they require special buildings or structures to simple devices that can be stored away in the test laboratory when not in use. An example of the former type is a large centrifuge for generating sustained linear acceleration while Helmholtz coils for magnetic-field generation and pressure domes for pressure-and vacuum-sensitivity tests are examples of the latter. Since the characteristics of these latter devices are generally well known, they will not be discussed further in this paper.

The effects of two environments on the precision gyro are of particular concern to the inertial-system engineer today. With the current emphasis on missile and rocket guidance, the acceleration-squared-sensitive terms of the gyro error model have taken on increased significance and must be accurately measured in the high-g environment. This has resulted in the use of linear vibrators and centrifuges to generate high linear-acceleration levels. Particularly in the strapdown application, but also in gimbaled systems, angular vibration can cause appreciable changes in gyro performance. Thus, a precision angular vibrator is used to check the effects of such an environment on the gyro performance. These three types of environment-simulation equipment - linear vibrator, centrifuge, and angular vibrator - are described in this section.

Linear Vibrator

The basic requirements of a test station for sinusoidal vibration testing are (12):

(a) to produce a pure sinusoidal rectilinear vibration with a high translational acceleration and a minimum amount of angular vibration at the gyro compliance calibration frequencies (less than 100 Hz); this frequency range is considerably below any structural resonant frequencies in current gyros and is usually lower than the wheel-rotation frequencies (200 to 400 Hz);

(b) to produce sinusoidal vibrations at high translational acceleration at frequencies from 100 to 2000 Hz to evaluate component and sub-component fragility;

(c) to produce sinusoidal vibrations at frequencies up to 5000 Hz to evaluate gyro structural-response characteristics.

Electrodynamic vibrators are commercially available to satisfy the requirements of items (b) and (c). These vibrators cannot generally satisfy the requirements of item (a) because of their relatively large amount of cross-axis vibration and angular vibration. The problem of meeting the requirements of item (a) was approached at the Instrumentation Laboratory by two specific test stations. The first approach was a precision linear vibrator and the second was an electrodynamic vibrator-slip table combination.

Precision Linear Vibrator. Figure 4-42 is a schematic diagram of the precision linear vibrator and figure 4-43 is a close-up view of a gyro mounted in the vibrating carriage in a fixture that is rotatable about a vertical axis. The fixture shown supports the case of the gyro at an angle such that the gyro output axis is accurately aligned parallel to the earth's polar axis of rotation. The gyro can be rotated about its output axis until its input axis is at any desired angle with respect to the acceleration field, which is horizontal. By changing fixtures, the gyro can be aligned to any other orientation with respect to the earth or with respect to the horizontal acceleration field.

The carriage is supported on guide shafts and is driven by an eccentric through a slider, which gives an action similar to that of a conventional Scotch yoke. Backlash, which would cause errors in the system, is eliminated through the use of preload springs. These force the carriage to follow the slider by keeping the slider in contact with the drive block even under the peak acceleration that occurs during any test. The springs have a natural resonant frequency between 400 and 500 Hz, while the maximum frequency of vibration is only 50 Hz.

In order to obtain the greatest possible precision in the system, cam-shaft deflection is made as small as possible by using shafts of substantial diameter. The drive shaft is carried between heavy inner and outer bearings that reduce bending distortion of the shaft to a minimum. The drive-shaft cams are rotated at constant speed by means of an electric-motor-powered drive unit.

Changes in linear-acceleration amplitude are made by changing the drive speed and by changing from one drive shaft to another with an eccentric giving a different amplitude. The drive speed is continuously adjustable from 600 to 3000 rpm, thereby giving a vibration frequency up to 50 Hz with an acceleration up to 10 g's.

All sliding surfaces are lubricated by oil supplied under high pressure. Sliding surfaces and hydraulic-pressurized bearings are used throughout rather than ball bearings in order to achieve smooth acceleration curves that are free from the erratic high-frequency-interference effects that may accompany the operation of ball bearings. The lubricating oil is cooled by passing it through a heat exchanger using water as a coolant.

Because of its all-mechanical construction, the precision linear vibrator is limited to 10g's for a 20-pound specimen (fixture plus instrument). In addition, this vibrator is a constant-displacement machine so that a change in acceleration requires a change in frequency. Thus, it is difficult to differentiate gyro-compliance-coefficient frequency dependency from acceleration dependency although interfering effects from angular vibrations due to lack of rigidity of the carriage or the bearings can be estimated by tests at reduced wheel speeds.

Electrodynamic Vibrator-Slip Table Combination. The second approach used at the Instrumentation Laboratory to meet the requirements of item (a) above was to use a commercially available high-force electrodynamic vibrator with its axis horizontal driving a precision slip table. With the vibrator decoupled from the slip table, items (b) and (c) above can be satisfied. Figures 4-44 and 4-45 are schematic diagrams of the setup, and figure 4-46 is a photograph of the vibrator inside its acoustically shielded room. The acoustically shielded room is necessary because the noise generated by the vibrator in operation might damage the hearing of test personnel in the area (see 'Acoustic Noise' page 173). Figure 4-47 shows a gyro mounted in a vibration fixture on the slip table during testing.

As indicated in figures 4-44 and 4-45, the vibrator and slip table are mounted in an air-spring-suspended seismic mount. The four air springs on bellows and the large seismic-mass base provide high test-system inertia and isolation from high-frequency input disturbances from the test-area environment during high-acceleration testing.

Since the entire test system is not geometrically symmetric, the system center of gravity does not coincide with its geometric center. This factor alone requires accurate balancing and leveling through precise control of each of the leveling elements, or air bellows. This control is accomplished by regulating the air pressure to the four bellows. Because of the different loading conditions

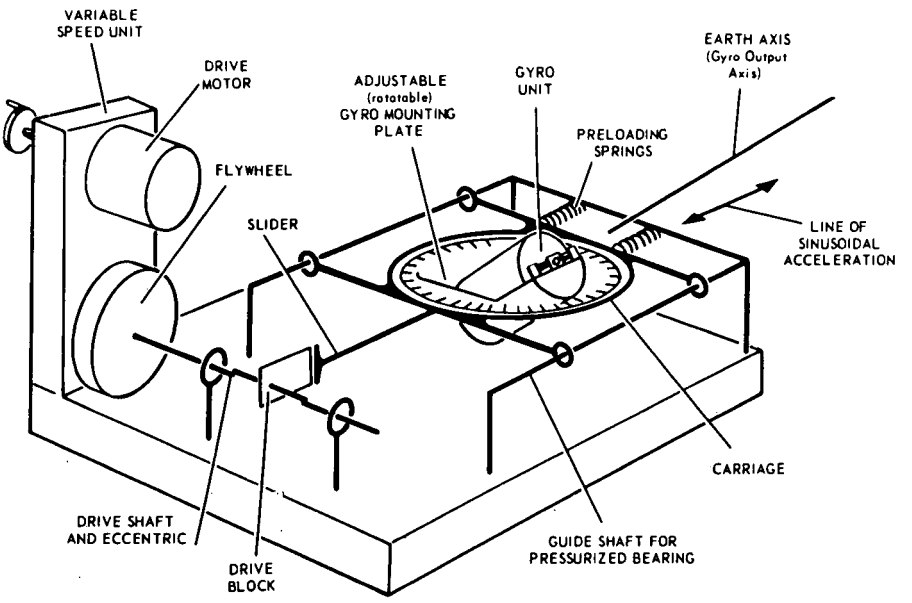

Fig. 4-42 Line schematic of the precision linear vibrator

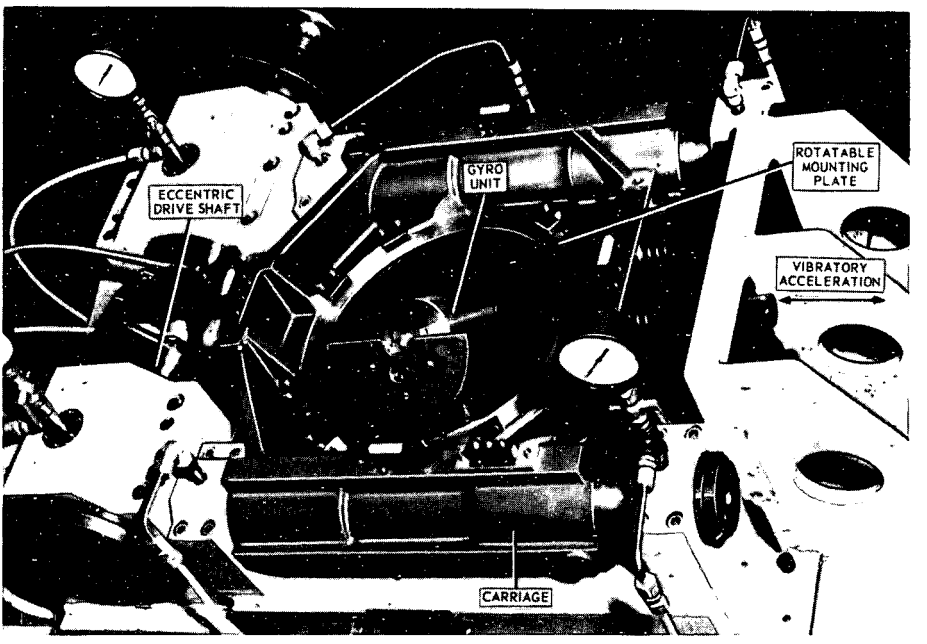

Fig. 4-43 Gyro unit mounted on precision linear vibrator

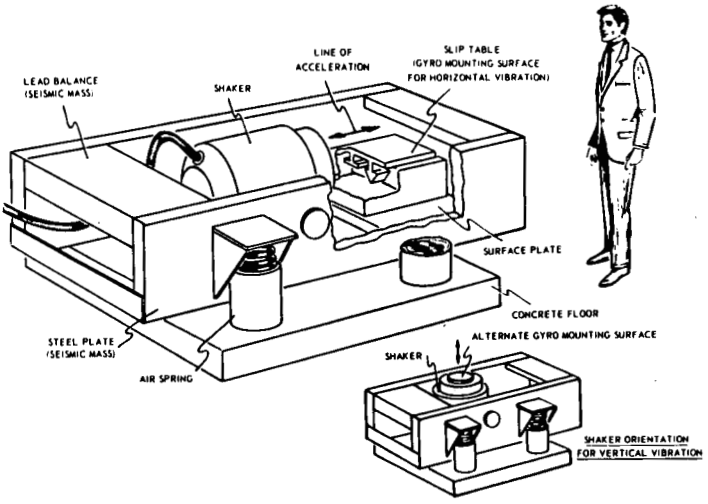

Fig. 4-44 Pictorial schematic of electrodynamic linear vibrator

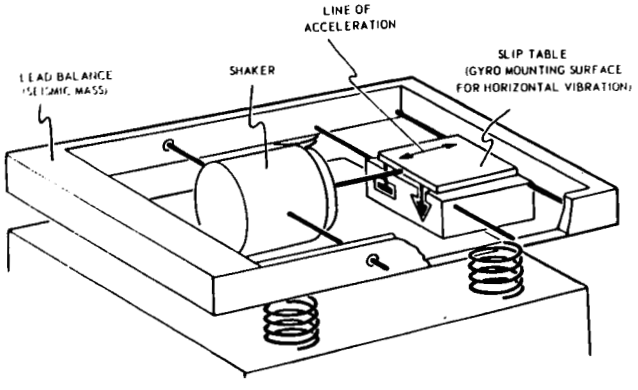

Fig. 4-45 Line schematic of electrodynamic linear vibrator

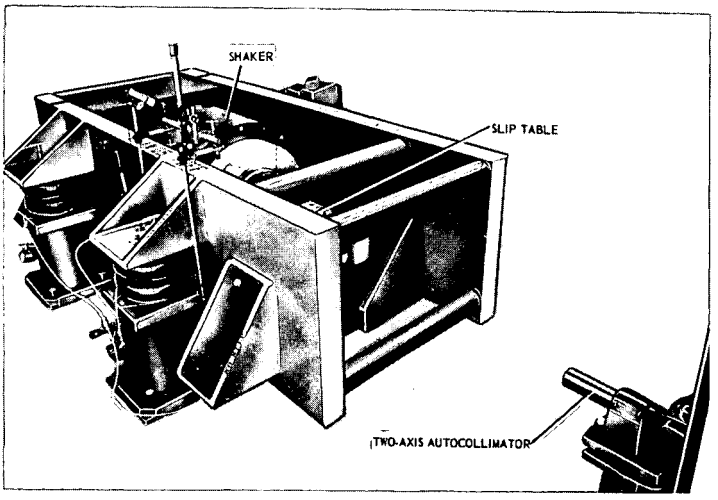

Fig. 4-46 Vibrator and slip table inside acoustically shielded room

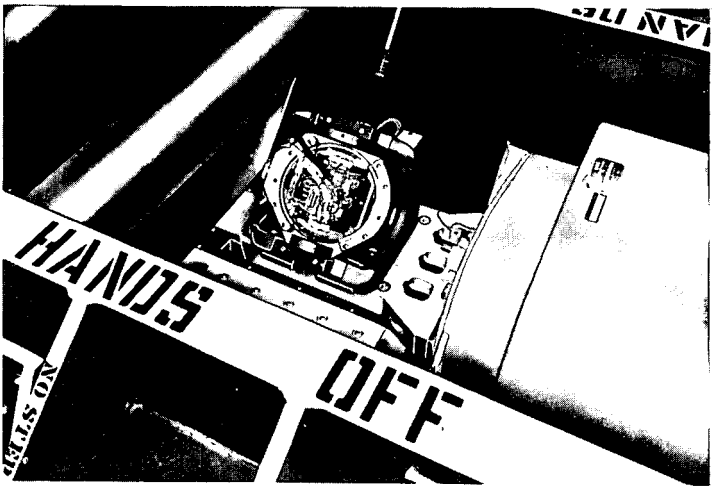

Fig. 4-47 Gyro unit on vibration test

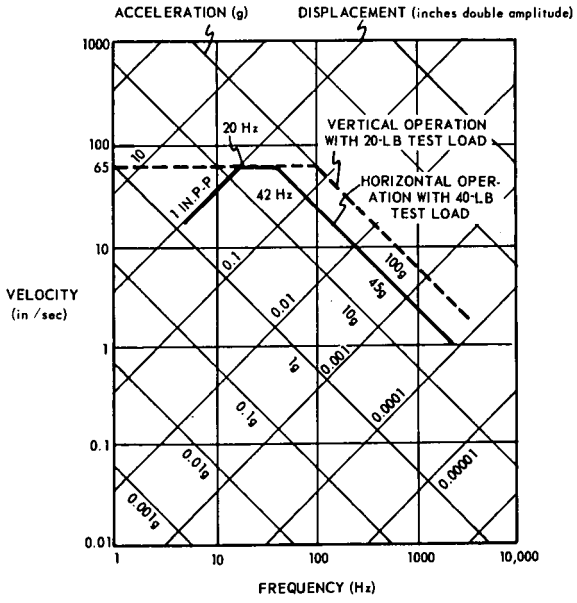

Fig. 4-48 Vibration-test-station performance nomograph

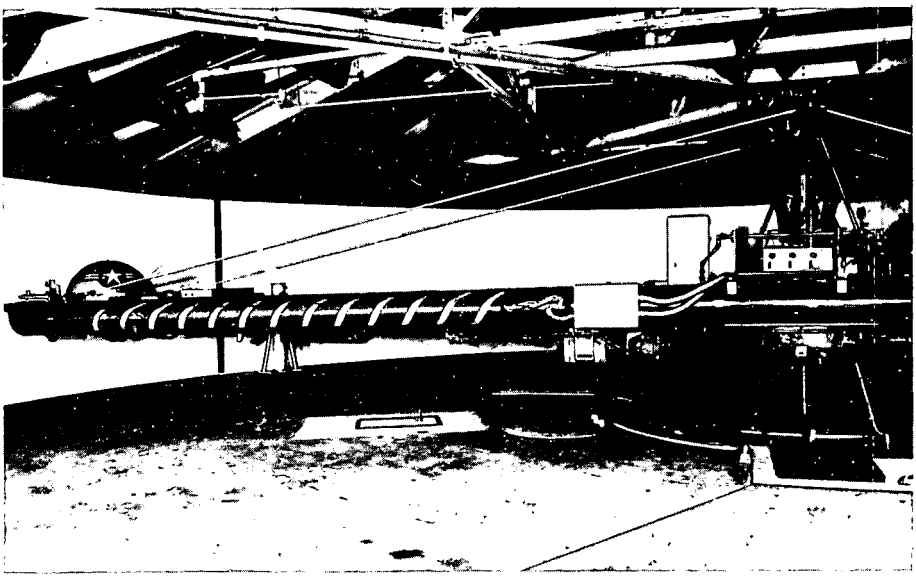

Fig. 4-49 MIT (U.S. Air Force) 980-cm-arm centrifuge

between the two sets of bellows, two independent-pressure air-supply systems are available. The main air-supply system comprises an air compressor, pressure regulators, fittings and air lines. To back up the main system in case of failure during a test, an auxiliary system composed of pressure tanks and regulators is connected in parallel with the main system. Check valves prevent reverse air flow into the compressor and thus direct the flow directly to the air bellows for proper regulation of supply pressure.

Environmental-temperature variations contribute to uneven air pressures due to density variations of the air in the bellows. This fact necessitates precise temperature control in the test area. In addition, dimensional stability of the entire system structure is gained through proper temperature control.

The slip table is designed to operate with minimum friction while being driven by the vibrator. This efficiency of operation is gained by use of a hydraulic system in conjunction with the slip table, i.e. the slip table rides on two low-friction hydraulic tracks. Their primary purpose is to restrict the table motion to the thrust axis only, in addition to providing a low-friction bearing surface for the table.

Checkout of the electrodynamic vibration system was accomplished through the use of autocollimators and mirrors to check the alignment about three axes (pitch, roll and yaw) while the system was in operation. Frequency levels and angular motions of the base were detected by monitoring the outputs of velocity transducers and crystal accelerometers positioned at several locations. In addition, transverse motion of the base was checked with respect to the table thrust axis.

The system was found to be, according to specifications, subject to a displacement limit of 1.0 inch peak-to-peak and a velocity limit of 65 inches/second. Cross-axis vibration was measured with accelerometers mounted transverse to the table thrust axis and is guaranteed to be less than 10 percent for the operating range of 20 to 1500 Hz, exceeding 10 percent in no more than two narrow frequency bands in the range of 1500 to 2000 Hz.

The total harmonic distortion is less than 5 percent from 20 to 2000 Hz, with the exception of the second and third submultiple of the axial resonance which did not exceed 20 percent. Distortion was measured with a commercial distortion analyzer.

Acceleration of the base for vertical operation of the vibrator is guaranteed to be less than 3 percent to 25 Hz and less than 0.5 percent above 25 Hz. Accelerometers, mounted on the seismic base, were used for this checkout.

As previously noted, the vibrator is capable of operating over a large range of frequencies (5 to 3000 Hz). The system geometry limits the physical size of the attached slip table to $13\frac{1}{4}$ inch diameter. A table-mounted test specimen (gyro and fixture) weighing approximately 40 lb reduces the acceleration output capability of the system. However, the system is capable of delivering a constant force output of 8000 lb. With this output force level, a 40-lb test specimen (combined with the 138-lb effective weight of the slip table and shaker armature) would be subjected to a 45-g acceleration loading. The performance characteristics are summarised in the nomograph of figure 4-48.

Since future vibration test programs may impose demands on the gyro and its positioning fixture to withstand acceleration inputs up to 100 g's, a mechanical modification has been proposed to upgrade the vibrator and slip table to that level.

After investigating a variety of possible schemes, the one finally chosen that seemed to be the most practical from the standpoint of fabrication, cost and dependability was a resonant structure mounted in series with the slip table. The resonant structure consists basically of two cantilever beams anchored to the vibrator's seismic walls and to the slip table. The spring effect of cantilever beams imparts a multiplying effect to the previously available maximum acceleration at a particular narrow range of operating frequencies (approximately 75 Hz).

The main objectives in the design of the structure are keeping the repeated stress level well below the endurance limit of the structural material, ease of fabrication and simplicity of installation and operation.

Centrifuge

The precision centrifuge offers the only means, on Earth, for applying a steady-state acceleration of 10 to 100 g's for indefinitely long periods. The principal interference to testing that must be accepted is the angular velocity of 10 rad/sec that even the largest centrifuges require to achieve 100 g's. This interference is particularly troublesome for gyroscopic instruments that generate torques proportional to input angular velocities. For gyros, this problem is so great that steps have to be taken to minimize even secondary interferences; that is, the gyro wheel is either stopped completely or is rotated at very low speed, or the gyro is mounted on a counter-rotating platform.

The principal requirements of a centrifuge for gyro testing are that its velocity, $W_{(c\,f)}$, remain stably vertical at all times, that its arm test platform be maintained at a fixed angular orientation with respect to $W_{(c\,f)}$, and that the arm be as long as possible (consistent with the second requirement). These requirements have been met at the Instrumentation Laboratory by means of the 980-cm-arm centrifuge shown in figure 4-49, which is capable of producing 100 g's.

In order to assure long-term vertical stability of the centrifuge-angular-velocity vector, the centrifuge rests on a stable foundation produced by driving steel pilings to bedrock and then pouring a heavy concrete mat on top. The bearing system of the spindle makes use of the natural centering action of a large tapered roller (apex down), which carries practically all of the vertical load, and a second tapered roller approximately 1.5 meters below, which is preloaded and stabilizes against any lateral unbalance forces. The spindle may be adjusted to the vertical and requires readjustment after several months running. The arm speed is controlled by variations in the flow rate to a hydraulic-power drive system for the spindle in response to the error between the called-for speed and the instantaneous tachometer-measured speed.

The natural tendency of the arm to uncurl its cantilever droop as speed increases would produce unwanted changes in the test-platform angular orientation. This effect is therefore compensated by countermoments adjusted with lead weights located on top of the steel table that is visible in figure 4-49 near the end of the arm. An optical system is used to observe changes in the test-orientation platform angle due to elevation or depression of the arm while centrifuging.

Angular Vibrator

The MIT precision angular vibrator is a two-gimbal device capable of producing

sinusoidal angular oscillations simultaneously about two orthogonal axes– figure 4-50 (13). When vibration is required about only one axis, the other gimbal may be locked in position. The gyro unit to be tested is mounted in the inner gimbal, which is pivoted in the outer gimbal. Different mounting plates afford selection of gyro orientation with respect to the vibrator axis. The vibrator outer-gimbal axis is permanently aligned east-west; thus it is perpendicular to the earth's rotational axis. The average position of the inner-axis is aligned north-south parallel to the earth's rotational axis. Microsyn signal generators are mounted on the gimbal axes of rotation to provide continuous monitoring of the amplitude and phase of the vibration inputs.

Drive blocks, riding on eccentric cams, generate sinusoidal angular oscillations of their respective gimbals. A pictorial representation of the drive shaft may be seen in the enlarged diagram at the bottom of figure 4-50. The phase adjustment between the oscillations of the two gimbals also may be seen in that diagram. Phase adjustment is accomplished by releasing the phase-locking clamp, turning the adjustment shaft to the desired phase difference, and relocking the clamp by tightening six bolts. The gimbal-vibration amplitudes may be varied by turning the amplitude-adjustment shaft by a method similar to that used to vary phase. Turning this shaft causes the drive-block eccentric to shift position with respect to the shaft eccentric.

The vibrator is designed to apply angular vibrations to the instrument under test in three ways:

(a) input from outer gimbal with the inner-gimbal amplitude set at zero

(b) input from inner gimbal with the outer gimbal locked in place

(c) input to both inner and outer gimbals.

These capabilities may be used to provide an input to any single defined gyro axis or to any combination of two axes. In addition, input to three axes is possible; for example, by mounting the gyro output axis along one of the vibrator's axes and by rotating the gyro in its support plate so that both the spin and the input axes will receive a portion of the gimbal-axes oscillation.

The angular vibrator has the following specifications:

(a) the inner-gimbal amplitude can be set from 0 to 2.5 milliradians.

(b) the outer-gimbal amplitude can be set from 0 to 5 milliradians.

(c) the frequency range is from 10 to 30 Hz using a small pulley of the drive and from 30 to 115 Hz using a larger pulley.

(d) the phase between the oscillations of the two axes is variable from 0 to ± 180 degrees.

Fixtures

Whenever a gyro and its holding fixture are anchored to a vibrator or a centrifuge, the structural characteristics of the fixture must be taken into account. In the ideal case, the fixture should behave as a rigid body throughout the frequency spectrum of the input and add or subtract nothing from the vibration or sustained acceleration. If the fixture is dynamically incompetent, however, resonances will appear and produce undesirable angular or linear motions about

and along each of the fixture axes. To prevent the desired input from becoming contaminated with these spurious inputs is a difficult task that becomes more critical as fixture size and complexity increase.

The gyro-holding fixture may take on various basic geometrical shapes for a particular application. However, the important design considerations include structural rigidity, light weight, and accessibility in terms of permitting the gyro to be monitored during the test. The use of basic fixture geometry aids in the dynamic analysis as part of an on-the-board fixture design effort. In other words, natural frequencies and mode shapes can be more accurately determined if basic design geometrics are assumed.

Unfortunately, the holding fixture usually must be rather complex in construction in order that meaningful test data may be obtained from the gyro. In other words, the fixture probably will be neither symmetric in geometry nor constructed as a one-piece member. In fact, since the gyro must be tested in various orientations with respect to gravity and the earth's polar axis, a two-or three-gimbaled fixture may be required. Figures 4-51 and 4-52 are photographs of a gyro centrifuge and a gyro vibration fixture, respectively.

Fixture complexity cannot be neglected in an error analysis since the fixture is essentially an elastic member subject to vibrational stresses, strains and deflections. If the test fixture were indeed symmetric in geometry, then an error analysis could be greatly simplified since basic beam theory could be applied. Even though this is not possible in the real world of complex test fixtures, some basic assumptions must be made if meaningful test results are to be achieved.

Fixture error analysis can start with the premise that basically the fixture and gyro package are an oscillating cantilever beam. The desired results of the analysis are vibration amplitudes, natural frequencies, and mode shapes. The analysis must be simplified because of complexities such as density or mass distribution due to geometry variations of the fixture structure. If the deflection of the beam is y,

$$\frac{dy}{dx} = \text{slope}$$

$$\frac{d^2y}{dx^2} = M = \text{bending moment}$$

$$\frac{d^3y}{dx^3} = V = \text{shear} \qquad \text{(Eq. 4-25)}$$

where the boundary conditions are (figure 4-53)

$x = 0$:	$x = \ell$:
$y = y_o \sin \omega t$	$\frac{d^2y}{dx^2} = 0$
$\frac{dy}{dx} = 0$	$\frac{d^3y}{dx^3} = 0$

(Eq. 4-26)

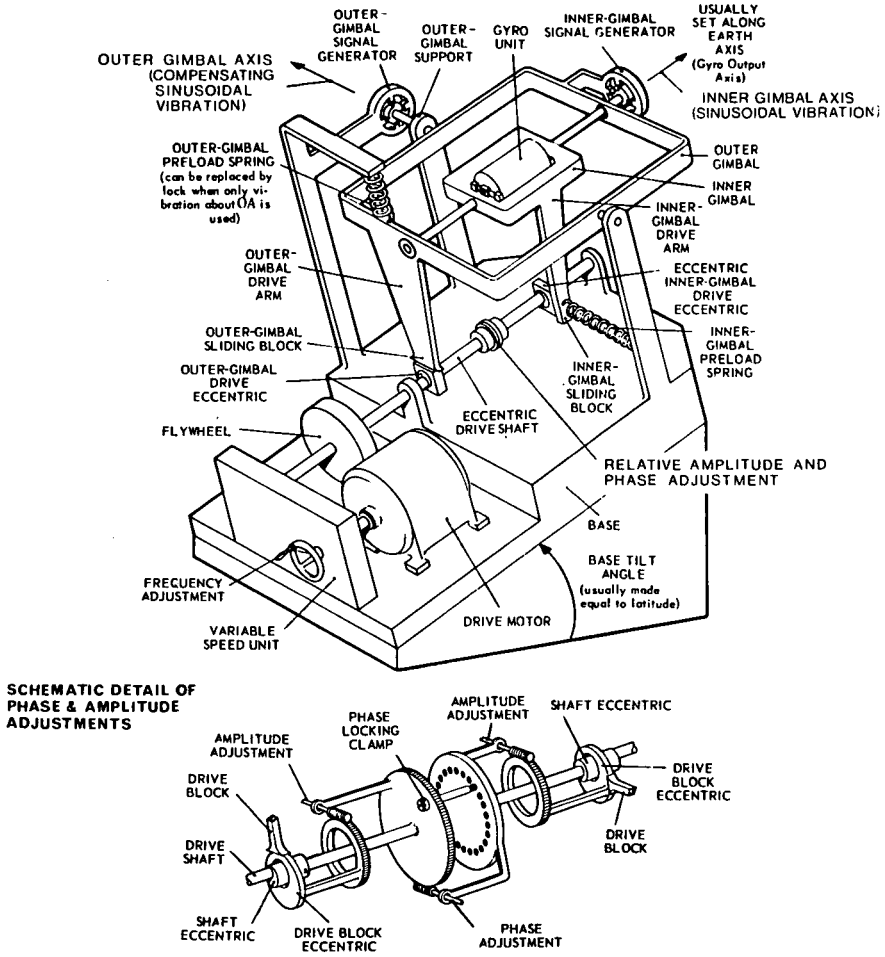

Fig. 4-50 Pictorial schematic diagram of precision-angular-vibration test table

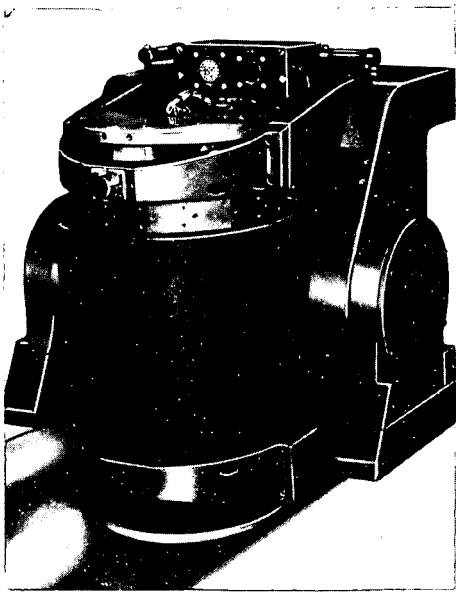

COMPLETELY ASSEMBLED FIXTURE WITH MAGNETIC SHIELDING IN PLACE

MAGNETIC SHIELDING REMOVED AND ACCESS PORT OPEN TO SHOW GYRO PROXIMITY PACKAGE

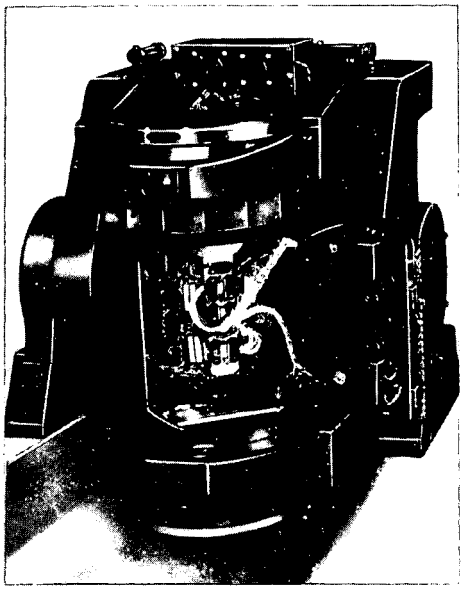

Fig. 4-51 Gyro centifruge fixture

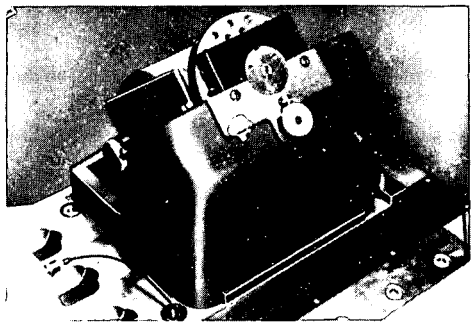

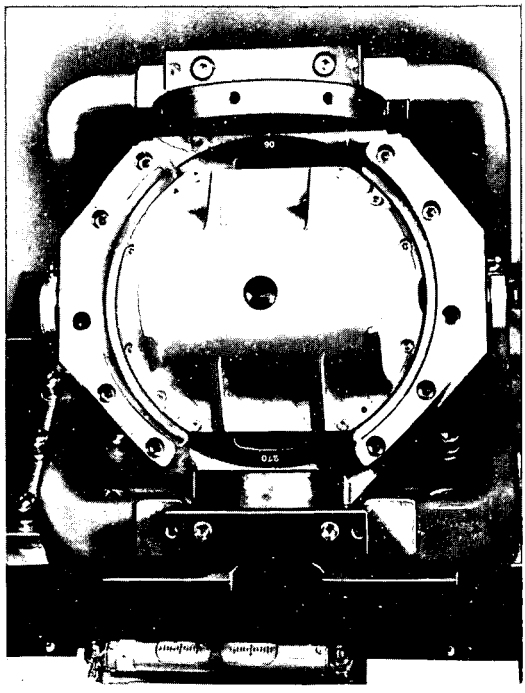

Fig. 4-52 Gyro vibration fixture

These are, of course, crude assumptions since it may not be possible to accurately determine the mass distribution throughout the fixture assembly. Also, if a large contribution of mass density is concentrated near the free end of the beam (or fixture), then the assumption can be made that

$$\frac{d^3y}{dx^3} = m_e \frac{d^2y}{dx^2} \qquad \text{(Eq. 4-27)}$$

at x = 0. Values for mode shapes and frequencies can be determined if the above boundary conditions are substituted into the general relation for beam analysis

$$y = A \sin mx + B \cos mx + C \sin hmx + D \cos hmx \qquad \text{(Eq. 4-28)}$$

where the constants are determined from the known end conditions of the beam. The process involves the reduction of a determinant to obtain the desired results.

The requirement for a good test fixture is maximum stiffness for the lightest possible weight. This seems reasonable since maximum stiffness permits testing over a larger range of frequencies and amplitudes than would otherwise be the case. A light-weight fixture permits testing at higher acceleration levels for a given force input since the effective driven mass of the test fixture and gyro package is smaller. However, a trade-off must usually be made in the area of stiffness versus weight.

If resonant levels do occur during testing, then relatively large amplitudes of fixture displacement are possible. Since purely analytical calculations are difficult in determining resonant frequencies and amplitudes for the test fixture, experimental means must be adopted if what actually happens under various test conditions is to be investigated. A method commonly used is to monitor the output of accelerometers mounted at various points on the test fixture and on a dummy gyro mounted in the test fixture to simulate an actual test situation. This is a simple but nevertheless effective method of determining test-fixture capabilities over various frequency and amplitude ranges.

Evaluation of the data from the accelerometers can be used as a basis for a more efficient fixture design. From this reasoning, it can be concluded that a gyro test fixture is designed to function over a specified range of amplitude and frequency levels only. Input levels outside this range will cause unwanted inputs to the gyro because of excessive fixture movement and distortion.

In order to facilitate the task of predicting the test fixture's dynamic behavior by using classical theory, it is necessary to design and fabricate the simplest, yet fully functional, fixture structure possible. In this way, dependable results can be obtained from a classical-theory approach. Actual testing will result, of course, in useful information about fixture behavior from accelerometers mounted on the fixture. An accurate prediction by classical means, however, will save much time in preventing the fabrication of useless fixtures. If means are available to construct a mathematical model of the fixture, then this approach should yield an even more complete analysis of the fixture characteristics and general behavior.

Electronics

The electronics required for gyro excitations and monitoring and for the rate-feedback loop are basically the same for environment-simulation test stations as for one-g test stations. The servo-turntable loop and optical pickoff electronics are usually not required because environment-simulation tests are generally conducted in the rate-feedback mode. In addition, the long-term-stability requirements of the electronics may be somewhat less stringent for the

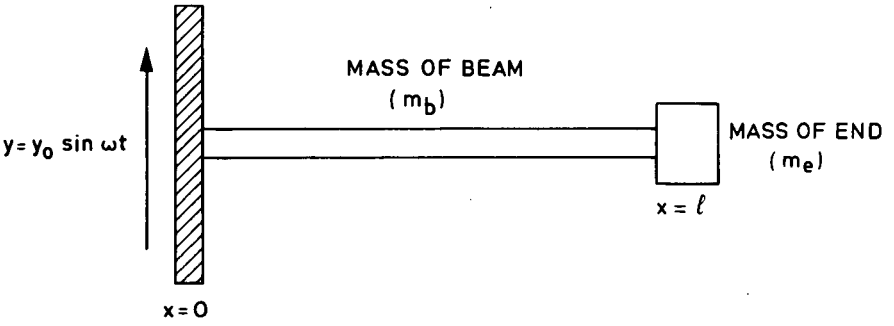

Fig. 4-53 Simply supported cantilever beam

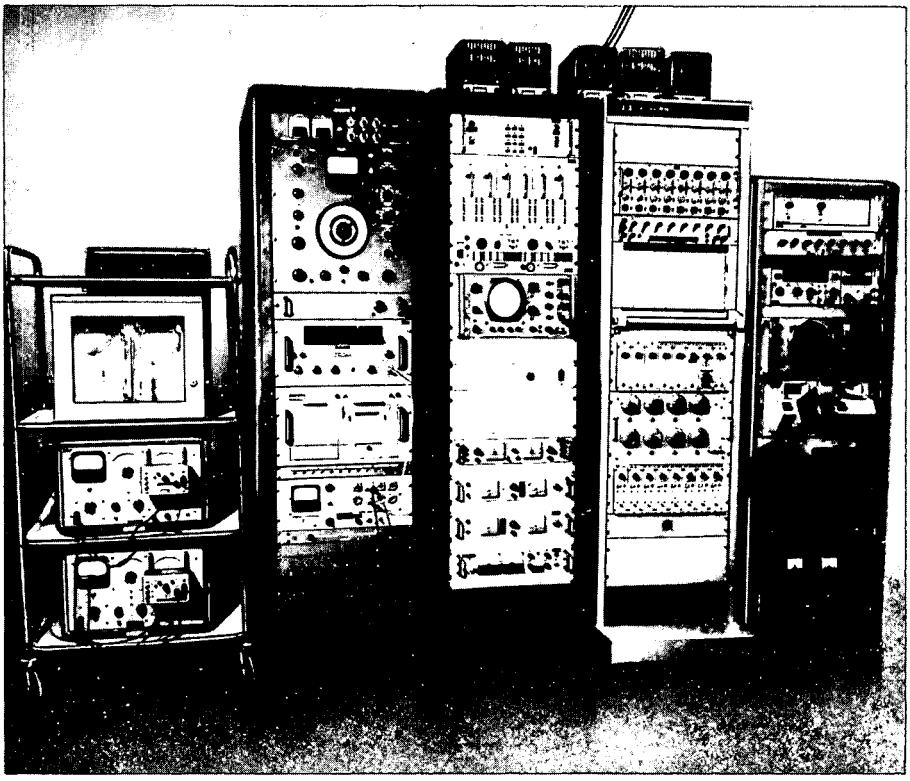

Fig. 4-54 Vibration test electronics

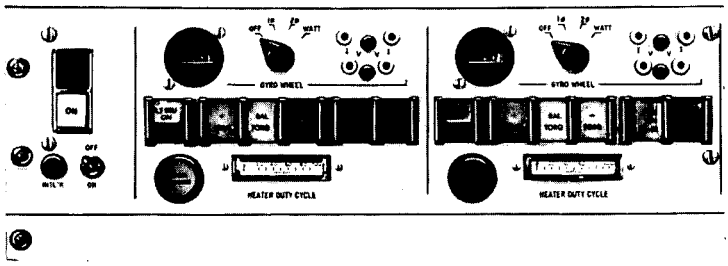

Fig. 4-55 Gyro control unit

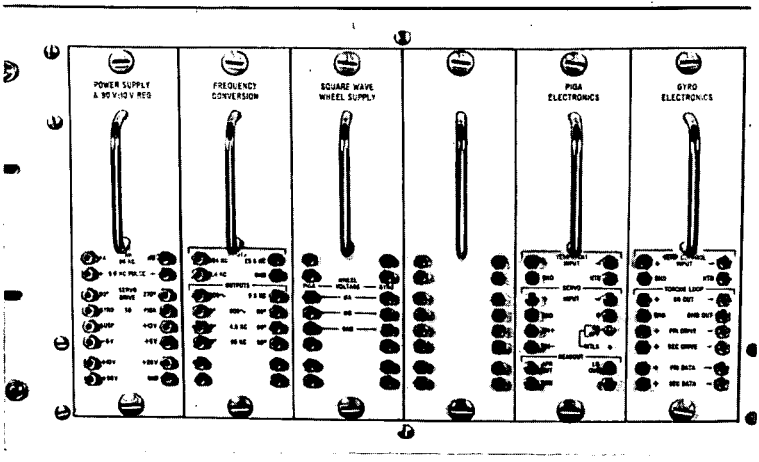

Fig. 4-56 Gyro electronics unit

environment-simulation test station because of the shorter duration of the tests.

Figure 4-54 shows the electronics consoles of the electrodynamic vibrator-slip table test station, which can be considered a typical example of the electronics required for an environment-simulation station. Looking at the racks in that photograph from left to right, only rack number 2 is unique to the vibration test station; the other four contain the various gyro-excitation, monitoring, control-loop, and data-acquisition equipment. Very briefly, the functions of the various racks are:

Rack No.	Function
1	Wave analyzers and recorders for gyro wheel and bearing-retainer noise.
2	Vibrator control console, which includes controls for operating the vibrator and monitoring electronics for vibrator operation, i.e. accelerometer outputs, etc.
3	D.c. and a.c. gyro-excitation sources and gyro-control electronics, which include rate-feedback loop, gyro temperature controller and mode-selection panel.
4	Eight-channel strip-chart recorder for recording test data in analog form.
5	Digital data-acquisition equipment for recording test data in digital form on punched tape.

Figures 4-55 and 4-56 are close-up views of two of the panels in rack number 3. Figure 4-55 shows the mode-selection panel, or gyro-control unit, which controls all gyro system functions. The left-hand section of the panel controls the application of power to the gyro electronics unit shown in figure 4-56. The two right-hand sections of the panel each control one gyro and contain rate-feedback loop controls, wheel-excitation mode selector, and a gyro-heater duty-cycle monitor. The gyro electronics unit shown in figure 4-56 contains d.c. power supplies, a frequency-conversion unit, a square-wave gyro-wheel supply, and PIGA and gyro rate-feedback loops.

As noted in section 2, it is desirable that some of the electronics be physically as close to the gyro on test as possible. The high-g equivalents of the table-top electronics units described in that section are the gyro proximity packages which are mounted in the vibration and centrifuge fixtures (Figs. 4-51 and 4-57). These proximity packages contain five modules:

(a) signal-generator preamplifier

(b) temperature-controller preamplifier

(c) gyro magnetic-suspension external circuitry

(d) torque-generator drive circuitry

(e) gyro caging circuitry.

5. Error Sources

The basic standards of reference against which gyro performance is measured are earth's rate, gravity, and sidereal time. Obviously, error and uncertainty in the values of these standards will mask the true performance of the gyro on test, but two other sources of error are of more significance to the instrumentation designer. These are errors and uncertainty generated by the instrumentation and those generated by the environment.

Since the inertial gyro is basically a precisely balanced electromechanical device, anything that upsets its balance or that generates a spurious angular rate will tend to obliterate the desired gyro-performance data. For example, the gyro will respond to angular rates generated by misalignment or platform tilt, to angular and linear vibration, to electrical-excitation changes, and to changes in its thermal or electromagnetic environment.

After briefly discussing the accuracy of the standards of reference, this section describes mechanical and electrical sources of error and uncertainty generated by the test instrumentation and techniques for their minimization. Error and uncertainty resulting from the environment are discussed in section 6.

Basic Standards

The only rate on earth constant enough to be used as a standard against which to measure gyro performance is the rate of the earth's daily rotation. The earth makes one revolution per day consistent to one part in 30×10^6 (14). While this accuracy is sufficient for testing today's gyros, it has been shown that if gyro performance approaches a level of 10^{-6} degrees per hour (0.000067 meru), fluctuations in the earth's spin rate must be taken into account (14).

A new absolute determination of the specific force of gravity has been made by the U.S. National Bureau of Standards, which indicates a value of g equal to 9.801018 m/s^2 with a standard deviation of 0.3×10^{-5} m/s^2 or 0.3 milligal (15). This standard deviation is approximately 0.3 ppm of the value of g. Reference 15 also states that the difference in the values of g at two locations can be measured more accurately (to $\pm$ 0.01 milligal in the best determinations) than the absolute values themselves.

Various manufacturers of frequency-counting time recorders are now specifying accuracy on the order of one part in 10^9 for a period of twenty-four hours and three parts in 10^7 for a period of seven days. Thus, inaccuracy in the basic standards of reference is not a significant source of error for the test-instrumentation designer today.

Mechanical-Instrumentation Error Sources

The basic concept of gyro testing with earth's rate and gravity as standards of reference requires that the gyro be accurately oriented with respect to the earth's polar axis and the local gravity vector. Any misalignment will result in erroneous test results.

The gyro is directly affected by misalignment anywhere in the set of building blocks making up the test-station complex: the table mounting surface, the table, the gyro holding fixture, or any parts related to this set. Misalignment can result from seismic or cultural disturbances that cause floor motion (see section 6). Long-term angular motion may be the result of machining stresses in the gyro test table or mounting fixture, or in overloading in excess of original

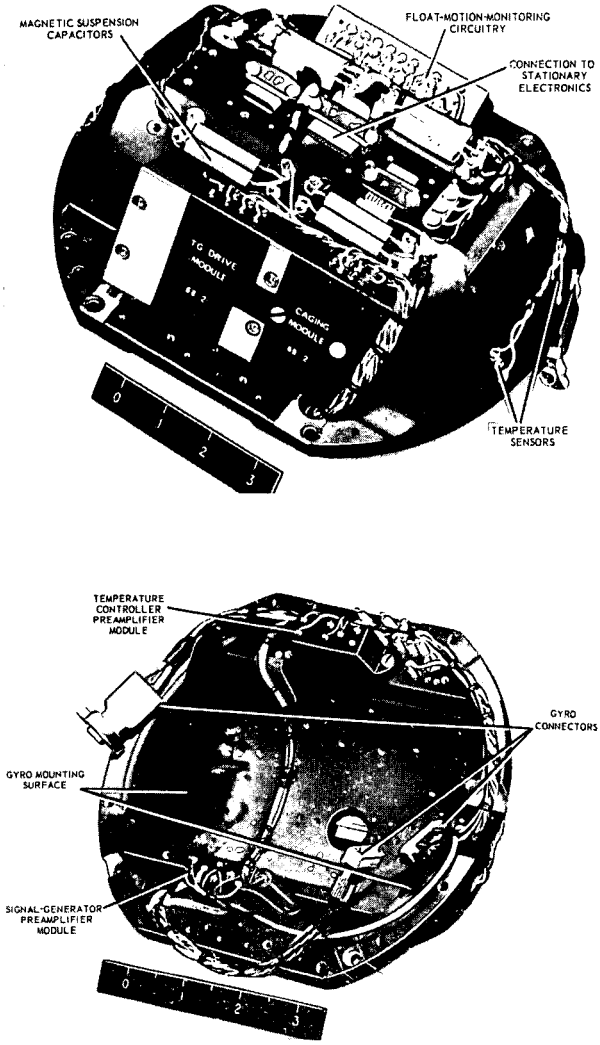

Fig. 4-57 Gyro proximity package

design loads. In addition, excessively high stresses in clamping or locking devices used to accurately position test equipment can produce plastic deformation over an extended period of time, thereby causing changes in azimuth or level of the test station.

Early testing procedures proved that the gyro was more capable of defining alignment of its input axis with the appropriate table axis by electrical means rather than by any other means. This was, and for that matter still is, accomplished by 'yozzling' the test table, which consists of oscillating the test table, and therefore the fixture and gyro, about the trunnion axis of the table. The error angle that the gyro input axis forms with the plane perpendicular to the trunnion axis introduces a component of the yozzling rate to the gyro through its input axis. Since the signal-generator output is proportional to the total angle accumulated about the trunnion axis, the gyro is considered aligned in the fixture with respect to the trunnion axis when the signal-generator signal is minimized by successive adjustments of the gyro orientation. This technique of aligning the gyro to the test-table axis requires that the test fixture be aligned within specific tolerances with the test table so that as the gyro is reoriented on the test table by manipulation of the test fixture, the alignment accuracy is maintained between the gyro and the test-table axis. The orientation of the test-table axis is also required to be within certain limits with respect to the earth's rotational axis and the local gravity vector.

The precision required for alignment of the various parts in the test-station complex is directly related to the type of test to be performed and the level of accuracy desired. For instance, a rate-feedback test, which is the test generally used for measurement of the error coefficients of the single-degree-of-freedom gyro, requires that the gyro input axis be accurately aligned perpendicular to both the test-table axis and the earth's axis so that the gyro is insensitive to the table rate and to the earth's rate. Even assuming that the gyro were aligned perfectly with respect to the test-table axis so that the gyro is insensitive to the table rate, misalignment of the table axis with respect to the earth's axis will introduce an error of approximately 0.3 meru per minute of arc misalignment (16).

In an effort to assign a value of error directly attributable to mechanical sources, it will be assumed that the gyro is aligned in the rate-feedback mode with its input axis perpendicular to both the table axis and the earth's axis. It should be understood that the gyro can, at times, be in a more disadvantageous position with respect to table motion or to the tolerance build-up of the component parts of the table. Various mechanical error sources and the value attributed to each are discussed in the following paragraphs, using the current Model E test station as an example.

Gyro End Mounts. A possible source of error contribution is the gyro end mounts. This condition can result from improper mating with the fixture mounting surface and/or the gyro end bosses on which they are clamped. Possible sources of alignment error which must be checked include the following areas:

(a) surface tolerances at interface between clamp and fixture

(b) surface finish at interface between clamp and fixture

(c) thermal coefficient of expansion

(d) hole clearances of attaching and mounting screws

(e) deflection due to gyro weight in test orientations

(f) stress induced by clamping

These precautionary measures will reduce the possibility of mounting misalignments associated with the gyro and mounting fixture.

Current machining limitations are such that a maximum misalignment of two seconds of arc (0.01 meru) could be introduced as a function of misalignment of the gyro with earth's axis because of the mating of the gyro with the end mounts and the end mounts with the test-fixture surface.

Two-Axis Test Fixture. Since the first connected member to the gyro unit is the test fixture, it can be suspected as contributing possible errors due to motion about the gyro input axis. The various orientations of the gyro as dictated by the test program can be easily accomplished with use of such a test fixture. Accurate alignment of the three gyro axes with respect to the local gravity vector and earth's rotational axis for any particular test orientation depends, of course, on the accuracy of the fixture itself. This includes gimbal errors, indexing errors, etc., which, if not properly controlled, can lead to the eventual misalignment of the gyro axis from its desired position for a specified test. The misalignment error in milliradians manifests itself in meru output error. Thus it can be seen that accurate positioning of the unit is mandatory for monitoring gyro performance and can only be accomplished with a highly accurate fixture device. A check of fixture quality can be made with the use of mirrors and autocollimators, while the fixture gimbals are being repositioned and indexed for the required gimbal test orientations.

The following parameters must be carefully checked for possible sources of error:

(a) surface tolerances at clamp interface

(b) parallelism of clamp mounting sources

(c) condition of mounting surface (roughness, etc.)

(d) thermal-expansion effects

(e) orthogonality of fixture axis

(f) positioning or indexing accuracies on table

(g) surface condition of base mounting surface

(h) deflection due to weight shifts and vibrations

(i) stress induced by clamping

A maximum tolerance build-up of five seconds of arc is possible in the gyro fixture. This would be the equivalent of 0.025-meru error introduced to the gyro in the rate-feedback mode.

Test Turntable. The test turntable can be broken down to the table top and its supporting structure which includes bearings, base ring, rotary table, trunnion axis, etc. It is difficult to determine accurately the relative movement between these table members because of bearing wobble, shaft runout, etc. However, with the use of appropriate test equipment, the accuracy of the table specifications can be checked.

Table Top - the mounting surfaces of both the table top and the test fixture must be accurately machined so that a pure interface condition is obtained. Clamping of the fixture to the table surface should receive careful attention since uneven bolt torques can lead to uneven fixture internal stresses which result in distortion or deflection of the fixture; required bolt torquing should be adjusted with precision torque wrenches. Machine finish on the table top can exhibit a one-second-of-arc error in perpendicularity to the turntable-shaft axis: this could introduce as much as 0.005- meru error to the gyro under appropriate conditions. The following items should be carefully checked as possible error sources:

(a) condition of mounting surface

(b) material thermal properties

i temperature gradients

ii thermal capacity

iii coefficient of expansion

(c) stress levels of surface

(d) symmetry about table axis

i mass unbalance

ii geometric unbalance

iii moment of inertia

Yoke Motion - any nonuniform expansion or contraction of the yoke arms will show up as a motion in the tilt axis, shaft axis, and table-top level. Temperature recordings on a typical table have shown a 2°F differential change. This is probably caused by the fact that oil is fed through one arm of the yoke and not the other. Approximate calculations indicate that for 1°F difference in yoke arms, a one-second-of-arc (0.005-meru) movement is translated to each of the above-mentioned axes.

Main Support Bearing - with a dimensional tolerance for roundness of the radial bearings and flatness of the thrust bearings of 25×10^{-6} inches total indicated runout, a shaft wobble of 0.4 second of arc (0.002 meru) is possible.

Table Trunnion Axis - the trunnion assembly is supported by air bearings at the end of each arm and is held in position by brake shoes at each bearing. The error attributable to the trunnion assembly (azimuth error) has a value of one second of arc (0.005 meru). The condition and performance of the bearings must be carefully checked for:

(a) runout

(b) axial movement

(c) axial alignment

(d) frictional torque level

Rotary Base - the rotary base, bolted to the stationary base on each of four corners, permits adjustment of the turntable yoke about the vertical with an accuracy of three seconds of arc (0.012 meru). Current alignment procedures permit alignment to local vertical to two seconds of arc (0.010 meru).

Stationary Base - the stationary base has a coefficient of linear expansion of 12×10^{-6} inches per degree F. The height of the base is $8\frac{1}{4}$ inches or 0.001 inch per degree F. Since 0.001 inch is one second of arc in 20 inches, a one degree F temperature gradient from one side of the base to the other will subject the entire table to a one second of arc tilt (0.005 meru). Current alignment procedures permit alignment to local vertical to two seconds of arc (0.010 meru).

Azimuth Positioning. Azimuth table alignment is usually made from references previously established. These references, which probably are not established to better than five seconds of arc (0.02 meru), determine the alignment. Ideally, the astro-azimuth technique which uses direct star observations can reduce this misalignment to within 0.2 second of arc (0.001 meru).

Summary. Table 4-2 summarizes the possible mechanical-instrumentation error sources. It is difficult to predict the cumulative effect of the errors since any attempt to algebraically sum these errors could result in an extreme error, or coincidental cancellation could produce no observable error.

Table 4-2 Mechanical-instrumentation error sources

Error Source	Maximum misalignment (second of arc)	Equivalent error (meru)
Gyro end mounts	2	0.01
Two-axis test fixture	5	0.025
Test turntable		
Table top	1	0.005
Yoke	1	0.005
Main support bearing	0.4	0.002
Trunnion assembly	1	0.004
Rotary base	5	0.02
Stationary base	3	0.015
Azimuth positioning	5	0.02

Electronic-Instrumentation Error Sources

The required performance characteristics of the test instrumentation utilized in testing gyros are directly dependent on the calibre of the instrument being tested and the desired accuracy and resolution of the performance data.

As mentioned previously, gyro testing is accomplished at MIT by determining a set of torque coefficients for the gyro error model. These coefficients describe the response of the instrument, in terms of torque about the output axis, to influences other than angular rate about the input axis. In other words, they are error torque coefficients. Variations in these coefficients caused by factors external to the gyro appear as uncertainty in the gyro performance data. In addition, the accuracy to which the performance data is known is dependent on the data acquisition technique and the capability of the monitoring or measuring equipment. The following paragraphs describe the major sources of performance error and data-acquisition error that may be attributed to the electronic instrumentation

Performance-Error Sources. The most significant equipment-induced contributions to error torque about the gyro output axis are variations in reaction torque and mass-unbalance torque. Reaction torque is a characteristic of the electromagnetic elements, i.e. the ducosyns which comprise the signal-generator, torque-generator, and magnetic-suspension components of the gyro. Variation in mass-unbalance torque is caused by displacement of the center of mass of the gyro float and is commonly the result of changes in the gyro temperature. (Mass-unbalance variations may also be due to other influences). The manner in which the electronic instrumentation is related to these errors is discussed in the following paragraphs as reaction torque, wheel-power sensitivity, and temperature sensitivity.

Reaction Torque - reaction torque is a magnetic effect caused by lack of symmetry in the flux distribution between separate pole pieces in the microsyn. This dissymmetry is caused by machining imperfections in the manufacturing process and the inability to wind identically equally effective ampere turns on each pole. Since magnemotive force or flux density in the magnetic circuit is proportional to current in the microsyn windings, reaction torque is dependent on excitation current and, in fact, is directly proportional to the square of the excitation current. Reaction torque is a property of the microsyn and hence cannot be an error attributable to the test equipment. However, changes in the microsyn-excitation current caused by variations of the excitation source will result in reaction-torque variations and thereby contribute uncertainty in the performance data. To reduce this uncertainty to acceptable levels, the output stability of the microsyn-excitation source must be very closely controlled. Since the signal-generator, torque-generator and magnetic-suspension elements are electromagnetic microsyns, all three can contribute to the total reaction torque.

Wheel-Power Sensitivity - the gyro wheel is driven by a two-phase hysteresis motor excited by a precision voltage source. Variations in the voltage-excitation level to the motor cause corresponding variations in the magnitude of the phase currents, thereby maintaining the constant total developed torque required to keep the wheel in synchronism. Since the motor windings possess resistance, incremental changes in the phase currents result in small variations in the total power dissipated within the motor structure in the form of heat or I^2R loss. The resulting expansion or contraction of the motor component parts may result in a shift in the location of the center of mass of the float and thereby contribute uncertainty to the determination of mass-unbalance torque. This effect is termed wheel-power sensitivity and is expressed in meru/watt, meru/volt or meru/amp. As was the case with reaction torque, the effect of wheel-power sensitivity is minimized by strictly controlling the output characteristics of the gyro-wheel-excitation source.

Temperature Sensitivity - the gyro float is buoyant in the flotation fluid at a specific temperature called the flotation temperature or unit operating temperature. Balancing of the float is a critical operation that is carried out at the unit's flotation temperature in order that mass-unbalance effects may be minimized. During operation, the temperature of the gyro is maintained as closely as possible to the flotation temperature by a heater-sensor configuration attached to the gyro case and a precision temperature controller. Since the gyro float is dimensionally sensitive to temperature, changes in the location of the float center of mass may result from temperature variations. This effect is similar to that described under wheel-power sensitivity; however, perturbations in the unit operating temperature may arise from causes outside the gyro case as well as from within. For this reason, the gyro temperature-control hardware should isolate the unit from ambient-or environmental-

temperature excursions as well as attempt to compensate for internal disturbances. Temperature sensitivity is expressed in meru/°F and its effect is minimized by closely controlling the gyro temperature.

Equipment Considerations - minimizing the sources of uncertainty in the performance data as discussed in the previous sections requires a high degree of stability and control in the electrical excitations or inputs to the gyro undergoing tests. In the case of reaction torque or wheel-power sensitivity, the undesirable effect is maintained within acceptable limits by providing excitation sources having exceptionally stable output-voltage characteristics. As stability requirements become more stringent, it is not sufficient to design or purchase a source with the required stability specification at its output terminals. Factors such as variation in connector contact resistance and slip-ring-resistance changes serve to degrade the stability of the excitation actually supplied to the gyro. Excitation sources employing a remote-sensing technique are used to overcome this problem. As the term implies, remote sensing provides for monitoring of the excitation signal at a point in close proximity to the gyro with the correction or feedback signal being returned to the source via low-current-carrying conductors. Stabilities on the order of 0.005 percent may be achieved by this method utilizing currently available commercial equipment.

Gyro-temperature-control electronics is also subject to proximity considerations. Normally, the gyro temperature is sensed by a resistance winding or sensor affixed directly to the case of the gyro. This sensor forms one leg of a precision bridge which generates the error signal for the heater circuitry. Stability of temperature control is largely dependent on the ability of this bridge circuit to accurately detect small incremental differences between set-point temperature and actual gyro temperature. In some instances, the fixed legs of the bridge are mounted directly on the gyro to take advantage of the relatively constant thermal environment and inherently short lead lengths. In other cases, the bridge is mounted nearby with suitable precautions taken to prevent excessive thermal disturbances. Whatever the configuration, error sources such as contact resistance, thermal emf's, lead resistance and temperature variations must be considered in designing and fabricating the temperature-control circuitry.

In addition to providing for control of the gyro excitations, means of monitoring the performance of the various circuits should be provided. Continuous monitoring of performance parameters such as signal-generator excitation, gyro-wheel excitation and gyro temperature not only provides information relative to equipment performance thereby assisting in reducing troubleshooting time, but also allows for correlation of anomalies in the gyro performance data with corresponding excursions in the monitored variable. In the past, high-resolution analog strip-chart recorders have been developed for this purpose. These multiple-channel recorders accept either ac or dc signals and possess zero-suppression circuitry with stability on the order of 20 ppm. Recording sensitivities of 0.01 percent of the input signal are easily achievable with these instruments.

Data-Acquisition Error Sources. As described in section 3, the two major modes of gyro evaluation at the MIT Instrumentation Laboratory are rate-feedback tests and servo-turntable tests. In the former, the performance data are a measure of gyro unbalance torque as a function of gyro position and in the latter, the performance data are deviations in turntable rate from a known reference.

Rate-Feedback Tests - with the analog rate-feedback loop, the unbalance torque is obtained by measuring the magnitude of the feedback current to the gyro torque generator. This measurement is made open loop and is dependent for accuracy

and resolution on the characteristics of the recording circuitry. Gain instabilities, phase shifts and electrical noise in the circuitry place a practical limit on torque resolution and must be considered in determining the error contribution of the test equipment. In addition, further uncertainty is injected into the data by the need for human interpretation of a strip-chart recording. Resolution capability of this configuration is on the order of 0.5 meru.

As an alternative to manually translating the unbalance-torque data to numerical form, an analog-to-digital converter is used to log the recording-circuit output directly on punched paper tape. This method also minimizes the effect of noise by averaging the data over predetermined time intervals. Significant improvement in resolution may be achieved by this method, and the data is in a form readily adaptable to computer reduction.

With the digital rate-feedback loop, the unbalance torque is obtained by accumulating the net number of discrete torque pulses of a given polarity on an electronic counter. Since total elapsed time for a data sample and the net pulse count of the data sample are the two variables required for torque calculation, either of two methods of instrumenting the readout may be used. The time interval may be predetermined and the pulse count over the time interval be the measured quantity, or the number of desired torque pulses may be preset and the elapsed time for the preset number of pulses to accumulate be measured. Instability in the clock frequency may result in lost data pulses in the first method; hence the latter readout configuration is commonly used. As the weight in meru-seconds of a specific torque pulse is dependent on the length of time over which data is gathered, torque resolution may be enhanced by expanding the data-accumulation time. Since the digital rate-feedback loop does not possess the data-acquisition errors inherent in the analog rate-feedback loop, it offers improved unbalance-torque-resolution capability.

Servo-Turntable Tests - various methods can be used to record the turntable rate during servo testing. The method employed at the MIT Instrumentation Laboratory utilizes a duplex photoelectric-scale-readout system consisting of an accurately engraved glass dial mounted concentrically with the turntable shaft and a pair of photoelectric readout devices. The engravings are sensed by the readout devices which trigger a clock. The readout devices, mounted 180 degrees apart, are so arranged that the trigger pulse to the clock is the average of both readouts. The reason for this is twofold. First, if only one readout was employed, a failure in the readout system would cause a lapse in data until the fault was remedied. This would result in an expensive and time-consuming rerun. Secondly, by averaging the readouts, most of the indicated error in table-rate caused by table-axis radial eccentricity and glass-dial concentricity with the table shaft is removed.

The glass dial is mounted on the rotating portion of the turntable so that the graduations are concentric with rotation of the turntable shaft within 3 arc seconds. The accuracy of graduation is ± 2 arc seconds. During performance runs, the primary interest is the comparison of the basic unbalance curve with the reference curve or with the previous revolution. Therefore, in this instance, the graduation accuracy does not play an important part except that the basic unbalance curve will have discontinuities if the graduation accuracy is poor. However, during short runs, such as multi-position or cogging tests, coefficients are being determined and excessive error in graduations will cause large errors in the coefficient magnitude.

Since the table drives at approximately earth's rate, it requires four minutes to travel 1 degree.

$$1°/4 \text{ min} = 3600 \widehat{\text{sec}}/4 \text{ min}$$
$$= 900 \widehat{\text{sec}}/\text{min}$$
$$\approx 1 \widehat{\text{sec}}/0.001 \text{ min}$$

At earth's rate, an error of 0.001 minute over a one-degree interval results in an error of 0.25 meru. Therefore, an error of 1 arc second in the glass dial can be indicated as an error of 0.25 meru in the unbalance coefficient.

To record the table rate for the servo mode of testing, a precise time source is required which is not normally a part of the test station. Since the table rate is a direct function of earth's rate, it is commonly measured utilizing sidereal frequency to drive a clock. A drift in the frequency source will cause errors in the indicated gyro unbalances because the clock is triggered by the photoelectric readouts. The frequency source should be at least one order of magnitude better than the performance requirements of the gyro. For example, if an accuracy of 0.3 meru (one part in 10 000 of earth's rate) is required, then the clock must have an accuracy of one part in 100 000. Therefore, the drift of the clock must be less than 0.8 second in 24 hours. For a one-degree table interval, timing accuracies necessary for corresponding error requirements are as follows:

Timing accuracy (min)	Error (meru)
0.01	2.5
0.001	0.25
0.0001	0.025

6. Environmental Considerations

Current philosophy of gyro-test-station design has been described in the previous sections along with the techniques for minimizing the errors generated by the test instrumentation itself. At this point, then, the instrumentation engineer may feel that he has devised the ultimate in a gyro test station, and perhaps he has. All he now needs is an isothermal room free of magnetic fields having an absolutely stable floor that is unaffected by earth tremors or cultural activity in which to set up the test station. Obviously such a room is unavailable today, at least on the earth, and therefore the instrumentation engineer must now direct his thinking toward subjects such as site selection and preparation and base-motion isolation. These and other environmental aspects of test-station design are covered in this section.

Site Selection and Preparation

The task of setting up an advanced inertial-test facility requires definition of the most sensitive device to be tested and, specifically, its sensitivity to as many disturbing inputs as it is possible to get data on by theoretical or empirical means. These disturbances may be constant or they may vary with some degree of predictability. If the disturbances are constant, then certain assumptions can be made and the performance of the inertial instrument can be evaluated with a certain degree of success. If the disturbances are varying, then assumptions are difficult, if not impossible, to make with regard to the effect the disturbance will have on the inertial instrument. It is for this last reason that it is necessary to perform a good investigation of the site to be used for a test facility. This does not imply that the site will be dependent on the results of the investigation alone since there may be overriding influences. It does mean, however, that the instrumentation engineer will have the basic knowledge and data available to him to define the particular disturbance problem facing him.

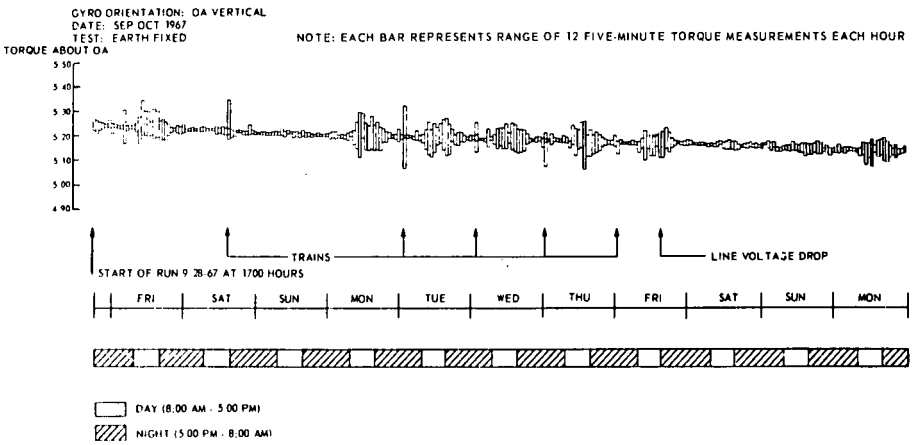

Fig. 4-58 Effect of cultural activity on gyro test data

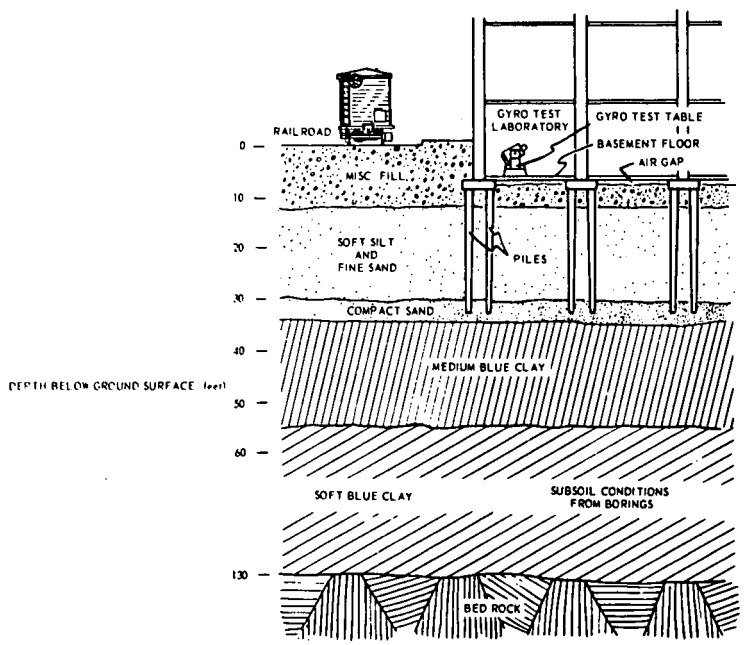

Fig. 4-59 Cross section showing soil conditions under the MIT Instrumentation Laboratory.

Once the sensitivity of the gyro to be tested has been defined, a location can be sought within the framework of the other restrictions that are bound to be imposed, namely, money, proximity to other facilities or to trained personnel, transportation availability, and all of the other economic factors governing any site selection.

Site evaluation within a given area can usually be best left to experienced seismological consultants once they have been informed of the maximum g and angular-displacement levels that can be tolerated. The reason for this is that the costly equipment and trained personnel necessary to do competent work in the field of seismology are usually not available within the inertial-component manufacturer's or R and D firm's organization. However, this is a decision which must be left to the individual setting up a test facility and which is dependent on the accuracy desired for the facility. At any rate, the precision of the investigation can be defined as ten times more precise in magnitude than the magnitude of the test information to be obtained in the next ten years. This precision and time relationship seem right to accommodate both economic considerations and the rate of advancement of technology.

Seismic activity is generally noticed by the layman only when it assumes the proportions of a large earthquake. However, the precision inertial gyro is sensitive to microseismic activity, particularly to angular disturbances in the 0.1-Hz range, although most seismic activity is predominantly translational in nature. Other natural disturbances which contribute to the microseismic disturbances and of themselves cause ground or structure angular motion are:

(a) variations in ground water level

(b) seasonal changes in soil characteristics (i.e. freezing and thawing)

(c) radiant energy from the daily transit of sunlight across a facility (this is thought to be a major contributor to the typical diurnal tilting found in most test facilities)

Cultural activity may cause translational motion and most of the tilting or angular motion sensed by a test facility. There is no standard relationship between cultural activity and quantity of angular displacement observed in any given test facility because each facility generally has unique geological and structural characteristics and, therefore, responds differently to the various typical inputs. The typical cultural inputs to a test facility include the following:

(a) personnel activity

(b) heavy machinery, including both manufacturing and utilities

(c) vehicular traffic inside or outside the facility

The combined effects of cultural activity on gyro test data are depicted dramatically in figure 4-58, which is a portion of the test data from a long-term earth-fixed test taken on a gyro test station which is mounted directly to the test-laboratory floor. Each vertical bar represents the range of twelve five-minute torque measurements made each hour. Note that the torque excursions are smallest over the weekends and at night when the cultural activity within and around the laboratory is at a minimum. The only exception to this is the large spike appearing just after midnight each weekday when a railroad train passes within about twenty feet of the test station. The fact that the torque range in general is greater in the afternoon each day than in the morning (even on weekends) may be the result of the sun heating the south wall of the test laboratory

and causing building tilt or it may be due to heavier afternoon traffic on the main highway that passes the laboratory.

Since both artificial and natural continuous disturbances are accentuated in soft ground, seismological stations are usually located in well-consolidated rock, preferably on granite or Paleozoic sediments (17). The implication here is that more consistent, repeatable phenomena can be recorded on a bedrock installation.

One gyro manufacturer in the United States, Northrop Nortronics, was able to reach a bedrock outcropping when they excavated for an addition to their facility in Massachusetts. They constructed a 16 x 16 x 10-foot concrete block weighing approximately 170 tons on the rock outcropping. The block, in turn, was surrounded by a trapezoidal retaining wall upon which a floor was constructed for personnel traffic. The concrete block has cylindrical passageways cast into it through which air maintained at a constant temperature (± 1°F) is circulated to minimize tilt caused by temperature gradients. This resulted in a reduction in typical tilt measurements from a few seconds of arc to less than 0.6 second of arc.

Another firm, LTV Aerospace Corporation in Michigan, has located an inertial-test facility in an unused portion of an operating salt mine located 1100 feet beneath the surface of the earth. The laboratory site, carved out of natural rock salt, is at least two miles removed from the main shaft and active mining operations. Noteworthy advantages of the underground location are:

(a) bedrock floor, which provides extreme resistance to seimic disturbances, very low test-pier-construction costs and no restriction on equipment size and weight

(b) constant 57 ± 1°F ambient temperature, which reduces heating and air-conditioning costs

(c) elimination of radio-frequency interference

(d) low laboratory-construction costs (if the mine is already available)

Initial measurements showed ambient vibration levels averaging from 1 to 5 micro-g's for frequencies below 20 Hz and from 10 to 30 micro-g's in the 20 to 200 Hz range. Floor stability is excellent: a 10-minute tremor recorded during initial observations moved the bedrock floor only ± 3 seconds of arc; heavy traffic within 20 feet and personnel movement within 6 feet produced no measurable disturbances (18).

One possible disadvantage of the salt-mine site is that it was necessary to use gyro compassing techniques to establish a prime meridian, which is accurate to 5 to 10 seconds of arc. Astro-azimuth techniques using direct star observations can result in accuracies within 0.2 second of arc.

Another manufacturer, Martin Company in Colorado, did just about everything that should and could be done in selecting a site for, designing and constructing a test facility. However, when their facility was complete and personnel were moved in to utilize it, it was found that personnel walking outside of the building could produce acceleration values at the test station in excess of the design goals. This was accomplished through an unfortunate tuning of the building structure. With some minor modification, they expect to achieve a 10 micro-g maximum acceleration ambient. Maximum floor tilt during a 13-day test was found to be 2.3 seconds of arc over a 24-hour period; total peak-to-peak change during the test was 3.3 seconds of arc (19).

In contrast to the examples just mentioned, all of which were located on bedrock, Honeywell Corporation's test facility is located in Florida on extremely sandy soil. They took particular care to lower the existing water table under their plant to keep the sand in a most advantageous dry condition to minimize transmissibility of cultural or seismic disturbances, even to the extent of constructing a moat around the facility. They also took care to minimize vibration internal to the structure by individually isolating any rotating or oscillating machinery.

Thus, site selection for an inertial-gyro test facility is primarily dependent on the sensitivity of the gyro to be tested and on the constraints imposed by management. Site selection and preparation is summarized in reference (19) as follows.

> 'Management should be informed that, because of the state-of-the-art limitations, it is impossible to guarantee what performance parameters can be met before the construction of critical components is complete. The difficulty in establishing reasonable funding estimates for facilities with predetermined performance criteria should be stressed.
>
> Ambient conditions should be determined before the site selection is made.
>
> The construction schedule should allow for field testing after completion of critical components and for probable remedial action.
>
> Design details should have flexibility which permits economical revisions to vary the damped natural frequencies of the structural components to avoid a resonant condition that may be produced by some unpredictable mode of vibration.
>
> All details should be carefully analyzed to reduce vibration transmission from normal building activity to the inertial test pad. The minuteness of vibrations which can cause accelerations in the micro-g range should be constantly remembered. It is essential to control load paths in order that the building components located adjacent to the inertial test pad perform as predicted.
>
> Generally, better control can be obtained by placing vibration-generating equipment on isolated foundations rather than supporting the equipment from building components that have more complex vibration modes.'

Base Motion

Each of the examples in the preceding subsection described a situation where a gyro manufacturer was setting up a complete new facility and where he had a certain amount of flexibility as to exact location within a given area. Now let us consider the situation where a high-precision test facility must be set up within an existing building, which is situated in what is perhaps a less-than-ideal location. For example, consider the Instrumentation Laboratory of MIT. It is a typical four-story brick-shell wooden New England mill-type structure, constructed about the turn of the century and used originally for the manufacture of shoe polish. It is situated between a city street and a railroad line and is less than 100 yards from a major highway. Figure 4-59 is a cross-section view of the Instrumentation Laboratory showing the ground conditions beneath the building. Some of the effects of this location have already been shown in figure 4-58.

In such a situation, and even in the case of a new specially designed and constructed facility where the ultimate in performance is desired, it is necessary to

control the environment in which the gyro is tested. Control, of course, does not always mean elimination of all troubles; but it does mean reducing unwanted inputs to acceptable levels, which for testing purposes should be at least an order of magnitude smaller than the signal level of the data being sought. For example, consider a test station that is being set up to test gyros for the next decade whose drift performance is assumed to be of the order of 0.0001 degree per hour. Even if all of the error budget is expended on angular motion of the test platform, angular motion must be less than 0.00001 degree per hour or 0.03 second of arc per hour. Since one second of arc is the angle subtended by 0.000058 inch at one foot, which is approximately equivalent to the thickness of this sheet of paper at 60 feet, the magnitude of the job necessary to stabilize the environment becomes more apparent.

Many and varied solutions have been attempted to control micro-g and tilt disturbances at a gyro test station. It is a classical observation that simultaneous isolation from both high-and low-frequency disturbances is quite difficult. One possible solution seems to be the spring mounting of a large mass for isolation from disturbing frequencies above 10 Hz and the use of a servo-controlled platform for isolation from lower frequencies.

The remainder of this subsection describes the approaches to the problem of control of base motion at MIT. MIT's solution is not pointed out as necessarily the best isolation technique because the environmental problems in each area will undoubtedly be quite different from those that were experienced at the Instrumentation Laboratory.

Effects of Base Motion. An error model equation has been developed that indicates the effects on the MIT single-degree-of-freedom floated integrating gyro of motions of the test-turntable base (20). It should be noted that this equation is applicable only to a gyro having characteristics similar to the following:

Gain ≈ 1

Characteristic time $\approx$ 1 millisecond

Lowest resonant frequency > 800 Hz

Anisoelasticity factor 1 to 1.6

Ratio of damping to critical damping ≈ 0.01

It is also assumed that cross compliances between the output and spin axes and between the output and input axes are negligible. For such a gyro the maximum possible error, E, in meru, due to turntable base motion is

$$E = 0.005\epsilon_o + 1.11e_o + 0.0035\epsilon_1^2 + 0.0035\epsilon_2^2 + 0.107\epsilon_3^2 + 5A_o^2 + 5.5A_1^2 + 7A_2^2 + 9A_3^2 + 11A_4^2 + 19.5A_5^2 + 54A_6^2 + 500A_7^2 + 850A_8^2 \quad \text{(Eq. 4-29)}$$

where

ϵ_o = maximum angular displacement of the platform in a three-month period (sec of arc) - assumed recheck of table alignment every three months.

e_o = largest rms value of the average angular rate of the platform (sec of arc/minute) measured over (averaged for) a time interval Δt for a set of representative periods of time T. For typical gyro-performance tests, Δt and T are specified as follows:

Test	Δt (minutes)	T (hours)
10 x ER tumbling 1°cogging 1°servo	4	1
1 x ER tumbling 10°cogging 10°servo	40	10
Fixed-azimuth or earth-reference drift tests where rate is averaged over one-hour periods	60	50

For example, for the 1°-servo test, the specification requires that the average rate of the platform be obtained by measuring the angular displacement during four-minute intervals. The rms value of the 15 consecutive measurements made during each hour is then obtained. The largest of the rms values that occurs during a representative 24-hour day is substituted in the specification.

$\epsilon_1^2, \epsilon_2^2, \epsilon_3^2$ =sum of the peak mean-squared angular oscillations measured about three orthogonal axes in the bandwidths of 1-10, 10-100, and 100-5000 Hz, respectively.

$A_0^2 \ldots A_6^2$ =sum of the peak mean-squared linear vibrations measured along three orthogonal axes in the bandwidths of 0-100, 100-200, 200-300, 300-400, 400-500, 500-600, 600-5000 Hz, respectively.

A_7^2, A_8^2 =largest value of the sum of the peak mean-squared linear vibrations along three orthogonal axes in the range between 600 and 5000 Hz in 150 and 50 Hz bandwidths, respectively.

Now let us analyze each of the error contributors to equation 4-29. The first term ϵ_o, represents the maximum angular displacement of the turntable over an assumed three-month interval between calibrations. The turntable may be mounted on a flexible or elastic foundation that can, and in fact does, distort and/or oscillate with a varying load such as personnel walking through the area (Fig. 4-60) or merely as the result of personnel activity in the building (Fig. 4-61). The possibility of disturbing the test table is also increased whenever any heavy equipment such as electronic consoles or hydraulic equipment is moved into or out of the area.

An additional problem can occur if the turntable base and the foundation on which it rests is actually shifted due to settling of the building foundation over a period of time. Such a case can occur when the building is located on a 'soft' land area such as is the case of the Instrumentation Laboratory. Shifting can occur, of course, if the turntable is subjected to accidental physical contact from personnel and/or other test equipment.

The fact that thermal gradients are present cannot be over-emphasized. The test environment itself is air-conditioned so that thermal gradients are minimized but the thermal gradients outside the test area can possibly contribute to disturbance displacements inside the test area. Radiational cooling of the building exterior can cause dihedral shifting of the walls. Unless the test area is completely isolated from the rest of the building, this problem cannot be ruled out. Even weather changes, if drastic enough, can cause thermal stresses and displacements in the building structure which are transmitted to the test area.

In addition to this phenomenon in the exterior environment, the simple case of vehicle movements such as automobile traffic, railroad trains, buses, heavy trucks, etc., can contribute enough disturbance to shift and/or vibrate the building and its foundation (Fig. 4-62). Tests using precision tilt sensors located in close proximity to a test turntable have shown both short-term and long-term tilt with the above factors as known inputs.

The second term of equation 4-29, e_o, is the largest rms value of the average angular rate of the platform measured over (averaged for) a time interval Δt for a set of representative periods of time T. For example, in a servo test the requirement is that the average angular rate be obtained by measuring the angular displacement during a time interval (Δt), of four minutes. If T = 1 hour is chosen, then the rms values of fifteen consecutive measurements are obtained during that time. The largest of the rms values that occurs during a representative 24-hour day is the value finally chosen.

All of the factors discussed in the case of the coefficient ϵ_0 can just as well contribute to the case of platform angular rate since the base or floor is subjected to the above excitations whereby motion can result in translation and/or rotation. Since the turntable and its base may be rigidly secured to the floor and little or no isolation exists through the structure, any floor motion is felt at the test platform.

The next three terms of equation 4-29, ϵ_1^2, ϵ_2^2, and ϵ_3^2 are the sum of the peak mean-squared angular oscillations measured about three orthogonal axes in the bandwidths of 1-10 Hz, 10-100 Hz, 100-5000 Hz, respectively. The maximum error that may be produced by angular vibration is, in meru

$$E_{(max)} = 0.324 \times 10^{-3} \left[\frac{(1 + h^2)^{1/2}}{4} \right] \int_0^\infty \frac{\omega}{(1+\tau^2\omega^2)^{1/2}} \epsilon^2(\omega)\, d\omega \quad \text{(Eq. 4-30)}$$

where

$\epsilon^2(\omega)$ = the peak power spectral density of the total angular vibration (seconds of arc)^2

τ = gyro time constant (sec)

ω = vibration frequency (rad/sec)

E = error in rate (radian/sec)

h = gyro gain

Equation 4-30 may be approximated by a numerical integration. Assuming an angular-vibration-measuring instrument whose gain is unity and whose time constant is 1 millisecond, the maximum error in meru is approximated as

$$E_{(max)} = 0.0035\epsilon_1^2 + 0.0035\epsilon_2^2 + 0.107\epsilon_3^2 \quad \text{(Eq. 4-31)}$$

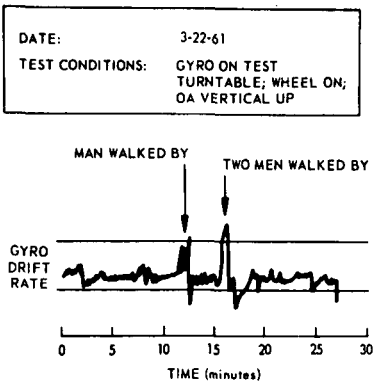

Fig. 4-60 Effect of personnel in area on gyro test data

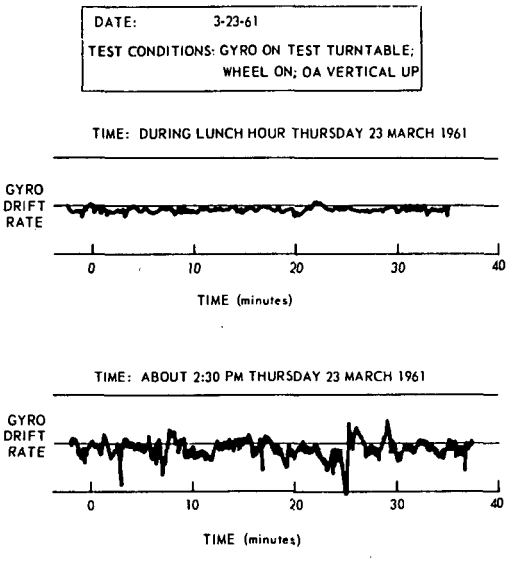

Fig. 4-61 Effect of personnel activity in building on gyro test data

Angular vibrations can exist about the spin, input and output axes as a result of floor oscillations. An acute form of oscillatory motion, for example, can be associated with any earth tremors that may occur in the vicinity of the test area and its surroundings. Of course, the test platform could oscillate in any number of modes and phases; but the total oscillation can be resolved into its components about the spin, input and output axes, which is treated in the above expressions.

The remaining terms of equation 4-29, A_0^2 through A_8^2, are the total peak mean-squared magnitude of linear vibratory acceleration (g^2 peak) in bandwidths from 0 to 5000 Hz. These terms represent errors in the compliance torques associated with translational acceleration along the input and/or spin axes. In actual practice, however, these terms can be virtually ignored. As mentioned in reference 21, under emphasis was placed on the steady-state translational errors introduced by high-frequency vibrations, since they do not occur in practice. The acceleration sensitivities of a well-designed gyro are such that accelerations of 0.01 g above 1 Hz produce negligible measurement errors after averaging the gyro output signal. At lower frequencies, the displacements required to produce a significant error are very much larger than those encountered in practice. It is concluded that no translational-vibration isolation is required for gyro testing. Accordingly, a translational vibration of 0.001 g is considered tolerable. Thus, the largest and more significant errors (in practice) in gyro testing are caused by the rates associated with angular vibrations of the test platform.

Isolation. Problems associated with test-station stability have been pursued by Instrumentation Laboratory personnel since 1957 because of large-magnitude disturbances that were showing up in the test data even then. These were found to be caused by the movement of railroad trains and by movement of large heavy pieces of equipment within the laboratory near a test station.

Preliminary investigations of the floor of the gyro test laboratory showed that the five-inch-thick concrete was acting like a membrane. People walking near a test station caused tilt of the order of seconds of arc, and a diurnal variation was detected on the order of two-to-four seconds of arc (Fig. 4-63). This work was tediously carried out with level vials calibrated to 1.42 seconds of arc sensitivity.

The first attempts at isolation of a test station from floor motion are depicted schematically in figure 4-64. The theory behind these endeavors was to support the test table at the nodal points in the floor membrane. These nodal points were the area immediately around the building-load-bearing columns, which in turn were supported by pile bents driven to refusal in the subsoil.

The first isolation platform comprised two parallel steel beams supported at the building nodal points as indicated at the left of figure 4-64. Data taken at an accelerometer testing table mounted midway on the two beams showed a substantial reduction in transient deflections caused by personnel, but the diurnal variations persisted.

An isolation platform for a gyro test turntable was then constructed in the same area. This platform consists basically of two steel beams welded together in an X pattern. The ends of the X are welded to 12-inch-diameter steel-tubing supports which support the X approximately one inch above the floor. The cylindrical supports are mounted around the building columns but do not touch the building columns. In this manner, the platform is supported by the building pilings beneath the floor. A turntable base ring is welded at the junction of the beams. This ring provides a mount for the turntable and also stiffens the structure. The accelerometer test platform was maintained at one side. Figures 4-65 and 4-66 are photographs taken before the false floor was constructed, and figure 4-67 shows the

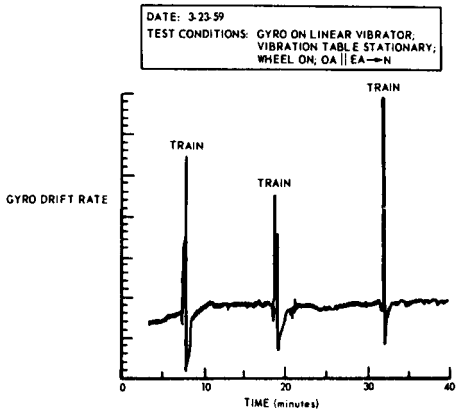

Fig. 4-62 Effect of passing trains on gyro test data

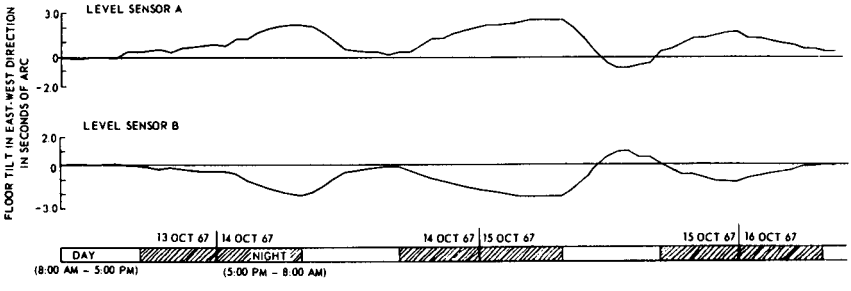

NOTE: LEVEL SENSORS A AND B WERE MOUNTED BACK TO BACK WHICH ACCOUNTS FOR MIRROR-IMAGE EFFECT

Fig. 4-63 Diurnal floor tilt along east-west axis

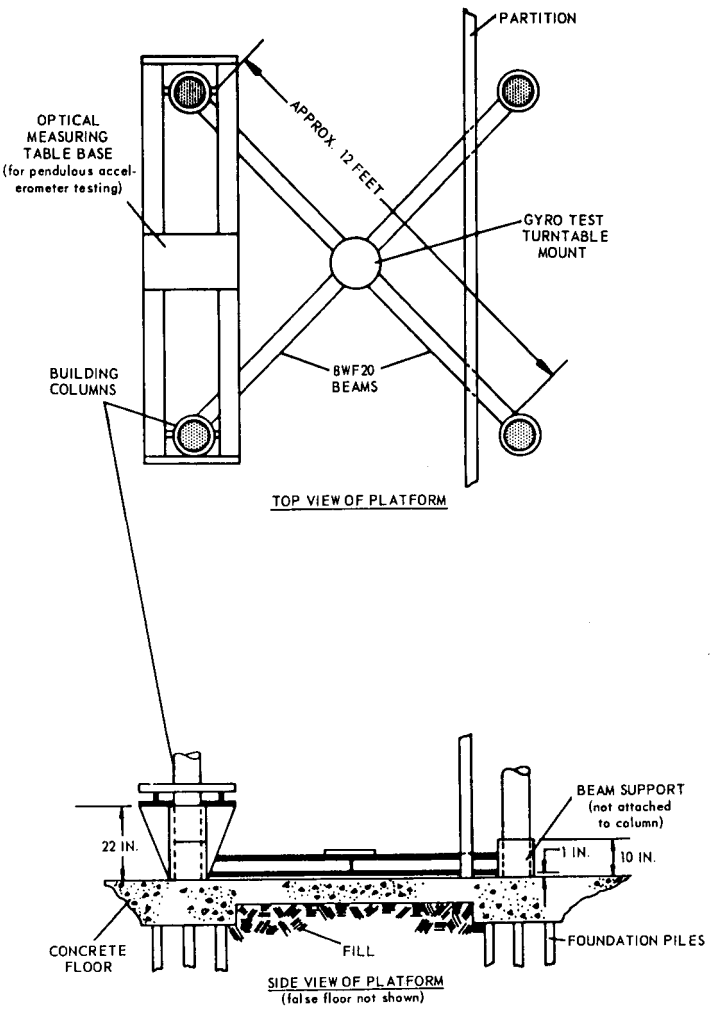

Fig. 4-64 Floor-isolation platforms

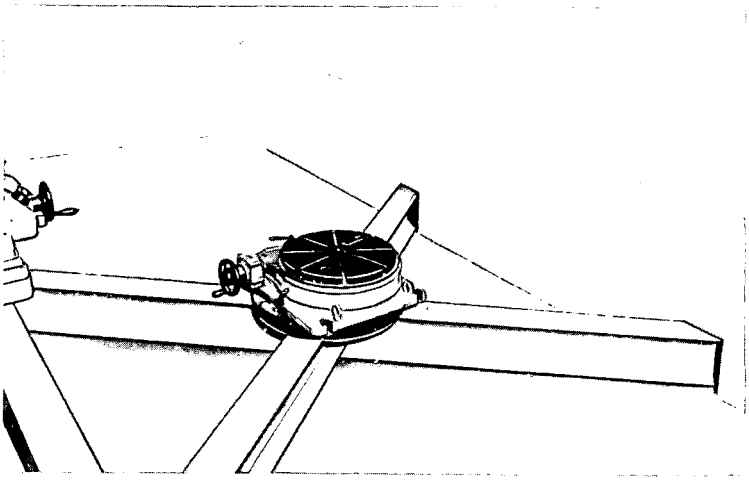

Fig. 4-65 Floor-isolation platform showing base for gyro test turntable

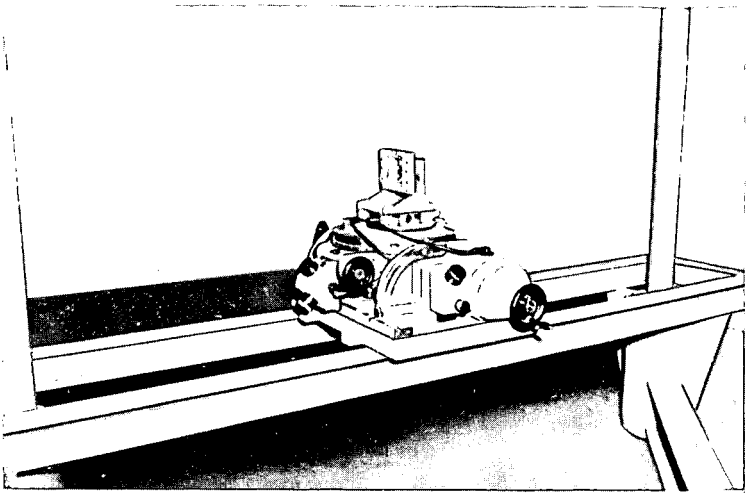

Fig. 4-66 Floor-isolation platform and optical measuring table for pendulous accelerometer testing

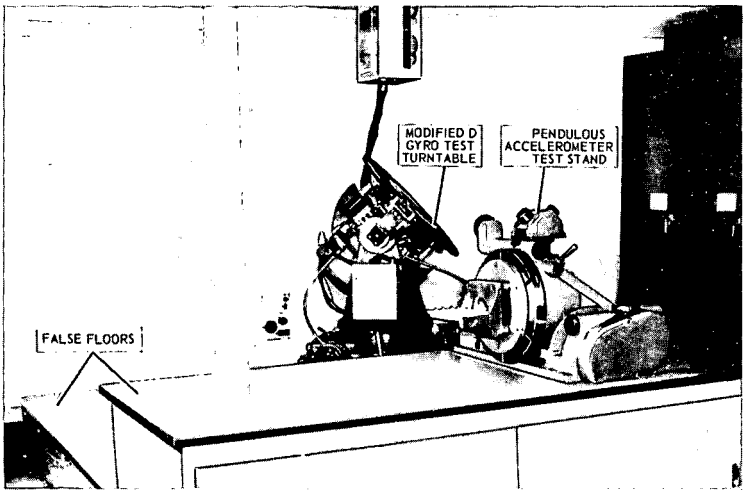

Fig. 4-67 Completed isolation-platform setup showing gyro and pendulous accelerometer test stands

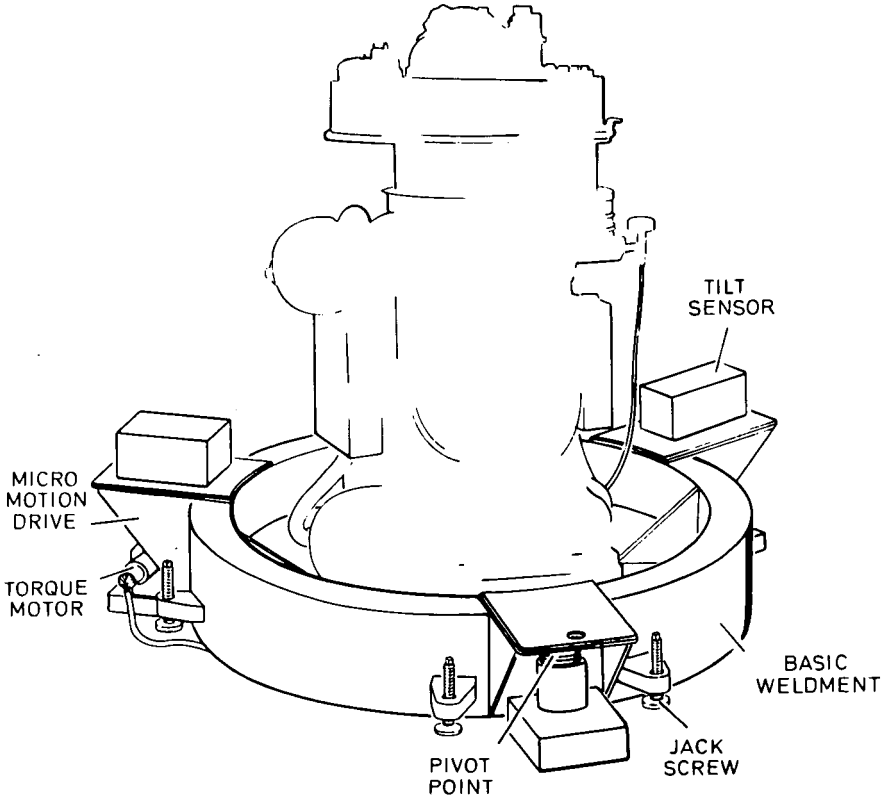

Fig. 4-68 Ground-tilt-isolation platform

complete setup after installation of the false floor. Some of the estimated parameters of the X-type isolation platform are:

Weight of platform 800 lb

Load to be placed on platform 2000 lb

Total load on floor 2800 lb

Load at each bearing area 700 lb

Area at bearing 26.5 in^2

Bearing stress 26.4 lb/in^2

The following calculations were made to define the platform's susceptibility to deformation and vibration. All computations concerning the beams were made assuming the beams to be simply supported. The deflection of a simply supported beam is

$$\Delta_1 = \frac{F\ell^3}{48EI} \qquad \text{(Eq.4-32)}$$

where

Δ_1 = deflection of beam (neglecting weight of beam)

F = force applied to beam = 2000 lb

ℓ = free length of beam = 11.85 ft

E = modulus of elasticity = 29×10^6 lb/in^2

I = moment of inertia of beam = 69.2 in^4

Substituting numerical values into equation 4-32 gives

$$\Delta_1 = 0.0597 \text{ in} \qquad \text{(Eq.4-33)}$$

Deflection due to weight of the beam itself is

$$\Delta_2 = \frac{5w\ell^4}{384EI} \qquad \text{(Eq.4-34)}$$

where

w = unit weight of beam = 20 lb/ft

Substituting numerical values into equation 4-34 gives

$$\Delta_2 = 0.0044 \text{ in} \qquad \text{(Eq.4-35)}$$

Total deflection, Δ_T, is the sum of Δ_1 and Δ_2 or

$$\Delta_T = 0.0641 \text{ in} \qquad \text{(Eq.4-36)}$$

Since two similar beams are sharing the load, the resisting moment of inertia is doubled and total deflection is halved. Using this fact, the natural frequency

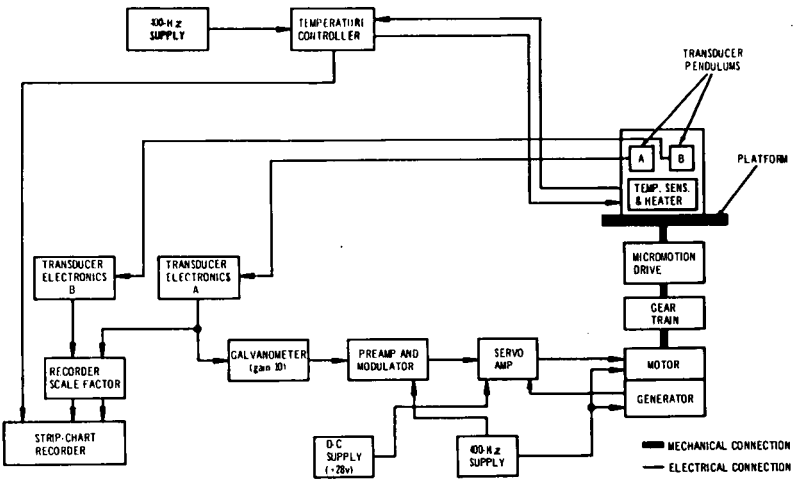

Fig. 4-69 Ground-tilt-isolation-platform block diagram (one of two horizontal axes)

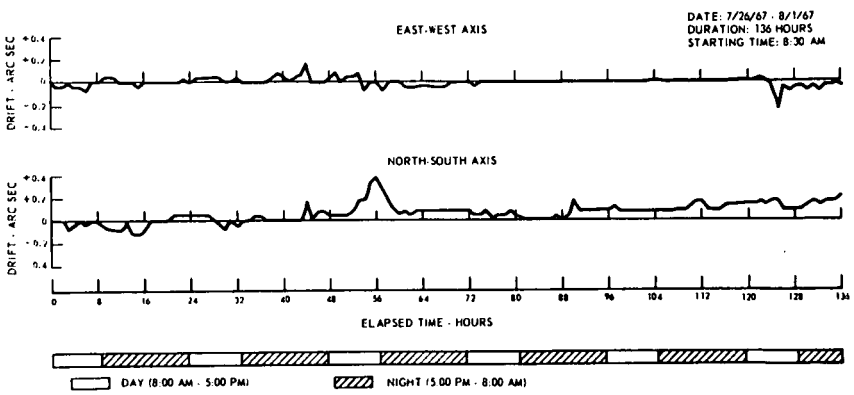

Fig. 4-70 Performance of the ground-tilt-isolation platform

of the isolation platform can be computed from the relationship

$$f_n = \frac{1}{2\pi}\sqrt{\frac{g}{\Delta}} \qquad \text{(Eq. 4-37)}$$

where

f_n = natural frequency

g = acceleration of gravity = 386 in/sec^2

$\Delta = \Delta_T/2 = 0.0321$ in

Substituting numerical values into equation 4-37 gives

$$f_n = 17.5 \text{ Hz} \qquad \text{(Eq. 4-38)}$$

Measurement of natural frequency with a velocity pickoff gave a value of 18 Hz, which agreed so well with the calculated value that computations for the other extreme (fixed-end beams) were deemed unnecessary. The setup closely approximates simply supported beams because the beam supports are not attached to either the floor or the building columns. The slightly higher value was expected because the assembly is actually stiffer than defined in the computations. However, this appears to be a sufficiently low natural frequency to avoid most of the transient vibrations of motors, etc.

Although a generally accepted method of obtaining a stable base is to sink a column into the ground to a depth at which a stable bearing is accomplished and then isolate the column from surrounding vibration sources and media, that method was ruled out at the Instrumentation Laboratory at the time. One reason was the condition of the water table, and another was the excellent results obtained from the earlier platform for accelerometer testing in eliminating transients caused by personnel. However, both platforms are susceptible to movement of the building pilings.

Servo-Controlled Isolation. Present-day control of base motion at the Instrumentation Laboratory comprises servo-controlled ground-tilt-isolation platforms upon which the gyro test turntables are mounted as shown in figure 4-68 (22). The ground-tilt-isolation platform consists basically of a circular steel weldment which is supported at three points - a fixed pivot point and two micromotion drives. The circular weldment is an annular ring of hollow rectangular cross section. A circular member, which is the support for the test table, is welded to the bottom of the annular ring. Three brackets with gussets to provide bearing points for the pivot point and micromotion drives are equally spaced on the circumference of the annular ring.

The circular base has two axes of motion at an included angle of sixty degrees. When a ground tilt causes the platform to rotate about one of these axes, the motion is sensed by a pendulous sensor, which is located in a temperature-controlled housing just over the micromotion drive. There are two tilt sensors on each of the two active axes. One is in the servo-control loop; the other monitors the actual tilt of the axis, thus indicating any shift in the null point of the controlling sensor. The voltage output of the pendulous sensor is proportional to the deviation of the pendulum from the zero-tilt position. This voltage is amplified and continuously fed to one phase of a two-phase servo motor. The servo motor drives a highly refined micromotion unit that converts the rotary motion to vertical translational motion, thereby leveling the platform. Each of the two servo systems consists of a tilt sensor, a servo motor, a gear train, a

micromotion drive, and the necessary electronics (Figs. 4-69 and 4-71). The servo loops can function either independently or simultaneously. The overall gear ratio in each servo loop is 1860:1; in other words, 1860 revolutions of the servo motor are required for one turn of the micromotion lead screw.

Test results have shown that the ground-tilt-isolation platform maintains a level base within ± 0.2 second of arc for periods ranging from many days to a few months. A typical segment of data is shown in figure 4-70. The intermittent jags in the data were found to be caused by stiction of the lead screws in the micromotion drive. This problem is being alleviated by replacing the ordinary micrometer screws with ball screws and ball-bearing thrust washers. Some of the basic parameters of the ground-tilt-isolation platform are:

Weight of base 1800 lb

Load-carrying capacity 22 000 lb

Annular-ring ID 48 in

Annular-ring OD 56 in

Annular-ring cross section 4 in x 10 in

Support bracket size 12 in x 12 in

Micromotion drive max. motion ± 0.030 in

Load on each drive 2000 lb

The ground-tilt-isolation platform has proven to be effective in isolating against low-frequency disturbances lower than 1/10 Hz. A recent attempt at the Instrumentation Laboratory to control high-frequency motion is depicted in figure 4-72. That figure shows concrete bases for seven ground-tilt-isolation platforms and accelerometer test tables. The bases are set in pea stone and are surrounded by a retaining wall, the combination of which is expected to effectively attenuate high-frequency culturally induced motion. Preliminary evaluation of this setup has shown a decrease in noise of less than an order of magnitude as compared to noise measured with the tables directly mounted to the building floor. This evaluation is continuing.

A proposed experimental design for soft mounting on the ground-tilt-isolation platform to isolate against high-frequency disturbances (>10 Hz) is shown in figure 4-73 (24). Soft elastic supports on the framework carry a granite-block mounting surface for the gyro test table. The soft elastic supports will isolate the gyro from high-frequency disturbances that are within the boundary of the ground-tilt-isolation-platform correction capability. The entire assembly is enclosed in a housing that provides control of temperature, acoustic noise, barometric pressure and radio-frequency interference. Although this proposed design is limited to the isolation of frequencies higher than 10 Hz, its operation will provide background knowledge for the isolation of low- and intermediate-frequency vibrations.

Other Considerations

In addition to the site-selection and base-motion considerations already discussed, the instrumentation engineer must evaluate the thermal, acoustic-noise, radio-frequency interference and magnetic environments in which he intends to set up his test station.

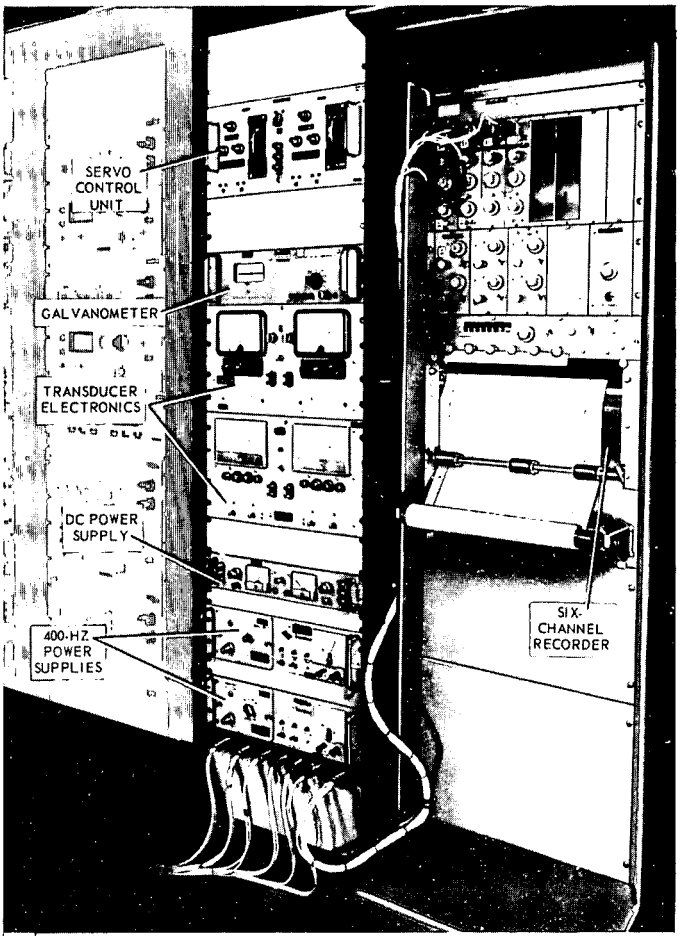

Fig. 4-71 Ground-tilt-isolation-platform electronics console

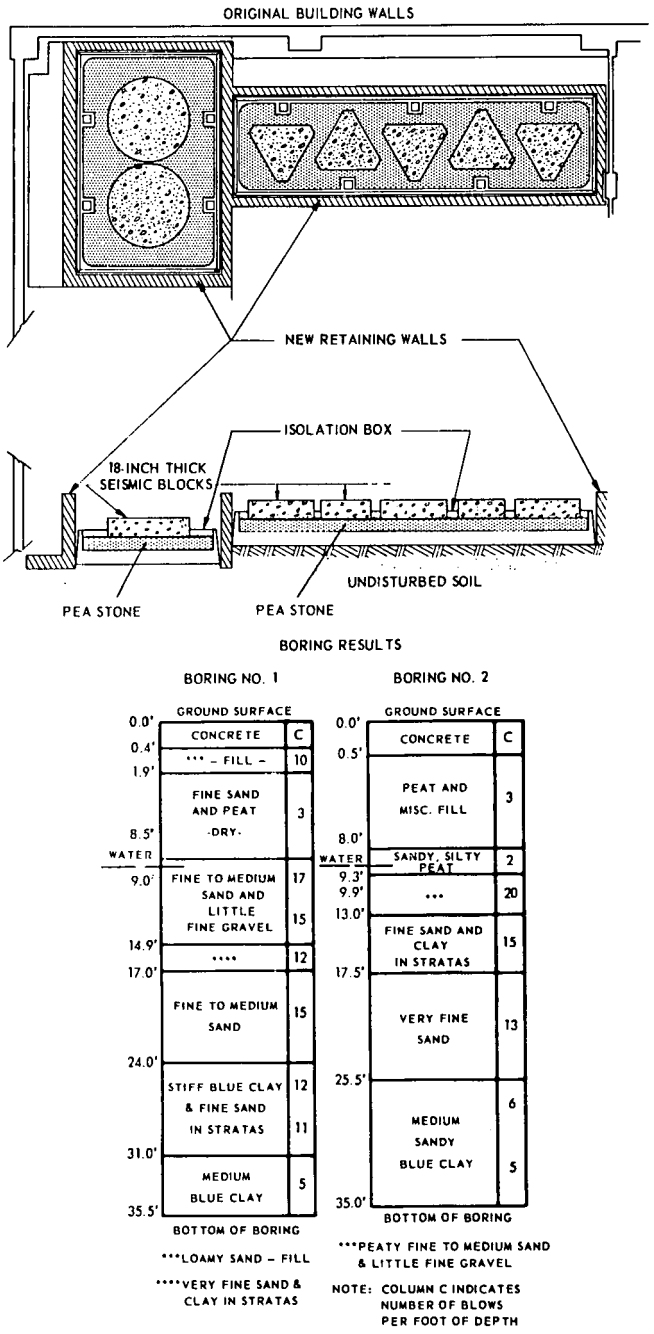

Fig. 4-72 Recent attempt at base-motion isolation at the Instrumentation Laboratory

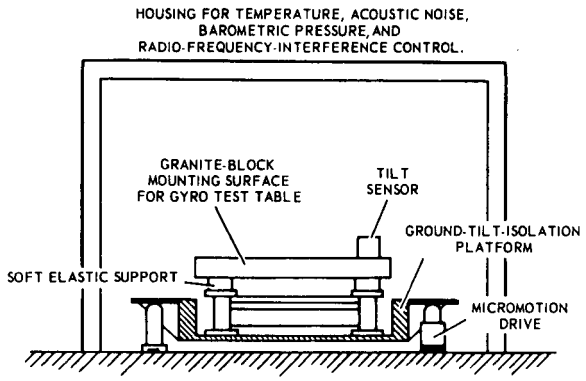

Fig. 4-73 Ground-tilt-isolation platform with soft elastic supports

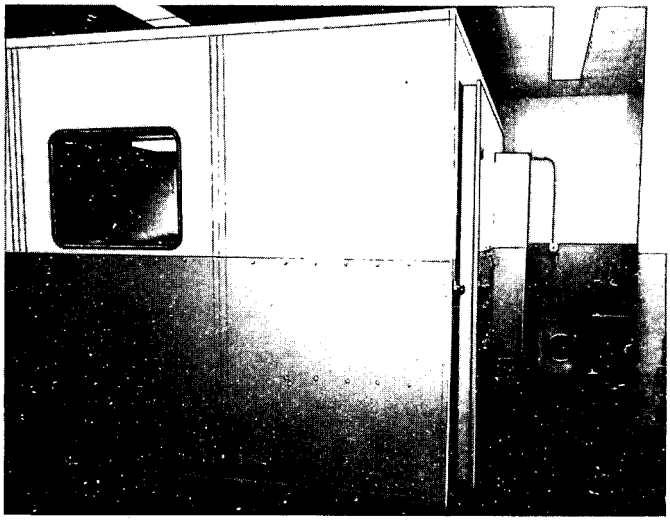

Fig. 4-74 Acoustically shielded enclosure

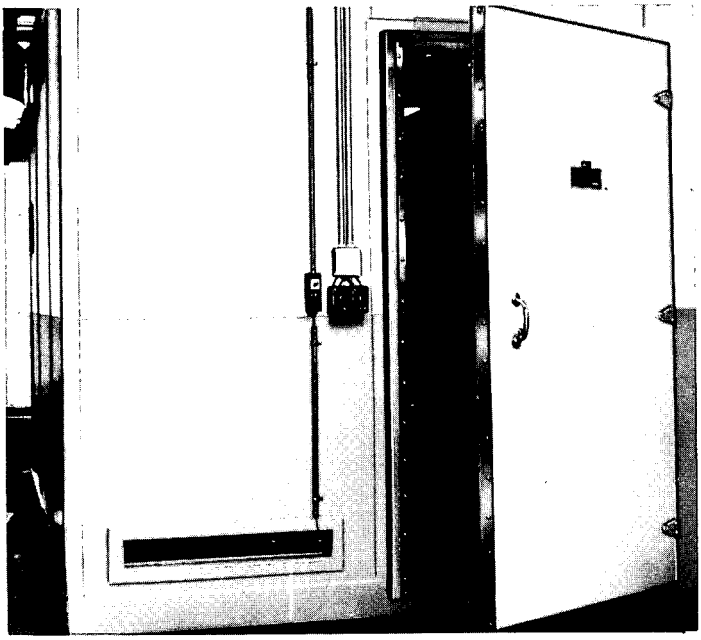

Fig. 4-75 R.f. shielded room

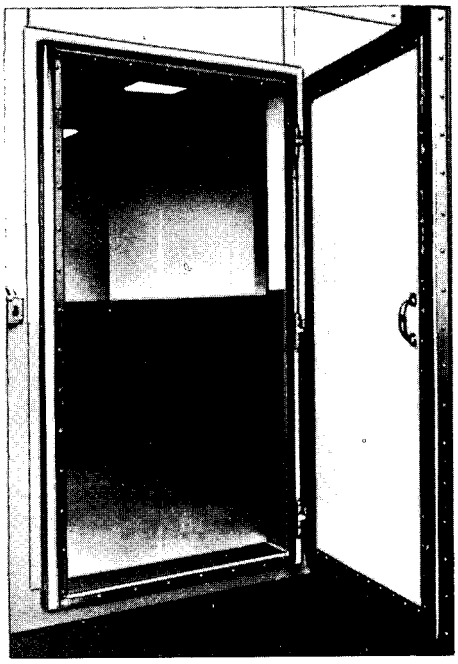

Fig. 4-76 Entrance to r.f. shielded room

Thermal Environment. Ambient temperature at a test station can cause problems in two ways: either by remaining constant at too high or too low a level or by varying erratically with time. If the temperature is constant at some level other than the ideal (and if a correction cannot be made), then the heat-sink interface to the gyro must be altered to provide the necessary potential for heat flow out of or into the gyro. Caution should be exercised in altering heat-sink interfaces in that the physical stability of the material used as insulator or conductor should be investigated along with its thermal stability. Varying temperature is not usually a problem because most large air-conditioning installations today are generally well planned and integrated with the test area. A smaller facility, however, with individual air-conditioning equipment may find that the air-conditioning cycle is apparent in their gyro test results.

Air motion can also result in anomalies in gyro performance, but well designed, positioned and baffled air conditioning usually minimizes or eliminates these problems. In the case of centrifuge testing, the device being tested is mounted inside a wind shroud to eliminate the direct effects of air velocity; however, cooling of the enclosure may be a problem.

Acoustic Noise. Sound is a form of vibration that may affect both the gyro and personnel working in the area. Ultra-high-precision gyro test facilities are therefore shielded acoustically to prevent noise from external machinery, etc., from reaching the gyro on test. In addition, some test devices themselves must be acoustically shielded to prevent acute discomfort or even injury to personnel. An example of such a device is a large electrodynamic vibrator such as that described on pages 126ff.

The vibrator and associated slip table are enclosed in the acoustical room shown in figure 4-74. The walls of the room are four-inches thick constructed of sixteen-gage galvanized-steel exterior sheet and twenty-gage perforated interior sheets and filled with Fiberglas to a density of 6 lb per cubic foot. The room contains a door for personnel and equipment access, a special port for theodolite sighting to check gyro alignment on the vibrator, and the necessary apertures for air-conditioning ducts, cables to the electronic consoles which are outside the room, electrical wiring and plumbing (for cooling the vibrator). Prior to installation of the shielding, the noise level near the vibrator was 107 db at 2000 Hz, which is equivalent to that generated by a subway train passing a station or by a punch press. After installation of the acoustical enclosure, the noise level was of the order of 60 db, which is equivalent to a quiet typewriter or a soft voice.

Radio-Frequency Shielding. Since certain types of gyros may be sensitive to radio-frequency interference, the instrumentation engineer may be called upon to provide shielding against such a disturbing input. One such room at the Instrumentation Laboratory is constructed of plywood which has zinc-coated steel permanently bonded to it (Fig. 4-75). The joints are specially treated as are all access ports, including the door, as shown in figure 4-76. R.f. attenuation within the enclosure is greater than 80 db at 21 MHz.

Magnetic Shielding. Magnetic fields must also be investigated by the instrumentation engineer and dealt with in a degree proportional to the sensitivity of the gyro being tested. Usually the gyro itself will include some magnetic shielding as part of its outer housing or thermal jacket, but additional shielding may have to be provided by the instrumentation engineer especially on fixtures to be used in close proximity to sources of high magnetic fields such as electrodynamic vibrators.

A variety of materials are on the market today for use as magnetic shields, and the instrumentation engineer must choose the material best suited to his particular requirements. Regardless of the material chosen, annealing procedures should be carefully adhered to and the shielding design should be as nearly 'water-tight', i.e. without apertures, as possible.

Testing of magnetic materials at the Instrumentation Laboratory has tended to dispel the widely held notion that mumetal is extremely sensitive to shock. Deformation of annealed mumetal by vibration, peening, drilling, cutting, sawing and filing did not produce significant changes in its shielding qualities (23).

7. Conclusions

Test equipment philosophy at the Instrumentation Laboratory of MIT considers individual pieces of equipment as interrelated parts of a complete system. In other words, each test station and the gyro or gyros to be tested thereon is considered as a complete system. The performance characteristics of each part or subsystem are carefully examined on an individual basis to determine their adequacy for the particular function involved and then re-examined from the standpoint of total system performance. In addition, the question of cost versus desired flexibility and degree of precision is continually weighed. The objective is to provide a complete gyro test station capable of accurately determining the performance of today's precision inertial gyros in the most efficient and economical manner.

Basically, a gyro test station comprises devices for gyro orientation and/or for environment simulation, electronics and environment-control devices. In the first category are test turntables for one-g testing, gyro holding fixtures, linear and angular vibrators and centrifuges. The electronics includes excitation, control and monitoring equipment. Environment control includes temperature control of ambient and equipment and various methods of base-motion isolation.

The mechanical portion of the gyro test station presents stringent machining and inspection requirements. For example, most precise mechanical interfaces are currently being finished to the limit of practical machining capability, which is in the range of 10^{-5} inches total indicated runout. It is not uncommon for a test-turntable top surface to be hand-lapped to 40×10^{-6} inches total indicated runout for a mounting diameter of eight inches with respect to the test-turntable rotational axis. This accuracy could still result in angular misalignment with respect to the turntable axis of approximately one second of arc. Obviously, then, the tolerance budget for the various pieces comprising a complete assembly must be kept under extremely strict control if the desired precise gyro test orientations are to be achieved.

Two of the major electronics subsystems of a gyro test station are the control loops used with the servo-turntable and rate-feedback (or tumbling) modes of gyro testing and their respective data-acquisition techniques. The servo turntable loop is closed to the gyro through rotation of the turntable top on which the gyro is mounted. The loop uses tachometer feedback for synchronization and stabilization. The rate-feedback loop, on the other hand, is closed to the gyro through the gyro torque generator. Either an analog or pulsed restraint loop may be used, each of which has advantages and disadvantages from the standpoint of data acquisition.

Environmental-control considerations for a gyro test station range from site selection and preparation to local isolation from interfering inputs. Site selection and preparation has run the gamut from one gyro manufacturer locating on sandy

soil and maintaining a stable water table under his test laboratory for maximum high-frequency damping of base motion to another manufacturer locating on ledge to minimize low-frequency disturbances. Local isolation from interfering inputs includes the use of base-motion-isolation devices such as those in current use at MIT, ambient air-conditioning systems, and temperature control of individual electronics consoles.

Acknowledgements

The authors wish to acknowledge Messrs. Howard M. Mussoff and Joseph G. Walsh for their contributions to the material on modes of testing and Messrs. Steven I. Kane and Ira C. Weymouth for their contributions to the material on mechanical test instrumentation. They also express their appreciation to Mr. Edward J. Carbrey and his associates of the Jackson and Moreland Division of United Engineers and Constructors for their help in compiling and editing the author's rough notes.

References

(1) **Lund, P. S.**, 'The Changing Emphasis and Future Trends in Navigational Gyros', paper presented at the SAE-NASA Aerospace Vehicle and Flight Control Conference, Los Angeles, California, July 1965.

(2) **Wing, W. G.**, 'Inertial Guidance and Navigation', Space/Aeronautics R and D Handbook, 1965.

(3) **Fink, D. J.**, 'Communications - Components - Guidance in Space Age of FY 2001', paper presented at the 4th Goddard Memorial Symposium of the American Astronautical Society, Washington, D. C., March 1966.

(4) **Denhard, W. G.**, 'Laboratory Testing of a Single-Degree-of-Freedom Integrating Inertial Gyro', Report R-105, App. 9, Instrumentation Laboratory, MIT, Cambridge, Massachusetts, Sept. 1956.

(5) **Ibid**, App. 10.

(6) **King, R. L.**, 'Two-Axis Universal Test Stand', Report E-1503, Instrumentation Laboratory, MIT, Cambridge, Massachusetts, Feb. 1964.

(7) **Gianoukos, W. A.**, 'Gyro Test Station Checkout and Evaluation', Report MDC-TR-66-66, Air Force Missile Development Center, Holloman Air Force Base, New Mexico, April 1966 (also published as Report E-1738, Instrumentation Laboratory, MIT, Cambridge, Massachusetts, April 1966).

(8) 'Automation of Holloman Test Station', unpublished internal memo from **N. H. Nathan to N. Polner**, Instrumentation Laboratory, MIT, Cambridge, Massachusetts, 6 Dec. 1967.

(9) **Draper, C. S., McKay, W.** and **Lees, S.**, 'Instrument Engineering', Vol. I, Ch. 9, McGraw-Hill Book Company, New York, 1952.

(10) **Spitzer, E. A.** 'Preliminary Analysis of a Digital Tumbling Loop', Master of Science Thesis T-320, Department of Aeronautics and Astronautics, MIT, Cambridge, Massachusetts, June 1962.

(11) **Hutchings, P. B.**, 'Compensation of a Sample Data Contactor Servo', Master of Science Thesis, Department of Electrical Engineering, MIT, Cambridge, Massachusetts, May 1959.

(12) **Marshall, R.E., and Palmer, P.J.**, 'Inertial Instrument Design Verification Tests for High-G Applications', paper presented at an International Symposium on Inertial Guidance Testing Techniques, Nov. 1965 at Weilheim, Germany (also published as Report E-1866, Instrumentation Laboratory, MIT, Cambridge, Massachusetts, Oct. 1965).

(13) **Smith, A.J.**, 'Two-Axis Angular Vibration Test Results on a Single-Degree-of-Freedom Integrating Gyroscope', Report MDC-TR-66-68, Air Force Missile Development Center, Holloman Air Force Base, New Mexico, Dec. 1966 (also published as Report E-1965, Instrumentation Laboratory, MIT, Cambridge, Massachusetts, Dec. 1966).

(14) **Kayton, M.**, 'Co-ordinate Frames in Inertial Navigation', Doctor of Philosophy Thesis T-260, Department of Aeronautics and Astronautics, MIT, Cambridge, Massachusetts, Aug. 1960.

(15) **Tate, D.R.**, 'Absolute Value of g at the National Bureau of Standards', J. Res. NBS 70C (Eng. and Inst.), April-June 1966.

(16) **Palmer, P.J.**, 'Notes on the Single-Degree-of-Freedom Floated Integrating Gyro', Report GL-250, Instrumentation Laboratory, MIT, Cambridge, Massachusetts, July 1959.

(17) **Richter, C.F.**, 'Elementary Seismology', W.H. Freeman and Company, San Francisco, 1958.

(18) **Weil, W.M., Srode, W.E., and Burrows, R.M.**, 'Description of an Inertial Test Facility Located 1100 Feet below the Surface of the Earth', Paper No. 67-538, American Institute of Aeronautics and Astronautics, New York, Aug. 1967.

(19) **Mathis, L.O., Stevens, J.R., and Wright, S.C.**, 'The Design and Construction of an Inertial Test Facility', paper presented at the AIAA/ION Guidance and Control Conference, Minneapolis, Minnesota, Aug. 1965.

(20) **Weinstock, H.**, 'Specification for the Permissible Motions of a Platform for Performance Evaluation of Single-Degree-of-Freedom Inertial Gyroscopes', Report E-1267, Instrumentation Laboratory, MIT, Cambridge, Massachusetts, Dec. 1962.

(21) **Weinstock, H.**, 'Limitations on Inertial Sensor Testing Produced by Test Platform Vibrations', NASA Technical Note TN D-3683, National Aeronautics and Space Administration, Washington, D.C., Nov. 1966.

(22) **Tsutsumi, K. and Merenda, F.S.**, 'Performance of a Ground Tilt Isolation Platform', paper presented at the AIAA/JACC Guidance and Control Conference, Seattle, Washington, Aug. 1966.

(23) **Banuk, R.**, 'Mumetal Shielding Investigation', Report GMF-102, Instrumentation Laboratory, MIT, Cambridge, Massachusetts, April 1965.

Bibliography

AIAA/IUN Guidance and Control Conference, pp 278-309 and 360-390, Minneapolis, Minnesota, Aug. 1965.

AIAA/JACC Guidance and Control Conference, pp 366-397 and 559-592, Seattle, Washington, Aug. 1966.

AIAA Guidance,Control and Flight Dynamics Conference, Papers 67-538 to 67-550,Huntsville, Alabama, Aug. 1967.

Blackburn, J.F., Reethof, G., and Shearer, J.L., 'Fluid Power Control', The Technology Press of MIT and John Wiley and Sons, Inc., New York, 1960.

Carlberg, N.E., and Herring, T.H., Designer's Guide,'Electrical Interference Reduction', Document No. D2-4156, Boeing Airplane Company, Seattle, Washington.

Curreri, J.R., 'Fundamentals of Vibrating Structures', MB Electronics, New Haven, Connecticut, 1961.

Den Hartog, J.P., 'Mechanical Vibrations', McGraw-Hill Book Company, Inc., New York, 1956.

Harris, C.M., and Crede, C.E., 'Basic Theory and Measurements', Shock and Vibration Handbook, Vol.I, McGraw-Hill Book Company, Inc., New York, 1961.

Hasse, H.O., 'Influence of Sun and Moon on the Magnitude and Orientation of the Earth's Gravity Vector', WP-MDSD-67-2, Central Inertial Guidance Test Facility, Holloman AFB, New Mexico, May 1967.

Hume, K.J., 'Metrology with Autocollimators', Hilger and Watts, Ltd., London, 1965.

Jakob, M., and Hawkins, G.A., 'Elements of Heat Transfer', John Wiley and Sons, Inc., New York, 1957.

King, R.L., 'Investigation of Transient and Long-Period Tilts and of Translation Vibration Characteristics of a Gyro Test Area', Report MDC-TR-66-67, Air Force Missile Development Center, Holloman AFB, New Mexico, April 1966 (also published as Report E-1732, Instrumentation Laboratory, MIT, Cambridge, Massachusetts, April 1966).

Maleev, V.L., and Hartman, J.B., 'Machine Design', International Textbook Company, Scranton, Pennsylvania, 1957.

Musoff, H., 'Varying Gyroscope Angular Momentum', Report GE-E-58, Instrumentation Laboratory, MIT, Cambridge, Massachusetts, Feb. 1966.

Roark, R.J., 'Formulas for Stress and Strain', McGraw-Hill Book Company, Inc., New York, 1965.

Seely, F.B., and Smith, J.O., 'Advanced Mechanics of Materials', John Wiley and Sons, Inc., New York, 1952.

Seismic Survey for Kearfott Company, Inc., The Geotechnical Corporation, Technical Report No. 59-3, Feb. 1962.

Shaw, M.C., and Macks, E.F., 'Analysis and Lubrication of Bearings', McGraw-Hill Book Company, Inc., New York, 1949.

Skalski, C.A., 'Comparison of Actively Leveled Test Platforms', IEEE Trans. on Instruments and Measurements, Vol. IM-17, No.1, March 1968.

Starling, S.G., 'Levels and Level Bubbles', Transactions of the Optical Society, Vol. XXIV, No. 5, 1922-23.

Weinstock, H., 'Design of a Precision Tilt and Vibration Isolation System', NASA Technical Report TR R-281, National Aeronautics and Space Administration, Washington, D.C., March 1968.

Weymouth, I.C., 'Design Considerations for Fluid Bearings Used on Gyro Test Turntables', Report E-939, Instrumentation Laboratory, MIT, Cambridge, Massachusetts, Aug. 1962.

5

Precision Inertial Gyro Testing at MIT

P.J. PALMER (Chapter Editor), W.A. GIANOUKOS, W.C. DONOVAN,
F.E. CARTWOOD, A.J. SMITH, R.H. WILKINSON
Instrumentation Laboratory, Massachusetts Institute of Technology,
Cambridge, Massachusetts, USA.

Summary

One philosophy of inertial gyro testing is that the test program should provide accurate measurements of the coefficients of a model equation that mathematically defines the gyro performance in any environment. The reduction of this philosophy to practice at the Instrumentation Laboratory of MIT is described in this chapter as it relates to the testing of the single-degree-of-freedom floated integrating gyro to today's high-performance, high-reliability and long-life specifications.

After defining basic terms and nomenclature, the error model for the gyro is developed. Laboratory testing in both the one-g and the higher-than-one-g environments is then described in considerable detail as are the data processing techniques involved. A discussion of two-degree-of-freedom gyro testing elsewhere is included as an Appendix.

1. Introduction - P.J. Palmer

The gyros of an inertial navigation or guidance system are a major determinant of the performance and reliability of the system. In a gimbaled or floated-type system, these gyros stabilize a controlled member or platform in a given coordinate system. Upon the platform are mounted accelerometers, the outputs of which are integrated to provide measurements of inertial velocity and then integrated again to provide measurements of distance. In a strapdown system, the gyros provide a reference frame to which the accelerometer outputs are referred.

As indicated by its title, this chapter is concerned with the test and evaluation of inertial gyros. But just what does the term 'inertial' mean when applied to a gyroscope ? One definition is that an inertial-quality gyro is one upon which the effect of earth's rotation is readily apparent. Dr. C.S. Draper has often suggested that the term 'inertial-quality' be applied only to gyros that have a drift rate less than one-thousandth of earth's rate (0.015 degree/hour), or one milli-earth-rate unit, commonly called one meru at the Massachusetts Institute of Technology (MIT). The latter definition will be used in this chapter.

At the equator, the earth's angular rate of rotation with respect to inertial space is 900 knots or 900 minutes of longitude per hour. Therefore a drift rate of one meru is equivalent to about one nautical mile per hour or one minute of arc per hour. The current state-of-the-art in commercial inertial-navigation systems

indicates that such performance can be achieved (1). It is certainly reasonable to expect a substantial improvement in the performance of inertial systems which will be available commercially in the future or which are still classified.

Philosophy of Gyro Testing at MIT

The high-performance, reliability and long-life requirements of inertial gyros dictate extensive and effective testing. The desired accuracy of the data and the cost of the required test equipment both have a significant impact on the selected test techniques. High accuracy is likely to require significant averaging times for each data point and to require data sets that cannot be completed in terms of a single day. Test equipment costs require that economic as well as technical factors be evaluated to determine the number and type of test stations required. Careful attention must be paid to equipment errors and uncertainties and to the thermal, magnetic, base motion and other environments to which an inertial gyro is sensitive. 'Error' is defined as the predictable component of inaccuracy which can be measured and compensated. 'Uncertainty' is the random component of inaccuracy, which is only predictable statistically (2).

No gyro testing standard exists today, and at least two distinct test philosophies are evident in reviewing inertial-gyro testing. One philosophy is that the test should simulate the actual environment in which the gyro will be used. Under this philosophy, the inertial-system designer must produce detailed information concerning the electrical, mechanical, thermal, magnetic, vibration, linear acceleration and other environments to which the gyro will be exposed when actually installed and operated in the system. The gyro test engineer, in turn, must produce detailed measurements of the performance of the gyro when subjected to these environments. As might be expected, this philosophy is of limited usefulness for several reasons, for example:

(a) the difficulties of accurately simulating the system environment even during one-gravity testing

(b) the difficulties of subjecting the gyro to several environments simultaneously

(c) the fact that gyros are often designed prior to a detailed knowledge of the environments expected in the system.

The gyro testing philosophy at MIT is that the test program should provide accurate measurements of the coefficients of a model equation that mathematically defines the gyro performance. Under this philosophy, the system designer is provided with a model of the gyro in its currently known functional form. This model contains the errors which have been measured over a wide range of environments for a given gyro family such as the MIT single-degree-of-freedom floated integrating gyro. Requirements which are unique to the particular system application are then included in the test and evaluation program to extend the model if necessary. The purpose is to obtain a 'complete' model of the gyro so that its behavior can be predicted in a given environment without the necessity of testing in that particular environment. The word 'complete' is enclosed in quotation marks since an adequate model for today's applications will probably not suffice for future applications. Experience has shown that, as the performance requirements become more stringent or as the environment is changed, more terms must be added to the model. In the early days of manned-aircraft navigation, the magnitude and stability of the acceleration-squared-sensitive errors of the gyro were no more significant than the magnitude and stability of the bias and

acceleration-sensitive errors. In the missile environment on the other hand, the magnitude and stability of the acceleration-squared errors become extremely significant because of the high-g levels involved. For the satellite application, where the system is not required for guidance during the boost phase, the bias error becomes the only term of significance.

Today's inertial systems are designed to be self-calibrating in the field. This is accomplished by moving the inertial instruments to several successive orientations with respect to gravity and then simultaneously solving the model equations for the instrument error coefficients. However, before reliance can be placed upon such a technique, it is necessary to demonstrate that the error coefficients obtained in such a benign environment can validly be extrapolated to cover the full range of variables to be encountered during operational usage. For example, the acceleration-sensitive error coefficients must be checked in a high-g environment by means of precision vibration and centrifuge testing. Instrument design limits have been above 50 g's, and new system applications exceed this value without significant increases in allowable instrument uncertainties. Such environments require more attention to nonlinear instrument errors than ever before. Therefore, tests at one gravity are conducted to verify the basic instrument design concepts and assembly techniques. Vibration tests are conducted to measure the acceleration-squared sensitivities and to search for nonlinearities in the sinusoidal or random acceleration environment. Centrifuge tests are conducted to measure the acceleration-sensitive errors in the sustained-linear-acceleration environment. These tests are conducted separately because it is assumed that linear superposition of the measured errors is a reasonable premise in instrument evaluation.

The purposes of gyro testing therefore include the following:

(a) verification of assembly procedures (commonly called acceptance tests)

(b) verification of design parameters (commonly called qualification or engineering evaluation tests)

(c) development of the gyro model equation

(d) development of advanced test techniques

(e) indication of the need for development of advanced test equipment (although test equipment *per se* is not covered in this chapter)

(f) determination of the reasons for failure to perform as expected (commonly called diagnostic tests)

Objective of this chapter

The objective of this chapter is to describe the reduction to practice of the gyro testing philosophy just presented. Emphasis throughout is on testing the single-degree-of-freedom floated integrating gyro at the MIT Instrumentation Laboratory, although two-degree-of-freedom gyro testing is discussed in Appendix A. The chapter is concerned primarily with the test and evaluation of inertial gyros for application in gimbaled or floated-type systems, but many of the test techniques and philosophies also apply to the test and evaluation of inertial gyros for application in strapdown systems (3).

After describing the MIT single-degree-of-freedom floated integrating gyro and

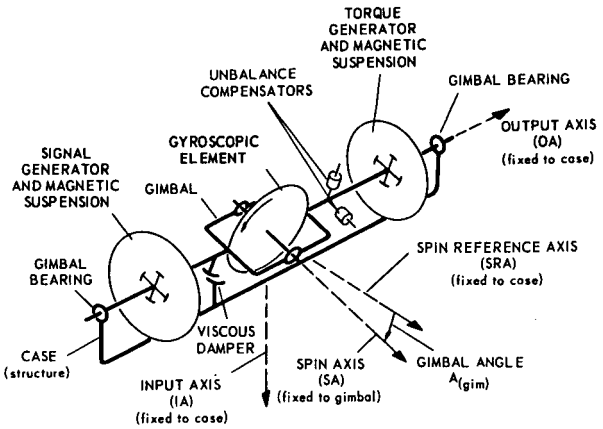

Fig. 5-1 Line schematic of the MIT single-degree-of-freedom floated integrating gyro

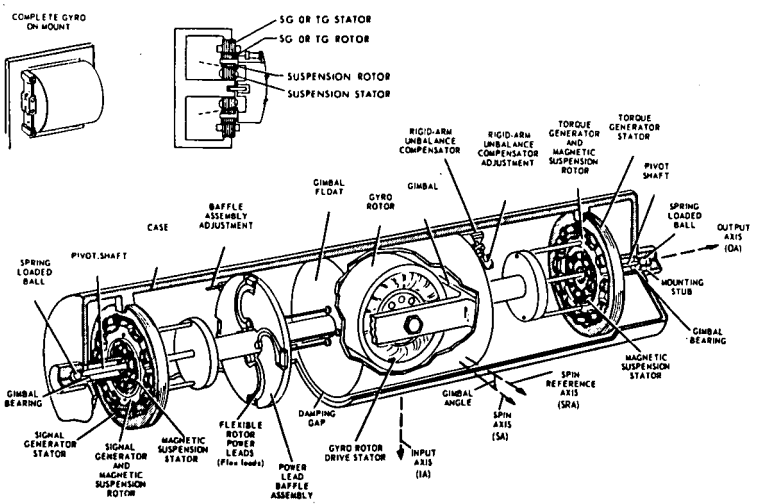

Fig. 5-2 Pictorial schematic of the MIT single-degree-of-freedom floated integrating gyro

certain basic terms in section 2, the gyro model equation is developed in section 3. Section 4 covers laboratory testing in the one-gravity environment. These tests include preliminary tests, which are intended to prove the integrity of the gyro assembly processes; calibration tests and short-term performance tests during which the gyro orientation is changed with respect to the local gravity vector while connected in a rate-feedback loop; and long-term performance tests on a servoed turntable. The tests are analyzed to compare their relative advantages and disadvantages, and multiple simultaneous gyro testing is discussed.

Testing in the higher-than-one-gravity environment is described in sections 5 and 6, which cover linear vibration and centrifuge tests. Section 7 describes angular vibration tests. Even at low amplitudes, these environments can cause appreciable changes in performance of the inertial-grade gyro.

Section 8 discusses the history of gyro data processing, the use of high-speed electronic computers in data processing and the application of digital techniques in gyro testing.

The overall basic philosophy and testing methods are summarized in section 9. A glossary of the terms and symbols used throughout is included at the end of the chapter.

2. Definitions - P. J. Palmer

Before proceeding to the development of the error model for the single-degree-of-freedom floated integrating gyro, it is well to describe the gyro itself and to establish standards (at least for this chapter) for certain items that to date are not standardized throughout the industry. Items that require definition are the concept of specific force and the polarity conventions for torque and drift rate.

The MIT Single-Degree-of-Freedom Floated Integrating Gyro (4-7)

Figures 5-1 and 5-2 are a line-schematic diagram and a pictorial-schematic diagram of the MIT single-degree-of-freedom floated integrating gyro. As figure 5-2 shows, the gyroscopic element (usually called the rotor or wheel) is mounted within the float. The float is supported by a highly viscous fluid inside the case. The float and case are hermetically sealed coaxial cylinders separated radially by a small damping gap. With this geometry, the damping restraint on the float about any radial axis is nearly 10 000 times greater than the value about the float axial or output axis (OA). The wheel spin axis (SA) is along a radial float axis and is therefore perpendicular to the float output axis. With the spin and output axes thus located by gyro construction, the most sensitive axis, the input axis (IA), is the radial axis positioned perpendicular to both the spin and output axes.

The direction of IA, OA and SA is in accordance with a right-handed Cartesian coordinate system. The spin axis is in the direction of the wheel spin vector when the wheel is rotating in its normal direction. In all cases, a positive direction may be determined by the right-hand rule in which the thumb is pointed along the vector toward the arrowhead. The fingers, when curled about the vector, point in the direction of positive rotation.

Since the gyro is operated within a few seconds of arc of the float null position, the spin and input reference axes can generally be considered to be synonomous

with the spin and input axes. This means that, for most practical purposes, IA, OA and SRA can be considered fixed with respect to the gyro case.

The gyro wheel is supported by either preloaded ball bearings or self-generating gas bearings. In operation, the wheel spins at a constant speed that is sustained by torque from a hysteresis-ring assembly within the rotor. This ring assembly is driven by an a.c. motor stator. The wheel assembly is enclosed in a hermetically sealed shell that forms an integral part of the gimbal, or float, as it is commonly called. The shell is filled with a gas at low pressure - helium, for example - which acts as a neutral atmosphere, tends to minimize windage losses, and thus serves as a thermal-conducting medium which tends to produce an even temperature distribution over all parts of the shell. Axial projections from either end of the float carry rotors for ducosyn electromagnetic units. A ducosyn unit is a dual electromagnetic device with an outer signal or torque generator and an inner, co-planar, magnetic-suspension device. The ducosyn stators are mounted in the gyro end housings. The signal generator is sensitive to rotation of the gimbal with respect to the case and produces an a.c. output voltage whose amplitude is proportional to the input angle and whose phase with respect to the excitation voltage depends on the direction of input-angle displacement. The torque generator receives an input current, which may be a.c., d.c., or pulses, and applies an output torque to the float proportional in magnitude to the product of the input-current magnitude and the excitation current magnitude. Both the input and the excitation current must be either a.c., or d.c. The direction of the output torque is determined by the relative phase or polarity, in the case of d.c., of the input current with respect to the phase or polarity of the excitation current. The rotors and stator cores of the dycosyn units are made of high-permeability low-hysteresis magnetic material in order to gain the maximum output and best response from given input currents.

Each of the ducosyn units also contains a magnetic-suspension device that senses radial or axial displacement of the rotors with respect to the stators and changes the magnetic-flux distribution in the gap so that a force acts on the rotors tending to return them to centralization with respect to the stators. Polished pivot shafts of tungsten carbide mounted on the outer ends of the float projections are accurately aligned with the float axis. These shafts fit inside watch-jewel-type bearings of polished tungsten carbide that are mounted in the case of the unit. Outside of these bearings, spring-loaded balls of polished tungsten carbide form end stones for the rounded ends of the pivot shafts.

The case of the gyro unit is hermetically sealed, and the clearance space between the outside of the gimbal float and the inside of the case is filled with a carefully degassed viscous fluid having a relatively high density. The mass of the float with respect to its volume is designed so that it has almost neutral buoyancy in the fluid. This condition depends on the average unit temperature, which is stabilized by means of a thermal-control housing that is assembled to the unit. Not shown in figure 5-2 are several expansion capsules that are partially depressed at the unit flotation temperature and maintain the fluid pressure at a small specified range with relatively large ($\pm 10^{\circ}$F) changes in temperature.

The fluid in the gyro unit supports the gimbal by flotation so that the residual weight supported by the magnetic suspension under one gravity is not more than a small fraction of a gram. Buoyancy and viscous-shear effects provide support for the float that automatically increases directly with the specific force due to shock, vibration and linear acceleration. This means that the force tending to move the float within the case depends on the residual unfloated mass, not on the total mass of the float. The residual force from one gravity is so small in comparison with the force acting on the float due to viscous effects in the fluid

that a long time period is required for the gimbal to move radially by a small amount. With this slow rate of response, the effects of shock, vibration and high acceleration in causing the float to move within the case are negligibly small, not only from the standpoint of damage to the gyro but also because there is no deterioration of performance. The combination of flotation and magnetic support from the ducosyn units makes it possible to keep the pivot shafts from making contact with their bearings even under the most severe environmental conditions. Starting with the shafts in contact with their bearings, some time (perhaps several minutes - depending, of course, on the magnetic-suspension stiffness, fluid viscosity and float mass) is required for the magnetic-suspension action to centralize the pivots. Once the pivots are centralized with the magnetic suspension remaining in action, the float remains free of rubbing-friction effects under any physically realizable environment of shock, vibration and acceleration; this statement ceases to hold if the mechanical abuse becomes so severe that the case is actually damaged. As long as the magnetic suspension is working (and, of course, the unit is at proper operating temperature), the uncertainty torque acting on the float is extremely small. It is important to note that the primary function of temperature control is to limit uncertainty torques by maintaining proper buoyancy of the float.

Viscous-shear forces acting across the damping gap between the case and the float provide the torque for the integrating action that gives the gyro unit its name, Starting with the spin axis in the position inside the case for which the signal generator has its null output level, a forced rotation of the gyro unit case about the input axis causes the gyro rotor to generate an output torque that tends to turn the spin axis toward the input axis. This torque is resisted by the inertia-reaction torque associated with accelerating the gimbal and by the drag torque due to viscous shear in the damping gap. When the case is given a constant angular velocity about the input axis, the gimbal movement with respect to the case goes through a transient period to finally reach a constant angular velocity. If the spin axis deflection angle is measured with respect to its initial position (as defined above) in the case (this initial position determines the spin-reference axis, a direction fixed to the case), the result is that the gimbal angle is proportional to the angular displacement of the case about the input axis, measured from its initial position, as the inertial-space reference. The net result of this action is that the gimbal angle is proportional to the rotation of the case with respect to inertial space about the input axis.

The gimbal angle produced by a given case rotation increases as the angular momentum of the gyro rotor is made greater and decreases as the viscosity of the fluid in the case is increased. In effect, the viscosity of the fluid controls the angle input-gimbal angle output sensitivity of the gyro unit. This sensitivity generally affects the overall gain of the system in which the gyro unit is used. Ordinarily, the unit is used in a feedback arrangement that continues to operate properly even if sensitivity changes of 10 to 20 percent occur. With a change of four percent in viscosity per degree Fahrenheit change in fluid temperature, several degrees of change in gyro unit temperature can be tolerated in practical applications of gyro units. This tolerance is somewhat wider than the tolerance determined by the flotation problem.

Inertia-reaction torque on the float interacting with viscous-shear torque causes the gimbal to behave as a first-order system. In practice, the characteristic time (equivalent to the time constant of a resistance-capacitance circuit) of a properly designed gyro unit is in the vicinity of one millisecond.

The power for driving the gyro rotor is carried to the gimbal by means of flexible semicircular metallic leads that are almost perfectly floated in the non-

conducting damping fluid. Immersion in the fluid greatly improves the cooling of the leads and so increases the safe current-carrying capacity. Flotation in the viscous fluid reduces the distorting effects that occur when the unit is subjected to changes in the direction of gravity or to high linear accelerations. The four flexible leads (three for the stator leads and one for grounding the float) have their outer ends mounted on insulated terminals around the circumference of a rotatable baffle plate. With the unit completely assembled and in normal operation, the angular position of the baffle in the case may be adjusted from outside the unit to minimize the torque on the gimbal due to elastic effects in the leads.

The power-lead baffle has clearance grooves along each flexible lead. These grooves are so small that solidification of the fluid at low temperatures cannot produce forces large enough to damage the flex leads.

As noted in section 1, inertial gyro units of reasonable performance must have extremely small drift rates. Let us assume a drift-rate specification of 1 meru. The basic gyroscope equation relating drift rate about the input axis to torque about the output axis is

$$\overline{M}_O = \overline{H} \times \overline{W}_{(IC)\,I} \qquad \text{(Eq. 5-1)}$$

where

$\overline{M}_O$ = torque about the gyro output axis in dyne-cm

$\overline{H}$ = angular momentum of the gyro rotor

= wheel inertia times speed of wheel rotation

= 2×10^6 gm-cm^2/sec (assumed value)

$\overline{W}_{(IC)I}$ = angular velocity of the gyro case with respect to inertial space about the gyro input axis

= 1 meru = 7.28×10^{-8} rad/sec (assumed drift specification)

Substituting values for H and $W_{(IC)I}$ in equation 5-1 and solving gives a torque about the gyro output axis of only 0.145 dyne-cm that will cause a gyro drift rate of one meru. An approximation that may be applied in describing the physical requirements is

$$m_w g \left[(U)d_{(Ocm)} \right] = 0.145 \text{ dyne-cm} \qquad \text{(Eq. 5-2)}$$

where

m_w = mass of wheel

= 250 grams (assumed value)

g = local gravity

= 980 cm/sec^2

$(U)d_{(Ocm)}$ = uncertainty in the distance between the output axis and the center of mass of the wheel in cm

Therefore, for this size wheel

$$(U)d_{(Ocm)} = \frac{0.145}{250 \times 980} \approx 6 \times 10^{-7} \text{ cm} \approx 0.24 \times 10^{-6} \text{ in.} \qquad \text{(Eq. 5-3)}$$

This result shows that, to maintain the uncertainty level in torque that may be realized in this case, the mass center of the wheel must maintain its position with respect to the output axis within about 6×10^{-7} centimeters. It is interesting to note that this arm-length uncertainty is only about ten times the crystal-lattice size of the materials ordinarily used for gimbal construction (aluminum, beryllium or iron - the crystal-lattice size of these lies in the range of 2 to 4 angstrom units: 2×10^{-8} to 4×10^{-8} cm). Techniques for balancing float assemblies within this dimensional tolerance before the complete gyro unit is tested do not exist. For this reason, it is necessary to provide externally available means for float unbalance compensation. The final settings for these compensators are made by observing the effects on the drift rate of the gyro unit under actual operating conditions that accompany changes in the compensator adjustments.

Table 5-1 presents the results of similar calculations carried out for four assumed performance specifications. For these calculations, it was assumed that the gyro wheel was moving along its spin axis. The table shows that to achieve gyro performance of 0.01 meru, for example, the wheel location must be stable to within 0.006 centimeter, or 0.6 angstrom unit. Obviously, measurements cannot be made directly to this order of accuracy; and therefore, the precision gyro must literally be used to test itself.

Table 5-1 Gyro-wheel center-of-mass stability requirements in the one-gravity field

For performance of:			Axial wheel stability must be better than:	
Meru	Deg/hr	$\widehat{\text{Sec}}$/hr	Centimeters	Angstroms
1	1.5×10^{-2}	54	0.6	60
0.1	1.5×10^{-3}	5.4	0.06	6
0.01	1.5×10^{-4}	0.54	0.006	0.6
0.001	1.5×10^{-5}	0.054	0.0006	0.06

Notes:
1. 1 second of arc on earth's surface ≈ 100 feet
2. 250-gm wheel with an angular momentum of 2×10^6 gm-cm^2/sec

Anisoelasticity of the gimbal and rotor-bearing assembly (that is, the condition that exists when the elastic coefficient for deflections of the rotor in the gimbal along the spin axis is different from the corresponding elastic coefficient for deflections at right angles to the spin axis) must be held within reasonable limits if good performance is to be realized. To reduce the effects of anisoelasticity, the gimbal is constructed of beryllium, which has an extremely high stiffness (modulus of elasticity - this in kg/cm^2 is 31.1×10^5 for beryllium, 20.5×10^5 for 52100 steel, and 7.3×10^5 for 2024 aluminum); and the most desirable bearing contact angle is chosen. In addition, anisoelasticity can be compensated by spring-mounted weights whose shift under acceleration balances the corresponding shift of the gyro element (8).

Specific Force

Specific force, ($\overline{SF}$), can be considered a vector specifying a quantity being sensed by an instrument in a vehicle. If the vehicle is stationary with respect to a nonrotating earth, a pendulum suspended within the vehicle will line up with the gravity vector, $\overline{G}$. On the other hand, if the vehicle is subjected to an acceleration,

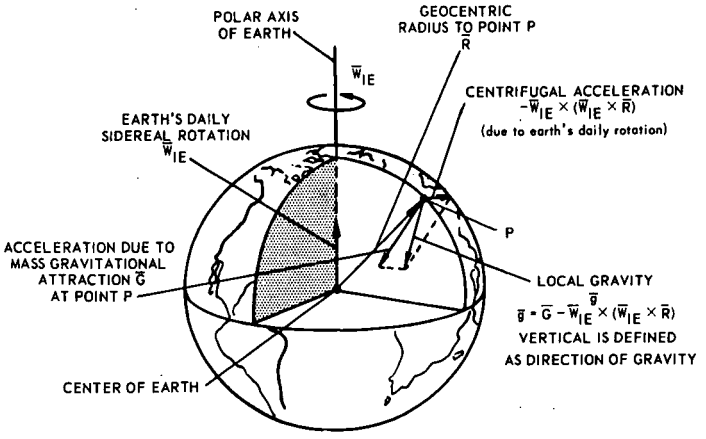

Fig. 5-3 Factors defining local gravity

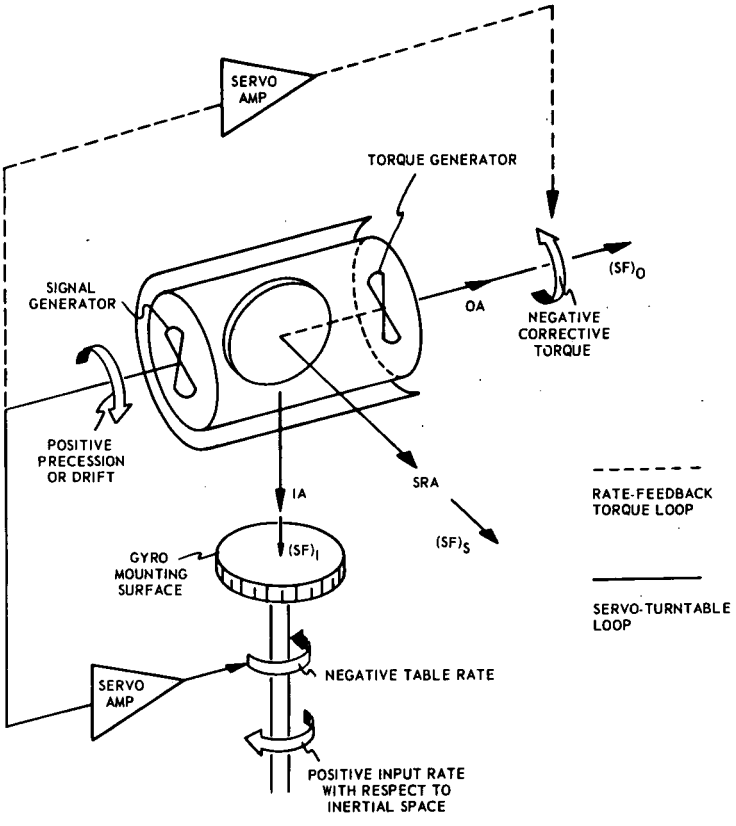

Fig. 5-4 Polarity conventions for gyro torque and drift rate

the pendulum will detect a change because of the additional force produced by the vehicle acceleration. If the vehicle accelerates forward, the pendulum will lag as a result of this additional force. The angle that the pendulum makes with the gravitational vector will be the result of the addition of the vectors $\overline{G}$ and $p_i^2\,\overline{R}$ (the vehicle acceleration vector with respect to inertial space). The resultant vector is the specific-force vector, which expressed in equation form is

$$\overline{SF} = \overline{G} - p_i^2\overline{R}$$

$$= \overline{G} - \overline{a} \qquad \text{(Eq. 5-4)}$$

where

$\overline{SF} = \overline{SRF}$ = specific mass reaction force at a point equal in magnitude and direction to the force that a unit mass with the location and acceleration of the point applies to its supporting structure. This is commonly called specific force.

$\overline{G}$ = acceleration due to mass gravitational attraction

$p_i^2\overline{R} = \overline{a}$ = second derivative with respect to inertial space of the vector $\overline{R}$ from the center of the earth to a point P on the surface of the earth (Fig. 5-3) (9).

Local gravity, $\overline{g}$, is the vector resultant of the acceleration due to mass gravitational attraction and the centrifugal acceleration due to the earth's daily rotation, or

$$\overline{g} = \overline{G} - \overline{W}_{IE} \times (\overline{W}_{IE} \times \overline{R}) \qquad \text{(Eq. 5-5)}$$

where

$\overline{W}_{IE}$ = angular velocity of the earth with respect to inertial space

$= 7.272205 \times 10^{-5}$ rad/sec (sidereal time) (10)

$\overline{R}$ = radius of the earth

$-\overline{W}_{IE} \times (\overline{W}_{IE} \times \overline{R})$ = centrifugal acceleration due to the earth's daily rotation

Solving equation 5-5 for $\overline{G}$ and substituting the result in equation 5-4 gives

$$\overline{SF} = \overline{g} + \overline{W}_{IE} \times (\overline{W}_{IE} \times \overline{R}) - \overline{a} \qquad \text{(Eq. 5-6)}$$

If a unit mass is stationary with respect to the earth, its acceleration, $\overline{a}$, with respect to inertial space is the centripetal acceleration $\overline{W}_{IE} \times (\overline{W}_{IE} \times \overline{R})$. Equation 5-6 then reduces to

$$\overline{SF} = \overline{g} \qquad \text{(Eq. 5-7)}$$

Torque and Drift Rate

Figure 5-4 illustrates polarity conventions for torque and drift rate. A positive input rate with respect to inertial space is arbitrarily defined as a positive rotation about the gyro input axis. This input rate causes the gyro to precess in the positive direction about its output axis as indicated at the signal-generator end of the gyro. In servo-loop operation, the resulting signal-generator output voltage is amplified and applied to the test-table-drive motor to drive the table in the negative direction about the input axis. In rate-feedback-loop operation, the signal-generator output is amplified and applied to the gyro torque generator, which torques the float in the negative direction back to the signal-generator null position.

Specific force directed along positive IA, OA and SRA is considered positive; along negative IA, OA and SRA, it is considered negative. Likewise, a mass unbalance along a positive axis, for example, is considered positive and along a negative axis, negative. This convention will result in a polarity of unbalance torque that will agree with the precessional torque generated by a positive rate input about IA. It is necessary to maintain these conventions if a consistent set of error model equations is to be developed.

In the discussion of gyro performance, it is desirable to convert easily from rate units to torque units. Since the gyro precessional torque about the output axis is equal to the angular momentum of the gyro wheel multiplied by the angular velocity about the input axis, an angular velocity of one earth-rate unit about the input axis results in one earth-rate torque about the output axis. The relationships are as follows:

Earth-Rate Units:	Torque Units:
1 eru = 15 deg/hr	HW_{IE} dyne-cm
1 meru = 0.015 deg/hr	$\frac{HW_{IE}}{1000}$ dyne-cm

With a gyro on servo test, the gyro drift, which is that part of the turntable rate due to gyro error and uncertainty, is, in meru

$$(U)W_{ET} = 1000 \left[\frac{W_{ET} - W_{IE}}{W_{IE}} \right] = 1000 \left[\frac{W_{ET}}{W_{IE}} - 1 \right] \qquad \text{(Eq. 5-8)}$$

where

W_{ET} = angular velocity of the test turntable with respect to the earth

$(U)W_{ET}$ = that part of the angular velocity of the test turntable with respect to the earth due to gyro error and uncertainty

However, the test turntable is rotating in a direction such as to cancel the earth's angular velocity input to the gyro and the gyro drift. In other words, the gyro drift is in the opposite direction from the test turntable rotation. Therefore, to obtain the gyro drift equation 5-8 must be multiplied by -1. Thus, gyro drift, W_d, in meru is

$$W_d = 1000 \left[1 - \frac{W_{ET}}{W_{IE}} \right] \qquad \text{(Eq. 5-9)}$$

3. Single-Degree-of-Freedom Gyro Model Equations - P.J. Palmer

As stated in section 1, gyro testing philosophy at MIT is predicated on knowledge of a model equation that accurately defines the gyro performance. The model equation is used to measure and specify gyro quality, to provide information for error compensation during the gyro's use in an inertial system, and as a basis for diagnostic testing.

For convenience, the model equation for the single-degree-of-freedom floated integrating gyro is treated in two separate parts - a so-called steady-state error

model and a so-called dynamic performance function. Both parts are derived in the following subsections.

Steady-State Error Model

History. Today's steady-state error model of the single-degree-of-freedom floated integrating gyro comprises ten terms. Not too many years ago, however, the gyro error model comprised only three terms: a bias term independent of specific force and two mass-unbalance terms proportional to specific force (for mass unbalance along SRA and IA). Gyro performance in those days was crude by today's standards and only the major terms could be measured. The others were masked by the gyro uncertainty.

As gyro performance improved, another term became evident in the test data that was a function of specific force squared. Analysis showed that this term was caused by anisoelasticity of the float assembly; in other words, the float was not equally stiff in all directions. At the time, it was assumed that the compliance axes were aligned with the gyro axes, and that there was a single compliance term. This added a fourth term to the model equation.

When tumbling tests with the gyro output axis parallel to the earth's axis and the table axis were started, it was assumed that a second harmonic sine term would be evident in the Fourier analysis of each revolution of unbalance data because of the gyro compliance. However, a second harmonic cosine term also appeared. This was explained by assuming that the compliance axes were not aligned with the gyro axes but were in the IA-SRA plane. The two compliance terms were called major and minor compliance, and the error model had grown to five terms.

Further analysis and testing led to the three-dimensional theory of compliance, which postulated that the compliance axes were neither aligned with the gyro axes nor in the IA-SRA plane. The error model then comprised eight terms.

Although it was believed that the gyro was completely described mathematically by the eight-term error model, discrepancies continued to be evident in the test data in certain orientations. Further extensive testing and analysis showed that first one and then another additional term should be considered in the error model, making a total of ten terms. These last two terms were functions of specific force and specific force squared along the output axis.

Up to this time, the gyro error model had usually been written in physical terms such as mass unbalances and compliances which could be easily visualized. With the addition of the last two terms, however, the state-of-the-art had advanced to the point where the physical situation could no longer be as easily visualized. For example, how can a specific force along an axis cause a torque about that axis ? In addition, error terms that heretofore had been designated simply as mass unbalance were now known to consist of not only mass-unbalance but also temperature-gradient effects, unit-average-temperature-change effects, wheel-power-change effects, etc. For these reasons, it was decided to convert from a strictly physical error model to a mathematical model, which is a description of the physical properties of the gyro in mathematical form.

Today's Model. From experience, we know that gyro drift is composed of three basic components: a component insensitive to specific force, a component proportional to specific force, and a component proportional to specific force squared, or

$$W_d = \frac{M_O}{HW_{IE} \times 10^{-3}} = C_O + C_1(SF) + C_2(SF)^2 \qquad \text{(Eq. 5-10)}$$

Rewriting specific force in terms of components along the gyro axes and including all possible combinations, equation 5-10 becomes

$$\begin{aligned} W_d = {} & +D_F + D_I(SF)_I + D_S(SF)_S + D_O(SF)_O \\ & +D_{II}(SF)_I^2 + D_{SS}(SF)_S^2 + D_{OO}(SF)_O^2 \\ & +D_{IS}(SF)_I(SF)_S + D_{OS}(SF)_O(SF)_S + D_{IO}(SF)_I(SF)_O \end{aligned} \qquad \text{(Eq. 5-11)}$$

where

D_F = gyro drift rate in meru that is insensitive to specific force

D_I, D_S, D_O = gyro drift rate in meru/g that is proportional to specific force along IA, SRA and OA, respectively

D_{II}, D_{SS}, D_{OO} = gyro drift rate in meru/g^2 that is proportional to specific force squared along IA, SRA and OA, respectively

D_{IS}, D_{OS}, D_{IO} = gyro drift rate in meru/g^2 that is proportional to the product of specific force along IA and SRA, OA and SRA, and IA and OA, respectively. The order of the subscripts is unimportant; in other words, it is assumed that $D_{IS} = D_{SI}$, etc.

$(SF)_I$, $(SF)_S$, $(SF)_O$ = specific force in g's directed along IA, SRA and OA, respectively

Equation 5-11 describes the steady-state operation of a single-degree-of-freedom floated integrating gyro assuming that (11):

(a) the gyro is operating in a closed servo or torque loop. This implies that the spin and spin reference axes are maintained so nearly coincident that cross-coupling effects are negligible.

(b) the gyro is isolated from linear and angular oscillations so that cylindrical and anisoelastic resonance effects as well as coning torques are negligible.

(c) no terms exist higher than second-order specific-force-dependent terms.

(d) gyroscopic torque due to angular rate inputs about the gyro input axis and command torque generated by the gyro torque generator are zero.

Substituting equation 5-4 into equation 5-11 gives

$$\begin{aligned} W_d = {} & +D_F + D_I(G_I - a_I) + D_S(G_S - a_S) + D_O(G_O - a_O) \\ & +D_{II}(G_I - a_I)^2 + D_{SS}(G_S - a_S)^2 + D_{OO}(G_O - a_O)^2 \\ & +D_{IS}(G_I - a_I)(G_S - a_S) + D_{OS}(G_O - a_o)(G_S - a_S) \\ & +D_{IO}(G_I - a_I)(G_O - a_O) \end{aligned} \qquad \text{(Eq. 5-12)}$$

where

G_I, G_S, G_O = components of acceleration in g's due to mass gravitational attraction directed along IA, SRA and OA, respectively

a_I, a_S, a_O = total acceleration in g's directed along IA, SRA and OA, respectively

Equation 5-12 is valid either for inertial system or test laboratory use. However, a more convenient equation for test laboratory use can be obtained by substituting equation 5-7 into equation 5-11 , which results in

$$W_d = +D_F + D_I g_I + D_S g_S + D_O g_O + D_{II} g_I^2 + D_{SS} g_S^2 + D_{OO} g_O^2 + D_{IS} g_I g_S + D_{OS} g_O g_S + D_{IO} g_I g_O \qquad \text{(Eq. 5-13)}$$

where

g_I, g_S, g_O = components of local gravity in g's directed along IA, SRA and OA, respectively

Equation 5-11 and 5-13 are the forms of the error model for the single-degree-of-freedom floated integrating gyro most useful to the gyro test engineer today. The word 'today' must not be neglected, because there is no reason to believe that the error model will not continue to expand as gyro performance is improved and as new and more stringent environments are encountered. For example, already there is some analytical evidence that additional terms exist that are proportional to the fourth power of specific force (12, 13). Although their magnitude is small at one-g, these terms may be significant in high-g environments.

The physical significance of the various terms comprising equation 5-11 is discussed in the following paragraphs.

Acceleration-Insensitive Drift. The fixed or bias term, D_F, of the error model equation comprises all of the effects causing gyro drift that are insensitive to acceleration. These effects include:

(a) power-lead torque

(b) signal-generator reaction torque, which is proportional to signal-generator excitation current squared

(c) magnetic-suspension reaction torque, which is proportional to magnetic-suspension excitation current squared

(d) time rate of change of the above three

(e) float radial and axial velocity effects

In equation form

$$D_F = R(1 + P_R t) + D_{dS}\dot{d}_S + D_{dI}\dot{d}_I + D_{dO}\dot{d}_O \qquad \text{(Eq. 5-14)}$$

where

R = drift in meru due to items (a), (b) and (c) above

P_R = time-dependent change in R in sec^{-1}

t = time in seconds

D_{dS}, D_{dI}, D_{dO} = gyro drift sensitivity to rate of linear float displacement along SRA, IA and OA, respectively, in meru/cm/sec

$\dot{d}_S$, $\dot{d}_I$, $\dot{d}_O$ = rate of linear float displacement along SRA, IA and OA, respectively, in cm/sec

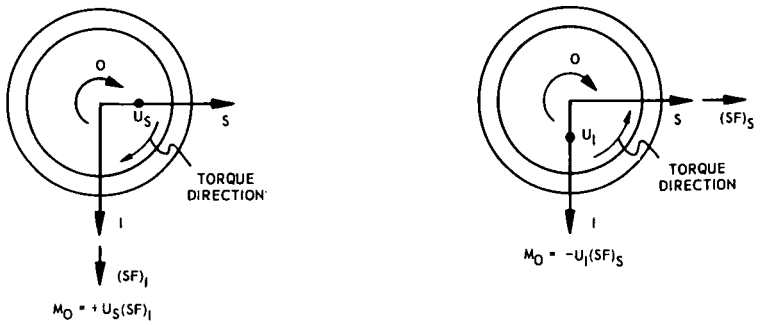

(a) Mass unbalances

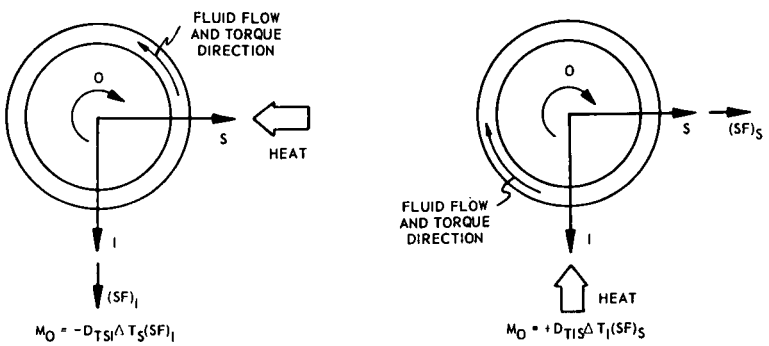

(b) Thermal gradients

Fig. 5-5 Polarity definitions of acceleration-sensitive terms

Acceleration-Sensitive Drift. The three acceleration-sensitive coefficients of the error-model equation comprise all of the effects causing gyro drift that are proportional to the first-power of acceleration. These include:

(a) mass unbalance torque

(b) mass unbalance torque change with time

(c) torque due to temperature gradients across the gyro. This torque is made up of fluid torque, torque due to float center-of-buoyancy shift and torque due to float center-of-mass shift.

(d) torque due to temperature gradients changing with time

(e) torque due to average gyro unit temperature change

(f) torque due to wheel voltage change

Average gyro unit temperature and wheel voltage, however, are usually held within closely prescribed limits. Neglecting torques due to these latter two effects, the steady-state acceleration-sensitive drift can be expressed in equation form as

$$D_I (SF)_I = [U_S (1 + P_S t) - D_{TSI} \Delta T_S] (SF)_I$$

$$D_S (SF)_S = [-U_I (1 + P_I t) + D_{TIS} \Delta T_I] (SF)_S \qquad \text{(Eq. 5-15)}$$

$$D_O (SF)_O = [U_O (1 + P_O t) + D_{TOO} \Delta T_O] (SF)_O$$

where

U_S, U_I = mass unbalance in meru/g along SRA and IA, respectively

U_O = proportionality coefficient in meru/g relating drift component to specific force along the output axis

P_S, P_I, P_O = time dependent change in U_S, U_I and U_O, respectively, in sec^{-1}

D_{Txy} = gyro drift sensitivity in meru/g°F to a combination of temperature gradient along x and specific force along y

ΔT_S, ΔT_I, ΔT_O = temperature gradients across the gyro along SRA, IA and OA, respectively

The algebraic signs of each of the terms has physical significance in that a plus sign denotes a positive torque or drift while a negative sign denotes a torque or drift in the opposite direction. The polarity of the $(SF)_O$ term was arbitrarily chosen as positive in the error model. The physical significance of the other polarities is illustrated in figure 5-5. Note that in figure 5-5a a mass unbalance along positive SRA, $+U_S$, reacts with a specific force along positive IA, $+ (SF)_I$, to give a torque in the positive direction about OA. A mass unbalance along positive IA, $+ U_I$, on the other hand, reacts with a specific force along positive SRA, $+ (SF)_S$, to give a negative torque about OA. When a thermal gradient is impressed across the gyro from +SRA to -SRA as in the left-hand sketch of figure 5-5b, the fluid at +SRA becomes hotter, less dense, and flows in the direction indicated as a result of $(SF)_I$. The resulting torque is in the negative direction. When heat is impressed on +IA as shown in the right-hand sketch, the fluid flow is such as to cause a positive torque about OA.

Acceleration-Squared-Sensitive Drift. The six acceleration-squared-sensitive drift terms of the error model are the gyro compliance terms, which result from the

fact that the gyro structure is not equally stiff in all directions. These terms are the most stable of all of the error terms and, to date at least, have shown no change with time or variation with environmental changes such as temperature. The physical significance of the various compliance terms is

$$
\begin{aligned}
D_{II}(SF)_I^2 &= K_{SI}(SF)_I^2 \\
D_{SS}(SF)_S^2 &= K_{IS}(SF)_S^2 \\
D_{OO}(SF)_O^2 &= K_{OO}(SF)_O^2 \\
D_{IS}(SF)_I(SF)_S &= (K_{SS} - K_{II})(SF)_I(SF)_S \\
D_{OS}(SF)_O(SF)_S &= (K_{OS} - K_{IO})(SF)_O(SF)_S \\
D_{IO}(SF)_I(SF)_O &= (K_{OI} + K_{SO})(SF)_I(SF)_O
\end{aligned}
\qquad \text{(Eq. 5-16)}
$$

where

K_{xy} = compliance along x due to a specific force along y in meru/g^2

$= m^2 K'_{xy}$

K'_{xy} = displacement along x due to a specific force along y

m = displaced mass (which may be different along each axis)

The algebraic signs of the compliance terms have physical significance similar to those of the acceleration-sensitive terms and may be determined in like manner. Let d_K be the displacement of the center of gravity of the float resulting from compliance of the wheel, bearing and gimbal assembly. Then

$$
\begin{aligned}
d_K = {} & [\text{displacement along SRA}] \\
& + [\text{displacement along IA}] \\
& + [\text{displacement along OA}] \\
= {} & [K'_{SS}\, m(SF)_S + K'_{SI}\, m(SF)_I + K'_{SO}\, m(SF)_O] \\
& + [K'_{IS}\, m(SF)_S + K'_{II}\, m(SF)_I + K'_{IO}\, m(SF)_O] \\
& + [K'_{OS}\, m(SF)_S + K'_{OI}\, m(SF)_I + K'_{OO}\, m(SF)_O]
\end{aligned}
\qquad \text{(Eq. 5-17)}
$$

Torque due to compliance, M_K, is

$$
\begin{aligned}
M_K = {} & m(SF)_I\, [\text{displacement along SRA}] \\
& - m(SF)_S\, [\text{displacement along IA}] \\
& + m(SF)_O\, [\text{displacement along OA}]
\end{aligned}
\qquad \text{(Eq. 5-18)}
$$

Substituting equation 5-17 into equation 5-18 and replacing the m^2K' in each term with K, the compliance torque equation becomes

$$
\begin{aligned}
M_K = {} & K_{SI}(SF)_I^2 - K_{IS}(SF)_S^2 + K_{OO}(SF)_O^2 + (K_{SS} - K_{II})(SF)_I(SF)_S \\
& + (K_{OS} - K_{IO})(SF)_O(SF)_S + (K_{OI} + K_{SO})(SF)_I(SF)_O
\end{aligned}
\qquad \text{(Eq. 5-19)}
$$

Dynamic Performance Function

Basic Equations of Motion. For the purpose of deriving a basic equation of motion for a single-degree-of-freedom floated integrating gyro, certain simplifying assumptions may be made that do not affect the useful validity of the results (4). These are:

(a) no gyro torque uncertainties exist

(b) the spin axis and the spin-reference axis remain essentially co-incident

(c) the gyro rotor spins about an axis of symmetry

(d) the gyro rotor spins at a constant speed

(e) the spin angular momentum is much greater than the nonspin angular momentum

(f) the center of mass of the rotor coincides with the center of mass of the float.

(g) the rotor-bearing structure is rigid

(h) the electromagnetic components, power leads, etc., are ideal

The basic equation of motion of the gyro float can be shown to be (Figs. 5-6 and 5-7)

$$I_O \ddot{A}_{(IF)O} + c_{(CF)O} \dot{A}_{(CF)O} = HW_{(IC)I} + M_{tg} \qquad \text{(Eq. 5-20)}$$

where

$A_{(IF)O}$ = $A_{(IC)O} + A_{(CF)O}$
= angle of the gyro float with respect to inertial space about the gyro output axis in radians

$A_{(IC)O}$ = angle of the gyro case with respect to inertial space about the gyro output axis in radians

$A_{(CF)O}$ = angle of the gyro float with respect to the case about the gyro output axis in radians

I_O = moment of inertia of the gyro float about the gyro output axis in gm-cm^2

$c_{(CF)O}$ = damping coefficient between the gyro float and case about the gyro output axis in dyne-cm/rad/sec

H = angular momentum of the gyro wheel in gm-cm^2/sec

$W_{(IC)I}$ = angular velocity of the gyro case with respect to inertial space about the input axis in rad/sec

M_{tg} = command torque applied to the float by the gyro torque generator in dyne-cm

Equation 5-20 can be rewritten in operational form as

$$p^2 I_O A_{(IC)O} + p^2 I_O A_{(CF)O} + p c_{(CF)O} A_{(CF)O} = HW_{(IC)I} + M_{tg} \qquad \text{(Eq. 5-21)}$$

Solving for $A_{(CF)O}$ and substituting τ for the ratio $I_O / c_{(CF)O}$, equation 5-21 becomes

$$A_{(CF)O} = \frac{1}{p(\tau p + 1)} \left[\frac{H}{c_{(CF)O}} W_{(IC)I} + \frac{M_{tg}}{c_{(CF)O}} - \tau p^2 A_{(IC)O} \right] \qquad \text{(Eq. 5-22)}$$

where

τ = the gyro first-order characteristic time

The gyro output signal, e_{sg}, is

$$e_{sg} = A_{(CF)O} S_{sg} \qquad \text{(Eq. 5-23)}$$

where

S_{sg} = signal-generator angle input - voltage output sensitivity in mv/mrad

Note from equations 5-22 and 5-23 that, in the absence of case angular acceleration about the output axis, the gyro output signal, e_{sg}, is directly related to the sum of the input-axis angular velocity and the command torque. Even if an angular acceleration exists about the output axis, the acceleration is multiplied by the first-order characteristic time, τ, which in present-day inertial gyro units is of the order of 0.001 second: the first-order characteristic time of the gyro can be measured by employing an angular vibrator (14, 15) or by applying a step change in angular velocity about the input axis (16). Also in a gimbaled inertial guidance system, the three gyros form a mutually defensive arrangement so that the interfering effects of inputs about the output axis are generally negligible. In applications where the gyro units are not so arranged, such as a strapdown system, the effects of these inputs may be important. Note also that the change in gyro output signal due to an input angular rate about the input axis is proportional to the time integral of the angular rate in the low-frequency region

$$A_{(CF)O} = \frac{H}{c_{(CF)O}} \int_0^t \frac{W_{(IC)I}}{(\tau p + 1)} \qquad \text{(Eq. 5-24)}$$

and in the steady-state case

$$A_{(CF)O} = \frac{H}{c_{(CF)O}} \int_0^t W_{(IC)I} \qquad \text{(Eq. 5-25)}$$

Since a constant of integration is required to solve this time integral, the ideal integrating gyro does not have a preferred position of output angle and must be used in a nulling-type servo loop.

If the initial conditions are taken as zero

$$\frac{W_{(CF)O}}{W_{(IC)I}} = \frac{A_{(CF)O}}{A_{(IC)I}} = \frac{H}{c_{(CF)O}} \qquad \text{(Eq. 5-26)}$$

where the ratio of H to $c_{(CF)OA}$ is commonly referred to as the angular gain or rate gain of the gyro.

Higher Order Effects. Some years, ago, Dr. Robert K. Mueller of the Instrumentation Laboratory explained a noted difference in the measured characteristic time of the single-degree-of-freedom integrating gyro unit and the characteristic time calculated from the angular momentum and the output-axis damping by including the effects of gimbal and spin-axis-bearing compliance about the input axis (17). If the lumped stiffness of the gyro spin-axis bearings and gimbal about the input and output axes, $K_{(FW)I}$ and $K_{(FW)O}$, are included, the gyro performance function can be shown to be the following third-order equation (18).

$$\frac{A_{(CF)O}}{A_{(IC)I}} = \frac{H}{c_{(CF)O}} \cdot \frac{1}{\frac{H^2 I_O}{K_{(FW)O} K_{(FW)I} c_{(CF)O}} p^3 + \frac{H^2}{K_{(FW)O} K_{(FW)I}} p^2 + \frac{I_O}{c_{(CF)O}} + \frac{H^2}{K_{(FW)I} c_{(CF)O}} p + 1} \qquad \text{(Eq. 5-27)}$$

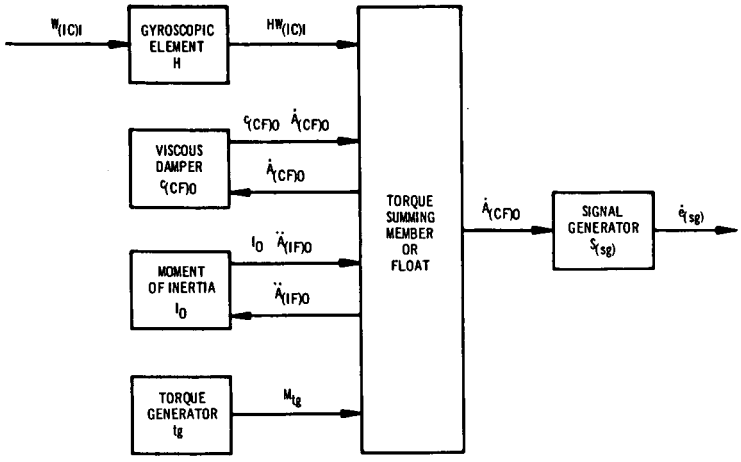

Fig. 5-6 Functional diagram for the single-degree-of-freedom floated integrating gyro

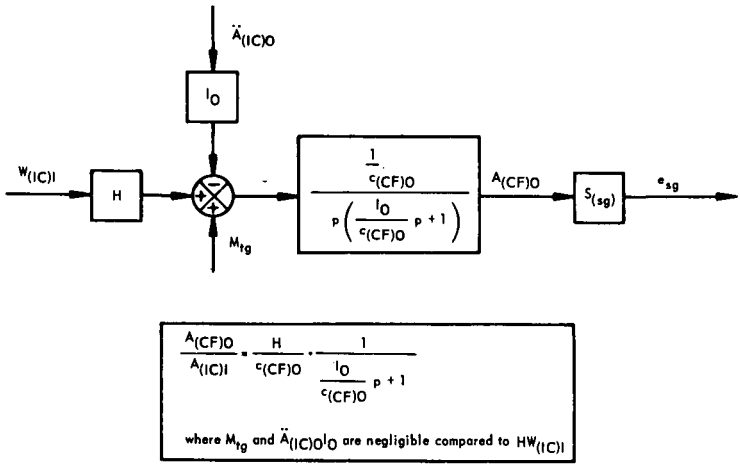

Fig. 5-7 Representation of first-order equation of motion of the single-degree-of-freedom floated integrating gyro unit

where

$K_{(FW)O}$ = lumped stiffness of the gyro wheel with respect to the float about the output axis in dyne-cm/rad

$K_{(FW)I}$ = lumped stiffness of the gyro wheel with respect to the float about the input axis in dyne-cm/rad

(a) as before, the steady-state (i.e., as $p \to 0$) sensitivity ratio of the gyro unit is

$$\frac{A_{(CF)O}}{A_{(IC)I}} = \frac{H}{c_{(CF)O}} \qquad \text{(Eq. 5-26) (repeated)}$$

(b) for relatively low frequencies, only the two lowest-order terms in the denominator of equation 5-27 are important. The performance function is then approximated by

$$\frac{A_{(CF)O}}{A_{(IC)I}} = \frac{H}{c_{(CF)O}} \cdot \frac{1}{1 + \tau p} \qquad \text{(Eq. 5-28)}$$

The magnitude of equation 5-28 can be expressed as

$$\left|\frac{A_{(CF)O}}{A_{(IC)I}}\right| = \frac{H}{c_{(CF)O}} \left(\frac{1}{1 + \tau^2\omega^2}\right)^{1/2} \qquad \text{(Eq. 5-29)}$$

and the phase angle as

$$DRA = -\tan^{-1}(\tau\omega) \qquad \text{(Eq. 5-30)}$$

where

ω = frequency in rad/sec

DRA = dynamic response angle in radians

$$\tau = \frac{I_O}{c_{(CF)O}} + \frac{H^2}{K_{(FW)I}c_{(CF)O}} = \frac{I_O}{c_{(CF)O}}\left[1 + \frac{H^2}{I_O K_{(FW)I}}\right] \qquad \text{(Eq. 5-31)}$$

The ratio $I_O/c_{(CF)O}$ is the first-order characteristic time of the gyro unit if $K_{(FW)I}$ is infinite. It can be seen from equation 5-31 that the first-order characteristic time is increased by the square of the angular momentum of the gyro wheel divided by the product $I_O K_{(FW)I}$. Thus, at low frequencies, $K_{(FW)I}$ is an important parameter in determining gyro dynamics.

(c) for medium frequencies, the effects of $K_{(FW)O}$ may become important.

(d) for high frequencies, the performance of the gyro must be approximated by a third-order system. The additional phase shift must be accounted for in the design of high-performance servo systems that use gyros.

The dynamic effects of adding output-axis suspension stiffness (for example, magnetic suspension or reed suspension) to the gyro dynamics has been investigated (20). The drift torques and dynamic effects due to angular vibrations are discussed in section 7.

The actual performance of the gyro is also distorted by motion of the case about

the output axis with respect to inertial space. If there is case motion, the equation relating the float-to-case motion about OA to the case-to-inertial space motion becomes

$$\frac{A_{(CF)O}}{A_{(IC)O}} = -\frac{\dfrac{I_O H^2}{K_{(FW)O}K_{(FW)I}C_{(CF)O}}p^3 + \dfrac{I_O}{C_{(CF)O}} + \dfrac{H^2}{C_{(CF)O}K_{(FW)I}}p}{\dfrac{I_O H^2}{K_{(FW)O}K_{(FW)I}C_{(CF)O}}p^3 + \dfrac{H^2}{K_{(FW)O}K_{(FW)I}}p^2 + \dfrac{I_O}{C_{(CF)O}} + \dfrac{H^2}{C_{(CF)O}K_{(FW)I}}p + 1} \qquad \text{(Eq. 5-32)}$$

(a) in the steady state as $p \longrightarrow 0$

$$\frac{A_{(CF)O}}{A_{(IC)O}} = 0 \qquad \text{(Eq. 5-33)}$$

(b) for relatively low frequencies, the input-output relationship may be expressed as

$$\frac{A_{(CF)O}}{A_{(IC)O}} = \frac{\tau p}{1+\tau p} \qquad \text{(Eq. 5-34)}$$

where

$$\tau = \frac{I_O}{C_{(CF)O}}\left[1 + \frac{H^2}{I_O K_{(FW)I}}\right] \qquad \text{(Eq. 5-31) (repeated)}$$

the magnitude of equation 5-34 can be expressed as

$$\left|\frac{A_{(CF)O}}{A_{(IC)O}}\right| = \left(\frac{\tau^2\omega^2}{1+\tau^2\omega^2}\right)^{1/2} \qquad \text{(Eq. 5-35)}$$

and the phase angle as

$$\text{DRA} = -\frac{\pi}{2} - \tan^{-1}(\tau\omega) \qquad \text{(Eq. 5-36)}$$

A comparison of equations 5-27 and 5-32 shows that the characteristic equation for case motion about the input axis is the same as the characteristic equation for case motion about the output axis. This is to be expected since the same physical system is being considered. For a first-order approximation, the stiffness of the gyro gimbal and the gyro wheel bearings about the input axis is shown to be important. The complete response of the gyro unit to case motions about the input and output axes may be quite complex, since, even with the simplifying assumptions made in this paper, the performance must be approximated by a third-order system.

4. One-Gravity Testing - W.A. Gianoukos and W.C. Donovan

The primary purpose of one-gravity gyro testing is to determine that the gyro on test meets the performance requirements for that environment as specified by its application. One-g testing not only measures the gyro's basic performance but also generates data to be used to advance the state-of-the-art.

One-g testing at MIT today is conducted on a test station similar to that shown in figure 5-8 (see chapter 4). The tests may be conducted open-loop, in the rate-feedback mode, or in the servo-turntable mode of testing. (The first mode is

self explanatory; the other two are described later in this section). Each of these testing modes has advantages and disadvantages; the choice of mode is determined primarily by the data required.

In general, the testing procedures described in this paper pertain to the MIT single-degree-of-freedom floated integrating gyro as described in section 2. The basic techniques and philosophy, however, are also applicable to other gyro types.

Types of Testing

All gyro testing can be divided into three basic categories or types:

(a) Acceptance tests, which are conducted on 100 percent of the gyros built. These tests ascertain that the gyro is assembled correctly, can be balanced, and will meet its basic performance requirements.

(b) Design verification tests (or qualification tests), which may be conducted on a sampling basis. These tests ascertain that the gyro's design is such that the unit will operate satisfactorily under the various environments and excitation variations to which it will be exposed.

(c) Engineering evaluation tests, which may also be conducted on a sampling basis. These tests are an expansion of the design verification tests and also include diagnostic and design improvement tests.

One-gravity tests in each of these categories are described in this section. Testing in the greater-than-one-g environment is described in section 5 and 6 and in the angular vibration environment in section 7.

Acceptance Tests. Acceptance tests are conducted on all of the gyros built in any program and thus constitute a major area of effort, especially in a production run of any quantity. As figure 5-9 shows, current acceptance-test time at the Instrumentation Laboratory is seven times what it was in 1959; and the best estimate for the near future is that this trend will continue. This is basically the result of more stringent requirements on gyro performance and life. In addition, as the gyro error model becomes better developed, the testing required to determine all the terms of the model becomes more complex.

Because of this trend to longer, more complex and therefore more expensive tests, automatic test stations are being developed; and simultaneous multi-gyro testing is being conducted. Of course, a trade-off is necessary between the very heavy equipment costs associated with automation on the one hand and the test-program costs on the other. Simultaneous multi-gyro testing can often be justified on strictly technical rather than economic grounds because of the fact that the gyros on test, in effect, monitor one another. Any simultaneous anomaly appearing in the data from all gyros can be dismissed as an environmental disturbance, for example, rather than as gyro uncertainty as might be the case if only one gyro were on test.

Acceptance testing in the one-gravity test laboratory can be divided into three categories: go/no-go tests, normalizing tests, and coefficient and performance determination tests. While the coefficient and performance determination tests are dominated by the requirements of the inertial system for which the gyro is destined, the go/no-go and normalizing tests are dictated by the specific features of the design of the particular gyro on test. Thus, a discussion of a concrete test program which has universal application is not possible. However,

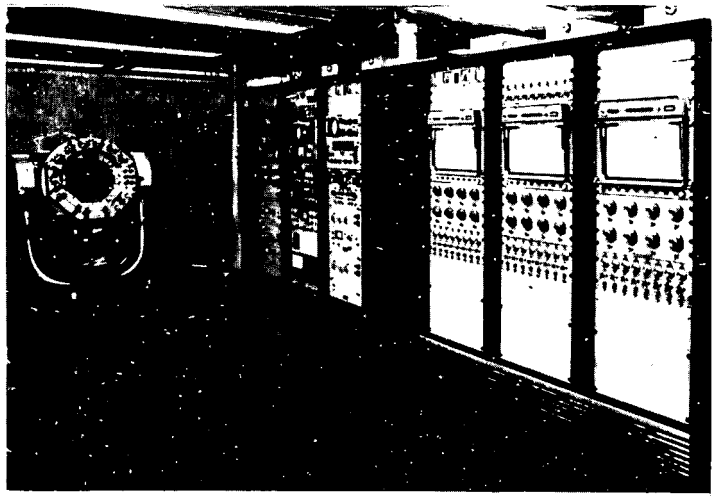

Fig. 5-8 Gyro test station in the one-g test laboratory

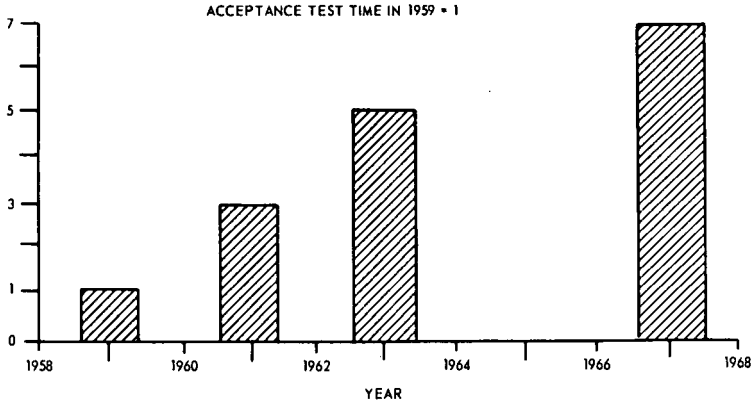

Fig. 5-9 Normalized one-gravity acceptance-test time for single-degree-of-freedom floated integrating gyros at MIT

Table 5-2 Typical gyro acceptance tests

Category	Test
Go/no-go	preliminary tests
	float freedom
	ducosyn operation
	uncertainty investigation
	deceleration
	signal-generator output analysis
	reaction torque and elastic restraint
Normalization	gyro gain
	torquer scale factor
	flotation
	coefficient adjustments
	gyro alignment
Coefficient and performance determination	final coefficient determination
	short-term performance

Table 5-3 Typical gyro design verification tests

Category	Test
Input excitation variations	wheel-power sensitivity
	operating-temperature sensitivity
	signal-generator resolution
	torque-generator linearity and stability
Environmental variations	ambient temperature
	ambient pressure
	magnetic fields
	linear vibration
	angular vibration
	linear acceleration
	shock

a 'for example' test program is described which utilizes the general design concepts of the gyros that are designed, built, and tested at the MIT Instrumentation Laboratory.

The test sequence must be arranged so that the anticipated problem areas are checked first; thus, a minimum of test time will be spent on unacceptable gyros. Since the sequence may vary depending on the gyro being tested, the discussion has not been arranged in any particular order; the tests are merely listed, not sequenced (see table 5-2).

Before beginning the acceptance tests, the completed gyro is thermal cycled. Past experience has shown that this tends to stabilize the assembly with the result that additional cycling to the same temperature has negligible effect on the unit balance. The component parts of the gyro are thermal cycled at various stages of the fabrication process, but the complete gyro unit must be thermal cycled from operating temperature to some lower temperature defined by its specific application. As a result, if heater power should be accidentally lost or intentionally removed at some future time (for example, during shipment, storage, or during some system standby condition), torque shifts will be minimal.

Preliminary tests are the final checks of the resistance and insulation of the electromagnetic elements (ducosyns and wheel-drive motor) and the polarities of the signal generator, the torquer and the wheel-drive-motor stator. These are relatively simple checks and much needless effort may be saved by determining early in the test program that the gyro is properly wired and assembled electrically.

Float freedom is a three-dimensional check that consists of determining that the float can be displaced axially along OA, perpendicular to OA, and rotational about OA. Since a complete check of all possible attitudes of the float with respect to the case is not practical, the freedom perpendicular to OA is checked in two planes only (the OA-SRA and OA-IA planes). Also, each of the four freedoms are checked independently, not in combinations. The axial displacement is critical in that an excessive value can result in a situation where one magnetic-suspension element ceases to suspend and produces a radial load. If the friction level between the pivot and jewel is greater than the suspension axial restoring force, the float will not erect to the zero-force point. The results of these checks in the one-g environment must be extrapolated to assure that the pivot will not come in contact with the jewel during the linear and angular vibrations and sustained linear accelerations that the gyro will experience during its application.

Ducosyn operation is the final electrical test of the magnetic-suspension operating point, quality factor, and saturation level. The most common operating point is the upper half-power point, which is the -3 db point on the resonance curve where the current through the ducosyn lags the excitation voltage by 45 degrees. If the operating point is too low, the danger of the erection problem discussed in the previous paragraph is increased. Saturation of the ducosyn results in radial float oscillations of the order of 1 Hz per minute, which in turn cause variation in the torque about the gyro output axis.

Uncertainty investigations are conducted to quickly ascertain that the damping fluid is uncontaminated. The basic concept of this test is to compare the unbalance torque at the signal-generator null of the gyro before and after driving the float slowly from stop-to-stop and before and after temporary changes in operating temperature. If necessary, the tests are repeated with the float displaced from its centered radial and axial position. These tests are performed with the gyro at various orientations with respect to the gravity vector and are conducted with the wheel at standstill.

Deceleration time can indicate impending spin-axis-bearing problems in a ball-bearing gyro. Deterioration in ball-bearing performance results in a decrease in the time required for the wheel to coast to standstill from synchronous speed. Thus, a comparison of the deceleration time with deceleration times measured during fabrication indicates the relative condition of the bearings and provides a reference for any subsequent tests.

Signal-generator output analysis is conducted to ascertain that the signal-generator null voltages and frequencies are within acceptable limits. The signal-generator null voltage is a complex wave form, which normally contains the spin motor and ducosyn excitation frequencies and their higher harmonics. It also contains frequencies caused by float oscillations generated by the rotating dynamic-unbalance vector of the wheel. In addition, the dynamic unbalance of the retainer-ball groups is present in ball-bearing gyros. During system application, these additional frequencies could cause servo-loop saturation and/or actual oscillation of the system. Therefore, a wave analyzer is used to measure the signal-generator output at frequencies from 50 Hz to three times the signal-generator excitation frequency.

Reaction torque and elastic-restraint torque is minimized by careful design and fabrication of the ducosyn elements. If reaction torque is high, changes in ducosyn excitation will cause changes in the acceleration-insensitive drift. With the signal generator at null, torque-generator reaction torque is a function of torque-generator elastic restraint and the angular separation between the signal- and torque-generator nulls. Therefore, the null separation is also measured.

Normalizing tests all have a common purpose and therefore it is not necessary that they be discussed independently as were the go/no-go tests. The purpose of normalizing tests is to yield a standardized gyro that requires no adjustments when it is mated with the system. The system can thus be simpler in design and the procurement of system parts can be considerably easier. In other words, the gyro-system interface is passive in nature. The normalizing procedures insure that all gyros of a program have a gain, torque-generator scale factor, thermal-control requirements, coefficients and alignment within specified limits. Thus, the gyro will be truly a 'plug-in' item.

Coefficient and performance tests comprise the final phase of all acceptance test programs. These tests consist of determining the magnitude of the error coefficients of equation 5-11 and indicate the stability and repeatability of these coefficients on a short-term basis. The long-term look is usually reserved for the engineering evaluation tests. In any particular test program, the duration of short-term and long-term tests is defined by the ultimate system application.

Design Verification Tests. The basic performance of a gyro is determined in the test laboratory under precisely controlled conditions. In application, however, the gyro may be expected to operate in an environment which is variable and with excitations that may not be controlled as precisely as in the laboratory. A series of design verification tests are therefore run to ascertain that the gyro meets the performance requirements of the real-world situation in which it will have to operate.

Design verification tests comprise basically the determination of the gyro's sensitivity to variations in input excitations and to the environment in which it is expected to perform (see table 5-3). Knowledge of the gyro's sensitivity to excitation or environmental changes permits:

(a) error compensation to be programmed into the system computer if the variations are predictable

(b) corrective measures to be taken to modify the gyro's environment or to increase the stability of the various excitations

(c) modification of the gyro design, if necessary

A separate test program can be generated for each of the tests listed in table 5-3. Each program would simulate the actual operating environments of a particular application, and the performance and sensitivities would be determined. In general, these tests all follow the general sequence:

(a) measure error coefficients

(b) change excitation or environment, usually in small increments

(c) remeasure error coefficients after each change

(d) remeasure error coefficients under the initial conditions

By repeating the sequence in various orientations, the effects of changes in excitation or environment on the various error coefficients are determined (see 'Rate Feedback Mode', below).

Engineering Evaluation Tests. A major objective of engineering evaluation testing is to evaluate gyro compatibility with system objectives and procedures using a single gyro rather than the three or four gyros that would be required to test a complete system. This concept has the advantage of demonstrating unit-system compatibility early in a program and removes component tests from the system development program. In addition, the cost of conducting these tests at the component level is significantly less than that of conducting them at the system level. Two examples of these tests are long-term performance tests (see 'Servo Turntable Mode', page 212) and single-axis tests using system calibration procedures.

Also included in the engineering-evaluation-test category are tests run for design improvement for use in advanced systems. If during any test series anomalies appear, then engineering evaluation tests are run to determine the cause of the anomaly and possibly suggest corrective measures to alleviate the condition causing the anomaly.

Test Modes

Rate-Feedback Mode (19). The rate-feedback mode of testing is primarily used to measure the gyro error coefficients and the gyro short-term repeatability. This mode of testing affords one of the most flexible methods of determining gyro unit sensitivities to environmental and excitation variations.

One of the most common tests conducted in the rate-feedback mode is the tumbling test. For a tumbling test, the turntable is usually oriented with its rotation axis (table axis, TA) parallel to earth's axis (EA). The gyro is rigidly mounted on the turntable so that its input axis is in the sterile plane; in other words, the gyro output axis or spin axis is parallel to the table axis. In these orientations, the gyro input axis is perpendicular to the angular velocity of the earth and of the turntable, which renders the gyro insensitive to both rates. The turntable shaft is driven by a synchronous drive at some multiple of earth's rate.

A torque about the gyro output axis causes the gyro float to rotate, which results in a voltage signal from the signal generator. This voltage is amplified and fed back to the gyro torque generator as a current or as pulses. This generates

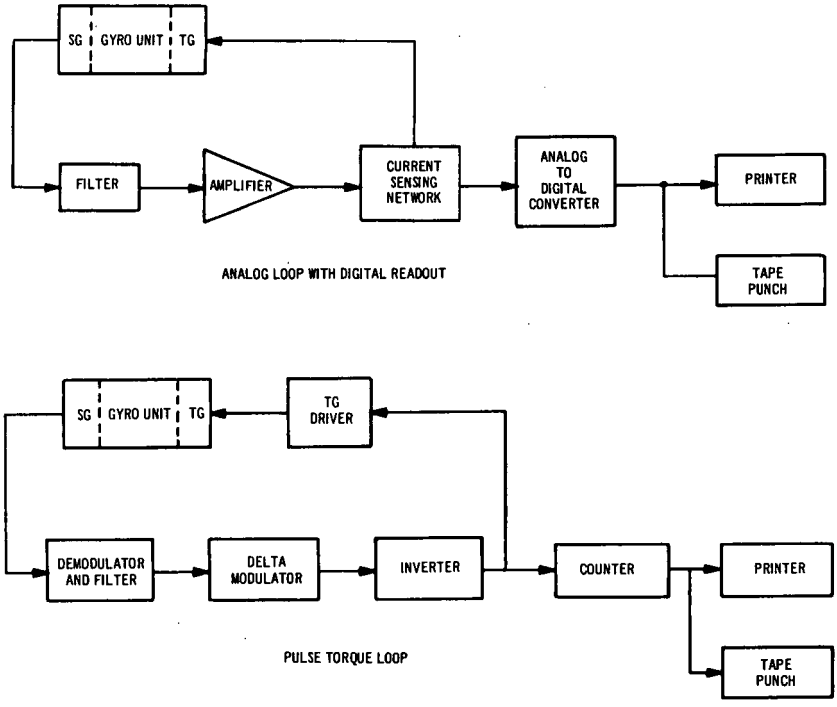

Fig. 5-10 Simplified diagrams of the rate-feedback loop

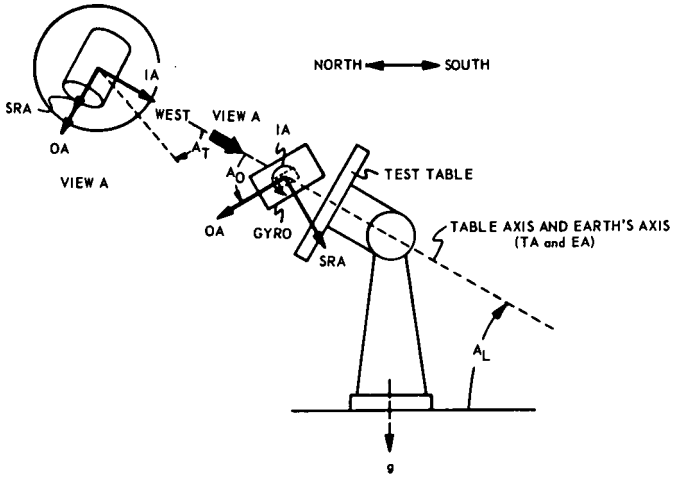

Fig. 5-11 Gyro orientation at start of tumbling test with OA at an arbitrary angle, A_O, to EA and TA

a torque equal to but opposite in polarity from the interfering torque that initially disturbed the float. The recording of this current or the pulse count can be converted easily to torque units. Simplified block diagrams of the rate-feedback loop are shown in figure 5-10. The upper diagram shows the analog loop with digital readout; the lower diagram is the pulse-torquing loop.

Since the turntable is synchronously driven at some constant multiple of earth's rate, the gyro tumbles with respect to gravity. The recording of the feedback current is sinusoidal with its peak determined by the magnitude of the gyro unbalances and compliances. A Fourier analysis of this current curve can therefore be used to compute the various gyro error coefficients. Comparison of contiguous revolutions yields the short-term repeatability or performance of the instrument.

If the gyro is aligned on a test turntable as depicted in figure 5-11, the components of specific force acting along each of its axes are (22)

$$\begin{aligned}(SF)_S &= g \cos A_L \cos A_O \cos A_T + g \sin A_L \sin A_O \\ (SF)_I &= g \cos A_L \sin A_T \\ (SF)_O &= g \sin A_O \cos A_L \cos A_T - g \sin A_L \cos A_O\end{aligned} \qquad \text{(Eq. 5-37)}$$

where

A_L = latitude angle at the test location

A_O = angle between OA and TA measured about +IA

A_T = turntable angle measured from a zero reference

Substituting equation 5-37 into equation 5-11 , then utilizing trigonometric identities, combining and rearranging terms gives

$$\begin{aligned}W_d = {} & \Big[D_F + gD_S \sin A_L \sin A_O + \tfrac{g^2}{2} D_{II} \cos^2 A_L - gD_O \sin A_L \cos A_O \\ & + \tfrac{g^2}{2} D_{SS} (\cos^2 A_L \cos^2 A_O + 2 \sin^2 A_L \sin^2 A_O) \\ & + \tfrac{g^2}{4} D_{OS} (\cos^2 A_L - 2 \sin^2 A_L) \sin 2A_O \\ & + \tfrac{g^2}{2} D_{OO} (\cos^2 A_L \sin^2 A_O + 2 \sin^2 A_L \cos^2 A_O)\Big] \\ & + \Big[gD_I \cos A_L + \tfrac{g^2}{2} D_{IS} \sin 2A_L \sin A_O - \tfrac{g^2}{2} D_{IO} \sin 2A_L \cos A_O\Big] \sin A_T \\ & + \Big[gD_S \cos A_L \cos A_O + gD_O \cos A_L \sin A_O + \tfrac{g^2}{2} D_{OS} \sin 2A_L (\sin^2 A_O - \cos^2 A_O) \\ & + \tfrac{g^2}{4} (2D_{SS} - D_{OO}) \sin 2A_L \sin 2A_O\Big] \cos A_T \\ & + \Big[\tfrac{g^2}{2} D_{IS} \cos^2 A_L \cos A_O + \tfrac{g^2}{2} D_{IO} \cos^2 A_L \sin A_O\Big] \sin 2A_T \\ & + \Big[\tfrac{g^2}{2} D_{SS} \cos^2 A_L \cos^2 A_O + \tfrac{g^2}{4} D_{OS} \cos^2 A_L \sin 2A_O - \tfrac{g^2}{2} D_{II} \cos^2 A_L \\ & - \tfrac{g^2}{2} D_{OO} \cos^2 A_L \sin^2 A_O\Big] \cos 2A_T\end{aligned} \qquad \text{(Eq. 5-38)}$$

By substituting fixed numerical values for A_O for specific orientations of the output axis, the torque equation for single-axis tumbling for that orientation can be obtained easily. For the two-axis tumbling case, both A_T and A_O vary simultaneously.

The magnitudes of the gyro error coefficients can be determined by various combinations of OA parallel to EA and SRA parallel to EA single-axis tumbling tests by themselves or used in conjunction with other auxiliary tests (Fig. 5-12). Ten error coefficients can be obtained from the data that is generated by four single-axis tumbling tests. Nine coefficients (D_{OO} excluded) can be obtained from three single-axis tumbling tests or two single-axis tumbling tests combined with an east-west survey with OA vertical up and OA vertical down (a four-position gyrocompass test). Depending upon how complex an error model is to be considered, which is a function of the application, the test requirements can be reduced to two single-axis tumbling tests and, in some instances, one tumbling test. Also, one two-axis step-tumbling test will yield the same nine gyro coefficients as the above tests if A_O is varied at a multiple of A_T. Ratios of 2 to 1 and 5 to 2 will generate the nine coefficients. One thing that the two-axis test lacks is the redundant readout of some torque coefficients that are inherent in the other tests. With the exception of the two-axis tests, the tests can be of the continuous-rate or the step-tumbling variety. The most common rate in use at this time is 10 times earth's rate although testing at earth's rate and at 100 times earth's rate has been performed successfully. Even higher rates should not be considered unfeasible. The two-axis tumbling test is confined to step or pause tumbling because, in order to maintain the gyro input axis in a sterile plane, the two axes of rotation are the gyro input axis and the table axis, which is perpendicular to IA and parallel to the earth's axis.

The repeatability of the error coefficients can be determined by conducting one of the above groups of tests before and after temporarily altering one or more of the gyro operating conditions or ambient. Some of the gyro parameters that are investigated are: wheel, microsyn, and thermal stand-by conditions. Some of the environment characteristics which fit conveniently into the before-and-after-checks category are: linear and angular vibration, sustained linear acceleration, shock, and thermal cycling.

Earth-fixed tests of various lengths (hours, days, weeks, or months) where the gyro remains stationary with respect to the earth appear to be an effective way of obtaining a quantitative look at the stability of the gyro error coefficients. The interpretation of the results of a series of earth-fixed tests run with the gyro in the three key orientations shown in figure 5-13 (OA vertical, IA vertical and SRA vertical) appears to be easier than extracting them from tests in which the gyro is subject to a rotating gravity vector. If it is assumed that the compliance coefficients are negligible, the simplified model equations for these three orientations are $D_F - gD_O$, $D_F + gD_I$ and $D_F + gD_S$, respectively.

By orienting the gyro with respect to gravity at certain fixed turntable positions, various gyro error coefficients can be isolated. Then, at these positions, the various gyro excitations may be varied to yield an immediate record of error-coefficient response to these variations. From the recording, the gyro coefficient sensitivities to these excitation changes can be computed. Similarly, sensitivities to environmental changes can be obtained.

The foundation of error-coefficient-sensitivity tests is data obtained from four basic orientations: OA up, OA down, IA vertical and SRA vertical (Fig. 5-14). Variations of these latter two orientations are OA parallel to EA with IA

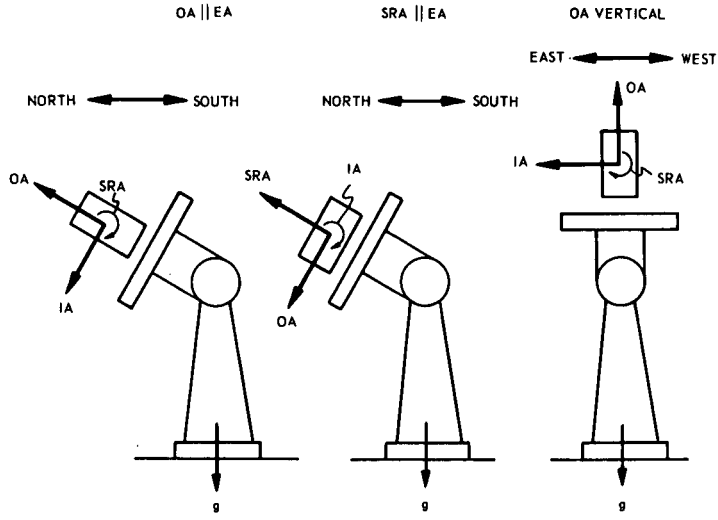

Fig. 5-12 Rate-feedback-mode test orientations

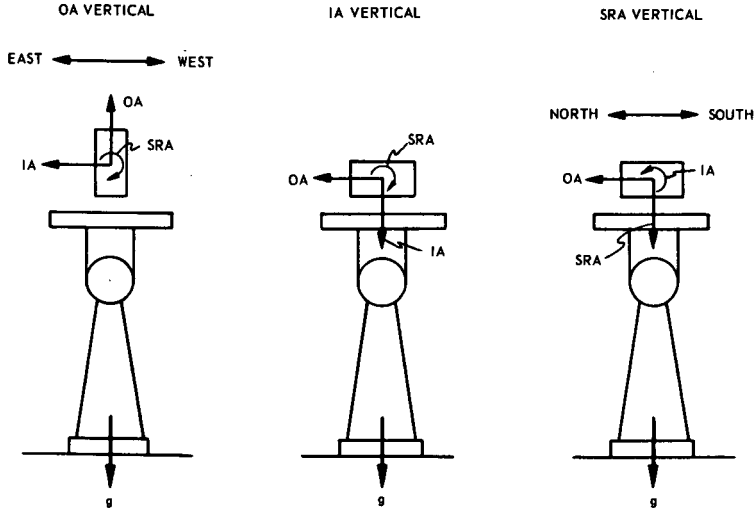

Fig. 5-13 Earth-fixed test orientations

horizontal and OA parallel to EA with SRA horizontal. The simplified model equations for the basic orientations are: $D_F - gD_O$, $D_F + gD_O$, $D_F + gD_I$, $D_F + gD_S$. The equations for the two alternative orientations are: $D_F + gD_S \cos A_L$ and $D_F + gD_I \cos A_L$. The results of these tests in conjunction with knowledge of the system environment and the performance of the system excitation supplies are necessary for the proper error analysis and budgeting of any system. These tests are similar to the error-coefficient-repeatability tests in that the same parameters are varied. However, the data is obtained at several levels of the parameters rather than before and after temporary changes in them. The parameters (wheel excitation, microsyn excitation, operating temperature, ambient temperature, external magnetic fields, thermal gradients) can be varied one at a time while keeping all others at their quiescent values or in the format of a fractional factorial experiment design. In the more sophisticated applications where the simplified error models are not adequate, the sensitivity tests must expand from the basic four-position concept to full-fledged tumbling tests, so that the effects on all of the error coefficients can be determined.

Servo-Turntable Mode (19). Servo-turntable-mode testing is primarily used to measure gyro long-term performance. Various orientations may be used, but one of the most common is with the gyro input axis parallel to the turntable axis which in turn is parallel to the earth's axis. The gyro senses earth rate about its input axis, which causes the float to rotate due to precession. This generates a voltage from the signal generator, which controls a servo motor that drives the turntable in the direction to cancel the effect of the earth's rotation (Fig. 5-15). In the ideal case, the turntable would rotate exactly at earth's rate, and the gyro would remain fixed with respect to inertial space. In the actual case, the turntable rate varies due to gyro and equipment errors and uncertainty. By measuring the table rate and subtracting earth's rate, a curve of these errors and uncertainties versus table position may be plotted. By comparing point-to-point, revolution-to-revolution, a deviation curve is obtained which yields the uncertainty of the gyro and test setup. In addition, the data from the first revolution of a multi-revolution test can be considered as error compensation and subtracted from the data for each succeeding revolution. The result is the long-term performance of the gyro.

Servo-turntable-mode testing uses two primary test configurations: inertial-reference drift runs and earth-reference drift runs. In one sense, these tests are counterparts to the tumbling test and earth-fixed tests which are conducted in the rate-feedback mode.

The inertial-reference drift run has the advantage over the earth-reference drift run of subjecting the gyro to varying components of gravity. The main purpose of the inertial-reference test is to obtain an indication of overall long-term gyro performance. The more common orientations are IA parallel to TA and EA, and IA rotated 45 degrees about SRA from TA, which is parallel to EA (Fig.5-17). In this latter orientation, varying gravity components act along all three major gyro axes.

In contrast to the repeatable periodic function of table rate that is generated by the inertial-reference test, the earth-reference test results in a near-zero table rate of the order of 1 minute of arc per hour. The normal orientations with IA parallel to TA are (Fig. 5-18).

(a) OA vertical, IA horizontal east-west

(b) SRA vertical, IA east-west

(c) IA vertical

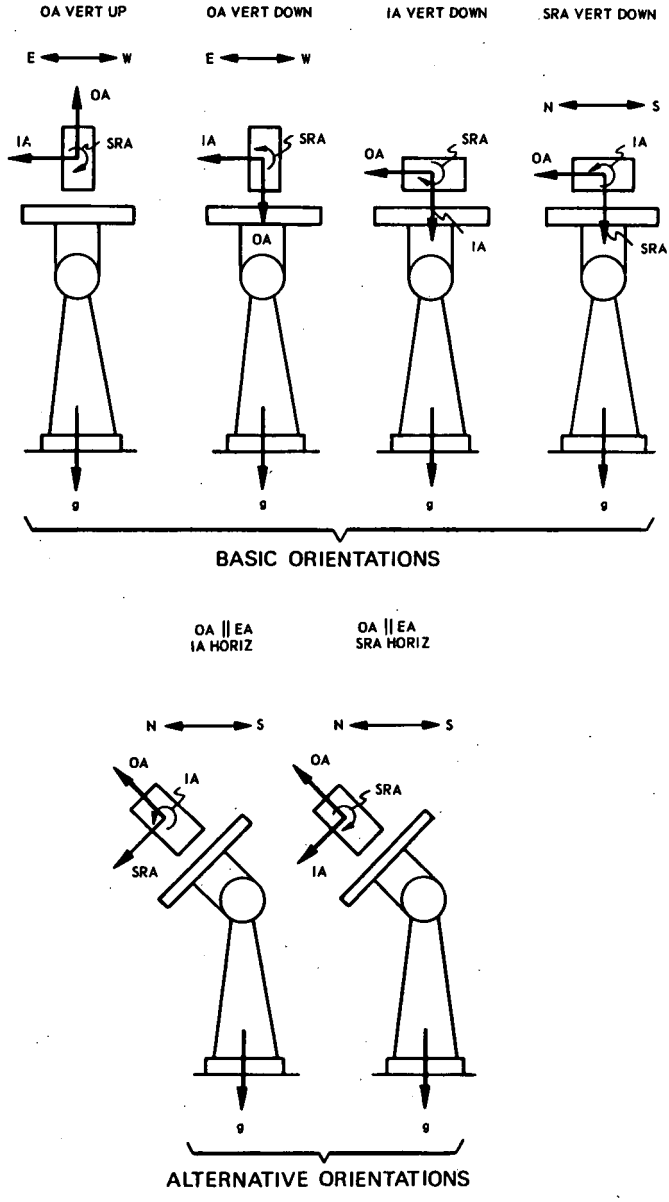

Fig. 5-14 Sensitivity-test orientations

In the first two orientations, the initial table rate which results from the gyro errors and uncertainty is compensated by changing the coupling between the gyro input axis and the earth's axis. The correction in the third test is obtained by using the gyro's torque generator.

Comparison of Modes. All present indications are that the rate-feedback mode of gyro testing is being used more and more and the servo-turntable mode less and less. The time duration of a test weighs heavily in favor of the rate-feedback mode where 10 or even 100 revolutions of data can be accumulated in one day as opposed to one revolution of a servo test. The advent of pulse and digital equipment has now virtually eliminated the resolution edge once held by the servo-turntable mode. Of course, the servo mode will always be useful since it more nearly simulates the system operation of the gyro. In addition, the servo mode permits torque-generator investigations because the torque generator is not part of the servo loop. The relative advantages and disadvantages of both modes are summarized in table 5-4.

Table 5-4 Comparison of rate-feedback and servo-turntable testing modes

Advantages	Disadvantages
Rate-Feedback Mode	
1. all error coefficients can be determined	1. torque generator nonlinearity
2. short-term performance can be measured	2. loop dynamics
3. effects of modifying inputs can be determined	3. gyro axes alignment is critical
Servo-Turntable Mode	
1. data is integrated	1. time consuming
2. performance testing is closer to system simulation	2. requires low-friction turntable bearing
3. use of the torque generator is eliminated	3. requires high-performance servo
4. gyro axes alignment not critical	4. short-term response of the gyro is restricted
	5. requires high-accuracy table-rate readout

The most attractive rate-feedback tests appear to be the two-axis step tumbling tests; two axis because one test does the work of two, three or four, and step because it eliminates the added complexity of the effects of rate-tumbling about two axes simultaneously. Also, the future role of the tumbling test seems to be centered around the determination of the acceleration-insensitive and acceleration-sensitive terms only; the linear-vibration technique appears more suitable for determining the terms sensitive to the high powers of acceleration (see section 5).

The earth-fixed test will be used extensively for the determination of gyro performance. Simultaneous multi-gyro testing goes hand-in-hand with the earth-fixed-test concept and seems necessary because the present state-of-the-art of environment control and/or monitoring is not commensurate with the gyro state-of-the-art. Figure 5-16 presents the results of an earth-fixed test run

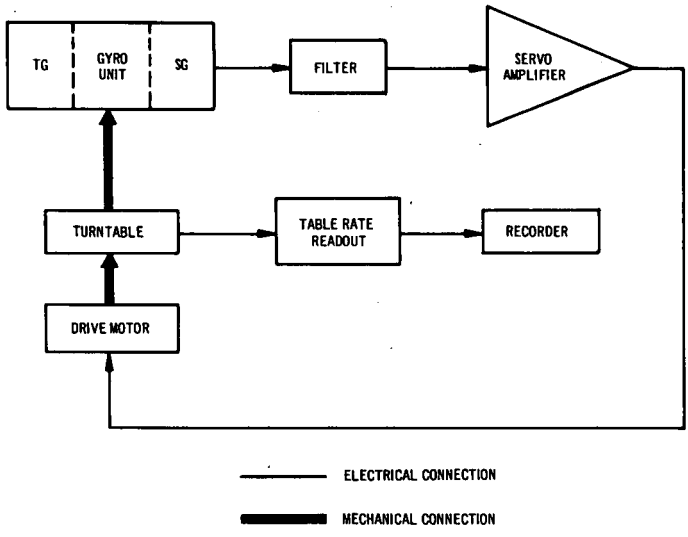

Fig. 5-15 Simplified diagram of the servo-turntable loop

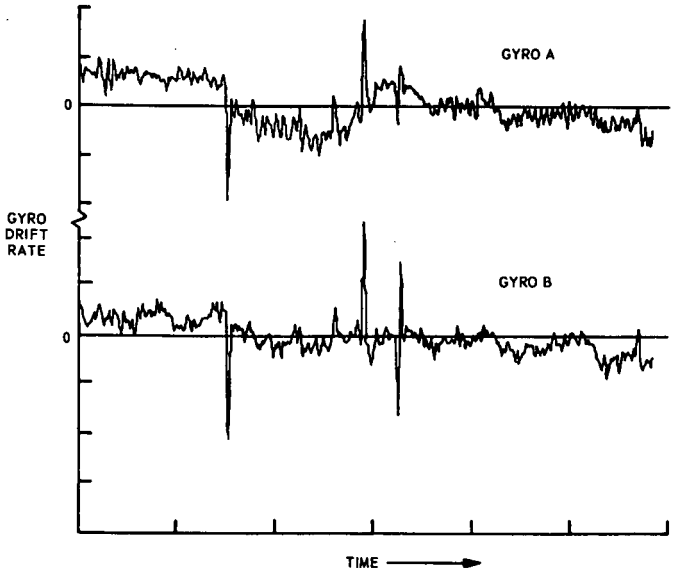

Fig. 5-16 Simultaneous data from two gyros on an earth-fixed test

simultaneously on two gyros. If at that time only one of these gyros had been on test, the simultaneous torque excursions exhibited by both gyros may have been attributed to the gyro rather than to the real cause, which was the environment.

One final item that should be mentioned is the possibility of a more efficient and effective use of all gyro output signals, for example, signal-generator output, radial magnetic-suspension signals, axial magnetic-suspension signals and wheel noise. The sensitivity of changes in torque about the output axis to changes in these signals could be measured during one-g testing and programmed into the system computer to compensate for changes occurring during system operation.

5. Linear Vibration Testing— P. J. Palmer and F. E. Cartwood

Linear vibration is but one of several experimental methods available for measuring acceleration-sensitive gyro drift rate or torque. Tumbling and centrifuging are the other common methods, although all three actually chart performance in different areas. As indicated in figure 5-19, tumbling tests are limited to one g at low frequency. Centrifuge testing can reach high-g levels, but again at low frequencies, even with the gyro mounted on a counter-rotating platform. Vibration testing permits exposure to the widest range of frequency and g levels.

The unique qualities of linear vibration that make it valuable during gyro testing are the following:

(a) the vibration can be applied and removed without introducing major interfering inputs

(b) the integrated effects of linear vibration on the gyro affect only the compliance, or higher powered acceleration-sensitive terms

(c) angular alignments are not critical

(d) the gyro can be tested with normal excitations

(e) a complete set of compliance coefficients can be determined in less time than with any other method

(f) precise gyro flotation is not required

(g) rotary power or signal transfer is not required

(h) the equipment is relatively inexpensive (compared to centrifuge equipment)

The following are the major disadvantages:

(a) cross-axis vibration results in relatively large but systematic (correctable) errors

(b) angular vibration is the predominant interference

(c) sustained linear acceleration cannot be simulated

Purpose

Almost all inertial navigation systems endure a significant level of vibration during some part of their operational lifetimes. This vibration, owing to the nature of flight-guidance applications, often accompanies high levels of sustained acceleration such as occur during rocket launchings and reentry. Generally speaking, linear vibration testing aims at two different aspects of gyro

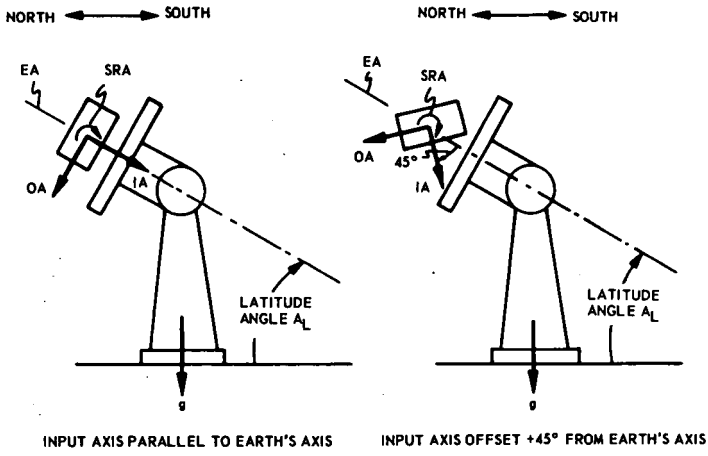

Fig. 5-17 Inertial-reference drift-test orientations

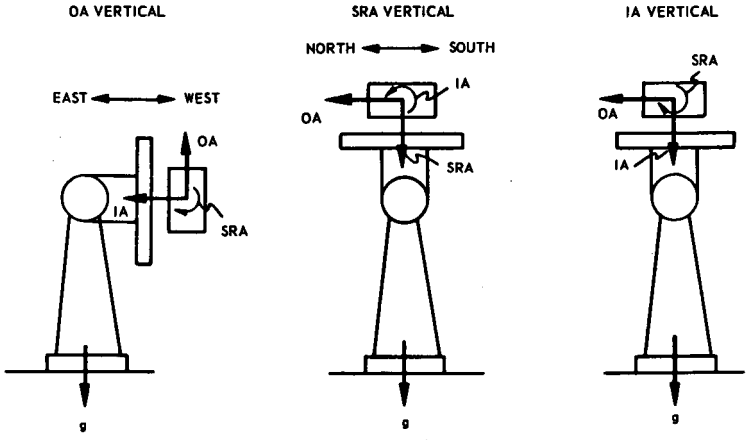

Fig. 5-18 Earth-reference drift-test orientations

performance. The first concerns a simulation of the vibratory environment encountered in operational life. (Random vibration testing represents another simulation technique.) This type of testing seeks to discover incipient failure resulting from permanent physical changes induced by vibration. Plastic deformation, for example, is an irreversible change corresponding to 'permanent damage' and perhaps a significant degradation in performance.

The second aim of linear vibration testing concerns the determinate response of the gyro to an applied acceleration. This type of testing seeks to measure the torques which reflect the sensitivity of the instrument to acceleration. Such error torques are the result of various reversible physical changes brought about by acceleration or high powers thereof. Mechanical deflection in the elastic range of deformation, for example, is a reversible change which can lead to such an error torque. While a measure of good design is low sensitivity to acceleration, a measure of ultimate performance is the level of precision with which that sensitivity is known.

Advances in inertial gyro design have brought instruments to the point where survival in the vibratory environment is not a critical problem. It is usual therefore to subject gyros to vibration for environmental simulation purposes and find no resultant degradation in performance. On the other hand, much emphasis has fallen upon linear vibration testing as a means to define instrument sensitivity to acceleration. This section revolves around this latter aspect of linear vibration testing.

Linear Acceleration Effects

Linear vibration provides a sinusoidal linear acceleration of the form $(SF)_v \sin \omega t$, where $(SF)_v$ = peak vibration amplitude in g's and ω = vibration frequency in rad/sec. In response to this acceleration, the steady-state gyro torque about the output axis depends only upon the instrument sensitivity to even powers of acceleration. This results from the fact that only even powers of a sinusoidal function have a nonzero average, i.e. the average value of $(SF)_v \sin \omega t$ is zero, the average value of $[(SF)_v \sin \omega t]^2$ is $(SF)_v^2/2$, and so forth. Linear vibration is therefore most useful in measuring gyro torques which are functions of g^2, g^4, etc.

An anisoelastic structure such as a gyro wheel assembly can be simulated by a mass mounted on four springs as is shown in figure 5-20 (12). The springs along the spin axis are assumed to be less stiff than the springs along the input axis. When such a structure is subjected to an acceleration, the resulting deviation of the effective center of mass is not along the line of action of the acceleration but is toward the softer of the two spring axes, in this case the spin axis. In figure 5-20, the center of mass is displaced along the negative spin and input axes by d_S and d_I as a result of the force components F_S and F_I. Since these forces and displacements are in the defined negative direction, they must be given a negative polarity for consistency. If the acceleration vector were reversed, the forces and displacements would all be directed along the positive axes and thus would carry positive polarities. Over a complete cycle of vibration, the drift torque about the output axis is therefore

$$M_O = \frac{(-F_I)(-d_S) - (-F_S)(-d_I)}{2} + \frac{F_I d_S - F_S d_I}{2} \qquad \text{(Eq. 5-39)}$$

$$= F_I d_S - F_S d_I$$

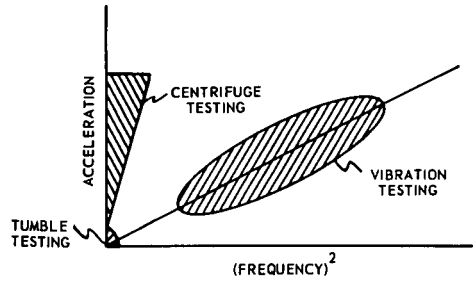

Fig. 5-19 Relative acceleration and frequency levels of tumbling, centrifuge, and linear vibration testing

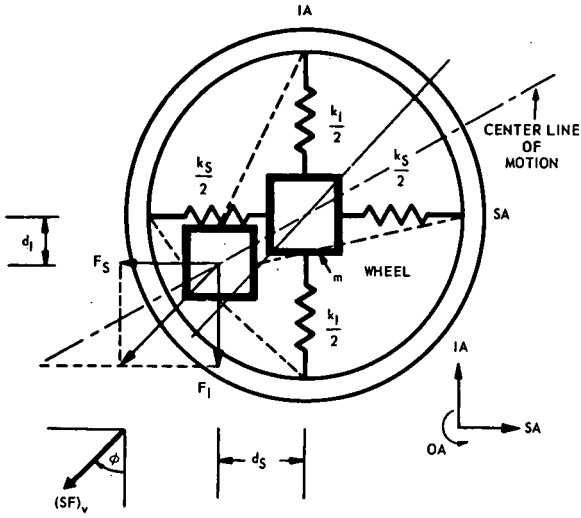

Fig. 5-20 Anisoelasticity torque model of gyro

where

F_S = force component along SRA in dynes
$= m[\ddot{d}_S + (SF)_S \sin \omega t]$

F_I = force component along IA in dynes
$= m[\ddot{d}_I + (SF)_I \sin (\omega t + \alpha)]$

d_I, d_S = displacement along IA and SRA, respectively, in cm

m = effective mass in gm of the displaced gyro wheel and bearing assembly

$(SF)_I$, $(SF)_S$ = maximum amplitude of the vibratory specific force components along IA and SRA, respectively, in cm/sec^2

α = phase angle between acceleration components along IA and SRA in radians

Equation 5-39 is expanded in Appendix A of reference (22) into a frequency-dependent relationship yielding

$$M_O = \frac{m(SF)_S(SF)_I \cos \alpha}{2}\left[\frac{\omega_{nS} - \omega^2}{(\omega_{nS}^2 - \omega^2)^2 + 4(DR)_S^2 \omega_{nS}^2 \omega^2} - \frac{\omega_{nI} - \omega^2}{(\omega_{nI}^2 - \omega^2)^2 + 4(DR)_I^2 \omega_{nI}^2 \omega^2}\right]$$
$$- \frac{m(SF)_S(SF)_I \sin \alpha}{2}\left[\frac{2(DR)_S \omega_{nS} \omega}{(\omega_{nS}^2 - \omega^2)^2 + 4(DR)_S^2 \omega_{nS}^2 \omega^2} + \frac{2(DR)_I \omega_{nI} \omega}{(\omega_{nI}^2 - \omega^2)^2 + 4(DR)_I^2 \omega_{nI}^2 \omega^2}\right] \quad \text{(Eq. 5-40)}$$

where

ω_{nI}, ω_{nS} = undamped natural frequency along IA and SRA, respectively, in rad/sec
$= \sqrt{k/m}$

k = equivalent bearing stiffness in dyne/cm

$(DR)_I$, $(DR)_S$ = damping ratio along IA and SRA, respectively
$= \frac{1}{2}\sqrt{c^2/mk}$

c = structural damping coefficient in dyne/cm/sec

The first term of equation 5-40 is usually referred to as anisoelastic torque and the second term as the cylindrical torque (11). As the phase angle α approaches zero, the cylindrical torque approaches zero, and the anisoelastic torque becomes maximum.

For the cylindrical torque, if the damping ratio is small, the frequencies at which the torque peaks occur can be computed by differentiating the equation for cylindrical torque with respect to ω and equating the derivative to zero, which results in

$$\omega_{(peak)S} = \omega_{nS}\left[\frac{1 - 2(DR)_S^2}{3}\left(1 \pm \sqrt{1 + \frac{3}{[2(DR)_S^2 - 1]^2}}\right)\right]^{1/2}$$

$$\omega_{(peak)I} = \omega_{nI} \left[\frac{1 - 2(DR)_I^2}{3} \left(1 \pm \sqrt{1 + \frac{3}{[2(DR)_I^2 - 1]^2}} \right) \right]^{1/2} \qquad \text{(Eq. 5-41)}$$

where

$\omega_{(peak)I}$, $\omega_{(peak)S}$ = frequencies at which peak torque occurs

As the forcing vibration frequency decreases, the cylindrical torque decreases to zero.

Figure 5-21 is a comparison of theoretical and experimental cylindrical torque data, and figure 5-22 is a similar comparison of anisoelastic torque data (23). To obtain the data of figure 5-21, two vibrators were used to apply simultaneous vibration along IA and SRA with the phase angle, α, set at 90 degrees so that the anisoelastic torque was zero. To obtain the data of figure 5-22, vibration was applied mid-way between IA and SRA. Since only one vibrator was used, the phase angle, α, was zero and the cylindrical torque was zero. The difference between the experimental and theoretical data of figure 5-22 at low frequencies (points 2, 3, 4 and 5 on the curve) is attributed to angular oscillations of the vibrator and to a fixture resonance at the frequency marked 1.

If the damping ratio is small, the frequencies at which the peak anisoelastic torques occur can be computed by differentiating the anisoelastic-torque equation with respect to ω and equating the derivative to zero, which results in

$$\omega_{(peak)S} = \omega_{nS} \sqrt{1 \pm 2(DR)_S}$$

$$\omega_{(peak)I} = \omega_{nI} \sqrt{1 \pm 2(DR)_I} \qquad \text{(Eq. 5-42)}$$

For the example given in figure 5-22, solution of equation 5-42 yields values of $(DR)_S$ and $(DR)_I$ of approximately 0.02 and 0.01, respectively. Then, for forcing frequencies ω, less than 10 percent of the undamped natural frequencies, ω_{nS} and ω_{nI}, $(\omega/\omega_{nS})^2$ and $(\omega/\omega_{nI})^2$ are each less than 0.01 and $4(DR)_S^2(\omega/\omega_{nS})^2$ and $4(DR)_I^2(\omega/\omega_{nI})^2$ are each much less than 0.004. The average anisoelastic drift torque may, therefore, be expressed within 1 percent as

$$M_O = \frac{m(SF)_S(SF)_I}{2} \left[\frac{1}{\omega_{nS}^2} - \frac{1}{\omega_{nI}^2} \right] \qquad \text{(Eq. 5-43)}$$

$$M_O = \frac{m^2(SF)_S(SF)_I}{2} \left[\frac{1}{k_S} - \frac{1}{k_I} \right] \qquad \text{(Eq. 5-44)}$$

where

$1/k$ = compliance

Data from commercially available gyro spin-axis ball bearings indicate stiffnesses of

$k_S = 2.6 \times 10^{10}$ dyne/cm

$k_I = 3.6 \times 10^{10}$ dyne/cm

Since the undamped natural frequency ω_n is $\sqrt{k/m}$, for a wheel mass of 250 grams,

$\omega_{nS} = 1.0 \times 10^4$ rad/sec

$= 1600$ Hz

$\omega_{nI} = 1.2 \times 10^4$ rad/sec

$= 1900$ Hz

To obtain the anisoelastic torque accurately to within 1 percent of its value at one gravity, the forcing frequency must be less than 10 percent of the natural frequency, or less than 1000 rad/second (160Hz). In addition, the gyro must be mounted in a fixture whose natural frequency is well above the test level. Thus, although engineering evaluation tests may be conducted at frequencies up to 5000 Hz to determine ruggedness and structural resonance points, vibration testing to measure error coefficients is limited to low frequencies.

The example just given indicates another use of linear vibration testing in addition to measurement of the error coefficients. Tests at low g levels to obtain torque vs frequency will indicate the resonant frequencies, from which the bearing stiffness can be calculated (in the case of ball bearings). This gives a check of possible changes in bearing preload or performance.

It should be noted at this point that the gyro model just described is the simplest case where it is assumed that the compliance axes and the principal axes of inertia are coincident with the gyro axes. It should be further noted that compliance (or stiffness) is tacitly taken to be independent of acceleration, which is another way of saying that the analysis assumes linear spring stiffness. Although linear analysis has thus far been very effective, high standards of performance may create the need for a quasi-linear model of behavior. For example, consider a ball-bearing-type gyro that is to be subjected to accelerations up to 100 g's (12). The axial load-deflection characteristic for a single angular-contact ball bearing is given by

$$F_c = Cd^n \qquad \text{(Eq. 5-45)}$$

where

F_c = the compressive force along the line of action of the ball

C = a constant determined by bearing dimensions and materials

d = deflection of the ball along the line of action of the ball

n = 3/2 for a ball loaded between two semi-infinite flat plates (a good approximation for many bearing designs)

For a preloaded pair of angular-contact ball bearings, the load-deflection characteristic is essentially linear. The nonlinear effects of one bearing tend to be compensated by the nonlinear effects of the other bearing. In other words, as the compliance of one bearing increases, the compliance of the other bearing decreases. At accelerations that are small compared to the breakout acceleration, drift rate due to compliance torque increases essentially as the square of the applied acceleration as indicated by equation 5-44 : the breakout acceleration is defined as that acceleration along the spin axis where the applied force to the rotor exceeds the original preload force. At higher accelerations, the drift rate due to compliance torque deviates from that which would be predicted by the analysis using linear spring constants for the ball bearings (13).

An estimate of the maximum deviation from linearity for an isoelastic or slightly nonisoelastic bearing package is given by

$$M_O = (0.06)(F_o d_o)\left[\frac{(SF)}{(SF)_b}\right]^4 \sin 4\phi \qquad \text{(Eq. 5-46)}$$

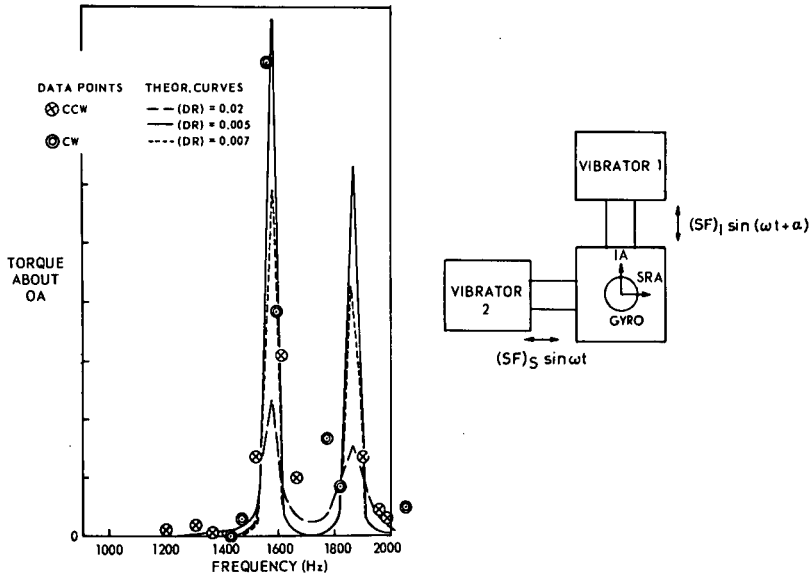

Fig. 5-21 Theoretical and experimental gyro cylindrical torque versus frequency

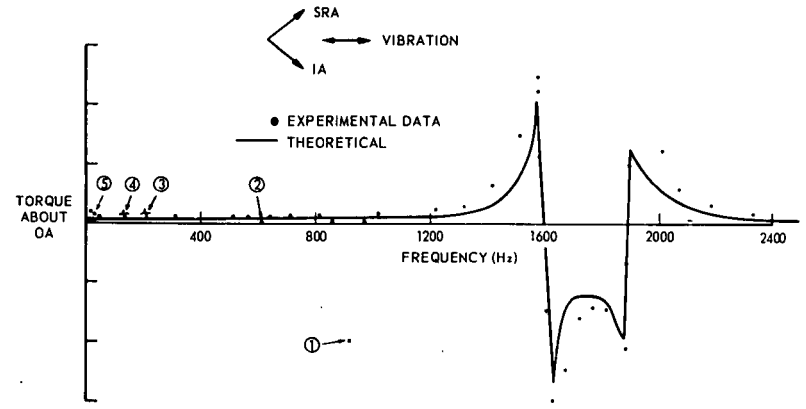

Fig. 5-22 Theoretical and experimental gyro anisoelastic torque versus frequency

Table 5-5 Deviation in gyro drift rate from linear analysis at various g levels

Applied acceleration (SF) in g's	$\frac{(SF)^*}{(SF)_b}$	Drift Rate in Meru*		Nonlinearity, percent
		Linear effect* f (sin 2ϕ)	Nonlinear effect, f (sin 4ϕ)	
1	0.01	1	1.4×10^{-5}	0.001
10	0.1	100	0.14	0.1
20	0.2	400	2.2	0.5
30	0.3	900	10	1.1
40	0.4	1600	40	2.5
50	0.5	2500	110	4.4
60	0.6	3600	240	6.7
70	0.7	4900	470	10
80	0.8	6400	850	13
90	0.9	8100	1400	17
100	1.0	10 000	2300	23

*Assumed parameters:

1. $(SF)_b$ = 100 g's
2. Linear effect = D_{IS} = 1 meru/g^2
3. Wheel angular momentum = 2×10^6 gm-cm^2/sec

Table 5-6 Extraction of compliance coefficients from linear vibration data

Orientation	VK_1	K_2	K_3
OA ∥ EA	D_{IS}	D_{II}	$-D_{SS}$
SA ∥ EA	D_{IO}	D_{II}	$-D_{OO}$
IA ⊥ EA	$-D_{OS}$	D_{SS}	$-D_{OO}$

V = +1 for OA, SA ∥ EA with OA, SA south or IA ⊥ EA with IA down

V = -1 for OA, SA ∥ EA with OA, SA north or IA ⊥ EA with IA up

for accelerations up to about 0.3 $(SF)_b$ and by

$$M_O = (0.1)(F_o d_o)\left[\frac{(SF)}{(SF)_b}\right]^{4.4} \sin 4\phi \qquad \text{(Eq. 5-47)}$$

for accelerations from about 0.3 $(SF)_b$ to breakout acceleration, where

F_o = preload force

d_o = initial bearing deflection as a result of F_o

(SF) = applied acceleration

$(SF)_b$ = breakout acceleration

ϕ = angle of the applied acceleration vector in the SRA-IA plane referenced to SRA or IA (Fig. 5-20)

Consider a case where the preload force is 6.65×10^6 dynes (15 pounds) and the resulting deflection is 5×10^{-4} cm. At the point where the applied acceleration is equal to one-half of the breakout acceleration, the deviation in torque from the linear analysis is 16 dyne-cm. This corresponds to a drift rate of 110 meru in a gyro with a wheel angular momentum of 2×10^6 gm-cm^2/sec. Table 5-5 indicates the percentage of nonlinearity at various g levels for the case of breakout acceleration of 100 g's and D_{IS} equal to 1 meru/g^2.

Table 5-5 is presented to point out that the nonlinearity in the bearings contributes a small torque compared to the nonisoelastic torque even in the example given. It should be noted, however, that the torque due to nonisoelasticity is a second harmonic of the angle ϕ while the torque due to nonlinearity is a fourth harmonic of the angle ϕ. Therefore, the maximum torques do not occur at the same angles.

Since the compliance of a preloaded pair of angular-contact ball bearings increases with the applied load (acceleration), the compliance of the wheel about the input and output axis increases with applied load. This increase in rotational compliance produces an increase in the characteristic time of the instrument. At the acceleration where the bearing preload is exceeded, the rotational stiffness decreases to about 0.2 percent of its value at zero acceleration; and the characteristic time may increase by a full order of magnitude.

Techniques

When a gyro unit is subjected to linear vibration, the components of specific force acting along each of its axes are (21)

$$\begin{aligned}(SF)_I &= (SF)_{g(I)} + (SF)_{v(I)} \sin \omega t \\ (SF)_S &= (SF)_{g(S)} + (SF)_{v(S)} \sin \omega t \\ (SF)_O &= (SF)_{g(O)} + (SF)_{v(O)} \sin \omega t\end{aligned} \qquad \text{(Eq. 5-48)}$$

where

$(SF)_{g(I)}$, $(SF)_{g(S)}$, $(SF)_{g(O)}$ = components of the specific force of gravity appearing along IA, SRA and OA, respectively, in g's.

$(SF)_{v(I)}$, $(SF)_{v(S)}$, $(SF)_{v(O)}$ = components of the specific force due to vibratory acceleration appearing along IA, SRA and OA, respectively, in g's

Substituting the relationships of equation 5-48 into equation 5-11 gives

$$
\begin{aligned}
W_d = {} & D_F + D_I[(SF)_{g(I)} + (SF)_{v(I)} \sin \omega t] + D_S[(SF)_{g(S)} + (SF)_{v(S)} \sin \omega t] \\
& + D_O[(SF)_{g(O)} + (SF)_{v(O)} \sin \omega t] + D_{II}[(SF)_{g(I)} + (SF)_{v(I)} \sin \omega t]^2 \\
& + D_{SS}[(SF)_{g(S)} + (SF)_{v(S)} \sin \omega t]^2 + D_{OO}[(SF)_{g(O)} + (SF)_{v(O)} \sin \omega t]^2 \\
& + D_{IS}[(SF)_{g(I)} + (SF)_{v(I)} \sin \omega t][(SF)_{g(S)} + (SF)_{v(S)} \sin \omega t] \\
& + D_{IO}[(SF)_{g(I)} + (SF)_{v(I)} \sin \omega t][(SF)_{g(O)} + (SF)_{v(O)} \sin \omega t] \\
& + D_{OS}[(SF)_{g(O)} + (SF)_{v(O)} \sin \omega t][(SF)_{g(S)} + (SF)_{v(S)} \sin \omega t]
\end{aligned}
$$

(Eq. 5-49)

Equation 5-49 can be expanded and then rewritten to group those terms that are:

(a) independent of specific force, that is, the D_F term.

(b) independent of vibration, that is, terms which result in a torque only as a function of gravity.

(c) dependent upon vibration and gravity. These terms are functions of sin ωt so that the average value of the torque produced is zero. However, these torques do act on the float and appear as sinusoidal signals on the output of the signal generator at a frequency equal to the frequency of the applied vibration.

(d) dependent upon vibration only, that is, terms that result in a torque only as a function of linear vibration. These are the terms that contain a sine-squared function. Since the average value of a sine-squared function is equal to one-half the peak value, these terms result in a steady-state average torque. Actually, since $\sin^2 A = (1/2)(1 - \cos 2A)$, the effect of the sine-squared term is a steady-state torque plus a cosinusoidal torque at a frequency equal to twice the frequency of the applied vibration.

Rewriting only those terms that result in a steady-state torque to produce a steady-state gyro drift, equation 5-49 becomes

$$
\begin{aligned}
W_d = {} & D_F && \text{acceleration independent} \\
& + D_I (SF)_{g(I)} + D_S (SF)_{g(S)} + D_O (SF)_{g(O)} \\
& + D_{II} (SF)^2_{g(I)} + D_{SS} (SF)^2_{g(S)} + D_{OO} (SF)^2_{g(O)} \\
& + D_{IS} (SF)_{g(I)} (SF)_{g(S)} + D_{IO} (SF)_{g(I)} (SF)_{g(O)} && \left.\begin{array}{l}\\ \\ \\ \\ \end{array}\right\} \text{gravity dependent} \\
& + D_{OS} (SF)_{g(O)} (SF)_{g(S)} \\
& + {}^1/_2 D_{II} (SF)^2_{v(I)} + {}^1/_2 D_{SS} (SF)^2_{v(S)} \\
& + {}^1/_2 D_{OO} (SF)^2_{v(O)} + {}^1/_2 D_{IS} (SF)_{v(I)} (SF)_{v(S)} \\
& + {}^1/_2 D_{IO} (SF)_{v(I)} (SF)_{v(O)} + {}^1/_2 D_{OS} (SF)_{v(O)} (SF)_{v(S)} && \left.\begin{array}{l}\\ \\ \\ \end{array}\right\} \text{vibration dependent}
\end{aligned}
$$

(Eq. 5-50)

The direction of vibratory acceleration with respect to the gyro coordinate system is arbitrary and, for that matter, so is the orientation of the gyro in the inertial reference frame. In an attempt to distinguish acceleration-induced torque, however, torques from other sources should obviously be minimized wherever possible. This points immediately to test orientations which position

the gyro input axis in the sterile plane, i.e. the plane perpendicular to earth's axis. There are three such orientations that have been employed in vibration testing at MIT. These three orientations locate OA or SRA parallel to earth's axis or IA perpendicular to it, as shown in figure 5-23. Also shown in that figure is the vibratory acceleration vector, which lies in the east-west direction. In each orientation, the gyro rotates about one fixed axis through a series of angular test positions. The analysis of reference (21) derives equations for all three orientations which, in terms of the compliance coefficients, relate gyro torque to acceleration amplitude, $(SF)_v$, and gyro position, A_F. Analysis of one orientation (OA parallel to EA) follows to characterize the method in depth. Only the compliance or g^2 - sensitive coefficients will be considered.

In the OA parallel to EA orientation shown in figure 5-23, the components of specific force due to vibratory acceleration along each of the gyro axes are

$$(SF)_{v(S)} = -V(SF)_v \sin A_F$$

$$(SF)_{v(I)} = -(SF)_v \cos A_F$$

$$(SF)_{v(O)} = 0 \qquad \text{(Eq. 5-51)}$$

where

V = +1 for OA pointed south

= -1 for OA pointed north

AF = mounting fixture angle that increases with rotation (about OA in this orientation) in the $-W_{IE}$ direction.

As far as vibration-dependent torque is concerned, only the last portion of equation 5-50 is important, and

$$W_{d(vib)} = W_d - D_F - \text{(gravity-dependent drift)} \qquad \text{(Eq. 5-52)}$$

where

$W_{d(vib)}$ = gyro drift rate due to vibration

Substituting equation 5-51 into equation 5-50, and considering only that torque which varies with vibratory acceleration,

$$W_{d(vib)} = \frac{(SF)_v^2}{4}(D_{II} + D_{SS}) + V\frac{(SF)_v^2}{4}(D_{IS}) \sin 2A_F + \frac{(SF)_v^2}{4}(D_{II} - D_{SS}) \cos 2A_F \qquad \text{(Eq. 5-53)}$$

where the remaining coefficients do not contribute torque in this orientation.

An evaluation of the compliance coefficients in equation 5-53 can be carried out by measuring torque at each of a complete cycle of angular positions. If equation 5-53 evaluated at 0° is called A_1, at 45° is called A_2, ... and at 315° is called A_8, solving for the compliance coefficients yields

$$VK_1 = A_2 - A_4 + A_6 - A_8$$

$$K_2 = A_1 + A_5$$

$$K_3 = -(A_3 + A_7) \qquad \text{(Eq. 5-54)}$$

Since all three orientations are similar geometrically, it can be shown that an algorithm exists in which the K_1, K_2 and K_3 above represent compliance coefficients in accordance with table 5-6. In actual practice the A coefficients of equation 5-54 are determined from a least-squares fit to the torque data that is collected at various vibration levels at fixed frequency. The compliance

coefficients are then extracted according to table 5-6; these are overall values for the corresponding range of acceleration. Thus, all six of the compliance coefficients are determined with redundant measurements of three of the six.

Automatic instrumentation records and accumulates the torque data during linear vibration testing. Torque data is recorded for the same set of acceleration levels at each angular position. Angular position changes are made manually as are the settings of the acceleration levels at each position. After a complete cycle of angular positions, the data from that orientation is processed to extract the appropriate compliance coefficients. All of the data processing takes place on a modern high-speed digital computer. More detailed information on the data processing equipment is given in section 8. The vibration equipment is described in chapter 4.

6. Centrifuge Testing - P. J. Palmer

Inertial system operation in high-g environments has focused attention on those terms of the gyro error model that are functions of acceleration squared or of the higher powers of acceleration. Nonlinearities in these terms - such as the example given in table 5-5 - must be investigated extensively to meet system performance requirements at high g levels.

The precision centrifuge offers the only means, on earth, of applying a sustained linear acceleration for an indefinitely long period. The centrifuge would thus seem ideally suited to the task of determining the sensitivity of a gyro to linear acceleration. A centrifuge has an obvious disadvantage, however, in that it generates relatively large angular velocities to which the gyro is extremely sensitive. The critical problem in gyro testing on a centrifuge, therefore, becomes that of isolating the gyro from this large angular velocity.

Interfering Inputs

The major interfering input during centrifuge testing is the high angular rate generated by the centrifuge. Even the largest centrifuges in existence today require an angular velocity of about 10 rad/sec to reach 100 g's.

The gyro's sensitivity to the centrifuge angular velocity can be minimized by:

(a) reduction of the angular momentum of the gyro wheel

(b) alignment of the gyro input axis perpendicular to the centrifuge angular-velocity vector

(c) location of the gyro on a counter-rotating fixture

The first method employs low (or zero) wheel speed to reduce (or eliminate) the gyroscopic action of the instrument which translates angular velocity into output torque. Although the acceleration-sensitive error coefficients are not a function of the wheel angular momentum, *per se*, they are phenomena of the wheel and its support mechanisms. Therefore, any change from normal wheel speed is apt to affect the gyro's error coefficients.

Alignment of the sensitive (input) axis of the gyro perpendicular to the centrifuge axis will certainly reduce angular-velocity inputs. In the case of precision gyros, however, the alignment accuracy necessary becomes a formidable problem. A 980-cm radius centrifuge, for example, operating at an acceleration of ten times gravity, requires gyro alignment to better than five seconds of arc to

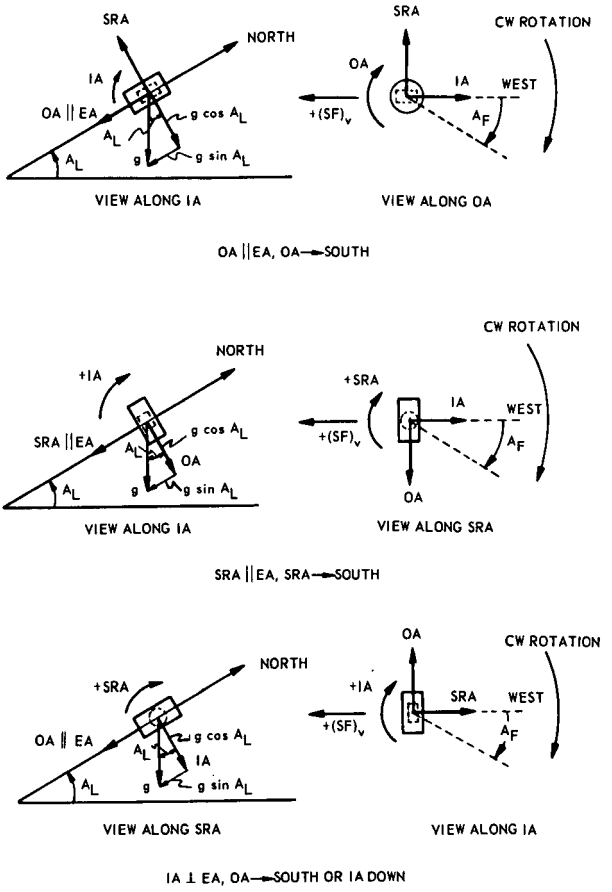

Fig. 5-23 Gyro orientations for linear-vibration testing

reduce interfering rates to below one earth rate. The situation is further complicated because the gyro actually has a plane, not just an axis, that is sensitive to angular velocity. Even though it is considered a single-degree-of-freedom gyro, the other restrained axis is usually incapable of withstanding the large gyroscopic torques that are generated during centrifuging. For example, gyroscopic torque generated by the centrifuge angular velocity about the output axis will precess the float about the input axis until restrained by the output-axis suspension. This precessional torque may exceed the restraining torque provided by the magnetic-suspension elements and result in pivot-to-jewel loading with its accompanying torque uncertainties. This then requires that the gyro's sensitive plane be aligned perpendicular to the centrifuge axis. Such a requirement becomes a major test limitation of this method because it eliminates the possibility of orienting the gyro to have the acceleration vector along the spin axis.

Even with the gyro wheel at standstill, the centrifuge angular velocity generates an anisoinertia (or dynamic-unbalance) torque. Anisoinertia torque is a gyroscopic torque that is developed whenever a rigid body is rotated with respect to inertial space about an axis not parallel to a principal axis of inertia. (See Derivation Summary 5-3 on pages 270-2. The torque generated about the float OA is a function of the angular velocities in the IA-SRA plane and of the difference in moments of inertia in the IA-SRA plane. Although output-axis anisoinertia torques are eliminated with OA parallel to the centrifuge axis, the entire centrifuge rate then appears about OA with the possibility of the problems discussed in the previous paragraph.

Table 5-7 Effect of interfering inputs during centrifuging without counter-rotation

Gyro orientation	IA senses centrifuge rate	Anisoinertia torque	Float precession about IA*
IA vertical	Yes	Yes	No
SRA vertical	No	Yes	No
OA vertical	No	No	Yes

*Can be minimized by testing with gyro wheel at standstill or rotating at low speed.

The effects of centrifuge rate on the gyro without counter-rotation are summarized in table 5-7. If a gyro is to be centrifuged without counter-rotation, wheel operation at low speed seems to be the most expedient method of minimizing the gyroscopic torques developed by the centrifuge angular velocity. Centrifuging with the gyro output axis parallel to the centrifuge axis eliminates the anisoiertia. Therefore, whenever possible, centrifuge testing without counter-rotation is conducted with the gyro output axis vertical. In this orientation, radial, axial, and a combination of radial and axial spin-axis-bearing loading can be investigated.

In all cases where tests are run at other than normal wheel speed, the test data must be related to data taken at normal wheel speed. When tests are run with the wheel at standstill, the centrifuge acceleration acting on the static mass unbalance of the wheel may cause the wheel to rotate to a new orientation with respect to the float. This would appear as a change in mass unbalance. In addition, the effects of wheel speed on bearing stiffness and on thermal gradients must be taken into account.

Counter-rotation seems to offer the best method for centrifuge testing of a gyro. In ideal operation, it places the gyro in a nonrotating acceleration environment without acceleration gradients, that is, all parts of the gyro are subjected to the same centripetal acceleration. In terms of the resultant environment, the centrifuge now resembles a two-axis linear vibrator with the characteristics of constant amplitude and orthogonal phasing. However, this method, like the others, has its own problems. Adequate isolation from the large centrifuge angular velocities ultimately depends on the stability of mechanical devices. One arc second misalignment of the axis of the counter-rotating fixture introduces five parts per million of the centrifuge angular velocity.

Improper gyro operating temperature also results in interfering torques during centrifuge testing whether or not counter-rotation is used. If the gyro operating temperature is not precisely at flotation temperature, the effects of acceleration acting on the unfloated mass of the float will load the output-axis suspension. In the case of a pivot-and-jewel type of suspension, frictional torque will result. Even in a magnetically suspended instrument, the force resulting from the centrifuge acceleration acting on the unfloated mass may be large enough to overcome the suspension force and cause frictional torque. In either case, fluid torques will be created from the motion (velocity) of the float, which is eccentric with respect to the case. These are transient torques that only occur while the float is in motion, but their characteristic time may be long. Thus, the gyro temperature must be maintained at flotation temperature within narrow limits throughout centrifuge testing. In the MIT gyro design, differential voltage signals from the magnetic suspension indicate the position between the rotor and stator. Changes in these signals indicate a change in relative float-to-case position. The operating temperature of the gyro can then be set within prescribed limits of flotation temperature by reading the suspension signals while the unit is centrifuged.

The various test interferences must be minimized and, if possible, their effects separated from the test results. In the case of centrifuge rate interferences caused by counter-rotation errors, both methods must be used. The counter-rotating fixture must therefore be rigid and, in general, capable of remote alignment.

Techniques

The objective in gyro centrifuge testing is to calibrate the terms of the gyro error model in a sustained high-acceleration environment. The goal is to complete the task with a minimum number of tests yet with a high degree of accuracy.

As is the case during linear-vibration testing, the gyro is calibrated in the one-g test laboratory before and after centrifuge testing. The purpose of these tests is to insure the validity of the centrifuge test data by monitoring the experiment controls across the acceleration exposure.

Without Counter-Rotation (12). As noted previously, gyro centrifuge tests without counter-rotation are usually conducted with the gyro wheel at standstill or rotating at low speed to minimize the gyroscopic torques generated by the centrifuge angular velocity. In addition, they are conducted whenever possible with the gyro output axis vertical (parallel to the centrifuge axis) to eliminate the anisoinertia torque.

A minimum of seven separate centrifuge tests must be conducted in two basic gyro orientations (OA vertical and SRA vertical) in order to extract ten error

terms from the test data. These tests are summarized in table 5-8.

Inspection of table 5-8 shows that the test data comprises terms that are not acted upon by the centrifuge acceleration, those that are acted upon by the centrifuge acceleration and those that are acted upon by the centrifuge acceleration squared. These are tabulated as the C_0, C_2 and C_4 terms of the power-series

$$W_d = C_0 + C_1 W_{(cf)} + C_2 r W^2_{(cf)} + C_3 W^3_{(cf)} + C_4 r^2 W^4_{(cf)} \qquad \text{(Eq. 5-55)}$$
$$= C_0 + \ldots\ldots\ldots + C_2 (SF)_{(cf)} + \ldots\ldots\ldots + C_4 (SF)^2_{(cf)}$$

where

r = centrifuge radius

$W_{(cf)}$ = centrifuge angular velocity

$(SF)_{(cf)}$ = centrifuge specific force = $rW^2_{(cf)}$

The C_1 and C_3 coefficients, which are misalignment terms, are not included. If misalignment is zero, they are both zero. The computation procedure for extracting the gyro error coefficients is given in table 5-9.

Note that an anisoinertia torque term appears in the C_2 coefficient when OA is not parallel to $W_{(cf)}$. Since anisoinertia torque is a function of $W^2_{(cf)}$ not $(SF)_{(cf)}$, it can be measured by running tests at two different centrifuge-arm lengths at two different values of $W_{(cf)}$ selected to result in the same $(SF)_{(cf)}$ at each radius. The change in the C_2 coefficient between the two tests is a measure of the anisoinertia torque alone.

As with most test procedures, this centrifuge test procedure has both advantages and disadvantages. Among the advantages are:

(a) the gyro is subjected to the maximum acceleration along four axes, SRA, IA, OA and 45 degrees to SRA and IA

(b) seven tests are the minimum number required to obtain ten coefficients

(c) the maximum coefficient information is obtained for each gyro position

(d) the number of lumped coefficients represented by each power-series term is minimized

(e) the number of changes in gyro orientation is minimized

(f) interfering inputs such as anisoinertia torques and precession torques due to centrifuge angular velocity are minimized

Some of the disadvantages are:

(a) D_{IO}, which is a compliance term resulting from displacement of the effective center of mass of the gyro float along SRA, is obtained with ± 1g acting along OA in tests 1 and 2. The same comment applies to D_{OS} in tests 3 and 4; but in tests 6 and 7, D_{OS} can be obtained with maximum acceleration along OA.

(b) D_{II} and D_{IS} cannot be cross checked with data obtained from another test. At least partial cross checking is possible for the other coefficients. In cases of data discrepancies, other test orientations can be used (21).

Table 5-8 Summary of gyro error coefficients obtained from centrifuge tests at specific gyro orientations without counter-rotation

	Gyro orientation		Error coefficients**		
Test	Vertical	$(SF)_{(cf)}$*	C_0	C_2***	C_4
1	OA ↓	IA ↓, SRA →	$D_F+gD_O+g^2D_{OO}$	$-D_I-gD_{IO}$	D_{II}
2	OA ↑	SRA ←, IA ↓	$D_F-gD_O+g^2D_{OO}$	$-D_I+gD_{IO}$	D_{II}
3	OA ↓	IA ←, SRA ↓	$D_F+gD_O+g^2D_{OO}$	$-D_S-gD_{OS}$	D_{SS}
4	OA ↑	SRA ↓, IA →	$D_F-gD_O+g^2D_{OO}$	$-D_S+gD_{OS}$	D_{SS}
5	OA ↓	IA ↙, SRA ↘	$D_F+gD_O+g^2D_{OO}$	$0.707(-D_I-D_S+gD_{IO}-gD_{OS})$	$0.5(D_{IS}+D_{II}+D_{SS})$
6	SRA ↑	IA ←, OA ↓	$D_F-gD_S+g^2D_{SS}$	$-D_O+gD_{OS}+\frac{\Delta I}{2}\sin 2\theta$	D_{OO}
7	SRA ↓	IA ↓, OA ←	$D_F+gD_S+g^2D_{SS}$	$D_O+gD_{OS}+\frac{\Delta I}{2}\sin 2\theta$	D_{OO}

* Directed outwards along centrifuge arm away from centrifuge axis.

** Error coefficients from power-series expansion of gyro drift rate about OA. See equation 5-55.

*** $(\Delta I/2)\sin 2\theta$ is anisoinertia torque where ΔI is the difference in moments of inertia about the principal inertia axes closer to SRA and IA, respectively, and θ is the angle between the smaller moment of inertia axis and the angular-velocity vector measured about OA. Anisoinertia torque is a function of $W^2_{(cf)}$ not $(SF)_{(cf)}$.

Table 5-9 Computation procedure for gyro centrifuge tests without counter-rotation

Required coefficient	Obtain from
D_{IO}	C_2 of tests 1 and 2
D_{OS}	C_2 of tests 3 and 4
D_{II}	C_4 of tests 1 and 2
D_{SS}	C_4 of tests 3 and 4
D_{IS}	C_4 of tests 5, 1, and 3
D_{OO}	C_4 of tests 6 and 7
D_F	C_0 of tests 1 and 2 and C_4 of tests 6 and 7
D_I	C_2 of tests 1 and 2
D_S	C_2 of tests 3 and 4
D_O	C_2 of tests 6 and 7

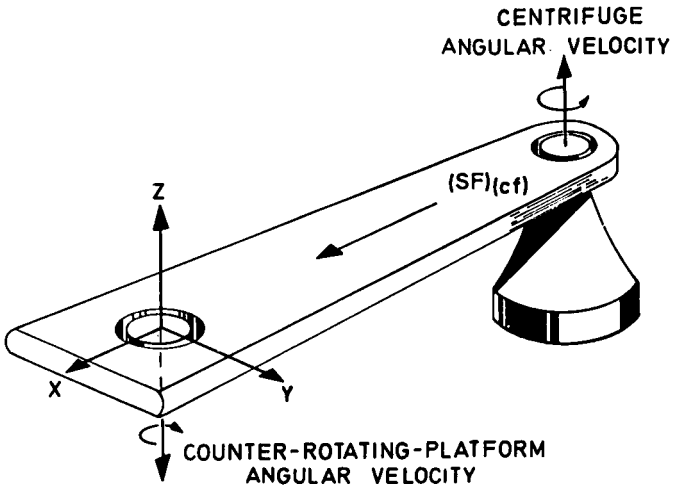

Fig. 5-24 Geometry definitions for gyro centrifuge testing on a counter-rotating platform

Table 5-10 Functional model for centrifuge test data with counter-rotation

Fourier series*	Power series** C_0	C_1	C_2	C_3	C_4
A_0	$D_F + gD_Z + g^2D_{ZZ}$	Counter-rotation rate error		Counter-rotation rate error caused by unbalance	$\frac{1}{2}(D_{XX} - D_{YY})$
A_1		Counter-rotation axis constant misalignment	$D_X + gD_{XZ}$	Counter-rotation axis misalignment caused by unbalance	
A_2					$\frac{1}{2}(D_{XX} + D_{YY})$
B_1		Counter-rotation axis constant misalignment	$D_Y + gD_{YZ}$	Counter-rotation axis misalignment caused by unbalance	
B_2					$\frac{1}{2}D_{XY}$

*Fourier series: $W_d = A_0 + A_1 \cos \omega t + A_2 \cos 2\omega t + B_1 \sin \omega t + B_2 \sin 2\omega t$

**Power series: $W_d = C_0 + C_1W_{(cf)} + C_2rW^2_{(cf)} + C_3W^3_{(cf)} + C_4r^2W^4_{(cf)}$

$= C_0 + C_1W_{(cf)} + C_2(SF)_{(cf)} + C_3W^3_{(cf)} + C_4(SF)^2_{(cf)}$

Note: See figure 5-24 for definition of X, Y and Z axes.

(c) the data must be taken with the gyro wheel at standstill or rotating at low speed

With Counter-Rotation. The geometry of a centrifuge test with the gyro mounted on a counter-rotating platform is as depicted in figure 5-24. The gyro coordinate system is represented by the X, Y, Z triad, which is fixed with respect to the counter-rotating platform. The specific forces along the X, Y, Z axes are

$$(SF)_X = (SF)_{(cf)} \cos \omega t$$
$$(SF)_Y = (SF)_{(cf)} \sin \omega t \qquad \text{(Eq. 5-56)}$$
$$(SF)_Z = -g$$

where

ω = centrifuge frequency in rad/sec

The gyro drift rate, truncated to acceleration-squared terms, may then be written as

$$\begin{aligned} W_d &= D_F + D_X (SF)_X + D_Y (SF)_Y + D_Z (SF)_Z \\ &+ D_{XX} (SF)_X^2 + D_{YY} (SF)_Y^2 + D_{ZZ} (SF)_Z^2 \\ &+ D_{XY} (SF)_X (SF)_Y + D_{XZ} (SF)_X (SF)_Z + D_{YZ} (SF)_Y (SF)_Z \end{aligned} \qquad \text{(Eq. 5-57)}$$

Centrifuging subjects the gyro to a rotating acceleration field, and this environment results in a gyro drift rate that can be expanded in a Fourier series with the fundamental frequency being the centrifuge rate. The separation of test interferences from gyro acceleration torques is simplified by the relationship between applied acceleration and centrifuge angular velocity, since centripetal acceleration increases as the square of centrifuge rate. Now, if the counter-rotating fixture misalignment is a pure power series in applied centripetal acceleration, the resultant interfering rates will all be odd powers of centrifuge rate while the gyro acceleration-sensitive error coefficients will all be proportional to even powers of centrifuge rate (that is, integer powers of applied acceleration). A separation can therefore be obtained by also expanding the test data into a power series of centrifuge rate. Table 5-10 summarizes these operations and makes apparent the coefficient-extraction process. Since power-series coefficients are not orthogonal, care must be taken to ensure that all powers that have a mechanism are included in the reduction model.

As an example, assume a gyro to be mounted on the centrifuge as shown in figure 5-24 with SRA aligned along X, IA along Y, and OA along Z. Equation 5-57 then becomes, after combining and rearranging terms

$$\begin{aligned} W_d &= D_F + D_{O}g + D_{OO}g^2 + 1/2(D_{SS} + D_{II})(SF)_{(cf)}^2 \\ &+ (D_S + D_{OS}g)(SF)_{(cf)} \cos \omega t + 1/2(D_{SS} - D_{II})(SF)_{(cf)}^2 \cos 2\omega t \\ &+ (D_I + D_{IO}g)(SF)_{(cf)} \sin \omega t + 1/2 D_{IS} (SF)_{(cf)}^2 \sin 2\omega t \end{aligned} \qquad \text{(Eq. 5-58)}$$

This orientation alone would therefore yield only three of the error coefficients, D_{SS}, D_{II}, and D_{IS}. Additional tests in other orientations would have to be run to determine the others.

The uncertainty associated with this method of centrifuge testing is very dependent on both the gyro and the test model. Confidence in results will increase with acceleration and, in general, be at a high level only for the extraction of acceleration-squared (or higher-order) gyro coefficients. If acceleration-squared or higher-order terms are the only ones of interest, then the test must rely either

on rectification effects, as in vibration testing, or on wide-bandwidth data acquisition. The latter has the advantage of minimizing the number of test orientations necessary to extract all higher-order coefficients. The bandwidth necessary must be sufficient to accurately extract the second harmonic component and phase. In the absence of such bandwidth, each orientation yields only one rectified acceleration term (A_O, C_4 in table 5-10) and, in general, this term comprises more than one gyro coefficient. The cross-compliance terms (D_{IO}, D_{OS} and the so-called major compliance D_{IS}) furthermore can only be extracted by orienting the gyro so that the two axes of interest have the same phase of acceleration. This requires that neither axis be in the plane of acceleration; an optimal position orients the two axes equidistant from the acceleration plane. This orientation has the disadvantage that it reduces the maximum effective test acceleration.

Centrifuge testing using counter-rotation has the major advantage of permitting the gyro to be operated normally, in other words, at full wheel speed, in any desired orientation with respect to the centrifuge specific-force vector. Its major disadvantage is the extremely precise match required between the centrifuge angular-velocity vector and the negative counter-rotation vector.

7. Angular Vibration Testing- A. J. Smith

In system operation, the inertial gyro not only may be subjected to linear vibration and sustained linear acceleration but also to angular vibration. Some of the sources of angular vibration in a gimbaled inertial system are:

(a) low-frequency and low-amplitude motion due to vehicle angular motion and imperfect inertial-platform stabilization

(b) high-frequency linear vibration in the vehicle environment that produces angular vibration due to pendulosity of the inertial platform and its imperfect stabilization

(c) high-frequency inertial-platform motion due to electronic or electromechanical sources of noise in the platform-stabilization loop.

These sources might indicate amplitudes of at least a few arc-seconds and frequencies up to about 100 Hz. In the case of strapdown applications where the gyro is rigidly mounted to the supporting structure of the guided vehicle, the amplitude and frequency environments are those of the vehicle structure and therefore are much greater.

Two angular-vibration effects with which the designer and user of an inertial single-degree-of-freedom floated integrating gyro should be familiar are aniso-inertia torque and coning rates. The physical and geometrical causes of both these effects have been analyzed by many authors (24-33). The emphasis in this section is on the utilization of the analytical results in gyro testing at MIT.

In addition to the measurement of gyro float anisoinertia torque and coning rates, angular-vibration testing of the single-degree-of-freedom floated integrating gyro is useful:

(a) to measure gyro frequency response to angular rates about IA or OA

(b) to determine gyro constructional parameters such as wheel angular momentum, gyro gain, float and wheel inertias, and float output-axis time constant

(c) to measure dynamic characteristics of the damping fluid and float suspension (34)

(d) to measure wheel-drive-motor characteristics as functions of bearing and/or inertia loading

(e) to observe gyro and servo loop saturation or other nonlinear effects

(f) to measure performance degradation, if any, as a result of angular vibration

Although gyro frequency response and angular-vibration torques can be observed using a single-axis sinusoidal angular vibrator, a two-axis machine capable of generating orthogonal sinusoidal vibrations at various phase relationships is necessary for a more complete comparison with theoretical calculations. A machine capable of applying random angular and linear vibrations simultaneously to the test specimen would, of course, more closely simulate the gyro operational environment. However, such a machine would be extremely difficult to design and construct and would not be as useful analytically as a machine that subjects the gyro to a single sinusoidal frequency at a time. Furthermore, if the random vibration environment in which the gyro is to be used is known, standard mathematical techniques can be used to determine anticipated coning and anisoinertia vibration-induced rates from sinusoidally generated test results (31). In any case, since angular-vibration test equipment must be precision devices so that spurious inputs or nonlinearities do not mask or modify the desired measurements, the design and construction of a two-or-three-axis sinusoidal angular vibrator of sufficient amplitude and frequency range is a formidable task limited primarily by the weight (inertia) and volume of the test specimen (35). At MIT, a two-gimbal device capable of producing sinusoidal angular oscillations simultaneously at any phase about orthogonal axes has been built and used to obtain test data satisfactorily accurate to affirm the theoretical expectations. A description of this machine and its associated electronics is included in chapter 4 and also may be found in references (36) and (37). The techniques used to check out the MIT angular vibrator and the results of this check-out are given in reference (38).

Typical gyro-frequency-response characteristics, the measurement of anisoinertia and coning rates, and the use of this data to determine gyro constructional parameters are discussed in the remainder of this section. Note should be taken at this point that, under angular vibration, the gyro float axes can no longer be assumed to be coincident with the gyro case axes. In other words, the spin, input, and output axes must be differentiated from the spin reference (SRA), input reference (IRA), and output reference (ORA) axes. Therefore, the complete notation for each axis is used with the symbols in this section.

Frequency Response Measurement

It was shown in 'Higher Order Effects', page 198, that for relatively low frequencies the gyro performance function for angular rate inputs about IA is approximated by

$$\frac{A_{(CF)OA}}{A_{(IC)IA}} = \frac{H}{c_{(CF)OA}} \cdot \frac{1}{1+\tau p} \qquad \text{(Eq. 5-28) (repeated)}$$

or

$$\frac{W_{(CF)OA}}{W_{(IC)IA}} = \frac{H}{c_{(CF)OA}} \cdot \frac{1}{1+\tau p} \qquad \text{(Eq. 5-59)}$$

with a magnitude, or dynamic amplitude ratio (DAR), of

$$\left|\frac{A_{(CF)OA}}{A_{(IC)IA}}\right| = \frac{H}{c_{(CF)OA}} \cdot \left(\frac{1}{1+\tau^2\omega^2}\right)^{1/2} \qquad \text{(Eq. 5-29) (repeated)}$$

and a phase angle, or dynamic response angle (DRA), of

$$DRA = -\tan^{-1}(\tau\omega) \qquad \text{(Eq. 5-30) (repeated)}$$

Also, in that section, it was shown that for relatively low frequencies the gyro performance function for angular rate inputs about OA is approximated by

$$\frac{A_{(CF)OA}}{A_{(IC)OA}} = -\frac{\tau p}{1+\tau p} \qquad \text{(Eq. 5-34) (repeated)}$$

or

$$\frac{W_{(CF)OA}}{W_{(IC)OA}} = -\frac{\tau p}{1+\tau p} \qquad \text{(Eq. 5-60)}$$

with a magnitude of

$$\left|\frac{A_{(CF)OA}}{A_{(IC)OA}}\right| = \left(\frac{\tau^2\omega^2}{1+\tau^2\omega^2}\right)^{1/2} \qquad \text{(Eq. 5-35) (repeated)}$$

and a phase angle of

$$DRA = -\frac{\pi}{2} - \tan^{-1}(\tau\omega) \qquad \text{(Eq. 5-36) (repeated)}$$

In the derivation of the above equations, it is assumed that:

(a) the gyro wheel and float structure is infinitely rigid, allowing wheel motion only about the spin axis. If the effects of wheel-to-float and float-to-case compliance are to be included in a more rigorous analysis, the gyro performance functions for inputs about IA or OA are seventh-order equations (20).

(b) float-to-case rotation is about the float output axis only; that is OA remains parallel to ORA. In the MIT inertial gyros, the rotational damping about a float radial axis (IA, SA, etc.) is four orders of magnitude greater than that for rotation about its output axis allowing this approximation.

(c) the float-to-case angular rotation about the output axis is limited to small angles. A float rotation of one degree about OA would cause an error in gyro-gain, $H/c_{(CF)OA}$ indication of $(1 - \cos 1^\circ)$ or 0.00015, which may be considered as negligible.

(d) the only reactive gyro parameters considered are the float-to-case damping and the float and wheel moment of inertias about the float output axis. That is, in addition to assumptions (a) and (b), any case-to-float elastic restraint about the float output axis is considered to be insignificant.

(e) the amplitude of angular vibration inputs is small (less than one degree maximum).

Since inputs are needed about a single axis only, gyro-frequency-response measurements may be made using a single-axis angular vibrator or a gyro test

turntable that can be driven over the necessary amplitude and frequency range. Accurate results, of course, require accurate measurements of input and output oscillation amplitudes and of the relative phase between them. Carefully calibrated signal-generator microsyns on the gyro output and vibrator gimbal axes are used at MIT to measure the amplitude of the input and output oscillations. The most accurate method of measuring the relative phase between the input and output oscillations that has been found to date is to use a counter to compare the time between the 'zero crossovers' of each microsyn output with the oscillation period time.

An alternative method that may be used with a two-axis vibrator to determine the gyro-frequency-response characteristics to inputs about IA is to set the output-axis external vibration to an amplitude and phase relationship that reduces the gyro microsyn output-signal oscillation to zero for each input oscillation. In this way, exact knowledge of the gyro microsyn voltage-output - angle-input sensitivity is not needed for the response measurement and may, if desired, be determined from the test.

Since the gyro precessional property is not used for frequency-response measurements for inputs about OA, this test may be run either with the gyro wheel running (for thermal purposes) or with the gyro wheel at standstill. In other words, this test is of the viscous integrating properties of the gyro, independent of the wheel-to-float coupling characteristics (which are assumed perfect for the reduced equation).

Typical nondimensionalized gyro response characteristics are shown in figures 5-25/26. As suggested by those figures, for accurate determination of gyro parameters, the test frequency range used should extend from at least one order of magnitude below to one order of magnitude above the first-order frequency breakpoint, $1/\tau$. The broken curves indicate how ball-bearing-gyro frequency-response characteristics might be modified if the above assumptions were not made. By plotting the data on log-log paper, it can be seen that:

(a) the gyro gain, $S_{(gu)}$ which is equal to $H/c_{(CF)OA}$, is the magnitude of $A_{(CF)O}/A_{(IC)IA}$ as the vibration frequency, ω, approaches zero (Fig. 5-25).

(b) the gyro first-order time constant, τ, which is equal to $I_{OA}/c_{(CF)OA}$, is the reciprocal of the angular frequency, ω_b, at which the phase shift is 45 degrees and at which the amplitude-ratio curves break (Figs. 5-25 and 5-26).

If the gyro wheel angular momentum (H), float inertia (I_{OA}), or damping coefficient ($c_{(CF)\,OA}$) is known, the other two parameters can be easily calculated.

Kinematic Rectification Rates

Theoretical background indicates that application of simultaneous angular vibrations about the spin and input or spin and output axes of a single-degree-of-freedom floated integrating gyro can produce appreciable steady-state float-input-axis rates. To produce this steady-state rate, the two angular vibrations must be of identical frequency but can be of any phase relationship. For constant-amplitude vibrations, the vibration-produced rate varies with the frequency of angular vibration and is a function of the gyro response characteristics. In the case of in-phase angular vibrations about the gyro spin and input axes, an additional torque rate proportional to the difference between the float principal moments of inertia in the IA-SA plane is also developed. (In most cases, the

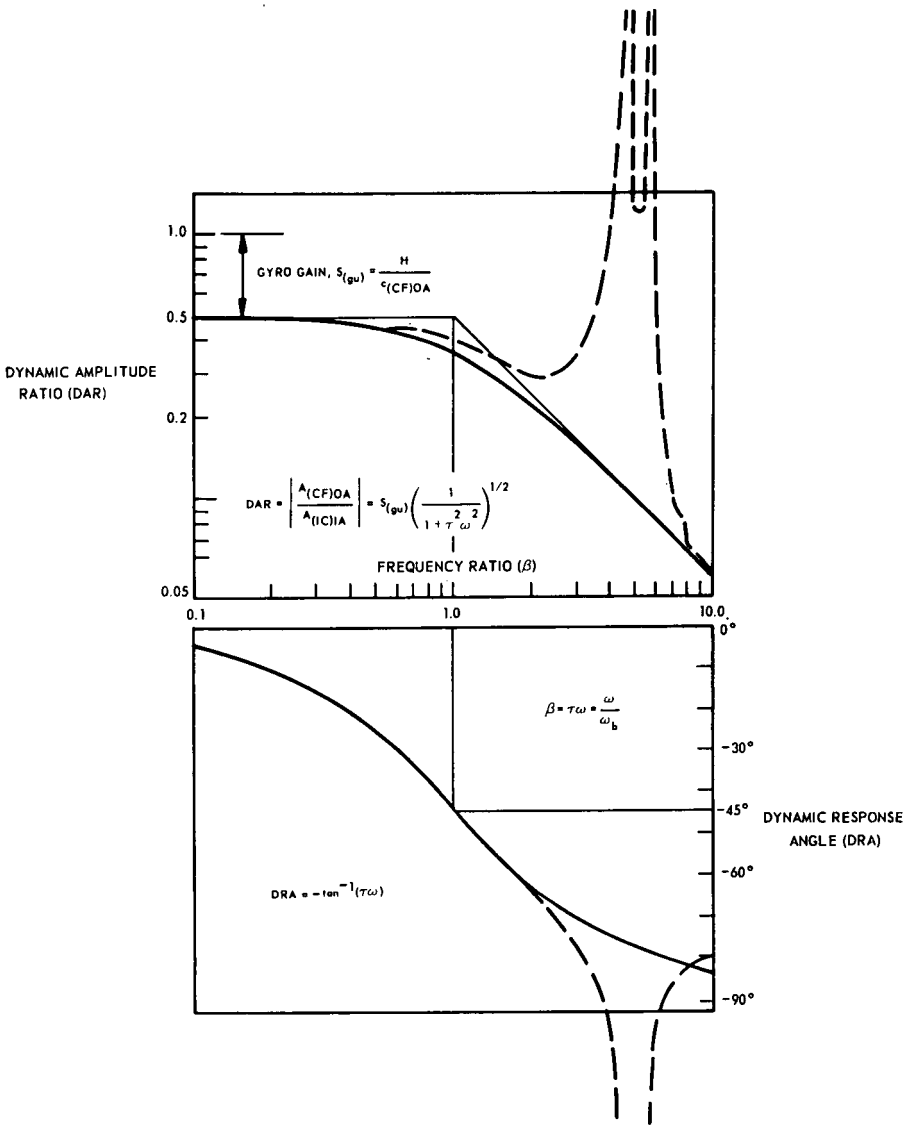

Note: Continuous curves are first-order approximations calculated from gyro parameters; broken curves indicate effects of bearing and float compliances.

Fig. 5-25 Gyro frequency response to angular vibration about IA

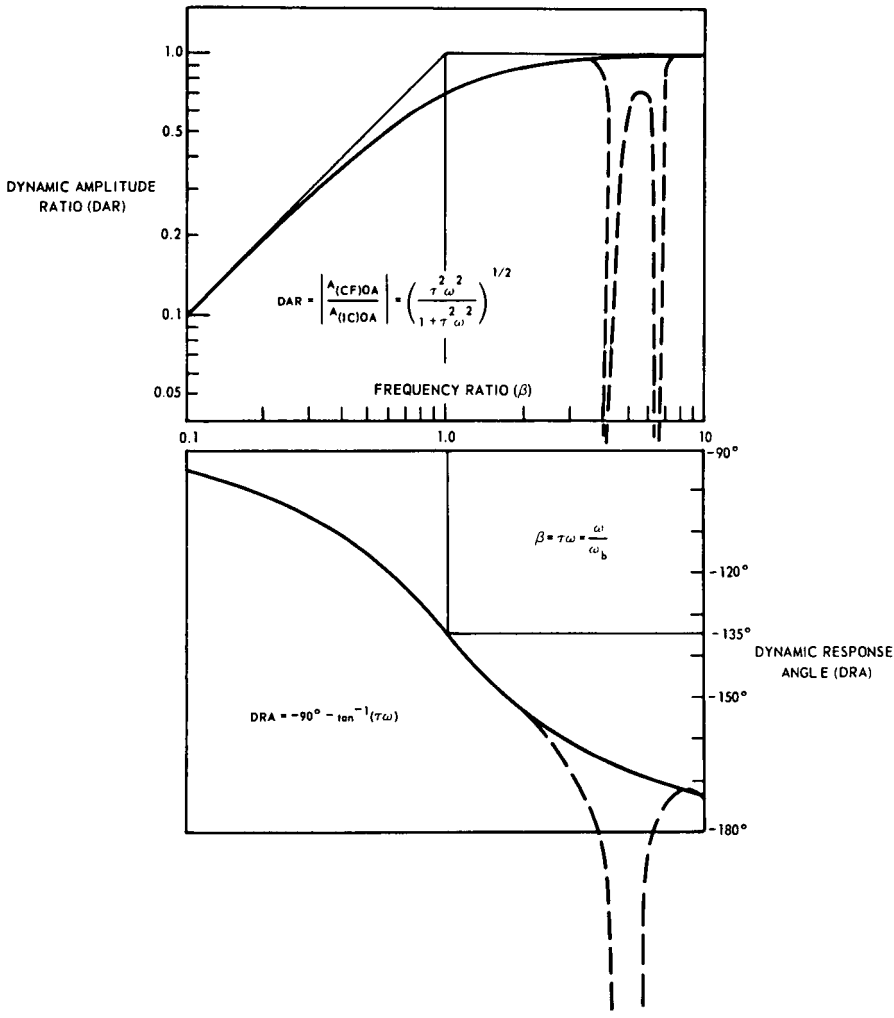

Note: Continuous curves are first-order approximations calculated from gyro parameters; broken curves indicate effects of bearing and float compliances.

Fig. 5-26 Gyro frequency response to angular vibration about OA

float principal axes of inertia are nearly coincident with the gyro case spin and input reference axes).

The angular-vibration-induced rate is commonly called the coning effect because the input axis of the gyro float traces a conical surface during the generation of the steady-state input-axis-sensed rate. The output-axis torque due to the difference of the float inertias is commonly called anisoinertia or dynamic-unbalance torque. The equivalent input-axis anisoinertia torque rate is determined by the gyro wheel angular momentum.

Model Equation. Derivation Summaries 5-1 through 5-3 (Appendix B of this chapter) outline how the coning and anisoinertia rate terms are generated by simultaneous angular vibration about two orthogonal gimbaled axes such as those of the MIT precision angular vibrator (see chapter 4). The magnitude of the quadrature coning terms for the strapdown (nongimbaled) situation may be up to two times greater depending on the structural dynamics of the gyro environment (24, 26). In addition, an extremely high servo-loop stiffness will also modify these equations to some degree. Thus, in the derivation summaries, normal servo-loop stiffness and a gimbaled gyro mount are assumed. Also, the assumptions stated on page 238 regarding gyro structural rigidity and low-amplitude-vibration are still taken as valid. With these assumptions, the average kinematic rectification rate produced about a gyro input axis by angular vibration about two orthogonal gimbaled axes is

$$W_{K(gim)} = \left(\frac{\tau\omega^2\cos\alpha_1 - \omega\sin\alpha_1}{2(1+\tau^2\omega^2)}\right)\left|A_{(IC)ORA}\right|\left|A_{(IC)SRA}\right| + S_{(gu)}\left(\frac{\tau\omega^2\cos\alpha_2 - \omega\sin\alpha_2}{2(1+\tau^2\omega^2)}\right)\left|A_{(IC)IRA}\right|\left|A_{(IC)SRA}\right| + \left[\frac{(I_{SA}-I_{IA})}{2H}\omega^2\cos\alpha_2\right]\left|A_{(IC)IRA}\right|\left|A_{(IC)SRA}\right| \quad \text{(Eq. 5-61)}$$

where

$W_{K(gim)}$ = angular-vibration-induced kinematic rectification rate in rad/sec

τ = gyro first-order time constant for rotational motion of the float with respect to the case about OA in seconds

$= I_{OA}/c_{(CF)OA}$

I_{OA} = moment of inertia of the wheel and float about OA in gm-cm^2

$c_{(CF)OA}$ = damping coefficient between float and case about OA in dyne-cm/rad/sec

ω = angular vibration frequency in rad/sec

α_1 = phase angle by which the angular vibration about ORA leads the angular vibration about SRA

α_2 = phase angle by which the angular vibration about IRA leads the angular vibration about SRA

$|A_{(IC)ORA}|$ = amplitude of the angular vibration in radians applied about the gyro case output reference axis with respect to inertial space

$|A_{(IC)\,SRA}|$ = amplitude of the angular vibration in radians applied about the gyro case spin reference axis with respect to inertial space

$|A_{(IC)\,IRA}|$ = amplitude of the angular vibration in radians applied about the gyro case input reference axis with respect to inertial space

$S_{(gu)}$ = gyro unit sensitivity or gain

$= H/c_{(CF)\,OA}$

$I_{SA} - I_{IA} = \Delta I$ = difference of the float principal moments of inertia in the IA-SA plane (the gyro input and spin axes are assumed to be principal axes of inertia)

Each of the three terms of equation 5-61 represents an input-axis rate due to a specific effect. The first term is the rate due to spin-output axis coning. That is, the input oscillations are those present about the gyro case spin reference and output reference axes, SRA and ORA. The first half of the term is the rate generated by in-phase oscillations, the second half is that due to quadrature oscillations. The second term is the rate due to spin-input axis coning; the input oscillations are about the gyro case spin reference and input reference axes. Similarly, the first half of this term is the rate due to in-phase oscillations, and the second half is that due to quadrature oscillations. Note that the first two terms differ only by the gyro gain, $S_{(gu)}$. The third term in equation 5-61 is the equivalent input-axis rate due to the anisoinertia torque. As stated previously, this torque is caused by in-phase oscillations only.

Equation 5-61 also shows that the coning rate can only be modified by changing the gyro design (the gyro gain or time constant), but that it cannot be eliminated. In other words, a coning rate is a true input rate, a result of the kinematic rectification of orthogonal angular oscillations. It is not the result of any gyro design characteristic. The third term of equation 5-61 shows that the anisoinertia torque is the result of gyro design characteristics and that it may be eliminated by designing the float such that the inertia difference is zero.

A more complete analysis of the coning effect would yield periodic and higher-order terms as well as the average-input-axis rate given in equation 5-61. It has been shown, however, that since these terms are functions of the higher powers of the input vibration angular amplitude, they are small enough to be neglected (26).

Vibration-Rate Measurement. As noted previously, a two-axis angular vibrator is needed to obtain a complete set of measurements to determine the various gyro parameters and to verify the angular-vibration model equation. With single-axis angular-vibration test equipment, in-phase oscillations may be applied about the defined gyro axes by introducing the vibration input between the axes (39, 14), but the quadrature parts of the error equation cannot be verified. In addition, since in-phase coning rates and anisoinertia torques are additive functions of the same inputs, they cannot easily be separated into individual effects.

At MIT, the average kinematic rectification rates are measured by connecting the gyro on test in a rate-feedback loop and recording the torque-generator current required to keep the gyro float at its average null position. In order to measure the input-axis rectification rate, the gyro torque generator's current-rate sensitivity is independently determined prior to the test. This is usually done by measuring the torque-generator current required to hold the gyro float

at its signal-generator null position when known portions of the earth's rate are applied about the gyro input axis.

The remainder of this section discusses typical gyro rates as a function of vibration frequency resulting from constant-amplitude angular-oscillation inputs. The following definitions and conversion factors are used to convert to the rate units used on the plots:

meru = rad/sec multiplied by 13.75×10^6

deg/hr = meru multiplied by 0.015

= rad/sec multiplied by 0.206×10^6

Since the coning and anisoinertia rate scales are generated by dividing the calculated or measured rates by the practical milliradian input angular-vibration amplitudes, the scale conversion factor is:

$\frac{\text{meru}}{\text{mr}^2}$ = rad/sec multiplied by 13.75

$\frac{\text{deg/hr}}{\text{mr}^2}$ = rad/sec multiplied by 0.206

Figure 5-27 shows the coning rate for quadrature angular-vibration inputs about either the spin and output reference axes or the spin and input reference axes for various gyro output-axis time constants. Figure 5-28 shows the coning rate for in-phase angular vibration inputs about either the spin and output reference axes or the spin and input reference axes for various gyro time constants, and figure 5-29 shows the anisoinertia-torque equivalent input-axis rate for various values of the ratio of the float inertia difference and the wheel angular momentum. Note that, at 100 Hz and τ equal to one millisecond, angular vibration of one milli-radian applied about two of the gyro axes generates an equivalent input-axis rate of approximately 3000 meru or 45 degrees/hour. Even at an amplitude as low as 0.1 milliradian, the equivalent input-axis rate that is generated is approximately 30 meru or 0.4 degree/hour.

As was the case for the frequency-response measurement, the gyro time constant, τ, for rotation about OA is the reciprocal of the coning-rate-curve angular-frequency breakpoint. The gyro gain, $S_{(gu)}$, is the ratio (the difference on log-log scales) of the input-spin axis and output-spin axis coning rate amplitudes at each frequency. Note, however, that knowledge of the magnitude of the input oscillations - as required during frequency response measurements - is not needed to determine gyro gain. All that is required is that the magnitude of the input vibrations be the same for the two test positions. (This is true for in-phase input-spin axis measurements only at test frequencies where the rate resulting from anisoinertia torque is negligible).

Figures 5-30 and 5-31 show a comparison of in-phase and quadrature output-spin and input-spin axis angular-vibration-generated rates. These figures are enlarged portions of figures 5-27 through 5-29 for a gyro with a float output-axis time constant of one millisecond. The broken curves show how the approximate curves representing the kinematic rectification rates would be modified if the assumptions stated on page 238 were not made in deriving the rate equations.

The quadrature output-spin coning rate shown in figure 5-30 is positive because in this example the vibrations applied about the gyro output reference axis lag in time the vibrations applied about the gyro spin reference axis by 90 mechanical degrees, i.e. $\alpha = 270°$. The diagram in figure 5-30 that depicts the gyro

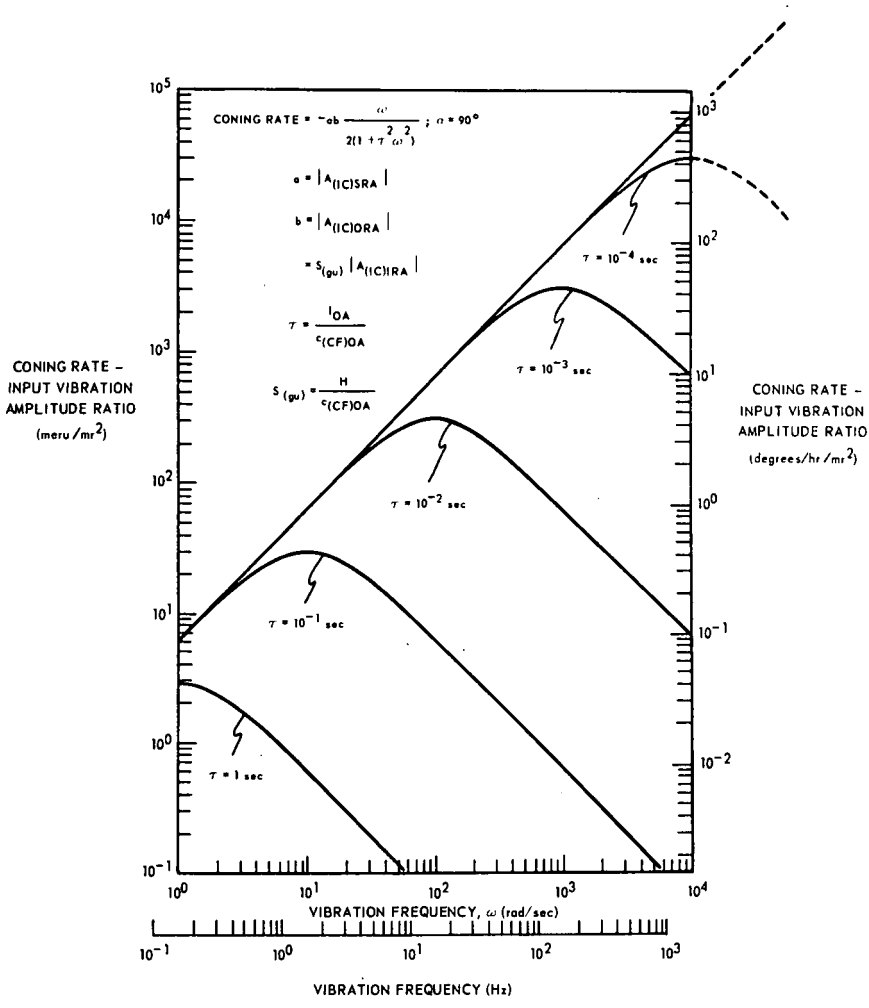

Fig. 5-27 Gyro coning rate due to quadrature angular vibrations about SRA and ORA or SRA and IRA

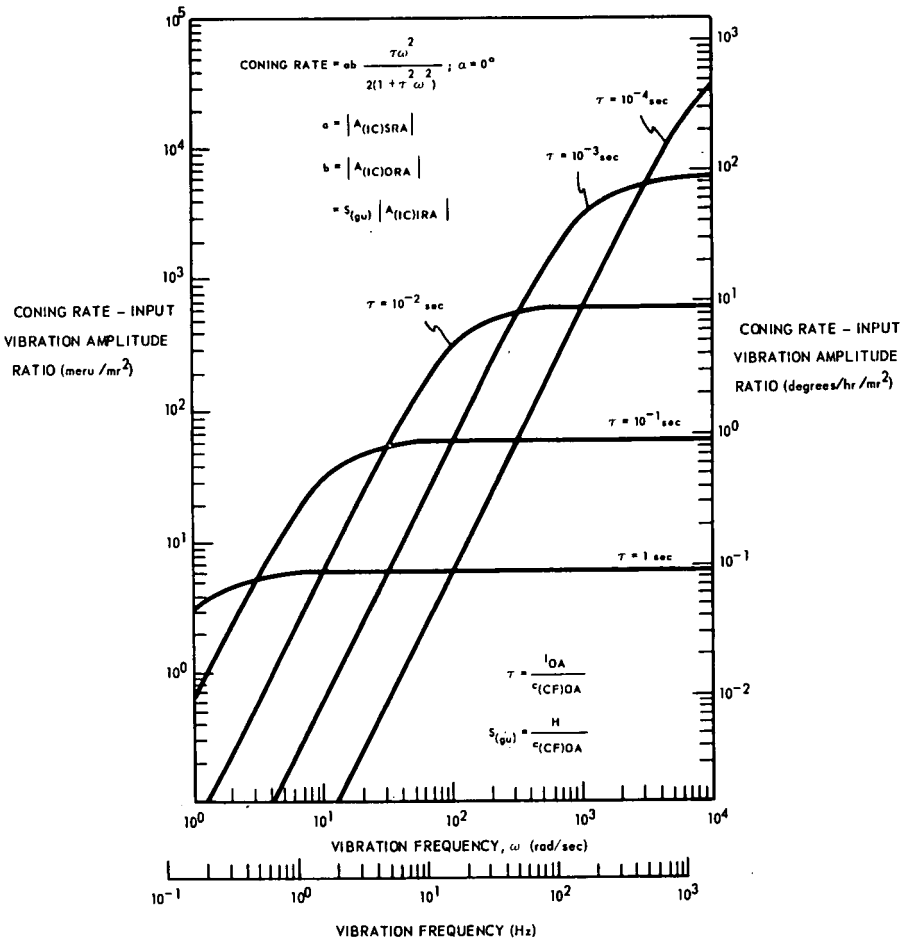

Note: Anisoinertia torque rate is not included; see figure 5-29

Fig. 5-28 Gyro coning rate due to in-phase angular vibrations about SRA and ORA or SRA and IRA

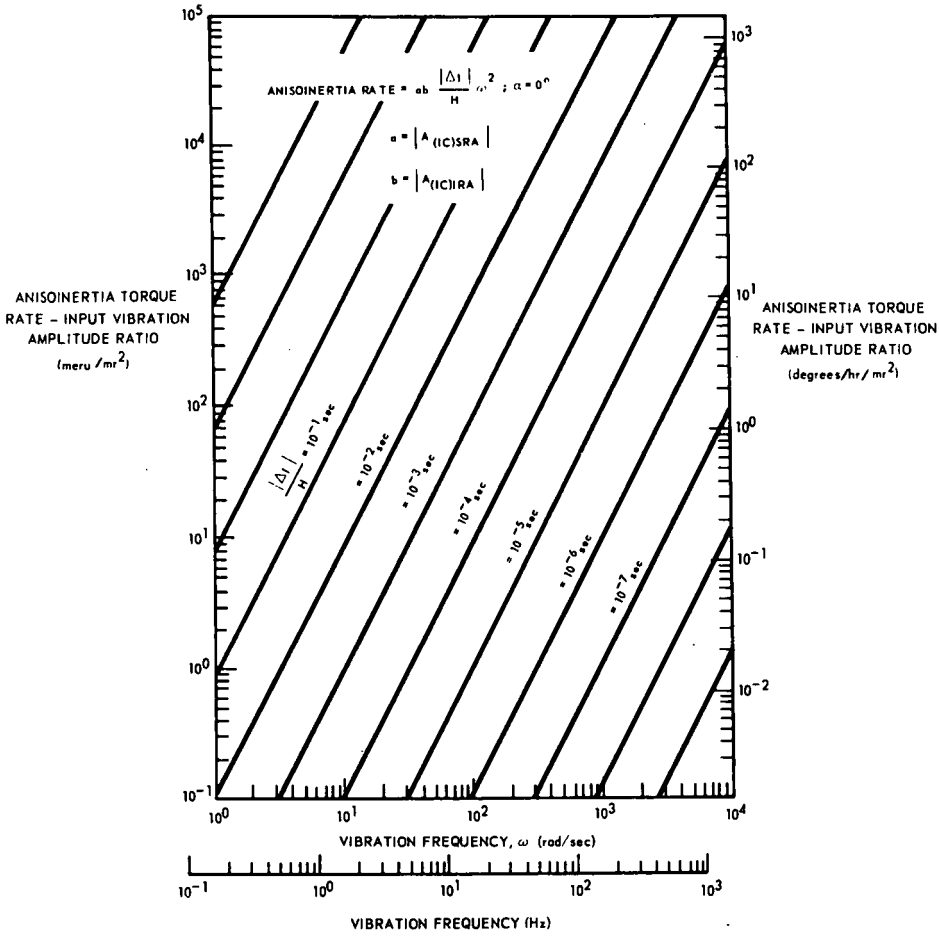

Note: Coning rate is not included; see figure 5-28.

Fig. 5-29 Gyro anisoinertia torque rate due to in-phase angular vibrations about SRA and IRA

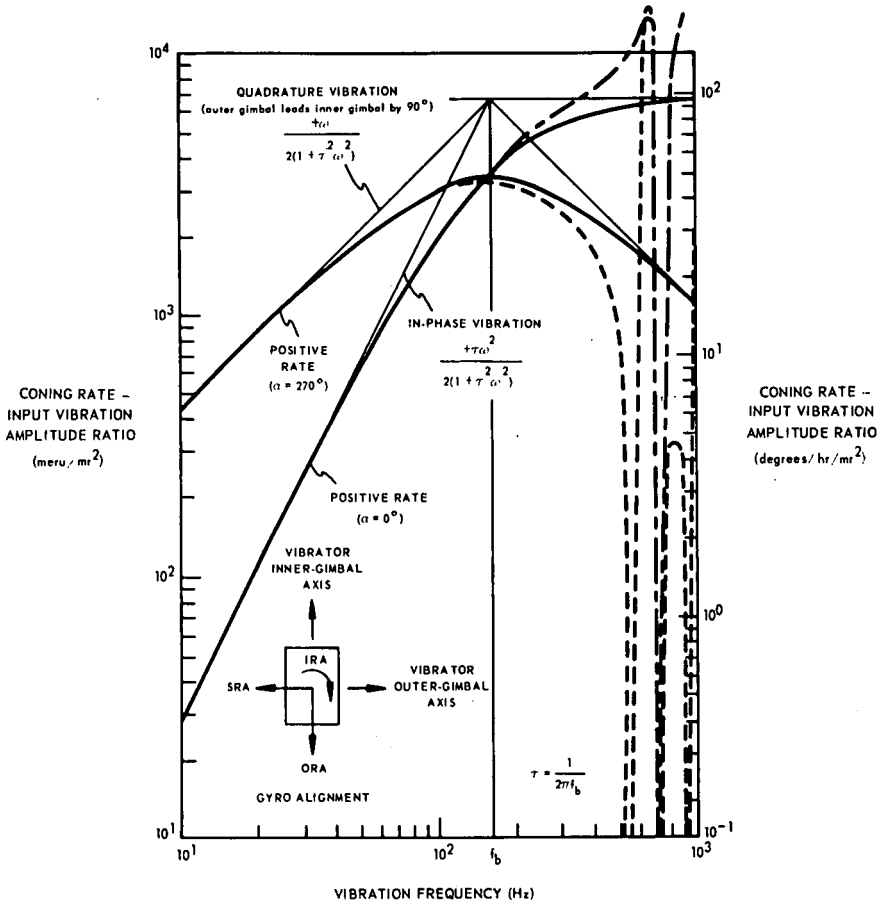

Note : Continuous curves are first-order approximations calculated from gyro parameters; broken curves indicate effects of bearing and float compliances

Fig. 5-30 Gyro coning rate due to simultaneous angular vibration about SRA and IRA

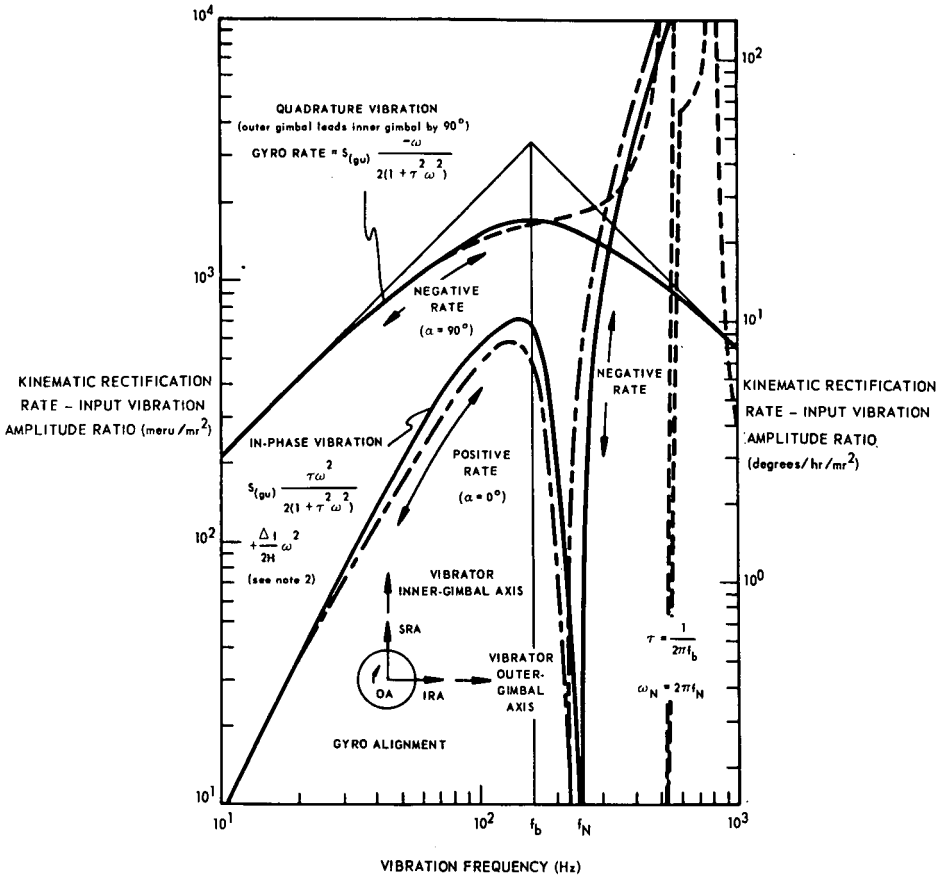

Notes: 1. Continuous curves are first-order approximations calculated from gyro parameters; broken curves indicate effects of bearing and float compliances.

2. For this gyro, $I_{IA} > I_{SA}$; therefore ΔI is negative.

Fig. 5-31 Gyro kinematic rectification rate due to simultaneous angular vibration about IRA and SRA

NONDIMENSIONAL CONING RATE = τ (coning rate)

$$= ab\left[\frac{\beta^2 \cos\alpha}{2(1+\beta^2)} - \frac{\beta \sin\alpha}{2(1+\beta^2)}\right]$$

$$a = \left|A_{(IC)SRA}\right|$$

$$b = \left|A_{(IC)ORA}\right|$$

$$= S_{(gu)}\left|A_{(IC)IRA}\right|$$

$$\tau = I_{OA}/c_{(CF)OA}$$

$$S_{(gu)} = H/c_{(CF)OA}$$

$$\beta = \tau\omega = \omega/\omega_b$$

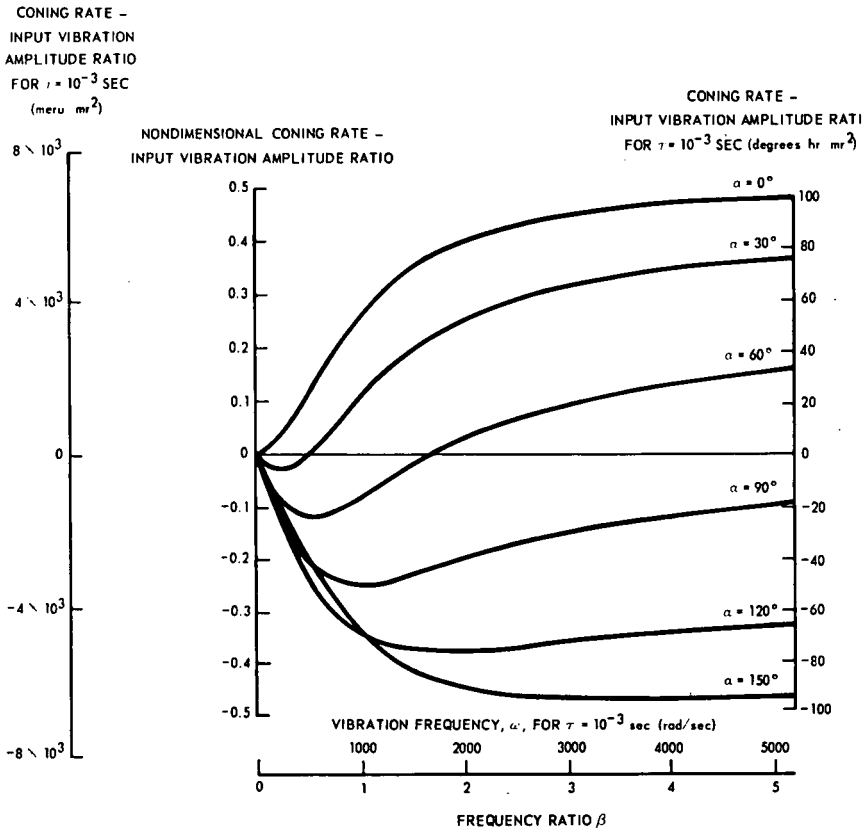

Fig. 5-32 Gyro coning rate for various phase angles at constant-amplitude angular vibration about SRA and ORA or SRA and IRA

alignment shows the output reference axis aligned parallel to the angular vibrator inner-gimbal axis but directed oppositely and the gyro spin reference axis parallel to the vibrator outer-gimbal axis and also directed oppositely. In addition, note that for quadrature vibration the vibrator outer gimbal leads its inner gimbal by 90 degrees. With this gyro alignment and vibrator gimbal phasing, the angular vibrations applied about the gyro output reference axis lag by 90 degrees those about the gyro spin reference axis; or, restating, the vibrations about ORA lead those about SRA by 270 mechanical degrees. The value of the sine of the phase angle, α, is then -1, and the quadrature coning rate is positive. If the direction of either (not both) of the gyro output or spin reference axes is reversed with respect to their aligned gimbal axis, or their spatial positions are interchanged, a negative instead of a positive coning rate would be applied about the gyro input axis.

Note in figure 5-30 that the first-order approximate curve break frequency, f_b, is the frequency at which both the in-phase and quadrature rates are of equal magnitude. This of course is not the case for the in-phase input-spin axis kinematic rectification rates unless the anisoinertia-torque rate is negligible at the break frequency. Figure 5-31 shows the situation when the anisoinertia torque rate is obviously not negligible; in fact, at higher frequencies the float anisoinertia changes the direction of and controls the magnitude of the in-phase-vibration rate. The lower amplitude of the input-spin quadrature coning (Fig. 5-31) from the output-spin quadrature coning (Fig. 5-30) is due to a gyro gain less than one. By comparing the two plots, it can be seen the gyro gain chosen for this example is about one-half.

From figure 5-31 or from the angular-vibration model equation it can be seen that, since the parameters τ and $S_{(gu)}$ can be found independently of the $\Delta I/2H$ parameter, the anisoinertia coefficient $\Delta I/H$ can be determined from the relationship

$$\frac{\Delta I}{H} = \frac{2}{\omega^2} W_{K(IRA)(SRA)\phi} - S_{(gu)} \left(\frac{\tau}{1 + \tau^2 \omega^2} \right) \qquad \text{(Eq. 5-62)}$$

where

$W_{K(IRA)(SRA)\phi}$ = the kinematic rectification rate in radians/second generated by in-phase angular vibrations about IRA and SRA

When the in-phase spin-input coning rate is of opposite polarity to the anisoinertia torque rate, as is the case shown in figure 5-31, the kinematic rectification rate will become zero at some input forcing frequency, ω_N, and equation 5-62 will reduce to

$$\begin{aligned} \frac{\Delta I}{H} &= -S_{(gu)} \frac{\tau}{1 + \tau^2 \omega_N^2} \\ &= -S_{(gu)} \frac{\tau}{1 + \left(\frac{\omega_b}{\omega_N} \right)^2} \\ &= -S_{(gu)} \frac{\tau}{1 + \left(\frac{f_b}{f_N} \right)^2} \end{aligned} \qquad \text{(Eq. 5-63)}$$

If any of the parameters H, $c_{(CF)OA}$, I_{OA}, or ΔI are known, the others may be easily determined from the $S_{(gu)} = H/c_{(CF)OA}$, $\tau = I_{OA}/c_{(CF)OA}$, and $\Delta I/H$ values.

Figure 5-32 is a linear scale plot showing how the coning rate varies as the phase between the input vibrations is varied from 0 to 150 degrees. The coning rate for 180 degrees would be represented by the negative of the coning rate for 0 degrees, and similarly that for 210 degrees by the negative of that for 30 degrees, etc. As indicated by the two additional scales on figure 5-32, the coning-rate expression may be completely nondimensionalized and displayed independently of an individual gyro's output-axis time constant by multiplying the expression by the gyro output-axis time constant and defining the nondimensional frequency ratio, β, equal to $\tau\omega$.

8. Data Processing - P.J. Palmer

Closed-loop gyro tests are usually conducted to obtain values of the coefficients of the gyro model equation and to obtain an indication of gyro performance. The basic raw data obtained during these tests, however, may be a recording of current, a pulse count, or a timer printout. A strip-chart recording of current or a punched-paper-tape count of pulses to the gyro's torque generator is the raw data obtained from the rate-feedback test in the analog and digital mode, respectively. A printed or punched-paper-tape record of the time required for the gyro turntable to rotate through predetermined angular increments is the output of the servo-turntable test. The conversion of this raw data into more usable form in the minimum time has required some fairly sophisticated data processing techniques.

The history of gyro data processing at the Instrumentation Laboratory is briefly traced in this section, after which the use of digital torquing techniques is explored. As noted in section 4, the use of digital equipment has virtually eliminated the resolution edge once held by the servo-turntable mode of testing. This fact, coupled with other advantages of the rate-feedback mode, such as less time required for a test and its adaptability to multiple simultaneous gyro testing, has resulted in the current popularity of that test mode.

History

In the earliest days of inertial gyro testing at the Instrumentation Laboratory, all data was laboriously recorded and processed by hand. During servo-turntable tests, the table rate was clocked by means of a stopwatch. Later, elapsed-time indicators were installed that stamped a paper tape after each degree of rotation of the table top. These tapes were read manually, and all data processing was carried out on a desk calculator. Data processing in those days comprised the calculation of correction torques and integrated drift to obtain a measure of the performance of the gyro.

During the earliest rate-feedback tests, the test technician read an ammeter measuring current to the gyro torque generator each 10 degrees of table rotation. A Fourier analysis of the test data was then performed, again only with the aid of a desk calculator, on two revolutions of the data, one clockwise revolution and one counterclockwise. From the Fourier coefficients, the five coefficients of the then-known error model were calculated.

One of the first attempts at automation of any of the data processing was the use of an electromechanical device somewhat like a planimeter. A stylus on the device was run over a plot of torque-generator current versus table angle; its output was coupled into an early computer, which was programmed to yield the Fourier coefficients.

This technique was soon supplanted by more modern methods. The raw data from rate-feedback tests was recorded on a strip-chart recorder, and this analog record was read manually at each ten degrees of table rotation. The results were transferred to punched cards, which in turn were fed into a digital computer. The computer performed a Fourier analysis of each revolution and was also programmed to give the residual unbalance as a function of turntable angle after the five Fourier coefficients were removed, the root-mean-square value and the average value of the residual unbalance, the deviation between any two successive revolutions as a function of turntable angle, the root-mean-square value and the average value of the deviation between two successive revolutions, the deviations as a function of turntable angle between a clockwise and a counterclockwise revolution, and the root-mean-square value and average value of the deviation between a clockwise and counterclockwise revolution (usually between the last two revolutions in each direction).

In the case of servo tests, the printed-paper-tape record of elapsed time was still read manually as before. After subtracting the correct component of earth's rate for the specific test orientation from the data and converting to equivalent torque units, the data was transferred to punched cards and analyzed in similar fashion as the rate-feedback-test data.

A major disadvantage of the method just outlined was that a human operator was still involved. In addition to the ever-present possibility of human error, the procedure was time-consuming, especially after a weekend during which data was recorded all day Saturday and Sunday. The resultant pile-up of tapes would have to be read Monday morning, the data manually transferred to punched cards, and the cards shipped to the computer location (about a mile away). Frequently it was Tuesday before the analyzed data was ready for evaluation; and at the very minimum, a 14-hour period was required between data acquisition and data availability for evaluation.

Another step forward was the installation of digital data-acquisition devices for both servo-turntable and rate-feedback tests. For the servo-turntable tests, these were timers whose output was punched-paper-tape record of the time required for the turntable top to rotate one degree. For the rate-feedback test, they were voltage-controlled oscillators which converted voltage changes to frequency changes that could be counted with standard electronic counters and converted to punched-paper tape. Punched cards were then automatically prepared from the punched tape, but the 14-hour turnaround time in sending cards to the computer and getting results back still remained. (In fairness, it should be pointed out that the primary function of the computer then being used was theoretical analysis work for the Apollo program; the computer was only available to other Instrumentation Laboratory groups for two hours a day).

The data acquisition and processing loop is now completely automated (40-42). At the beginning of each workday, the data on the punched tapes is automatically transmitted via teletype over a leased telephone line to a computer setup 16 miles away that specializes in data processing. The computer calculates the gyro error coefficients and their uncertainty, the trend per day in the coefficients, a standard deviation, the mean standard deviation and the trend in the standard deviation. In addition, it plots automatically the gyro drift, the unbalance during the last revolution, and the deviation between the last two revolutions. Turnaround time between data transmission and receipt of results is normally two hours and up to 10 000 bits/day have been processed. This equipment is described in chapter 4.

The current computer program is highly structured, which means among other things that it is written to eliminate anomalies in the data. For example, a data

point more than some specified limit from the mean will be automatically discarded, and the number of such points will be recorded on the computer printout. Use of this highly structured program has had an important by-product in that it has forced the test engineer into developing a thoroughly structured test program. He must devise a well-thought-out test plan and decide what data, how much data, what processing, what type of presentation, etc., he desires long before he flicks a switch.

Digital torquing

The gyros under discussion in this paper are angular velocity integrating devices, wherein the signal generator output angle is proportional to the time integral of the torque applied about the output axis. If the torque is applied in bits or pulses over a specified time period, the resolution limit is set by the size of one bit. For example, assume binary pulse torquing at a constant pulse height which applies a torque somewhat larger than that needed to cancel earth's rate, say 1400 meru and a constant pulse width of 5 milliseconds (100 positive and 100 negative pulses per second for zero net torque). The weight of one pulse is then 1400×0.005 or seven meru-seconds. This single pulse would command a servo-stabilized platform to rotate 0.105 arc second about an axis parallel to the input axis of the gyro. (Binary can be defined as existing in two states; in this case, either positive or negative pulses. In ternary pulsing, three states exist: positive, negative, and zero.)

During gyro testing in the rate-feedback mode, pulse-torquing loops can be employed in earth-fixed tests or in step-tumbling tests. For such applications, the number of pulses in a given time is a measure of the total torque acting on the gyro float. The objective is to obtain the maximum resolution in the minimum time.

An example is useful here to illustrate the operation of a binary pulse-torquing scheme. Assume that the gyro is fixed with respect to the earth and that the signal-generator output signal is applied to a binary-pulsing torque-generator driver. Since the pulse frequency is constant, it is only necessary to count either the total number of positive pulses (or the total number of negative pulses). Assume that the positive pulses are to be counted and that the number of pulses (in a given time) for zero net torque is taken as a reference. A pulse count greater than this value will indicate a positive torque, and a pulse count smaller than this value will indicate a negative torque. Let

M_C = torque loop constant (pulse height) in meru: the pulse height is a characteristic of a gyro (a function of the torque-generator sensitivity and current) and must be determined by calibration

M = actual gyro torque in meru

t = time in seconds for a prespecified number of positive pulses

t_o = time in seconds for a prespecified number of positive pulses occurring at zero net torque

and let

$$t_o = \frac{p}{r} \qquad \text{(Eq. 5-64)}$$

where

p = the number of prespecified or present positive pulses

r = positive pulse rate in pulses/sec at zero net torque

Figure 5-33 represents the process in graphical form, where all positive pulses and all negative pulses are grouped into areas and where t_s is the switch time from one group of pulses to another group of pulses. At a given positive torque M over the time t

$$Mt = M_C(t - t_s) - M_C t_s$$
$$= M_C t - 2M_C t_s \qquad \text{(Eq. 5-65)}$$

Considering the total time interval t_o, the following relationships can be written by referring to figure 5-33:

$$M_t = 0 = -M_C t_s + M_C(t - t_s) - M_C(t_o - t) \qquad \text{(Eq. 5-66)}$$

or

$$-2M_C t_s = 2M_C t + M_C t_o \qquad \text{(Eq. 5-67)}$$

Combining equations 5-65 and 5-67 gives

$$Mt = M_C t_o - M_C t \qquad \text{(Eq. 5-68)}$$

Solving for M

$$M = M_C\left[\frac{t_o}{t} - 1\right] \qquad \text{(Eq. 5-69)}$$

For illustration, assume

M_C = 1400 meru

t = 8 seconds

p = 1000 pulses

r = 100 pulses/sec

$\Big\}\ t_o = 10$ seconds

Substituting these values into equation 5-69 gives a value of M equal to 350 meru.

Equation 5-69 shows that if the time, t, for a prespecified number of positive pulses is less than the time, t_o, required for the prespecified number of positive pulses at zero net torque, the torque being applied is positive. The limit is reached when t becomes equal to $t_o/2$, or in other words, when only positive pulses occur and M is equal to or greater than M_C. If t is greater than t_o, the torque being applied is negative. The time t increases without limit when the measured torque approaches $-M_C$ (all the pulses are negative). The above remarks are illustrated in figure 5-34 where the ratio of M/M_C is plotted against the ratio of t/t_o.

Turning now to the question of resolution, the rate of change of the measured torque M, as a function of the time, t, for a prespecified number of positive pulses can be found by taking the partial derivative of equation 5-69 with respect to t

$$\frac{\partial M}{\partial t} = -\frac{M_C t_o}{t^2} \qquad \text{(Eq. 5-70)}$$

Note that for zero net torque, $t = t_o$ and

$$\left.\begin{aligned}\frac{\partial M}{\partial t} &= -\frac{M_C t_o}{t_o^2} = -\frac{M_o}{t_o}\\ \partial M &= -\frac{M_C}{t_o}\,\partial t\end{aligned}\right\} \qquad \text{(Eq. 5-71)}$$

or, for small finite intervals near zero net torque,

$$\Delta M = - \frac{M_C}{t_o} \Delta t \qquad \text{(Eq. 5-72)}$$

where Δt is the width of a single pulse.

Substituting numerical values from the example above,

$$\Delta M = - \frac{(1400)(0.005)}{(10)} = -0.7 \text{ meru}$$

For illustration, the change or error in the measured torque due to a timing error equal to one pulse is shown in figure 5-35, where the resolution limit, also called the quantization uncertainty, is plotted as a function of the time t. Measured torque as a function of the time t is shown in figure 5-36.

As shown in figure 5-36, when the sample time is equal to the time required for the preset number of positive pulses, that is, when t is ten seconds and t_o is also ten seconds (the time required for 1000 positive pulses), the measured torque is zero regardless of the pulse height. For the pulse height of 1400 meru and the time of 10 seconds used in the example, the resolution as shown by figure 5-35 is 0.7 meru-second. Now let us assume that the pulse torquing loop is to be used in a test where the torque to be measured is a significant fraction of the torque produced by earth rate, say ± 700 meru (the value of the horizontal and vertical components of earth rate at 45 degrees latitude). Referring to figure 5-36 note that, with a pulse height of 1400 meru, the time for a preset number of positive pulses to measure + 700 meru is 6.7 seconds and that to measure - 700 meru it is 20 seconds. Figure 5-35 shows that, at a pulse height of 1400 meru and a 6.6-second time, the resolution limit is 1.7 meru-seconds; for 20 seconds, it is 0.15 meru-second. Thus the dynamic resolution, which is a function of the magnitude of the torque being measured, must be considered in the data analysis.

When the performance of a gyro is to be measured in an orientation where the total torque about the gyro output axis is essentially zero- for example, with OA vertical and IA east to measure the stability of the D_F and D_O terms - equation 5-72 indicates that ΔM is inversely proportional to t_o or t and directly proportional to M_C and Δt. Figure 5-37 is a plot of the resolution limit as a function of time for essentially zero net torque and a plot of assumed data, where over 3000 one-second samples of data were assumed. By averaging the sequential samples, the standard deviation of the data was computed over 1, 2, 4, 8, 16, 32, 64, 128 and 256 seconds. The indications are that the gyro uncertainties are lower than the resolution limit for sampling periods less than about 16 seconds, while for longer samples the gyro uncertainties are larger than the resolution limit. For periods of about four minutes, gyro uncertainties of the order of 0.1 meru could be attained.

It is interesting to note that $M_C \Delta t$ is a fixed characteristic for a given pulse-torquing system since it represents the resolution limit at zero net torque. For the example given after equation 5-69 and used throughout this section, a preset of 100 pulses makes a single pulse worth 7 meru-seconds. A preset of 1000 pulses makes a single pulse worth 0.7 meru-second. In this case, resolution is obtained at the expense of decreased bandwidth since data is obtained less often. In reverse, increased bandwidth can be obtained but, on an individual piece of data, only at the expense of decreased resolution. Simultaneous high resolution and wide bandwidth can be achieved by continuous data averaging where a sliding-window technique is used and any given piece of data will be contained in several window-sized averages.

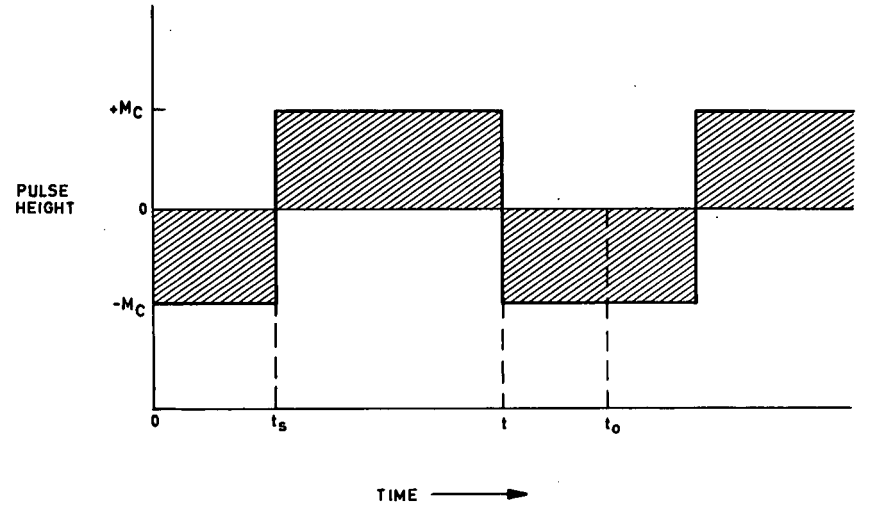

Fig. 5-33 Graphical representation of pulse torquing

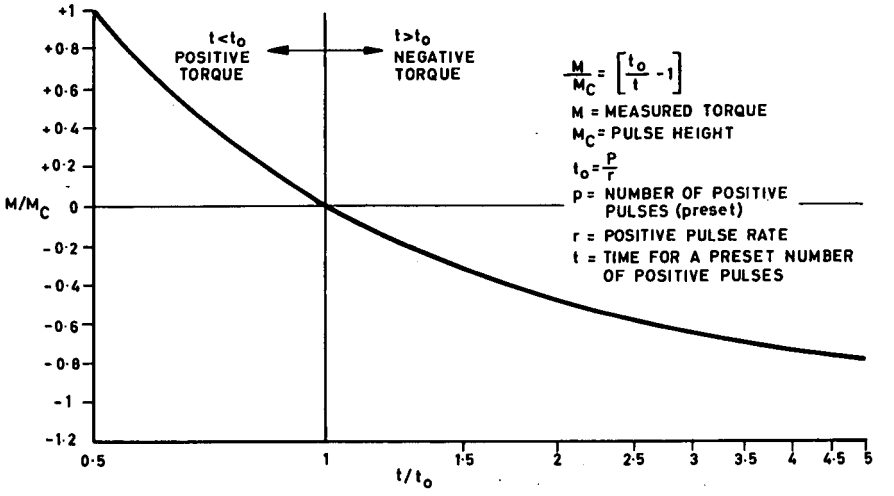

Fig. 5-34 M/M_c vs t/t_o

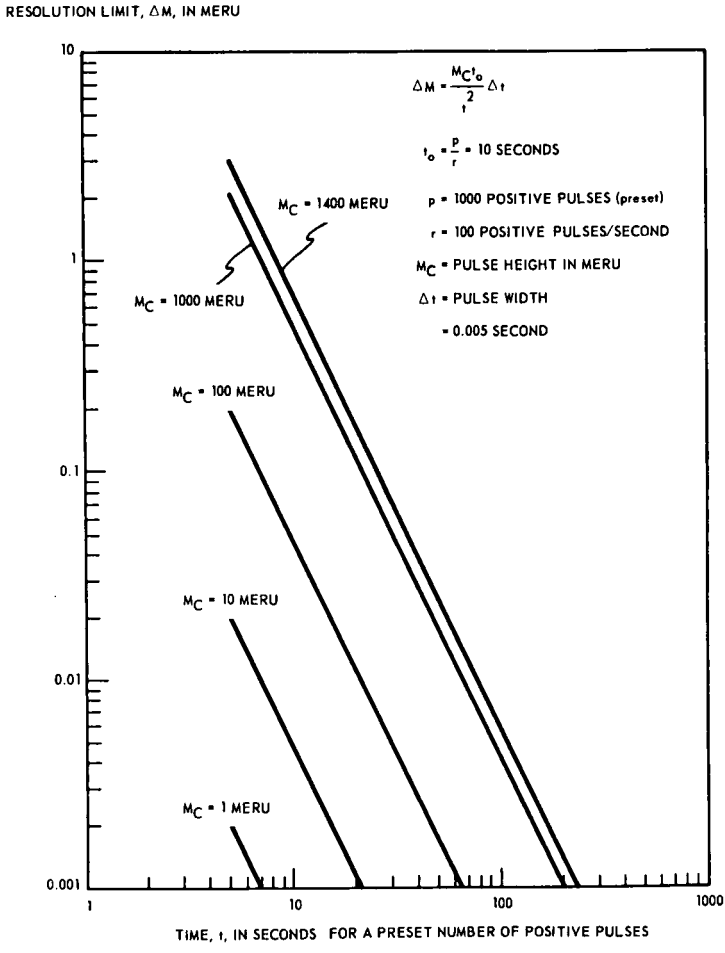

Fig. 5-35 Resolution limit for a preset number of positive pulses

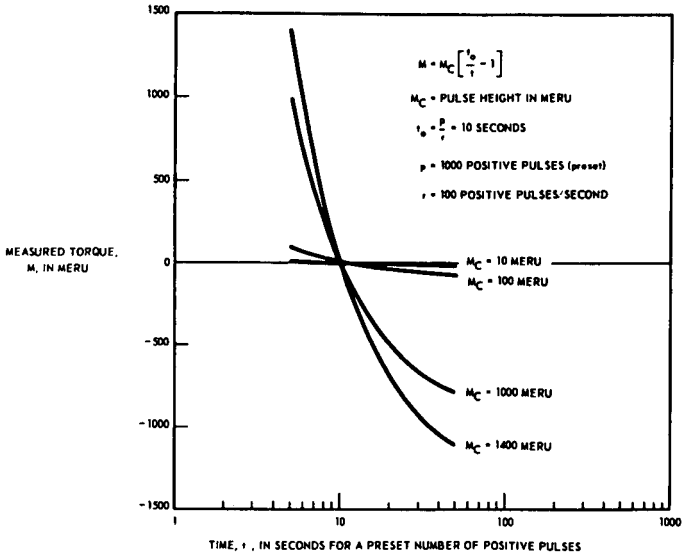

Fig. 5-36 Measured torque versus time for a preset number of pulses

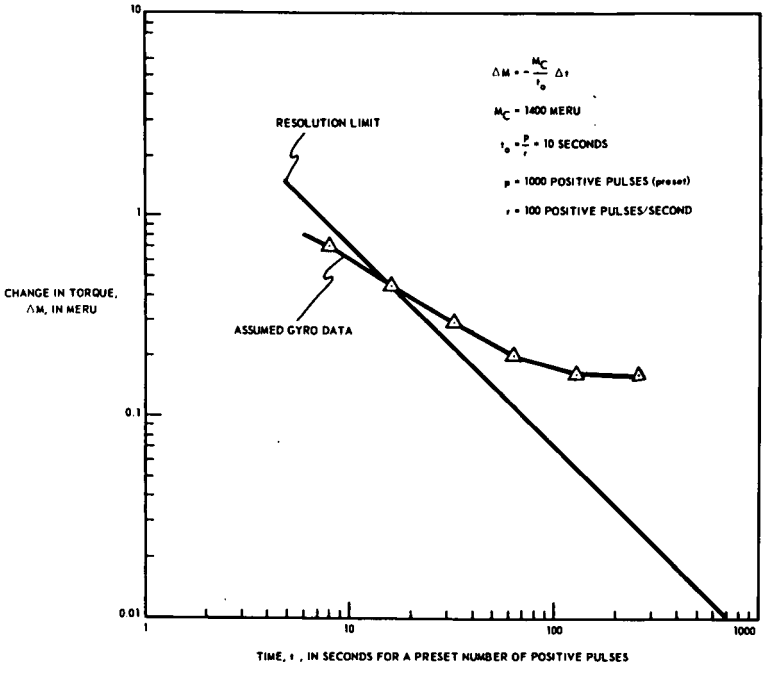

Fig. 5-37 Change in torque versus time for a preset number of positive pulses

9. Summary and Conclusions - P.J. Palmer

One philosophy of inertial gyro testing is that the test program should provide accurate measurements of the coefficients of a model equation that mathematically defines the gyro performance in any environment. The reduction of this philosophy to practice at the Instrumentation Laboratory of MIT has been described as it relates to the testing of the single-degree-of-freedom floated integrating gyro to today's high-performance, high-reliability, and long-life specifications. The test and evaluation of the inertial gyro for application in gimbaled or floated-type systems has been emphasized, but many of the techniques and philosophies apply also to the test and evaluation of inertial gyros for use in strapdown systems.

Evolution of the current steady-state and dynamic error models was traced and testing techniques for determining the coefficients of these model equations were presented. No one test program can be considered optimum for all applications, however. A judicious choice of one-g laboratory tests, linear vibration tests, centrifuge tests and angular vibration tests must be made by the responsible test engineer with factors such as gyro application, length of time between field calibrations and cost being carefully evaluated. Thus, economic as well as technical factors must be considered during the formulation of the test program.

Frequently a trade-off must be made between economic and technical considerations, but occasionally a happy situation arises where such is not the case. An example of this latter situation is the current popularity of rate-feedback testing. From the economic viewpoint, this mode of testing was always looked upon with favor because of the less time required for a test, but data resolution on servo tests had always been superior. With the advent of digital equipment and techniques, the resolution advantage of servo-turntable testing has been virtually eliminated. In addition, the rate-feedback mode lends itself admirably to multiple simultaneous gyro testing, which not only cuts cost but also adds to the data reliability.

Advances in inertial gyro design have brought the instruments to the point where survival in a high-g environment is no longer a critical problem. However, with increased emphasis on system operation in high-g environments, attention has become focused on those terms of the error model that are functions of acceleration squared or higher powers of acceleration. Linear vibration and centrifuge testing is therefore being used extensively to measure these terms to precision levels that would be unnecessary to meet system requirements for a low-g application.

Angular vibration can result in coning rates and anisoinertia torques. Even at low input amplitudes, these effects can cause appreciable changes in the performance of the inertial gyro. In addition to the measurement of these effects, angular vibration is useful in the measurement of gyro frequency response, constructional parameters and dynamic characteristics.

The time interval between system field calibrations increases as instruments and systems show better performance and more reliability. However, as the requirements for improved performance become more demanding and the instrument coefficients must be determined more accurately, data must be averaged over increasingly longer time periods. The data obtained at each calibration period must be shown to relate accurately to the steady-state performance of the system during the time up to the next calibration period and to the instrument performance during flight. As the performance range of the system is extended, more accurate knowledge of the instrument coefficients is required, and the total effort is multiplied to the point where serious economic considerations must be investigated. These operational and economic factors appear to be one of the major determinants of instrument quality. This is equivalent to saying that instruments can be test limited (12).

Appendix A

Testing of Two-Degree-of-Freedom Gyros - R. H. Wilkinson

The Two-Degree-of-Freedom Gyro

The two-degree-of-freedom gyro is basically similar to the single-degree-of-freedom gyro in that both consist of a spinning wheel contained in an outer case. They differ in the degree to which the wheel axis is constrained to the case. In the single-degree-of-freedom gyro, the wheel axis is almost rigidly restrained from rotating about the input axis and is free to rotate about the output axis, although the rate of rotation about the output axis is heavily restrained by damping fluid. In the two-degree-of-freedom gyro, much less restraint is applied to the wheel about the two axes perpendicular to the spin axis. The gyro is constructed so that both of the axes perpendicular to the spin axis are practically identical, and both can serve simultaneously as input and output axes. The two sensitive axes are usually designated X and Y or (as in this chapter) A and B. In the two-degree-of-freedom gyro, torque applied about one input axis causes a rotation about the other.

Two-degree-of-freedom gyros in current use can be classified into two major categories: those with a gimbaled wheel and those with free rotors. The gimbaled variety are often constructed similarly to the single-degree-of-freedom type, having a wheel contained in a floated gimbal. However, the float of the two-degree-of-freedom gyro is usually spherical rather than cylindrical and the damping gap is larger. In the free-rotor type, the wheel is contained directly in the case with no inner gimbal, and the wheel is mounted so that it can rotate about the A and B axes with respect to the case. The displacement of the angular momentum vector with respect to the case is picked off directly from the rotating wheel. Considerable ingenuity has been applied in the design of free-rotor gyros so that some variety exists in the physical form taken by current production types.

In spite of the differences, all gyros are found to be susceptible to the same types of error when subject to translational accelerations, although the relative significance of various terms in the error equation is greatly affected by the design of the gyro concerned. Each of the two output axes is susceptible to drift, so a pair of equations is necessary to represent the two-degree-of-freedom gyro. The following error equations cover all practical cases (43):

$$\begin{aligned} W(A)_d = {} & +D(A)_F + D(A)_A(SF)_A + D(A)_B(SF)_B + D(A)_S(SF)_S \\ & +D(A)_{AA}(SF)_A^2 + [D(A)_{BB}(SF)_B^2] + D(A)_{SS}(SF)_S^2 \\ & +D(A)_{AB}(SF)_A(SF)_B + D(A)_{AS}(SF)_A(SF)_S + D(A)_{BS}(SF)_B(SF)_S \end{aligned} \qquad \text{(Eq. 5-A1)}$$

$$\begin{aligned} W(B)_d = {} & +D(B)_F + D(B)_A(SF)_A + D(B)_B(SF)_B + D(B)_S(SF)_S \\ & +[D(B)_{AA}(SF)_A^2] + D(B)_{BB}(SF)_B^2 + D(B)_{SS}(SF)_S^2 \\ & +D(B)_{AB}(SF)_A(SF)_B + D(B)_{AS}(SF)_A(SF)_S + D(B)_{BS}(SF)_B(SF)_S \end{aligned} \qquad \text{(Eq. 5-A2)}$$

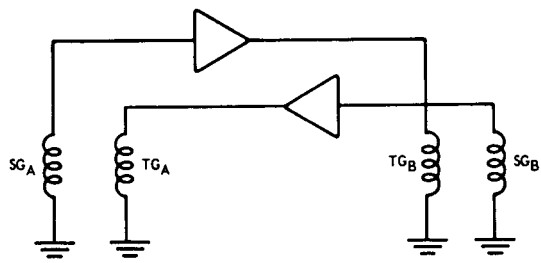

Fig. 5-A1 Torque-to-null loops for testing a two-degree-of-freedom gyro

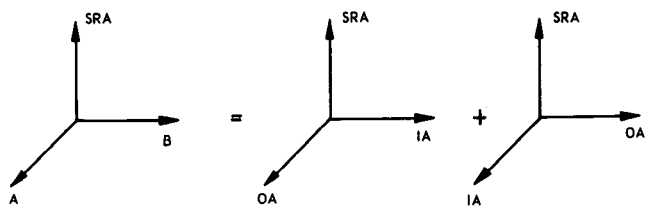

Fig. 5-A2 Single-degree-of-freedom gyro equivalents to a two-degree-of-freedom gyro

where

$W(A)_d$	= gyro drift rate about A in meru
$D(A)_F$	= gyro drift rate about A in meru that is insensitive to specific force
$D(A)_A, D(A)_B, D(A)_S$	= gyro drift rate about A in meru/g that is proportional to specific force along A, B and SRA, respectively
$D(A)_{AA}, D(A)_{BB}, D(A)_{SS}$	= gyro drift rate about A in meru/g^2 that is proportional to specific force squared along A, B and SRA, respectively
$D(A)_{AB}, D(A)_{AS}, D(A)_{BS}$	= gyro drift rate about A in meru/g^2 that is proportional to the product of specific force along A and B, A and SRA, and B and SRA, respectively
$(SF)_A, (SF)_B, (SF)_S$	= specific force in g's directed along A, B and SRA, respectively
$W(B)_d$	= gyro drift rate about B in meru, etc.

The two terms in brackets in the equations are required for completeness but are not measurable by one-g test methods alone. Consequently, they must be assumed negligible if only one-g testing is contemplated. This assumption is frequently valid. In fact, for many purposes, only a few terms need be retained. The reduction of the equations by judicious elimination of minor terms can make testing simpler and quicker.

Equations 5-A1 and 5-A2 are not independent; some of the terms are strongly coupled by the presence of mass unbalances along the spin axis, for example. Nevertheless, the coefficients in practice may be all different. As for the single-degree-of-freedom case of equation 5-11, the equations assume that drift angles remain very small, and this is normally assured by the use of nulling loops around both axes. If the H vector is permitted to move from null, restraint torques may become significant and cross-coupling errors will enter. In particular, the gyro may be subject to coning error under angular vibration. The two-degree-of-freedom gyro is much less susceptible to coning error than the single-degree-of-freedom type, however, due to the lighter coupling between wheel and case.

Test Procedures

In point of time, the single-degree-of-freedom inertial gyro was the first to be developed, followed by the two-degree-of-freedom inertial gyro. It is natural therefore that two-degree-of-freedom gyro test methods have been adapted from those already established for the single-degree-of-freedom types. Most of the test procedures for two-degree-of-freedom gyros are identical with those outlined in the body of this chapter, and are performed on the same type of test tables, having one axis of rotation (44). In some instances, tables having two orthogonal axes have been used, on which the gyro can be simultaneously servoed about both its axes, but this is not commonly done and will not be discussed further.

By amplifying the output signal of the A-axis pickoff and applying it with appropriate sense to the B-axis torquer, the instrument is reduced to a single-

degree-of-freedom gyro, having the A axis as electrical input axis while the B axis serves as pickoff output axis and mechanical input axis. Although there are obvious differences between the two-degree-of-freedom gyro connected this way and a conventional single-degree-of-freedom gyro, the instrument can nevertheless be subjected to all the tests discussed in the body of the chapter in order to establish the coefficients in equation 5-A2 (drift about the B axis, or equivalently, the null torque applied to the A axis). In order to complete evaluation of the gyro, the entire test must then be repeated with the gyro reconnected so that pickoff B drives torquer A. This will yield the coefficients in equation 5-A1.

This is the customary procedure for testing two-degree-of-freedom gyros with one exception. In the case of tumbling tests, it is possible by proper design of the test to attain considerable economy by utilizing the signals of both A and B torquers simultaneously. To do this, the gyro is connected in two identical torque-to-null loops as indicated in figure 5-A1. Drift torques about the A axis are automatically compensated and measured by the A torquer current, and similarly the B torquer current measures B-axis drift torque. The gyro can be considered conceptually equivalent to two single-degree-of-freedom gyros as indicated in figure 5-A2 which are being tested simultaneously.

Since there are two input axes, it is desirable to take as much data as possible with both of these axes orthogonal to the table axis, i. e. with the spin axis aligned with the table axis. In this way, the outputs of both torque loops can be used as data. One rotation with the spin axis along the table axis and a second with the spin axis rotated through 180 degrees are sufficient to determine all coefficients in equations 5-A1 and 5-A2, provided that $D(A)_{SS}$ and $D(B)_{SS}$ can be neglected (43). If all terms are to be included, some additional data can be obtained by aligning one of the sensitive axes along the table axis. For this additional information, each gyro must be tested separately, according to the procedures outlined in the body of this chapter. The output of the torquer on the axis aligned with the table is not usable, of course, since it is required to compensate for the large input rate. Some gyro torquers cannot develop the high torques required, in which case a reduced table rate, or stepped testing, may be resorted to. In addition, to avoid loss of alignment, the required torquer current should be injected from a separate supply so that the pickoff is not required to hang off null. In any case, the presence of a large torquer current means that the gyro is operating under somewhat abnormal circumstances in this phase of the test. An alternative procedure is to obtain this portion of the data by servo testing.

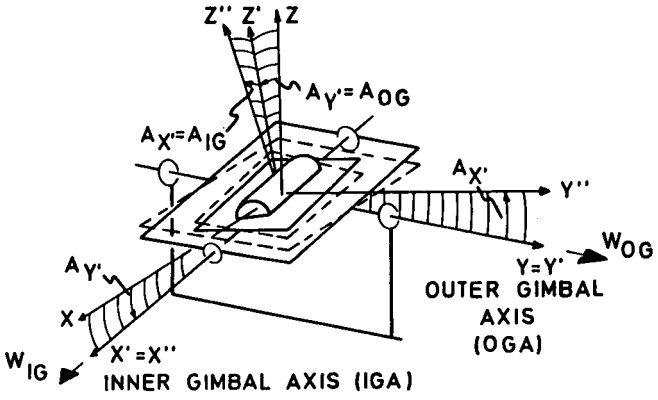

Fig. 5-D 1

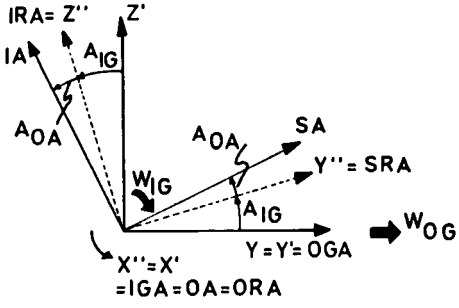

Fig. 5-D 2a

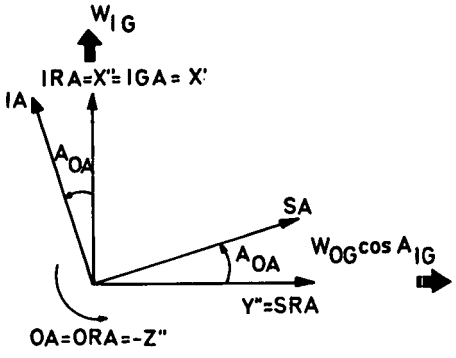

Fig. 5-D 2b

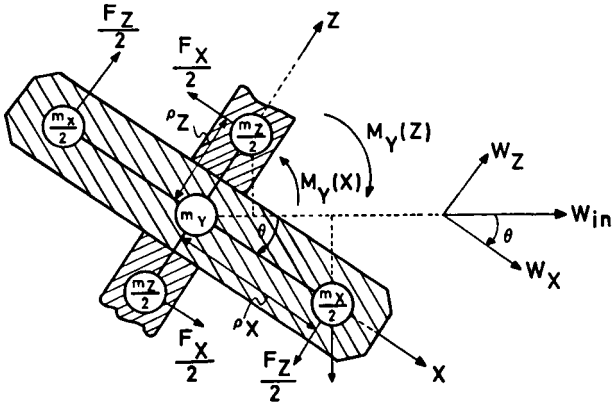

Fig. 5-D 3

Appendix B

Derivation Summary 5-1 Gimbaled system coning rate - a geometric effect

If out-of-phase angular vibrations of the same frequency are simultaneously applied to a body about two orthogonal space-fixed axes, or one space-fixed and one body-fixed axis, a nonzero-average angular velocity will be generated maximum about a third 'orthogonal' body-fixed axis. As a demonstration of this effect, the average rate developed for the case of small-amplitude sinusoidal angular oscillations applied about one space-fixed and one body-fixed axis is developed below.

Consider a gimbal system such as that shown in figure 5-D1. The instantaneous rate about the nonoscillating Z (body) axis, W_Z'', is given by

$$W_Z'' = -W_{OG} \sin A_{IG} \simeq -W_{OG} A_{IG} \quad \text{(small angle approximation)} \qquad \text{(Eq. 5-D1)}$$

Assuming an environment of general sinusoidal angular oscillations,

$$A_{IG} = A_X' = a \sin(\alpha + \omega t) = a[\sin\alpha \cos\omega t + \cos\alpha \sin\omega t]$$

and

$$A_{OG} = A_Y' = b \sin\omega t$$

$$W_{OG} = b\omega \cos\omega t$$

Equation 5-D1 becomes

$$W_Z'' = -ab\omega[\sin\alpha \cos^2\omega t + \cos\alpha \sin\omega t \cos\omega t] = -\frac{ab\omega}{2}[\sin\alpha + \sin(\alpha + 2\omega t)] \qquad \text{(Eq. 5-D2)}$$

Equation 5-D2 shows that W_Z'' is composed of a nonzero-average (coning) rate

$$-\frac{ab\omega}{2} \sin\alpha$$

plus a zero-average sinusoidal term. Any instrument mounted on this gimbal system will be subjected to this rate.

Derivation Summary 5-2 Coning rate modified by gyro dynamics

If a single-degree-of-freedom floated integrating gyroscope is in an angular-vibratory environment, the coning rate sensed by the gyro float input axis will be modified by the gyro dynamics. Two examples are given below.

Case 1: Output-spin axis coning

If the gyro is mounted on the inner gimbal of a gimbal system such as that shown in Derivation Summary 5-1 with its output axis parallel with the inner gimbal axis and its spin reference axis in the outer-gimbal-axis direction, the modified output-spin axis coning rate sensed by the gyro float may be approximated to the first order as follows.

Looking along the inner gimbal axis, IGA, as in figure 5-D2a, the instantaneous gyro input axis rate is given by

$$W_{IA} = -W_{OG} \sin (A_{IG} + A_{OA})$$
$$\simeq -W_{OG} (A_{IG} + A_{OA}) \qquad \text{(small angle approximation)}$$
(Eq. 5-D3)

The single-degree-of-freedom gyro performance equation for this orientation is

$$I_{OA} \ddot{A}_{(IF)OA} + c_{(CF)OA} \dot{A}_{(IF)OA} = HW_{(IF)IA} + c_{(CF)OA} \dot{A}_{(IC)OA}$$
(Eq. 5-D4)

where

$$\dot{A}_{(IF)OA} = \dot{A}_{(IC)OA} + \dot{A}_{(CF)OA}$$
$$= W_{IG} + W_{OA}$$

and

$$W_{(IF)IA} = W_{IA} = -W_{OG} A_{(IF)OA}$$

Substituting the above identities into equation 5-D4 and dividing through by $c_{(CF)OA}$, equation 5-D4 becomes

$$\tau \ddot{A}_{(IF)OA} + \dot{A}_{(IF)OA} = -S_{(gu)} W_{OG} A_{(IF)OA} + W_{IG} \qquad \text{(Eq. 5-D5)}$$

where

$$\tau = \frac{I_{OA}}{c_{(CF)OA}}$$

and

$$S_{(gu)} = \frac{H}{c_{(CF)OA}}$$

Equation 5-D5 is a Matheau equation and must be solved by an iteration process, or, since the angle $A_{(IF)OA} = A_{IG} + A_{OA}$ is small, may be approximated under the following conditions: (a) the input angular velocities, W_{IG} and W_{OG}, are of the same order of magnitude and (b) the gyro gain is approximately one or less.

$$\tau \ddot{A}_{(IF)OA} + \dot{A}_{(IF)OA} \simeq W_{IG} \qquad \text{(Eq. 5-D6)}$$

which is directly solvable. The steady-state solution of equation 5-D6 for an inner-gimbal angular-oscillation input of $A_{IG} = a \sin(\omega t + \alpha_1)$ is

$$A_{(IF)OA} \simeq \frac{a \sin(\omega t + \alpha_1) - a\tau\omega \cos(\omega t + \alpha_1)}{1 + \tau^2\omega^2} \qquad \text{(Eq. 5-D7)}$$

Expanding and rearranging terms equation 5-D7 becomes

$$A_{(IF)OA} \simeq a \left[\left(\frac{\sin \alpha_1 - \tau\omega \cos \alpha_1}{1 + \tau^2\omega^2} \right) \cos \omega t + \left(\frac{\cos \alpha_1 + \tau\omega \cos \alpha_1}{1 + \tau^2\omega^2} \right) \sin \omega t \right]$$
(Eq. 5-D8)

To determine the output-spin axis coning rate sensed by the gyro float input axis, the expression for $A_{(IF)OA}$ derived in equation 5-D8 and the outer gimbal sinusoidal angular oscillation rate, $W_{OG} = b\omega \cos \omega t$, are substituted into equation 5-D3. This substitution results in

$$W_{IA} \simeq -ab\omega \left[\left(\frac{\sin \alpha_1 - \tau\omega \cos \alpha_1}{1 + \tau^2\omega^2} \right) \cos^2 \omega t + \left(\frac{\cos \alpha_1 + \tau\omega \cos \alpha_1}{1 + \tau^2\omega^2} \right) \sin \omega t \cos \omega t \right]$$
(Eq. 5-D9)

or by trigonometric expansion,

$$W_{C[OA+SA]} \simeq \left[\frac{\tau\omega^2 \cos \alpha_1 - \omega \sin \alpha_1}{2(1+\tau^2\omega^2)}\right] ab + (\text{zero-average sinusoidal terms}) \qquad \text{(Eq. 5-D10)}$$

where

$W_{C[OA+SA]}$ = output-spin axis coning rate

$a = |A_{IG}| = |A_{(IC)OA}|$

$b = |A_{OG}| = |A_{(IC)SRA}|$

A similar derivation can be applied for the orientation where the gyro output axis is mounted in the outer-gimbal direction, and the spin axis is parallel with the inner-gimbal axis.

Case 2: Input-spin axis coning

If the gyro is mounted with its input reference axis parallel with the inner-gimbal axis and its spin reference axis again in the direction of the outer-gimbal axis, the following derivation may be used to approximate to the first order the gyro input-spin axis coning rate.

Looking along the plus Z″(body) axis (perpendicular to the plane of the inner gimbal), as in figure 5-D2b, the instantaneous gyro input axis rate is given by

$$W_{IA} = -W_{OG} \cos A_{IG} \sin A_{OA} + W_{IG} \cos A_{OA}$$
$$\simeq -W_{OG} A_{OA} + W_{IG} \qquad \text{(small angle approximation)} \qquad \text{(Eq. 5-D11)}$$

The single-degree-of-freedom gyro performance equation for this orientation is

$$I_{OA}\ddot{A}_{(CF)OA} + c_{(CF)OA}\dot{A}_{(CF)OA} = HW_{(IF)IA} - I_{OA}\ddot{A}_{(IC)OA} \qquad \text{(Eq. 5-D12)}$$

where

$$\ddot{A}_{(CF)OA} = \ddot{A}_{OA}$$
$$W_{(IF)IA} = W_{IA} \simeq -W_{OG} A_{OA} + W_{IG}$$
$$\ddot{A}_{(IC)OA} = \ddot{A}_{OG} \sin A_{IG} \simeq \ddot{A}_{OG} A_{IG} \qquad \text{(small angle approximation)}$$

Substituting the above identities into equation 5-D12 and dividing through by $c_{(CF)OA}$, equation 5-D12 becomes

$$\tau\ddot{A}_{OA} + \dot{A}_{OA} = S_{(gu)}(W_{IG} - W_{OG} A_{OA}) - \tau\ddot{A}_{OG} A_{IG} \qquad \text{(Eq. 5-D13)}$$

which is again a Matheau equation and must be solved by iteration, unless the following conditions exist under the restraint that A_{OA} and A_{IG} are small angles: (a) the input angular velocities, W_{IG} and W_{OG}, are of the same order of magnitude and (b) the gyro gain is approximately one or more. Under these conditions

$$\tau\ddot{A}_{OA} + \dot{A}_{OA} \simeq S_{(gu)} W_{IG} \qquad \text{(Eq. 5-D14)}$$

which is directly solvable.

The steady-state solution of equation 5-D14 for an inner-gimbal angular oscillation input of $A_{IG} = a \sin(\omega t + \alpha_2)$ is

$$A_{(CF)OA} = A_{OA} \simeq S_{(gu)} \frac{a \sin(\omega t + \alpha_2) - a\tau\omega \cos(\omega t + \alpha_2)}{1 + \tau^2\omega^2} \qquad \text{(Eq. 5-D15)}$$

Expanding and rearranging terms, equation 5-D15 becomes

$$A_{OA} \simeq aS_{(gw)} \left[\left(\frac{\sin \alpha_2 - \tau\omega\cos \alpha_2}{1 + \tau^2\omega^2} \right) \cos \omega t + \left(\frac{\cos \alpha_2 + \tau\omega \sin \alpha_2}{1 + \tau^2\omega^2} \right) \sin \omega t \right] \qquad \text{(Eq. 5-D16)}$$

To determine the input-spin axis coning rate sensed by the gyro float input axis, the expression for A_{OA} derived in equation 5-D16, the outer and inner gimbal oscillation rates, $W_{OG} = b\omega \cos \omega t$ and $W_{IG} = a\omega \cos (\omega t + \alpha_2)$ are substituted into equation 5-D11. This substitution results in

$$W_{IA} \simeq -S_{(gw)} ab\omega \left[\left(\frac{\sin \alpha_2 - \tau\omega \cos \alpha_2}{1 + \tau^2\omega^2} \right) \cos^2 \omega t + \left(\frac{\cos \alpha_2 + \tau\omega \sin \alpha_2}{1 + \tau^2\omega^2} \right) \sin \omega t \cos \omega t \right] + a\omega \cos(\omega t + \alpha_2) \qquad \text{(Eq. 5-D17)}$$

or by trigonometric expansion,

$$W_{C\,[IA+SA]} \simeq S_{(gw)} \left[\frac{\tau\omega^2 \cos \alpha_2 - \omega \sin \alpha}{2(1 + \tau^2\omega^2)} \right] ab + (\text{zero-average sinusoidal terms}) \qquad \text{(Eq. 5-D18)}$$

where

$W_{C\,[IA+SA]}$ = input-spin axis coning rate

a = $|A_{IG}| = |A_{(IC)IRA}|$

b = $|A_{OG}| = |A_{(IC)SRA}|$

A similar derivation can be applied for the orientation where the gyro input reference axis is mounted in the outer-gimbal-axis direction, and the spin reference axis is parallel with the inner-gimbal axis.

Derivation Summary 5-3 Anisoinertia or dynamic unbalance torque - a gyroscopic torque

If a rigid body is in rotation with respect to inertial space about a body axis that is not a principal axis of inertia, a torque must be applied to the body if the direction of the axis of rotation is to be held stationary with respect to the inertial (fixed) frame. This torque is required to produce the change in the angular momentum of the body that is needed to maintain the body's angular-velocity vector motionless in space. It is represented by Euler's Dynamical Equations for the motion of a rigid body in terms of body-axis components as

$$\begin{aligned} -M_{(app)X} &= M_{(P)X} = -I_X \dot{W}_X + (I_Y - I_Z) W_Y W_Z \\ -M_{(app)Y} &= M_{(P)Y} = -I_Y \dot{W}_Y + (I_Z - I_X) W_Z W_X \\ -M_{(app)Z} &= M_{(P)Z} = -I_Z \dot{W}_Z + (I_X - I_Y) W_X W_Z \end{aligned} \qquad \text{(Eq. 5-D19)}$$

where

$M_{(app)X}$, $M_{(app)Y}$, $M_{(app)Z}$ = applied torque about the X, Y and Z axes, respectively.

$M_{(P)X}$, $M_{(P)Y}$, $M_{(P)Z}$ = precession reaction torque about the X, Y and Z axes respectively.

I_X, I_Y, I_Z = principal moments of inertia about the X, Y and Z axes, respectively.

W_X, W_Y, W_Z = components of angular velocity of the body about the X, Y and Z axes, respectively

X, Y, Z = orthogonal set of principal body axes

In the case of a single-degree-of-freedom gyro, consider the situation where the gyro is in rotation with respect to inertial space about some axis through the gyro float center of mass in the float IA-SA plane. In other words, the gyro float output axis is positioned perpendicular to the input angular velocity vector. For simplicity (and since most single-degree-of-freedom gyros are designed and constructed so that it is approximately true), it is assumed that one of the float principal central moments of inertia is about the gyro output axis and the other two are in the float IA-SA plane. It is also true that the single-degree-of-freedom gyro input and spin axes are nearly coincident with principal central axes of inertia of the gyro float. The torque about the gyro float output axis is determined from Euler's Dynamical Equations as

$$M_{P(IF)OA} = -I_{OA}\dot{W}_{(IF)OA} + (I_Z - I_X)W_Z W_X \qquad \text{(Eq. 5-D20)}$$

where

$M_{P(IF)OA}$ = precession inertial reaction torque of the float about its output axis

$I_{OA} = I_Y$ = principal central moment of inertia of the float about OA

I_X, I_Z = principal moments of inertia of the float in the IA-SA plane

$\dot{W}_{(IF)OA}$ = angular acceleration of the float about OA with respect to inertial space

W_X, W_Z = components of input angular velocity about the float IA-SA plane principal inertia axes

In order for the input angular velocity and thus its body-axis components, W_X and W_Z, to remain in the same direction with respect to an inertial reference system, the gyro float must not rotate with respect to that reference system about its output axis; in other words, $W_{(IF)OA}$ and thus $\dot{W}_{(IF)OA}$ must be zero. This constraint results in the so-called anisoinertia or dynamic unbalance torque

$$\begin{aligned} M_{(\Delta I)OA} &= (I_Z - I_X)W_Z W_X \\ &= H_Z W_Z - H_X W_X \end{aligned} \qquad \text{(Eq. 5-D21)}$$

where

H_Z, H_X = components of float angular momentum about the Z and X axes, respectively.

It can be seen from equation 5-D21 that, when the gyro float is in rotation with respect to inertial space, the anisoinertia torque will be zero only if the input angular velocity is about one of the float's principal axes or when the float inertia is the same about any axis in the IA-SA plane (the isoinertia condition)-that is, $I_X = I_Z$.

Equation 5-D21 may be rewritten for a single angular velocity input such as that during centrifuge testing as

$$M_{(\Delta I)(cf)} = |I_Z - I_X|\, W_{in}^2 \, \frac{\sin 2\theta}{2} \qquad \text{(Eq. 5-D22)}$$

where

W_{in} = input angular velocity

θ = angle measured about the gyro float output (Y) axis from the direction of the input angular velocity vector to the smaller principal moment of inertia axis, I_X or I_Z.

To determine the expression for the anisoinertia torque developed in an angular-vibration environment, the angular velocity inputs, W_X and W_Z, are defined to be

$$W_X = a\omega \cos(\omega t + \alpha)$$

$$W_Z = b\omega \cos \omega t$$

Substitution into equation 5-D21 gives the anisoinertia torque resulting from angular vibration or

$$M_{(\Delta I)(\text{ang. vib.})} = (I_Z - I_X)\frac{ab\omega^2}{2}[\cos \alpha + \cos 2(\omega t + \alpha)] \qquad \text{(Eq. 5-D23)}$$

which has a time average of

$$M_{(\Delta I)(\text{ang. vib.})} = \frac{(I_Z - I_X)}{2} ab\omega^2 \cos \alpha \qquad \text{(Eq. 5-D24)}$$

As for any output axis torque, the anisoinertia torque may be expressed as an equivalent gyro input axis rate by dividing by the gyro wheel spin angular momentum, H, or

$$W_{(\Delta I)} = \frac{(I_Z - I_X)}{2H} W_Z W_X \qquad \text{(Eq. 5-D25)}$$

where

$W_{(\Delta I)}$ = equivalent input axis anisoinertia rate.

The anisoinertia torque equation may be developed from Newton's second law, F = ma, by describing the central ellipsoid of inertia of a rigid body as point masses displaced along the principal axes by lever-arm distances (radii of gyration) from the body's center of mass. A cross section of such an ellipsoid in the X-Z principal axis plane is shown in figure 5-D3. Inspection of the figure shows that

$$\begin{aligned} M_{\Delta I} &= M_Y(Z) + M_Y(X) = \rho_X F_Z + \rho_Z F_X \\ &= (\rho_X^2 m_X - \rho_Z^2 m_Z) W_{in}^2 \sin\theta \cos\theta \\ &= (I_Z - I_X) W_{in}^2 \frac{\sin 2\theta}{2} \end{aligned} \qquad \text{(Eq. 5-D26)}$$

or

$$\begin{aligned} M_{\Delta I} &= (I_Z - I_X) W_Z W_X \\ &= (I_Z W_Z) W_X - (I_X W_X) W_Z \\ &= H_Z W_X - H_X W_Z \end{aligned} \qquad \text{(a gyroscopic torque) (Eq. 5-D27)}$$

Symbols and Abbreviations

a	acceleration = second derivative with respect to inertial space of the vector $\bar{R}$ from the center of the earth to a point P on the surface of the earth = $p_I^2 \bar{R}$
a_I, a_S, a_O	total acceleration directed along IA, SRA and OA, respectively
A	one of the two sensitive axes of a two-degree-of-freedom gyro. (The other axes are B and SRA)
$A_{(CF)O}$	angle of the gyro float with respect to the case about the gyro output axis = $A_{(gim)}$
A_F	mounting fixture angle measured from zero reference
$A_{(gim)}$	gimbal angle
$\lvert A_{(IC)IRA} \rvert$	amplitude of angular vibration applied about the gyro case input reference axis with respect to inertial space
$A_{(IC)O}$	angle of the gyro case with respect to inertial space about the gyro output axis
$\lvert A_{(IC)ORA} \rvert$	amplitude of angular vibration applied about the gyro case output reference axis with respect to inertial space
$\lvert A_{(IC)SRA} \rvert$	amplitude of angular vibration applied about the gyro case spin reference axis with respect to inertial space
$A_{(IF)O}$	angle of the gyro float with respect to inertial space about the gyro output axis
A_{IG}	inner gimbal angle
A_L	latitude angle at the test location
A_O	angle between the gyro output axis and the test table axis measured about + IA
A_{OA}	output axis angle
A_{OG}	outer gimbal angle
A_T	turntable angle measured from a zero reference
A_X, A_Y	angle about the X and Y axes, respectively
A_0	constant term of a Fourier analysis
A_1, A_2	first and second harmonic cosine terms of a Fourier analysis, respectively
α	phase angle
α_1	phase angle by which the angular vibration about ORA is leading the angular vibration about SRA
α_2	phase angle by which the angular vibration about IRA is leading the angular vibration about SRA
B	one of the two sensitive axes of a two-degree-of-freedom gyro. (the other axes are A and SRA).
B_1, B_2	first and second harmonic-sine terms of a Fourier analysis, respectively

β frequency ratio $= \omega/\omega_b$

c structural damping coefficient

$c_{(CF)O}$ damping coefficient between gyro float and case about the gyro output axis

C_O, C_1, C_2, C_3, C_4 coefficients of a power series

d_b ball displacement

d_I, d_S, d_O linear displacement along IA, SRA and OA, respectively

d_K displacement of the center of gravity of the float resulting from compliance of the wheel, bearing, and gimbal assembly

d_o initial bearing deflection as a result of a force, F_o

D gyro drift coefficient

D_{dS}, D_{dI}, D_{dO} gyro drift sensitivity to rate of linear float displacement along SRA, IA and OA, respectively

D_F gyro fixed drift rate that is insensitive to specific force

D_I, D_S, D_O gyro drift rate that is proportional to specific force along IA, SRA and OA, respectively

D_{II}, D_{SS}, D_{OO} gyro drift rate that is proportional to specific force squared along IA, SRA and OA, respectively

D_{IS}, D_{OS}, D_{IO} gyro drift rate that is proportional to the product of specific force along IA and SRA, OA and SRA, and IA and OA, respectively. The order of subscripts is unimportant; in other words, it is assumed that $D_{IS} = D_{SI}$, etc.

D_{TIS} gyro drift sensitivity to a combination of temperature gradient along IA and specific force along SRA

D_{TOO} gyro drift sensitivity to a combination of temperature gradient along OA and specific force along OA

D_{TSI} gyro drift sensitivity to a combination of temperature gradient along SRA and specific force along IA

D_X, D_Y, D_Z gyro drift rate that is proportional to specific force along X, Y and Z, respectively

D_{XX}, D_{YY}, D_{ZZ} gyro drift rate that is proportional to specific force squared along X, Y and Z, respectively

D_{XY}, D_{XZ}, D_{YZ} gyro drift rate that is proportional to the product of specific force along X and Y, X and Z, and Y and Z, respectively.

$D(A)_F, D(B)_F$ gyro drift rate about A and B, respectively, that is insensitive to specific force

$D(A)_A, D(A)_B, D(A)_S$ gyro drift rate about A that is proportional to specific force along A, B and SRA respectively

$D(B)_A, D(B)_B, D(B)_S$ gyro drift rate about B that is proportional to specific force along A, B and SRA, respectively

$D(A)_{AA}, D(A)_{BB}, D(A)_{SS}$ gyro drift rate about A that is proportional to specific force squared along A, B and SRA, respectively

$D(B)_{AA}, D(B)_{BB}, D(B)_{SS}$ gyro drift rate about B that is proportional to specific force squared along A, B and SRA, respectively

$D(A)_{AB}$, $D(A)_{AS}$, $D(A)_{BS}$ gyro drift rate about A that is proportional to the product of specific force along A and B, A and SRA, and B and SRA, respectively

$D(B)_{AB}$, $D(B)_{AS}$, $D(B)_{BS}$ gyro drift rate about B that is proportional to the product of specific force along A and B, A and SRA, and B and SRA, respectively

DAR dynamic amplitude ratio

DRA dynamic response angle

$(DR)_I$, $(DR)_S$ damping ratio along IA and SRA, respectively

$e_{(sg)}$ signal-generator output voltage

E east

EA earth's polar axis

f_b first-order approximate break frequency

f_N node frequency

F force

F_c compressive force

F_I, F_S force directed along IA and SRA, respectively

F_o preload force

F_X, F_Y, F_Z force directed along the X, Y and Z axes, respectively

g local gravity, which is the vector resultant of the acceleration due to mass gravitational attraction and the centrifugal acceleration due to the earth's daily rotation

g_I, g_S, g_O components of local gravity along IA, SRA and OA, respectively

G acceleration due to mass gravitational attraction

G_I, G_S, G_O components of the acceleration due to mass gravitational attraction along IA, SRA and OA, respectively

H angular momentum of the gyro rotor = wheel inertia times speed of rotation

H_X, H_Z angular momentum about the X and Z axes, respectively

I = IA input axis of the single-degree-of-freedom gyro unit; mutually perpendicular to OA and SA. Its sense is such that a positive input about the input axis results in a positive output about the output axis. In all cases, a positive rotation may be determined by the right-hand rule in which the tumb is pointed along the vector towards the arrowhead. The fingers, when curled about the vector, point in the direction of positive rotation. IA, SA and OA are fixed with respect to the gyro float.

IRA input reference axis of the single-degree-of-freedom gyro unit; in the same direction as the input axis when the condition of zero angular displacement with respect to the case occurs (float is at the signal generator null). Since the gyro is operated within a few seconds of arc of null, IRA can usually be considered synonomous with IA. IRA, SRA and ORA are fixed with respect to the gyro case.

IGA inner gimbal axis

I_{IA}, I_{SA} principal moment of inertia axes of the gyro float in the IA-SA plane nearer to IA and SA, respectively

I_O moment of inertia of the gyro float about the gyro output axis

I_X, I_Y, I_Z moments of inertia about the X, Y and Z axes, respectively

ΔI $I_{SA} - I_{IA}$

k equivalent bearing stiffness

k_I, k_S bearing stiffness along IA and SA, respectively

$K_{(FW)I}, K_{(FW)O}$ lumped stiffness of the gyro wheel with respect to the float about the input and output axes, respectively

K_{II} compliance along IA due to a specific force along IA

K_{OO} compliance along OA due to a specific force along OA

K_{SS} compliance along SA due to a specific force along SA

K_{IS} compliance along IA due to a specific force along SA

K_{SI} compliance along SA due to a specific force along IA

K_{OS} compliance along OA due to a specific force along SA

K_{SO} compliance along SA due to a specific force along OA

K_{IO} compliance along IA due to a specific force along OA

K_{OI} compliance along OA due to a specific force along IA

K'_{II} displacement along IA due to a specific force along IA

K'_{OO} displacement along OA due to a specific force along OA

K'_{SS} displacement along SA due to a specific force along SA

K'_{IS} displacement along IA due to a specific force along SA

K'_{SI} displacement along SA due to a specific force along IA

K'_{OS} displacement along OA due to a specific force along SA

K'_{SO} displacement along SA due to a specific force along OA

K'_{IO} displacement along IA due to a specific force along OA

K'_{OI} displacement along OA due to a specific force along IA

m mass

m_w wheel mass

m_X, m_Y, m_Z displaced mass along the X, Y and Z axes, respectively

$M_{(app)X}, M_{(app)Y}, M_{(app)Z}$ applied torque about the X, Y and Z axes, respectively

M_C torque loop constant (pulse height)

M_K torque about the gyro output axis due to compliance

M_O torque about the gyro output axis

$M_{P(IF)OA}$ precession inertial reaction torque of the float about the output axis

$M_{(P)X}, M_{(P)Y}, M_{(P)Z}$ precession reaction torque about the X, Y and Z axes, respectively

M_{tg} torque developed by the gyro torque generator

$M_{\Delta I}$ anisoinertia torque

$M_{(\Delta I)(ang.vib.)}$ anisoinertia torque resulting from angular vibration

$M_{(\Delta I)(cf)}$ anisoinertia torque resulting from centrifuging

$M_{(\Delta I)OA}$ anisoinertia torque about the gyro output axis

N north

O = OA output axis of the single-degree-of-freedom gyro unit; fixed with respect to the gyro float and directed from the signal-generator end to the torque-generator end

OGA outer gimbal axis

ORA output reference axis of the gyro unit; fixed with respect to the gyro case and directed from the signal-generator end to the torque-generator end. ORA can usually be considered to be synonomous with OA

p differential operator

p number of prespecified or preset positive pulses

p_i^2 second derivative with respect to inertial space

P a point on the surface of the earth

P_I, P_S, P_O, P_R time dependent change in U_I, U_S, U_O and R, respectively

ϕ angle of the applied acceleration vector in the IA-SA plane referenced to IA or SA

r centrifuge radius

r positive pulse rate at zero net torque

$\bar{R}$ radius of the earth

R gyro drift caused by power-lead torque and microsyn reaction torque

ρ_X, ρ_Z radii of gyration along the X and Z axes, respectively

S south

S = SA spin axis of the gyro wheel; fixed with respect to the gyro float

SF = SRF specific mass reaction force at a point equal in magnitude and direction to the force that a unit mass with the location and acceleration of the point applies to its supporting structure. This is commonly called specific force.

$(SF)_b$ breakout acceleration

$(SF)_{cf}$ centrifuge specific force

$(SF)_{g(I)}$ $(SF)_{g(S)}$, $(SF)_{g(O)}$ specific force of gravity components along IA, SA and OA, respectively

$(SF)_A$, $(SF)_B$ specific force components along A and B, respectively

$(SF)_v$ vibration specific force

$(SF)_{v(I)}$, $(SF)_{v(S)}$, $(SF)_{v(O)}$ vibration specific force components along IA, SA and OA, respectively

$(SF)_I$, $(SF)_S$, $(SF)_O$ specific force components along IA, SA and OA, respectively

$(SF)_X$, $(SF)_Y$, $(SF)_Z$ specific force components along X, Y and Z, respectively

SG signal generator

$S_{(gu)}$ gyro unit angle input - angle output sensitivity

SRA spin-reference axis of the gyro unit; fixed with respect to the gyro case, SRA is in the same direction as the spin axis of the gyro

wheel when the condition of zero angular displacement with respect to the case occurs (float is at the signal-generator null). Since the gyro is operated within a few seconds of arc of null, SRA is usually considered synonomous with the spin axis.

$S_{(sg)}$ signal generator angle input - voltage output sensitivity

t time

t_o time for a prespecified number of positive pulses occurring at zero net torque

t_s switch time from one group of pulses to another

TA table axis

TG torque generator

$\Delta T_I, \Delta T_S, \Delta T_O$ temperature gradients across the gyro along IA, SA and OA, respectively

τ gyro first-order characteristic time

θ angle between the smaller moment of inertia axis in the IA-SA plane and the angular velocity vector measured about OA

$(U)d_{(Ocm)}$ uncertainty in the distance between the output axis and the center of mass of the wheel

$(U)W_{ET}$ that part of the angular velocity of the test turntable with respect to the earth due to gyro error and uncertainty.

U_I, U_S mass unbalance along IA and SRA, respectively

U_O proportionality coefficient relating drift component to specific force along the output axis

$W_{(cf)}$ centrifuge angular velocity

W_d gyro drift rate

$W_{d(vib)}$ gyro drift rate due to vibration

W_{in} input angular velocity

$W(A)_d, W(B)_d$ gyro drift rate about the A and B axes, respectively

$W_{C[IA+SA]}$ input-spin axis coning rate

$W_{C[OA+SA]}$ output-spin axis coning rate

W_{ET} angular velocity of the test turntable with respect to the earth

$W_{(IC)I}$ angular velocity of the gyro case with respect to inertial space about the gyro input axis

W_{IE} angular velocity of the earth with respect to inertial space

$W_{(IF)O}$ angular velocity of the gyro float with respect to inertial space about the gyro output axis

W_{IG} angular velocity of the inner gimbal

$W_{K(gim)}$ angular-vibration-induced kinematic rectification rate

$W_{K(IRA)(SRA)\phi}$ kinematic rectification rate generated by in-phase angular vibrations about IRA and SRA

W_{OA} angular velocity about the output axis

W_{OG} angular velocity of the outer gimbal

W_X, W_Y, W_Z angular velocity about the X, Y and Z axes, respectively

$W_{\Delta I}$	equivalent input axis anisoinertia rate
ω	angular frequency $= 2\pi f$
ω_b	approximate first-order break frequency
ω_n	undamped natural frequency
ω_{nI}, ω_{nS}	undamped natural frequency along IA and SRA respectively
$\omega_{(peak)I}, \omega_{(peak)S}$	frequencies along IA and SRA, respectively, at which peak torque occurs
ω_N	node frequency
X, Y, Z	a set of three mutually perpendicular axes

References

(1) 'Wide Use of F-111 Mk 2 Avionics Seen', Aviation Week and Space Technology, pp 93-100,June 6, 1966 and 'Inertial Navaid Business Expands Sharply', pp 136-145,August 15, 1966.

(2) **Draper, C.S., McKay, W. and Lees, S.**,'Instrument Engineering', McGraw-Hill Book Company, Inc., New York, Vol. 1,Ch. 9, 1952.

(3) **Wheaton, G.M.**, 'Strapdown Systems and Components - Test Procedures', Report MDC-TR-66-71, Vol. II, Holloman AFB, New Mexico, Jan. 1967 (also published as Report E-2063, Vol. II,Instrumentation Laboratory, MIT, Cambridge, Mass., Jan. 1967).

(4) **Wrigley, W.W.**, 'Single-Degree-of-Freedom Gyroscopes', paper presented at a symposium on gyrodynamics at Celerina, Switzerland, sponsored by the International Union of Theoretical and Applied Mechanics, Aug. 1962, and included as pp 62-91 of 'Gyrodynamics (Kreiselprobleme)', Springer-Verlag, Berlin, 1963 (also published as Report R -375, Instrumentation Laboratory, MIT, Cambridge, Mass., July 1962).

(5) 'Space Navigation Guidance and Control, AGARDograph 105, pp 29-46, Technivision Ltd., Maidenhead, England, 1966.

(6) **Draper, C.S., Wrigley, W.W., and Hovorka, J.**, 'Inertial Guidance', Pergamon Press, New York, 1960.

(7) **Palmer, P.J.**, '3-D Compliance Study on the Single-Degree-of-Freedom Floated Integrating Gyro and Test Results from the Precision Linear Vibrator', Report R-243, Instrumentation Laboratory, MIT, Cambridge, Mass., May 1959.

(8) **Ernst, C.M., and Samborsky, J.M.**, 'Reduction of Anisoelastic Error in a Single-Degree-of-Freedom Integrating Gyroscope Subjected to Translational Vibration', Master of Science Thesis T-336, Department of Aeronautics and Astronautics, MIT, Cambridge, Mass., May 1963.

(9) **Wrigley, W.W., Woodbury, R.W., and Hovorka, J.**, 'Inertial Guidance', Sherman M. Fairchild Fund Paper FF-16, Institute of Aeronautical Sciences, New York, 1957.

(10) 'Explanatory Supplement to the Astronomical Ephemeris and the American Ephemeris and Nautical Almanac', Her Majesty's Stationery Office, London, 1961.

(11) **Palmer, P. J. and Gianoukos, W. A.**, 'Seminar Notes - Inertial Gyro Testing', paper presented at the First Advanced Testing Seminar, Air Force Missile Development Center, Holloman AFB, New Mexico, Nov. 1966 (also published as Report GY-452, Instrumentation Laboratory, MIT, Cambridge, Mass., Nov. 1966).

(12) **Marshall, R. E. and Palmer, P. J.**, 'Inertial Instrument Design Verification Tests for High-G Applications', paper presented at an International Symposium on Inertial Guidance Testing Techniques, Nov. 1965 at Weilheim, Germany (also published as Report E-1866, Instrumentation Laboratory, Cambridge, Mass., Oct. 1965).

(13) **Weinstock, H.**, 'Effects of High Accelerations on Ball Bearing Gyroscope Performance', Report E-1568, Instrumentation Laboratory, MIT, Cambridge Mass., May 1964.

(14) **Whitman, H. R., Wales, R. L., and Andersen, J. P.**, 'The Type-H Gyro, Computing and Accelerometer Units', Report R-17, Instrumentation Laboratory, MIT, Cambridge, Mass., Sept. 1953.

(15) **Irlbeck, D. H. and Raroha, G. H.**, 'Experimental Investigation of the Effects of Angular Vibration on a Single-Degree-of-Freedom Floated Integrating Gyroscope', Master of Science Thesis T-345, Department of Aeronautics and Astronautics, MIT, Cambridge, Mass., May 1963.

(16) **Hoag, D. G.**, 'Suggested Specifications for the BuOrd Standard Integrating Gyro 20IG', Report R-91, Instrumentation Laboratory, MIT, Cambridge, Mass., Dec. 1955.

(17) **Mueller, R. K.**, 'Proposed Method for Producing a Lead Performance Function in Integrating Gyros', Report E-38, Instrumentation Laboratory, MIT, Cambridge, Mass., March 1951.

(18) **Fertig, K. and Palmer, P. J.**, 'The Dynamics of the Single-Degree-of-Freedom Gyroscope', Report GL-205, Instrumentation Laboratory, MIT, Cambridge, Mass. (published as Appendix 5 of reference 19).

(19) **Denhard, W. G.**, 'Laboratory Testing of a Floated, Single-Degree-of-Freedom, Integrating Inertial Gyro', Report R-105, Instrumentation Laboratory, MIT, Cambridge, Mass., Sept. 1956.

(20) **Hendrickson, J. F.**, 'The Effect of Gyroscope Parameters on Control-Loop Performance, Report GL-242, Instrumentation Laboratory, MIT, Cambridge, Mass., Dec. 1959.

(21) **Palmer, P. J.**, 'Gyro Torque Coefficients', Report E-1601, Instrumentation Laboratory, MIT, Cambridge, Mass., Jan. 1966.

(22) **Spitzak, A. W.**, 'An Investigation of Gyro Drift Caused by an Applied Rotating Linear Acceleration, Master of Science Thesis T-314, Department of Mechanical Engineering, MIT, Cambridge, Mass., June 1962.

(23) **Napier, N. C., III**, 'Vibration Testing of a Single-Degree-of-Freedom Floated Integrating Inertial Gyro', Bachelor of Science Thesis T-232, Department of Mechanical Engineering, MIT, Cambridge, Mass., Jan. 1960.

(24) **Cannon, R. J., Jr.**, 'Kinematic Drift of Single-Axis Gyroscopes, Paper No. 57-A-72, presented at the Annual Meeting of the American Society of Mechanical Engineers, New York, Dec. 1957.

(25) **Goodman, L. E., and Robinson, A. R.**, 'Effect of Finite Rotation on Gyroscopic Sensing Devices', Paper No. 57-A-30, presented at the Annual Meeting of the American Society of Mechanical Engineers, New York, Dec. 1957.

(26) **Weinstock, H.**, 'A Study of the Response of the Single-Degree-of-Freedom Integrating Gyroscope to Angular Vibrations', Master of Science Thesis T-233, Department of Mechanical Engineering, MIT, Cambridge, Mass., Jan. 1960.

(27) **Haff, W. B. and Meltzer, M.**, 'Effects of Angular Vibration on the Performance of a Single-Degree-of-Freedom Integrating Gyroscope', Master of Science Thesis T-257, Department of Aeronautics and Astronautics, MIT, Cambridge, Mass., May 1960.

(28) **Arutyunov, S. S.**,'Errors of a SDF Integrating Gyro Due to Angular Oscillations of Its Base', ARS Journal Supplement, July 1960.

(29) **Feldman, J.**, 'Errors of a Linear Integrating Accelerometer under a Vibration Environment', Master of Science Thesis T-279, Vol. I, Department of Aeronautics and Astronautics, MIT, Cambridge, Mass., May 1961.

(30) **Thomas, I. L.**, 'Wander Rate Changes in Single-Degree-of-Freedom Gyros Induced by Angular or Conical Vibration', Tech. Memo No. IAP 746, Royal Aircraft Establishment, Farnborough, England, Dec. 1961.

(31) **McCubbin, E. and Reid, D. F.**, 'Errors of a Single-Degree-of-Freedom Integrating Gyroscope in a Vibration Environment', Master of Science Thesis T-301, Department of Aeronautics and Astronautics, MIT, Cambridge, Mass., May 1962.

(32) **Weinstock, H.**, 'Specification for the Permissible Motions of a Platform for Performance Evaluation of Single-Degree-of-Freedom Inertial Gyroscopes', Report E-1267, Instrumentation Laboratory, MIT, Cambridge, Mass., Dec. 1962.

(33) **Bedford and Cashmore**, 'Inertial Platform Coning Drift Due to Angular Vibration', English Electric Tech. Memo 15XS/LI5063 (British).

(34) **Draper, C. S., Finston, M., Denhard, W. G., and Goldenberg, D.**, 'Dynamic Support of Instrument Components by Viscous Fluids', paper given at the First International Congress of the International Federation of Automatic Control, Moscow, USSR, 1960.

(35) **Sher, L. and Weinstock, H.**, 'Performance Requirements for a High-Frequency Two-Axis Angular Vibrator', Report R-514, Instrumentation Laboratory, MIT, Cambridge, Mass., Sept. 1965.

(36) **Smith, A. J.**, 'Two-Axis Angular Vibration Test Results on a Single-Degree-of-Freedom Integrating Gyroscope', Report MDC-TR-66-68, Holloman AFB, New Mexico, Dec. 1966 (also published as Report E-1965, Instrumentation Laboratory, MIT, Cambridge, Mass., Dec. 1966).

(37) **Hamilton, K. A.**, 'Precision Angular Vibrator Readout Electronics', Report GE-E-49, Instrumentation Laboratory, MIT, Cambridge, Mass., Jan. 1965.

(38) **Cross, J.**, 'Precision Angular Vibrator Checkout Methods', Report MDC-TR-68-27, Holloman AFB, New Mexico, Feb. 1968 (also published as Report E-2213, Instrumentation Laboratory, MIT, Cambridge, Mass., Feb. 1968).

(39) **Buchanan, J.**, 'Single-Degree-of-Freedom Gyro Drift Due to In-Phase Angular Vibration', Report E-1348, Instrumentation Laboratory, MIT, Cambridge, Mass., June 1963.

(40) **Cartwood, F. E.**,'Data Processing for Tumbling Tests and Drift Runs in OAO Gyro Acceptance Tests', Report E-2178, Instrumentation Laboratory, MIT, Cambridge, Mass., Sept. 1967.

(41) **Cartwood, F.E.**, 'Linear Vibration Test Station (LVTS) Data Reduction Program', Report E-2116, Instrumentation Laboratory, MIT, Cambridge, Mass., April 1967.

(42) **Klein, S.I.**, 'Automatic R and D Data Acquisition', Report SOSS-CMP-9-21-67, Instrumentation Laboratory, MIT, Cambridge, Mass., Sept. 1967.

(43) **Russell, J.F.**, 'Gyroscope Standard Torque-to-Balance Test', Report MDC-TR-67-79, Holloman AFB, New Mexico, June 1967.

(44) **Osband, S.**, 'The Testing of Rate-Integrating and Free Gyros:. A Comparison of Test Methods and Techniques for Two Types of Precision Stabilization Gyros', paper presented at the IRE National Winter Convention on Military Electronics in Los Angeles, California, Feb. 1963 (copies available from the author at Arma Division, American Bosch Arma Corp., Garden City, New York).

6

Testing the Precision Accelerometer

M.S. SAPUPPO, P.J. PIJOAN and J.H. BUCHANAN
Instrumentation Laboratory, Massachusetts Institute of Technology, Cambridge, Massachusetts, USA

Summary

The success of inertial guidance systems for vehicles navigating anywhere between outer space and the deepest sea bottom is directly dependent on the performance of the inertial reference gyro and the specific force receiver (accelerometer) as the primary position and motion sensing transducers. This chapter is a presentation of what, why, where and how to test the inertial quality accelerometer, based on experience with the pendulous integrating gyro accelerometer (PIGA) and the pulsed integrating pendulous accelerometer (PIPA), both designed and developed by MIT/IL.

As part of the development of an accelerometer, tests must be designed to determine the magnitude and stability of the performance parameters. A general review of the philosophy of testing the PIGA and PIPA is presented, including the major testing emphasis, the parameters to be measured, the optimum level of assembly at which to apply a test, the factors causing changes in the tests and the method of performing tests.

Measurement of an accelerometer output using components of gravity as an input by tumbling the accelerometer (positioning the accelerometer input axis) with respect to the local vertical is a standard and basic test of performance. An error analysis of the one-gravity PIGA tumble test, the mathematical model of the PIGA long-term performance and a special PIGA tumble test using an air bearing rate table to determine the effects of cross-axis acceleration are presented.

An air bearing rate table, which was designed and developed by MIT/IL for evaluation of PIGA performance, is described. The testing techniques and the advantages accrued through use of this table are also described.

The need for development of accelerometers having greatly increased sensitivities in order to meet the latest demands of oceanographic and space exploration has imposed problems of testing accelerometers at very low levels of acceleration input — as low as 10^{-9}g. This imposes stringent requirements on isolation of noise such as traffic and seismic noise, the generation and measurement of a low-level input signal and the recovery of the accelerometer output signal in the presence of noise. Suggested solutions to these problems are presented, including isolation of the accelerometer under test by an active servo-controlled isolation platform, generation and measurement of a low-level acceleration input and recovery of the low-level accelerometer output signal by the statistical techniques of autocorrelation and cross-correlation.

Vibratory motion (translational or angular, single-axis or double-axis) of the accelerometer produces detrimental effects on performance due to basic dynamics

as well as limit conditions such as mechanical resonance, electronic saturation, and mechanical fatigue. These effects are reviewed, and vibration tests for the accelerometer and special instrumentation required for the vibration test facility are described.

The centrifuge is an obvious source of acceleration input for evaluating nongyroscopic accelerometers such as the PIPA under sustained acceleration greater than one gravity. However, the same choice for a gyroscopic accelerometer such as the PIGA is not as obvious due to the high angular velocities of the centrifuge. This requires adequate solutions to the equations for the complex motion of the gyroscopic element in the centrifuge environment. The test techniques that have been successfully used and the basic restrictions and assumptions for the accelerometer and centrifuge are described. Mathematical models of expected performance are reviewed and recommended data analysis techniques are presented. The importance of complete definition of expected accelerometer performance, based on fundamental mechanics and other testing, before making an arbitrary or generalized analysis of observed performance on the centrifuge is stressed. In addition, the need for data analysis which allows inspection for unexpected but systematic deviations from expected performance prior to fitting the data to an assumed mathematical model is demonstrated. The chapter is concluded with a description of the instrumentation of some precision centrifuges.

1. Introduction

The Instrumentation Laboratory at the Massachusetts Institute of Technology (MIT/IL) has pioneered in the development of inertial guidance systems for navigational control and guidance of interplanetary vehicles, orbital vehicles, suborbital vehicles, supersonic aircraft, subsonic aircraft, vertical takeoff and landing craft, ships, submarines and deep sea submergence vehicles. Over the years of pioneering development, the inertial reference integrating gyro and the specific force integrating receiver have emerged as the primary position and motion sensing transducers for the inertial measurement units of the inertial guidance system.

Accelerometer development at the Instrumentation Laboratory has focused on two pendulous types: the pulsed integrating pendulous accelerometer (PIPA) and the pendulous integrating gyro accelerometer (PIGA). The PIPA and PIGA are single-degree-of-freedom transducers with fully-floated, purposely-unbalanced gimbals acting as the torque-summing members. In the PIPA, the pendulous torques as a result of an applied acceleration to the unbalanced gimbal are restrained by constant-current pulses applied to a current-to-torque transducer through a closed-loop servo system. In the PIGA, the pendulous torques as a result of an applied acceleration to the unbalanced gimbal are restrained by a gyroscopic torque through a closed-loop servo system.

Since the initial application of the PIGA by Germany in 1940, the PIGA has progressed to the point where it is the most accurate and reliable specific force resolver available for application to inertial navigation systems. Many successful inertial navigation systems have been developed by the MIT Instrumentation Laboratory, based on operation of the PIPA and PIGA.

The progress made in development of the PIPA and PIGA has placed continuous demands on the requirements of the associated test equipment and test techniques to determine the performance of the PIPA and PIGA. It is an awareness of today's performance, reinforced by anticipated improvements, that necessitates discussion of today's testing techniques, as presented in subsequent sections of this chapter.

The accelerometer testing techniques discussed are those associated with determination of an instrument's acceptability for use in a system, commonly known as acceptance tests, and those techniques associated with special tests to determine the magnitude and short and long term stability of instrument performance coefficients, commonly known as design verification tests; the measurement of the accelerometer performance coefficients by means of tumble testing in the earth's gravity field, through use of an air bearing rate table, and by acceleration inputs generated by a centrifuge are discussed. Also, determination of the ultra-low acceleration response of the accelerometer and the effect of vibratory motion on the instrument's performance are discussed.

2. Test Program

An effective test program to support the initial development and subsequent production of a high-quality instrument is best achieved when the test program is (a) derived from a thorough knowledge of the particular instrument to be tested and (b) influenced and updated as a result of the changing requirements of both the instrument and its application. The purpose of this section is to review the general philosophy of testing the PIPA and the PIGA, answering the questions what, why and how the decisions are made in determining a refined set of acceptance tests for these accelerometers.

During the research and development of PIPA and PIGA instruments, many tests are applied to materials, piece-parts, subassemblies and completed assemblies of prototype models to assure that new materials, new processes and new assembly techniques, or different application of standard assembly techniques, meet the specified requirements. In addition, many qualitative and quantitative design verification tests are performed on completed prototype models to determine response to various conditions. The first production models fabricated by a given manufacturer are placed on life test to determine wear-out modes and performance degradation for reliability analyses and prediction. From this compilation of test data must be chosen the acceptance tests to be applied to materials, piece-parts, subassemblies, and completed assemblies for acceptance by the user. This test selection is influenced by several factors:

(a) major testing emphasis

(b) parameters to be measured

(c) optimum level of assembly to apply a test

(d) factors causing change in tests

These topics are reviewed in the following paragraphs, based on the development of the PIPA and PIGA by MIT/IL over the past years.

Major Testing Emphasis

The major emphasis in testing PIPA and PIGA units is determined by:

(a) field operational requirements of the user

(b) reliability requirements

(c) previous experience

(d) quantity of units

The parameters specified by the field requirements of the user must be determined. However, the extent to which a given parameter is emphasized over another depends on how the accelerometer is used in the field. As an example, the magnitudes of the scale factor and acceleration bias may be required in the field, but the acceleration bias may be updated so frequently in the field that placing significant importance to acceleration bias stability becomes unnecessary. Rather, it would be more important to gain confidence in the stability of the scale factor.

The reliability requirements have a great deal of influence on the selection of an acceptance test program. High reliability requirements demand increased testing, including redundant tests, and the attendant increase in cost. High reliability requirements may mean that certain design verification tests, which are normally performed on prototype or first-production units only, are performed on all units produced. For example, these units may be subjected to thermal change, shock and vibration tests, which require expensive equipment and highly skilled personnel.

Previous experience is a factor that has the major impact on the types of tests to be performed. In other words, the experience obtained from a PIPA and PIGA developmental program greatly influences the test program for a PIPA or PIGA designed under a subsequent developmental program.

The quantity of units in a given developmental program also affects the test program, based on cost versus effectiveness. As an example, testing a small number of units for a given parameter may be too expensive due to the high investment cost in equipment. This means that a less expensive method must be found to measure a parameter that by experience implies compliance to another test. Compromises such as these are usually detrimental to the reliability of the instrument.

Parameters to be Measured

The parameters to be measured in a test program are determined by:

(a) field operational requirements of the user

(b) computation requirements of higher-order assemblies

(c) process and assembly requirements

(d) anticipated changes in parameters during assembly

As a minimum, the magnitude and stability of the following parameters are required by the user for field operation: (a) scale factor, (b) acceleration bias, (c) nonlinearities, (d) input axis-to-mounting flange misalignment, (e) transfer function.

In some applications, the sensitivity of the accelerometer to its environment is required. This includes the sensitivities to: (a) variations in the power source, (b) thermal variations, (c) vibration, (d) shock, (e) atmospheric pressure, (f) magnetic fields, (g) acoustic noise, (h) r.f. radiation, (i) storage.

Measurement of the magnitude of these parameters may be rather simple, but determination of the stability of these parameters is relatively difficult and expensive, tying up test equipment for long periods of time.

Many parameters of particular subassemblies can be determined only at the time prior to becoming part of another assembly. In many instances, these parameters must be known in order to compute some of the accelerometer parameters. As an example, the sensitivity of the signal generator (microsyn) can be measured only at the microsyn assembly level. This sensitivity is required to compute the velocity storage, coefficient of damping and transfer function of the accelerometer.

Tests to determine the adequacy of a process and an assembly of piece-parts are obviously required in a test program. Examples of this type of test include measurement of PIG float leak rate, magnitude and stability of the torque required to rotate the float, and the axial and radial position of the float.

Processes such as potting, impregnation, final machine grinding and filling with a gas or fluid cause changes in parameters such as sensitivity, maximum torque developed, flotation temperature and damping coefficient. For example, the coefficient of damping should be measured after filling of the PIG unit. However, due to the change in environment, the coefficient of damping changes when the PIG is completed as a PIGA and, therefore, must be measured again.

Level of Assembly

Acceptance tests may be performed at several levels of assembly, including materials, piece-parts, minor assemblies, major assemblies and final assembly. The level of assembly at which an acceptance test must be performed is determined by:

(a) the lowest assembly level at which the test can be performed and still be effective

(b) the personnel and test equipment available and the attendant cost at a given level of assembly

(c) previous experience.

Generally it is desirable to measure parameters at the lowest possible level of assembly, starting with the raw material through piece-parts, subassemblies, final assembly, system use and field use. Testing at the lowest possible level of assembly usually provides the following advantages: (a) it requires less skill from personnel, (b) it requires less complexity in supporting test equipment, (c) an incorrect parameter is determined at the earliest possible time, (d) any schedule impact caused by an incorrect parameter is determined at the earliest possible time.

The performance of a gas bearing gyro wheel is determined by its ability to withstand slewing. Normally, the ability to withstand slewing is determined after assembly of the gas bearing gyro wheel. However, through the use of state-of-the-art surface inspection and geometric measuring techniques, the probability of a given set of parts yielding a good assembly can be determined at the piece-part level. Therefore, subjecting a completed gas bearing gyro wheel to tests for determining the slew rate capability and for rundown characteristics only determines that no contamination has been introduced during the assembly process.

Recent advances in the determination of PIG float freedom are examples of reducing the skill required by personnel and reducing the requirements of test equipment, along with the attendant cost reduction. Until recently, the float freedom test was performed by torquing the float to a given rotational position and allowing the

pendulous float to return to a stable position under the influence of gravity. The quality of float freedom was determined by the operator's judgement of the smoothness of float rotation as indicated by monitoring the signal generator output voltage and by the repeatability of the final stable position of the float. Depending on the inertia of the float and the damping coefficient, the operator had to wait one, two or three time constants before recording the stable position of the float. In heavily damped units, the operator had to wait as long as fifteen minutes to record a data point. As a result, only gross errors in float freedom were observed and intermittent obstructions were missed completely, leaving the full effectiveness of this parameter to a PIGA closed-loop test, which is a test at a higher level of assembly requiring an elaborate test stand and test electronics. Recently, the float freedom test was changed to measure the float freedom by a closed torque-to-balance analog servo loop in which the float is caused to rotate back and forth between the float stops by a ramping signal with a triangular waveshape applied to the torque-to-balance loop. The current required by the torque generator to balance the loop is recorded on a zero-suppressed strip-chart recorder. Deviations in the torque trace on the strip-chart recorder are an indication of contamination or air bubbles in the damping fluid that impede the motion of the float. Adoption of this float freedom test has reduced human error through automatic operation, reduced the sophistication and attendant cost of the test equipment, and provided a permanent record of the results.

Measurement of the alignment between the PIGA input axis and its mounting surface is a typical example of a test being lowered to the next subassembly. In the past, this alignment has been measured on the completed PIGA unit in closed-loop operation using a sophisticated dividing head and relatively complex test equipment. Recently, measurement of this misalignment has been made on the prior subassembly, the input axis assembly, using an autocollimator. As a result, discrepancies are discovered earlier, making any required corrective action less costly.

Factors Causing Changes in Tests

Updating a test program is equal in importance to the initial selection of a test program so as to minimize testing without sacrificing effectivity of the test program or quality of the accelerometer. The parameters to be measured in a given acceptance test program are outlined on pp. 286-7. The effects of test program changes on these parameters are described in the following paragraphs.

If the stability and the error terms of the accelerometer performance (sensitivity to higher-order terms, cross-axis terms and extraneous environments) can be held to the level where they no longer have to be considered by the user in the error analysis for field operation, measurement of these parameters at final assembly of the accelerometer may be eliminated from the acceptance test program. As an example, the second-order nonlinearity term (the response of the accelerometer to the square of the acceleration input) is being reduced at the present time to a value within the prior uncertainty in measurement. This is being accomplished by inertia adjustments of the float, and will permit elimination of a test for simulation of acceleration inputs in excess of one g. As other examples, the sensitivity of the acceleration bias to magnetic fields and the temperature sensitivity of the scale factor have been minimized by new materials and assembly techniques, eliminating the need for two complex tests.

Tests to determine the stability of parameters with respect to an environment may be eliminated if experience proves that the environment does not affect the parameter. For example, repetition of a test sequence following a storage period has

been eliminated, providing a considerable saving in test time. On the other hand, if the user has experienced an abnormally high number of rejects during a certain mode of operation, a test may have to be added to eliminate rejections from this cause, thus lengthening the test program.

Normally, tests that are performed to provide data for computations at a higher order of assembly are difficult to eliminate from the acceptance test program. Even though a parameter of the higher-order assembly can be determined without the knowledge of the lower assembly parameters, the test is usually much more complex and it is therefore simpler to make the test at the lower order of assembly.

The acceptance test program must establish confidence in specific processes and assembly techniques. Tests of this type may be deleted from the program if factors affecting these techniques, such as changes in material, manpower and tooling, are watched carefully. However, if fabrication is controlled by some means such as a configuration-control or data-bank system, these tests may be deleted without any loss of confidence.

A test devised to measure a parameter that is known to change a given amount as the result of a fabrication process is difficult to eliminate from an acceptance test program. When a parameter is known to shift, it must be monitored.

The factors affecting change in an accelerometer acceptance test program are as follows:

(a) examination of the effectiveness of a test based on experience

(b) change in method of test or test equipment, e.g. manual versus automated

(c) change in the requirement of the user

(d) change in material, manufacturing process, assembly process, tooling or personnel

(e) confidence gained in a supplier, minimizing incoming inspection.

The effectiveness of a given acceptance test program must be evaluated continuously, based on the acceptance test data and the data on field operation, e.g. field calibrations. The best way to accomplish this task is to establish a data bank at the beginning of the developmental program (Fig. 6-1). This consists of storing, either manually or by computer, the build configuration data, assembly data, test data, field operating data and repair data accumulated on each accelerometer. Using a computer data bank, the data are recorded only once and keyed directly for the applicable assembly test and repair data forms, reducing the amount of paperwork and human error and providing faster reaction time for compilation of recorded data. These data can be analyzed for:

(a) distribution of a measured parameter with respect to its specification

(b) correlation between field and acceptance test data

(c) correlation between subassembly test data and final assembly test data

(d) effects of design and process changes on acceptance test data and field data.

For this program to be successful, both in-specification and out-of-specification data must be stored.

For example, based on examination of field data, a recent short-term acceptance test to determine long-term stability of the scale factor and acceleration bias was found to be totally inadequate; the test was an all-pass filter with no value. As a result, a new short-term test was devised. Unfortunately, the revised short-term test requires twice the test time of the original short-term test, but the accelerometers meeting the requirements of this test also meet the long-term stability requirements in field use.

As an example of a change in test method and test equipment, the test equipment used to perform acceptance tests on the 16 PM PIP Mod B was changed recently from digital to analog, reducing the cost of the test equipment to one-third the cost of digital test equipment. However, analog closed-loop testing was not adequate for determining the difference in scale factor as the result of positive and negative inputs of acceleration. Therefore, a simulated test was devised to measure this parameter with the analog test equipment, completely eliminating the need for any digital test equipment.

Automated acceptance test methods are the most desirable. In testing accelerometers, this means automatic programming of the dividing head, automatic scanners, analog-to-digital conversion of data and data recorded on punched tape or magnetic tape instead of printed tape. Automation provides a uniform method and reduces human error, minimizing judgement by the operator. The float freedom test, described on pp. 287-8, is also an example of automation of a test method. Currently, automatic test stations for performing PIGA tumble tests are in operation at MIT/IL, requiring no personal attention for days and weeks at a time. These stations lend themselves to long-term stability tests of the accelerometer performance coefficients. It is becoming increasingly apparent that advancing state-of-the-art of automated test equipment is one of the ways to reduce test uncertainties. In one military application, the test equipment is automated to the extent that one computer is controlling four test stations simultaneously. Operator instructions and the test being performed are presented visually on a slide viewer. Unless interrogated, the output indicates whether or not a unit passed a given test. If desired, the automated equipment can be operated manually and a test repeated.

3. Testing in One-Gravity Field

The primary purpose of testing inertial-grade accelerometers in the gravitational field of the earth is to determine the magnitude, the short-term uncertainties and the long-term uncertainties of the coefficients describing the mathematical model of the accelerometer performance. To evaluate the data obtained from these types of tests:

(a) A mathematical model of the short-term performance of the accelerometer must be selected and evaluated.

(b) A mathematical model of the long-term performance of the accelerometer must be selected and evaluated.

(c) The limitations and errors associated with the individual tests must be understood.

(d) The data must be interpreted in accordance with any special test conditions.

An error analysis of the one-gravity tumble test, the mathematical model of a PIGA long-term performance, and a special tumble test using the air-bearing rate table (see section 4) are described in this section of the chapter.

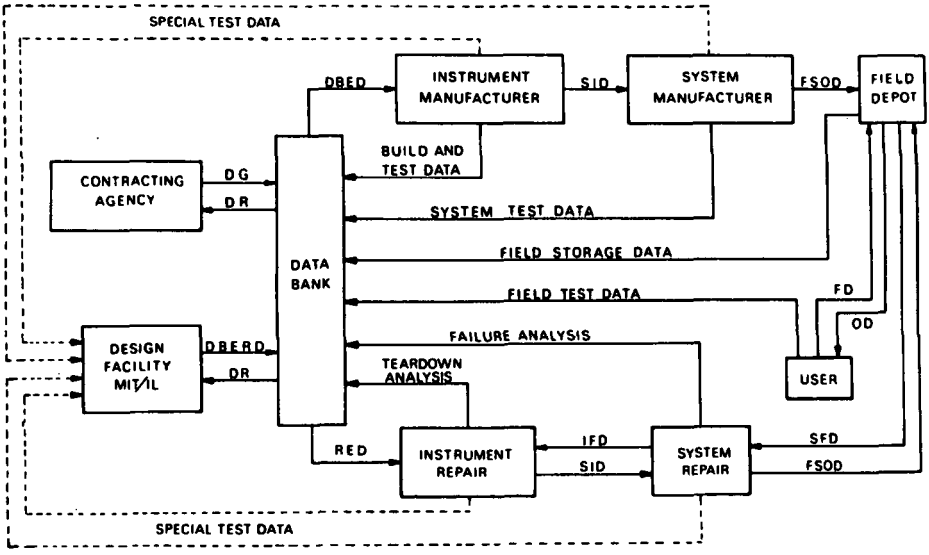

KEY

DBED	Design, build and evaluation data	IFD	Instrument failure data
DBERD	Design, build, evaluation and repair data	OD	Operating data
DG	Design goals	RED	Repair and evaluation data
DR	Data retrieval	SFD	System failure data
FD	Failure data	SID	System interface data
FSOD	Field storage and operating data		

Fig. 6-1 Idealized automated data handling

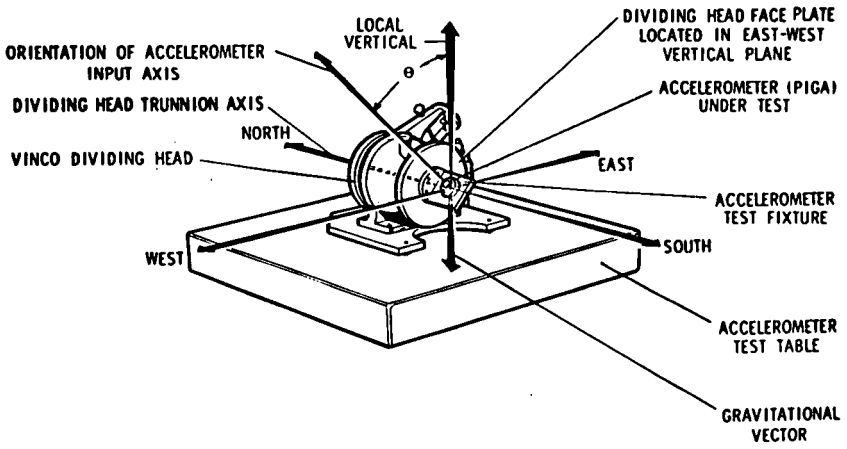

Fig. 6-2 Orientation of PIGA on index head

Table 6-1 Conditions during PIGA tumbling tests

Dividing head angle, θ_1, deg	Acceleration input, g	Time period for n revolutions	Time to midpoint of data, t_i
0	- 1	T	1/2 T
60	- 1/2	2 T	2 T
120	+ 1/2	2 T	4 T
180	+ 1	T	11/2 T
240	+ 1/2	2 T	7 T
300	- 1/2	2 T	9 T

Table 6-2 Definitions of coefficients affected by bias

Actual value of coefficient	Biased value of coefficient	Error in coefficient
A_0	$\hat{A}_0$	$(\Delta A_0)_b = \hat{A}_0 - A_0$
A_1	$\hat{A}_1$	$(\Delta A_1)_b = \hat{A}_1 - A_1$
A_2	$\hat{A}_2$	$(\Delta A_2)_b = \hat{A}_2 - A_2$
B_1	$\hat{B}_1$	$(\Delta B_1)_b = \hat{B}_1 - B_1$

Error Analysis of One-Gravity Tumble Test

A typical test station for testing an accelerometer in a one-gravity field consists of:

(a) a precision rotary dividing head supporting a test fixture with the capacity of mounting a single or multiple number of accelerometers on a precisely temperature-controlled mounting surface

(b) instrumentation such as a programmer-sequencer to program the automated dividing head and test data, digital monitoring instruments, analog recording equipment and general-support commercial equipment

(c) excitation sources and electronics for environmental control, such as thermal control of the accelerometer under test

The accelerometers to be tested are mounted in the test fixture with their input axes perpendicular to the dividing head trunnion axis, which is horizontal as shown in figure 6-2. The accelerometer is tumbled (rotated) in the vertical plane about the trunnion axis of the dividing head, and measurements of the accelerometer output are made at several angle settings of the dividing head. Each setting of the dividing head places the accelerometer input axis at some angle with respect to the direction of the earth's gravitational field.

The theoretical performance equation for the accelerometer, expressed as a power series, is

$$Y = a_0 + a_1 a_{in} + a_2 a_{in}^2 + \ldots \qquad \text{(Eq. 6-1)}$$

where

Y = accelerometer output

a_0 = coefficient insensitive to acceleration input (acceleration bias)

a_1 = first-order coefficient sensitive to acceleration input (scale factor)

a_2 = second-order coefficient sensitive to square of acceleration input (nonlinearity coefficient)

a_{in} = component of acceleration along PIGA input axis

The acceleration input may be expressed as

$$a_{in} = g \cos (\theta_i + \alpha) \qquad \text{(Eq. 6-2)}$$

where

g = local gravitational constant

θ_i = dividing head angle with respect to its vertical reference position

α = misalignment angle between the vertical reference position of the dividing head and the true vertical.

The effects of the following error sources on the coefficients of the accelerometer performance equation as obtained from the tumble test are considered in this error analysis:

(a) a linear drift of the acceleration bias, a_0, with respect to time, K_b

(b) a linear drift of the scale factor, a_1, with respect to time, K_s

(c) linear pier motion

Substituting equation 6-2 into equation 6-1 and applying trigonometric identities, the performance equation becomes

$$Y = a_0 + \frac{a_2}{2} g^2 + a_1 g \cos \theta_i - a_1 g \alpha \sin \theta_i + \frac{a_2}{2} g^2 \cos 2 \theta^i$$

$$- a_2 g^2 \alpha \sin 2\theta_i \qquad \text{(Eq. 6-3)}$$

Application of Least Squares Curve Fit to the Tumble Test Data. Several methods of curve-fitting data yield consistent estimates of parameter values if sufficient measurements are made. The method of least squares is the most efficient and will minimize parameter uncertainty if:

(a) The input values are known exactly.

(b) The measured set of output values for each input value vary randomly about some mean which is constant.

(c) The distribution of each set of measured values approaches a normal distribution asymptotically.

(d) The variance of the output as a function of the input value is known.

(e) The form of the theoretical performance equation is known and is linear with respect to the parameters.

The method of least squares is most efficient because it minimizes the sum of the squares of the deviations between the theoretical and empirical curves. The most efficient or the best estimates of the parameters are those that are normally distributed about the true mean value and have the smallest possible variance.

For the case where g = 1, the theoretical equation to which the method of least squares will be applied is:

$$Z_i = A_0 + A_1 \cos \theta_i + B_1 \sin \theta_i + A_2 \cos 2\theta_i + B_2 \sin 2\theta_i \qquad \text{(Eq. 6-4)}$$

Comparing equation 6-4 with equation 6-3:

$$A_0 = a_0 + \frac{a_2}{2} \qquad \text{(Eq. 6-5)}$$

$$A_1 = a_1 \qquad \text{(Eq. 6-6)}$$

$$B_1 = - a_1 \alpha \qquad \text{(Eq. 6-7)}$$

$$A_2 = \frac{a_2}{2} \qquad \text{(Eq. 6-8)}$$

$$B_2 = -a_2 \alpha \qquad \text{(Eq. 6-9)}$$

Compared to the other coefficients, the coefficient B_2 may be discarded as being insignificant.

Using N angle settings of the dividing head, the sum of the squares of the deviations for a least square curve fit is

$$\sum_{i=1}^{N} (Y_i - Z_i)^2 = \sum_{i=1}^{N} (Y_i - A_0 - A_1 \cos\theta_i - A_2 \cos 2\theta_i - B_1 \sin\theta_i)^2 \qquad \text{(Eq. 6-10)}$$

Taking partial derivatives with respect to each parameter and setting them equal to zero, the matrix form of the resulting set of equations is

$$\begin{bmatrix} \sum_{i=1}^{N} Y_i \\ \sum_{i=1}^{N} Y_i \cos\theta_i \\ \sum_{i=1}^{N} Y_i \cos 2\theta_i \\ \sum_{i=1}^{N} Y_i \sin\theta_i \end{bmatrix} = \begin{bmatrix} \sum_{i=1}^{N} 1 & \sum_{i=1}^{N} \cos\theta_i & \sum_{i=1}^{N} \cos 2\theta_i & \sum_{i=1}^{N} \sin\theta_i \\ \sum_{i=1}^{N} \cos\theta_i & \sum_{i=1}^{N} \cos^2\theta_i & \sum_{i=1}^{N} \cos 2\theta_i \cos\theta_i & \sum_{i=1}^{N} \sin\theta_i \cos\theta_i \\ \sum_{i=1}^{N} \cos 2\theta_i & \sum_{i=1}^{N} \cos\theta_i \cos 2\theta_i & \sum_{i=1}^{N} \cos^2 2\theta_i & \sum_{i=1}^{N} \sin\theta_i \cos 2\theta_i \\ \sum_{i=1}^{N} \sin\theta_i & \sum_{i=1}^{N} \cos\theta_i \sin\theta_i & \sum_{i=1}^{N} \cos 2\theta_i \sin\theta_i & \sum_{i=1}^{N} \sin^2\theta_i \end{bmatrix} \begin{bmatrix} A_0 \\ A_1 \\ A_2 \\ B_1 \end{bmatrix}$$

(Eq. 6-11)

Using N equally-spaced angle settings of the dividing head, the following relationships exist:

$$\sum_{i=1}^{N} \cos\theta_i = \sum_{i=1}^{N} \sin\theta_i = \sum_{i=1}^{N} \sin\theta_i \cos\theta_i = \sum_{i=1}^{N} \cos 2\theta_i = \sum_{i=1}^{N} \sin\theta_i \cos 2\theta_i = \sum_{i=1}^{N} \cos\theta_i \cos 2\theta_i = 0$$

(Eq. 6-12)

$$\sum_{i=1}^{N} 1 = N \qquad \text{(Eq. 6-13)}$$

$$\sum_{i=1}^{N} \cos^2\theta_i = \sum_{i=1}^{N} \sin^2\theta_i = \sum_{i=1}^{N} \cos^2 2\theta_i = N/2 \qquad \text{(Eq. 6-14)}$$

Using the entities given in equations 6-12 through 6-14, the matrix given in equation 6-11 becomes simplified as follows:

$$\begin{bmatrix} \sum_{i=1}^{N} Y_i \\ \sum_{i=1}^{N} Y_i\cos\theta_i \\ \sum_{i=1}^{N} Y_i\cos 2\theta_i \\ \sum_{i=1}^{N} Y_i\sin\theta_i \end{bmatrix} = \begin{bmatrix} N & 0 & 0 & 0 \\ 0 & N/2 & 0 & 0 \\ 0 & 0 & N/2 & 0 \\ 0 & 0 & 0 & N/2 \end{bmatrix} \begin{bmatrix} A_0 \\ A_1 \\ A_2 \\ B_1 \end{bmatrix} \qquad \text{(Eq. 6-15)}$$

The inverted equations for N equally-spaced angle settings of the dividing head are

$$\begin{bmatrix} A_0 \\ A_1 \\ A_2 \\ B_1 \end{bmatrix} \begin{bmatrix} 1/N & 0 & 0 & 0 \\ 0 & 2/N & 0 & 0 \\ 0 & 0 & 2/N & 0 \\ 0 & 0 & 0 & 2/N \end{bmatrix} \begin{bmatrix} \sum_{i=1}^{N} Y_i \\ \sum_{i=1}^{N} Y_i\cos\theta_i \\ \sum_{i=1}^{N} Y_i\cos 2\theta_i \\ \sum_{i=1}^{N} Y_i\sin\theta_i \end{bmatrix} \qquad \text{(Eq. 6-16)}$$

The equations expressed in this matrix are the equations for the Fourier analysis, which is a special case of least squares.

The number of revolutions of the PIGA in time, T, is a function of the acceleration input.

$$\frac{n}{T_j} = K_1 a_{in} \qquad \text{(Eq. 6-17)}$$

where

n = number of revolutions

T_j = time for n revolutions of PIGA at the acceleration level of a_{in}

K_1 = constant

The uncertainty in the PIGA output for a given acceleration input is inversely proportional to the number of revolutions of data.

$$\sigma_n = \frac{\sigma_1}{n} \qquad \text{(Eq. 6-18)}$$

where

σ_n = normalized uncertainty in PIGA n-revolution data

σ_1 = normalized uncertainty in PIGA one-revolution data

As proven by actual test data, the normalized uncertainty of the PIGA output is a constant for a given number of revolutions of the PIGA over the range of 1/2 to 1 g used in one-gravity tumble tests.

$$\sigma_n \neq f(a_{in}) \text{ from } 1/2 \text{ to } 1 \text{ g} \qquad \text{(Eq. 6-19)}$$

One of the requisites of the method of the least squares is that the data points have a constant uncertainty, σ_n. Equations 6-17, 6-18 and 6-19 imply that n is constant for all levels of acceleration input. Modifying equation 6-17:

$$\frac{1}{T_j} = K_2 a_{in} \qquad \text{(Eq. 6-20)}$$

where

$$K_2 = K_1/n$$

If $T_1 = T$ when $a_{in} = 1$ g, then $T_{1/2} = 2T$. The PIGA output is measured at six equally-spaced angles of the dividing head (N = 6), 0 deg, 60 deg, 120 deg, 180 deg, 240 deg and 300 deg. If t_i is defined as the midpoint of an ith set of data taken at a given level of acceleration, the conditions expressed in table 6-1 will exist during the tumble tests, starting with the position of 0 deg, t_i equal to zero at the beginning of this data set and rotating the dividing head counterclockwise. As indicated in table 6-1, the total test time for the tumbling test is 10T.

Coefficient Errors Resulting from Bias Drift. If a drift exists in the acceleration bias equivalent to K_b expressed in g per unit of time t_i, the PIGA output Y_i will be in error by the amount $K_b t_i$, independent of the dividing head angle (acceleration input). Under these conditions, the PIGA output is:

$$Y_i = y_i + K_b t_i \qquad \text{(Eq. 6-21)}$$

The coefficients of the performance equations as affected by the bias are defined in table 6-2. Substituting equation 6-21 for Y_i in equation 6-16, evaluating the matrix at the values of θ_i and t_i given in table 6-1, applying the value N = 6, and defining the coefficients in accordance with table 6-2 results in the following error matrix:

$$\begin{bmatrix} (\Delta A_0)_b \\ (\Delta A_1)_b \\ (\Delta A_2)_b \\ (\Delta B_1)_b \end{bmatrix} = \begin{bmatrix} \\ I \\ \\ \end{bmatrix} \begin{bmatrix} 4.6\, K_b T \\ -\frac{5}{3} K_b T \\ -\frac{5}{3} K_b T \\ -\frac{5\sqrt{3}}{3} K_b T \end{bmatrix} \qquad \text{(Eq. 6-22)}$$

where

I = unity matrix

Table 6-3 Conditions during two six-point tests

Dividing head angle, θ_i, deg	Acceleration input, g	Time period for n revolutions	Time to midpoint of data, t_i
0	- 1	T	1/2 T
60	- 1/2	2 T	2 T
120	+ 1/2	2 T	4 T
180	+ 1	T	11/2 T
240	+ 1/2	2 T	7 T
300	- 1/2	2 T	9 T
300	- 1/2	2 T	11 T
240	+ 1/2	2 T	13 T
180	+ 1	T	29/2 T
120	+ 1/2	2 T	16 T
60	- 1/2	2 T	18 T
0	- 1	T	39/2 T

Table 6-4 Coefficient errors in two six-point tests

Coefficient	Bias error K_b (m = b)	Scale factor error K_s (m = s)
$(\Delta A_0)_m$	20 K_b T	0
$(\Delta A_1)_m$	0	20 K_s T
$(\Delta A_2)_m$	0	0
$(\Delta B_1)_m$	0	0

Table 6-5 Coefficient errors in one six-point test

Coefficient	Bias error K_b (m = b)	Scale factor error K_s (m = s)
$(\Delta A_0)_m$	4.6 K_b T	- 5/6 K_s T
$(\Delta A_1)_m$	- 5/3 K_b T	+ 23/6 K_s T
$(\Delta A_2)_m$	- 5/3 K_b T	- 5/3 K_s T
$(\Delta B_1)_m$	- $5\sqrt{3}/3$ K_b T	- $\sqrt{3}/3$ K_s T

Coefficient Errors Resulting from Scale Factor Drift. If a drift exists in the scale factor equivalent to K_s expressed in units of output data per g per unit of time t_i, the PIGA output Y_i will be in error by the amount $K_s t_i \cos\theta_i$. Under these conditions, the PIGA output is

$$Y_i = y_i + K_s t_i \cos\theta_i \qquad \text{(Eq. 6-23)}$$

In other words, the amount that each data point is in error is a function of the acceleration input at that data point. Substituting equation 6-23 for Y_i in equation 6-16, evaluating the matrix at the values of θ_i and t_i given in table 6-1, applying the value N = 6, and defining the coefficients $(\Delta A_0)_s$, $(\Delta A_1)_s$, $(\Delta A_2)_s$, and $(\Delta B_1)_s$ in the same manner as the definitions in table 6-2 results in the following error matrix:

$$\begin{bmatrix} (\Delta A_0)_s \\ (\Delta A_1)_s \\ (\Delta A_2)_s \\ (\Delta B_1)_s \end{bmatrix} = \begin{bmatrix} \\ I \\ \\ \end{bmatrix} \begin{bmatrix} -\frac{5}{6} K_s T \\ \frac{23}{6} K_s T \\ -\frac{5}{3} K_s T \\ -\frac{\sqrt{3}}{3} K_s T \end{bmatrix} \qquad \text{(Eq. 6-24)}$$

Coefficient Errors Resulting from Drift of Bias and Scale Factor with Two Six-Point Tests. As an effective method of reducing the effect of bias and scale factor drift in the resulting coefficients, a six-point test and a repetition of the six-point test obtained by rotating the dividing head clockwise (mirror image of first six-point test) are applied to the accelerometer under test. During these tests, the conditions expressed in table 6-3, the equivalent of the conditions expressed in table 6-1, will exist. As indicated in table 6-3, the total test time for this tumble test is 20T. Applying the procedures described in the two preceding subsections, except evaluating the matrices at the values of θ_i and t_i given in table 6-3 instead of table 6-1, the errors in the coefficients due to bias and scale factor drift will be in accordance with table 6-4. The coefficient errors of the bias and scale factor are as expected, i.e. the error in the bias coefficient is $20TK_b$, which is the change in magnitude of the bias over the test time 20T due to a linear drift, K_b, and similarly for the scale factor. The advantages of two six-point tests is obvious by comparing the coefficient error in table 6-4 with the coefficient errors of one six-point test as indicated in table 6-5.

Using the coefficient errors defined in table 6-4, the actual measured coefficients of the accelerometer as defined by equations 6-5 through 6-9 are

(a) with a drift in bias

$$\Delta a_0 = 20\, K_b T \qquad \text{(Eq. 6-25)}$$

(b) with a drift in scale factor

$$\Delta a_1 = 20\, K_s T \qquad \text{(Eq. 6-26)}$$

Coefficient Errors Resulting from Linear Pier Motion. Floor instability is a gross source of input inaccuracy in the accelerometer tumbling tests. This error can be anywhere from 10 to 30 seconds of arc at various frequencies, depending on the type of floor or pad and depending on the source of the disturbance such as machinery or pedestrian traffic.

If all the input uncertainties are assumed to be randomly distributed, independent of one another, and asymptotically approach a normal distribution, the curve fit contains N + n statistical parameters. There are N input values and n instrument parameters, all having mean squared deviations from the true mean. Therefore, partial derivatives of the curve-fit squared deviations must be taken with respect to each of the N + n variables and set to zero. The N + n normal equations must then be solved simultaneously, involving the inversion of the N + n square matrix.

In general, this process is too involved to be worthwhile, even if a high-speed digital computer is used. About the only curve for which a standard solution exists in the literature is Y = a + bx. If N is sufficiently large, the standard least-squares curve fit is probably the best to use.

There is one approach that can be taken with the harmonic analysis of the accelerometer tumbling-test data. The errors in input setting can be converted into errors in output through the use of the standard least-squares equations and trigonometric substitutions. Starting with the theoretical performance equation:

$$Y = A_0 + A_1\cos\theta + B_1\sin\theta + A_2\cos 2\theta + B_2\sin 2\theta \qquad \text{(Eq. 6-27)}$$

The empirical equation, with the dividing head providing exact input angles, is

$$Y_i + E_i = A_0 + A_1\cos\theta_i + B_1\sin\theta_i + A_2\cos 2\theta_i \qquad \text{(Eq. 6-28)}$$

With random errors in the input angles δ_i, the empirical equation is

$$Y_i + E_i = A_0 + A_1\cos(\theta_i + \delta_i) + A_2\cos 2(\theta_i + \delta_i) \qquad \text{(Eq. 6-29)}$$

Using small-angle approximations and trigonometric identities:

$$\cos(\theta_i + \delta_i) = \cos\theta_i\cos\delta_i - \sin\theta_i\sin\delta_i = \cos\theta_i - \delta_i\sin\theta_i \qquad \text{(Eq. 6-30)}$$

$$\sin(\theta_i + \delta_i) = \cos\theta_i\sin\delta_i + \sin\theta_i\cos\delta_i = \delta_i\cos\theta_i + \sin\theta_i \qquad \text{(Eq. 6-31)}$$

$$\cos^2(\theta_i + \delta_i) = \cos 2\theta_i\cos 2\delta_i - \sin 2\theta_i\sin 2\delta_i = \cos 2\theta_i - 2\delta_i\sin\theta_i \qquad \text{(Eq. 6-32)}$$

Substituting equations 6-30, 6-31 and 6-32 into equation 6-29:

$$Y_i + E_i = A_0 + A_1\cos\theta_i - A_1\delta_i\sin\theta_i + B_1\sin\theta_i + B_1\delta_i\cos\theta_i + A_2\cos 2\theta_i - 2A_2\delta_i\sin 2\theta_i \qquad \text{(Eq. 6-33)}$$

Summing over a set of equally-spaced angles:

$$\begin{aligned}\Sigma Y_i = {} & NA_0 + A_1\,\Sigma\cos\theta_i - A_1\,\Sigma\delta_i\sin\theta_i \\ & + B_1\,\Sigma\sin\theta_i + B_1\,\Sigma\delta_i\cos\theta_i \\ & - A_2\,\Sigma\cos 2\theta_i - 2A_2\,\Sigma\delta_i\sin 2\theta_i\end{aligned} \qquad \text{(Eq. 6-34)}$$

The three terms in the second column of equation 6-34 go to zero because equally-spaced input angles were used. None of the three terms in the third column of equation 6-34 go to zero, but the coefficient A_1 is larger than the coefficients B_1 and A_2. Only the terms $A_1\,\Sigma\delta_i f(\theta_i)$ will be carried in each of the equations.

Simplifying equation 6-34:

$$Y_i = NA_0 - A_1 \Sigma \delta_i \sin\theta_i \qquad \text{(Eq. 6-35)}$$

Since the least squares fit for equally-spaced exact input angles has

$$\Sigma Y_i = N\hat{A}_0 \qquad \text{(Eq. 6-36)}$$

the equations can be combined to obtain

$$N\hat{A}_0 = NA_0 - A_1 \Sigma \delta_i \sin\theta_i \qquad \text{(Eq. 6-37)}$$

The deviation between A_0 and $\hat{A}_0$ is

$$A_0 - \hat{A}_0 = A_1/N \sum_{i=1}^{N} \delta_i \sin\theta_i \qquad \text{(Eq. 6-38)}$$

The deviation over m runs with m going to infinity is

$$A - \hat{A}_0 = \sqrt{(1/m) \sum_{j=1}^{m} (A_0 - \hat{A}_0)^2}$$

$$= (A_1/N) \sqrt{(1/m) \sum_{i=1}^{m} \left(\sum_{i=1}^{N} \delta_i \sin\theta_i \right)^2} \qquad \text{(Eq. 6-39)}$$

If the magnitude of the error angles is independent of the value θ, and the error angles are randomly distributed with a zero mean:

$$\left(\sum_{i=1}^{N} \delta_i \sin\theta_i \right)^2 = \sigma_{(\delta)}^2 \Sigma \sin^2\theta_i = \sigma_{(\delta)}^2 (N/2) \qquad \text{(Eq. 6-40)}$$

Therefore

$$\sigma(A_0 - \hat{A}_0) = (A_1/N)\, \sigma_{(\delta)} \sqrt{N/2} = (A_1/\sqrt{2N})\, \sigma_{(\delta)} \qquad \text{(Eq. 6-41)}$$

Continuing in the same manner for the equations of the other three parameters, and using equation 6-28 to establish the least-squares fit for equally-spaced input angles, the equations for the parameters are

$$\Sigma Y_i \cos\theta_i = (N/2)\hat{A}_1 \qquad \text{(Eq. 6-42)}$$

$$\Sigma Y_i \sin\theta_i = (N/2)\hat{B}_1 \qquad \text{(Eq. 6-43)}$$

$$\Sigma Y_i \cos 2\theta_i = (N/2)\hat{A}_2 \qquad \text{(Eq. 6-44)}$$

where

$\hat{A}_0$, $\hat{A}_1$, $\hat{A}_2$, and $\hat{B}_1$ are the values computed with exact inputs.

$$\Sigma Y_i \cos\theta_i = NA_1/2 - A_1 \Sigma \delta_i \cos\theta_i \sin\theta_i \qquad \text{(Eq. 6-45)}$$

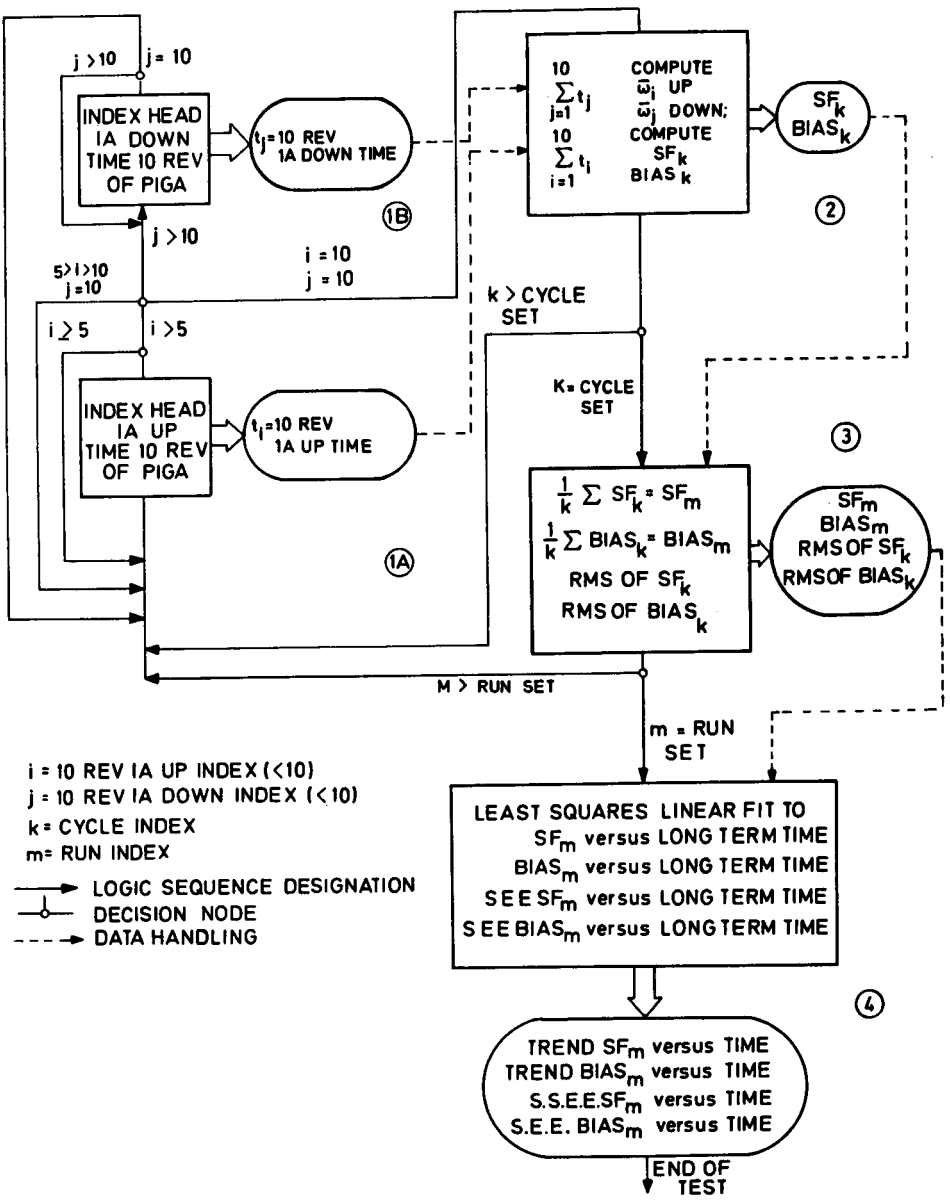

Fig. 6-3 Flow diagram of data acquisition procedure

$$\Sigma Y_i \sin\theta_i = NB_1/2 - A_1 \Sigma \delta_i \sin\theta_i \cos 2\theta_i \quad \text{(Eq. 6-46)}$$

$$\Sigma Y_i \cos 2\theta_i = NA_2/2 - A_1 \Sigma \delta_i \sin\theta_i \cos 2\theta_i \quad \text{(Eq. 6-47)}$$

The deviations in the parameters between exact and inexact input angles are

$$A_1 - \hat{A}_1 = (2A_1/N)\Sigma \delta_i \cos\theta_i \sin\theta_i \quad \text{(Eq. 6-48)}$$

$$B_1 - \hat{B}_1 = (2A_1/N)\Sigma \delta_i \sin^2\theta_i \quad \text{(Eq. 6-49)}$$

$$A_2 - \hat{A}_2 = (2A_1/N)\Sigma \delta_i \sin\theta_i \cos 2\theta_i \quad \text{(Eq. 6-50)}$$

Assuming again that the error-angle magnitudes are independent of angle and that the deviations are random:

$$\Sigma \sin^4\theta = 3N/8 \quad \text{(Eq. 6-51)}$$

$$\Sigma \cos^2\theta \sin^2\theta = N/4 \quad \text{(Eq. 6-52)}$$

$$\Sigma \sin^2\theta \cos^2 2\theta = N/8 \quad \text{(Eq. 6-53)}$$

$$\sigma_{(A_1 - \hat{A}_1)} = [(2A_1/N)\sqrt{N/4}\,]\,\sigma_{(\delta)} = (A_1/\sqrt{N})\sigma_{(\delta)} \quad \text{(Eq. 6-54)}$$

$$\sigma_{(B_1 - \hat{B}_1)} = [(2A_1/N)\sqrt{3N/8}\,]\sigma_{(\delta)} = (A_1/\sqrt{3/2N})\sigma_{(\delta)} \quad \text{(Eq. 6-55)}$$

$$\sigma_{(A_2 - \hat{A}_2)} = [(2A_1/N)\sqrt{N/8}\,]\,\sigma_{(\delta)} = (A_1/\sqrt{2N})\sigma_{(\delta)} \quad \text{(Eq. 6-56)}$$

Summary. The conclusion could be drawn from this presentation that the shorter the test time or the shorter the data acquisition time, T, the less the effect of scale factor drift and bias drift on the measured coefficients. This is not entirely true because the shorter the time, T, the fewer the number of revolutions of the PIGA during the time, T, and the higher the uncertainty of the rate measurement (see equations 6-17 and 6-18). This increases the least-squares curve-fit variance, σ_{cf}, which is reflected in an increase in the uncertainty of the curve fit coefficients as follows:

$$\sigma_{A_0}^2 = \sigma_{cf}^2 (1/N); \quad \sigma_{A_1}^2 = \sigma_{B_1}^2 = \sigma_{A_2}^2 = \sigma_{cf}^2 (2/N)$$

Therefore, the value selected for the time, T, is based on the values of σ_n, K_b and K_s.

Mathematical Model of Long-Term Performance

The method of least squares curve fitting is used frequently as the best measure of long-term PIGA performance. However, this practice can produce misleading results if assumptions implicit in the method are not confirmed. The purpose of this section of the chapter is to investigate the conditions for validity of the method

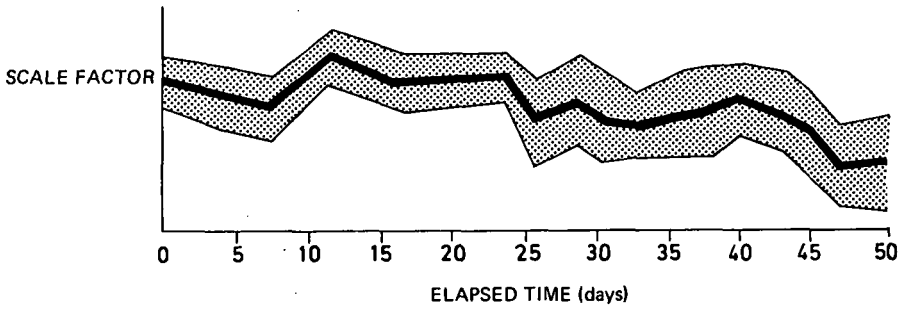

Fig. 6-4 Scale factor as a function of elapsed time

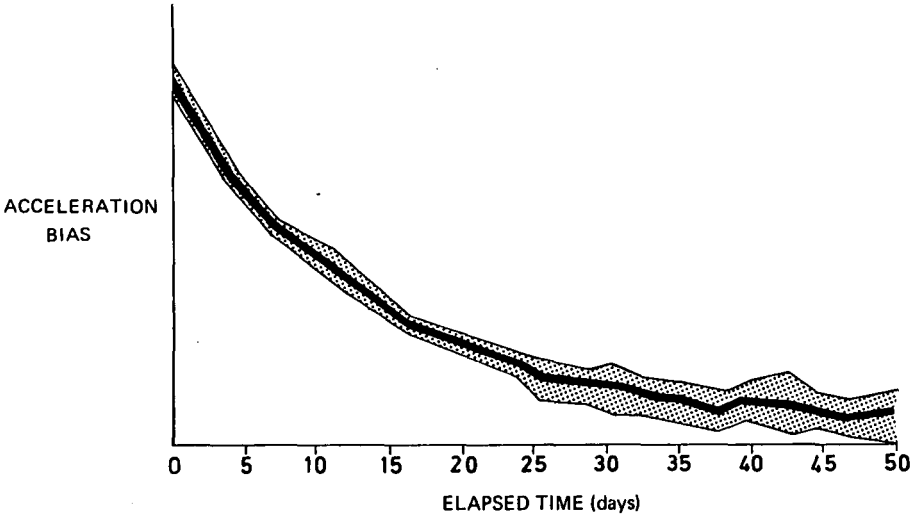

Fig. 6-5 Acceleration bias as a function of elapsed time

of least squares. As a test case, the data gathered on a 16 PIGA over a 49-day period are analyzed in detail.

First, the data at the point of generation are examined and characterized. From this point, the analysis follows the data handling procedure to the next phase, the calculation of short-term scale factor and short-term acceleration bias. The analysis is extended further to include and to evaluate the long-term scale factor and the long-term acceleration bias. At each phase of the data acquisition and evaluation, the data are characterized by distribution function through the use of the appropriate statistical techniques. At the point where the method of least squares is applied to the PIGA data, the method is examined for validity. Alternative tests are then described for possible evaluation of the PIGA data.

Generation of Test Data. A flow diagram of the data acquisition procedure is shown in figure 6-3. This procedure provides for automatic testing of the PIGA with a minimum amount of monitoring by the operator. Data generation points 1A and 1B shown in figure 6-3 are at the test station and data generation points 2, 3 and 4 are at the computer.

Each number is the time period for ten revolutions of the PIGA when sensing an acceleration of one g. One cycle consists of five numbers with IA up, ten with IA down and five more with IA up. Successive up or down numbers are not generated continuously, but are separated by one revolution of the PIGA. The scale factor, SF_k, and acceleration bias, $bias_k$, are calculated for each cycle of data in accordance with the standard formulae.

A successive number of cycles is defined as a run, and each run consists of approximately 15 cycles per run. The scale factors for each cycle, SF_k, and the acceleration bias for each cycle, $bias_k$, are averaged to obtain the mean scale factor, SF_m, and the mean acceleration bias, $bias_m$. In addition, the rms values of the deviations from the mean scale factor, rms of SF_k, and from the mean acceleration bias, rms of $bias_k$, are computed.

Successive runs, referred to as calibrations, are examined over a relatively long period of time, usually 30 days, or in this case 49 days (Figs. 6-4 and 6-5). A least squares linear fit is performed in the values of scale factor and acceleration bias. Trends and the rms value about the trends (the latter referred to as standard error of estimate, S. E. E.) are computed. Current evaluation procedures of the PIGA performance place heavy emphasis upon the trend and rms values about the trend as the parameters that best describe the PIGA performance. This practice will be examined critically in the following three subsections.

Statistical Analysis of Test Data. A list of the runs examined during this particular study is shown in table 6-6. When averaging the scale factors calculated for each cycle, the assumption is made that data gathered for all cycles are from the same population. If not, associating a mean scale factor with each run is misleading. The Kruskal-Wallis non-parametric test was applied successively to run nos. 368, 386, 395 and 409 to verify the assumption that each cycle of data comes from the same or identical populations.

Consider all the time periods measured with the PIGA IA up during run no. 368. As indicated in table 6-6, run no. 368 contains 12 cycles of data, making a total of 120 values of time periods measured with IA up as indicated in table 6-7. The time periods, t_{ik}, are ranked from the smallest to the largest values. When ties occur between two or more time periods, the mean of the tied ranks is assigned to each. If the time periods are from the same or identical populations, the sum of the rank values for each cycle should be nearly the same. Application of the

Kruskal-Wallis test indicates statistically whether or not this is the case. The null hypothesis, H_o, for this application indicates no significant difference in data between cycles K = 1, K = 2, K = 3, . . . K = 12. Rejecting the null hypothesis indicates that this assumption cannot be made, and would cast doubt on the procedure of averaging the scale factor values within each run. Table 6-8 is a summary of the application of the Kruskal-Wallis test to the time periods for IA up and IA down of run nos. 368, 386, 395 and 409.

As indicated in table 6-8, the null hypothesis was acceptable for all data selected except for run no. 409. Therefore, averaging scale factors calculated for each cycle appears to be justified.

Statistical Analysis of Scale Factor and Bias Distribution Functions. Application of the Kruskal-Wallis test to the PIGA data has resulted in support for the contention that successive cycles of data in any one calibration run are from the same or identical populations. While this is a powerful conclusion, justifying such standard data handling techniques as averaging or grouping of run data, no information as to the exact nature of population is offered. One of the strengths of the Kruskal-Wallis test is precisely that it does not depend upon the data following any particular distribution function, such as the Gaussian or binomial, for its validity. The only requirement is that the data in question come from a population with a continuous distribution.

Standard procedure for utilizing the data is to consider the mean scale factor as one point in time. Successive calibration runs are made and a linear least squares fit performed on these successive scale factors as a function of elapsed time. This procedure is justified only if each mean scale factor is obtained from a normally distributed population. If the scale factors are not normally distributed, a linear least squares fit is invalid - see p529 of reference (1). The assumption of normality is a necessary but not sufficient condition for a valid use of curve fitting. Additional conditions are considered in the subsection following.

The vertical variance is computed also. For this quantity to be a meaningful measure of dispersion of the scale factors, the assumption of normality is again required. For these two important considerations, the distribution function for scale factor and bias as well must be determined.

The Kolmogorov-Smirnov test of maximum absolute difference facilitates the comparison of a sample of experimental data with any assumed distribution function. It is a completely general tool applicable to distribution functions such as exponential, Poisson and binomial, as well as to the normal or Gaussian distribution. It compares the cumulative distribution function of the experimental data in question with the assumed theoretical distribution function.

The null hypothesis for this particular case states that no significant difference exists between the distribution of cycle scale factors or bias within any one run and an assumed normal distribution. The test is constructed so that rejection of the null hypothesis is accompanied by a confidence level. For example, rejection of H_o, the null hypothesis, at a 0.05 confidence level means that there are about five chances in 100 of rejecting the hypothesis - in this case the hypothesis of normality - when it should be accepted. Stated differently, the confidence level that the correct decision has been made is 95 percent. Rejecting the null hypothesis erroneously is conventionally designated as a Type I error.

The results of applying the Kolmogorov-Smirnov test to the scale factor values and acceleration bias values of each run are listed in table 6-9. In accordance with table 6-9, successive cycle scale factors collected over a short period of time

Table 6-6 List of runs examined

Run no. *	Cycles per run
368	12**
372	12
374	10
379	9
383	9
386	17**
389	14
391	16
393	20
395	19**
397	18
399	12
401	10
403	14
405	17
407	15
409	17**

* These runs are successive.
** These runs were examined in detail.

Table 6-7 Matrix of t_{ik} for run no. 368

Cycle no. (k)	Index within cycle (i)			
	1	2	. . .	10
1	$t_{1,1}$	$t_{2,1}$	. . .	$t_{10,1}$
2	$t_{1,2}$	$t_{2,2}$	. . .	$t_{10,2}$
.	.	.	.	.
.	.	.	.	.
.	.	.	.	.
12	$t_{1,12}$	$t_{2,12}$	. . .	$t_{10,12}$

(less than 24 hours) are normally distributed, at least for this PIGA unit. With the hypothesis of normality established, the scale factor standard deviation becomes a meaningful measure of dispersion and, used in conjunction with the mean scale factor, completely defines the parameters of the distribution. In addition, the hypothesis of normality provides a necessary condition for applying least squares techniques to successive mean run scale factors.

The consistent departure of cycle bias distributions from normality casts serious doubt on the usefulness of the bias standard deviation statistic and prohibits the use of least squares linear fitting to the successive mean bias values. The reason for the non-normal distribution of bias in this case appears to stem, at least in part, from the bias drift rate.

Statistical Analysis of Scale Factor and Bias Over the Long Term. Justification for fitting data plotted in figures 6-4 and 6-5 with a linear least squares function rests on the following assumptions - see pp526-527 of reference (1):

(a) The value Y, in this case scale factor or bias, is normally distributed for every value of X, in this case elapsed time in days.

(b) The mean value of Y, corresponding to a given value of X, is a linear function of X.

(c) The variance of Y, corresponding to a given value of X, is constant or proportional to a given function of X.

As indicated in the preceding subsection, the bias values are not normally distributed. Therefore, the preceding assumption (a) has been violated, and the least squares curve fit has been rejected as invalid. However, the values of scale factor were normally distributed so that the assumption (a) is justified. To verify compliance with assumption (c), the Bartlett test - see pp290-291 of reference (1) - was applied to determine if the scale factor variances $S^2_{SF(368)}$, $S^2_{SF(372)}$, $S^2_{SF(372)}$, . . . $S^2_{SF(409)}$ are from the same or identical populations. The results of the Bartlett test indicated that the null hypothesis must be rejected at the 0.005 confidence level. The variances cannot be considered equivalent, and a least squares linear fit cannot be justified.

Alternative Tests to the Linear Least Squares Curve Fit. Since the data do not meet the requirements for a linear least squares fit, data evaluation techniques must be chosen that do not depend on such stringent assumptions for validity. In other words, tests that do not presuppose the condition of normality or that do not require constant variance with time must be utilized. The analysis of variance and the runs test are two tests of this type. The analysis of variance does not require the constant variance assumption, but actually utilizes the changing variances as an indication of performance with time. The runs test does not require the normality assumption and, as a type of distribution-free statistic, it provides maximum statistical power with a minimum of necessary assumptions. It allows detection of any nonrandom component in the data.

Analysis of Variance Test – this test, a powerful and widely used statistical technique, permits the isolation of patterns such as trends or periodicities within a group of data samples. While requiring a fairly large amount of computational effort, the procedure is explicit. Constructing a digital computer program to perform the analysis is not difficult. The following application of analysis of variance is a limited application of the general technique; specifically, a two-way classification with only one observation per set.

Table 6-8 Results of Kruskal-Wallis test

Run no.	Input axis orientation	Null hypothesis	Confidence level
368	up	Accept	-
368	down	Accept	-
386	up	Accept	-
386	down	Accept	-
395	up	Accept	-
395	down	Accept	-
409	up	Reject	95%
409	down	Accept	-

Table 6-9 Results of Kolmogorov Smirnov test

Run	Null hypothesis		Confidence level	
	SF	Bias	SF	Bias
368	Accept	Reject		0.05
372	Accept	Accept		-
374	Accept	Accept		-
379	Accept	Reject		0.05
383	Accept	Reject		0.05
386	Accept	Reject		0.01
389	Accept	Accept		-
391	Accept	Reject		0.10
393	Accept	Reject		0.05
395	Accept	Accept		-
397	Accept	Reject		0.01
399	Accept	Reject		0.10
401	Accept	Accept		-
403	Accept	Reject		0.10
405	Accept	Reject		0.01
407	Accept	Reject		0.10
409	Accept	Reject		0.01

t*

Table 6-10 Scale factor matrix for analysis of variance test

Cycle no.	Run number			
	368 (m = 1)	372 (m = 2)	. . .	409 (m = 17)
1	$SF_{368,1}$	$SF_{372,1}$	. . .	$SF_{409,1}$
2	$SF_{368,2}$	$SF_{372,2}$	. . .	$SF_{409,2}$
.	.	.	. . .	.
.	.	.	. . .	.
.	.	.	. . .	.
9	$SF_{368,9}$	$SF_{372,9}$	. . .	$SF_{409,9}$

Table 6-11 Analysis of variance table

	Sum of squares	Degrees of freedom	Mean square
Column means	II - III	16	$\frac{II - III}{16}$
Row means	I - III	8	$\frac{I - III}{8}$
Remainder	IV + III - II - I	16 × 8	$\frac{IV + III - II - I}{16 \times 8}$
Total	IV - III	17 × 9 - 1	

Table 6-12 Testing randomness of grouping in a sequence of alternatives (3)*

n \ m	6	7	8	9	10	11	12	13	14	15	16	17	18	19	20
6	3														
7	4	4													
8	4	4	5												
9	4	5	5	6											
10	5	5	6	6	6										
11	5	5	6	6	7	7									
12	5	6	6	7	7	8	8								
13	5	6	6	7	8	8	9	9							
14	5	6	7	7	8	8	9	10							
15	6	6	7	8	8	9	9	10	10	11					
16	6	6	7	8	8	9	10	10	11	11	11				
17	6	7	7	8	9	9	10	10	11	11	12	12			
18	6	7	8	8	9	10	10	11	11	12	12	13	13		
19	6	7	8	8	9	10	10	11	12	12	13	13	14	14	
20	6	7	8	9	9	10	11	11	12	12	13	13	14	14	15

*Notes (a) value 'm' is always taken as the smaller number of cases
(b) probability of equal or smaller number of runs than that listed is P=0.05

The matrix shown in table 6-10 illustrates the application of this test to the scale factors. The objectives of the test are to determine if the scale factors change over a long-term period of time (row effects), and to determine if the scale factors change over a short term from cycle to cycle (column effects). One distortion of the data introduced by this method of analysis should be noted. Whereas table 6-6 indicates that all runs have at least nine cycles of data, requirements of symmetry necessitate limitation of all runs to only the first nine cycles of computed scale factors. While this limitation means discarding some scale factors in the runs with up to 20 cycles of data, it can be argued that always selecting the first nine samples in any given run does not introduce any systematic error into the analysis. The conclusions given above(pp. 305-6) support this contention for scale factor.

The following quantities are computed from the test matrix given in table 6-10, and an analysis of variance table, table 6-11, is constructed.

$$\left\{ \frac{\sum_{k=1}^{9} (\text{row sum}_k)^2}{\text{No. of columns} = 17} \right\} \quad \underline{\Delta}\ (\text{I}) \qquad \text{(Eq. 6-57)}$$

$$\left\{ \frac{\sum_{m=1}^{17} (\text{column sum}_m)^2}{\text{No. of rows} = 9} \right\} \quad \underline{\Delta}\ (\text{II}) \qquad \text{(Eq. 6-58)}$$

$$\left\{ \frac{\left[\sum_{k=1}^{9} \text{row sum}_k\right]^2}{\text{Product of row and column} = 9 \times 17} \right\} = \left\{ \frac{\left[\sum \text{column sum}_m\right]^2}{\text{Product of row and column} = 9 \times 17} \right\} = \underline{\Delta}\ (\text{III}) \qquad \text{(Eq. 6-59)}$$

$$\sum_{m=1}^{17} \sum_{k=1}^{9} (\text{element of matrix}_{km})^2 \quad \underline{\Delta}\ (\text{IV}) \qquad \text{(Eq. 6-60)}$$

The null hypotheses to be tested are:

$H_{o(c)}$: the column effects are zero; i.e. short-term changes of scale factor do not appear to exist

$H_{o(r)}$: the row effects are zero; i.e. long-term changes of scale factor do not appear to exist

To test these hypotheses, the following F ratios are computed from the quantities given in table 6-11:

$$F_{(\text{column})} = \frac{\left[\frac{\text{II} - \text{III}}{16}\right]}{\left[\frac{\text{IV} + \text{III} - \text{II} - \text{I}}{16 \times 8}\right]} \qquad \text{(Eq. 6-61)}$$

$$F_{(\text{row})} = \frac{\left[\frac{\text{I} - \text{III}}{8}\right]}{\left[\frac{\text{IV} + \text{III} - \text{II} - \text{I}}{16 \times 8}\right]} \qquad \text{(Eq. 6-62)}$$

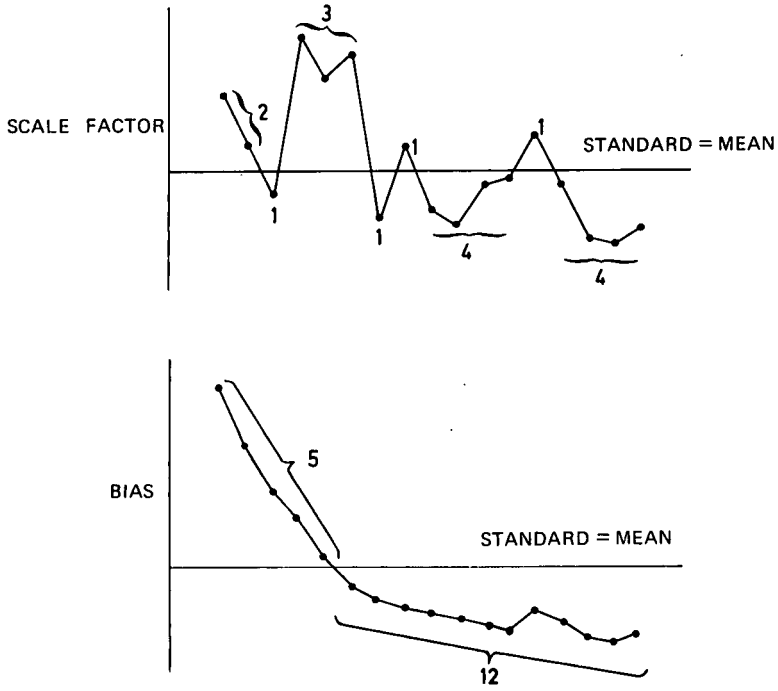

Fig. 6-6 Method one - runs above and below standard

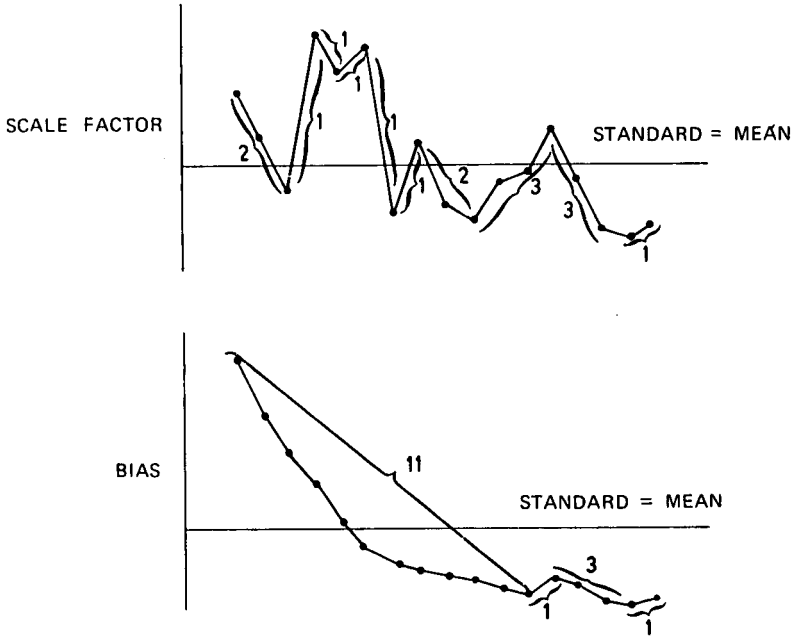

Fig. 6-7 Method two - runs up and down

If the ratio $F_{(column)}$ is greater than the value given in an analysis of variance table (see reference (2) which also contains a helpful description of the analysis of variance technique) at a preselected confidence level, the hypothesis $H_{o(c)}$ is rejected. If the ratio $F_{(row)}$ is greater than the value given in an analysis of variance table at a preselected confidence level, the hypothesis $H_{o(r)}$ is rejected.

Application of this test to the values of both the scale factors and bias yielded the following results:

(a) For the scale factor, both hypotheses were accepted. In other words, the scale factor of the accelerometer is not drifting.

(b) For the bias, both hypotheses were rejected at the confidence level of 0.05. In other words, the bias of the accelerometer is drifting, which further strengthens the conclusions made on pages 306, 308.

Runs Tests – the analysis of variance test described in the previous paragraph requires considerable computational effort. Application of the runs tests described in the following paragraphs can be applied to the values of the mean scale factor and mean bias with much less effort to obtain significant conclusions to the long-term performance of these parameters. Several types of nonparametric runs test are described, and applying more than one to each data sample increases the confidence of the conclusions. The null hypothesis for all the runs tests is that the data has no significant departure from randomness.

(a) Method One - Runs Above and Below the Standard: application of this method is illustrated in figure 6-6. The mean values of the scale factor and acceleration bias for each run are compared to a standard value, which in this case is the 49-day mean values of the scale factor and bias. As shown in figure 6-6, seven values of scale factor are above the standard value and ten values are below. Referring to table 6-12 for values of m = 7 and n = 10, the null hypothesis is rejected if the data contains five or fewer groupings of runs. As indicated in figure 6-6, there are four scale factor groupings of runs above the standard and four groupings below, making a total of eight groupings of runs. Therefore, the hypothesis of randomness for the scale factor is accepted at the 0.05 level of confidence. As also shown in figure 6-6, five values of bias are above the standard value and twelve values are below. Even though the values m = 5 and n = 12 are off table 6-12, the null hypothesis is rejected at the 0.05 level of confidence because the data contains a total of only two groupings of runs, one above and one below the standard, indicating a definite nonrandom component in the bias data.

(b) Method Two - Runs Up and Down: this method is similar to Method One except that the data are grouped in accordance with increasing and decreasing magnitude as shown in figure 6-7. As indicated in this figure, there are nine decreasing values of scale factor and seven increasing values of scale factor. Referring to table 6-12 for values m = 7 and n = 9, the null hypothesis is rejected if the data contains five or fewer groupings of runs. As indicated in figure 6-7, there are five groupings of increasing values of scale factor and five groupings of decreasing values, making a total of ten. Therefore, the hypothesis of randomness of the scale factor is accepted at the 0.05 level of confidence. As also shown in figure 6-7, fourteen values of bias are decreasing in value and two values are increasing. Even though the values of m = 2 and n = 14 are off the table 6-12, the null hypothesis is rejected at the 0.05 level of confidence because the data contains a total of only four groupings of runs, two increasing and two decreasing in value.

(c) Method Three - Longest Run: application of this test requires only the isolation of the longest increasing or decreasing run of data. As indicated in figure 6-8,

the longest scale factor run is an increasing run of three scale factor values. Extrapolating from the abridged table 6-13, the probability of an increasing or decreasing run of five values from a data sample with 17 values is approximately 0.0285. A run of three would be much more probable. For any probability greater than 0.05, the null hypothesis would be accepted. Therefore, a weak conclusion from this test is that the scale factor does not appear to depart significantly from randomness. As with the previous tests, the bias is clearly nonrandom. The longest bias run has eleven values as indicated in figure 6-8, which is completely improbable for data varying randomly. Therefore, the null hypothesis for the bias is rejected.

(d) Method Four - Longest Run Above or Below Standard: this test is based on the longest run of values above or below the standard. As indicated in figure 6-9, the longest scale factor run has four values below the standard. A decision cannot be made on the null hypothesis based on table 6-13. Future extension of this table will eliminate this problem. However, the bias is clearly nonrandom, as indicated by this method.

A summary of the results from these four methods of nonparametric runs tests is given in table 6-14.

Summary. This analysis of the long-term PIGA performance has emphasized the fact that application of data analysis techniques must include a careful investigation of assumptions implicit in these techniques. A misapplied statistic leads to false conclusions. The risk of misapplication of statistical methods resulting in false conclusions can be minimized by taking the following precautions:

(a) The assumptions of validity should be isolated and tested before the statistic is applied.

(b) Techniques that require as few assumptions as possible should be used. Distribution-free statistics are good examples of such techniques.

(c) More than one statistical test should be applied to the same data. Corroboration between two statistics, particularly if they take radically different approaches to the data, provides strong conclusions.

PIGA Tumble Test on Air Bearing Rate Table

During the normal six-point tumble test described on pp. 293ff, the PIGA is subjected to several different components of cross-axis acceleration (component of gravitation normal to the PIGA input axis). Cross-axis acceleration causes the float to wobble as the PIGA rotates about its input axis. As an example, with the PIGA input axis oriented 30 degrees above the horizontal as shown in figure 6-10, the PIGA is sensing 0.5 g along its input axis, and the gravitational component normal to the PIGA, 0.866 g, is applied along the +SRA, +OA, -SRA and -OA of the PIG unit as it rotates about IA. The test described in the following paragraphs provides a means for measuring the effect of cross-axis acceleration on the coefficients of the mathematical model that describes the PIGA performance as the result of a six-point test in a one-g field.

OA Tumble Test. In this OA tumble test, the PIGA IA is mounted and always maintained parallel with the rotating axis of the air bearing rate table (Fig. 6-11). The air bearing rate table is operated in the slave mode of operation where the PIG is servoed to the air bearing rate table and no relative motion exists between the PIG and PIGA (see section 4). A normal six-point test is performed where the PIGA IA

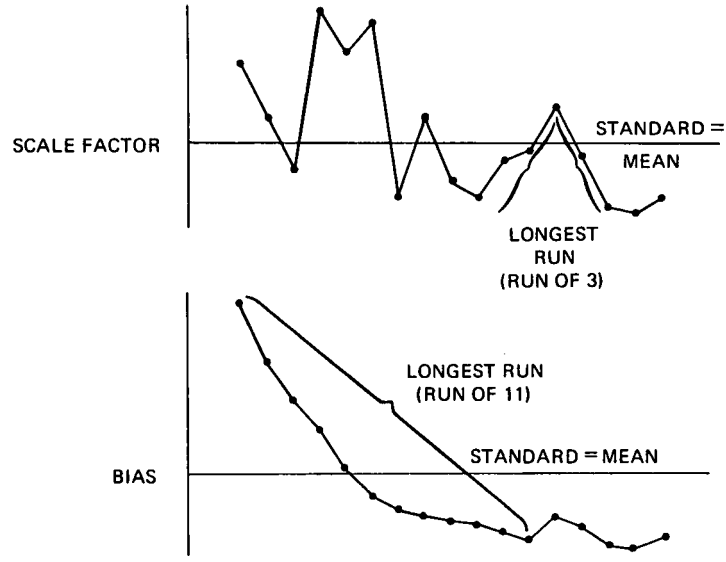

Fig. 6-8 Method three - Longest run

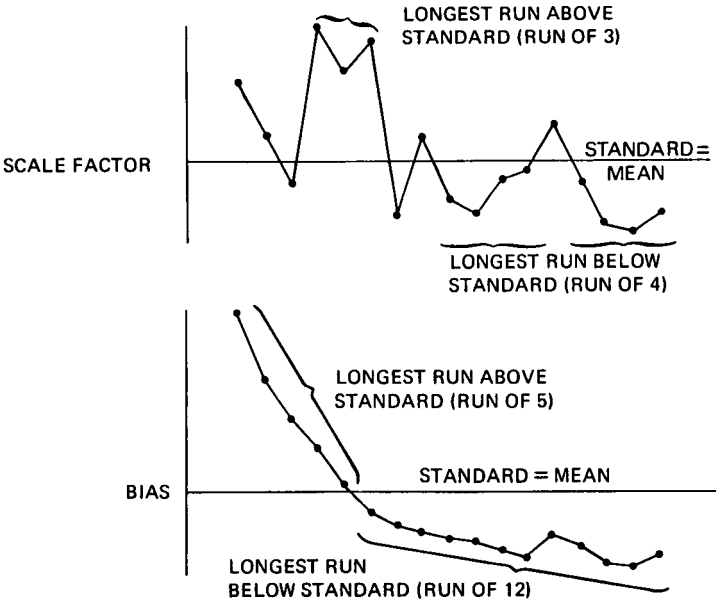

Fig. 6-9 Method four - Longest run above or below standard

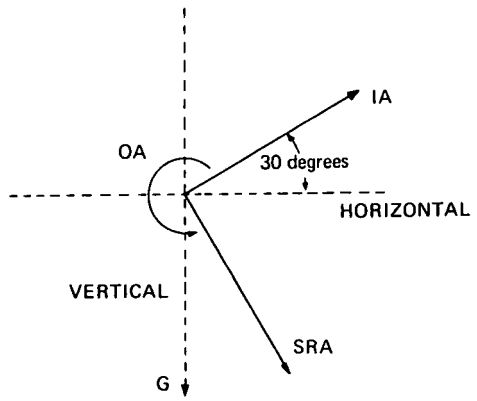

Fig. 6-10 PIG reference axes

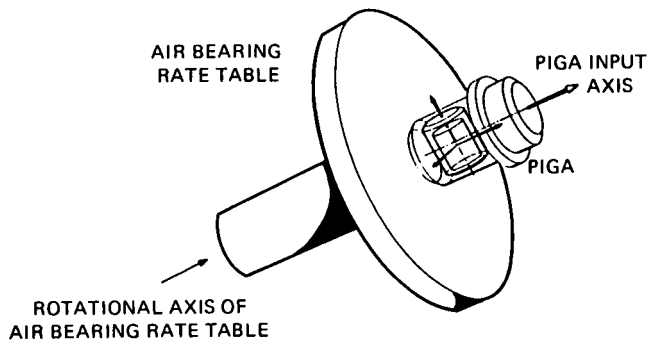

Fig. 6-11 Alignment of axes during OA tumble test

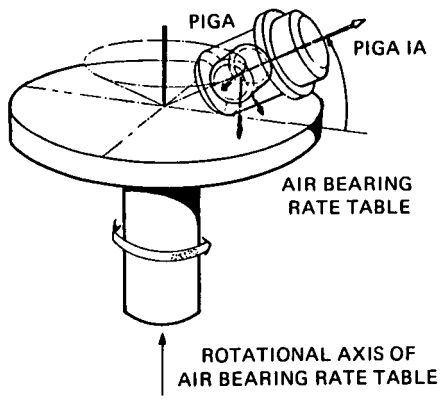

Fig. 6-12 Alignment of axes during OA horizontal test

Table 6-13 Limiting values for lengths of runs up and down in a series of N cases (4)

N	Run	Probability of an equal or greater run
4	4	0.0028
5	4	0.0165
6	4	0.0301
7	4	0.0435
8	4	0.0567
9	5	0.0099
10	5	0.0122
11	5	0.0146
12	5	0.0169
13	5	0.0193
14	5	0.0216
15	5	0.0239
20	5	0.0355
40	6	0.0118
60	6	0.0186
80	6	0.0254
100	6	0.0322
200	7	0.0085
500	7	0.0215
1000	7	0.0428
5000	8	0.0245

Table 6-14 Results of runs tests

Type Test	Scale factor	Bias
Runs above and below standard	Accept	Reject H_o, 0.05
Runs up and down	Accept	Reject H_o, 0.05
Longest run	Accept (weak)	Reject H_o, < 0.0285
Longest run above or below standard	Inconclusive	Reject H_o, < 0.0285

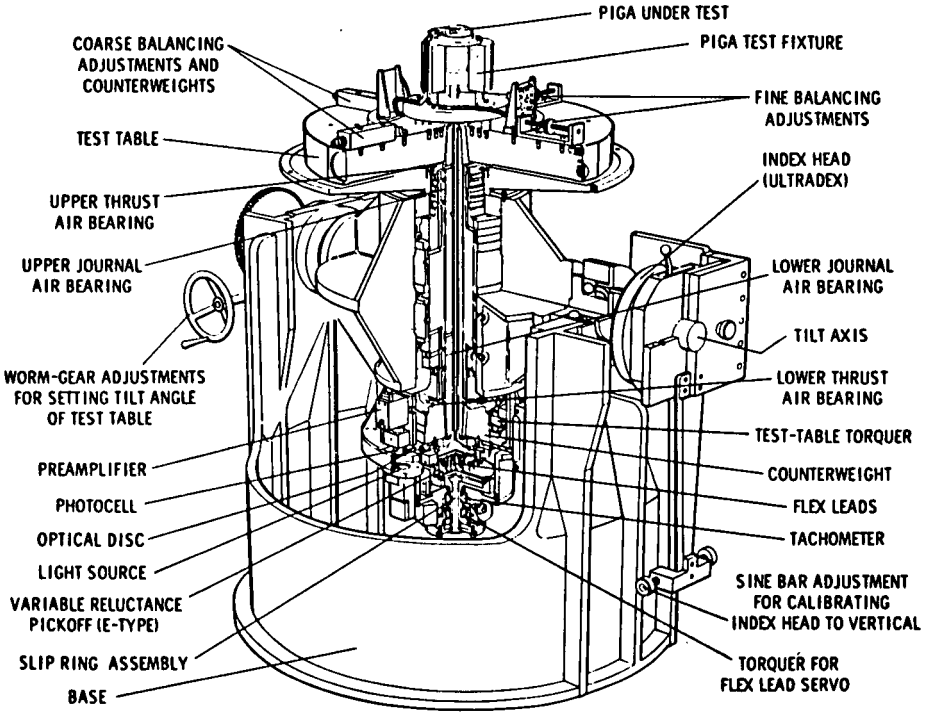

Fig. 6-13 Air bearing rate table

is tumbled in the vertical plane. Measurements are made with the PIGA sensing -1 g, -0.5 g, +0.5 g, +1 g, +0.5 g, and -0.5 g along with repetition of these measurements in the reverse order (mirror image). Under these conditions, the float is subjected to varying torques about SRA and OA due to cross-axis acceleration when the PIGA IA is in the ±0.5 g positions. The data from these measurements are curve fitted as described previously, and the coefficients A_0, A_1, A_2 and B_1 are obtained.

OA Horizontal Test. In this OA horizontal test, the rotating axis of the air bearing rate table is always maintained along the vertical and the PIGA IA is tumbled in the vertical plane (Fig. 6-12). As in the previous test, the air bearing rate table is operated in the slave mode of operation where the PIG is servoed to the air bearing rate table and no relative motion exists between the PIG and PIGA. As in the previous test, a normal six-point test and its mirror image are performed. Under these conditions, the orientation of OA and SRA is always fixed with relation to the cross-acceleration. Therefore, the float does not wobble and is not subjected to varying torques as the result of cross-acceleration. When the PIGA IA is along the vertical (sensing ±1 g), the PIGA input axis is parallel with the rotational axis of the air bearing rate table. Under these conditions

$$W_{(ABRT)} = W_{(PIGA)} = (SF)(g) \qquad \text{(Eq. 6-63)}$$

where

$W_{(ABRT)}$ = angular velocity of air bearing rate table with respect to earth

$W_{(PIGA)}$ = angular velocity of PIGA about IA with respect to inertial space

SF = scale factor of PIGA

g = gravitational constant (acceleration input)

When the PIGA IA is 30 degrees above or below the horizontal (sensing ±0.5 g)

$$W_{(ABRT)}(\sin 30^\circ) = W_{(PIGA)} + (ER)f(\phi,\theta,\ell) = (SF)(g)(\sin 30^\circ) \qquad \text{(Eq. 6-64)}$$

where

ER = earth's rate of rotation

ϕ = angle of rotational axis of air bearing rate table with respect to some arbitrary reference, usually $\phi = 0$ when PIGA IA is east

θ = angle of PIGA IA with respect to horizontal

ℓ = length of pendulous arm

As the PIGA is rotated by the air bearing rate table, the PIGA is subjected to varying components of earth rate along IA and SRA. Therefore, the angular velocity of the air bearing rate table and the angular momentum of the gyro wheel will not be constant during one revolution of the air bearing rate table. However, corrections can be made for these variations. The data from these measurements are curve fitted, and the coefficients are obtained.

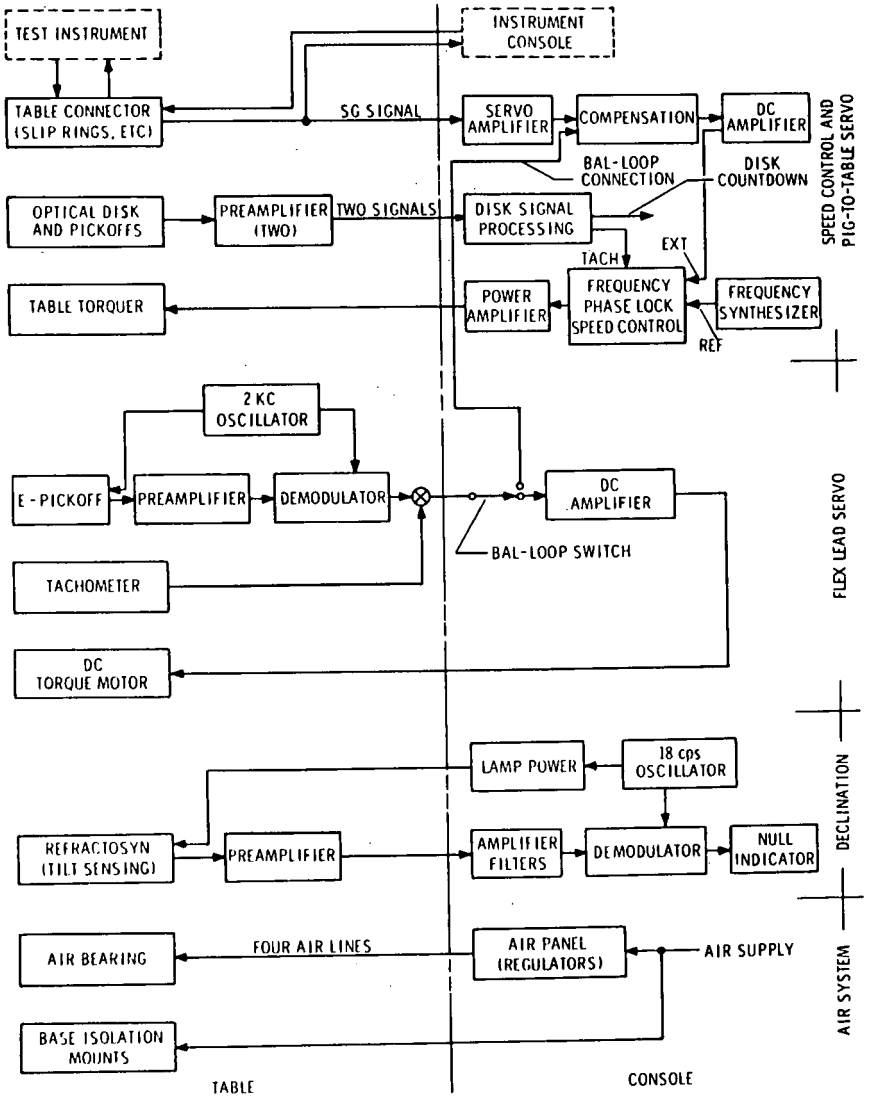

Fig. 6-14 Air bearing rate table systems

Correlation of Coefficients. To determine the effects of cross-axis acceleration, the coefficients determined in the OA tumble test are compared with the coefficients determined in the OA horizontal test. These tests must be repeated a number of times to be certain that the differences between the coefficients obtained from each test are significant and are not the uncertainty of the coefficients.

4. Testing on the Air Bearing Rate Table

The air bearing rate table (Fig. 6-13) is a research and test tool designed and developed by MIT/IL to evaluate performance of the PIGA. The air bearing rate table provides a very stable axis of rotation supported by an essentially frictionless air bearing. The PIGA is mounted on the table with its input axis parallel to the table axis, and one of two modes of operation may be used:

(a) the slave mode where the PIG is servoed to the rotary table and no relative motion exists between the PIG and PIGA

(b) the rate mode where the table is driven at a precise fixed rate and the relative motion between the PIG and PIGA is a stable value.

The slave mode eliminates the friction torques and instabilities of the PIGA drive axis. The rate mode provides different PIG-to-PIGA rates at a fixed level of acceleration input or constant PIG-to-PIGA rates at different levels of acceleration input.

Both modes of operation have been used in tests on the PIGA. Tests in the slave mode of operation permit separation of the PIG performance characteristics from the PIGA performance characteristics, and tests in the rate mode of operation permit precise alignment between the PIG and PIGA input axes.

Description of the Air Bearing Rate Table

As shown in figure 6-13, the air bearing supports a 21-inch diameter table. The bearing assembly is mounted on a tilting trunnion that is supported on a cast aluminium base. This assembly is set on a one-ton concrete slab. The slab, on a pneumatic isolation mount, provides the inertial characteristics to isolate the table from higher frequency earth motion.

The air bearing rate table is comprised of five major function systems (Fig. 6-14):

(a) Air system consisting of the axial and radial air bearings.

(b) Table declination system to tilt the air bearing axis ±180 degrees about the horizontal axis.

(c) Flex-lead servo system to follow the air bearing shaft so that the slip ring will not disturb the air bearing.

(d) Speed control system to provide precise speed control by phase-locking a digital encoder signal to a variable reference frequency.

(e) PIG-to-table servo system that commands the rate of the table to maintain a balance of the PIG signal generator error signal at null. This servo loop is functionally similar to the servo loop that operates the PIGA; however, the time constants of the two loops are vastly different, resulting in significant differences in dynamic characteristics.

Application of the Air Bearing Table for Precise PIG-to-PIGA Input Axis Alignment

The ideal PIGA has an angular velocity that is proportional to the acceleration sensed along the PIGA input axis. Such acceleration may be gravitational, inertial, or a combination of both. If the acceleration vector does not coincide with the PIGA IA, the angular velocity output of the PIGA will be proportional to the dot product of the acceleration vector and the input axis. Thus, an ideal PIGA sensing only a gravitational acceleration will precess with maximum velocity when the input axis is vertical, and have zero precessional velocity when the input axis is horizontal.

In actual practice, the PIGA input axis will not coincide with the PIG IA (Fig. 6-15). Such a misalignment affects the performance of the PIGA as follows:

(a) PIGA precessional velocity will not be constant for a constant input acceleration.

(b) The capacity of the PIGA to sense small accelerations will be limited.

As the PIG precesses, its input axis sweeps out a cone about the PIGA IA. Therefore, the PIG IA bears a varying periodic relationship to the constant input acceleration. Since the precessional rate of the PIG is determined by the component of acceleration sensed, the precessional rate will vary periodically.

The performance equation for the PIGA with PIG-to-PIGA misalignment is separable into two components; one represents a constant average value and the other is periodic and sinusoidal as the PIG precesses through one revolution.

$$W_p = SF[\,\bar{g}\sin\theta + \bar{g}\cos\theta\ \gamma\ \cos(\psi + A)\,] \qquad \text{(Eq. 6-65)}$$

where

W_p = angular velocity of the PIGA

SF = PIGA scale factor

$\bar{g}$ = gravitational vector

θ = angle between the PIGA IA and the horizontal

γ = PIG-to-PIGA IA misalignment

ψ = $\tan^{-1}\dfrac{\text{misalignment in the PIG IA-OA plane}}{\text{misalignment in the PIG IA-SRA plane}}$

A = angular rotation of the PIG about IA, which is zero when the PIG SRA is at its lowest point as the PIG rotates

Equation 6-65 is composed of a constant component and a periodic component. The term $[\,\bar{g}\sin\theta\,]$ is the component of acceleration parallel to the PIGA IA, sometimes designated as a_{in}. Similarly, $[\bar{g}\cos\theta\,]$ is the component of acceleration perpendicular to the PIGA IA, designated $a_{\perp}$.

From equation 6-65, the undesirable consequences of PIG-to-PIGA misalignment on PIGA operation may be illustrated. Equation 6-65 may be rewritten in a completely generalized form:

$A_{(IA\ mis)(IA-OA)}$ = COMPONENT OF IA MISALIGNMENT ABOUT SRA IN IA-OA PLANE

$A_{(IA\ mis)(IA-SRA)}$ = COMPONENT OF IA MISALIGNMENT ABOUT OA IN IA-SRA PLANE

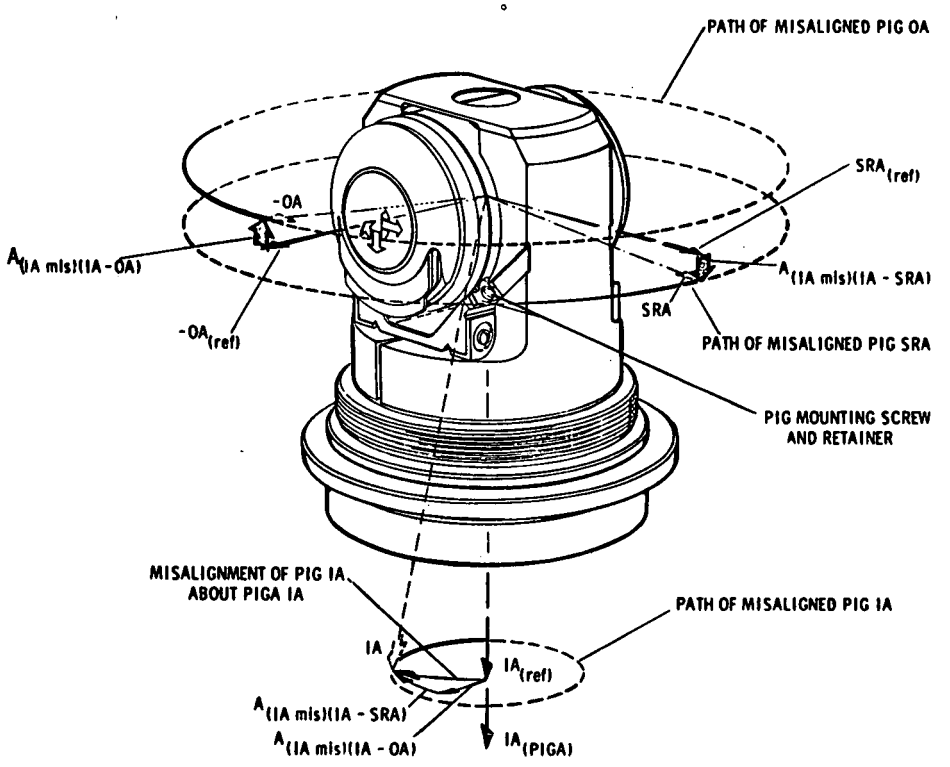

Fig. 6-15 Relationship of PIG and PIGA axes showing a misalignment angle

$$W_p = SF\,[a_{in} + a_{\perp}\ \gamma \cos(\psi + A)] \qquad \text{(Eq. 6-66)}$$

$$= SF\,a_{\perp}\left[\frac{a_{in}}{a_{\perp}} + \gamma \cos(\psi + A)\right] \qquad \text{(Eq. 6-67)}$$

where

a_{in} = component of total acceleration acting on PIG sensed along PIGA IA

$a_{\perp}$ = component of total acceleration perpendicular to PIGA IA (i.e., cross-axis acceleration)

Equation 6-67 takes into account the fact that the PIGA may be subjected to multiple accelerations simultaneously, i.e. both gravitational and inertial accelerations may exist. However, the resultant acceleration acting on the PIGA may always be resolved into a_{in} and $a_{\perp}$. The ratio of $(a_{in}/a_{\perp})$ becomes a limiting factor when the PIGA possesses a PIG-to-PIGA misalignment. Such a misalignment determines a minimum threshold of PIGA operation. From equation 6-67 the average value of W_p may be found as

$$W_p(avg) = SF\,a_{\perp}\sqrt{\left(\frac{a_{in}}{a_{\perp}}\right)^2 - \gamma^2} \qquad \text{(Eq. 6-68)}$$

From equations 6-67 and 6-68, it is apparent that if

$$\left(\frac{a_{in}}{a_{\perp}}\right)^2 \leq \gamma^2 \qquad \text{(Eq. 6-69)}$$

the PIG will not precess. Therefore, this relation, equation 6-69, sets a definite limit to unit operation.

To align the PIG IA to the PIGA IA, the misalignment is first measured by placing the PIGA IA two degrees above the horizontal as shown in figures 6-16 and 6-17. Data points are obtained by timing equal intervals of the PIG as it precesses. One precessional revolution of the PIG is divided into n (where n is usually 35) equal angular segments and timed during each segment. The value of elapsed time for each interval may be converted into a precessional angular velocity from the following expression:

$$W_p = \frac{2\pi}{t_i \times n} \qquad \text{(Eq. 6-70)}$$

where

t_i = elapsed time for portion of revolution

n = number of angular segments per revolution of PIG

The data points W_{p_i} versus position of the PIG SRA is least squares curve fitted by computer (Fig. 6-18).

The ability to measure and therefore to adjust the PIG-to-PIGA alignment angle γ to a minimum is limited by the input axis noise generated by the torque motor

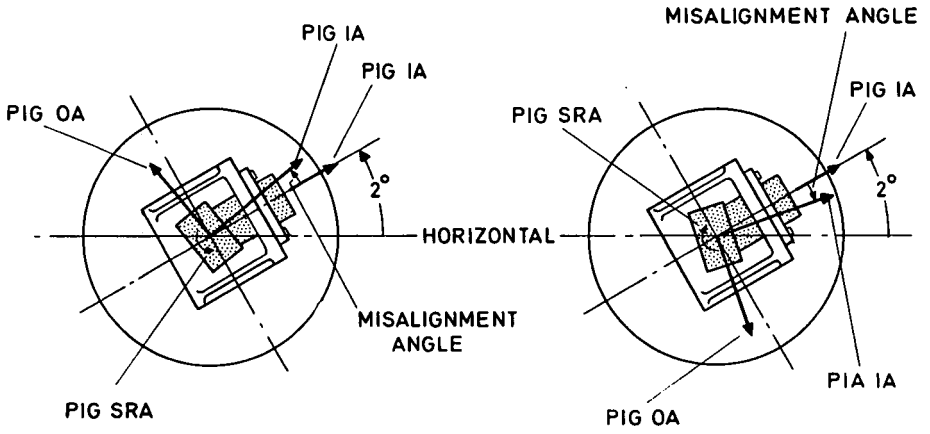

Fig. 6-16 Relation of PIG and PIGA axes showing misalignment of PIG IA and PIGA IA about SRA in IA-OA plane

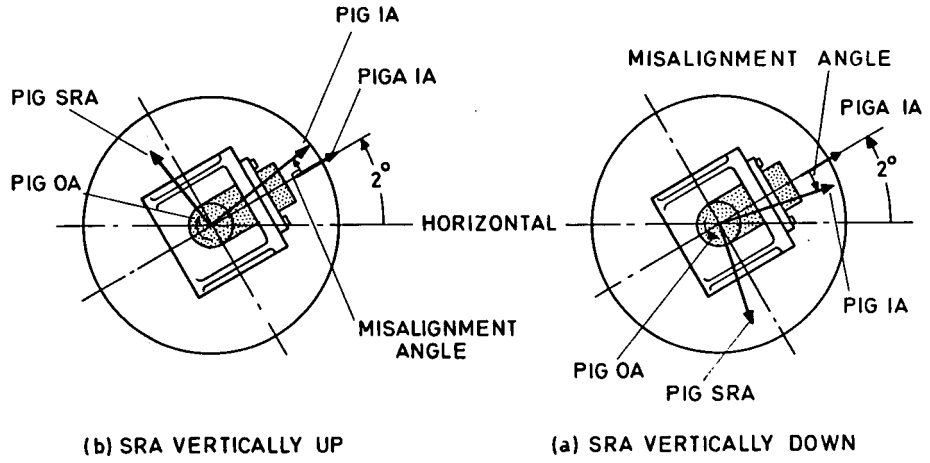

Fig. 6-17 Relation of PIG and PIGA axes showing misalignment of PIG IA and PIGA IA about OA in IA-SRA plane

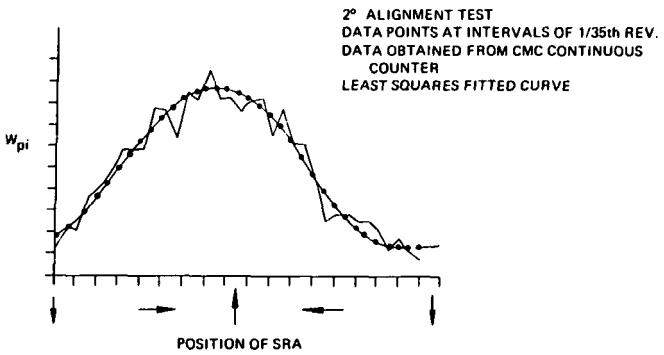

Fig. 6-18 Curve fit from a miniature components group program

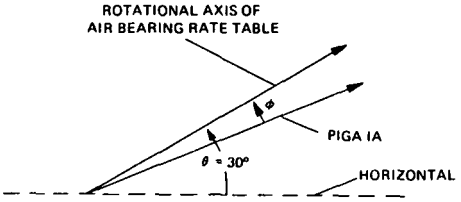

Fig. 6-19 Misalignment angle between PIGA IA and rotational axis of air bearing rate table

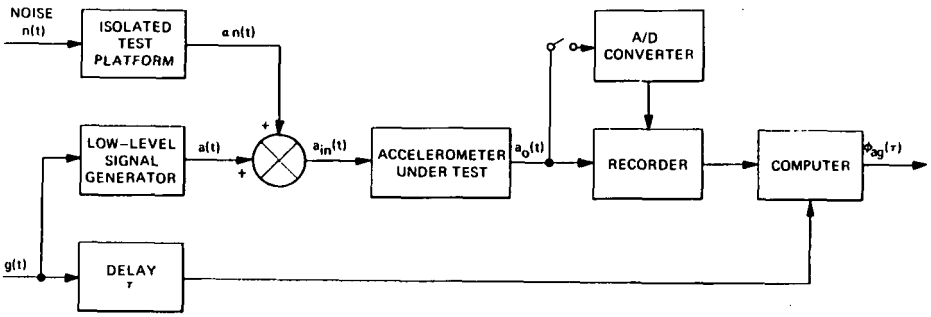

Fig. 6-20 Block diagram of total system required to evaluate ultra-low level accelerometers

cogging, the tooth-to-tooth encoder errors, and the duplex bearing imperfections. A measure of the uncertainty in γ caused by this noise is the rms of the curve fit residuals expressed in seconds of arc. Thus, to reduce the PIG-to-PIGA alignment masked in the noise, the noise must be eliminated. To minimize the noise, the air bearing table is used with its near perfect air bearing, d. c. torque motor and multi-line optical readout, corresponding to the duplex pair, torque motor and digital gear encoder of the PIGA.

The PIG-to-PIGA alignment procedure utilizing the air bearing rate table (Fig. 6-13) is accomplished by first aligning the PIGA IA to the rotational axis of the air bearing rate table. To align the PIGA IA to the rotational axis of the air bearing rate table, the rotational axis of the air bearing rate table is oriented at an angle of 30 degrees above the horizontal, and the PIGA is operated in the PIGA mode. The misalignment angle ϕ can be determined in magnitude and direction by taking integral revolution PIGA data with the air bearing rate table oriented at positions in four quadrants about its rotational axis. As an example, if the misalignment angle is only in the plane of the paper as shown in figure 6-19, the PIGA will precess at an average rate proportional to g sin $(\theta - \phi)$. When the air bearing rate table is rotated 90 degrees about its rotational axis from the position shown in figure 6-19, the PIGA will precess at an average rate proportional to g sin θ. When the air bearing rate table is rotated to a position 180 degrees from the position shown in figure 6-19, the PIGA will precess at an average rate of g sin $(\theta + \phi)$. Tests have indicated that the misalignment angle ϕ can be made extremely small by adjusting differential screws that control the angle between the surface of the PIGA mounting flange and the rotational axis of the air bearing rate table. To align the PIG IA to the rotational axis of the air bearing rate table, the rotational axis of the air bearing rate table is oriented at an angle of two degrees above the horizontal (Figs. 6-16 and 6-17), and the PIGA is operated in the slave mode. The misalignment angle is measured by the previously described PIG IA to PIGA IA alignment procedure, except that under these conditions the PIGA is slaved to the air bearing rate table and the misalignment angle can be measured with considerably greater certainty. The misalignment angle is reduced by adjusting the mounting hardware of the PIG to the PIGA. At the completion of these alignment adjustments, the PIG IA is aligned with the PIGA IA with considerably less uncertainty because both have been aligned with the rotational axis of the air bearing rate table.

Conclusions

Based on the results from testing the PIGA in the slave and PIGA modes on the air bearing rate table, the following conclusions can be drawn:

(a) The PIGA uncertainty versus level of acceleration input is constant from 0. 02 g to one g based on integral revolution data.

(b) When operating the PIG with an air-bearing rate table, the high inertia input axis (slave mode) decreases the PIG uncertainty by an order of magnitude compared to PIGA data. The PIGA input axis drive assembly is the major contributor to PIGA uncertainty.

(c) The PIGA uncertainty does not increase with decreasing PIG-to-PIGA rate, but remains relatively constant. The PIGA input axis bearing assembly does not further degrade the data at low PIG-to-PIGA rates.

(d) The air bearing rate table may be used effectively as a tool to perform diagnostic PIGA testing.

(e) Through the use of the air bearing rate table, the angle between the PIGA IA and the PIG IA may be made an order of magnitude smaller than by means of conventional methods.

5. Testing at Low Levels of Acceleration Input

Testing and calibrating accelerometers at low levels of acceleration arises from the related need to design and develop accelerometers with markedly increased sensitivity for such applications as oceanographic and space exploration. Accelerometers that can sense inputs as low as 10^{-9}g can be used to: (a) control the thrust of electric engines, (b) detect underground nuclear explosions, (c) map the ocean floor, (d) provide for a self-contained vehicle-borne range tracking measurement system.

Testing accelerometers at low levels of acceleration requires a determination of the response of the accelerometer under test due to a known input in the presence of noise. Since the magnitude of environmental noise at a relatively quiet test site is approximately 10^{-4}g over the frequency range of 0 to 10 cps, constant or time varying acceleration inputs below 10^{-4}g become buried in the noise. Frequencies above 10 cps can be attenuated by passive filtering. Signals imbedded in noise demand a technique to extract them. Signal recovery techniques, namely the methods of autocorrelation and cross-correlation, can be utilized to determine the response of an accelerometer to signals smaller than noise. The method considered to separate the output signal from the noise by correlation techniques requires a periodic input signal to the accelerometer. The extraction of a signal from noise is limited, however, by present day general purpose computing facilities, which can handle signal-to-noise ratios in the order of 10^{-2}. Hence, to accomplish signal recovery to levels of 10^{-9}g, the noise level must be reduced to 10^{-7}g. An isolated test platform that uses closed-loop control systems to minimize the translational motion and angular motion of the test platform can reduce the noise to the levels required. The degree of isolation provided by the test platform is dependent on the sensitivity of the platform sensors themselves. Accordingly, the sensing elements must possess an adequate sensitivity to translational accelerations of 10^{-7}g and to angular motions of 10^{-7} rad.

Solutions to the problem of noise do not of themselves enable the user to test ultra-low level accelerometers. Consider a hypothetical situation in which the environment is noise-free. Although there no longer would be a need for the sophisticated approaches to reduce the noise, the problem of verifying that the accelerometer under test is capable of sensing an input of 10^{-9}g remains. Its solution requires the generation of a precisely known input at a level of 10^{-9}g to the accelerometer under test. Concomitant with the requirement of generating a known input is the requirement of developing a method for measuring it.

In summary, the determination of the response of an accelerometer at a level of 10^{-9}g imposes stringent requirements on signal recovery, noise isolation, and generation and measurement of a known acceleration input. Signal recovery from noise requires statistical techniques employing the most advanced computing facilities; noise isolation requires an isolated test platform that reduces the noise level to 10^{-7}g; acceleration generation and measurement requires the capacity to accurately generate a known input to levels of 10^{-9}g.

The proposed system for testing accelerometers at ultra-low acceleration levels is described in this section. The necessary instrumentation is composed of (a) an isolated test platform, (b) an ultra-low level signal generator, (c) a signal recovery system. Figure 6-20 shows a block diagram of the total system.

Isolated Test Platform

In the testing of accelerometers at low levels of acceleration, an isolated test platform is required to minimize the undesirable inputs (noise) to the accelerometer. The noise level input to an accelerometer under test must be reduced to the level where statistical filtering techniques become practical for extracting the output signal from the random noise present at the accelerometer output. Statistical filtering is the more effective means for extracting the output signal at the low frequencies involved. However, extracting output signals buried deeper in noise than 40 db places stringent requirements on the computing facilities. An isolated test platform is required to reduce the noise level to within 10^{-7}g to accomplish signal recovery to levels of 10^{-9}g.

The isolated test platform must be designed to isolate the accelerometer from as many as possible of the following terrestrial and cultural disturbances: (a) earthquake waves, (b) earth tides, (c) microseismic waves, (d) earth tremors and local earth disturbances, (e) wandering of earth's poles, (f) precession of earth's polar axis, (g) change in speed of earth's rotation, (h) thermal distortion of buildings, (i) subsidence of buildings in soft clay, (j) acoustic noise, (k) stray radio frequencies, (l) temperature, humidity, barometric pressure and dust particles, (m) cultural noise - traffic, etc.

These disturbances can be divided generally into low frequency sources, which are arbitrarily set at frequencies less than one cps, and high frequency sources, which are arbitrarily set at frequencies higher than one cps.

Earthquakes at great distances may exhibit waves through the earth's interior of ground amplitudes over 0.0004 inch with time periods of approximately five seconds per cycle and surface waves of ground amplitudes of 0.40 inch with time periods of approximately 20 seconds per cycle. Much greater amplitudes occur nearer the source of the earthquake.

Earth tides have periods of approximately 12 hours, and their corresponding temporal variations in gravity are approximately a few parts in 10^{-7}g, depending on location. The sensitivity of gravimeters for observing these variations is of the order of fractions of 10^{-9}g.

Microseismic waves, or microseisms, are minute waves that continually move through the entire surface of the earth and correlate with meteorological storms and ocean waves. The most prominent and important microseisms have periods of four to seven seconds and amplitudes ranging from 0.0004 to 0.001 inch. There are other microseisms of much shorter periods and smaller amplitudes.

Earth tremors and local earth disturbances consist of local disturbances such as highway traffic, railroad traffic, building machinery, construction, loading of adjacent soil by construction, changes in ground water level and movement of personnel in the vicinity of the test area. Usually these disturbances are of a relatively high frequency (time periods less than 0.5 second) and are of short duration. As an example, a man weighing about 100 kilograms and moving about at a distance of approximately one meter from the accelerometer will cause a disturbing input in the order of 10^{-9}g.

The wandering of the earth's poles at irregular intervals within a plot less than 100 feet square results in small but measurable variations in latitude.

The precession of the earth's axis is very slow, requiring approximately 26 000 years for the earth's axis to complete a circle. This precession is equivalent to approximately 50.2 seconds of arc per year.

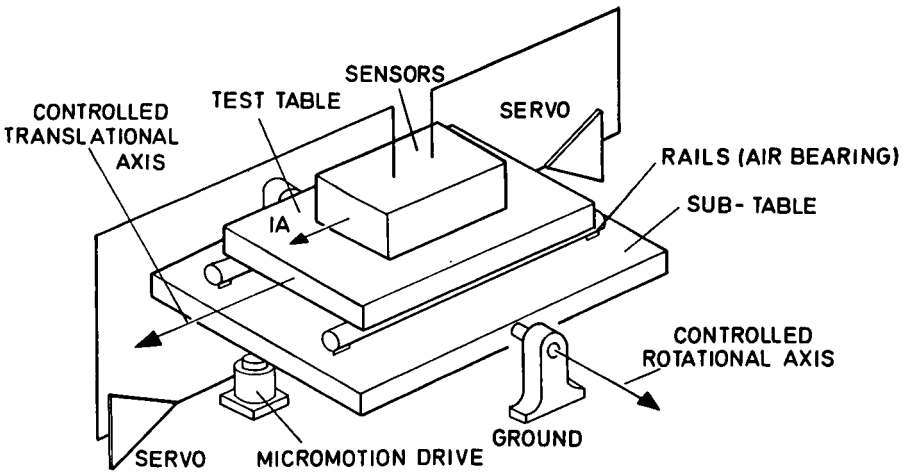

Fig. 6-21 Translational and rotational servomechanisms for the isolated test platform

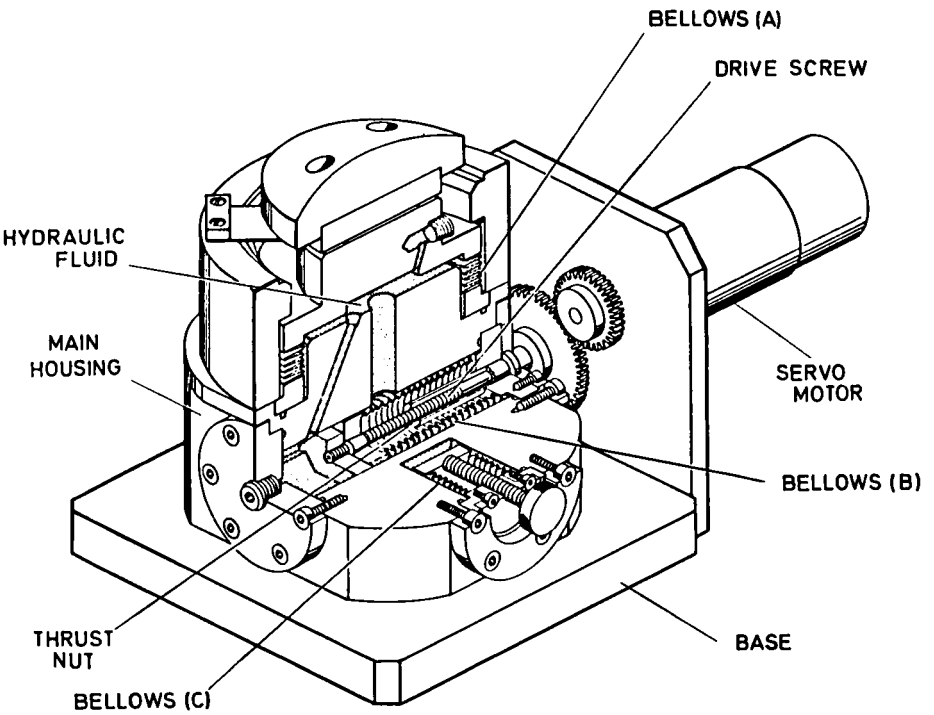

Fig. 6-22 Micromotion drive unit

The speed of the rotation of the earth has varied over the years. The change in the length of day corresponds to the speed of the earth's rotation and appears to vary in a very irregular manner.

The thermal distortion of buildings due to solar radiation varies with the building dimensions, materials of construction, and the character of the foundation. As an example, in a one-story reinforced concrete building, daily measurements of a concrete pillar which penetrated about 15 feet from the ground level into clay indicated day-to-day variations attributed to temperature changes. The maximum tilt angle was 22 seconds of arc. In addition to the day-to-day variations, a peak-to-peak change in the tilt angle of approximately 90 seconds of arc existed between summer and fall.

A thick layer of soft clay is the least desirable type of underlying soil for the foundation of a building. In an improperly designed building foundation, the weight of the structure on the clay causes a gradual subsidence of the building, which may continue indefinitely.

The modern addition to acoustic noise is the sonic boom. The effect on the ground from aircraft in level flight at Mach 1.2 and 10 000 feet is a wave of suddenly compressed air, a shock wave, with a pressure jump of approximately seven pounds per square foot.

Shielding from radio frequencies and from the effects of temperature, humidity, barometric pressure and dust particles can be eliminated or filtered to acceptable levels by proper construction of test housings.

One method of isolating an accelerometer from these disturbances is to locate the test platform on a massive structure in a suitably shielded building at a relatively isolated and quiet locale. The massive structure would have only a limited response to the random forces received by contact with the earth. In addition, the massive structure can be supported by material that will further isolate the test platform from the earth. This approach can be made increasingly effective with progressively larger and costlier structures. This method is a passive mechanical filtering system that is directly subject to each element of disturbance, i.e. if any part of the massive structure changes for any reason, the platform will change its orientation accordingly. At acceleration levels below 10^{-7}g, this mechanical filtering system becomes impractical and difficult to move if a more selective locale is required.

MIT/IL is currently developing an isolated platform through the use of closed-loop servomechanisms (Fig. 6-21). The isolated test platform consists of a two-axis servomechanism for translational stabilization of the test platform and a two-axis servomechanism for roll stabilization of the test platform. The two-axis servomechanism for translational stabilization is a closed-loop control system that isolates the accelerometer under test from horizontal seismic disturbances. Horizontal accelerations caused by ground motion and other sources are held to a minimum by the servo system, which consists of a wide-band translational acceleration sensing unit (TASU), a servo amplifier, a servo motor and a micromotion drive unit. The micromotion drive unit (Fig. 6-22) is a highly refined screw-driven hydraulic jack that is powered by the servomotor. The micromotion drive provides precise control of a small motion with minimum backlash, is small in size and has a large load-carrying capacity. The degree of isolation provided to the test platform is dependent on the degree to which the servomechanism can maintain acceleration of the test platform at a null value. This places the burden of performance on the TASU used to sense the platform motion. Therefore, the TASU must possess an adequate sensitivity to accelerations of 10^{-7}g. The air-bearing torque tester, a recent development by the Electromagnetic Section of

MIT/IL, and the analog torque-to-balance pendulum developed by the Miniature Components Group of MIT/IL are being considered as the TASU. To illustrate the sensitivity required, consider a typical pendulosity of 40 gm-cm(20 gram mass with a 2 centimeter eccentricity) employed as a pendulum on the test platform. A horizontal acceleration, normal to the eccentric arm, of 10^{-7}g, will produce a torque of 3.92×10^{-3} dyne-cm. Therefore, a device is required that can measure this magnitude of torque. The air-bearing torque tester has measured torques of this magnitude and can be applied and utilized in the proposed isolated platform. The analog torque-to-balance pendulum presently is capable of sensing accelerations of 10^{-6}g and, if refined, will be improved to 10^{-7}g.

The two-axis servomechanism for roll stabilization is a closed-loop system that isolates the accelerometer under test from long-period ground-tilt disturbances about the horizontal east-west and north-south axes. Angular motion of the platform (tilt) caused by ground motion and other sources is held to a minimum by the servo system which consists of a tilt-angle transducer, servo amplifier, servo motor and micro-motion drive unit. Assuming that translational stabilization is controlled to within 10^{-7}g, roll stabilization of the isolated test platform to at least 10^{-7} rad is necessary for the overall system to have an isolation capability of 10^{-7}g to both translational and rotational motion. The tilt-angle transducer developed by Dr. Kurt Lion of American Science and Engineering Company is a completely transistorized state-of-the-art device capable of measuring angular displacements of 0.02 arc-seconds (10^{-7} rad). Stabilization of the platform in both rotation and translation must have at least this degree of isolation capability to recover signals of 10^{-9}g from noise.

Generation of Low-Level Acceleration Test Signals

The development of an ultra-low level acceleration generator is required to provide a precisely known small acceleration test input for the purpose of calibration and threshold determination. Numerous ways of generating a known acceleration may be considered, such as: (a) tilting of test platform, (b) simple harmonic motion, (c) gravitational attraction, (d) centrifugal acceleration, (e) Coriolis acceleration, (f) electromagnetic radiation pressure, (g) acoustic radiation pressure.

Regardless of the method used, the generated acceleration must be periodic in order to use the proposed correlation techniques to recover the signal from the noise.

Tilting of Test Platform. In the method of tilting the test platform, a component of gravity on the weight of the sensitive mass of the accelerometer is used as the input to the accelerometer. The use of a tilt table or a bending beam both fall into the category of the tilt method. For the tilt table, the input axis of the accelerometer is moved through the necessary angle by rotating the table. The variation in the gravitational component sensed by the accelerometer is determined by measuring the angle traversed. The bending beam applies a periodic input by placing the accelerometer on the end of a beam supported on both ends and deflecting the beam by varying the force applied at the beam's center. For a variation in input acceleration of 10^{-9}g, the input axis of an accelerometer, using the tilt table, must be rotated through an angle of 10^{-9} radians, which is equal to 2.06×10^{-4} arc-sec. High angular resolution is an obvious necessity for the tilt table method, as well as the bending beam method, which essentially translates displacement (beam deflection) to angle. However, to circumvent the need for high angular resolution, the beam, for example, can be calibrated by applying sufficient force at the center to enable measurement of the deflection. The magnitude of the applied force is varied in discrete steps and the deflection measured for each corresponding applied force until the threshold of measuring the deflection is reached. From this,

a calibration chart can be obtained and extrapolated to lower levels provided certain conditions are met, e.g. Young's modulus remains constant. In both methods, the constancy of gravity to nine significant places is assumed at one g input levels. However, this is not true. It can be shown that the variation in the gravitational field due to the presence and relative motion of the heavenly bodies (sun, moon, etc.) is in the order of 10^{-7}g. Therefore, the use of these methods would require detailed knowledge of the variations in gravity.

Simple Harmonic Motion. In the method of simple harmonic motion, an input signal is generated by forcing the entire accelerometer to undergo small periodic translation oscillations in the direction of its input axis. The maximum amplitude of input signal obtained is determined by the maximum translational displacement, frequency of oscillation and manner of oscillation - i.e. sinusoidal or otherwise. Assuming sinusoidal oscillation, the maximum input signal is related to the maximum translation displacement and frequency of oscillation in the following manner.

$$x = x_{(max)} \sin \omega t \qquad \text{(Eq. 6-71)}$$

$$\dot{x} = \omega x_{(max)} \cos \omega t \qquad \text{(Eq. 6-72)}$$

$$\ddot{x} = -\omega^2 x_{(max)} \sin \omega t \qquad \text{(Eq. 6-73)}$$

$$\ddot{x}_{(max)} = 4\pi^2 f^2 x_{(max)} \qquad \text{(Eq. 6-74)}$$

The maximum translation is inversely related to the frequency squared. When the frequency becomes too high for a given desired resolution power, the maximum translation becomes too small to be measured. As an example, if the desired resolution is 10^{-8}g (4×10^{-6} in/sec^2) and if the desired translational frequency of oscillation is 10 cps, the maximum translation is

$$x_{(max)} = \frac{4 \times 10^{-6}}{4\pi^2 (10)^2} \qquad \text{(Eq. 6-75)}$$

$$= 10^{-9} \text{ inches}$$

On the other hand, when frequencies become low, translational displacements become measurable and, in this case, difficulties are encountered in insuring that only translation exists since small rotations introduce relatively large components of gravity, such undesired inputs being of exactly the signal generation frequency and therefore indistinguishable. As an example, if the desired resolution is 10^{-8}g (4×10^{-6} in/sec^2) and if the desired frequency of oscillation is 0.01 cps, the maximum translation is

$$x_{(max)} = \frac{4 \times 10^{-6}}{4\pi^2 (0.01)^2} \qquad \text{(Eq. 6-76)}$$

$$= 10^{-3} \text{ inches}$$

From this it can be seen that at very low frequencies (less than 1 cps), the measurement of displacement for 10^{-8}g is not extremely difficult. However, at high frequencies, measurement of displacement for 10^{-8}g becomes very difficult.

To circumvent the problem of measuring a very small displacement at the high

frequency end of the operating spectrum (10 cps), displacement magnification can be realized by applying the principle of action and reaction (Newton's first law). The idea basically consists of a very small mass (m_1) initially located adjacent to a much larger mass (m_2) that contains the accelerometer at its center of mass, and where the small mass is forced to move along an axis coincident with the input axis of the accelerometer by an ideally massless contrivance connecting m_1 and m_2. Measurement of the time-varying distance between the large and small masses together with the application of Newton's laws of acceleration and reaction forces determine the time-varying acceleration of the large mass, which is the acceleration sensed by the accelerometer. The measurement of very small displacement associated with accelerations of 10^{-9}g can be realized from the measurement of a much larger displacement as seen from the following:

$$F_i = 0 \qquad \text{(Eq. 6-77)}$$

$$m_1 x_1 - m_2 x_2 = 0 \qquad \text{(Eq. 6-78)}$$

where

m_1 = small mass

m_2 = large mass

x_1 = displacement of small mass

x_2 = displacement of large mass

For a displacement of the small mass of 10^{-5} inch, and a mass ratio, m_1/m_2, of 10^{-3}, the displacement of the large mass is

$$x_2 = (10^{-3})\ (10^{-5}) \qquad \text{(Eq. 6-79)}$$

$$= 10^{-8} \text{ inch peak-to-peak}$$

Using equation 6-74

$$\ddot{x}_{2(max)} = 4\pi^2(1/T)^2\, x_{2(max)} \qquad \text{(Eq. 6-80)}$$

Using sinusoidal motion and a time period of one second, the acceleration input to the accelerometer is

$$x_2 = \frac{4\pi^2(10^{-8})}{2(12)(32.2)} \qquad \text{(Eq. 6-81)}$$

$$= 5 \times 10^{-10}\text{g (peak)}$$

Gravitational Attraction. In the gravitational attraction method of generating a low-level acceleration input signal, the gravitational attraction between two masses is used as a means of generating an acceleration input to an accelerometer under test. In accordance with Newton's law of gravitation

$$F = G\ \frac{m_1 m_2}{r^2} \qquad \text{(Eq. 6-82)}$$

where

r = distance between two masses, m_1 and m_2

G = universal gravitational constant

If the magnitude or the direction of the distance between the two masses, r, is changed, the force will change. If a mass, m, is initially aligned with the accelerometer input axis (Fig. 6-23) at a distance, r, from the accelerometer seismic mass, m_s, and if the mass, m, is caused to rotate about the accelerometer in a circular path at a constant rate, ω, the force sensed by the accelerometer seismic mass will vary sinusoidally as

$$f_{IA} = \frac{F}{m_s} \cos \omega t \qquad \text{(Eq. 6-83)}$$

Substituting equation 6-82 into equation 6-83

$$f_{IA} = \frac{Gm}{r^2} \cos \omega t \qquad \text{(Eq. 6-84)}$$

The mass required to provide a maximum force along the input axis of 10^{-9}g at a distance of 100 cm is

$$10^{-9}(980) = \frac{(6.6)(10^{-8})m}{100^2} \qquad \text{(Eq. 6-85)}$$

$$m = \frac{1}{7} \times 10^6 \text{ gm}$$

A mass of this size is very difficult to obtain. If the distance, r, is decreased, the mass can be made smaller. Along with this difficulty of obtaining the required mass at a practical distance, the center of the accelerometer seismic mass is difficult to determine for accurate determination of the distance, r. In addition, the gravitational constant is known accurately to only six decimal places. These same uncertainties arise when the magnitude instead of the direction of the distance, r, is varied sinusoidally about some mean value. However, this method appears to be quite useful at acceleration levels less than 10^{-9}g.

Centrifugal Acceleration. In the method of centrifugal acceleration, the acceleration input is generated by aligning the accelerometer input axis along the radius of a test table that is rotating at a constant speed. The location of the accelerometer along the radius is movable from point P along the test table diameter to an equivalent point P on the opposite side of the test table center (Fig. 6-24).

When the radial location of the accelerometer is changed or modulated in this manner, a change occurs in the centrifugal force applied to the accelerometer. The angular rate of the earth and the angular rate of the table, ω, are assumed to be constant so that no acceleration is due to these angular rotations. The velocity at point P is

$$\bar{V}_P = p_i \bar{r} = p_o \bar{r} + \bar{\omega}_{IO} \times \bar{r} \qquad \text{(Eq. 6-86)}$$

where

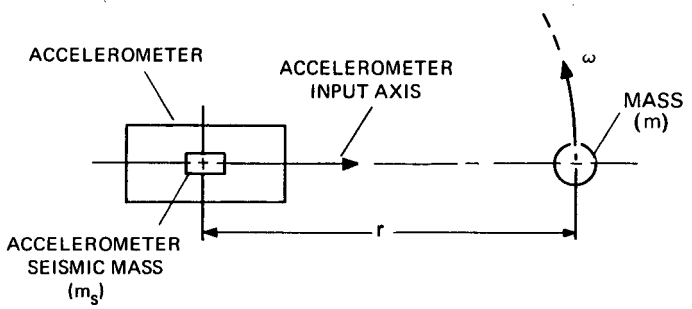

Fig. 6-23 Simplified line schematic of the gravitational attraction method for generating a low-level acceleration input signal

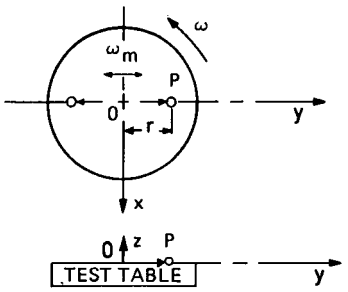

Fig. 6-24 Simplified line schematic of the centrifugal acceleration method for generating a low-level acceleration input signal

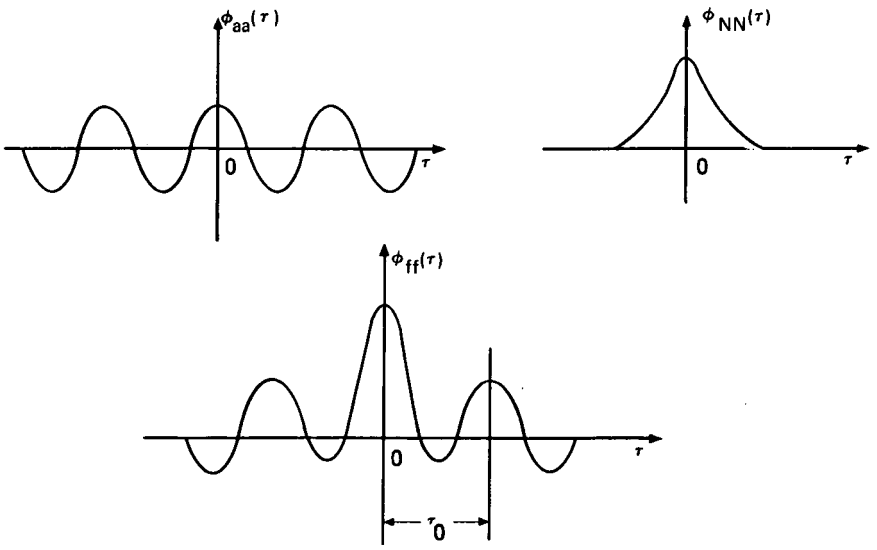

Fig. 6-25 Graphical representation of autocorrelation functions

$\bar{V}_P$ = velocity at point P

$p_i = \left[\frac{d}{dt}\right]_I$ = time rate of change with respect to inertial frame

$p_o = \left[\frac{d}{dt}\right]_0$ = time rate of change with respect to test table frame

$\bar{\omega}_{IO}$ = angular rate of test table with respect to inertial frame

The acceleration at point P is

$$\bar{a}_P = p_i \bar{V}_P = p_o \bar{V}_P + \bar{\omega}_{IO} \times \bar{V}_P \qquad \text{(Eq. 6-87)}$$

Substituting equation 6-86 into equation 6-87

$$\bar{a}_P = p_o^2 \bar{r} + 2\bar{\omega}_{IO} \times p_o \bar{r} + \bar{\omega}_{IO} \times \bar{\omega}_{IO} \times \bar{r} \qquad \text{(Eq. 6-88)}$$

Assuming sinusoidal motion, the radial location of the accelerometer, r, as the accelerometer moves along the test table diameter is

$$r(t) = R \cos \omega_m t \qquad \text{(Eq. 6-89)}$$

where

R = maximum value of r

ω_m = angular frequency of modulation of the accelerometer position along the test table diameter

The radius vector is

$$\bar{r}(t) = \bar{j} R \cos \omega_m t \qquad \text{(Eq. 6-90)}$$

$$p_o \bar{r} = -\bar{j} \omega_m R \sin \omega_m t \qquad \text{(Eq. 6-91)}$$

$$p_o^2 \bar{r} = -\bar{j} \omega_m^2 R \cos \omega_m t \qquad \text{(Eq. 6-92)}$$

$$\bar{\omega}_{IO} = \bar{k} \omega \qquad \text{(Eq. 6-93)}$$

$$\omega_{IO} \times r = \begin{bmatrix} 0 & -\omega_z & \omega_y \\ \omega_z & 0 & -\omega_x \\ -\omega_y & \omega_x & 0 \end{bmatrix} \begin{bmatrix} r_x \\ r_y \\ r_z \end{bmatrix} \qquad \text{(Eq. 6-94)}$$

$$= \begin{bmatrix} 0 & -\omega & 0 \\ \omega & 0 & 0 \\ 0 & 0 & 0 \end{bmatrix} \begin{bmatrix} 0 \\ R\cos\omega_m t \\ 0 \end{bmatrix} \qquad \text{(Eq. 6-95)}$$

$$= \bar{i}\,\omega R\cos\omega_m t \qquad \text{(Eq. 6-96)}$$

$$\omega_{I0} \times \omega_{I0} \times r = \begin{bmatrix} 0 & -\omega & 0 \\ \omega & 0 & 0 \\ 0 & 0 & 0 \end{bmatrix} \begin{bmatrix} -\omega R\cos\omega_m t \\ 0 \\ 0 \end{bmatrix} \qquad \text{(Eq. 6-97)}$$

$$= -\bar{j}\,\omega^2 R\cos\omega_m t \qquad \text{(Eq. 6-98)}$$

$$\omega_{I0} \times p_o r = \begin{bmatrix} 0 & -\omega & 0 \\ \omega & 0 & 0 \\ 0 & 0 & 0 \end{bmatrix} \begin{bmatrix} 0 \\ -\omega R\sin\omega_m t \\ 0 \end{bmatrix} \qquad \text{(Eq. 6-99)}$$

$$= \bar{i}\,\omega^2 R\sin\omega_m t \qquad \text{(Eq. 6-100)}$$

Substituting equations 6-92, 6-98 and 6-100 into equations 6-88, the acceleration applied to the accelerometer is

$$a_p = -j\omega_m{}^2 R\cos\omega_m t - j\omega^2 R\cos\omega_m t$$

$$+ i\,2\omega^2 R\sin\omega_m t \qquad \text{(Eq. 6-101)}$$

As given in equation 6-101, two components of acceleration exist along the accelerometer input axis; one is due to simple harmonic motion and one is due to centrifugal acceleration.

Coriolis Acceleration. The term $2\omega^2 R\sin\omega_m t$ in equation 6-101, the Coriolis acceleration, is at right angles to the centrifugal component. If the accelerometer input axis is oriented perpendicular to the radius of the test table, the accelerometer will sense the Coriolis component.

Data Analysis - Recovery of Signal from Noise

In the testing of accelerometers at the low levels of acceleration under consideration, the indicated acceleration signal at the output of the accelerometer as a result of a known acceleration input is considerably smaller than the noise level. Consequently, to recover the accelerometer output signal from the high noise level, autocorrelation and cross-correlation techniques will be utilized. Separation of the output signal from the noise by autocorrelation and cross-correlation techniques requires a periodic input signal to the accelerometer. The test or calibrating signal will be made periodic in such a way as to differ in essential character from the larger but principally random noise accelerations also entering the accelerometer under test. This difference in character permits extracting the periodic response of the accelerometer due to the input test signal from its random output response due to the noise by an averaging process. The process is basically to correlate the accelerometer output with a reference signal (cross-correlation) or with itself (autocorrelation). Accordingly, there is generated a cross-correlation or an autocorrelation function, which reveals the periodic component with the same frequency as the reference signal.

In the detection of a periodic signal from noise by autocorrelation, the accelerometer output may be considered as

$$f(t) = a(t) + N(t) \qquad \text{(Eq. 6-102)}$$

where

$a(t)$ = output acceleration due to a forced input

$N(t)$ = output noise

The definition of autocorrelation is

$$\phi_{ff}(\tau) = \lim_{T \to \infty} \frac{1}{2T} \int_{-t}^{t} f(t)\, f(t+\tau)\, dt \qquad \text{(Eq. 6-103)}$$

The autocorrelation function is the expected value of the product of $f(t)$ and $f(t+\tau)$ as

$$\phi_{ff}(\tau) = \overline{f(t)\, f(t+\tau)} \qquad \text{(Eq. 6-104)}$$

Substituting equation 6-102 into equation 6-104

$$\phi_{ff}(\tau) = \overline{[a(t) + N(t)]\,[a(t+\tau) + N(t+\tau)]} \qquad \text{(Eq. 6-105)}$$

If $f(t)$ and $f(t+\tau)$ are statistically independent, the expectation of the sum equals the sum of the expectation. Statistical independence is obtained if the time delay, τ, is made large enough. Then

$$\phi_{ff}(\tau) = \phi_{aa}(\tau) + \phi_{NN}(\tau) + \phi_{aN}(\tau) + \phi_{Na}(\tau) \qquad \text{(Eq. 6-106)}$$

If $a(t)$ or $N(t)$ has a zero mean value

$$\phi_{aN}(\tau) = \phi_{Na} = 0 \qquad \text{(Eq. 6-107)}$$

Then

$$\phi_{ff}(\tau) = \phi_{aa}(\tau) + \phi_{NN}(\tau) \qquad \text{(Eq. 6-108)}$$

As τ becomes very large, $\phi_{NN}(\tau)$ theoretically tends to zero if the mean value of N(t) is zero or tends to the square of the mean if the mean value of N(t) is non-zero. In a practical case, $\phi_{NN}(\tau)$ tends to zero or to the square of the mean after some time, τ_o. Assuming that the mean value of N(t) is zero, the plot of $\phi_{ff}(\tau)$ is shown in figure 6-25. As indicated in this figure, the technique of autocorrelation will determine whether or not a periodic component exists in the function f(t). Autocorrelation provides a gain in the signal-to-noise ratio at the accelerometer output as

$$\frac{S_o}{N_o} = 10 \log_{10} \frac{n}{1 + 4p_i^2 + 2p_o^4} \qquad \text{(Eq. 6-109)}$$

where

$\frac{S_o}{N_o}$ = output signal-to-noise ratio (db)

n = number of samples (data points)

p_i = input noise-to-signal ratio

The gain in the signal-to-noise ratio as given in equation 6-109 applies when the autocorrelation function is determined by the process of random sampling. This retains the statistical property of the function with respect to time when the function has a periodic component. The effective gain in the signal-to-noise ratio can be obtained by computing the autocorrelation function using a digital computer. The operations will be multiplication, summation and division as given by

$$\phi_{11}(T_k) = \frac{1}{n + 1} \sum_{m=1}^{n-m} y_n y_{(n + m)} \qquad \text{(Eq. 6-110)}$$

The amount of gain in the signal-to-noise ratio will be dependent on the number of data points, y_n and $y_{(n + m)}$ (see equation 6-109). Using the autocorrelation technique, no theoretical limit exists on the gain in the signal-to-noise ratio; however, some practical limits exist. For example, the time required to extract the signal from the noise increases as the signal-to-noise ratio increases. In addition, the noise level of any analog-to-digital conversion system imposes a practical limitation. As the signal-to-noise ratio decreases, the requirements of the computer become more stringent.

Detection of a periodic signal from noise by cross-correlation is also possible. One advantage of cross-correlation over autocorrelation is that a fewer number of data points are required to obtain the same gain in the signal-to-noise ratio. This will save computation time of the correlation function, thereby extracting the signal from the noise more quickly.

Since computation is performed using the statistical properties of the noise, the characteristics of the noise at a given test site must be known. Using the isolated

test platform, the expected signal-to-noise ratio will be in the order of 10^{-7} which is within the capabilities of present data instrumentation.

6. Vibration Tests

The precision accelerometer must perform satisfactorily under time-varying linear and vibratory acceleration inputs. One of the objectives in performance testing is to determine at least the first-order nonlinearity of the accelerometer, the coefficient proportional to the square of the acceleration input, a_{in}^2. A second objective is to determine the extent of permanent change, if any, in scale factor and bias due to the accelerations. Some possible means of applying the acceleration inputs are:

(a) Time-limited acceleration generators

1. aircraft in high acceleration maneuvers
2. test rocket flights
3. rocket-propelled sled on tracks
4. shock test machines

(b) Sustained acceleration generators

1. linear and angular vibration test machines
2. centrifuge machines

The accuracy of determining the first-order nonlinearities is proportional to $\int a_{in}^2\, dt$, because a_{in}^2 must be large enough and exist long enough to produce a detectable error in the accelerometer output. Therefore, a basic accuracy limit exists when time-limited acceleration generators are used to determine performance. Figure 6-26 is a comparison of $\int a_{in}^2\, dt$ generated by some examples of time-limited acceleration generators. In contrast, the vibration test machine and the centrifuge machine do not have this basic accuracy limitation. The usefulness of the vibration test machine is described in the following paragraphs, and the usefulness of the centrifuge machine is described in section 7.

Some Expected Effects of Vibration on Accelerometer Performance

Table 6-15 is a list of some of the theoretical errors in indicated acceleration that can be expected when subjecting a nongyroscopic pendulous accelerometer such as the PIPA to vibration inputs. These may be grouped as errors:

(a) due to differences in compliance along the input and pendulum axes of the structure on other support that determines the pendulum pivot point

(b) due to finite torque rebalance loop gain

(c) due to inaccuracies in setting and maintaining the electrical null reference of the error signal generator, which defines the input axis and cross-axis of the accelerometer

(d) due to finite moment of inertia of the pendulous element about the pivot axis.

Errors of the type in the preceding items (b) and (c) occur because the finite angular error causes the component of cross-axis acceleration to produce a torque that must be rebalanced by the servo loop. Since the error angle, e, to the first order is proportional to a_{in}/K_t, a term $(a_\chi a_{in})/K_t$ must exist in the output.

Problems in Vibration Testing the Accelerometer

Digital Readout Under Vibration. Accelerometers that have an analog readout of a_{ind} present no problem under vibration. However, testing accelerometers that have digital readouts does present a problem because the integrated acceleration has a discrete threshold that can be exceeded cyclically at the vibration frequency. This can give rise to a false readout due to the finite hysteresis purposely built into the electronics and to other effects of pulse jitter generated in the electronics. The problem should not exist if the vibratory acceleration is held below the sustained acceleration input because there will never be an instantaneous reversal of a_{ind}. Therefore, with both IA and $a_{vb(pk)} < 1$ directed vertically on a vibration machine, the PIGA error coefficient proportional to $a^2_{in(vb)}$ can be evaluated at low levels. No readout problems exist for errors that are excited only by cross-axis vibration with one g of sustained input acceleration because the instantaneous vibratory input will always be very small.

Extraneous Inputs at the Vibration Facility. As in all testing, measurements are made and signals are monitored to insure that only the desired inputs exist and any unwanted inputs are known and taken into account. The major extraneous environments in testing at a linear vibration facility (electrodynamic) are:

(a) test-fixture structural resonances, providing larger inputs to the accelerometer than expected

(b) angular vibration inputs due to resonances in either the fixture or vibration exciter

(c) angular orientation changes during test

(d) d.c. magnetic fields

Vibration pickoffs are mounted as close as possible to the defined input, and pretest surveys eliminate any unknowns caused by test-fixture structural resonances. Angular vibration inputs are measured by high-frequency autocollimators monitoring a mirror on or very near the accelerometer. If angular oscillations are significant, the frequencies at which they occur are avoided. Similar monitoring is used to verify angular stability of the test platform before, during, and after testing. The magnetic field problem is usually solved by use of thick-walled magnetic shields, demagnetizing coils, and precautions to keep rapid rates of change in the magnetic field from occurring during start-up of the vibration equipment.

Use of Linear Vibration Generator to Determine Frequency Response of Accelerometer

Since the accelerometer is subjected to time-varying inputs, it is important to know and specify the time response of the accelerometer to such inputs. Assuming that the dynamics of the accelerometer servo loop are linear, this time response can be found from the frequency response, using well-known transform methods. The linear vibration machine provides a means of determining the frequency response. A block diagram of this arrangement is shown in figure 6-27. In this example, the

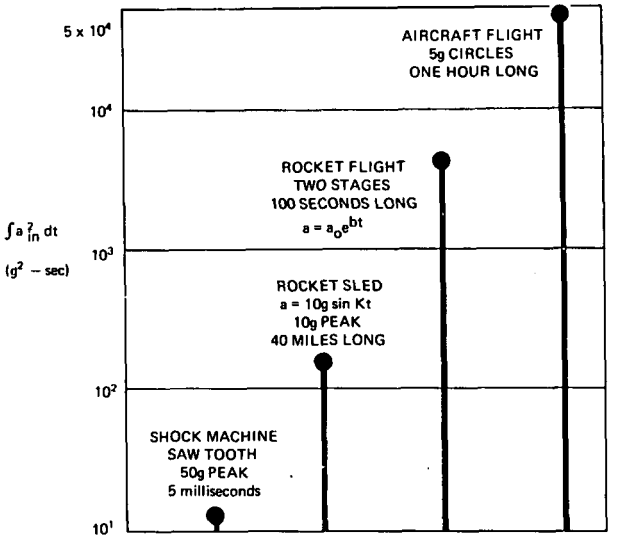

Fig. 6-26 Comparison of $\int a_{in}^2 dt$ generated by some time-limited acceleration generators

Table 6-15 Some theoretical errors in PIPA output due to vibration

Acceleration input	Error in indicated acceleration, $(E)a_{ind}$
1. Combined cross-axis and input linear vibratory acceleration	1. $\frac{a_X a_{in}}{2} \cdot \frac{(K_{pp} - K_{ii})}{P_p}$ mg
2. If inputs are in zero time phase	2. $\frac{a_X a_{in}}{2} \cdot \frac{e_{o(pulse)}}{a_{(pulse)}} \cdot [F_{(servo)}(j\omega)]^2$
3. Cross-axis linear vibration only	3. $\frac{a_X^2}{2} \cdot \frac{P_i}{P_p} \cdot \frac{e_{o(pulse)}}{a_{(pulse)}} \cdot [F_{(servo)}(j\omega)]^2$
4. Combined cross-axis linear vibration and sustained linear input accelerations	4. $\frac{a_X^2(vb)\ a_{in(sus)}}{2} \cdot [F_{(servo)}(j\omega)]^2 \cdot \left\{\left[\frac{e_{o(pulse)}}{a_{(pulse)}}\right]^2 + \left[\frac{K_{pp} - K_{ii}}{P_p}\right]\left[\frac{e_{o(pulse)}}{a_{(pulse)}}\right]\right\}$

Notes: (a) refer to symbols (pp 362-4) for definition of terms
(b) a_X is along pendulum case reference axis only

response of the gyro error signal to $a_{in(vb)}$ is measured under closed-loop conditions. The response of the accelerometer to input accelerations is

$$\frac{a_{ind}}{a_{in(vb)}}(j\omega) = F_{(servo)}(j\omega) = 1 - \frac{K_1 G_1(j\omega)}{P_s} \cdot \frac{e_o}{a_{vb}}(j\omega) \qquad \text{(Eq. 6-111)}$$

$$= K_2 G_2(j\omega) \cdot \frac{H}{P_s} \cdot \frac{e_o}{a_{vb}}(j\omega) \qquad \text{(Eq. 6-112)}$$

The frequency response of one of the two forward-loop components – K_1G_1, the gyro dynamics, or K_2G_2, the electronic amplifier and platform dynamics — must be known to complete the determination. One of these can be measured separately under open-loop conditions.

7. Testing at High Levels of Acceleration Input

As indicated in section 6, the problem of properly evaluating the precision accelerometer under acceleration inputs greater than one gravity is difficult. The rocket-flight itself is inadequate, not only because it is time-limited, but also because the problem of separating accelerometer errors from stable platform gyro errors is difficult (if not impossible). The centrifuge machine is a natural choice for evaluating the nongyroscopic pendulous accelerometer under high acceleration inputs, and the test problems reduce to those of accurately measuring radius change, average speed, and orientation angle of the centrifuge. However, for the gyroscopic pendulous accelerometer, a major problem exists in separating effects due to centrifuge angular velocity from those due to radial acceleration. This problem is both analytical, in that the error model for this environment must be completely determined, and practical, in that the sensitivity of the PIGA to angular orientation change is many times that of the PIPA-type accelerometer.

Two types of tests are considered in this section:

(a) accelerometer input axis parallel with the centrifuge arm

(b) accelerometer input axis perpendicular to the centrifuge arm

Therefore, the major purpose of testing is to determine the deviations in the output of the accelerometer from:

(a) an expected linear variation with the square of the centrifuge angular velocity, $\overline{W}^2_{cf}$

(b) an expected constant output despite the cross-axis acceleration

If the theory or the mathematical model of performance predicts deviations, then the purpose is redefined to determine deviations from the expected output under high acceleration inputs.

Linearity Tests

Linearity tests are performed with the accelerometer input axis, AIA, aligned parallel with the centrifuge radial acceleration, a_{cf} (Fig. 6-28). Under these conditions, the output of a gyroscopic accelerometer such as the PIGA can be stated generally as

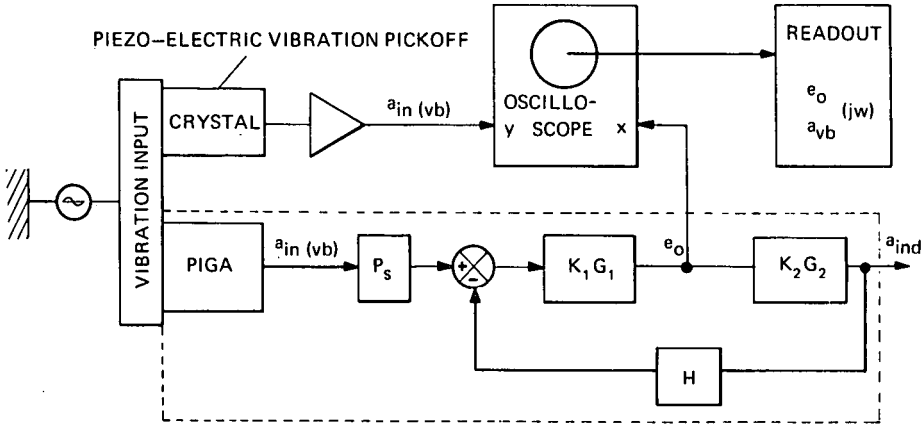

Fig. 6-27 Block diagram showing arrangement for determining frequency response of the accelerometer

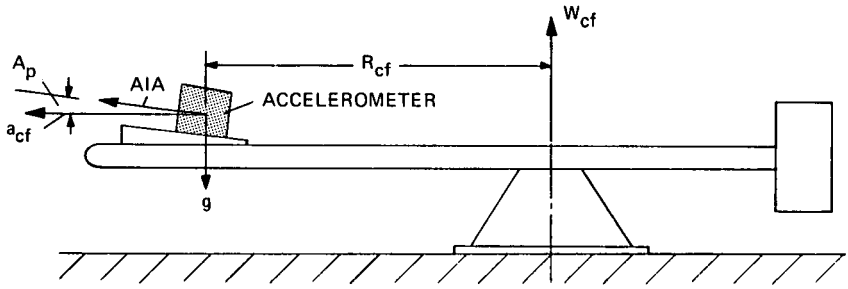

Fig. 6-28 Line schematic of accelerometer input axis aligned parallel with centrifuge radial acceleration

$$a_{ind} = B + W_{cf}^2 (R_{cf}/g)(1 + \Delta R) + [1 \mp (W_{cf}/SF)](A_p + \Delta A) + (E)a_{ind} \qquad \text{(Eq. 6-113)}$$

where

a_{ind} = acceleration indicated by accelerometer

B = accelerometer bias

W_{cf} = centrifuge angular velocity

R_{cf}/g = centrifuge radius per gravity unit at a selected reference g level

ΔR = measured change in centrifuge radius from reference value of R_{cf}

SF = accelerometer scale factor

W_{cf}/SF = additional input to a gyroscopic accelerometer due to the angular velocity existing on the test platform

A_p = initial alignment angle between the accelerometer input axis and the centrifuge radial acceleration axis at the reference level

ΔA = measured change in the alignment angle from the reference value of A_p

$(E)a_{ind}$ = error in indicated acceleration

The object of the linearity tests is to determine the error in indicated acceleration, $(E)a_{ind}$, over a given range of acceleration input. Before proceeding with the linearity tests, preliminary procedures must be performed to determine the initially unknown radius and alignment angle, R_{cf}/g and A_p. The practice at MIT/IL has been to let the accelerometer indicate these two references rather than attempt to locate the accelerometer at a measured radius or attempt alignment with optical instruments. These latter procedures simply add to the number of assumptions that have to be made about the test.

For nongyroscopic accelerometers such as the PIPA, the simplest procedure for determining A_p is to measure a_{ind} for two positions of the centrifuge arm that are 180 degrees apart, and calculate A_p from

$$A_p \approx \frac{a_{ind(0)} + a_{ind(180)}}{2} - B \qquad \text{(Eq. 6-114)}$$

where the accelerometer bias B as well as the accelerometer scale factor have been determined previously in one-gravity tests. This procedure for determining A_p eliminates the effect of any misalignment of the centrifuge with the vertical. The radial reference may be determined by setting the centrifuge speed at a value where

$$a_{ind(ref)} - B - A_p = 1\ g \qquad \text{(Eq. 6-115)}$$

$$= (R_{cf}/g) W_{cf(ref)}^2 \qquad \text{(Eq. 6-116)}$$

and calculating R_{cf}. The assumptions made in the linear tests for the PIPA are:

(a) A_p at standstill equals $A_{p(ref)}$. Optical monitoring is used to verify or correct this assumption.

(b) Nonlinearities in a_{ind} are insignificant at the reference g-level or, if known, are estimated and subtracted from a_{ind}.

(c) The scale factor and bias of the accelerometer remain unchanged from the one-gravity measurement conditions in the tumble tests to the one-gravity measurement conditions on the centrifuge.

(d) The centrifuge instrumentation provides adequate measurement of ΔA.

(e) The centrifuge instrumentation provides adequate measurement of ΔR.

(f) The average $(W_{cf})^2$ = (average W_{cf})^2 over the data time.

For gyroscopic accelerometers such as the PIGA, the alignment angle A_p determines both the component of g and W_{cf} to which the accelerometer responds. Therefore, to determine the references for A_p and R_{cf}/g, the indicated accelerometer output, a_{ind}, is measured for both clockwise and counterclockwise rotation of the centrifuge at a speed where W_{cf} = SF. Under these conditions

$$A_p = \frac{a_{ind(cw)} - a_{ind(ccw)}}{1 + [W_{cf(ref)}/SF]} \qquad \text{(Eq. 6-117)}$$

$$R_{cf}/g = \frac{a_{ind(ccw)} - B}{W^2_{cf(ref)}} \qquad \text{(Eq. 6-118)}$$

The assumptions made in the linear tests for the PIGA are the same as those listed for the PIPA except the first assumption, with the following additional assumptions:

(a) Nonlinearities or other errors in indicated acceleration are identical for clockwise and counterclockwise rotation of the centrifuge.

(b) The alignment angle A_p is the same for both clockwise and counterclockwise rotation of the centrifuge. Optics are used to verify or correct this assumption.

(c) The radial reference R_{cf}/g is the same for both clockwise and counterclockwise rotation of the centrifuge. If not, this is corrected by instrumentation.

Cross-Axis Tests

Cross-axis tests are performed with the accelerometer input axis along the vertical, perpendicular to the centrifuge radial acceleration, a_{cf}. Under these conditions, the alignment angle, A_p, is $\pm \pi/2$. Precise alignment can be made by the procedures just described and rotating the accelerometer 90 degrees. A cube with two well-machined flat surfaces at right angles to each other provides a relatively inexpensive test fixture for this purpose. Since the purpose of this test is to evaluate the small effects of cross-axis acceleration on the accelerometer indicated acceleration, accurate knowledge of the centrifuge radius, R_{cf}, is not necessary unless the alignment angle, A_p, differs greatly from 90 degrees. The expected PIGA indicated acceleration contains the alignment term

$$[g \pm (W_{cf}/SF)] \times 1 \qquad \text{(Eq. 6-119)}$$

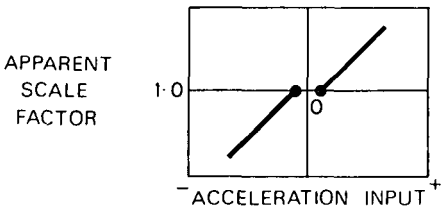

(a) $(E)a_{ind} = C_2 a_{in}^2$

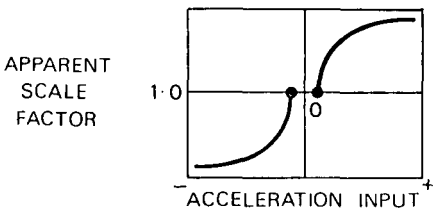

(a) BIAS OR PIPA ALIGNMENT

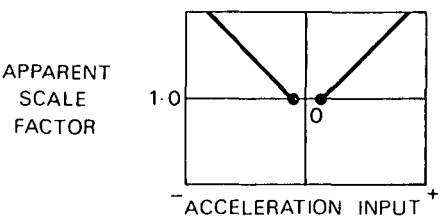

(b) $(E)a_{ind} = C_2^1 a_{in} |a_{in}|$

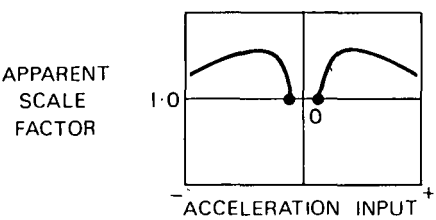

(b) PIGA ALIGNMENT

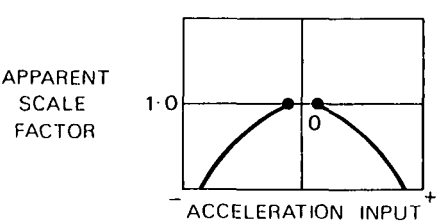

(c) $(E)a_{ind} = C_3 a_{in}^3$

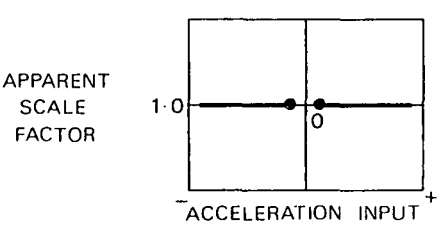

(c) SCALE FACTOR

SCALE FACTOR ERROR CAN BE DETERMINED ONLY BY COMPARISON OF $R_{cf(ind)}$ WITH $R_{cf(meas)}$

Fig. 6-29 Possible error shapes in apparent scale factor due to nonlinearity errors

Fig. 6-30 Possible error shapes in apparent scale factor due to reference determination errors

Therefore, the PIGA rotation can be zero for some centrifuge speeds and directions. The latter are chosen to avoid this condition.

Data Analysis Methods

After determining the initial conditions for the test at some low level of acceleration input, the indicated acceleration, a_{ind}, and the centrifuge angular velocity, W_{cf}, are measured at higher levels of acceleration input along with measurement of the appropriate correction data, ΔR and ΔA. After making measurements, the next step is to process and analyze the data. A number of quite different test procedures have been used in the past by various investigators with equally different success. Success in this application is obtaining a high correlation between measured error coefficients and error coefficients predicted from theory, obtained from known parameters of the accelerometer, and obtained from other tests that exercise a particular error in a manner different from the centrifuge input. The procedures described in this section are recommended because test experiences have resulted in very good correlation and for the following particular reasons:

(a) Preliminary analysis is made so that the expected types of nonlinearity (e.g. square, cubic) and the expected types of errors in the preliminary assumptions (e.g. bias and scale factor) can be recognized readily and so that the unexpected but systematic errors are clearly apparent when they exist.

(b) No prior assumption is made that the accelerometer output is of a general mathematical form such as a power series, and the data is not forced to fit any assumed mathematical model before the preliminary inspection.

(c) Normalizing the data for differences of the centrifuge radius in the two-position test (e.g. $A_p = 0$ and π) or the multiposition test is inherent in the analysis.

(d) The coefficients that involve the centrifuge radius and the alignment angle are derived from accelerometer indications at levels of one g or less where the assumptions are minimized.

The preliminary analysis consists of calculating the quotient called the apparent scale factor as follows:

$$\frac{SF_a}{SF} = \frac{a_{ind} - B - (\text{misalignment effects})}{W_{cf}^2 \, (R_{cf}/g) \, (1 + \Delta R)} \qquad \text{(Eq. 6-120)}$$

This reduces the degree of the equation for indicated acceleration, equation 6-113, by one. When the apparent scale factor is plotted as a function of acceleration input, the shape of the curve will indicate generally the type of error or nonlinearity present (Figs. 6-29 and 6-30). The errors in the assumptions that $SF_{1g} = SF_{cfg}$ and $B_{1g} = B_{cfg}$ do not exist at the reference level because compensating errors occur in R_{cf}/g and A_p. By definition, errors are zero at the reference level.

Following the preliminary procedure of inspecting the apparent scale factor, SF_a, coefficients of an error equation that is justified from physical theory are obtained by standard least-squares methods. The coefficients from this analysis can be refined by iteration, whereby the error in indicated acceleration, $(E)a_{ind}$, based on coefficients from the first analysis are removed from the indicated acceleration, a_{ind}, before performing a second least-squares fit, etc. This procedure is necessary because determinations at the reference g-level are not made for the condition of the centrifuge radial acceleration, a_{cf}, equal to zero.

Expected Errors in Indicated Acceleration

The preceding paragraphs contain a recommended test procedure, an approach to data analysis, and the general form of expected errors in the indicated acceleration when subjecting an accelerometer to centrifuge inputs. Some specific errors expected from a non-gyroscopic accelerometer such as the PIPA are given in table 6-16. The sources of these errors are the same as the sources of the errors when the PIPA is subjected to vibration (see pp. 341-2), e.g. lack of infinite loop gain, anisoelasticity in the suspension, etc.

Some of the specific errors expected from a gyroscopic accelerometer such as the PIGA are given in table 6-17. Similarly, the sources of these errors are the same as the sources of the errors when the PIGA is subjected to vibration. The error designated no. 2 in table 6-17 is due to a rectification caused by the presence of vertical angular velocity on the centrifuge platform. A schematic diagram of a PIGA on a centrifuge with its input axis, AIA, aligned with the centrifuge radial acceleration is shown in figure 6-31. The PIG output axis, OA, is subjected to components of the centrifuge angular velocity, W_{cf}, varying as the sine of the PIGA rotation angle. Therefore, the PIG is subjected to an angular acceleration about OA, resulting in a torque, $I_{OA} \cdot \dot{W}_{OA}$, that varies as W_{cf} times the cosine of the PIGA rotation angle times the rate of change of this angle. This torque and a similarly time-varying component of W_{cf} caused by finite friction of the PIGA rotational axis combine to produce an error. In this instance, the friction torque is assumed to vary linearly with the input acceleration. Derivation of these errors is beyond the scope of this paper. However, the purpose in presenting them is to emphasize that the end point of the precision testing process is to account precisely for what is observed. Therefore, a very complete and thorough analytical investigation of what is expected to be observed should be made prior to the testing operation.

Unexpected Errors in Indicated Acceleration

A point is reached at which systematic but unexplained deviations are seen consistently despite extensive analysis of the dynamic and kinematic conditions and despite careful evaluation tests to verify that the centrifuge instrumentation provides true information. Thermal changes are the most likely deviations that defy analysis. In both the PIGA and the analog-torqued PIPA, the effect of power input changes on the sensitive gyroscopic and pendulous elements causes changes in the indicated acceleration. This effect is eliminated in the pulse-torqued PIPA. During tests on the centrifuge, the input power to the PIGA torquer, the gyro wheel and the thermal-control heaters changes with the input acceleration. One way of determining unexpected errors is to simulate at one g the thermal conditions that are known or expected to occur during centrifuge tests.

Instrumentation of the MIT/IL Centrifuge

The instrumentation of the MIT/IL 32-foot radius precision centrifuge (Fig. 6-33) is described and evaluated in the following paragraphs. This centrifuge has been in operation since 1956 and was upgraded recently to perform precision tests up to 100 g. Further refinements contemplated for this centrifuge and other new features are being incorporated in a high-precision centrifuge for the Air Force Central Inertial Guidance Test Facility (Fig. 6-34). This centrifuge consists of a cylinder with a 50-foot diameter rotating within a stationary cylinder. The heat dissipation and thermal changes at the test area are extremely low compared to the open construction of the MIT/IL centrifuge.

Table 6-16 Some theoretical errors in PIPA output when subjected to centrifuge radial acceleration (*Pivot axis is horizontal)

Acceleration input	Error in indicated acceleration, $(E)a_{ind}$
1. Combined input and cross-axis centrifuge acceleration	1a. $-(1/4)a_{cf}^2 \left[\frac{e_{o(pulse)}}{a_{(pulse)}}\right] \sin 2A_p$ 1b.* $+(1/2)a_{cf}^2 \left[\frac{(K_{pp} - K_{ii})\ mg}{P_p}\right] \sin 2A_p$ 1c. $+(1/2)a_{cf} g \left[\frac{e_{o(pulse)}}{a_{(pulse)}}\right] (\sin A_p)^2$
2. Cross-axis centrifuge acceleration only ($A_p = \pm \pi/2$)	2. $+(1/2)a_{cf}^2 \left\{ (P_i/P_p) + g \left[\frac{e_{o(pulse)}}{a_{(pulse)}}\right] \right\}^2$
3. Centrifuge angular velocity	3.* $+(1/2)\ (\Delta I_p/P_p) W_{cf}^2 \sin 2A_p$

Table 6-17 Some theoretical errors in PIGA output when subjected to centrifuge radial acceleration

Acceleration input	Error in indicated acceleration, $(E)a_{ind}$
1. Centrifugal acceleration ($A_p = 0$)	1. $-a_{cf}^2\ (P_s/H)[(I_i - I_s)(A_s - A_o) + \Delta I_{is}]$
2. Combined centrifugal acceleration and angular velocity	2. $(1/2)a_{cf}^2 W_{cf}^2 (\cos A_p)^3 \left[(K_f I_o)/(K_{lc} P_s) \right]$
3. Cross-axis centrifugal acceleration ($A_p = \pm \pi/2$)	3. $-(1/2)a_{cf}^2 (P_{piga-o}/K_{lc}) \left| G_c^{-1} \left[j\left(\frac{P_s}{H} g \pm W_{cf}\right) \right] \right|$
4. Centrifuge angular velocity ($A_p = \pm \pi/2$)	4. $-[W_{cf}^2/P_s]\ [(I_i - I_s)(A_s - A_o) + \Delta I_{is}]$

Refer to Symbols (pp.362-4) for definition of terms.

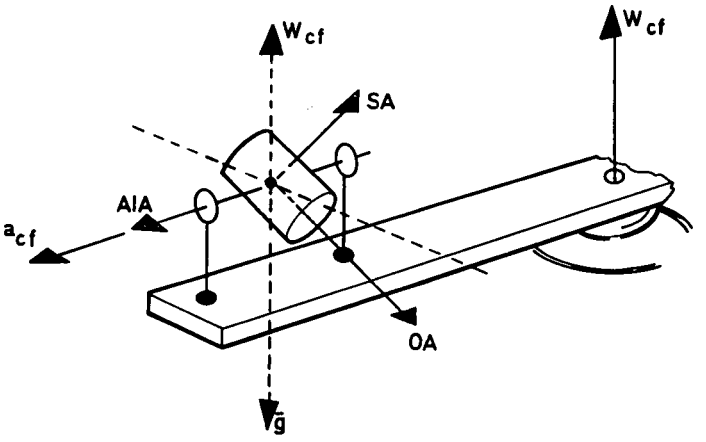

Fig. 6-31 Line schematic of PIGA on centrifuge with its input axis aligned parallel with the centrifuge radial acceleration

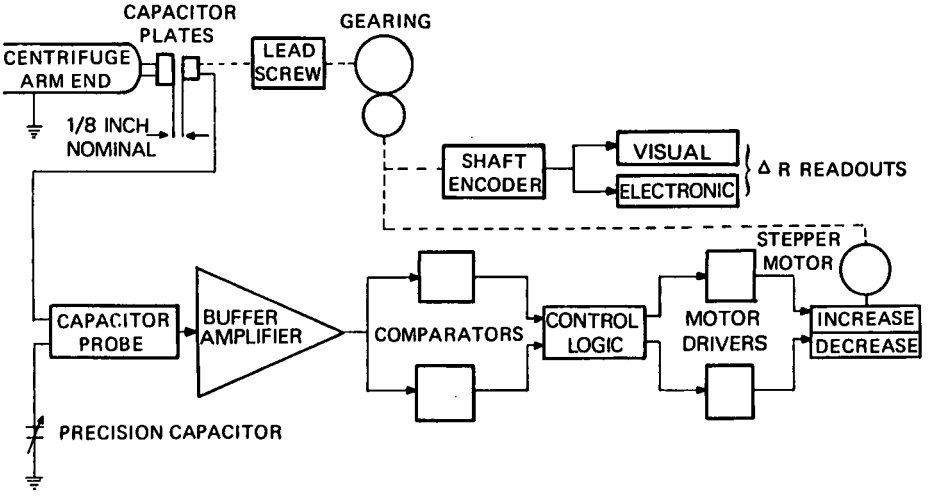

Fig. 6-32 Functional block diagram of centrifuge radius change measurement system

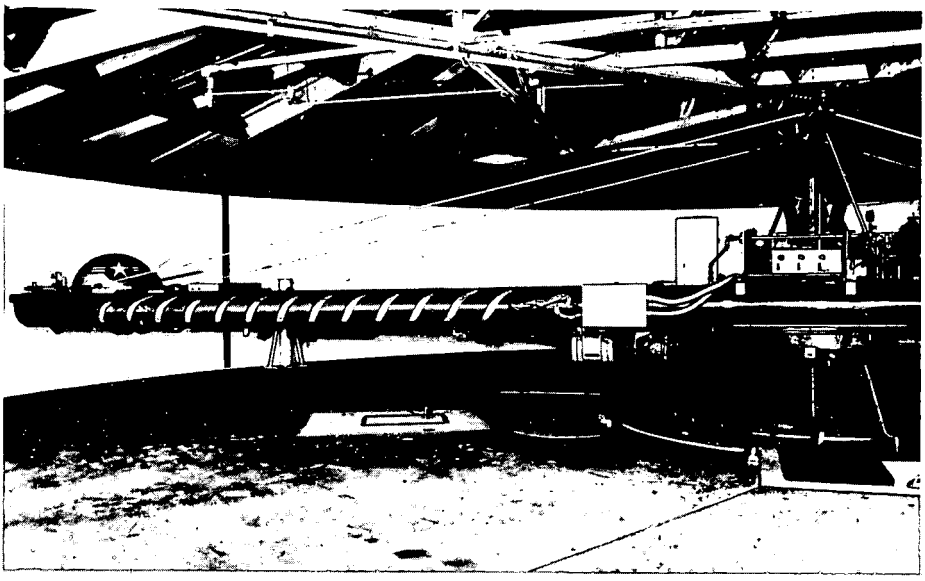

Fig. 6-33 MIT/IL 32-foot precision centrifuge

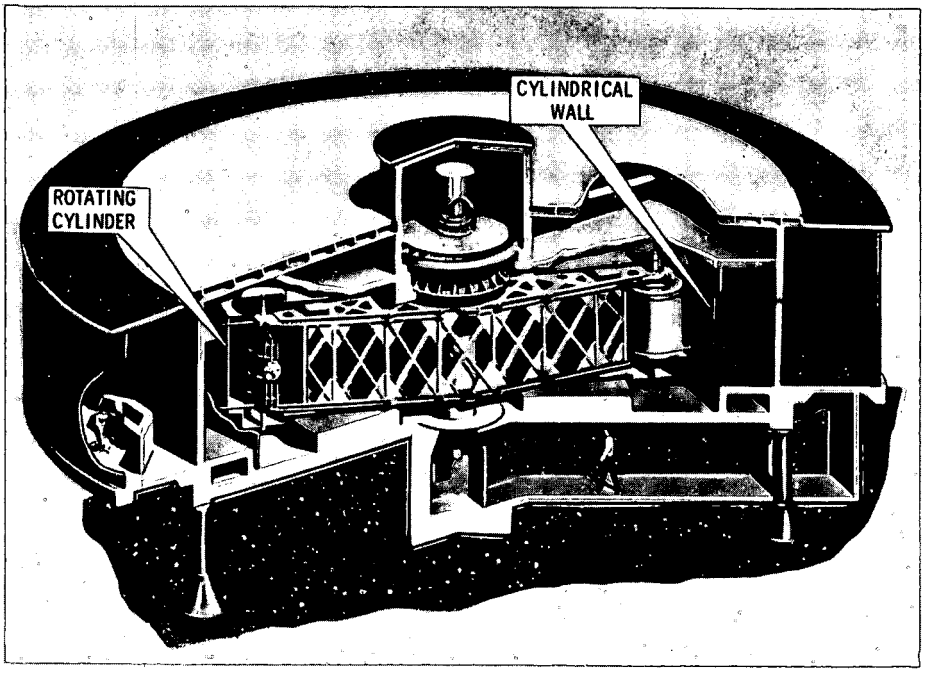

w Fig. 6-34 Air force central inertial guidance test facility

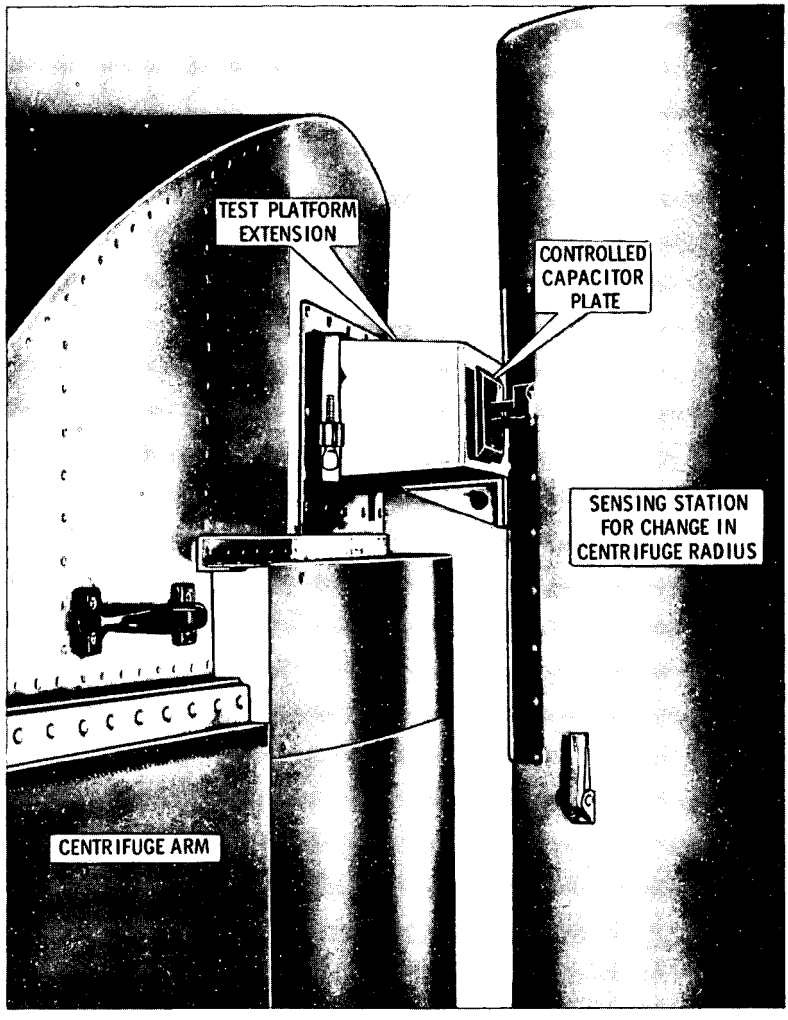

Fig. 6-35 Noncontacting radius monitor

Radius Readout of Centrifuge Arm. In the past, measurement of the change in radius of the centrifuge arm, ΔR, has been made by noting changes in the reading of a micrometer actuating a finger that contacts the end of the centrifuge arm with a known uncertainty. Generally, this method has worked well in the range of 0 to 20 g on the MIT/IL centrifuge and other centrifuges. However, mechanical failures due to impact shock, fatigue and wear gave reason to improve the method from a maintenance and reliability standpoint. In addition, during the upgrading of the MIT/IL centrifuge to 100 g, permanent mechanical sets and more frequent failures occurred in the mechanical fingers at the higher impacting arm velocities and windage. Readout of the radius change on the MIT/IL centrifuge is made from an encoder of a shaft rotation geared to the micrometer rather than from reading a manually-made micrometer setting.

To improve the reliability of radius change measurement over the 0-100 g range, a system has been developed that does not require physical contact with the rotating machine and indicates changes in the length of the centrifuge arm to a possible uncertainty of ± 200 microinch or ± 1/2 ppm of the total length. As in the past, two measurement stations diametrically opposite each other (north and south) are used so that translation of the center of rotation as well as radius changes can be detected. A second pair (east and west) having go/no-go contacts are used also to provide comparative information and to aid reliability. A functional block diagram of the system is shown in figure 6-32. A plate mounted on the end of the centrifuge arm and a second plate mounted on a platform that is radially movable with respect to the measuring station form one leg of a capacitance bridge. A balancing leg consists of an extremely stable fixed capacitor. A signal proportional to the amount of bridge unbalance drives a bi-directional stepping motor to move the second plate so as to maintain balance, keeping its distance from the first plate constant. Thus, any radial motion of the end of the rotating centrifuge arm is duplicated in the stationary measurement station. The stepping motor also serves to quantize this motion, relaxing the requirements on a shaft encoder that converts it to electrical signals for transmission to the control room where they actuate visual readouts and also are available as inputs to data recording equipment. The mechanical contact stations are identical in principal except for the sensing of the change in radius. Figure 6-35 shows the radius measuring system with the centrifuge arm at a position for measurement of the change in radius.

The principal factors that affect the performance of the radius readout are:

(a) sensitivity of capacitance bridge

(b) frequency response of capacitance bridge

(c) null drift of capacitance bridge

(d) minimum required spacing between the capacitor plates

(e) area of capacitor plates

(f) radius of centrifuge arm

(g) change in dielectric of air with pressure and temperature

(h) maximum acceleration of centrifuge

(i) stability of measuring station base with respect to center of rotation

(j) thermal and structural conditions between the measuring point and the reference radius of the test platform

To qualify this radial measurement system, the following two types of tests were made:

(a) pier stability

(b) comparison of the contacting and noncontacting systems

To determine the pier stability, daily comparisons of the radius readout were made for nearly identical conditions of the centrifuge arm. The results of this evaluation are indicated in figure 6-36, which shows a daily record of the contacting type readout at one g after one hour of rotation, stabilizing conditions to some extent. This data indicates that over a period of one month of accelerometer testing, the combined stability of the radius sensor, pier and thermal conditions were such that the arm radius was a constant with ±2 ppm rms. Since the stability of radius readout observed here is the sum of three contributors, and has not been corrected for thermal changes, it can be surely stated that the stability of the station piers is better than 2 ppm.

Figure 6-37 shows the difference between the radius readouts of the contacting and noncontacting types (normalized to the same scale factor) over the range of 0 to 100 g. With the exception of the 100 g point, where a permanent set occurred in the contact-type readout as indicated by post-test data at one g, the discrepancies between measurements by the two methods were:

Peak:	-1.8 ppm at 25 g
RMS:	0.96 ppm
Correlation:	0.99994

Speed Readout of Centrifuge. Precise measurement of average centrifuge speed is required in testing accelerometers. On the MIT/IL centrifuge, the speed is not controlled to an accuracy that permits elimination of speed averaging, nor is such control considered necessary for accelerometers with a digitalized output. The averaging for testing gyroscopic accelerometers such as the PIGA requires that the centrifuge shaft rotation be digitalized to a fine degree due to the requirement that integral PIGA shaft revolutions set the speed-averaging period. This technique eliminates certain dynamic PIGA outputs from the data. Nongyroscopic accelerometers such as the PIPA require only one pulse per revolution for speed averaging. The least increment of centrifuge shaft readout sets the accuracy level for a given speed averaging period or reduces testing time for a given accuracy. A major improvement in the speed readout has been made recently on the MIT/IL centrifuge by applying a frequency multiplier to the shaft rotation pulses as described in the following paragraphs. The result has been to reduce the acceleration error due to speed averaging to 1/10 and the testing time per data point by 1/4 of that which would exist in the absence of the (100×) multiplier.

The speed readout of the centrifuge is initiated by a photocell (Fig. 6-38) generating pulses proportional to the number of interruptions of a light path made by a radially scribed, silver-backed glass disc mounted on the centrifuge shaft. The disc generates 3600 interruptions per revolution to an accuracy of ± 2 arc-seconds. The centrifuge pulses, f_c, are fed to a pulse rate multiplier that reproduces the pulses at 100, 10 and one times the original rate. The outputs originate from a voltage-controlled oscillator producing the 100× rate. Secondary control voltage is applied from a rate logic that generates a voltage proportional to the centrifuge rate. The primary precise control is obtained through the phase-lock loop as follows. The output of the voltage-control oscillator is divided twice by ten. The phase of the resulting 1× rate, f_{co}, is compared to the phase of the incoming centrifuge pulse, and an analog voltage is produced proportional to the phase difference. Phase

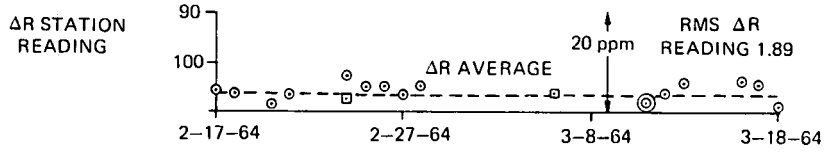

Fig. 6-36 Stability of radius measurement station over 30-day period

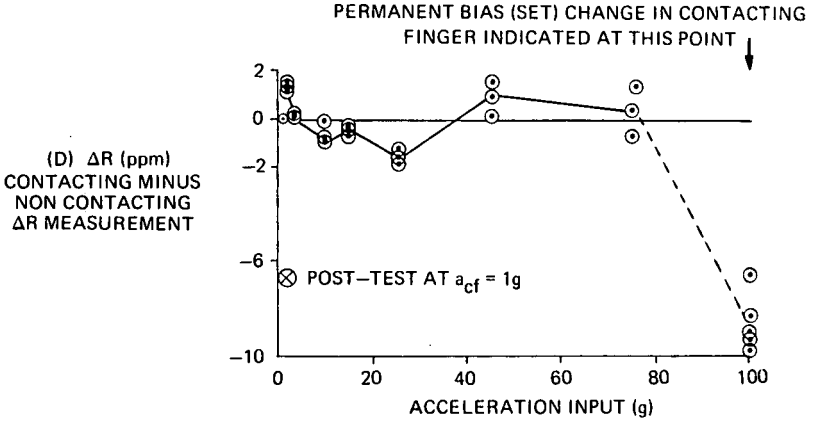

Fig. 6-37 Deviations between contacting and noncontacting radius measurement systems

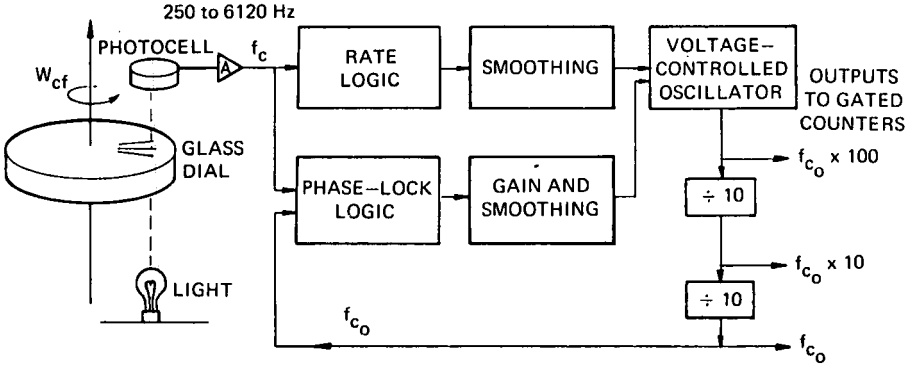

Fig. 6-38 Block diagram of centrifuge speed readout and pulse rate multiplier

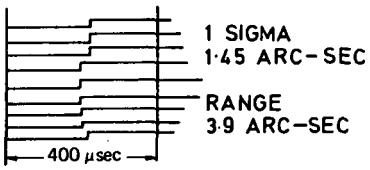

Fig. 6-39 Oscilloscope traces illustrating pulse-to-pulse jitter

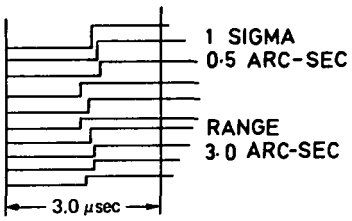

Fig. 6-40 Oscilloscope traces indicating glass dial to pulse multiplier uncertainty

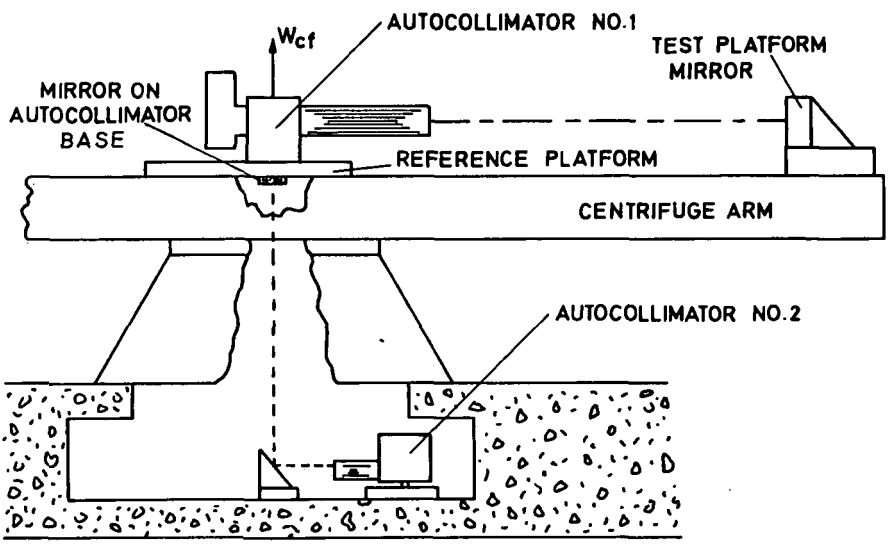

Fig. 6-41 Angular orientation readouts

error is allowed such as to give the voltage-controlled oscillator a total control voltage producing the exact 100× frequency. Smoothing compensation is applied to both control voltages for the voltage-controlled oscillator.

The principal parameters of the speed readout are:

Readout range:	0.2 to 120 g
Equivalent 1× frequency range (low range switched):	250 to 6120 pps
Equivalent centrifuge angle at 100×:	3.6 arc-sec/bit
Equivalent phase error bias:	120 arc-sec
Phase-lock loop gain, 1× cps/deg error:	3 cps/deg
Phase-lock loop response time delay:	6 millisec
Rate-logic linearity:	1% at 100 g
VCO linearity:	1/2%

To evaluate the centrifuge speed readout along with the pulse rate multiplier, the following three types of test were made:

(a) pulse-to-pulse uncertainty of glass dial centrifuge position output

(b) glass-dial pulse to 1× multiplier pulse uncertainty

(c) apparent multiplication accuracy over the test range of 100 g

The glass dial pulse-to-pulse uncertainty is illustrated in figure 6-39, which is a reproduction of successive oscilloscope traces showing pulse-to-pulse jitter for nine randomly-selected pulse pairs. One pulse triggers the horizontal time sweep and the succeeding pulse is reproduced vertically. A change in centrifuge speed during one pulse has negligible effect on this data. Due to the huge arm inertia and estimates of torque disturbances, an angle no greater than 10^{-2}/ac arc-sec is expected. Therefore, the observed pulse jitter is primarily due to the scribing errors made in manufacture of the dial. The results show:

One-sigma uncertainty = 1.45 arc-second of centrifuge rotation

Range of uncertainty = 3.9 arc-seconds

The glass dial to 1× pulse multiplier uncertainty is illustrated in figure 6-40, which is a reproduction of successive oscilloscope traces of the multiplier pulses made during high-acceleration tests. They are referenced to the centrifuge glass dial, which triggered the horizontal time base of the oscilloscope. The uncertainty between these pulses is:

One-sigma uncertainty = 0.5 arc-second

Range of uncertainty = 3.0 arc-seconds

This uncertainty is only slightly less than the glass dial jitter and is due to the fact that the multiplier does not follow the higher frequency glass dial errors.

Multiplication accuracy over the acceleration range of 100 g is shown in table 6-18, which is a tabulation of data from an electronic counter measuring ten times the ratio of the 100× pulse train to the pulse train from the digitalized centrifuge rotation. The data indicates that the glass dial pulses are being multiplied × 100 ± 1.2/100 pulses rms after removing the ±1 pulse uncertainty due to the counter.

However, the multiplier contains smoothing of the control voltages to the voltage-controlled oscillator, which tends to hold the frequency of the voltage-controlled oscillator constant despite changes in input frequency. Therefore, the multiplied pulse train is producing a better average of the centrifuge position than the glass dial.

Angular Orientation Readout of Centrifuge. The angle of major concern for accelerometer testing is the angle between the centripetal acceleration vector and the input axis of the accelerometer in the elevation direction. This angle produces a component of gravity during IA parallel tests or a component of centripetal acceleration during IA cross-axis tests as an input to the accelerometer that must be accounted for in precision testing. The gyroscopic accelerometer is affected also by the angular velocity component. Instrumentation for measurement of this angle has existed on the MIT/IL centrifuge since 1957, as has the policy of including this measurement in the data analysis. Unfortunately, such measurement and use have not been applied to other precision centrifuges until recently. Instead, assumptions have been made as to the stability and repeatability of the orientation angle that would require validation in high-precision tests. In 1964, instrumentation of this angle was improved by replacing a manually-read optical system with a commercially available, automatic tracking autocollimator. In addition, monitoring of angle orientation changes of the autocollimator platform has been added to verify integrity of this reference during the test run. Previous verifications, made by theodolite observation of a shaft-mounted mirror, indicated stability within 2 arc-seconds. The other two test platform orientation angles are of lesser concern. Azimuth changes with respect to centripetal acceleration are important only for accelerometer cross-axis tests in which IA is both horizontal and perpendicular to the centrifuge arm. Twist of the platform about the radial direction also has an effect in such accelerometer tests. Stability of both angles is expected to be excellent compared to elevation, because the centrifugal forces do not tend to produce changes in those directions on a symmetrical structure.

A line diagram of the angular orientation readouts is shown in figure 6-41. Autocollimator no. 1 is mounted on a reference platform at the center of rotation and determines changes in the orientation of a mirror on the test platform with respect to the autocollimator reference. Its output is available in the control room as an analog voltage or an analog-to-digital converted frequency. Autocollimator no. 2 measures any changes in the reference for the elevation measurement that may occur if the coning motion of the main bearing changes or if parameters such as acceleration forces, temperature and metal creep affect the reference platform on which autocollimator no. 1 is located. Autocollimator no. 2 is earth-referenced and closely follows instantaneous deflections of the horizontal mirror mounted in the base of the elevation autocollimator no. 1. This deflection varies sinusoidally with arm rotation and can be resolved into arm coordinates in the elevation and twist directions.

To evaluate the angular orientation readouts, the following two types of tests were performed:

(a) evaluation of a stable reference for elevation-angle measurements

(b) evaluation for possible systematic errors in autocollimator sight line due to centrifuge generated thermal and pressure gradients in turbulent air

To evaluate the stability of the reference for the elevation-angle, a comparison was made of the $A_{p(ref)}$ indicated by autocollimator no. 2 and by two precision accelerometers oriented for cross-axis tests, IA up and down. Measurement by using the accelerometers was made essentially by determining the difference between

Table 6-18 Counter printout at various levels of acceleration input indicating accuracy of multiplier

Acceleration input (g)	$1000f_{co}/f_c$
1	1003
	999
	999
	1000
	1000
	1004
10	998
	1004
	999
	1005
	1001
	997
	1005
20	997
	1000
	1002
	999
	1000
	1004
	999
	1000
50	1001
	1000
	1000
	1002
	1004
	1002
	999
	1007
	1000
100	995
	998
	1000
	999
	1003

Average = 1000.7
RMS = 2.5
Range = 12

the reading of the elevation autocollimator no. 1, and the alignment angle indicated by the accelerometers:

$$A_{p(ref)} = A_{p(meas)} - \frac{[W_{pd} - W_{pu} + 2\,\overline{SF}\,]}{2\,\overline{SF}\,a_c} \qquad \text{(Eq. 6-121)}$$

where

$A_{p(ref)}$ = alignment angle reference

$A_{p(meas)}$ = alignment angle measured by autocollimator no. 1

W_{pd}, W_{pu} = measured accelerometer output with IA down and IA up, respectively

SF = assumed accelerometer scale factor

a_c = centripetal acceleration

This measurement is in error at least by an inaccuracy in assumptions made concerning the accelerometer scale factor and bias:

$$(E)A_{p(ref)} = \frac{1}{a_c}\,[\,1 - (SF_u + SF_d + B_u - B_d) / \overline{SF}\,] \qquad \text{(Eq. 6-122)}$$

where

$(E)A_{p(ref)}$ = error in the reference alignment angle

SF_d, SF_u = actual accelerometer scale factor with IA up and IA down, respectively

B_d, B_u = actual accelerometer bias with IA up and IA down, respectively.

Acknowledgements

The authors wish to acknowledge the assistance of the people who contributed to the preparation of this paper. In particular, the authors wish to thank: Mr. J.E. Lebo for his assistance in the error analysis of the one-gravity tumble test; Mr. S.R. Carpenter for his work on the mathematical model for the long-term PIGA performance; Mr. C.R. Kochakian for his work on testing accelerometers at low levels of acceleration; Mr. J. Meehan and Mr. J.A. Miola for their work on the air bearing rate table.

Symbols

a_{cf} centripetal acceleration established by centrifuge

a_{in} input acceleration to accelerometer

a_{χ} cross-axis acceleration, perpendicular to a_{in}

a_{ind} indicated acceleration output of accelerometer

$a_{(pulse)}$	value of torque rebalance pulse of PIPA in units of acceleration per pulse
$a_{\chi(vb)}$	cross-axis vibratory acceleration
$a_{in(sus)}$	sustained input acceleration to accelerometer
A_{vb}	amplitude of angular vibration input
a_o, A_s	misalignment angle of PIG input axis to PIGA input axis due to rotation
$e_{o(pulse)}$	PIPA output axis error angle required to produce $a_{(pulse)}$
$(E)a_{ind}$	errors in indicated acceleration output
f_{vb}	frequency of vibration input
$F_{(servo)}$	transfer function (closed-loop response of controlled-member servo, a_{ind}/a_{in})
g	value of gravity at test site
G_c	transfer function of PIGA servo compensation
H	angular momentum of PIG established by its spin motor and wheel
I_i, I_o, I_s	moment of inertia of PIG gyroscopic element about input, output and spin axes, respectively
ΔI_p	product of inertia and other inertia dissymmetry of PIPA pendulous element proportional to mass distributions along input and pendulous axes
ΔI_{is}	product of inertia of PIG gyroscopic element proportional to the product of mass distributions along input and spin axes
m	mass of PIPA pendulous element
$K_{pp} - K_{ii}$	difference in compliance of PIPA pendulous element support from case along the directions of the pendulum and input axes
K_t	torque gain constant of PIGA servo
K_f	PIGA platform bearing friction torque per gravity (for this example, friction torque assumed linear with a_{in})
PIG	pendulous integrating gyro
PIGA	pendulous integrating gyro accelerometer
PIPA	pulse integrating pendulous accelerometer
P_p	pendulosity along PIPA pendulous axis
P_s	pendulosity of PIG gyroscopic element along spin axes
P_{piga-o}	pendulosity of PIGA platform (controlled member) along PIG output axis
R_{cf}/g	centrifuge radius per unit of gravity

T_F bearing friction torque of PIGA platform (controlled member) axis, positive for positive a_{in}

W_{cf} angular velocity of centrifuge

References

(1) **Hald, A.**, 'Statistical Theory With Engineering Applications', pp 290, 291, 526, 527, John Wiley and Sons, Inc., New York, 1952.

(2) **Dixon, W.J., and Massey, Jr., F.J.**, 'Introduction to Statistical Analyses', McGraw-Hill, New York, 1957.

(3) **Swed, F.S., and Eisenhart, C.**, 'Tables for Testing Randomness of Grouping in a Sequence of Alternatives', Annals of Mathematical Statistics, Vol XIV, pp 66-87, 1943.

(4) **Olmstead, P.S.**, 'Distribution of Sample Arrangements for Runs Up and Down', Annals of Mathematical Statistics, Vol XVII, p 29, 1946.

(5) **Hero, J.R. and Wilterdink, B.W.**, 'Air Bearing Rate Table Instruction Manual', Report No. MCR-75, Miniature Components Group, Instrumentation Laboratory, MIT, Cambridge, Mass., Feb. 1966.

(6) **Carpenter, S.**, 'Interpretation and Evaluation of P-A Alignment Test Data', Report No. MCR-45, Miniature Components Group, Instrumentation Laboratory, MIT, Cambridge, Mass., Dec. 1964.

(7) **Tsutsumi, K.**, 'A Ground Tilt Isolation Platform', Report No. E-1508, Instrumentation Laboratory, MIT, Cambridge, Mass., Jan. 1964.

(8) **Tsutsumi, K., and Kochakian, C.R.**, 'Design of a Stable Test Platform for Attenuation of Disturbances Due to Rotational and Translational Components of Ground Motion', Technical Memo No. 400, Miniature Components Group, Instrumentation Laboratory, MIT, Cambridge, Mass., Jan. 1968.

(9) **Colman, G.**, 'Generation of Calibrating Signals for Ultra-Sensitive Accelerometers', Thesis No. T-437, Instrumentation Laboratory, MIT, Cambridge, Mass., Sept. 1965.

(10) **Buchanan, J.M.**, 'Some Effects of Vibration on Gyroscopic Equipment Performance', Report No. R-369, Instrumentation Laboratory, MIT, Cambridge, Mass., July 1962.

(11) **Buchanan, J.M.**, 'Principle Types of Centrifuge Tests of Inertial Guidance Equipment', Report No. E-1223, Instrumentation Laboratory, MIT, Cambridge, Mass., Oct. 1962.

(12) **Weinstock, H.**, 'Laboratory Test Equations for a Pendulous Integrating Gyroscope and the Linear Integrating Accelerometer', Report No. E-1400, Instrumentation Laboratory, MIT, Cambridge, Mass., Aug. 1963.

(13) **Grohe, L.R., Hall, E.J., Sapuppo, M.S., Scoville, A.E.**, 'The MIT 25 Series Inertial Instruments', Report No. R-141, Instrumentation Laboratory, MIT, Cambridge, Mass., Feb. 1958.

(14) **Barry, J.,** 'Development of PIGA Functional Block Diagram and Preliminary Study of 11 PIGA Dynamic Performance', Report No. MCR-65, Miniature Components Group, Instrumentation Laboratory, MIT, Cambridge, Mass., June 1965.

(15) **Draper, C.S., Sapuppo, M.S., Hughes, L.,** 'Accelerometer Operation in a Low-G Environment', Report No. R-402, Instrumentation Laboratory, MIT, Cambridge, Mass., Dec. 1962.

7

Testing and Acceptance of Instruments at a System Level

KENNETH FERTIG
Associate Director, Instrumentation Laboratory, Massachusetts Institute of Technology, Cambridge, Massachusetts, USA

Summary

In the course of an inertial system development, when the instruments arrive and the platform with its electronics is to be assembled, a trade-off arises; to what level should the instruments be 'acceptance' tested and calibrated as components rather than integrated into the platform and tested together in a system-like environment?

The philosophical point of view presented in this chapter is that overall system costs are decreased when most of the instrument testing is done in the final use environment. The savings result through a decrease in expenditure for test equipment, and a requirement that instruments work properly in the final assembly prior to being accepted and that the greater fraction of total test and acceptance time spent in the system environment provide more useful data to operationally deploy the system.

The philosophy of system level testing is expanded as to be applicable to the research, development and prototype phases of system and instrument development as well as the production phase.

1. Introduction

An inertial system can perform no better than its internal instruments perform. Moreover, the system must be properly conceived and implemented or the capabilities inherent in instrument performance will not be realized. If the system concepts and implementation are carefully monitored, then system performance is quite directly a measure of instrument performance. Testing of the instruments in the system certainly is a test of instruments in their real environment and against their real mission. Therefore, system testing can be looked upon quite properly as the ultimate in instrument testing and not as an auxiliary effort with differing goals. The objective of this paper is to demonstrate the benefits of instrument test and acceptance at a system level. As a collateral objective, aspects of the philosophy and methods of system level testing and the use of system equipment are presented as a means whereby instruments and instrument testing can be improved.

System level testing is the payoff, and the quicker instruments are brought to system level testing the quicker the payoff - which can be expanded to mean incentive payments for instruments which pass all tests in the system without replacement and recycle. Instruments which pass contractual acceptance tests but do not perform well in a system are not worth buying (assuming confidence that the mechanization of the system in concept and hardware is correct).

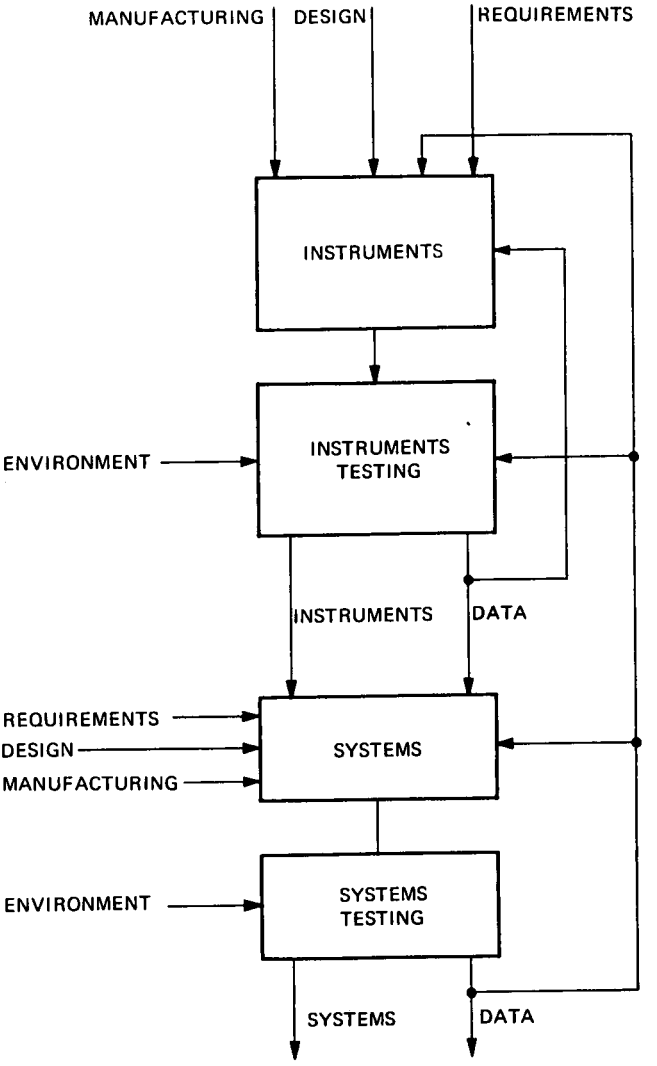

Fig. 7-1 The feedback influence of system testing

System level testing involves not only equipment but also a philosophical point of view applied to regular instrument testing, particularly in the conceptual and prototype stages of a system. This is the same critical point of view that is applied to instrument testing during the production phase as a result of experiences fed back from system testing. This attitude of looking for instrument environment, hardware, and mission interactions as they affect actual and potential system performance is the heart of system level thinking and testing.

Is this philosophy really new? And have instrument testing approaches lagged? Unfortunately, the answer is yes. While the tone of the companion chapters presented by the members of the MIT Instrumentation Laboratory (MIT/IL) suggests that new techniques of analysis, improved models and a new generation of equipment are coming into play, the progress is largely a result of the push of systems and largely borrowing from systems efforts. The dynamic influence of system testing through feedback everywhere in the system, including instrument design, is shown in figure 7-1.

Although the instrument testing situation has improved, testing in systems is stressed because system and instrument requirements are not static. As more refined information about the instruments is obtained from testing, the systems proposed and implemented are being refined and the performance goals are increased. System/instrument interface specifications are inherently incomplete to totally specify and permit (if one could afford it) the verification by instrument test alone of the probable performance of instruments when incorporated in a system.

Even for production systems, the testing situation should not be static. The most rigid change control procedures still can permit incorrect and undesired changes to creep into the instruments and the system. As the system goes through various block models, integrated performance must be checked to assure total and sustained compatibility. The most rigid quality control on programs will still permit instruments to be shipped which do not perform in the system. Most quality assurance programs in production attempt to control performance by manufacturing techniques and to eliminate, as much as possible, the verification of performance of components by test.

The trend in production is to maximize profit and to reduce costs to meet competition by reducing the number of specifications that must be verified prior to shipment and payment. If acceptance can be delayed until performance in a system is verified (even a reduced version of the system) incremental costs may be higher for the units which really are acceptable, but funds are not wasted on poor units. Tremendous leverage is exerted back through production to obtain good instruments measured by delivered performance, as compared to those which have merely passed interface specifications. The leverage exists because of the desire to receive payment (and perhaps incentive fees) and because the system level test should pinpoint problem areas to make correction a rational process.

This chapter expounds the philosophy of testing inertial instruments in systems and/or using system techniques in order that time and funds are saved and improved performance realized. The chapter is structured so as to show initially the phases of inertial system development and how system testing of inertial instruments fits into each phase. After describing some of the problems of specifying system-to-instrument interfaces, the hardware of a system is described briefly to show how in a system the hardware availability and functional characteristics ideally support instrument testing.

The flexibility inherent in a system to support instrument testing in a variety of orientations and environments is described at some length. The concept is developed of improving the model of instrument in order that performance be

improved. By using system monitoring procedures and analysis, an extended model can be used to compensate instruments in the system and to influence design and manufacturing procedures. The concept of model/monitor is extended to consider aids to testing and performance assessment at both instrument and system level by mixing data from a variety of background environmental sensors.

Two examples of systems testing - gyro compassing and centrifuging - are presented to show how and why improved instrument data may be obtained by testing in a system.

A brief survey of cost estimation with attending difficulties is presented to compare grossly the costs of testing instruments separately and in systems.

A philosophical review and summary concludes the chapter.

2. Inertial System Development

Phases of Development

The development of inertial equipment may be classified in three phases as new systems and instruments in the conceptual or proposal stage, in prototype development, and in production. In each phase, the system development can be improved if more is known about the instruments as they are used in the system and as they react with respect to each other, the total system environment, and the systems goals.

Testing, analysis and simulation are used to gain the insight, initially, and the knowledge, finally, as to how a system should be mechanized and how well it will perform. The peculiarities of particular instruments and the availability of alternatives pressure the system designer to follow certain configuration paths which may restrict applications of final hardware.

Through instrument testing, instrument peculiarities may be understood sufficiently well to be removed by design or circumvented by system mechanization. It is incumbent upon the system designer to truly understand the instruments to be used in a system. Excepting only in a closed and non-competitive environment, the instrument supplier must equally well understand the system level problems of instrument use and performance.

Definitions

In a philosophical chapter, definitions are desirable for terms repeatedly used, particularly if they have subjective connotations. The terms 'system', 'system level', and 'testing at a system level' are defined in an operational sense applicable to all phases of system development. While the definitions are personal (as may be the objective and many of the views expressed in this chapter) they serve as a frame to show how system development supports and spurs instrumentation efforts.

System. 'System' may be defined as the unifying concept of coherent goals and methodology for the use of several existing or new instruments and associated equipment. An understanding of missions and applications of the unifying concept and its flexibility and timeliness is implicit in the definition of system. Furthermore, equipment, partial or complete, in the field, factory, or yet in design constitute elements of a system appropriate to the particular developmental phase of the system. Finally, an appreciation of costing is a necessary element of a system since the rules governing the trade-offs which establish the configuration of a

system have cost estimation as a dominant factor.

System Level. By 'system level' is meant efforts motivated by appreciation of system requirements, or to provide information for decisions to the system designer. As an example, this effort could be design, fabrication and cost studies carried out for gyro electronics to verify the desirability of common electronics versus individual instrument electronics for suspension, signal generator and wheel power supplies. With respect to testing the effort could be the construction of a test complex, using system electronics, to test several instruments and verify commonality of environment and electronic interactions and appropriateness of instrument model, the actual testing, and the interpretation and resulting system decision.

Testing to System Level. The term 'testing to system level' means testing to all or part of a system specification, utilizing as much as possible parts of representative system equipment up to and including the entire system. If instruments are tested this way, real specifications can be generated which measure delivered performance. Incentives and penalties may be generated which reward good performance and which punish performance degraded from that previously agreed to and met. Sources of degraded instrument performance may also be pinpointed and corrective action initiated because of the sophistication of equipment available in system level testing.

System acceptance level testing can be a one way proposition and this is unfortunate. Unacceptable instruments are rejected, which is proper. If some instruments are significantly better than the system requires, they can pass without any real knowledge gained of how much better these instruments are. This situation is depicted in figure 7-2a. It is important that instrument vendors and designers of instruments and systems recognize the situation and test in sufficient depth to know the performance distribution. If the instruments are well defined and properly made, most will pass. However, before the value engineers get to work on the instrument to save potential incremental costs and cut corners which affect performance distribution, as shown in figure 7-2b, a review should be made and supported by test data and mission analysis to examine, from a system point of view, the effective methods of cost saving and the real performance trade-offs and attendant risks.

Improved system performance as a rewarded incentive should be considered as a candidate cost effective measure. Further, the system application can be reviewed and new options and increased flexibility obtained, as the most cost effective measure. Cost may be reduced when the instruments are culled as shown in figure 7-2c for systems requiring differing performance either by selection or because the mean performance is sufficiently high. The instrument design remains cost effective because the instrument may be produced in quantity and be broadly used.

Premature relaxation of goals and reduced depth of testing may be ultimately the least effective and most costly approach. Proper system level testing, even for production systems, should permit engineering data to be taken to establish the 'quality' of performance in a quantitative sense. Moreover, operational systems on location should be capable of being interfaced with an off-line monitor system without degrading the system or removing it from an operational status. This permits field verification of performance or discovery of problems not previously apparent or understood.

If the system as a whole is to be equal to or greater than the sum of its parts, then something must be introduced at system level. That something typically is an appreciation of instruments in greater depth than is typical at the level of instrument testing. For example, complete three-axes systems can be made largely self-calibrating. The system level testing results in more than just the several

individual coefficient sets for the instrument models. In addition, the instrument models can be readily expanded and additional coefficients derived which yield better performance. Lastly, the coefficients for the model which represents the relative coordinates of the instruments within the triads of accelerometers and gyros may be determined as well as the alignment of the triads to each other. These test procedures are dealt with in detail later on in this chapter.

System analysis is not some magical process whereby poor instruments are miraculously transformed into perfect instruments. The use of modern filter theory to minimize noise and uncertainty does not eliminate problems within a system but can help maintain an appropriate level of performance and help to pinpoint some cause-effect relations previously obscured, ignored, or unexpected and unmodeled. Also, filter theory can give deceiving answers if the noise and uncertainty models are wrong.

3. Examples of System Impact on Instrument Testing

Instruments have been misapplied in systems due to misunderstandings between the instrument and system developers concerning their relative roles and mutual requirements. In general, personal experience and some opportunities for an overview of the experience of others lead the author to the conclusion that system level testing has underscored shortcomings in instrument designs, testing, or recommended usage and has led to corrective modifications. While examples are legion, two will be cited where system level testing has led to improved instrument testing. The examples are chosen to illustrate the range of the feedback of system testing into the instrument area.

PIGA Calibration

PIGAs (Pendulous Integrating Gyro Accelerometers) - see chapter 6 - are classically calibrated on the basis either of time to complete an integral number of turns or of the angular change over a set time interval while being subjected alternately to positive and negative gravity. Because of system applications and testing needs, new procedures have been developed which examine total PIGA output as a function of time and with greater resolution. This has resulted in refinements to the instrument model, an appreciation of noise sources, and subsequent design improvements to the instrument and the system.

Present data gathering techniques influence the instrument indication by introducing short term quasi-random or specular noises into the steady state estimate. The effects of these noise sources can be presented from both the time and frequency domain viewpoints. In figure 7-3, a time domain interpretation is presented where the instrument indication is shown as a slight oscillation superimposed about an ideal ramp. (Note: oscillations are exaggerated for purpose of illustration.) These oscillations are, in reality, the result of internal phenomena such as servo noise, encoder noise, etc. and have a zero mean. How such noise can be introduced into instrument data and performance estimates becomes apparent when one analyzes the two data gathering techniques shown in figure 7-3.

In technique 1, integral angle data is taken at precisely known $\Delta\theta$s at, say, 10-turns, 50-turns or 150 turns. But in so doing, unfortunately, the uncertainty in δt and noises introduced not by the instrument but by the servo, etc., will also be strobed into the readout ($\Delta T + \delta T$) of the precise angle. In addition, if the time quantization is not fine enough, additional short and long term quantization errors will be introduced.

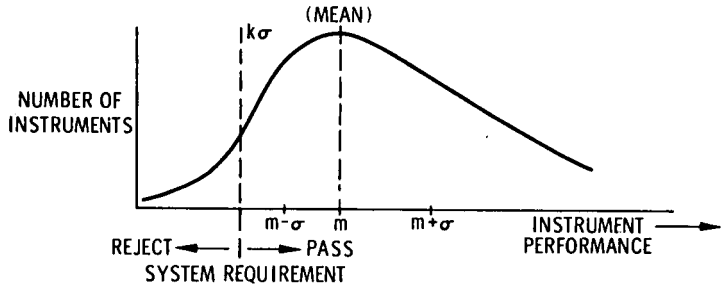

(a) DISTRIBUTION OF INSTRUMENT PERFORMANCE

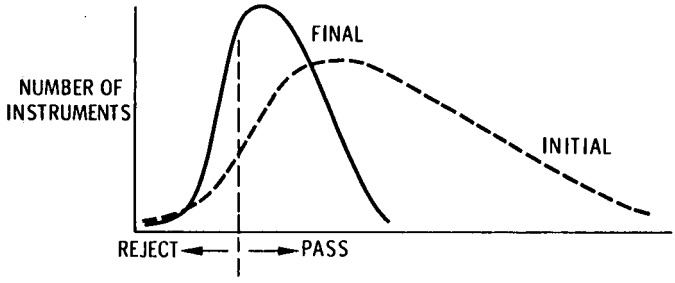

(b) EFFECT OF VALUE ENGINEERING ON PERFORMANCE

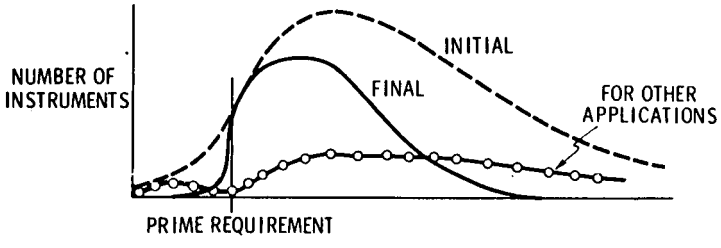

(c) DISTRIBUTION AFTER CULLING OF INSTRUMENTS FOR APPLICATIONS REQUIRING DIFFERING PERFORMANCE

Fig. 7-2 Distribution of instrument performance

In technique 2, because of the typical organization of the computer, quantization is performed precisely in time. However, it is possible to come out in the middle of the quanta of the angle at either end of the integral and, in so doing, strobe into the data an uncertainty that has nothing to do with the instrument but only with the inherent quantization and noise sources. The introduction of such quantization and oscillation disturbances presents a misleading interpretation of the instrument's performance. Long duration and time consuming testing and computational techniques may be required just to reduce the noise introduced by the method of data collection. In figure 7-4, the noise sources are presented in the frequency domain. Present readout techniques hetrodyne high frequency noise into the calibration estimate.

The problem illustrated in figures 7-3 and 7-4 is that if there is an oscillation, and strobing occurs at some arbitrary time, it is very likely that noise will be strobed into the output indication whereas, in fact, the very next instant of time will have had a cancelling noise. The average will have been zero. However, if one considers the use of low-pass filters as an appropriate form through which all of the indication data would go, then it would be the output of the filter that would be strobed to make the calibration estimate. By processing the data through the low-pass filter, it would be possible to make adjacent noise pulses or oscillations in effect cancel themselves out. The filter would attenuate such oscillations and the strobed readout would then show very little noise in its readout when the reading was taken.

Recent testing has demonstrated that the situation can be improved by taking the data through digital filters (which are the analog of low-pass filters) rather than through strobe filters. Note that the RSS (Root-Sum-Square) quantization noise equals ΔV for a PIGA bit over a computation cycle time divided by $\sqrt{12}$, the RSS factor for a quantum change. For example, if quantization equalled ΔV ft/sec as indicated and the data gathering time equalled T, the noise would be approximately $\frac{\Delta V}{T} \frac{1}{\sqrt{12}}$ ft/sec^2. In figure 7-5, the present and proposed data gathering and processing techniques are summarized. The present data gathering techniques are shown as

$$\frac{\Delta\theta}{\Delta T + \delta t} \quad \text{or} \quad \frac{\Delta\theta + \delta\theta}{\Delta T}$$

with the information really contained in the variation for either case.

In present data processing techniques, the average is taken of successive tests, i.e. of ten 50-turn samples. Recently, it was proposed that the equivalent of several 50-turn samples could be obtained in the same time period normally taken by two 50-turn samples. This is accomplished by taking ten 10-turn samples and computing the average of averages or 50 turns sliding 10 turns at a time, resulting in an improvement in reducing the noise effects. These sampling techniques, however, often introduce high frequency noises into the low frequency regime by strobing the several noise sources which are in the form of a gaussian curve centered about some frequency. These new techniques may be called 'weighted' or non real-time low-pass filters.

The recommended filtering techniques will take advantage of recent experiences in system and instrument testing and should materially shorten the time to perform a calibration estimate with minimal response to all noise sources. In future systems, data will be handled through real-time digital low-pass filters so that the noise is not allowed to affect the estimate, while the total data base is increased and the time for an estimation is reduced. Furthermore, it is recommended that facilities

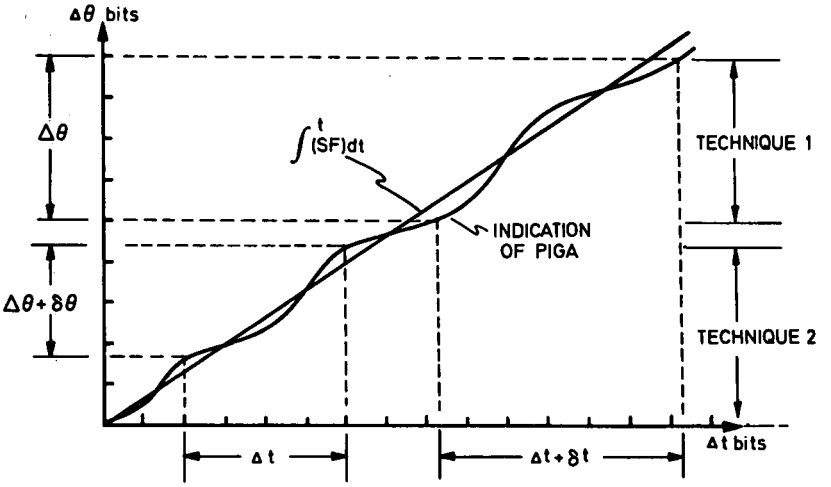

Fig. 7-3 PIGA interface - calibration and use in time domain

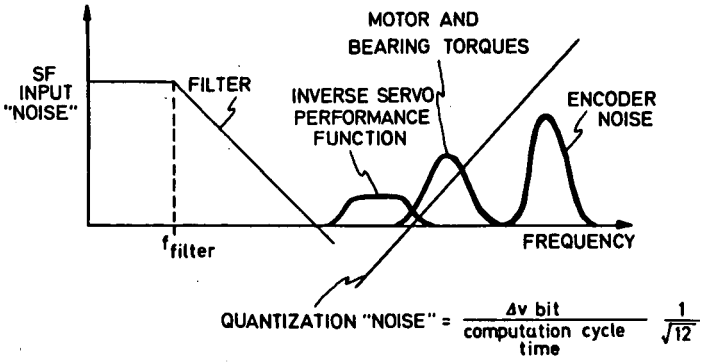

INSTRUMENT BETTER THAN DATA GATHERING TECHNIQUES;

PRESENT TECHNIQUES HETERODYNE HIGH FREQUENCY "NOISE" INTO CALIBRATION ESTIMATE

Fig. 7-4 PIGA interface - calibration and use 'noise' in frequency domain

which are primarily oriented toward supporting instrument testing should obtain some small general purpose computer in order to do real-time filtering prior to mass data transfer to large central computers. An additional benefit obtained with the use of the local small computer is that instrument coefficient modeling efforts are more readily pursued experimentally.

Gyro and PIGA Electronics

Gyros and PIGAs classically are tested in the laboratory on instrument test stands with associated electronics racks, all interconnected by cables with multiple test points. Instruments would exhibit stability in place but change calibration numbers upon being moved to a new stand. The results of system testing indicated (a) significant change in test stand wiring was required because wiring practices had not remained in step with raised carrier frequency excitation used in newer instruments, (b) test stand servos should and could be improved and (c) coupling and subsequent instrument calibration instability could be reduced by operating the signal generators and magnetic suspensions of instruments at the different frequencies.

Initially, the test group involved was loath to consider the changes because the instruments appeared to pass, quite well, individual acceptance tests performed on separate pieces of test equipment. They were prepared to accept data discontinuities as the instrument was moved to different test stations.

Sensor/Computer Interface

A third case where system level thinking has impacted on instrument design will not be discussed in depth in this chapter. Briefly, however, as the understanding grew of the several interfaces, i.e. between the platform, the instruments, the electronics, and the computer, a new approach to general purpose sensor data transfer to a computer developed. Angle encoding and general analog-to-digital (A/D) conversion techniques have been generated which yield signal rate as well. The interface technique is described in the literature (1, 2) and utilizes phase locked loop techniques.

4. System/Instrument Interface Specifications

Specifying System/Instrument Interfaces

The purpose in accepting instruments is for use in a system. Consider what happens if the instruments are accepted just on the basis of Instrument Test and Acceptance data. How can the customer be assured of usability? One way, clearly, is by inserting the instruments into a system and then testing. Another way which is often proposed is the use of a 'system/instrument interface specification.' Unfortunately, specifications do not totally define an instrument nor its interaction with its environment.

Product improvement changes, skipped inspections, eased tests, etc., appear to save money and are pushed by instrument vendor/design teams to improve delivery and profit. But will the instrument, after acceptance and as an instrument, then fit, function, and perform in the system? Costs in lost interchangeability, in matching or tuning of the electronics to the instruments, or in total unusability in a system of instruments which meets specification can be much greater than costs of instrument testing (or of better instruments) in systems prior to acceptance of instruments. As a minimum, system level testing will insure that change control

procedures for systems in production are more scrupulously followed and important and that appropriate specifications are created for instrument test prior to shipment.

By the same token, the appreciation of the benefits of system level testing by vendors and designers of instruments and systems will help develop better methods for specifying instrument test prior to acceptance. Further, this appreciation, rather than restricting design and product improvement, will lead to the real improvements in yield, performance flexibility, application and lowered cost.

Typical Problems of Inadequate Specifications

As an example of how inadequate system/instrument interface specifications create problems, the following two examples will be cited. One was developed during a block change of a production system, the other during an R & D (Research and Development) program.

The production system went through several block changes and finally through a major system revision and updating. The gyros in the system had developed a remarkable record of reliability through the block changes and were to be used in the updated system. The gyros were gas bearing units which typically require greater starting power compared to running power. In the design of the updated system, the wheel power supplies were specified for the run condition and did not have the required and well known (but unspecified) high voltage for start. The result was that, for system purposes, not all gyros would reliably start and one of the most reliable elements - the gyro, with a long history of good performance - became a major source of reliability problems in the updated system. The specifications did not keep pace with the actual hardware interfaces. The problem here, most likely, was that knowledgeable engineers who knew the 'unwritten' rules and reasons for decisions had become managers and a new group of engineers had inherited the direction and design of the system. A more subtle aspect of the problem was that the various divisions of the company communicated but, at a design and working level, the communication seemed to be in the form of paper-specifications and not the information feedback of people concerning hardware.

The second example is a little closer to home: on an R & D system in which the interface between an accelerometer and the system was to be improved, the interaction, in the form of discussions and memoranda, took place between the Instruments and Systems Groups. However, the interaction was mainly tangential. A consistent problem with the instrument had been large amounts of harmonic and quadrature voltages at the secondary. A system request had been expressed for a center-tap on the signal generator (SG) secondary and for the suspension excitation to be changed from 4800 Hz to 9600 Hz, to reduce the coherent leakage coupling of the suspension into the SG. This situation is depicted in figure 7-6.

Signal generators without center-taps are of long standing design and a reluctance for change existed. The frequency change was accommodated. The problem of large coherent voltage was reduced. Servo stand-off was reduced and an improvement was effected. However, the noncoherent voltages increased and the servo preamp, although differentially connected, tended now to block because of the large common mode signal present at its input. The center-tap would have eliminated this. The Instrument Test Group was totally unaware of the problem because the shielded pair of wires from the instrument to the test console were long and contributed significant capacitance and a virtual center-tap to ground. In the system however, no such long leads really existed and some sort of retrofit was required or the servo was likely to block.

This problem, an instrument/system interface, arose because the Instrument Test

Group could not relate their own experience to that of the System Group and naturally viewed a problem unreal to them as esoteric. In fact, the problem is real; instruments can be damaged and, as a minimum, short-term performance degraded. The example also demonstrates that groups, exchanging opinions and paper and appearing to cooperate, in fact may not accomplish major objectives until hardware and people are exchanged to operate in new environments for some minimal time.

This second example serves to illustrate the sort of communication gap which exists between instrument and system groups seen in many organizations: 'use the instrument as it was tested' contrasted with 'test the instrument as it will be used'. The arguments between groups often extend beyond just comments on the testing level to criticism at the design level where, of course, the vital parochial prejudices and considerations of each group reside. Recall that this chapter stresses, both philosophically and by example, that testing as well as test and acceptance should be performed at a system level and in a system-like as well as systematic manner.

Instrument groups which create families and generations of instruments tend to have a larger capital investment in test equipment which is geared to testing by existing methods. On the other hand, system testing tends to be less of a residual capital equipment problem and, because of competition, the systems thinking, design and testing tends to be more advanced and structured for change. The message should be clear - test it at system level and borrow techniques and equipment from the system.

5. System Hardware

The inertial instruments of a system are supported in a mechanical structure called a platform which provides the thermal environment, stability of mechanical mount, and vehicle interface. The electronics of a system provide the various a.c. and d.c. power supplies required by instruments and readout interpretation and supply the interface to the computer and control subsystems.

Interface Environment

The mechanical and electronic supporting hardware together generate the interface environment for instruments. As these hardware elements vary from set points, the instrument performance is likely to vary. For example, if the platform temperature varies totally or in a gradient sense, the gyros (or accelerometers) are liable to show a change in the coefficients of the drift model. The ranges for the drift model as well as the coupling coefficients to describe the platform vehicle interface can only be determined in a system test; test stand data is typically inapplicable. Similarly, electronic changes such as system wheel supply voltage variations can result in coefficient changes which can only be established in the system.

It is increasingly evident that as instrument capabilities improve, applications environments become increasingly severe in terms of vibration, temperature, allowed volume, etc. The price of environmental control increases as the need for the control to achieve performance increases. The alternative is to increase model complexity and monitor more variables for inputting deviations to the instrument model. The price for added model complexity is in the additional monitor circuits and added computer requirements. The monitor/control trade-off is a constant system concern and will be referred to again.

A reason for stressing this issue here is to note that, typically, only in system

level testing are the computer and monitoring circuits available or is the hardware environment close to that of application.

Computer

The availability of the general purpose digital computer presents a significant increase in system capability and in the opportunities to test the system. Improved instrument performance now available might not be useful or applicable to many missions without the digital computer which is the basic sequencer, communication link, controller, and data processer for present and future systems.

Similarly, on-line, real-time computers will be the control means and data formatter for system level testing. While much has been done and will continue to be done effectively by laboratory instrument testing, data recording is relatively manual in nature. Manual techniques in the long run tend to be naturally restrictive in terms of the amount and quality of data taken. Fewer environmental monitor circuits will be operative and less frequent data readings made. The instrumentation will be restricted and calibration of performance will exhibit greater apparent noise and uncertainty. As on-line computers are utilized in instrument testing, such testing becomes more like system level testing.

Digital computer interface equipment can be expensive for real-time applications and certainly the computer software represents considerable costs. For production or even prototype equipment, the availability of a system computer eases certain problems and adds others. The system programs are available (but may require trouble-shooting during prototype development) and cut down on extra software development. However, system programs may be too restrictive in terms of the test programmed, the amount and type of data processing, and the available space in memory, computing time, or priority input/output channels. Moreover, many small and inexpensive computers are on the market which readily interface with systems and other computers.

These commercial computers represent costs which are not significantly greater than present test stand recording equipment. Furthermore, they are adapted to real-time data processing and communication with and control by large central recorder/processers. These computers are relatively easy to program flexibly and suitably replicate the probable system computer repertoire. Many of them can be programmed by using a larger machine as the simulator to further reduce software costs and complexity, and to build up a software library applicable to several system programs. Current literature must be used in this rapidly developing field to maintain an appreciation for the availability of applicable hardware, techniques and software.

The use of computers during each phase of system development - new, prototype, or production - whether it be a total system or merely a subsystem or instrument level test, will improve understanding of the instrument in the system.

Scanning the literature and borrowing heavily from the excellent summary of aerospace computer characteristics by Baechler (3), an estimate may be gained of probable test computer requirements, useful in the laboratory and possessing most of the characteristics of system computers. Such a computer would have between 8000 and 32 000 words of memory. The word length would be 18 to 32 bits. Add-times should be a few microseconds. Multiply-times should be approaching 10 microseconds. A scratch pad memory of about 100 to 1000 words is a necessity, as is a reasonably complete instruction repertoire. The computer-to-test system interface (I/O) should be reasonably flexible and contain several buffer registers to store data and cut down the number and frequency of priority interrupts.

A general situation is shown in figure 7-7 in which both a system computer and an off-line computer are used. In fact, the system computer may be replaced by any computer that can simulate it sufficiently well such that similar instructions and times are required to carry out the particular test sequence. In this case, the off-line and system computers may be commoned if this is considered to be advantageous. The essential thought stressed is that the utilization of computers increases the flexibility in dealing with instruments in the system, or simulated system testing, to the point that more testing should be performed at a system level.

In the USA, a recent computer development by IBM (International Business Machines) suggests the availability of modular computer capability in their 4π line, in which increasingly larger machines are available as measured in word length, memory size and instruction repertoire but that all are similar to each other and to the large IBM 360 family. The smaller machines can be programmed via IBM 360 routines. Increasingly, manufacturers are designing computers as families or having compatibility with others by using simple interfaces and common languages and instruction repertoire.

6. System Testing

System Test Positions

The discussion in much of this chapter is concerned with how well instruments may be tested in systems. It seems appropriate, therefore, to illustrate in this section a few geometrical aspects of system testing and how instruments are calibrated and their performance verified.

Instrument acceptance by system test is not difficult since the procedures for instrument calibration and measurement of system performance are regularly part of the system function. At most, simple and superficial changes are all that are required for acceptance testing. Modeling, monitoring, and aided testing activities may require additional computing capability and software but no fundamental changes to the basic platform or system.

A system laboratory test setup is depicted in figure 7-8. An inertial measurement unit (IMU) is mounted on a test stand with one or more degrees of freedom. A computer and control console, autocollimators, and a monitor console as shown in figure 7-9, complete the facility. In production, there may be several such setups with some of the major equipment shared between test stations. Data logging between individual stations and associated computers and a larger central computer is often desirable for record keeping, data retrieval, and comparison purposes, particularly if the systems and components are recycled.

The monitor console permits diagnostic access to internal system signals to a greater or lesser degree, depending upon the system and whether the test station is for production, engineering, or prototype testing. The displays permit simultaneous viewing and recording of several signals.

The 'burn-in' and regular system test procedures evolve as indicated in figure 7-10. The philosophy of system testing is that to a large degree a system is self-contained and, by a choice of simple test orientations and references, capable by automatic procedures of calibrating its components. This philosophy is indicated in figure 7-11, which further indicates that field calibration and checkout procedures can be verified in the laboratory.

For platforms with three gyros and three accelerometers, as shown in figure 7-12, calibration is similar to erection and alignment. In fact, performance may be

Present data gathering techniques:

Time for integral turn $\sim \frac{\Delta\theta}{\Delta t + \delta t}$

Angle for fixed time $\sim \frac{\Delta\theta + \delta\theta}{\Delta t}$

Filtering techniques:

Average of successive tests

Average of averages

Sliding average of averages $\rightarrow \sqrt{N}$ improvement

Proposed data gathering techniques:

Use quasi continuous filter $\rightarrow \frac{f_{filter}}{f_{noise}}$ improvement

Fig. 7-5 PIGA interface - filtering

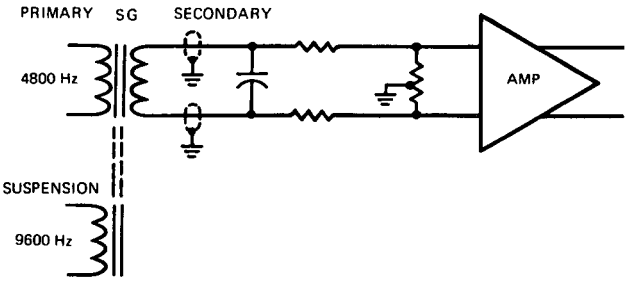

Fig. 7-6 Accelerometer ducosyn circuit

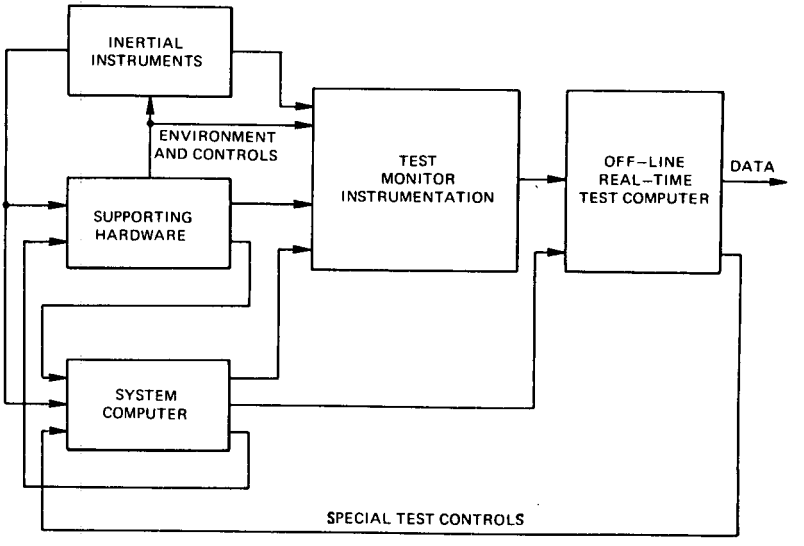

Fig. 7-7 Computer usage in testing

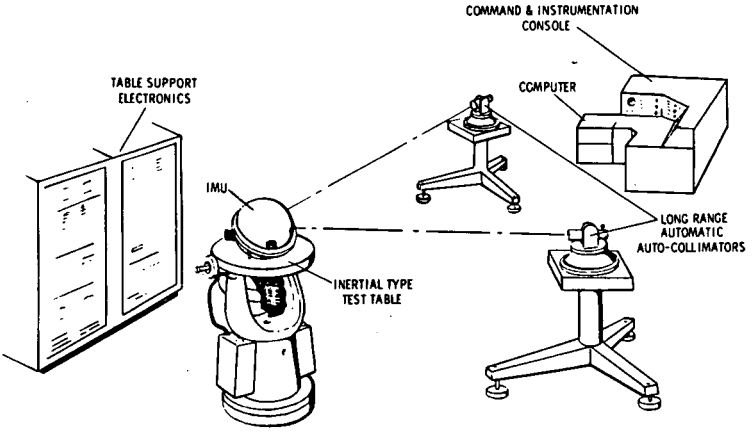

Fig. 7-8 System laboratory test facility

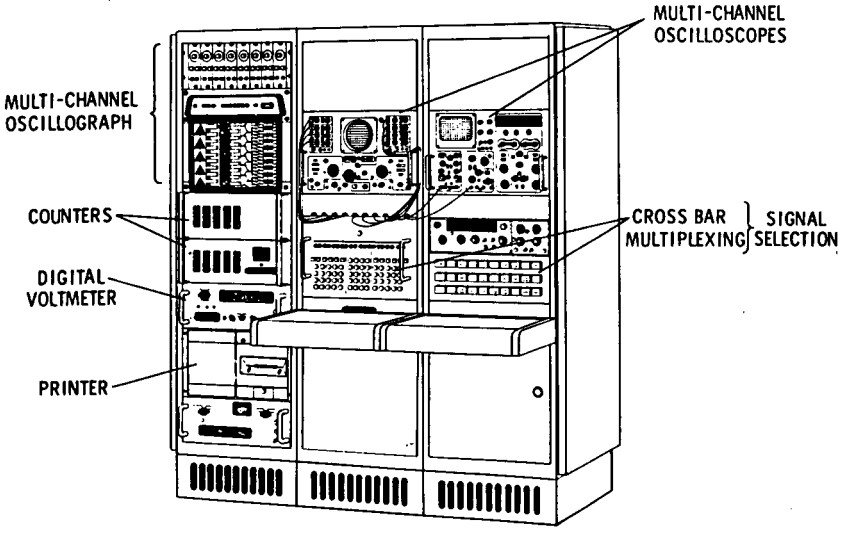

Fig. 7-9 Monitor console

System test is dependent on mission application

- –Time
- –Accuracy
- –Stability
- –Resolution

Instrument test should reflect system techniques

Planned effort required to improve system and instrument

- –Test procedures
- –Flexibility
- –Range of application

Fig. 7-10 Evolving test techniques

1. System operation

   –Computer controlled-integral system part

   –Carries its own time base — crystal clock

   –System aligned and calibrated system-wise versus assembled calibration components

2. Alignment and calibration

   –Similar techniques in the field as in the laboratory

   –Non-linear instrument terms determined in laboratory-assumed constant for system use, and may be verified

   –Three axis optical alignment versus optical azimuth and pendulums

   –Field system to be devised such that optical reference system is available

Fig. 7-11 Test philosophy

–IMU platform has 3 gyros and 3 accelerometers
–Calibration similar to erection /// alignment
–Two vector matching, gravity and earth rate
–Discrete versus quasi-continuous time filtering of data
–Establish laboratory and field procedures
–Natural orientations
–Redundant orientations
–Analysis and computer simulation

Fig. 7-12 Calibration

verified by first calibrating the instruments in a platform and then observing how well the platform erects and aligns itself. The availability of autocollimators makes the verification signal readily available and also can supply orientation data for those platforms with only two accelerometers.

Analysis and simulation are important adjuncts to system testing because they assist in planning the tests, in 'quick look' estimates of performance and in post test analysis evaluations and recommendations for acceptance of the components and the system.

Platform Orientation

The platform of modern inertial equipment acquires many forms. The conventional platform with three or four gimbals is well known. The gimbals may be used to assist the test stand (or use a less complicated one) in going through the several calibration orientations. A strapdown system requires a table with versatility and fixturing in order that appropriate orientations may be accommodated. More recently, a new platform configuration called the 'Flip' has been announced by Nortronics (a division of Northrop Corporation, Hawthorne, California). The Flip is a floated inner ball containing instruments and electronics; it contains no gimbals but does possess internal torquing techniques to control orientation relative to the outer support sphere. The freedom of the Flip permits the inner ball to assume a command orientation or clamp to reference marks on the outer sphere. As a result, Flip can assume calibrations and orientations as well as traditionally gimballed systems. The treatment of required orientations and resulting calibration equations is presented in this paper, therefore, independently of particular platform characteristics and focused directly on the vector attitude of the individual instrument axes.

Each instrument, itself, must be described by more than one attitude quantity. For example, a gyro must have its input, spin, and output axes defined nominally relative to the platform axes and other instruments. This nominal attitude relationship must be known and stored in the computer for all classes of instruments such as single and two-degree-of-freedom gyros, carouseling gyros, vibrating string accelerometers, restrained accelerometers, PIGAs, etc. Some applications may even require finer than nominal knowledge of relative instrument axis alignment. Once the attitude data of each instrument are defined relative to the platform axes, testing to evaluate the particular coefficients of an instrument requires that the instrument be placed in orientations relative to gravity, $\bar{g}$, and earth rate, W_{IE}, as in conventional single instrument testing (see chapters 5 and 6).

Because the number of possible choices of platform instrument alignment is so large, only one case will be presented in this paper as illustrative of a single-degree-of-freedom gyro calibration. The techniques are generally applicable to other instrument configurations. Furthermore, if the test stand or platform has sufficient freedom of motion, tests completely analogous to servo tumbling may be performed, if desired, rather than fixed position testing.

The set of calibration positions chosen for the example is presented in figures 7-13 through 7-16. Each figure has four sketches: the upper left-hand corner shows the orientation of the three gyro input axes, earth rate, W_{IE}, and gravity down. Also shown are the reference platform mirrors M_1, M_2 and M_3 which might be acquired by autocollimators and used for holding the platform when measuring performance. The remaining three diagrams in each figure show the orientations of the remaining axes of each gyro.

The listed torque unbalance equations for gyro 1 may be listed as follows in equa-

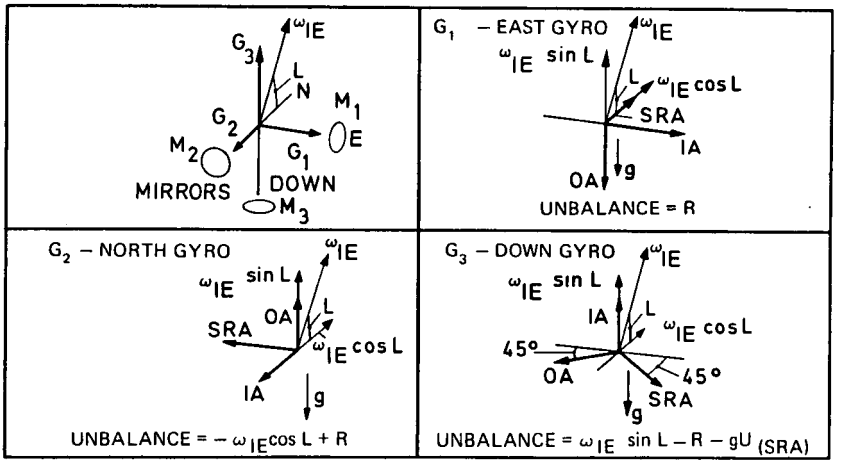

Fig. 7-13 Calibration positions - set 1

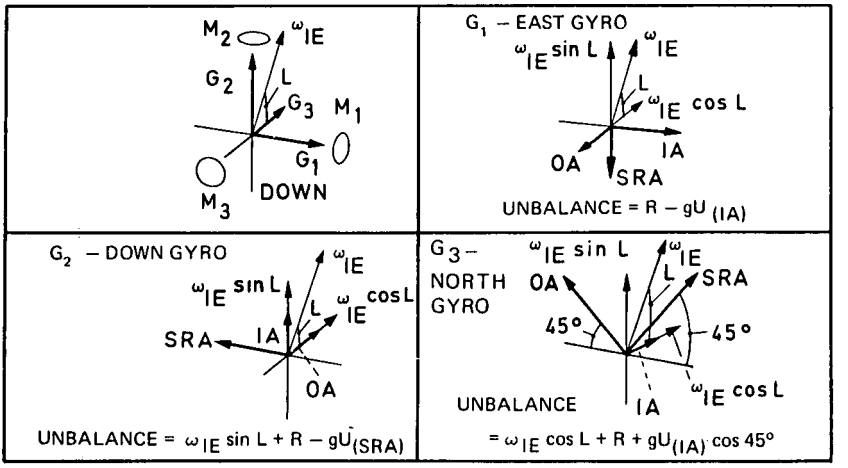

Fig. 7-14 Calibration positions - set 2

tions 7-1 through 7-4:

$$U_1 = R \qquad \text{(Eq. 7-1)}$$

$$U_2 = R - g\,U_{IA} \qquad \text{(Eq. 7-2)}$$

$$U_3 = -W_{IE} \sin L + R + gU_{sa} \qquad \text{(Eq. 7-3)}$$

$$U_4 = W_{IE} \cos L + R - g\,U_{IA} \cos 45 \qquad \text{(Eq. 7-4)}$$

From equations 7-1 and 7-2, R and U_{IA} are determined with this result and from equation 7-4 the torque generator scale factor may be determined. Knowledge of torque scale factor, inserted into equation 7-3, determines U_{sa}. If more instrument coefficients are to be determined, such as compliance, more test orientations are added with the condition that the position yield new data on undetermined coefficients.

There is a strategy to the choice of test orientations, i.e. positions are picked, when possible, from which the data are relatively insensitive to slight errors in orientation. An example of this is equation 7-1, where R is relatively easy to calibrate if the platform is oriented such that the input axis (IA) is close to east and the output axis (OA) is close to vertical. Another example is calibrating accelerometers, where bias and scale factor are easily separated by placing the platform such that the accelerometer sensitive axis is close to vertical and the antivertical. The strategy of platform orientations for calibrating instruments in a system is seen to be similar to that used for regular instrument testing. An additional aspect of the strategy is the choice of a minimal number of orientations to a total measurement set on all instruments. Sometimes, the minimal number of orientations exceeds the number of coefficients per instrument to be determined because in a certain number of the required orientations, say for one gyro, no new coefficients are excited on another gyro. The redundant data obtained on the other gyros are useful in verifying the stability of previously determined coefficients.

At the same time that the data are extracted in the positions required to resolve the coefficients of gyro 1, data are collected on the remaining two gyros and three accelerometers such that their coefficients may be resolved. Thus, in the time required to test and calibrate one gyro, a total of six instruments has been tested and largely calibrated. Some care must be used in selecting positions in order that a determinable set is obtained. Depending upon the system application, a few additional positions may be required for system testing purposes to establish the relative alignment of instruments. These additional positions yield data which can be used sometimes to provide additional validation of several coefficients of the instrument set.

In summary, the several positions required to test a system have been shown to be equivalent to the same positions required to test individual instruments. The relative ease in a system of acquiring the positions and the fact that several instruments are tested simultaneously and in the final environment recommend system test and acceptance of instruments as a valid and useful process. Further, the multiplicity of positions which are available in a system permits redundancy checks on instrument calibration and higher order instrument model term determination. This system test effort generally supports engineering and R & D requirements in as much as modeling experiments may be performed and research instruments inserted.

7. Monitor/Model

A purpose of testing that is becoming increasingly important is to establish the

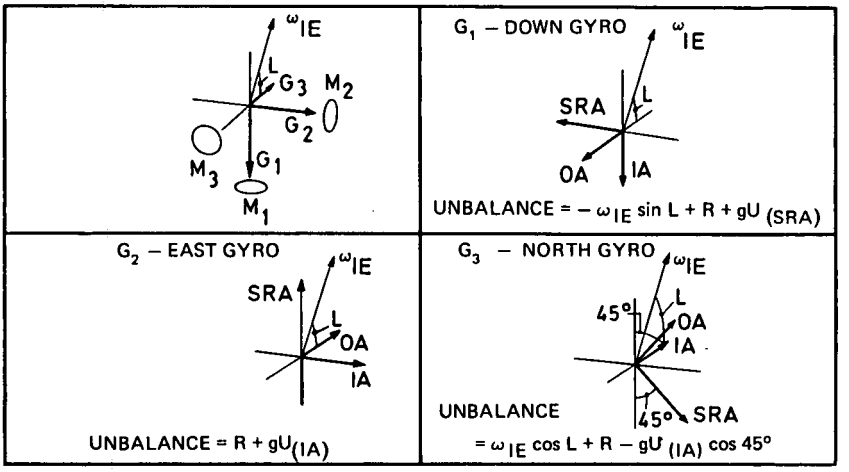

Fig. 7-15 Calibration positions - set 3

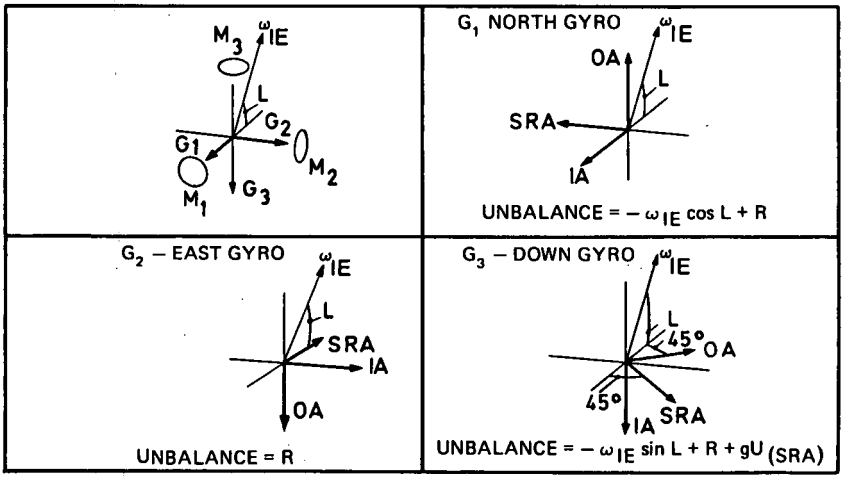

Fig. 7-16 Calibration positions - set 4

coefficients for filtering an instrument error model and verifying the model. These models for accelerometers or velocity meters and gyroscopes have been detailed in companion papers from MIT and will not be restated at length here.

The models for instruments typically involve scale factor, bias, acceleration-dependent nonlinearities, inter-axis cross-coupling, etc., and their associated residual uncertainties. The system designers use the one sigma value of the uncertainty in the coefficients in an error analysis of the system to arrive at a one sigma uncertainty estimate for the system response with respect to several mission profiles. In the case of the ballistic missile, for example, the traditional CEP (Circular Error Probable) (4) would be carried out for several ranges, for varying lofting angles, different flight times and booster thrust and, perhaps, for differing azimuths. Similarly, the propagation of errors through a navigation system may be studied and verified by simulation and test (5).

The customer's requirement for systems accuracy and flexibility improvements results in forcing the systems designers to refine the uncertainty model of the instruments and trim the error budget. Continuously, whether the system is a production, a block change, competitive procurement or R & D, the pressure exists to make improvements.

For the instrument designers, the same customer pressures translate into product improvements, intensive test programs to gather valid statistics to justify coefficient estimates, and programs which develop new instruments out of understanding achieved from research and testing.

Unfortunately for both the instrument and system designers, and sometimes for the customer, pressures for cost reduction tend to reduce the effort expended on testing and continuous validation of coefficient assumptions without relaxing requirements for maintaining and improving performance and flexibility.

An instrument is a transducer which responds to multiple inputs, to the several dimensions of its background electrical, thermal and mechanical environment. By design, the response is strong to its design input and, hopefully, quite weak to the background.

New system requirements do come up which require extended models of instrument performance, i.e. more coefficients are required. To achieve greater accuracy in a system, the bias and acceleration-sensitive terms, etc., may be tested to resolve temperature or temperature gradient dependence of these coefficients. The time constants for the error model response to the environmental inputs may be evaluated. Mission application of the resulting model requires increased system computer capacity to achieve the desired results. Testing at the instrument level requires significantly increased data processing compared to that typically performed.

An alternative approach to improving system accuracy against background environment could be to control the environment, i.e. control the various power supplies, the temperature, etc. to the ultimate. Certainly, while this might work, it is probably an expensive and difficult approach. A middle ground would be to resolve, by testing, the sensitivity to environmental and subordinate inputs and to determine which elements require control and to what degree.

An extension of the middle ground is to control the background to a level which is reasonably consistent with design practice and capabilities and, of course, cost, and to monitor the rest of the background to introduce monitored deviations as inputs to the residual coefficient model.

Instrument test groups are almost doing this now. However, typically they force a variation to one input which is large to establish a first estimate of a drift coefficient but do not take into account that other control and environmental variables might be interacting. For example, wheel voltage might be varied and monitored but wheel power, internal temperature, temperature controller response, suspension signals, etc., are ignored, or at best crudely monitored but not tied into the estimate of torque drift. A properly monitored situation might be described by equation 7-5:

$$dM = \frac{\partial M}{\partial(e_{sg},\ e_{susp},\ e_{wheel},\ \ldots\ Temp_{\omega h},\ T_{case\ \ldots 1\,x,\,y,\,z})}\ \delta(v) \qquad \text{(Eq. 7-5a)}$$

or

$$dM = K_1\ \delta e_{sg} + K_2\ \delta e_{sp} + \ldots\ldots \qquad \text{(Eq. 7-5b)}$$

A set of monitored data, say for j tests on i variables, V_i, would be processed to arrive at the coefficient matrix K of equation 7-6:

$$\overline{dM_j} = \overline{K_i}\ [V_{ij}] \qquad \text{(Eq. 7-6)}$$

The tacit assumption in equation 7-6 is that the variations about the set point are sufficiently small that first order analysis will suffice.

How might the testing proceed to determine the extended model? The procedure is similar to conventional testing, except that more inputs are monitored in addition to the instrument indication and the prime input. Enough data is taken to perform a model fit and to verify that the model contains enough coefficients to suit the purpose. Regression analysis, least squares or, today's panacea, Kalman filtering, are standard techniques which are applied. *A priori* estimates of time constants and of some of the coefficients in the model help to speed the process, reduce the computation, and serve as initial conditions on iterative estimation procedures.

Consider the case of the single-degree-of-freedom gyro, OA vertical, IA east, depicted in figures 7-17 and 7-18. Typically, the coefficients of interest are bias and g-dependence along OA. The variations of the background environment which may be monitored are the power supplies for the spin wheel, the signal generator, etc., the temperature of the instrument and the mount, the heater duty cycle, and the temperature gradients. The monitored quantities are compared to the torque changes. A sequence of equations with unknown coefficients but known inputs and outputs is obtained. If enough measurements are made (greater than or equal to the number of coefficients to be determined), the coefficients may be determined by matrix manipulation and appropriate error minimization techniques.

A similar test may be carried out with the gyro oriented with OA and IA horizontal and SA vertical. This test is usually carried out to evaluate the SA mass imbalance coefficient and the background dependency.

Clearly, one may go through a sequence of tests in the appropriate positions used to determine the traditional instrument coefficients and, by taking the background data samples, determine the extended instrument model.

If the testing is done at an instrument level, valuable information is obtained but the time and equipment expenditure is large and the determination about an operating point may be incorrect to apply in a system if the system environment is substantially different than the instrument test stand. The operation is worthwhile for

R & D determination of the relative importance of model terms, coefficient ranges and initial values. Standard test and acceptance procedures may or may not require the extended model. However, the system itself provides the best test stand environment and provides capability for simultaneously testing several instruments.

Within the system, the environment, the computer capacity, the mechanization of a test stand (for a gimbaled system) is largely accomplished. The use of offline data processing can be used to augment or simulate present or future computer capability. In fact, the procedures employed may logically develop into a 'Field Calibration' procedure which permits minimal time for appropriate data acquisition, assurance of proper total system functioning, etc.

One of the reasons the procedures can be fast is that, as the platform containing the instruments is exercised in various attitudes with respect to gravity and earth rate, the SA influence of one instrument is determined while the IA or R term effects are determined for other instruments, etc. Both gyros and accelerometers are simultaneously calibrated for coefficients and uncertainty estimates. The inertial platform containing the instruments may be mounted on a test stand as indicated in figure 7-19 (with one or more degrees of freedom) or utilize the platform's own gimbal freedom if sufficient. In fact, the contrast between the two methods - test stands versus platform - of gimbal exercise is often revealing with respect to thermal and gravity-sensitive environmental terms in the platform structure, which must be assessed rather early in a program so as not to assign incorrectly system problems to instruments.

Procedures which are entirely analogous to torque-to-balance, step tumble, or servo table runs may be performed which can be assessed to yield required information about both instruments. Where appropriate, increased weight may be given to instrument indications in certain positions which are sensitive to specific model terms in those orientations. This results usually in more rapid convergence for initial and iterative model coefficient estimates.

Nonmission environments, such as vibrators and centrifuges, are used to augment the forcing function for particular inputs. The monitored variables become important as they often contribute in particular test environments out of proportion to their stationary one - g values. For example, high - g centrifuge testing may bring into account higher order terms in the compliance model. The same test may also cause wheel power, current, torque angle, suspension signals, etc., to vary significantly and cause drifts. The tests must be properly assessed to see what data is environment-peculiar and not validly reproduced in the mission.

The application of monitoring to a system is relatively straightforward and limited only by instrumentation, computer capacity, ingenuity, and perseverance.

The modeling may be carried out for accelerometers as well as for gyros. Suitable monitoring must be provided for the important parameters. The assessment of the quality of the model in accuracy and completeness may be verified by test as well as by mathematical procedures to improve the choice of parameters and to indicate compromises between control and monitoring.

Such a modeling program is ambitious but it promises the opportunity to move instruments from the test lab into a system with minimum difficulty. In the design phase of the instrument, excessive sensitivities are quickly brought to focus and corrected. Furthermore, sensitivities derived from such modeling define many of the requirements for electrical, mechanical and thermal interfaces between the instruments and the platform and the computer software load. An ultimate goal of modeling is the ability to carry out instrument testing and to deliver instruments

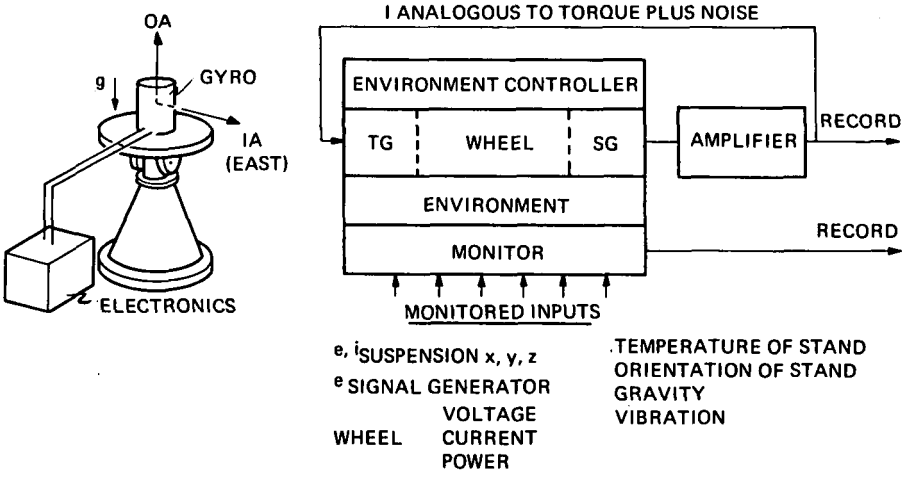

Fig. 7-17 Monitoring a gyro for coefficient determination

Classical Model of Drift

$$M = R + U_{SRA}\, A_{IA} + U_{IA}\, A_{SRA} + U_{OA}\, A_{OA}$$

$$+ \sum_{ijk} K_{ijk} \quad (A_{ijk}) \quad (A_{ijk})$$

Extended model of drift for a fixed position

$$dM_i = \frac{\partial M}{\partial (P_w, P_H, i_w, i_w{}^2, T_G, \Delta T_G, \ldots \text{susp}, x, y, z)} \delta(P_w, P_H, \ldots \text{susp}, x, y, z)$$

- gyro is a multidimensional transducer
- not possible (nor desirable) to provide absolute control of all gyro inputs
- can measure, determine significant, and control range of inputs
- can monitor deviations from absolute control point
- determine matrix for computer to model error terms

$$[M_j] = [K_i][V_{ij}]$$

Test in several positions

- to derive extended model of R, U, K terms

Fig. 7-18 SDF gyro drift model

and data packages such that system 'burn-in' is shortened without performance compromise.

An example of monitor/modeling is a system built by Autonetics (a division of North American Rockwell) called the 'N16 Inertial Navigation'. The platform, instruments, and electronics were modeled over an extremely wide temperature range (6). Monitored variables were used as excitations to model equations programmed in the system computer. As a result, the aircraft navigation system can be turned on from a cold start. The relevance to this chapter of the example is the fact that, early in the program, testing at an instrument level proved insufficient in terms of completeness of the model in establishing the coefficients; testing at a system level was the only answer. The situation in crossing department lines within a company in defining instrument test and acceptance or rejection is difficult enough; imagine the situation existing between companies in defining modes of operation, test techniques and criteria for acceptance or rejection.

Modeling and monitoring may prove to be the optimum method of assessing and controlling costs, of determining incentive by relating measured performance, modeled errors and the ideal performance, and of establishing a set of criteria to which both system and instrument personnel can test and deliver.

8. Aids to System Testing

The concept of 'aided systems' is well established and much commercial and military equipment functions in a manner which utilizes several information sources for control and navigation. The examples of Doppler and Loran equipment coupled to inertial equipment is a fairly well publicized example. With these aids, the velocity and/or positional indication of an inertial system can be updated, initialized, or dumped. Star trackers furnish an example where line-of-sight data is used to initialize or calibrate relatively high performance inertial equipment.

The application of monitor/modeling techniques may be extended to the degree that additional monitoring of the external environment aids in calibration, alignment and verification of the stability of calibration, alignment and general performance.

The many techniques developed in the course of operating aided systems have not been applied (to the author's knowledge) to instrument testing. While the background may have been noted, the data were not used in a model to affect the estimate of instrument coefficients. For example, consider a test environment with a gyroscope on a test stand in the torque-to-balance mode, as shown in figure 7-20. The monitored signals go into a model stored in the computer and are mixed, either directly with the gyro's torque-to-balance signal (Fig. 7-20a) or with the gyro's output signal (Fig. 7-20b). In either case, the aiding signal is used to subtract the effect of local disturbances such as floor tilt from the indication of the instrument's true performance. Trains, tides, weather, even personnel moving about, affect the floor and those test stands which can move. Often, the motion is sufficient to change the component of earth rate sensed by the gyro and to result in a change in the required torque-to-balance. If accelerometers, tilt meters, etc., had been mounted on the stand, their outputs could have been appropriately added to the gyro signal to generate the torque command, or the level shift signal could have been transmitted into a computer, where, appropriately weighted, it could have corrected the interpretation of the torque-to-balance. Similar remarks about aided interpretation of test environments may be made with respect to accelerometer testing. Recent proposals for precision testing include tilt meters to dynamically control the attitude of the test stand. What if the test stand space conditions had called for a complete step-tumble or clock-controlled tumble in which the gyro could change its attitude with respect to gravity? How

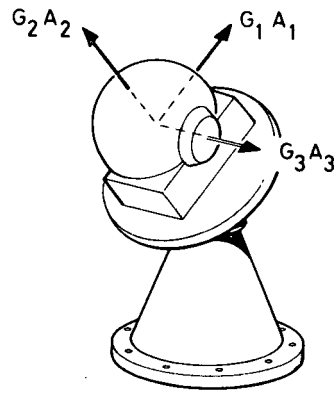

Fig. 7-19 IMU on test stand for servo run

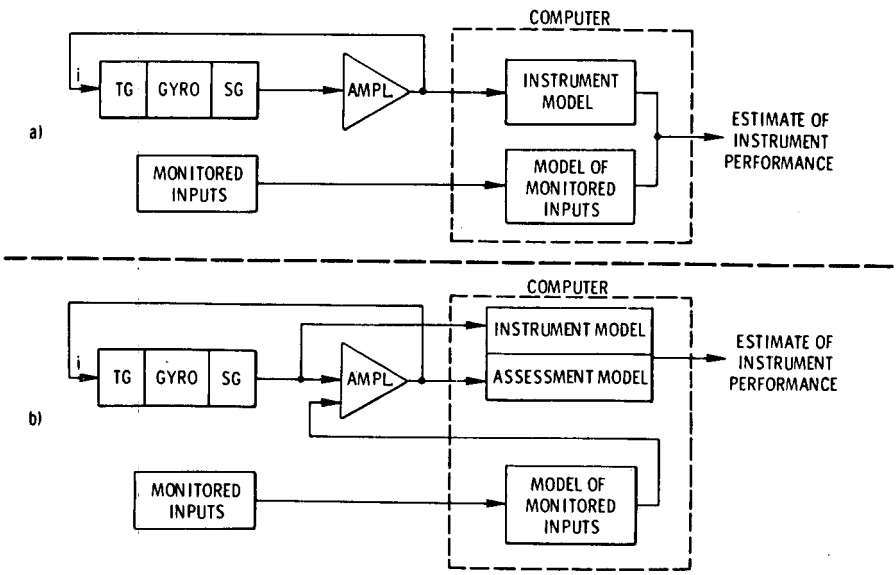

Fig. 7-20 Aided testing of gyros

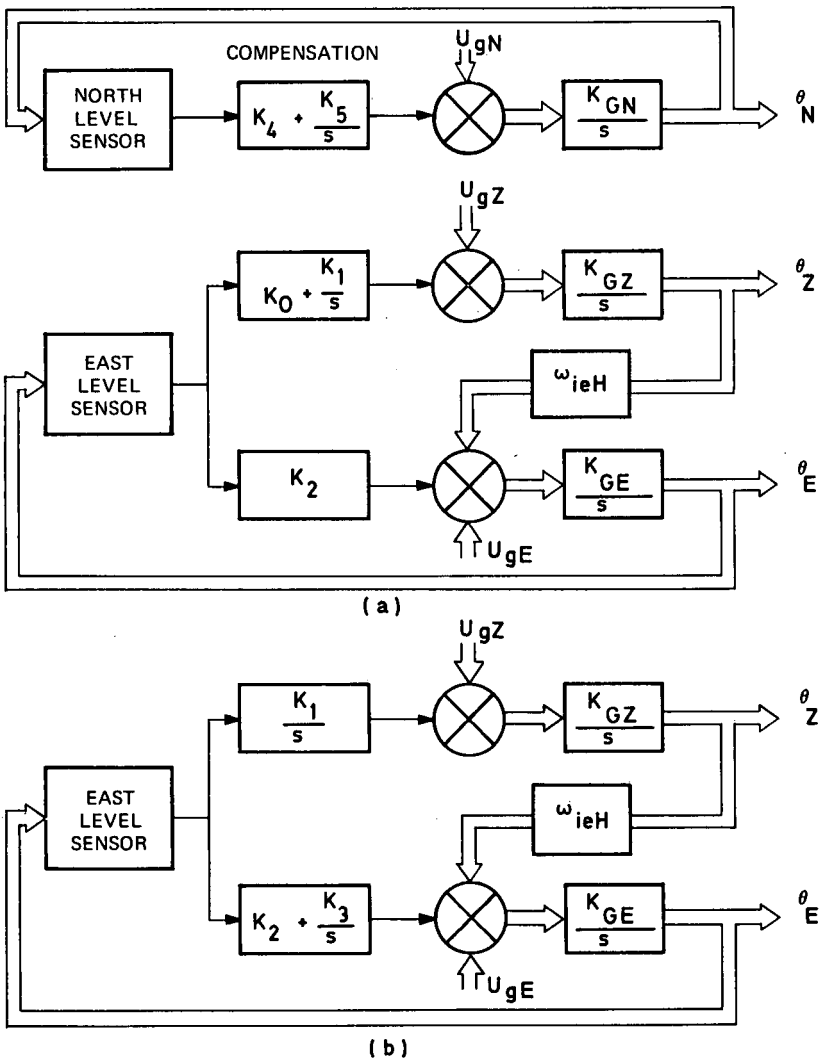

Fig. 7-21 Two gyro compass compensation schemes

many tilt meters would or could one use? The test stand conceivably could be mounted on a table whose verticality was continuously monitored and/or controlled to some fine tolerance. Clearly, the single gyro could have its indication corrected with a sensitive aid.

The instrument manufacturer, depending upon the customer's requirements, can test and pass acceptance at a broader specification or pay the extra costs to instrument properly. However, unless he instruments the test the broad tolerance may permit poorer gyros to pass. The instrument developer, presuming he is after accuracy, cannot long avoid the increased instrumentation.

Both the developer and manufacturer must consider the system-like implications of the testing. Clearly, by testing in a system both would achieve better calibrations, as would the customer, because the instrumentation and computer interfaces are present in the system and contain the aiding signals and the equipment to utilize them.

The resolution required from aids should be considered in a test. For our simple example, a rotation about north of 20 arc/sec or 10^{-4} radians results in a steady rate of angular velocity input to the gyro of 0.1 meru times the sine of latitude. This may or may not be important in terms of the instrument and its designed usage. However, if the angle were acquired in an oscillatory manner, say because of nearby equipment, people, or traffic, the small angle might be quite significant. Assuming a sinusoidal oscillation of $10^{-4} \sin\omega t$, where ω equals 1/60th of a second, the resulting angular velocity seen by the gyro is 1.6×10^{-6} rad/sec peak and is in the form $1.6 \times 10^{-6} \cos\omega t$, i.e. 23 meru.

The point of the discussion, without regard to the numbers for the example chosen, is that oscillatory background mechanical noise (particularly if it is more or less random and comes from several sources) can cause enough torque disturbance to mask the true behavior of a gyro. If the torque-to-balance loop is digital, such relatively high frequency noise can be heterodyned into low frequency readings, further complicating the testing of the gyro.

The conclusion is clear enough; the testing of single instruments must be aided by system-like use of additional sensors and appropriate computer interfaces. Computer interfaces for instruments are discussed in section 5 of this chapter. The aspects of the system-like test, the requirements for a relatively sophisticated test stand and set of sensors suggest that the test might be performed best and least expensively in a system, perhaps very much like the user's system, or in the user's platform.

9. Gyro Compassing

Gyro compassing is not only a traditional application of inertial systems, but also a method whereby a system level test may be used to derive instrument data for acceptance. In this section, gyro compasses are discussed which use accelerometers to establish the level of a platform and then null a gyro in an effort to determine east (or west). In such mechanizations, the north and east gyros also provide rate gyro damping of the platform motion and act as space integrators.

A simplified view of gyro compassing is presented in figure 7-21, where coupling between level and the Z gyro is introduced so that the platform is caused to rotate about vertical to null the east gyro against the projection in the horizontal plane of the earth rate vector. Note that the north loop is essentially decoupled from the east and azimuth loops. Two options are given for torquing the azimuth of the Z gyro and the east gyro. In figure 7-21a, there is no integration in the leveling action

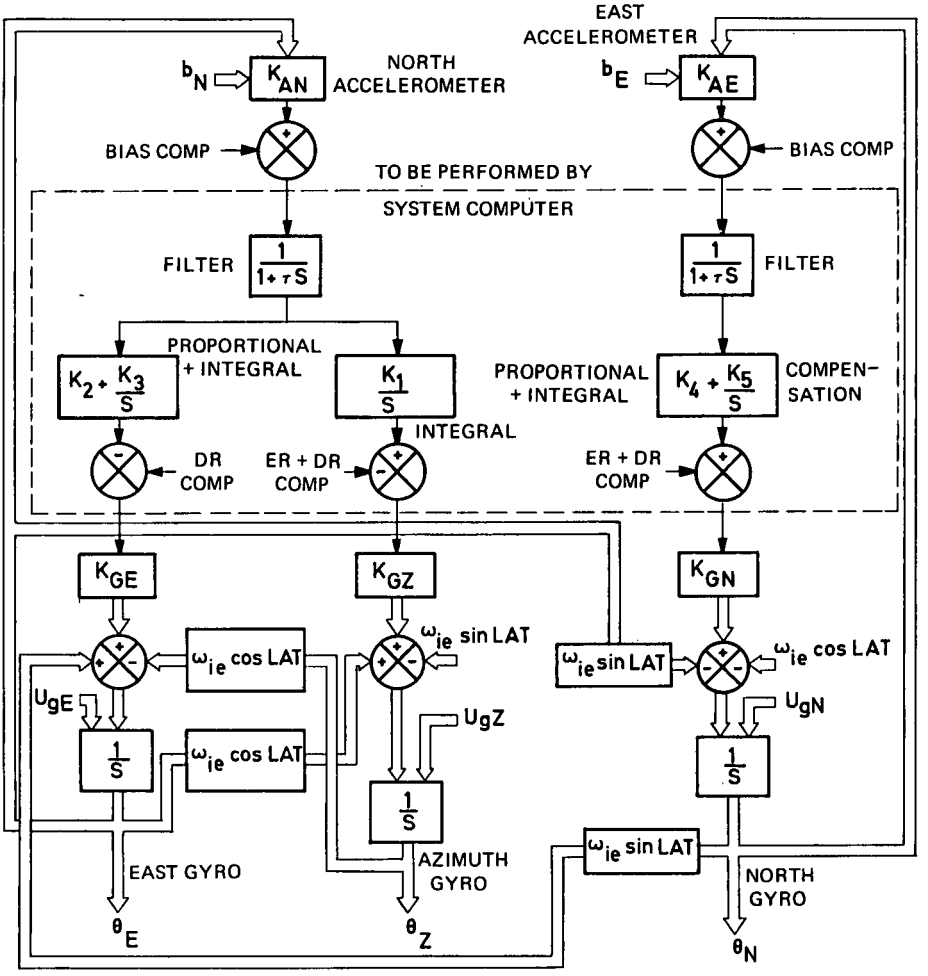

KEY:		
	$U_{gN, E, Z}$	GYRO DRIFT
	$b_{E, N}$	ACCELEROMETER BIAS
	ER + DR COMP	EARTH RATE + GYRO DRIFT RATE COMPENSATION

Fig. 7-22 Gyro compass loop linear model with East and North accelerometers

about east; instead, a proportional plus integral channel controls the Z gyro. In figure 7-21b, the proportional plus integral control is applied to the east gyro and simple integration is applied to the Z gyro. The requirement for dynamic stability of the coupled loops necessitates the either/or choice in the manner of control. The mechanization shown in figure 7-21b is considered an improvement because the extra integration in the east leveling loop permits not only the gyro but also the accelerometer signal, interpreted as level, to be nulled in the steady state. The description of the action of leveling with an accelerometer applies, with relatively slight changes, equally well to mechanization utilizing PIGAs. The advantage of applying integration at different points in the gyro compass loops assumes the availability of a digital computer performing the integrations; some of the mechanization and conclusions would change if only analog computer integration were available.

Accelerometer uncertainties and incorrectly scaled biases and scale factors will tilt the platform and change the component of earth rate to which the gyro is nulled. Similarly, gyro uncertainties and incorrectly scaled quantities such as bias, mass unbalance, etc., can cause platform angular deviations about the gyro input axes. The purpose of integration in the leveling loops before the gyro is to reduce the angular deviations to zero in the steady state. The steady state stored output quantities on the leveling loop integrators represent approximate components of earth rate and gyro drift seen by the gyros and nulled by the leveling loop action.

A more detailed presentation of gyro compassing is shown in figure 7-22, which includes the components of earth rate and instrument uncertainty. By observing a gyro compass and measuring the angular deviations in vertical and azimuth against a reference, say with suitably referenced autocollimators and monitoring mirrors on the platform, a calibration of instrument uncertainties may be performed, particularly if there is an ordered permutation sequence of which instruments are vertical and east. If the deviations are forced to null, the quantities stored in the computer taken from the steady state outputs of the integrators may be used to resolve the several instrument coefficients. In effect, by gyro compassing, the platform automatically goes to the required test orientations.

A particular gyro compassing scheme has been presented in this section merely as a vehicle for demonstrating that system mechanization, including the computer, can be extended to include calibration as a modification of regular operation rather than as a totally separate operation. By so doing, the calibration of instruments is carried out analogous to the manner in which they will be used in the system and in the operating environment. Further, it may be expected that system software will be reduced and calibrations become more accurate.

10. Centrifuge Testing of Instruments in a System

The testing of instruments on a centrifuge is a difficult and expensive art. Some of the difficulty arises because of a lack of quantitative precision in knowledge of the environment being imposed upon the instruments. In many instances, the instruments tested are of greater precision than those providing the background instrumentation.

As examples of the difficulties of quantitatively assessing performance and establishing coefficients, consider that slight tilts of the centrifuge, both static and dynamic, change the actual input to a gyro and that varying centrifuge arm deflection changes the angular rate coupling into the gyro as well as the acceleration environment. Because of this and other difficulties, gyros are sometimes tested in pairs (to establish by coherence the degree of tilt) on controlled tables which have angle adjustment capabilities, etc. Similar arrangements are carried out for

accelerometers. Often, the instruments cannot be operated in a normal manner. Gyros are sometimes run at slow speed in a torque-to-balance mode so as to reduce the effect of centrifuge arm deflection coupling the high centrifuge rate into the gyro. The torque commands stay within the bounds of the gyro torquer capability while still permitting resolution of the torque variations. However, the g-dependence of the gyro is probably changed with the gross change in wheel speed, as is its internal thermal environment. In fact, for some gas bearing instruments, slow speed operation may so reduce the bearing stiffness as to preclude the testing altogether except at normal speed in a stabilized platform. In general, instruments to be tested on a centrifuge over a wide range, but in a non-stabilized environment, have the conditions of operation so altered as to shed some doubt with respect to a quantitative coefficient data and performance assessment.

Traditional and novel approaches to instrument level centrifuge testing are described in other chapters in this volume. One approach considered in the past at MIT/IL has been to build up a special purpose inertial platform with an appropriate complement of gyros (and accelerometers) to control and indicate the g environment of the instrument under test (which itself may have been in the control system). In effect, this is a special purpose inertial system but has not been exploited to any degree.

A sample computation is presented to demonstrate the performance trade-off involved between the fixture support and the inertial platform support for a gyro undergoing a centrifuge environment. Assume a 32-foot radius centrifuge and a 100-g environment, which corresponds to an angular velocity of 10 radians per second. If the gyros on the platform have a mass unbalance term in the order of 10 meru/g, the platform drift is one eru. If compliance terms exist in the order of 1 meru/g^2, the drift will be in the order of 10 eru. The total drift of the platform might be 11 eru (a good part of which is expected) which is about 10^{-3} radians per second. If the gyro were tested in a fixture and the misalignment of the fixture and 'wobble' of the centrifuge totaled only 20 arc seconds (or 10^{-4} radians), the coupled centrifuge rate into the gyro would be

$$10^{-4} \text{ radians} \times 10 \text{ radians/second} = 10^{-3} \text{ radians/second}$$

The point of the comparison is that fixturing and centrifuge alignment must be known very well to be competitive with platform support for gyro testing on the centrifuge. Similar computations could be carried out for accelerometer testing.

The testing of systems in unusual environments to partially simulate mission environments (and the introduction of nonmission environments) taxes the ingenuity of the system developer. But in many ways, instrument evaluation by system testing on vibrators and centrifuges is easier than at the individual instrument level. The testing of an accelerometer on a gyro stabilized platform on a centrifuge may subject the accelerometer (or velocity meter) to an input of acceleration with a first derivative or 'jerk' term significantly greater than that imposed by the mission. Correct monitoring of the environment and of the several inputs to the instruments is essential for really understanding the instrument model. High-g testing is imposed to evaluate scale factors and nonlinearities. For example, an accelerometer may have a cubic nonlinearity or the integration of the jerk-to-position may be inaccurate either in the integration or estimating the 'jerk' input. Wide dynamic range accelerometers are typically nulling action instruments, as in the case of the PIGA and the pulse integrating pendulous accelerometer. Incomplete nulling introduces cross axis coupling and errors.

Complete system or platforms have been tested on centrifuges at MIT and elsewhere and a new facility has been under development for some time at the USAF Missile Development Center at Holloman AFB, New Mexico. For testing systems, the

centrifuges are generally equipped with a counter-rotating table at the place on the arm where the system platform is attached. The counter-rotating table removes the gross centrifuge rotation from the environment of the test system and, to a degree, relieves the platform servo. However, care must be exerted that the table does not insert large amplitude high frequency angular vibration because of its control parameters.

The system is usually operated in an inertial mode with fixed torques commanded on the gyros derived from quiescent requirements to fix the platform to the earth. Additional torque commands may be inserted to the platform gyros according to the g-sensitive model coefficient estimates, with the g-measurement supplied by the accelerometers. In this way, the platform coordinate frame is substantially known and constant except for incompleteness in the model implemented or errors in the coefficients. An alternative to gyro torquing is to keep the platform inertial and compute the rotating coordinate frame of the accelerometer's indication and perform the required computations in that frame. For either approach or mix of approaches, before and after measurements may be made of the platform alignment by traditional optical means to check the boundary conditions on the computation.

When the test system platform is mounted on a counter rotating table on the centrifuge, the situation is similar to testing the platform on a test stand which varies its orientation with respect to the gravity and earth rate vectors. Although the centrifuge's acceleration and rate environment may not be known precisely, the instruments' indication can help in a 'boot strap' manner to calibrate the various instrument model coefficients. For example, the cyclic nature of centrifuge acceleration plus gravity can help determine the centrifuge-imposed environment and the accelerometer coefficients by consistency checks on the root sum square acceleration. Techniques akin to 'vector matching', i.e. determining the variation of accelerometer alignment with time while in the centrifuge environment, help to check gyro g-dependent drift model. Coefficient sensitivity to thermal and electrical parameters may be used and validated as part of the centrifuge testing.

As further test techniques, the counter-rotating table or the platform servos (via gyro torquing) may be commanded to go through cyclic or complete rotations so as to introduce into the environment of the instruments a low frequency modulation of the g environment. This can serve to help in the partitioning of the environment and 'boot strapping' of the calibration/modeling process.

The techniques are not discussed here at great length because they are peculiar to the facilities available, the platform and instruments to be tested, and the proposed mission of the system. However, the system platform and supporting hardware serve not only as a very convenient test vehicle for the instruments, but also probably at least cost provide the most realistic environment contributed by supporting hardware and the greatest possibility for the proper mode of instrument operation.

Another aspect of centrifuge testing is the high rate of data flow from the instruments and environment sensors and the need for fine resolution to prevent computer round-off problems, etc. For example, consider testing a PIGA at 10-g on the 32-foot radius MIT Centrifuge (Fig. 7-23) with the arm rotating at approximately 3 radians/second. (Note: The sphere at the end of the centrifuge arm contains a counter-rotating table which is capable of supporting an entire system or fixture with instruments.) The horizontal acceleration seen on a stabilized platform is 320 sin 3t $(ft/sec)^2$. The resulting velocity is 107 cos 3t (ft/sec). If the quantization resolution of indicated velocity is 0.1 ft/sec, the computation is limited per cycle to 10^{-4} resolution, with added computational difficulties if the instrument were supposed to be tested and coefficients determined to one part in 10^5. PIGA bias error will cause the instrument to pass through resolution thresholds imposed

by quantization but a problem has been indicated, i.e. high data flow which can choke the data processer and fineness of required quantization. If the PIGA rate can be obtained, it can be used to improve the resolution without saturating the computer. Here again data from the computer and other PIGAs on the platform permit better modeling of the acceleration field and bypassing some quantization difficulties. If two PIGAs are substantially in the plane of the centrifuge rotation and are orthogonal to each other, the velocity indication of one may be scaled for quick estimation purposes at the acceleration of the other. This and other 'boot strapping' tricks can be implemented if a computer, an appropriate program and also a system-like platform are available.

Much of the discussion in this section applies to all three levels of system effort: R & D, prototype and production. Furthermore, the techniques are adaptable to the needs of the instrument developer. While the initial costs of an equipped system may seem high relative to the costs of specially constructed test tables, careful examination might reveal that the system approach using a stabilized platform is less costly than several special fixtures, most repeatable, and most realistic in simulating real instrument performance under valid operating conditions. Many of the remarks made in this section with respect to the advantages of inertial platform mounting, rather than special fixtures for instruments under centrifuge testing, apply equally to other harsh environment simulation testing such as vibration and shock.

11. Costs

The estimation of costs related to testing improvements as a function of test method is complicated because the influence of precision and performance goals dominates the costs, which are also influenced by the rate of testing. One expects that costs are greater to test performance to one meru than to 10 meru for gyroscopes. Similar remarks may be made for accelerometer testing.

Questions arise as to personnel costs versus automation, flexible and accurate test stands versus a multiplicity of fixtures, test stands versus system platforms, flexible electronics versus system electronics, and in-depth testing of selected units versus fast scan testing of many units. The list of questions can be so extensive that considerations will be presented here only in the context of high performance requirements and a comparison of system testing to component testing for instrument evaluation.

The surprising fact is that improved performance does not add incremental costs in proportion to the performance increase. The starting production base and the degree of competition present, not only in the first selection but also throughout a program, seem to influence costs as much as performance level. Moreover, proper planning for the fact that problems will arise can keep the cost of solving problems in bound. Unfortunately, costing figures are very much the private preserve of the contracting parties and not to be quoted. Moreover, R & D costs when factored into delivered item costs confuse overall program costing figures.

However, some insight and useful cost estimates may be made in terms of test equipment relative to real or simulated system hardware. For example, the precision test stands made by J.W. Fecker, Inc. (Pittsburg, Pennsylvania), Wayne-George Corporation (Newton, Massachusetts), etc., cost between $50 000 and $150 000. The cost of the test stand includes the associated electronics required for servicing the stand. Precision electronics units are required to excite and interpret signals from the instrument under test. Although these electronic units are fabricated by techniques different from system electronics, their costs are comparable or greater. A high performance system platform with its comple-

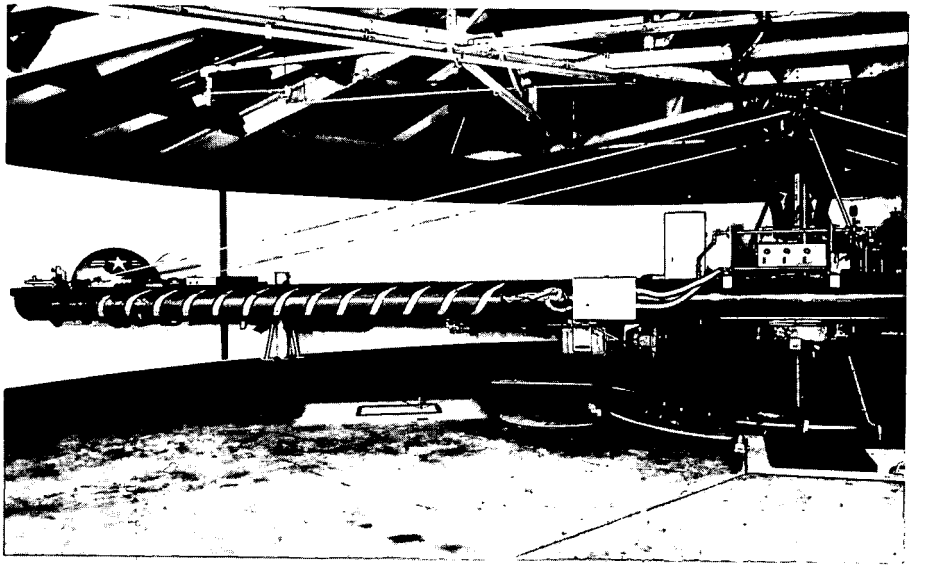

Fig. 7-23 MIT centrifuge

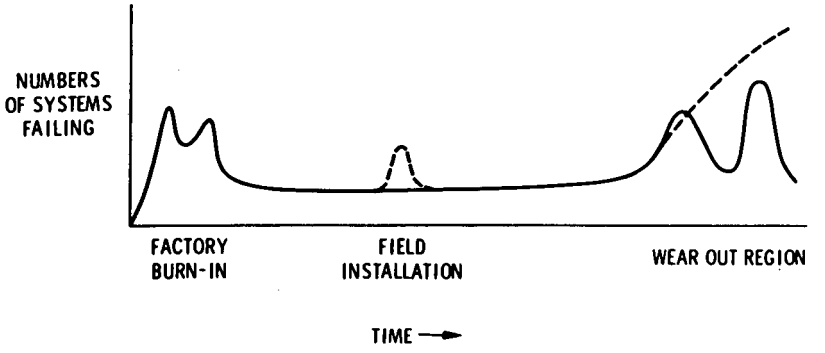

Fig. 7-24 Failure curve for a system

Table 7-1 Costs estimates

Instrument Level Testing

Capital equipment:

Test stands	150 K
Instrument support electronics	50 K
Computer (a fraction allotment)	30 K
Interface and recording equipment	20 K
Total	\$250 K *

*Multiplied by 2 for gyros and accelerometers = \$500 K

and $500 \times \frac{3}{n} \times R$ = Millions of Dollars

to support delivery rate through Test and Acceptance

where n = number of instruments on one stand
R = delivery rate

Minus fraction used on later programs or carried over from previous programs (assuming equipment is appropriate).

System Testing

Capital equipment:

Test stand (stand may be relatively simple)	50 K to 150 K
Computer (a) fraction allotment	30 K
(b) system computer	0
Total	\$50 K to 180 K *

*Multiplied by R to support delivery rate through Test and Acceptance date and Burn-In

where R = delivery rate

Minus fraction used on later programs or carried over from previous programs (simpler requirements).

Common costs (not included above):

Proper building with maintenance
Surveys, etc
Testing personnel
Data reporting

ment of instruments and electronics costs between $100 000 and $250 000. Thus, the equipment costs for testing instruments on a stand or in a system platform are comparable.

The degree of automated monitoring and direct interface with computers affects costs in a parallel manner. Here, if the monitor modes are part of the system's normal operation, the costs are low; if not, costs and flexibility of approach can be compromised.

Flexibility of component testing on a test stand superficially seems very high. In fact it can be high, but experience and review at a number of facilities indicates that all too often the available flexibility is not utilized and that monitoring is skimpy and quasi-manual. Further, the computer interface is not as well handled as it is in a system. As the instrument testing is improved in quantity and depth of testing and monitoring, the techniques become more and more like system level testing.

Estimation of costs in this chapter is largely philosophical for the many reasons stated, although such estimation is a 'life or death' problem in the real world. Table 7-1 shows some gross estimates related primarily to capital equipment costs. Personnel, test laboratory construction and maintenance, surveys, etc., are assumed common to both methods of textured accepting instruments, either as instruments or in systems. In fact, an instrument test and acceptance laboratory may have to be physically larger for handling the equivalent number of instruments.

The author's personal opinion on controlling costs and delivering reliable systems of expected performance follows. Instrument manufacturers should do sufficient testing to instill confidence when delivering instruments for incorporation into a system. After a short period of 'burn in' for a system, scoring on performance evaluation of the instruments in the system should begin. Penalties for instruments rejected for performance or failure should be counter-balanced by rewards for good instruments and for benefits of extra data taken in an assembled system. Instruments destined for maintenance depots to support a repair pipeline should also go through some sort of system acceptance, perhaps by lot sampling, to insure performance will be obtained when required.

If this form of costing - reward and penalties - forces the instrument manufacturer to become more insistent on knowing how his instruments are to be used in a system and results in the upgrading of his in-house capability, so much the better. Although the upgrading and rewards may increase unit instrument costs (to cover costs of rejects), net real system costs are likely to be reduced to the customer since problems are detected sooner and pipeline activities and operational and 'in the field' life can be properly estimated.

Another parallel may be drawn between test stand testing and acceptance of instruments and system level testing. Typically, hundreds of hours of testing may be required at a system level in a so called 'burn-in' period. During this time, 'infant mortality' on various system elements is used to find and eliminate probable early failures when the system goes into operational use. Figure 7-24 shows a typical failure curve for a system. These early failures, due to component problems (instrument, mechanical or electrical), are corrected and the system then works for a period until the conventional 'mean-time-to-failure' statistics influence useful life. The 'burn-in' period is used to provide prolonged installed life. Also, the 'burn-in' period is used to establish instrument coefficients according to a model predetermined for the mission. Thus, a platform will exercise the instruments against gravity and earth rate as described previously. A bank of data is built up through successive calibration cycles to achieve a level of confidence in coefficient data.

The 'burn-in' period may be of the order of five percent of the installed life prior to a programmed (or required) maintenance cycle. Clearly, 'burn-in' time is expensive, although no dollar cost is estimated here. Premature failure in the field is really expensive, especially if insufficient 'pipeline' support exists to sustain the system in the field.

In chapter 3, a strong and valid plea is made for greater testing, quantitatively and qualitatively, of instruments prior to their acceptance in a system. With the cost of testing high and representing a significant fraction of useful life, both as an individual instrument and within the system, the suggestion is made here that overall program costs can be significantly reduced and data management improved by increasing the fraction of instrument testing time within a system. Most important, performance and confidence are expected to be improved, particularly if rewarded by incentives.

A significant feature of costing a program is the expected growth in equipment performance, application, and life as the program matures. In order to realize this growth, it is essential that equipment be reserved for test and evaluation in engineering (not production) where extra monitoring and computer programs of increased complexity may be implemented. Unfortunately, but in fact, too little engineering testing seems to be permitted in support of production programs at either an instrument or system level. While it is a moot point to consider which type of testing — instrument or system — is more effective, it is imperative to recognize that in-depth engineering testing is a required part of a production system and the costs will be paid, either as planned initially or many times over in a crash effort to solve problems and to maintain a sick system in the field while a retrofit cure is effected.

All too often, in order to meet equally culpable competition, all is not told to the customer. Even as the customer knows the probable deficiencies of a product, he sells the program to higher echelons of authority in order to get a program moving. Protective penalty clauses do not really protect the customer or recover losses in a competitive commercial venture and, for the military, security may be compromised.

12. Summary and Conclusions

In the course of an inertial system development, when the instruments arrive and the platform with its electronics is to be assembled, a trade-off arises; to what level should the instruments be 'acceptance' tested and calibrated as components rather than integrated into the platform and tested together in a system - like environment?

The point of view presented in this chapter is that overall system costs are decreased to the user when most of the instrument testing is done in the final use environment and performance is rewarded.

The instrument vendor clearly wishes to be paid, and quickly, for instruments delivered as acceptable and meeting an interface specification. The postponement of payment until adequate performance is measured in a system may be made less painful by incentive payments, but the real incentive is that bought instruments truly work and perform in the system. Rejecting poorly performing units will serve to cause the vendor and customer to improve specifications and reinforce diagnostic component level testing and provides the only possible corrective feedback. While interim costs might be higher to cover vendor fees, real customer costs are reduced because he has bought only real performance and the user knows he has what he has planned for or has implemented alternatives quickly. The requirement

for testing in a system environment becomes more important when multiple vendors are employed.

Instrument developers are becoming increasingly aware of the user requirements and instrument test techniques are becoming more like flexible systems in themselves. The sophistication in instrument testing, however, is in itself not sufficient because it is without the real environment. Ultimately, the proof of acceptability of the instruments is performance in the system. Adequate safeguards by design, test, and continual verification must insure that the particular system used as the test and acceptance vehicle does not itself contribute to poor performance.

Instruments which undergo system tests and acceptance in a platform may stay with that platform in which they are tested or may be taken out of the platform and put on the shelf: the two alternatives affect cost of testing. However, multiple testing of instruments in one system can be less expensive than testing using multiple test installations.

The savings result through a decrease in expenditure for test equipment, and a requirement that instruments work properly in the final assembly prior to being accepted and that the greater fraction of total test and acceptance time spent in the system environment provide more useful data to operationally deploy the system.

The philosophy and approach of system level testing is applicable through all phases of development of systems and instruments, from the conceptual research and development phase through prototype design and into production.

In summation, this chapter has attempted to show how the testing of inertial instruments in a system, or using system testing techniques in Research & Development, can not only be more efficient and economical but also provide improved and more valid instrument performance data. It has been shown that gyro compassing, monitoring/modeling, centrifuge testing, aided systems and the recognition that system/instrument interface specifications can possibly be inadequate, are all important factors to be considered when testing inertial instruments and cause the stress on testing in a system.

Symbols and Abbreviations

A_{IA}	acceleration along the input axis
A/D	analog-to-digital conversion
A_{OA}	acceleration along the output axis
A_{SRA}	acceleration along the spin reference axis
b	accelerometer bias
M	torque drift
E	east axis which is in the level plane
eru, meru	earth-rate-unit: angular velocity of the earth equals one eru; meru equals milli-earth-rate unit or 0.001 eru
ER + DR	earth rate + gyro drift rate compensation
e_{sg}	signal generator voltage

e_{susp}	suspension voltage
e_{wheel}	wheel voltage
g	gravity constant
G_1, G_2, G_3	gyros 1, 2 and 3
i	current
IA	input axis of the gyro unit; mutually perpendicular to OA and SRA. Its sense is such that a positive input about the input axis results in a positive output about the output axis. In all cases a positive rotation may be determined by the right-hand rule in which the thumb is pointed along the vector towards the arrowhead. The fingers, when curled about the vector, point in the direction of positive rotation.
I/O	input/output stage
i_w	wheel current
L	latitude angle
M_1, M_2, M_3	platform mirrors
N	north axis which is in the level plane
OA	output axis of the gyro unit; fixed with respect to the case and directed from the signal generator end to the torque generator end.
P_w	wheel power
P_H	heater power
R	gyro constant bias drift coefficient
RSS	root-sum-square; total vector
SA	spin axis of the gyro wheel; fixed with respect to the gyro float
SF	specific mass reaction force at a point equal in magnitude and direction to the force that a unit mass with the location and acceleration of the point applies to its supporting structure. This is commonly called specific force.
SFIR	specific force integrating receiver
SG	signal generator
SRA	spin-reference axis of the gyro unit; fixed with respect to the gyro case, SRA is in the same direction as the spin axis of the gyro wheel when the condition of zero angular displacement with respect to the case occurs (float is at the signal-generator null). Since the gyro is operated within a few seconds of arc null, SRA is usually considered synonymous with the spin axis.

t	time
T	data gathering time
TG	torque generator
T_G	temperature of gyro
U	unbalance
U_{IA}	g - sensitive gyro drift coefficient due to mass unbalance along input axis
U_{SRA}	g - sensitive gyro drift coefficient due to mass unbalance along spin reference axis
U_{OA}	g - sensitive gyro drift coefficient due to mass unbalance along output axis
V	velocity
W_{IE}	angular velocity of the earth with respect to inertial space
Z	azimuth axis; perpendicular to the level planes

References

(1) **Fertig, K. and Cox, Jr., D.B.,** 'A New High-Speed General Purpose Input/Output Mechanism With Real-Time Computing Capability', E-2175, Instrumentation Laboratory, MIT, Cambridge, Mass., Aug. 1967.

(2) **AFIPS** (American Federation of Information Processing Society) Conference Proceedings, Vol. 31, p. 281, 1967 Fall Joint Computer Conference, Thompson Books, Washington, D.C., 1967. Distributor: Academic Press, Berkeley Square, London, W.1.

(3) **Baechler, D.O.,** 'The State-of-The-Art of Aerospace Digital Computers — 1962 - 1967', IEEE Computer Group News, Vol. 2, No. 1, Jan. 1968.

(4) **Pitman, Jr., G.R.,** 'Inertial Guidance', p. 340, John Wiley & Sons, Inc., New York, 1962.

(5) **O'Donnell, C.F.,** 'Inertial Navigation Analysis And Design', McGraw - Hill Book Company, 1964.

(6) **Powers, Jr., H.B. and Henderson, V.D.,** 'Analytical Thermal Compensation of Fast Reaction Inertial Navigation Systems', Presented at the National Aerospace Electronics Conference, Dayton, Ohio, A/N Document X6-957/3111, May 1966.

8

Gyro Testing Techniques in the UK

J. V. CARTER
Royal Aircraft Establishment, Farnborough, UK

Summary

Practical interest in the problems associated with inertial quality gyros started in the UK in 1955 and a permanent laboratory devoted to the testing and development of testing techniques on inertial gyros was created.

This laboratory at the Royal Aircraft Establishment, Farnborough, has maintained contact with all organisations in the UK that are allied to this subject and many independent firms and government agencies throughout the world.

This chapter, written by a member of the staff of this laboratory, will discuss the philosophy of testing and testing techniques as applied to the RAE and to Industry where they are directly working on Government supported projects.

The performance model and nomenclature used is relatively new; it has been developed by the Central Inertial Guidance Test Facility at Holloman, USA, and agreed by an interservice panel composed of UK, USA and Canadian members. It is offered as an alternative to the well established MIT nomenclature, since it can be applied to any type of inertial quality gyro without implying a specific source for the drift coefficient.

Two basic test methods are discussed and several types of tests commonly in use in the UK are described, with a full analysis given in the appendices.

The test data and the possible uses made of it when taken under simulated platform conditions are examined to establish the suitability of a gyro design for a particular application.

The chapter concludes with a review of the more important British designed gyro test equipment in relation to the tests discussed; it looks at the problems of laboratory facilities and layout, including the siting of working test pads and the realistic requirements for their stability.

1. Introduction

Testing of inertial quality gyros in the UK has been carried out since 1955, and, because all the designs tested so far have their origin in America, it has been expedient to base many of the techniques for testing on those used by the original manufacturer.

Nevertheless once a learning period has elapsed it is understandable that a pattern of testing develops in line with national projects and policies; hence in the UK the

emphasis, both in Industry and in Government establishments, has been to align the testing of gyros to aeroplane and submarine inertial applications. There are now many designs of gyros whose claimed performance makes them suitable for inertial navigation projects. Not all of these are single-degree-of-freedom floated gyros and where applicable they will be discussed in the text.

This chapter will attempt to outline the philosophy of gyro testing that has developed at the Royal Aircraft Establishment and the influence this has had on production testing in Industry on some Government-sponsored projects.

2. Philosophy of Testing

The terms of reference to which any gyro test programme of any testing laboratory is tied can be many and varied. Perhaps the most common concept is of a continuous cycle of design, build, test; in this role the testing and interpretation of test data play a vital part, dictating modification to the design and manufacturing procedure until improvement in performance meets or exceeds the original design goals.

Any competent gyro manufacturer, to some extent, must subscribe to this policy. Where a gyro is in production to an agreed performance specification, however, meet delivery promises and an agreed price the testing specification must be closely followed.

This leads to a second aspect of testing philosophy that can be difficult to resolve. It is only with considerable experience and first hand knowledge that an agency can talk to a gyro manufacturer or system designer about the required gyro performance and test specification.

Since most engineers have a realistic limit set on performance and price the experience of an active gyro test laboratory can be of great help. This is perhaps the most important reason why, in the UK at RAE, a gyro test laboratory is sponsored by the Government. The advice from a laboratory of this nature is also very effective if a gyro evaluation is undertaken prior to or in parallel with an evaluation of stable platform performance using the same type of gyro.

A second task for this laboratory is to keep itself informed of the latest state-of-the-art development. This can be achieved, to some extent, by the purchase of samples of new gyro designs, when they become available, for detailed evaluation. In this context close collaboration between test laboratory and manufacturer can result in advantages to both. During the planning of an evaluation full use should be made of the firm's experience and advice - there is no substitute for a personal visit - and throughout the evaluation, certainly at the end, a full transfer of test results back to the manufacturer completes the cycle discussed in the first paragraph.

3. Gyro Performance

First it must be established that it is impossible to quote one number which represents a gyro's performance: even when a more enlightened manufacturer gives up to twenty or more numbers related to a gyro's characteristics they seldom give the test conditions under which they can be obtained. The performance of a gyro as an instrument is very dependent on the test conditions. Mechanical, electrical and thermal environment all have significant effects on the test figures obtained.

Nevertheless, when gyro performance is discussed the first and most important

aspect that is considered is drift. In talking of drift the assumption is made that the gyro is a stabilising element defining an axis or axes in space and it is the rate at which these axes wander that is loosely called drift. In practice there are three aspects of gyro drift.

(a) Absolute drift. Since no gyro is perfect it will drift at a rate depending on the quality of certain adjustments that are made during manufacture. Provided this rate meets the specification its value is not of great importance since it is nominally constant and can be compensated.

(b) Switch-on to Switch-on Random Drift. With each successive switch-on of a gyro there will be a variation in the measured value of the absolute drift. The degree of variation can give an indication of the gyro's long term stability and is often a significant characteristic in platform design. Its magnitude will be affected by the treatment of the gyro between tests.

(c) Random Drift. During any one switch-on any unassignable drift changes are classified as random drift (also called in-test or short-term drift). This characteristic is also significant in platform design particularly if related to real time from switch-on.

Before continuing with a more detailed discussion of gyro drift there are two aspects of gyro performance that may be important when used on a platform. These are both related to the performance of the gyro torquer. The first is the stability and linearity of the torquer scale factor, the second is the stability of orthogonality of the torquing axes in a two-degree-of-freedom gyro.

4. Mathematical Error Model and Drift Rate

It is essential from a manufacturing standpoint that if the concept of design - build - test is to result in improvement in performance then the short-comings of the gyro causing it to drift must be accounted for and understood. As a result a performance model is required and the best-known nomenclature used is that developed by MIT. This is, however, based on a single-degree-of-freedom (SDF) floated gyro and gives symbols to gyro coefficients that associate them with mechanical phenomena operating in the gyro to cause drift.

An alternative nomenclature has been proposed by the Central Inertial Guidance Test Facility in America (1): each drift coefficient is identified by the component or components of acceleration of which it is a function. So, for a single-degree-of-freedom gyro:

$$\Omega = D_F + D_I a_I + D_O a_O + D_S a_S + D_{II} a_I^2 + D_{SS} a_S^2 + D_{IO} a_I a_O + D_{IS} a_I a_S$$

$$+ D_{OS} a_O a_S + \omega_I$$

where

Ω - total gyro precession

a_I, a_O, a_S - accelerations with respect to inertial space of the gyro case along the three principal axes I (input), O (output), S (spin)

D_F - gyro drift coefficient (°/hr) independent of acceleration

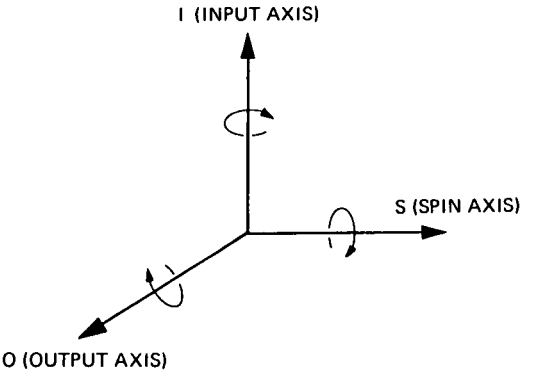

SINGLE DEGREE OF FREEDOM GYRO
(S.D.F.)

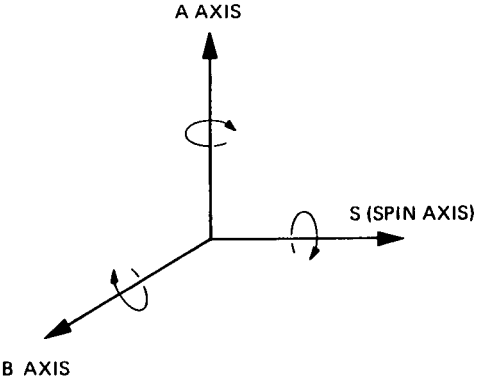

TWO DEGREE OF FREEDOM GYRO
(T.D.F.)

Fig. 8-1 Definition of axes

D_I, D_O, D_S - gyro drift coefficient (°/hr/g) proportional to acceleration

D_{II}, D_{SS} - gyro drift coefficient (°/hr/g^2) proportional to the square of acceleration

D_{IO}, D_{IS}, D_{OS} - gyro drift coefficient (°/hr/g^2) proportional to the product of accelerations

ω_I - angular velocity (°/hr) with respect to inertial space, of gyro case about input axis

g - local acceleration due to gravity, defined positive upwards.

A similar pair of equations can be written for a two-degree-of-freedom (TDF) gyro; these are discussed in Appendix A.

In order to apply this equation to gyro data a few basic definitions must be made. The axes of both a single and two-degree-of-freedom gyro are illustrated in figure 8-1. The three gyro axes form a right-handed, orthogonal co-ordinate frame such that $\bar{I} \times \bar{O} = \bar{S}$ or $\bar{A} \times \bar{B} = \bar{S}$.

The spin reference axis is the position of the spin axis when the pick-off output(s) are at null. Since in all the test methods discussed the pick-off output is very near to null, the spin axis and the spin reference axis can be considered to be coincident and the term 'spin axis' will be used.

Gravity can be considered either as a specific force with its vector directed downwards or as an upward apparent acceleration. The second convention is chosen since it is consistent with the application of inertial instruments in vehicles subjected to accelerations.

5. Methods of Operating Gyros for Test Purposes

Single Axis Servo Table Test

There are two principal test configurations used to operate a gyro. In the first, the gyro is provided with a third degree of freedom by mounting in a gimbal such that the gyro input axis is parallel to the gimbal axis. When a servo is closed from gyro pick-off to gimbal torque motor, such that the pick-off is held at null, the gyro is then acting as a stabilising transducer and defining an axis in space. Gyro drift can then be measured as the rate of rotation of the frame holding the gimbal relative to the gimbal holding the gyro.

The drift rate of inertial gyros is small and since the measurement of small rates can present problems the gyro is usually positioned such that a component of earth's rotation comes into the measurement.

The rate of rotation of the earth with respect to inertial space is 15·041 degrees per hour and the vertical and horizontal (north/south) components are $\omega \sin \lambda$ and $\omega \cos \lambda$ respectively, where λ is the local latitude. If then the test positions are chosen to have the gimbal axes of the test table either vertical or horizontal north/south, the rates to be measured at mid-latitudes are of the order of ± 10 degrees per hour plus or minus gyro drift. For a one-degree angle the times to be measured are around six minutes.

The principal advantage of this test configuration is that the gyro operation is

SDF GYRO

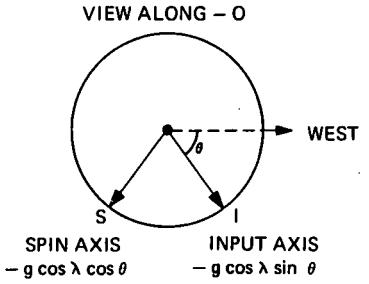

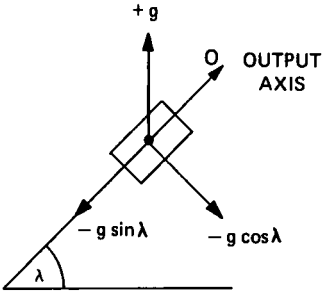

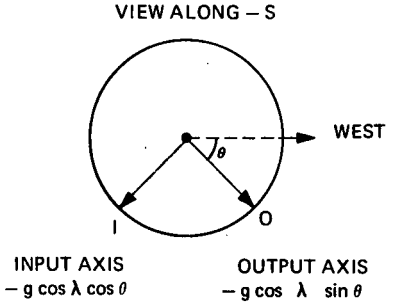

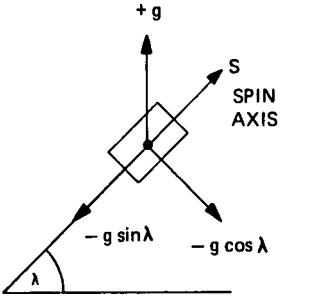

TDF GYRO

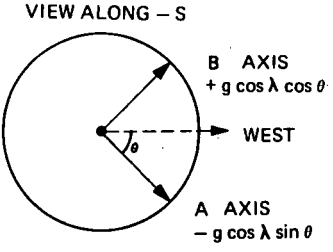

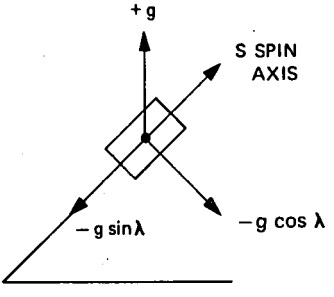

Fig. 8-2 Diagram of tumble test axes

similar to that of a gyro in an inertial platform and drift data can be measured without the use of the gyro torque motor. It can also be claimed that since the important feature of gyro performance is that the long term average drift should be satisfactory the long measuring time of six minutes is no disadvantage.

In relating this test to a TDF gyro it has not been necessary to provide a two-degree-of-freedom test table. Each axis of the gyro in turn can be used to stabilise the test table while the second axis can be held orthogonal by a simple servo feeding pick-off to appropriate gyro torquer.

Rate Mode Servo Test

The second and by far the most common test method is known by various names – rate mode, torque to balance mode and torquer feedback mode - but since the servo used takes the pick-off signal and feeds the appropriate current to the gyro torque motor (torquer), thus making the gyro a rate gyro with an electrical spring, the term 'rate mode' will be used in this chapter.

The assumption is made that the current flowing in the torquer necessary to hold the pick-off at null (or very nearly null, depending on servo gain) is a function of the total gyroscopic torques, i.e. input rates due to the motion of the case with respect to inertial space and error drift rate torques internal to the gyro.

The first obvious advantage of the method is that the expensive, complicated, servo gimbal test table is not necessary for operation of the gyro and that if a means of recording the current with the necessary resolution and accuracy is provided, a ready means of measuring instantaneous gyro drift continuously is available. The analysis of the test data does, however, rely on knowledge of the torquer scale factor (S_T) and its stability and linearity.

It is perhaps fortunate that in the development of modern inertial quality gyros high accuracy has been demanded from the gyro torquer - certainly in the SDF floated gyro 0.01 per cent for stability and linearity is not uncommon.

The many advantages of this test mode become apparent when considering testing under a variety of environments; measurements of the effect on gyro performance of accelerations applied by a shaker or a centrifuge cannot be made in any other way.

6. Types of Test

Before discussing various types of test that are applied to inertial gyros in the UK it is worth stressing again that at least some of the tests must bear relation to the application for which the gyro is intended. There seems little relevance in testing a gyro continuously for five days when the application intended is in an aeroplane flying two-hour sorties, or subjecting a gyro to severe acceleration environment when the system will be used in a civil airline type of environment.

Nevertheless there is one particular type of test that is worthwhile applying to any gyro irrespective of its application and this we call the 'polar axis tumble test'.

Polar Axis Tumble Test

To perform a tumble test the gyro is mounted on a rotating table so that the table

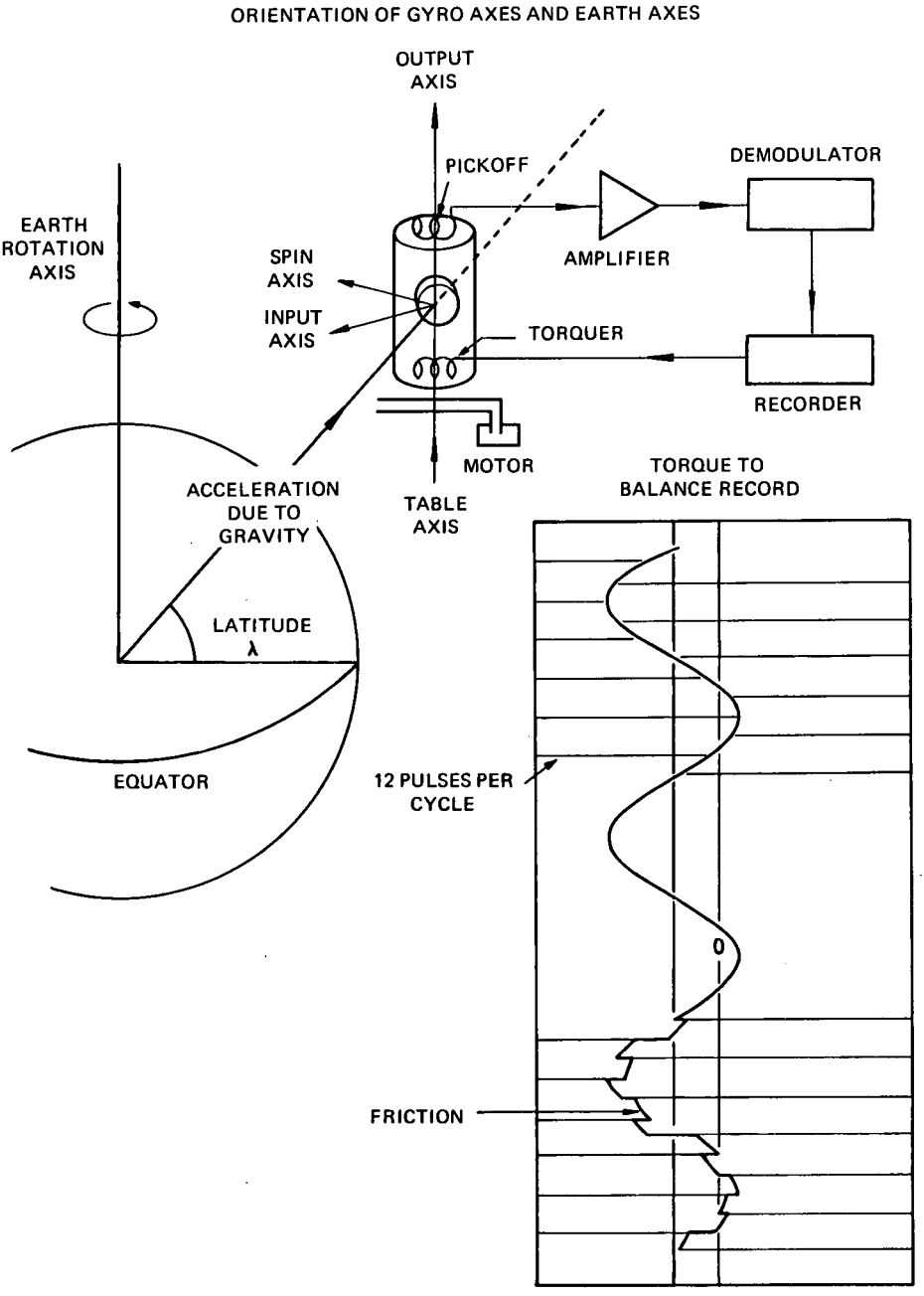

Fig. 8-3 Polar axis tumble test

axis and the gyro output axis in an SDF gyro or the spin axis in a TDF gyro are parallel to the axis about which the earth rotates (Fig. 8-2). In this arrangement the gyro does not sense either the earth's rotation or the table rotation since input axes remain perpendicular to both axes.

When the rate mode servo is closed to maintain the pick-off at null the spin axis is maintained orthogonal to the input axis (axes) and the current in the torque motor is a measure of the torques acting on the gyro.

Once the gyro has stabilised thermally (it is common to temperature control all types of inertial gyros, not just floated types) the test is started by switching on the table rotation with the input axis in a known position. The choice of table speed is not critical: for an SDF gyro it must be low enough to ensure that no large forces act on the pivots due to the rotation about the output axis. A rotation speed of 150 degrees per hour is commonly used and the test can continue for as many revolutions as is considered necessary.

There have now developed two independent philosophies on this type of test; in the first it is used in a qualitative sense and in the second for quantitative measurements of the maximum number of gyro coefficients obtainable in a single gyro test.

In the qualitative sense the table rotates continuously and at every 30-degree position of the table electrical contacts inject a pulse of current into the gyro torquer to rotate the float against the servo through a small angle (say 2 arc minutes). The direction of the float rotation is reversed by alternating the sign of the pulses and the disturbances show clearly on the analogue record (Fig. 8-3). Inspection of the recorded output reveals sinusoidally varying torque changes at table rotation frequency, caused by the component of acceleration due to gravity, in a plane normal to the sensitive axis of the gyro, acting on any unbalanced moment. Any offset of the sine wave from the recorder zero indicates the magnitude of non-acceleration-sensitive torques. Because the chart must contain the peak to peak torque changes it is understandable that the sensitivity is usually too low to observe the torque changes due to cross-compliance effects attributed to a gyro in the complete error model.

The effectiveness of this test in this form is its ability to search out manufacturing faults in a gyro quickly and avoid unnecessary waste of test time. Dr. Wyatt, in his chapter on diagnostic testing and design shortcomings, will illustrate this aspect in greater detail.

This test, performed for three cycles of rotation in both possible attitudes (OA up and down for SDF gyros and SA up and down for TDF gyros), is used by every gyro manufacturer in the UK and by many customers who require a quick test for quality assurance before installation on a platform.

The major problem that this test presents is one of specification, permitting suitable gyros to proceed in production and rejecting any that are suspect.

In the final analysis the test is an artifical one and does not operate the gyro as a stabilising transducer; on the other hand with respect to our error model it is easy to predict the output from a well made gyro. The problem then is one of deciding, when a gyro shows anomalous behaviour, if at some time in the future this fault will cause the gyro performance to fall below that required by the system.

The most common fault that occurs is a step change in rebalance current (gyro torque) as a result of the applied pulses and is often referred to as friction, but

a

random deviation in the expected torque pattern unrelated to any disturbances is also found.

Since production gyro testing must be reduced to an inexpert qualitative specification it is worth quoting from one such document that was applied to an SDF gyro in the UK.

"(a) Tests shall continue for three complete revolutions of the table with the gyro mounted OA up, followed by three revolutions with the OA down.

(b) The performances of the gyro as determined by these tests shall reach the following standards:

Friction -

Friction steps of less than $\frac{1}{4}$ degree per hour can be ignored.

The gyro shall be rejected if any friction step exceeds 1 degree per hour. Friction steps between $\frac{1}{4}$ and 1 degree per hour shall be added over each set of three cycles and the sum must not exceed 2 degrees per hour.

A friction step is measured as the deviation of the record from that which would be expected by interpolation from the adjacent part of the record.

Deviation from sine wave -

The current recorded shall at no place depart from the mean sine wave by more than the equivalent of 0·5 degree per hour except for the case of friction steps already covered. It will be sufficient to judge this by eye and relates only to the possible appearance of humps on the record."

This quoted extract illustrates one attempt to compromise with the problems that have in the past existed, and to some extent still exist, in the production of floated gyros.

It is quite feasible to perform a detailed analysis of these records to calculate the more important gyro coefficients, but the accuracy is limited to uncertainty of greater than 1 per cent of full scale of the recorded output and if this has to contain swings of up to ±3 degrees per hour then the resolution is limited to some hundredths of one degree per hour.

A possible source of error in the test is the misalignment between gyro axis and table axis; since the table rate is high (150 degrees per hour), an angular error of 1 arc minute will allow the input axis to sense more than 0·04 degree per hour. An estimate of the magnitude of this error can easily be established by reversing the direction of table rotation but, for this and other reasons, when the test is performed in a quantitative sense the table is stopped in each of the attitudes from which data is required.

Twelve Position Polar Axis Tumble Test

Appendices B and C give in detail the results of Fourier analysis of this test for both SDF and TDF gyros and it can be seen that an estimate of a large number of the gyro drift coefficients can be made from this one test.

To overcome the problem of lack of resolution in the analogue record the torquer current can be digitised and, provided sufficient time is allowed to count the pulses, resolution to 1/1000 degree per hour and better can be achieved. The application

of an integrating digital instrument to gyro testing will be discussed in detail later.

The test table is programmed to move from one 30 - degree position to the next at a relatively fast rate of 600 degrees per hour; a table contact then starts a clock that inhibits the table drive motor for a preset period of time, depending on (a) the time required for the gyro to recover from the table rotation and (b) the integration time required to digitise the output to give adequate resolution (typically several minutes to settle and five or ten minutes for the integration).

This brings up a debatable aspect of gyro testing philosophy – that is, the period of time taken to perform a particular test. The error model we use is a relatively simple one and from a practical point of view quite rightly so, but the degree to which it applies to a particular gyro will vary greatly, since all gyros possess drift characteristics that vary with time. If the sensitive element touches a limit stop this can put a step change in drift and our error model makes the rash assumption that if we reverse the acceleration vector we exactly reverse an acceleration-sensitive torque affecting gyro drift.

Therefore it is worth remembering that the estimate of drift coefficients will only be as valid as the gyro allows in respect of its sensitivity to (a) the test conditions, (b) its fit to the error model and (c) time.

Nevertheless a twelve position stopped polar axis tumble test with the output axis north and south for an SDF gyro and spin axis north and south for a TDF gyro can give a calibration of more gyro drift coefficients than any other single test.

Other Multi-Position Tests

From the beginning of our work on inertial gyros some form of multi-position test has been used to measure the more important drift coefficients. This requirement resulted in the design and development of a test table having complete rotational freedom about each of three axes.

The manufacturer of the early SDF gyros tested in the UK used a six-position test in servo mode to calibrate the gyro for non-acceleration-sensitive and first order acceleration-sensitive drift coefficients. The six positions were simply OA up and down, SA up and down and IA up and down. As mentioned previously, the input axis was positioned such that $\pm \Omega \sin$ or $\cos \lambda$ acted as the rate input to give practical values of rates for measurement and the gyro torquer, although not used during the actual measurement, was used to precess the gimbal back for the start of the next measurement through the same 1 degree angle. Five measurements of rate were made in each position to give an estimate of the in-test stability. Confidence in the table angular read-out system soon eliminated the use of a single 1 degree angle, so to reduce the test time five adjacent 1 degree angles were adopted with an interval counter operated at the end of each degree.

With some designs of torquer it was found that drift could be modified as a function of the polarity of the precession current prior to switch-off and, thanks to our three - degree - of - freedom table design, a test procedure was developed whereby the complete test could be performed without using the torquer: the input axis was alternately positioned to see positive and negative earth's rate by rotation about the gyro output axis. Figure 8-4 sketches the gyro positions for each of these tests.

Testing in servo mode is to some extent obsolescent, for with the increased confidence in torquer stability the majority of multi-position testing is now performed

in torquer feedback mode and the number of positions increased to eight to enable calibration of the torquer scale factor. This test, which is written into a current specification for a British SDF floated IN gyro, takes the following form (Fig. 8-5).

Warm-up position - 1 Rotor on 10 minutes after heaters. Test starts 1 hour after switch on.

Position - 1	OA up	IA south	Record for 30 min, measure mean level over last 15 min.
+ 1	OA up	IA north	Record for 15 min, measure mean level. Record for 1 hour with 2 arc min pulses every 10 min (use value of 6 × 10 min means to compute in-test standard deviation as vertical gyro).
3	IA up	SA south	Record for 30 min. Measure mean level over last 15 min.
4	IA down	SA north	Record for 30 min. Measure mean level over last 15 min. Record for 1 hour with pulses (use values of 6 ×10 min means to compute in-test standard deviation as azimuth gyro).
5	SA up	IA north	Record for 15 min. Measure mean level.
6	SA down	IA south	Record for 15 min. Measure mean level.
+ 2	OA down	IA north	Record for 30 min. Measure mean level over last 15 min. Record for 1 hour with pulses (use values of 6 ×10 min means to compute standard deviation)(only if required).
- 2	OA down	IA south	Record for 15 min. Measure mean level.

First, one criticism of this test in the light of previous remarks is the length of time taken to perform. A full working day of nine hours is necessary but as a result of the test the data contains a large amount of information.

In the error model equation written for each position in figure 8-5 the coefficients D_O, D_{II} and D_{SS} are neglected and by taking one half sum and difference of appropriate pairs of equations the following coefficients are derived:

(a) torquer scale factor S_T for both OA up and down.

(Note: gyros with end play in the pivots and inadequate torquer design may show a marked difference.)

(b) values for D_F for OA up and down and, if one believes this to be the most stable drift coefficient, then by substitution –

(c) value of D_F for IA up and down,

(d) value of D_S for SA up and down.

(Note: it is surprising how the degree of equality of the values of the same coefficient measured in two attitudes can vary with the design of gyros. A design that

ORIGINAL SIX POSITION SERVO-TABLE TEST

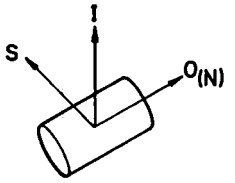

POSITION 1

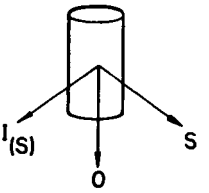

POSITION 3

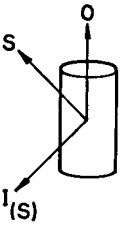

POSITION 5

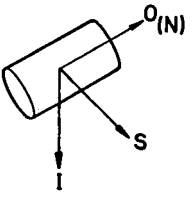

POSITION 2

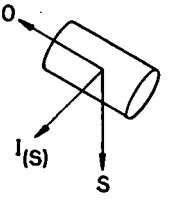

POSITION 4

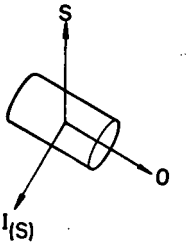

POSITION 6

MODIFIED SIX POSITION SERVO-TABLE TEST

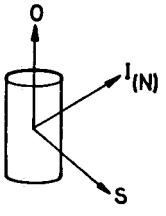

POSITION 1

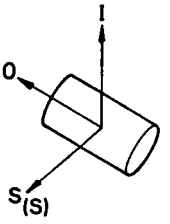

POSITION 3

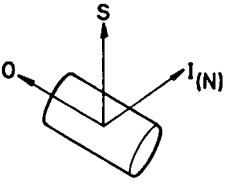

POSITION 5

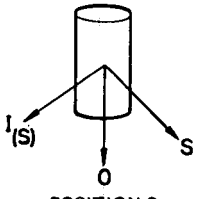

POSITION 2

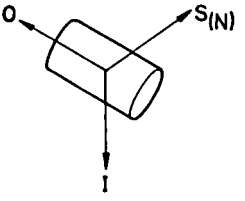

POSITION 4

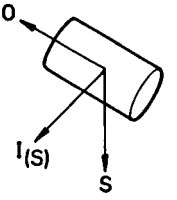

POSITION 6

– NO ROTATION ABOUT I WHEN CHANGING POSITION
– EXCITATION OF TORQUER NOT REQUIRED

Fig. 8-4 Gyro positions for servo-table test

fits the error model is likely to inspire confidence but a bad fit need not necessarily be a prediction of bad performance in a particular application. Extension of the error model to include D_{II} and D_{SS} can, at least mathematically, account for this discrepancy.)

(e) from positions +1, 4 and +2 an estimate of the in-test stability as a vertical gyro (positions 1 and 2) and an azimuth gyro (position 4). This is normally computed as a standard deviation. The pulses alternately applied to rotate the float of the gyro make the test more severe but do search for torque changes that could affect the gyro drift.

When this test procedure is repeated five or six times on separate days with complete shut-down between tests the computed data can be analysed to give an estimate of the day-to-day variation of the drift coefficients.

This procedure illustrates how in practice a multi-position test is used as part of the specification in the production of an SDF gyro and is helping to ensure high quality performance.

Single-Position Vertical and Azimuth Gyro Long Runs

In the multi-position test a period of one hour each is spent in the output axis and input axis vertical attitudes. These are the two attitudes in which gyros are used in conventional aeroplane platforms. It is therefore very relevant that in gyro testing these attitudes should receive special attention. This is particularly so when the gyro under test can be subjected to simulated platform thermal warm-up conditions and the drift of the gyro related to real time from switch-on and an established ambient temperature. The application and design of thermal jackets to achieve this will be discussed later.

Simulated warm-up tests are always performed in rate mode with the gyro sitting in the appropriate attitude. Prior to the start of the test the servo-electronics and recording equipment are energised and allowed to stabilise and at zero time the programmed heating procedure started. The gyro rotor is started at a point in time dictated by the platform system or, on a new type of gyro, on the manufacturer's recommendation.

Inspection of any record will show when, within the randomness of the gyro performance, settled conditions are established. Analysis of the record can give, say, the 10 to 20 minute mean drift and the rms value of successive 10 minute means from the 10/20 minute mean until the end of the test, which may go on for several hours. If the test is repeated many times the changes in the 10/20 minute mean give an indication of the switch-on to switch-on variation to be expected.

With the introduction into aided IN systems of optimised filtering techniques it may be necessary to establish an auto-correlation time for the gyro drift and it is data from a test of this type that could be used to establish the auto-correlation function.

Stability of Torquer Scale Factor and Torquer Linearity

Some inertial navigation systems demand knowledge of the torquer scale factor and the torquer linearity to 0·01 per cent; to guarantee measurement to 1 part in 10^4 even under laboratory conditions is not an easy task. The measurement is

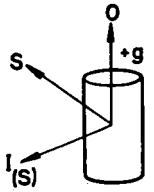

POSITION – 1

$S_T\ i_{-1} = D_F + D_O - \omega \cos \lambda$

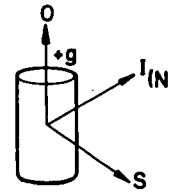

POSITION + 1

$S_T\ i_{+1} = D_F + D_O + \omega \cos \lambda$

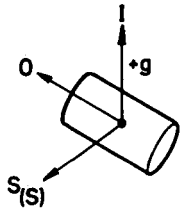

POSITION 3

$S_T\ i_3 = D_F + D_I + D_{II} + \omega \sin \lambda$

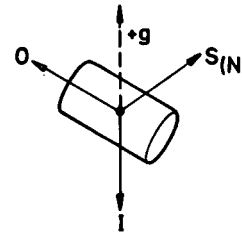

POSITION 4

$S_T\ i_4 = D_F - D_I + D_{II} - \omega \sin \lambda$

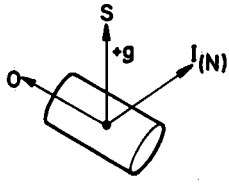

POSITION 5

$S_T\ i_5 = D_F + D_S + D_{SS} + \omega \cos \lambda$

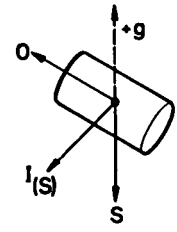

POSITION 6

$S_T\ i_6 = D_F - D_S + D_{SS} - \omega \cos \lambda$

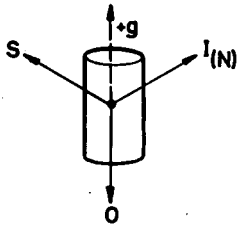

POSITION + 2

$S_T\ i_{+2} = D_F - D_o + \omega \cos \lambda$

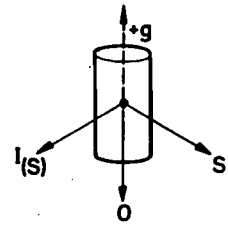

POSITION – 2

$S_T\ i_{-2} = D_F - D_o - \omega \cos \lambda$

Fig. 8-5 Gyro positions for eight-position test

made more difficult in this case because it cannot be divorced from the gyro drift stability. It has been demonstrated that during a multi-position test, using the earth as a precise rate table, the change in torquer current as a result of changing the rate input through $\pm \Omega \cos \lambda$ can give a measurement of S_T, but in solving the equations the assumption is made that the gyro drift $D_R + D_Q$ remains constant throughout the time spent in the two positions and in spite of the change from one to the other. Therefore, if adequate resolution in measuring the current and high accuracy in positioning the gyro are achieved, the S_T can only be determined as well as the gyro will allow.

The use of the earth as a rate table limits us to 15 degrees per hour or between 10-12 degrees per hour as a practical maximum, but knowledge of linearity up to 100 degrees per hour is necessary for many applications. Since a precision rate table has not been available this test has been performed on a servo table.

The table rate resulting from the application of accurately known currents or pulse rates to the gyro torquer in both a positive and negative sense is measured. The data is analysed by fitting the best straight line and computing the deviation from that line of the individual measurements. Again, because changes of gyro drift will modify the table rate the overall test accuracy will be limited by drift stability.

Rotor Power and Power Interrupt

The measurement of rotor power variations on gyros, particularly those with ball-bearing designs, has proved very worthwhile, for erratic drift characteristics have often been attributable to abnormal rotor performance that could only be detected by recording the power.

We are fortunate in the UK in having a British instrument available (a design sponsored by the RAE) whose output is a function of total three-phase power and can be applied to a recorder. By suitable backing-off techniques the recorder, with a 25 cm chart, can have a sensitivity of 75 mW full scale when the rotor is taking a total of several watts. It is also true to say that as a result of having this instrument we have also been able to be very critical of our own three-phase rotor supplies.

In a routine evaluation of a number of gyros rotor tests would be performed, say, every month or every 200 rotor hours or at any time if there were indications of this being a problem area. A typical test routine would be:

(a) With the gyro at stable operating temperature, record power during rotor run-up (at synchronism the hysteresis motor gives a characteristic drop in power level). Measure run-up time from record.

(b) Apply three 5-second power interrupts and observe any change in running power.

(c) Back off and increase recorder sensitivity to record at milliwatt level for 15 minutes.

(d) Switch off rotor and measure run-down time (from synchronism to stop) using motor back emf.

The milliwatt record will be a function of a particular wattmeter/recorder set-up, since the frequency response of such a set-up is limited above 1 Hz. However, from a national point of view, if we all use the same instrument all is well for this again is very largely a qualitative test.

Run-down time from synchronism to stop again can only give an indication of changing conditions in the gyro rotor; a more sophisticated test measuring high speed rundown (function of windage losses) and low speed rundown (function of bearing friction) may be necessary. Usually more consistent measurements can be made by reducing voltage to zero before switch-off.

With a gas spin bearing design it is often rewarding to perform this test in various attitudes depending on the design.

A power interrupt of very short duration can affect the gyro drift coefficient and it is recognised as a magnetic effect associated with the position of the poles on the hysteresis rotor. Many gyro designs have eliminated this problem, but a search for this effect is worthwhile in a new gyro design. A test can be performed automatically by programming to interrupt the rotor for a few milliseconds every few seconds. A record of gyro drift will then change sinusoidally if the effect is present and the peak to peak change in drift gives the bounded magnitude. This problem was given publicity by Honeywell (2) in 1962 and the error averaging technique given the title 'SMIT' (spin motor interruption technique).

Sensitivity to External Magnetic Fields

Many gyro designs include a magnetic shield as part of the outer case to minimise the effect of external fields. The extent to which any gyro is susceptible to external fields can be quickly assessed in a qualitative sense by observing on a recorder any change in torquer current when a hand held bar magnet is brought near to the gyro operating in rate mode.

If an accurate measure of the effect is required, the gyro is placed in the field generated by a Helmholtz coil arrangement; then the result of reversing a known field directed along each of the three principal gyro axes in turn can be measured. A maximum field strength of ten times that of the earth's total magnetic field is considered sufficient.

Sensitivity to Vibration Acceleration

The application of vibration to a gyro is one of the more difficult tests to perform because of the limitation of conventional vibration generators. The conventional electromagnetic loudspeaker type shakers can fall short of the requirements in two respects: first, they may produce very strong external magnetic fields which may vary with the excitation level and, second, the axis of vibration does not remain constant with frequency. Still, with the limits set by the equipment this test environment is used for two main purposes:

(a) to search through a practical frequency range (20 to 2000 Hz) for any resonance in the gyro construction that may adversely affect the gyro drift;

(b) to calibrate, under greater than 1g levels of acceleration, the drift coefficients that are either a function of the square of the acceleration or the product of accelerations.

The gyro is operated in rate mode and mounted directly on the shaker with a bracket that is designed not to resonate in the frequency range used. Brackets are normally machined from solid bar and separate brackets are made for each attitude in which the gyro is to be tested.

Having established the presence or otherwise of gyro resonances, spot frequencies are chosen (well away from the frequencies of resonance if they exist) to perform the calibration of specified drift coefficients.

The positions of gyro and axis of vibration normally investigated are:

Axis of applied vibration		Coefficient calibrated
SDF Gyro	I	$D_{I\,I}$
	S	$D_{S\,S}$
45°	I and S	$D_{I\,S}$ (anisoelastic coefficient)
45°	O and S	$D_{O\,S}$ (gas spin bearing cross compliance)
TDF Gyro	A	$D(A)_{A\,A}$
	B	$D(B)_{B\,B}$
	S	$D(A)_{S\,S}\,D(B)_{S\,S}$
45°	A and S	$D(A)_{A\,S}$ (major compliance)
45°	B and S	$D(B)_{B\,S}$ (major compliance)

Because many gyros have been known to change their value of calibrated coefficients as the result of vibration environment, it is prudent to perform a calibration test (eight-position test) just before and immediately after any vibration testing.

7 Thermal Jackets

A gyro of any design is certain to have coefficients that are a function of temperature, and close control of the ambient in which the gyro is operating will improve the performance. Even an SDF gyro using flotation techniques which has elevated temperature control as an integral part of its design can have a modified performance as the result of a change in thermal gradients.

It has been common practice for some time in British platform design to attempt to supply uniform controlled temperature conditions, and it is therefore necessary to stimulate these conditions, as far as possible, for at least some laboratory gyro tests.

Jacket designs are in use in Industry and at the RAE but in our own organisation other important advantages have come out of this philosophy. We have the problem of testing and evaluating a variety of gyro designs all of which differ in the method of mounting and yet are tested in either of two standard test tables. The concept of a casting to carry the gyro complete with thermal enclosure and to provide a standard flanged-type mounting design has enabled many forms of gyro design to be tested in a common set of test table brackets. Figure 8-6 illustrates one form of this design and figure 8-7 three test table brackets used. A complete description

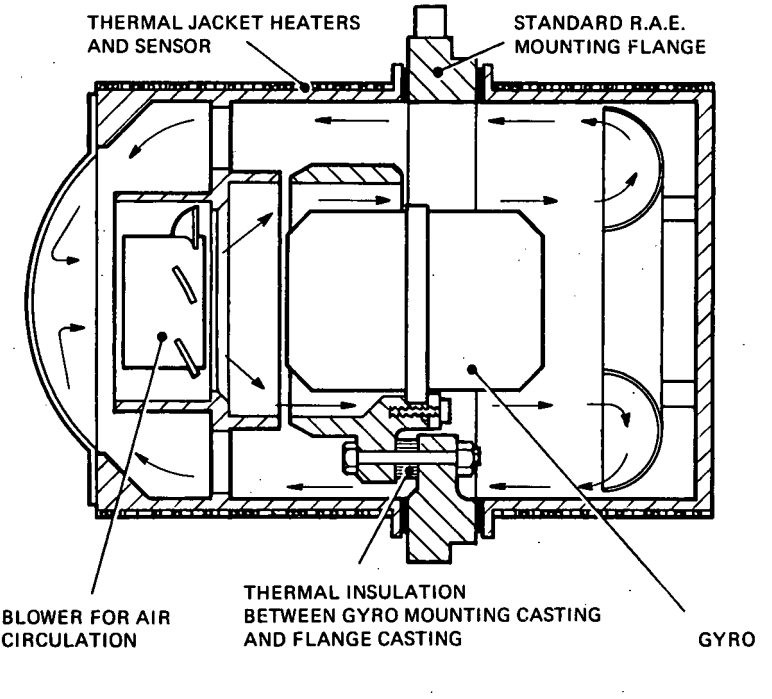

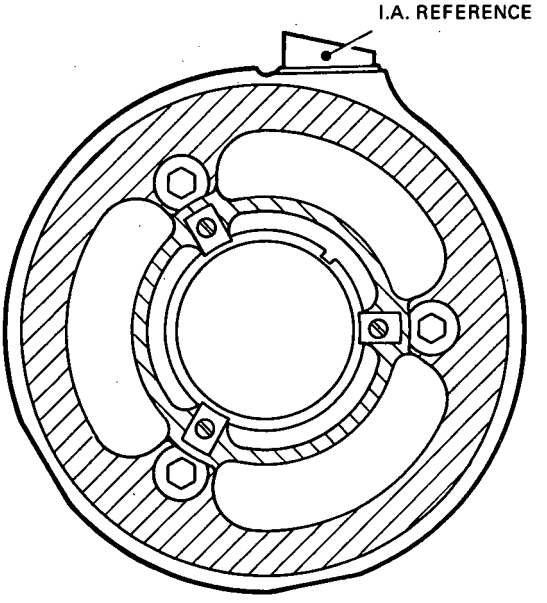

Fig. 8-6 Thermal jacket for test purposes typical central flange mounted gyro

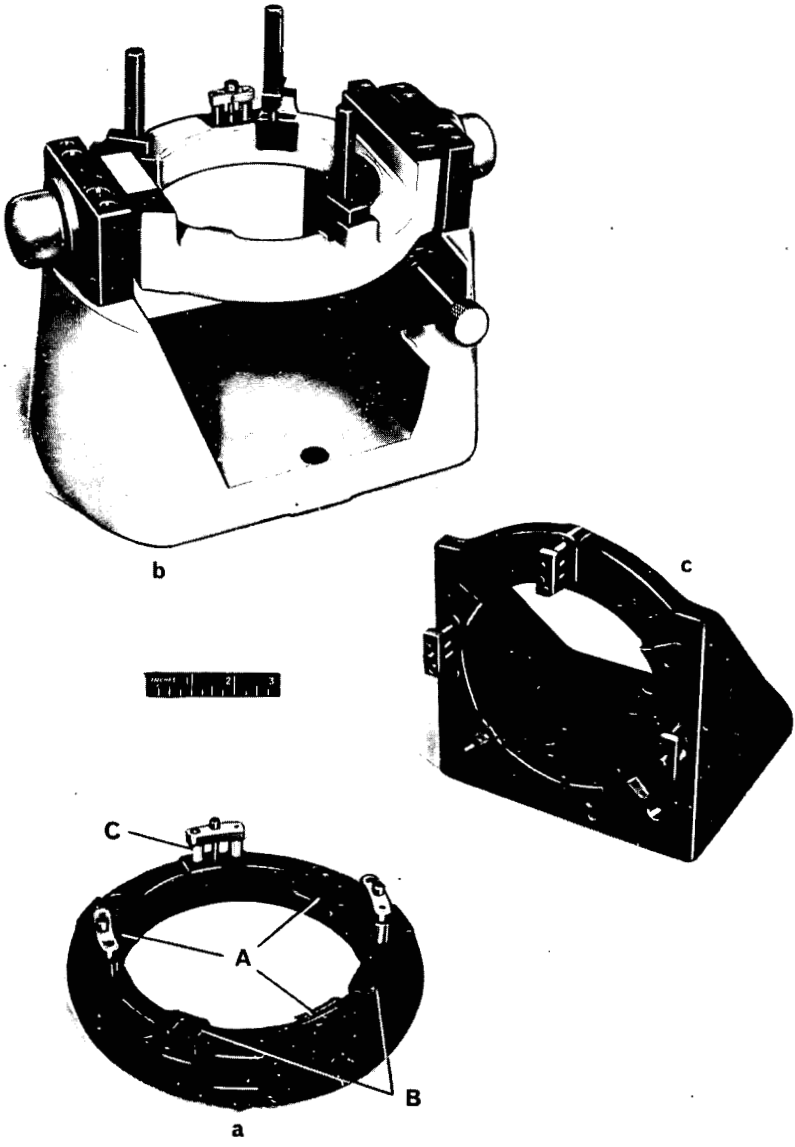

Fig. 8-7 Brackets for mounting thermal jackets

of thermal jacket designs is given in reference (2) but the principle aims of the design are repeated here:

(a) an easy but accurate method of mounting the gyro under test in a variety of test tables.
Note: A significant difference between platform conditions and test conditions is that the gyro is not removed from the platform between flights. Nevertheless, provided the test gyro is handled with care and the gyro can be aligned in the test stand to a high degree of repeatability, the difference between the two sets of conditions can be minimised.

(b) uniform controlled thermal environment for the gyro during a large part of its testing life.

(c) protection for the gyro when being handled. Not all gyros are enclosed in black boxes: some have exposed electrical connections and pre-amplifiers and it is important to avoid damage during a long evaluation.

(d) ability to assess the warm-up characteristics of the gyro from a variety of initial temperatures, with heat input to the gyro from its own heater and the thermal jacket in such a way that platform conditions are simulated.

(e) the feasibility of incorporating in the design a heat exchanger to enable low temperature storage tests to be made without removal of the gyro from the test stand.

Low Temperature Storage and Warm-up

Many military specifications for systems incorporating IN require rapid warm-up capability from low temperatures, say -20°C to -40°C. As well as the possibility of having an adverse effect on gyro coefficient stability and overall gyro reliability, the low temperatures involved do aggravate the problem of rapid warm-up.

The concept of a thermal jacket that incorporates a heat exchanger in the form of a large surface area copper tube and the availability of a portable refrigeration unit that can pump methanol cooled by solid CO_2 has made both storage and warm-up tests in the laboratory possible without removal of the gyro from the test table.

The latest design of jacket also provides vacuum tight sealing so that the air inside may be dry to eliminate condensation problems; alternatively the air can be enriched with helium to simulate the improved thermal conductivity incorporated in many platforms.

8. Special-Design Gyro Test Equipment

Test Tables

The concept of an all-purpose, super-precision, fully automatic, reasonably cheap test table still remains a dream. All the interested parties in the UK met a few years ago to discuss the subject and the main conclusion was that because of the very high cost and complexity of such a table all organisations were happy to continue with the tables already available, or if necessary to design their own special purpose table to meet particular needs. As a result, one organisation has designed a pressure air bearing, fixed latitude table which works well, and a second company uses precision spirit levels instead of optical scales on two axes since

Single axis servo test table

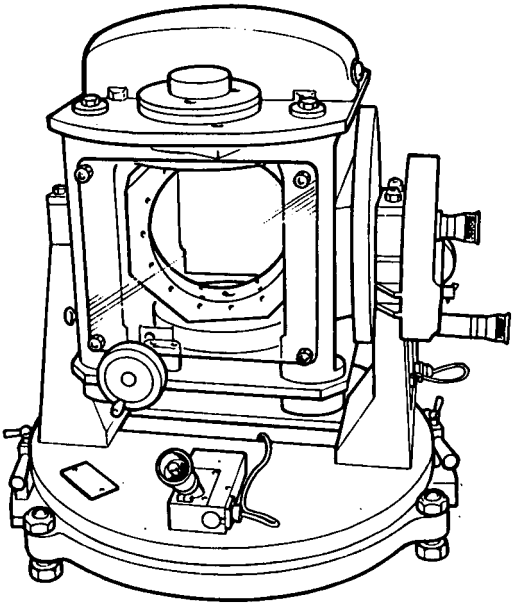

Polar axis tumble test table

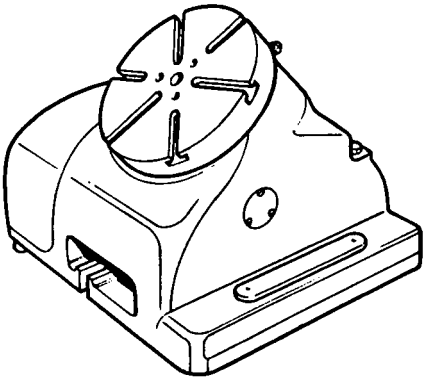

Fig. 8-8 Gyro test tables

the table positions required can use gravity in the alignment. These are just two examples where capital cost is reduced, at the expense of flexibility but with no detriment to the present tasks of the companies.

The two types of tables available commercially are the servo gimbal gyro tester and the polar axis test table. Each type is illustrated in figure 8-8. The servo table is used to test SDF gyros and TDF gyros (one axis at a time) in servo mode and because of the three degrees of freedom can orient a gyro in any position when testing in rate mode. The polar axis test table is a simple rate table with speeds of 1, 10, 40 times earth's rate. Table contacts can command pulses for either float disturbance in a qualitative sense or table stopping in discrete positions if required.

Electronic Equipment

The gyro and accelerometer group at RAE are fortunate in having the support of a very strong electronic design team. All test equipment is now transistorised and a very good MTBF has been built up with increased reliability. A recent design achievement by this group is a digital integrating milliammeter.

The requirement for this instrument arose out of the problem of obtaining adequate resolution from conventional analogue recording techniques used when testing in rate mode, particularly since the trend in gyro design has increased the torquer scale factor sensitivity so that to detect changes down to 1000th degree per hour has meant the resolution of very small currents in the presence of the noise both outside and inside the gyro servo loop.

The milliammeter is basically a servo system which maintains the net current into its input terminals at zero by feeding back current pulses which exactly cancel any input current from the source to be measured. The pulses are precisely defined in amplitude and duration but are reversed in sign as required to obtain balance at the input.

The difference between the number of positive and negative pulses in any given time is a very accurate measure of the mean input current during that time.

The complete specification is given in Appendix F. For gyro testing on ±1 milliamp and 10^6 full scale count, a resolution of 1 nanoamp with an accuracy of 1 part in 10^5 and an integration time of 10 minutes will go a long way to solving many of our gyro test data recording problems. This instrument, being an analogue-to-digital converter, can form the basis of an interesting data logging complex for gyro test data.

9. Gyro Test Laboratory Facilities

All engineers who have been exposed to the problems of gyro testing have formulated their own ideas of the perfect laboratory for this work. In practice the work is carried out under conditions that vary greatly and one does not know whether to be jealous or sorry for those American engineers now testing down a salt mine (LTV Aerospace, Detroit). There are three special aspects of such a laboratory that may be discussed: (a) temperature and humidity control, (b) alignment to geographic north, (c) design of concrete test pads.

Temperature and Humidity Control

Because so much of the equipment associated with the testing is of a high precision

nature, i.e. 0·01 per cent or better, it is obviously desirable to work under closely controlled temperature and humidity conditions but how difficult this is to achieve in practice. Gradients from floor to ceiling and airstreams directed at test stands are common faults.

Relative humidity between 45 per cent and 48 per cent and temperatures of 20°C ±1°C are probably ideal.

Alignment to Geographic North

Knowledge of true north to ● 10 arc seconds is all that is necessary for most applications. An error in alignment of 20 arc seconds results in an error of earth rotation component of 1000th degree per hour. It is much more important that any test table alignment should be stable to a few arc seconds.

The most satisfactory method for determination of north is by direct sighting of Polaris by theodolite but an alternative method using one of the many theodolites fitted with a gyro compass attachment can provide a solution when the building arrangements make direct sighting impossible.

Because of climatic conditions and the computation delays it is desirable to store this information in the laboratory rather than observe Polaris for every table alignment or check. There are three methods of storing an azimuth reference: (a)target, (b) optically flat mirror, (c) poroprism.

(a) Target. The bearing of a target from a fiducial mark over which the theodolite is centred is a popular method of storing an azimuth reference. The accuracy to which the theodolite has to be positioned is a function of the distance to the target; in practice this distance may have to be larger than is practicable. The advantage is that the theodolite can view the target from any height.

(b) Optically Flat Mirror. An optical flat can define a plane and the bearing of the normal to this plane can be established by an autocollimating theodolite. Accuracy is a function not of distance from the mirror but of resolution of the theodolite optics. A practical disadvantage is that the range of heights over which the theodolite can work is limited by the size of mirror.

(c) Poroprism. The poroprism operates in a similar manner to the optical flat but greatly extends the range of height at which the theodolite can be used. Note: The height of the theodolite will be dictated by the height of the reflecting surface mounted on the test table since azimuth alignment is performed by horizontal autocollimation. If a variety of tables are in use in a laboratory then flexibility in the position and height of the theodolite is necessary.

Design of Test Pads

The majority of gyro testing demands reasonable stability both in tilt and azimuth and the most common and cheapest solution to the problem is to mount the test table on a cast concrete test pad. The specification for a test pad includes three important aspects: (a) short term stability, (b) long term stability, (c) vibration.

(a) Short Term Stability. With present day inertial quality gyros random drift rates down to 0·001 degree per hour or less have to be measured in tests of a few hours' duration. It is therefore necessary, if input rates due to base motion disturbance are not to modify the gyro data, that these should be less than a few seconds of arc per hour change of tilt (5 arc seconds per hour equals 0·0014 degree

per hour). There are two common sources causing input rates of this order. The first is due to movement of personnel around the test station and the second is caused by solar heating where small building movements are transmitted to the test pad. Obviously, isolation of the test bed from the building structure will go some way to eliminating these effects.

(b) Long Term Tilt Stability. The error introduced into gyro data as a result of long term tilts is not so serious. The gyros under test are positioned with respect to earth's rotation axis and gravity. A tilt change of 20 arc seconds results in a 0·001 degree per hour change in earth's rotation component and 1 part in 10^4 in the acceleration effect due to gravity. Long term tilt changes may be caused by settling of the soil under the test area. Stability may also be affected within a one year period depending on the building reaction to summer/winter cycling. Relatively simple monitoring by spirit levels may be used to dictate re-levelling of the test stand when tilt reaches a specified amount.

(c) Vibration. Typical levels of vibration due to seismic noise are tens of micro gs at up to 30 Hz. Accelerations of this type are unlikely to affect gyro coefficients but do contribute to the general background noise and can make resolution of the test records less accurate. In general, it is preferable to choose a site where the vibration is acceptable without the use of anti-vibration mounts, since the introduction of any such system can seriously affect the tilt stability.

10. Conclusions

This chapter describes the principal tests used in the UK and attempts to justify their use and the philosophy behind them. The requirements for gyro testing call upon many disciplines and often use known techniques to their very limit of accuracy.

Detailed mathematical analysis of various tests in terms of the performance error model is contained in the appendices.

Appendix A

Nomenclature and Definition of Error Model

Single-Degree-of-Freedom Gyro (SDF)

Consider a gyro in which the sign convention for gyro axes and corresponding rotations is as shown in figure 8-1 such that $\bar{I} \times \bar{O} = \bar{S}$. Consider accelerations a_S, a_I and a_O (measured in units of g) acting along the three major axes. The gyro drift may be analysed into four types of components thus:

(a) a component independent of acceleration - D_F °/hr;

(b) components proportional to the accelerations (a_S, a_I, a_O) having magnitudes $D_I a_I$, $D_O a_O$, $D_S a_S$ °/hr where D_I, D_O and D_S are three drift coefficients having dimensions °/hr/g;

(c) components proportional to the squares of accelerations (a_S^2 and a_I^2) having magnitudes $D_{SS}\, a_S^2$ and $D_{II}\, a_I^2$ °/hr where D_{SS} and D_{II} are drift coefficients having dimensions °/hr/g^2.

(d) components proportional to the products of accelerations ($a_I a_S$, $a_I a_O$, $a_O a_S$) having magnitudes $D_{IO} a_I a_O$, $D_{IS} a_I a_S$ and $D_{OS} a_O a_S$ °/hr where D_{IO}, D_{IS} and D_{OS} are drift coefficients having dimensions °/hr/g^2.

The total gyro precession Ω is thus:

$$\begin{aligned}\Omega = {} & D_F \\ & + D_I a_I + D_O a_O + D_S a_S \\ & + D_{II} a_I^2 + D_{SS} a_S^2 \\ & + D_{IO} a_I a_O + D_{IS} a_I a_S + D_{OS} a_O a_S \\ & + \omega_I\end{aligned}$$

where ω_I is the angular velocity, with respect to inertial space, of the gyro case about the input axis.

Two-Degree-of-Freedom Gyro (TDF)

Consider a gyro in which the sign convention for gyro axes and corresponding rotations is as shown in figure 8-1. Consider it acted on by accelerations a_A, a_B and a_S; then, as in the case for an SDF gyro, a drift error model can be written for each axis:

$$\begin{aligned}\Omega_A = {} & D(A)_F + D(A)_A\, a_A + D(A)_B\, a_B + D(A)_S\, a_S \\ & + D(A)_{AA}\, a_A^2 + D(A)_{SS}\, a_S^2 \\ & + D(A)_{AB}\, a_A\, a_B + D(A)_{AS}\, a_A\, a_S + D(A)_{BS}\, a_B\, a_S + \omega_A\end{aligned}$$

$$\Omega_B = D(B)_F + D(B)_B\ a_B + D(B)_A\ a_A + D(B)_S\ a_S + D(B)_{BB}\ a_B^2 + D(B)_{SS}\ a_S^2 + D(B)_{BA}\ a_B\ a_A + D(B)_{BS}\ a_B\ a_S + \omega_B$$

where Ω = total gyro drift with respect to inertial space

$D(A)$ = drift coefficient of the A axis

$D(B)$ = drift coefficient of the B axis

a_A, a_B, a_S = acceleration, with respect to inertial space, of the gyro case along the A axis, B axis and spin axis respectively

ω_A, ω_B = angular velocity, with respect to inertial space, of the gyro case about the A axis and B axis respectively.

Note: ω_A and ω_B are both given the same sign. The A axis of the TDF gyro corresponds to the input axis of the SDF gyro. Thus a positive input is cancelled by a positive torque about the orthogonal axis. A positive input to the B axis is cancelled by a negative torque but in rate mode the current that cancels a positive input to both axes is labelled positive.

Appendix B

Single-Degree-of-Freedom Gyro Tumble Tests with Output Axis along Earth's Polar Axis: Fourier Analysis of Data

The arrangement for axes is defined in figure 8-2, where λ is the latitude angle and θ the angle between input axis and west. The accelerations acting on the gyro as a function of table angle are as follows:

Output axis north (up)	Output axis south (down)
$a_S = - g \cos \lambda \cos \theta$	$a_S = + g \cos \lambda \cos \theta$
$a_I = - g \cos \lambda \sin \theta$	$a_I = - g \cos \lambda \sin \theta$
$a_O = + g \sin \lambda$	$a_O = - g \sin \lambda$

In rate mode the drift error model equation is:

$$S_T \times i = D_F + D_I a_I + D_O a_O + D_S a_S + D_{II} a_I^2 + D_{SS} a_S^2 + D_{IO} a_I a_O + D_{IS} a_I a_S + D_{OS} a_O a_S$$

where S_T is the torquer scale factor (°/hr/mA) and i is the measured torquer current in mA.

Note: Since input axis is maintained normal to earth's polar axis and table axis, ω_I does not appear in the equation. If, due to error in alignment, the input axis lies at an angle α to the axis of rotation, then

$$\omega_I = \sin \alpha (\omega_T + \omega_E)$$

where ω_T is table rate with respect to earth and ω_E is earth's rotation rate with respect to inertial space.

Substituting the actual accelerations in the error model equation and collecting terms results in, for output axis north,

$$\begin{aligned} S_T i = {} & D_F + D_O \sin \lambda + \tfrac{1}{2}(D_{II} + D_{SS}) \cos^2 \lambda \\ & - D_I \cos \lambda \sin \theta - \tfrac{1}{2} D_{IO} \sin 2\lambda \sin \theta \\ & - D_S \cos \lambda \cos \theta - \tfrac{1}{2} D_{OS} \sin 2\lambda \cos \theta \\ & + \tfrac{1}{2} D_{IS} \cos^2 \lambda \sin 2\theta \\ & - \tfrac{1}{2}(D_{II} - D_{SS}) \cos^2 \lambda \cos 2\theta \end{aligned}$$

and for output axis south,

$$
\begin{aligned}
S_T i \;=\; & D_F - D_O \sin\lambda + \tfrac{1}{2}(D_{II} + D_{SS}) \cos^2\lambda \\
& - D_I \cos\lambda \sin\theta + \tfrac{1}{2} D_{IO} \sin 2\lambda \sin\theta \\
& + D_S \cos\lambda \cos\theta - \tfrac{1}{2} D_{OS} \sin 2\lambda \cos\theta \\
& - \tfrac{1}{2} D_{IS} \cos^2\lambda \sin 2\theta \\
& - \tfrac{1}{2}(D_{II} - D_{SS}) \cos^2\lambda \cos 2\theta
\end{aligned}
$$

Each expression contains a term independent of table angle θ, sine and cosine terms a function of table angle and sine and cosine terms a function of twice table angle. No higher harmonics should be present according to the simple assumptions of the present analysis. The following expressions for the Fourier coefficients can then be written:

For OA north

Mean level	A_0ON	$D_F + D_O \sin\lambda + \tfrac{1}{2}(D_{II} + D_{SS}) \cos^2\lambda$
Coeff. of sin θ	B_1ON	$- D_I \cos\lambda - \tfrac{1}{2} D_{IO} \sin 2\lambda$
Coeff. of cos θ	A_1ON	$- D_S \cos\lambda - \tfrac{1}{2} D_{OS} \sin 2\lambda$
Coeff. of sin 2θ	B_2ON	$+ \tfrac{1}{2} D_{IS} \cos 2\lambda$
Coeff. of cos 2θ	A_2ON	$- \tfrac{1}{2}(D_{II} - D_{SS}) \cos^2\lambda$

and for OA south

Mean level	A_0OS	$D_F - D_O \sin\lambda + \tfrac{1}{2}(D_{II} + D_{SS}) \cos^2\lambda$
Coeff. of sin θ	B_1OS	$- D_I \cos\lambda + \tfrac{1}{2} D_{IO} \sin 2\lambda$
Coeff. of cos θ	A_1OS	$+ D_S \cos\lambda - \tfrac{1}{2} D_{OS} \sin 2\lambda$
Coeff. of sin 2θ	B_2OS	$- \tfrac{1}{2} D_{IS} \cos^2\lambda$
Coeff. of cos 2θ	A_2OS	$- \tfrac{1}{2}(D_{II} - D_{SS}) \cos^2\lambda$.

By computing $\frac{1}{2} \times$ sym or difference of the Fourier coefficients and using the known value for λ, certain gyro coefficients or combinations of coefficients can be calculated:

$$
\begin{aligned}
\tfrac{1}{2}(A_0ON + A_0OS) &= D_F + \tfrac{1}{2}(D_{II} + D_{SS}) \\
\tfrac{1}{2}(A_0ON - A_0OS) &= D_O \\
\tfrac{1}{2}(B_1ON + B_1OS) &= -D_I \\
B_1OS - B_1ON &= D_{IO} \\
\tfrac{1}{2}(A_1OS - A_1ON) &= D_S \\
A_1ON + A_1OS &= -D_{OS} \\
B_2ON - B_2OS &= D_{IS} \\
A_2ON + A_2OS &= -(D_{II} - D_{SS})
\end{aligned}
$$

To achieve complete separation it is necessary to perform an additional tumble

test about the spin axis, although it is probable that the coefficients in question are likely to be small.

In a conventional SDF floated gas spin bearing gyro the relation between the new nomenclature and the established mechanical phenomena is:

D_F - restraint drift

D_I - mass unbalance (spin axis)

D_S - mass unbalance (input axis)

D_{IS} - anisoelastic coefficient

D_{OS} - gas spin bearing cross compliance (attitude angle)

Single-Degree-of-Freedom Gyro Tumble Tests with Spin Axis along Earth's Polar Axis: Fourier Analysis of Data

If λ is the latitude angle and θ the angle between input axis and west (Fig. 8-2), the accelerations acting on the gyro as a function of table angle are as follows:

Spin axis north (up)	Spin axis south (down)
$a_S = + g \sin \lambda$	$a_S = - g \sin \lambda$
$a_I = - g \cos \lambda \cos \theta$	$a_I = g \cos \lambda \cos \theta$
$a_O = - g \cos \lambda \sin \theta$	$a_O = - g \cos \lambda \sin \theta$.

Substituting these accelerations in the error model and collecting terms results in, for spin axis north,

$$\begin{aligned} S_T i = {} & D_F + D_S \sin \lambda + D_{SS} \sin^2 \lambda + \tfrac{1}{2} D_{II} \cos^2 \lambda \\ & - D_O \cos\lambda \sin \theta - D_{OS} \sin \lambda \cos \lambda \sin \theta \\ & + D_I \cos \lambda \cos \theta - D_{IS} \sin \lambda \cos \lambda \cos \theta \\ & + \tfrac{1}{2} D_{IO} \cos^2 \lambda \sin 2\theta \\ & + \tfrac{1}{2} D_{II} \cos^2 \lambda \cos 2\theta \end{aligned}$$

and for spin axis south,

$$\begin{aligned} S_T i = {} & D_F - D_S \sin \lambda + D_{SS} \sin^2 \lambda + \tfrac{1}{2} D_{II} \cos^2 \lambda \\ & + D_{OS} \cos \lambda \sin \lambda \sin \theta - D_O \cos \lambda \sin \theta \\ & + D_I \cos \lambda \cos \theta - D_{IS} \sin \lambda \cos \lambda \cos \theta \\ & - \tfrac{1}{2} D_{IO} \cos^2 \lambda \sin 2\theta \\ & + \tfrac{1}{2} D_{II} \cos^2 \lambda \cos 2\theta. \end{aligned}$$

Each expression contains a constant term, sine and cosine terms of fundamental frequency and sine and cosine terms of the second harmonic. The following expressions for the Fourier coefficients can then be written:

For SA north

Mean level	A_0SN	$D_F + D_S \sin \lambda + D_{SS} \sin^2 \lambda + \tfrac{1}{2} D_{II} \cos^2 \lambda$
Coeff. of $\sin \theta$	B_1SN	$- D_O \cos \lambda - D_{OS} \sin \lambda \cos \lambda$

Coeff. of cos θ	A_1SN	$+ D_I \cos\lambda - D_{IS} \sin\lambda \cos\lambda$
Coeff. of sin 2θ	B_2SN	$+ \frac{1}{2}D_{IO} \cos^2\lambda$
Coeff. of cos 2θ	A_2SN	$+ \frac{1}{2}D_{II} \cos^2\lambda$

and for SA south

Mean level	A_0SS	$D_F - D_S \sin\lambda + D_{SS} \sin^2\lambda + \frac{1}{2}D_{II} \cos^2\lambda$
Coeff. of sin θ	B_1SS	$- D_O \cos\lambda + D_{OS} \sin\lambda \cos\lambda$
Coeff. of cos θ	A_1SS	$+ D_I \cos\lambda - D_{IS} \sin\lambda \cos\lambda$
Coeff. of sin 2θ	B_2SS	$- \frac{1}{2}D_{IO} \cos^2\lambda$
Coeff. of cos 2θ	A_2SS	$+ \frac{1}{2}D_{II} \cos^2\lambda.$

By computing $\frac{1}{2} \times$ sum or difference of the Fourier coefficients and using the known value for λ, certain gyro coefficients or combinations of coefficients can be calculated:

$$\begin{aligned}
\tfrac{1}{2}(A_0SN + A_0SS) &= D_F + D_{SS} + D_{II} \\
\tfrac{1}{2}(A_0SN - A_0SS) &= D_S \\
\tfrac{1}{2}(B_1SN + B_1SS) &= -D_O \\
\tfrac{1}{2}(B_1SN - B_1SS) &= -D_{OS} \\
\tfrac{1}{2}(A_1SN + A_1SS) &= D_I - D_{IS} \\
B_2SN - B_2SS &= D_{IO} \\
A_2SN + A_2SS &= D_{II}
\end{aligned}$$

Appendix C

Two-Degree-of-Freedom Gyro Tumble Tests with Spin Axis along Earth's Polar Axis: Fourier Analysis of Data

The arrangement for axes is defined in figure 8-2, where λ is the latitude angle and θ the angle between A axis and west. The accelerations acting on the gyro as a function of table angle are as follows:

Spin axis north (up)	Spin axis south (down)
$a_S + g \sin \lambda$	$a_S - g \sin \lambda$
$a_A - g \cos \lambda \sin \theta$	$a_A - g \cos \lambda \sin \theta$
$a_B + g \cos \lambda \cos \theta$	$a_B - g \cos \lambda \cos \theta$.

In torquer-feedback mode the drift error model equation for the A axis is

$$\begin{aligned} S_{TB} i_B = {} & D(A)_F + D(A)_A a_A + D(A)_B a_B + D(A)_S a_S \\ & + D(A)_{AA} a_A^2 + D(A)_{SS} a_S^2 \\ & + D(A)_{AB} a_A a_B + D(A)_{AS} a_A a_S + D(A)_{BS} a_B a_S \end{aligned}$$

where S_{TB} is the B axis torquer scale factor and i_B is the measured B axis torquer current.

Substituting the actual accelerations in the error model equation and collecting terms results in, for spin axis north,

$$\begin{aligned} S_{TB} i_B = {} & D(A)_F + D(A)_S \sin \lambda + D(A)_{SS} \sin^2 \lambda + \tfrac{1}{2} D(A)_{AA} \cos^2 \lambda \\ & - D(A)_A \cos \lambda \sin \theta - \tfrac{1}{2} D(A)_{AS} \sin \lambda \sin \theta \\ & + D(A)_B \cos \lambda \cos \theta + \tfrac{1}{2} D(A)_{BS} \sin \lambda \cos \theta \\ & - \tfrac{1}{2} D(A)_{AB} \cos^2 \lambda \sin 2\theta \\ & - \tfrac{1}{2} D(A)_{AA} \cos^2 \lambda \cos 2\theta \end{aligned}$$

and for spin axis south,

$$\begin{aligned} S_{TB} i_B = {} & D(A)_F - D(A)_S \sin \lambda + D(A)_{SS} \sin^2 \lambda + \tfrac{1}{2} D(A)_{AA} \cos^2 \lambda \\ & - D(A)_A \cos \lambda \sin \theta + \tfrac{1}{2} D(A)_{AS} \sin 2\lambda \sin \theta \\ & - D(A)_B \cos \lambda \cos \theta + \tfrac{1}{2} D(A)_{BS} \sin 2\lambda \cos \theta \\ & + \tfrac{1}{2} D(A)_{AB} \cos^2 \lambda \sin 2\theta \\ & - \tfrac{1}{2} D(A)_{AA} \cos^2 \lambda \cos 2\theta \end{aligned}$$

and similarly for the B axis. The following expressions for the Fourier coefficients can then be written:

For SA north

Mean level	$A_0(A)SN\ \ D(A)_F + D(A)_S \sin\lambda + D(A)_{SS} \sin^2\lambda + \frac{1}{2}D(A)_{AA} \cos^2\lambda$
Coeff. of sin θ	$B_1(A)SN - D(A)_A \cos\lambda - \frac{1}{2}D(A)_{AS} \sin\lambda$
Coeff. of cos θ	$A_1(A)SN + D(A)_B \cos\lambda + \frac{1}{2}D(A)_{BS} \sin\lambda$
Coeff. of sin 2θ	$B_2(A)SN - \frac{1}{2}D(A)_{AB} \cos^2\lambda$
Coeff. of cos 2θ	$A_2(A)SN - \frac{1}{2}D(A)_{AA} \cos^2\lambda$

and for SA south

Mean level	$A_0(A)SS\ \ D(A)_F - D(A)_S \sin\lambda + D(A)_{SS} \sin^2\lambda + \frac{1}{2}D(A)_{AA} \cos^2\lambda$
Coeff. of sin θ	$B_1(A)SS - D(A)_A \cos\lambda + \frac{1}{2}D(A)_{AS} \sin 2\lambda$
Coeff. of cos θ	$A_1(A)SS - D(A)_B \cos\lambda + \frac{1}{2}D(A)_{BS} \sin 2\lambda$
Coeff. of sin 2θ	$B_2(A)SS + \frac{1}{2}D(A)_{AB} \cos^2\lambda$
Coeff. of cos 2θ	$A_2(A)SS - \frac{1}{2}D(A)_{AA} \cos^2\lambda$

and similarly for the B axis. By computing $\frac{1}{2}$ × sum and difference of the Fourier coefficients and using the known value for λ, certain gyro coefficients or sum of coefficients can be calculated.

For the A axis

$$\frac{1}{2}(A_0(A)SN + A_0(A)SS) = D(A)_F + D(A)_{SS} + \frac{1}{2} D(A)_{AA}$$

$$\frac{1}{2}(A_0(A)SN - A_0 A)SS) = D(A)_S$$

$$\frac{1}{2}(B_1(A)SN + B_1(A)SS) = - D(A)_A$$

$$B_1(A)SN - B_1(A)SS = - D(A)_{AS}$$

$$A_1(A)SN + A_1(A)SS = D(A)_{BS}$$

$$\frac{1}{2}(A_1(A)SN - A_1(A)SS) = D(A)_B$$

$$B_2(A)SN - B_2(A)SS = D(A)_{AB}$$

$$A_2(A)SN + A_2(A)SS = - D(A)_{AA}$$

and for the B axis

$$\frac{1}{2}(A_0(B)SN + A_0(B)SS) = D(B)_F + D(B)_{SS} + \frac{1}{2} D(B)_{BB}$$

$$\frac{1}{2}(A_0(B)SN - A_0(B)SS) = D(B)_S$$

$$\frac{1}{2}(B_1(B)SN + B_1(B)SS) = - D(B)_B$$

$$B_1(B)SN - B_1(B)SS = - D(B)_{BS}$$

$$A_1(B)SN + A_1(B)SS = D(B)_{AS}$$

$$\tfrac{1}{2}(A_1(B)SN - A_1(B)SS) = D(B)_A$$

$$B_2(B)SN - B_2(B)SS = D(B)_{BA}$$

$$A_2(B)SN + A_2(B)SS = -D(B)_{BB}$$

It will be noted that this test above does not allow determination of all the drift coefficients. To obtain complete separation it is necessary to perform additional tests.

In a conventional two degree of freedom gyro the relationship between this nomenclature and simple mechanical phenomena is:

$D(A)_A D(B)_B$ represents mass unbalance along the spin axis

$D(A)_S$ represents mass unbalance along the A axis

$D(B)_S$ represents mass unbalance along the B axis

$D(A)_{AS}$ represents major compliance

$D(B)_{BS}$ represents major compliance

Appendix D

Measurement of Misalignment Angle between Nominal IA and True IA and an Estimate of the Error between Nominal IA and Geographic North (SDF Gyro)

The definition of axes and sign conversion is given in figure 8-9.

Let ϵ be error (radians) between true IA and nominal IA, positive when measured ACW from nominal IA to true IA. Let ϕ be error (radians) between nominal IA and geographic north, positive when measured ACW from north to nominal IA. The equations are, for a four position test, OA up and down, nominal IA 90°and 270°on base scale:

OA up nominal IA 90°

$$S_T i_{90}\text{up} = D_F + D_O - (\phi + \epsilon)\,\omega \cos \lambda$$

and nominal IA 270°

$$S_T i_{270}\text{up} = D_F + D_O + (\phi + \epsilon)\,\omega \cos \lambda$$

OA down nominal IA 90°

$$S_T i_{90}\text{down} = D_F - D_O + (\phi - \epsilon)\,\omega \cos \lambda$$

and nominal IA 270°

$$S_T i_{270}\text{down} = D_F - D_O - (\phi - \epsilon)\,\omega \cos \lambda.$$

By addition and subtraction the following expression for the unknowns may be extracted:

$$\epsilon = \tfrac{1}{4} S_T \frac{(i_{270}\text{up} + i_{270}\text{down} - i_{90}\text{up} - i_{90}\text{down})}{\omega \cos \lambda}$$

$$\phi = \tfrac{1}{4} S_T \frac{(i_{270}\text{up} + i_{90}\text{down} - i_{90}\text{up} - i_{270}\text{down})}{\omega \cos \lambda}$$

$$D_F = \tfrac{1}{4} S_T (i_{90}\text{up} + i_{270}\text{up} + i_{90}\text{down} + i_{270}\text{down})$$

$$D_O = \tfrac{1}{4} S_T (i_{90}\text{up} + i_{270}\text{up} - i_{90}\text{down} - i_{270}\text{down})$$

Analysis of Eight Position Test (SDF Gyro)

Assuming that the misalignment angles ϵ and ϕ have been measured and adjustments made to make them significantly small, then for the eight positions the accelerations and components of earth's rotation are as follows:

Posn.	Direction of axes			Acceleration along axes (g)			Earth's Rotation
	S	I	O	S	I	O	
-1	W	S	Up	0	0	+1	$-\omega \cos \lambda$
+1	E	N	Up	0	0	+1	$+\omega \cos \lambda$
3	S	Up	W	0	+1	0	$+\omega \sin \lambda$
4	N	Down	W	0	-1	0	$-\omega \sin \lambda$
5	Up	N	W	+1	0	0	$+\omega \cos \lambda$
6	Down	S	W	-1	0	0	$-\omega \cos \lambda$
-2	W	N	Down	0	0	-1	$+\omega \cos \lambda$
+2	E	S	Down	0	0	-1	$-\omega \cos \lambda$

The equations in terms of torquer current are then

$$-1 \quad S_T i_{-1} = D_F + D_O - \omega \cos \lambda$$

$$+1 \quad S_T i_{+1} = D_F + D_O + \omega \cos \lambda$$

$$3 \quad S_T i_3 = D_F + D_I + D_{II} + \omega \sin \lambda$$

$$4 \quad S_T i_4 = D_F - D_I + D_{II} - \omega \sin \lambda$$

$$5 \quad S_T i_5 = D_F + D_S + D_{SS} + \omega \cos \lambda$$

$$6 \quad S_T i_6 = D_F - D_S + D_{SS} - \omega \cos \lambda$$

$$-2 \quad S_T i_{-2} = D_F - D_O - \omega \cos \lambda$$

$$+2 \quad S_T i_{+2} = D_F - D_O + \omega \cos \lambda.$$

In a simple analysis D_O, D_{II} and D_{SS} are considered small and are neglected. The following expressions can be extracted:

$$S_{T_{OA\ up}} = \frac{2\omega \cos \lambda}{(i_{+1} - i_{-1})} \qquad S_{T_{OA\ down}} = \frac{2\omega \cos \lambda}{(i_{+2} - i_{-2})}$$

$$D_{F_{OA\ up}} = \tfrac{1}{2} S_T (i_{+1} + i_{-1}) \qquad D_{F_{OA\ down}} = \tfrac{1}{2} S_T (i_{+2} - i_{-2})$$

$$D_I = \tfrac{1}{2} S_T (i_3 - i_4) \qquad D_S = S_T (i_5 - i_6).$$

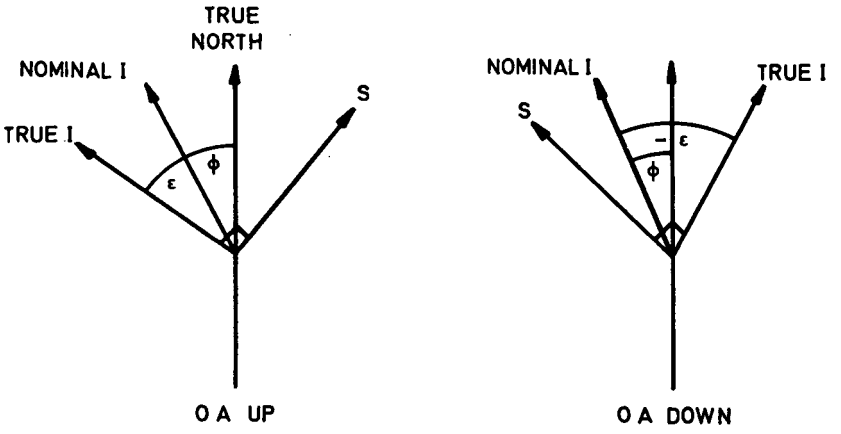

SDF GYRO

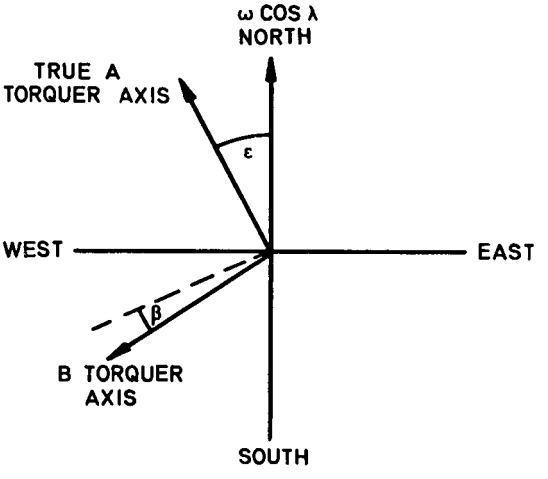

TDF GYRO

Fig. 8-9 Definition of misalignment angles

A more extensive analysis gives:

$$D_F = \tfrac{1}{4}S_T(i_{-1} + i_{+1} + i_{-2} + i_{+2})$$

$$D_0 = \tfrac{1}{4}S_T(i_{-1} - i_{+1} - i_{-2} - i_{+2})$$

$$D_{II} = \tfrac{1}{2}S_T(i_3 + i_4) - D_F$$

$$D_{SS} = \tfrac{1}{2}S_T(i_5 + i_6) - D_F$$

Appendix E

Analysis of Eight-Position Test Data TDF Gyro

1. Measurement of torquer scale factors and torquer misalignment angles

Let the misalignment angle between the A torquer axis and the nominal A torquer axis indicated by the mounting casting be ϵ radians and let the angle between the A and B torquer axes be $\pi/2 + \beta$ radians.

In the first four positions of this test the spin axis is vertical and the nominal A axis pointing north, west, south and east in turn. If we take as reference axes the true A torquer axis and the B axis orthogonal to this, the accelerations and components of earth's rotation acting along the various axes are:

Posn.	Direction of axes			Acceleration along axes			Earth's rotation	
	S	A	B	S	A	B	A	B
1	Up	N	W	+1	0	0	$\omega \cos \lambda$	$-\epsilon\omega \cos \lambda$
2	Up	W	S	+1	0	0	$-\epsilon\omega \cos \lambda$	$-\omega \cos \lambda$
3	Up	S	E	+1	0	0	$-\omega \cos \lambda$	$+\epsilon\omega \cos \lambda$
4	Up	E	N	+1	0	0	$+\epsilon\omega \cos \lambda$	$\omega \cos \lambda$

Substituting these accelerations and rate inputs results in the following equations:

Position 1
$$S_{TB} i_{B1} = D(A)_F + D(A)_S + D(A)_{SS} + \omega \cos \lambda$$
$$S_{TA} i_{A1} - \beta S_{TB} i_{B1} = D(B)_F + D(B)_S + D(B)_{SS} - \epsilon\, \omega \cos \lambda$$

Position 2
$$S_{TB} i_{B2} = D(A)_F + D(A)_S + D(A)_{SS} - \epsilon\, \omega \cos \lambda$$
$$S_{TA} i_{A2} - \beta S_{TB} i_{B2} = D(B)_F + D(B)_S + D(B)_{SS} - \omega \cos \lambda$$

Position 3
$$S_{TB} i_{B3} = D(A)_F + D(A)_S + D(A)_{SS} - \omega \cos \lambda$$
$$S_{TA} i_{A3} - \beta S_{TB} i_{B3} = D(B)_F + D(B)_S + D(B)_{SS} + \epsilon\, \omega \cos \lambda$$

Position 4
$$S_{TB} i_{B4} = D(A)_F + D(A)_S + D(A)_{SS} + \epsilon\, \omega \cos \lambda$$
$$S_{TA} i_{A4} - \beta S_{TB} i_{B4} = D(B)_F + D(B)_S + D(B)_{SS} + \omega \cos \lambda.$$

By addition and subtraction the following expression for the unknowns may be extracted:

$$S_{TB} = \frac{2\omega \cos \lambda}{i_{B1} - i_{B3}} \qquad S_{TA} = \frac{2\omega \cos \lambda}{i_{A4} - i_{A2}} \qquad (\text{if } \epsilon\beta \ll 1)$$

$$\epsilon = \frac{i_{B4} - i_{B2}}{i_{B1} - i_{B3}} \qquad \epsilon + \beta = \frac{i_{A3} - i_{A1}}{i_{A4} - i_{A2}} \qquad (\text{if } \epsilon\beta \ll 1)$$

2. The Complete Eight-Position Test

In the analysis of a complete eight position test it is assumed that ϵ is adjusted so that the A axis is aligned in the correct position and that β is negligible. If a correction has to be applied for β then

for S_{TA} substitute $S_{TA} - \beta S_{TB}$

The accelerations and input rates have been tabulated for positions 1-4. For positions 5-8 they are as follows:

Posn.	Direction of axes			Acceleration along axes			Earth's rotation	
	S	A	B	S	A	B	A	B
5	N	E	Down	0	0	-1	0	$-\omega \sin \lambda$
6	N	Up	E	0	+1	0	$\omega \sin \lambda$	0
7	N	W	Up	0	0	+1	0	$\omega \sin \lambda$
8	N	Down	W	0	-1	0	$-\omega \sin \lambda$	0

The equations for the eight positions in terms of torquer current are:

Posn.	A axis		
1	$S_{TB}\, i_{B1}$	=	$D(A)_F + D(A)_S + D(A)_{SS} + \omega \cos \lambda$
2	$S_{TB}\, i_{B2}$	=	$D(A)_F + D(A)_S + D(A)_{SS}$
3	$S_{TB}\, i_{B3}$	=	$D(A)_F + D(A)_S + D(A)_{SS} - \omega \cos \lambda$
4	$S_{TB}\, i_{B4}$	=	$D(A)_F + D(A)_S + D(A)_{SS}$
5	$S_{TB}\, i_{B5}$	=	$D(A)_F - D(A)_B$
6	$S_{TB}\, i_{B6}$	=	$D(A)_F + D(A)_A + D(A)_{AA} + \omega \sin \lambda$
7	$S_{TB}\, i_{B7}$	=	$D(A)_F + D(A)_B$
8	$S_{TB}\, i_{B8}$	=	$D(A)_F - D(A)_A + D(A)_{AA} - \omega \sin \lambda$

Posn.	B axis		
1	$S_{TA}\, i_{A1}$	=	$D(B)_F + D(B)_S + D(B)_{SS}$
2	$S_{TA}\, i_{A2}$	=	$D(B)_F + D(B)_S + D(B)_{SS} - \omega \cos \lambda$
3	$S_{TA}\, i_{A3}$	=	$D(B)_F + D(B)_S + D(B)_{SS}$
4	$S_{TA}\, i_{A4}$	=	$D(B)_F + D(B)_S + D(B)_{SS} + \omega \cos \lambda$
5	$S_{TA}\, i_{A5}$	=	$D(B)_F - D(B)_B + D(B)_{BB} - \omega \sin \lambda$
6	$S_{TA}\, i_{A6}$	=	$D(B)_F + D(B)_A$
7	$S_{TA}\, i_{A7}$	=	$D(B)_F + D(B)_B + D(B)_{BB} + \omega \sin \lambda$
8	$S_{TA}\, i_{A8}$	=	$D(B)_F - D(B)_A$

The acceleration squared terms are neglected in a simple analysis, so by addition and subtraction the following unknowns may be extracted:

A axis		
$S_{TB} = \dfrac{2\omega \cos \lambda}{i_{B1} - i_{B3}}$		
$D(A)_F$	=	$\frac{1}{4} S_{TB} (i_{B5} + i_{B6} + i_{B7} + i_{B8})$
$D(A)_F + D(A)_S$	=	$\frac{1}{4} S_{TB} (i_{B1} + i_{B2} + i_{B3} + i_{B4})$
$D(A)_A$	=	$\frac{1}{2} S_{TB} (i_{B6} - i_{B8}) - \omega \sin \lambda$
$D(A)_B$	=	$\frac{1}{2} S_{TB} (i_{B7} - i_{B5})$
B axis		
$S_{TA} = \dfrac{2\omega \cos \lambda}{i_{A4} - i_{A2}}$		
$D(B)_F$	=	$\frac{1}{4} S_{TA} (i_{A5} + i_{A6} + i_{A7} + i_{A8})$
$D(B)_F + D(B)_S$	=	$\frac{1}{4} S_{TA} (i_{A1} + i_{A2} + i_{A3} + i_{A4})$
$D(B)_A$	=	$\frac{1}{2} S_{TA} (i_{A6} - i_{A8})$
$D(B)_B$	=	$\frac{1}{2} S_{TA} (i_{A7} - i_{A5}) - \omega \sin \lambda$

Appendix F

Digital Integrating Milliammeter

Description

Many instances arise in which it is necessary to obtain a precise measurement of the mean value of a direct current which is subject to superimposed fluctuations many times larger than the permitted measurement error. A digital integrating milliammeter was developed to meet this need.

The milliammeter is basically a servo system which maintains the net current into its input terminals at zero by feeding back current pulses which exactly cancel any input current from the source to be measured. The pulses are precisely defined in amplitude and duration but are reversed in sign as required to attain balance with the input. The difference between the number of positive and negative pulses in any given item is a very accurate measure of the mean input current during that time.

Specification

Input current	±10 mA or ±1 mA full scale
Input resistance	10 ±0.01 ohms
Full scale count number	10^6, 10^5 or programmed
Resolution	1 digit = 1 nA (on 1 mA range)
Linearity	$\pm 2 \times 10^{-6}$
Accuracy	1×10^{-5}
Integration periods (preset)	2, 5 or 10 minutes from 10^6 counts 12, 30 or 60 seconds for 10^5 counts
Output	Numeric display and Binary coded decimal store

Availability

The instrument is being engineered for production by

Watesta Electronics Ltd.
34 Cambridge Park,
London E.11, UK

Information from

I. E. E. Department,
Royal Aircraft Establishment,
Farnborough, Hants, UK
Telephone: Aldershot 24461, Extension 3810
Patent Application No. 37961/67

Acknowledgement

This chapter is British Crown Copyright, reproduced with the permission of the Controller, Her Majesty's Stationery Office.

Note: This chapter expresses the opinions of the author and does not necessarily represent the official views of the Royal Aircraft Establishment.

References

(1) **Carter, J.V., and Evans, R.H.**, 'Testing of Gyros for Aircraft Inertial Navigation Application', Presented at the Third Inertial Guidance Test Symposium, Holloman AFB, New Mexico, Oct. 1966.

(2) 'Power Interruption Slashes Gyro Drift', Aviation Week and Space Technology, p. 63, July 23, 1962.

Bibliography

Cawood, W., 'Some Design Problems in Inertial Navigation', ONERA Aeronautical Congress, Paris, May 1957.

Stratton, A., 'Gyroscopes for Inertial Navigation' (James Clayton lecture), Institution of Mechanical Engineers, Feb. 1964.

Shuttlewood, G.D., 'Testing of Inertial Quality Gyroscopes' (Symposium on Gyros), Institution of Mechanical Engineers, Feb. 1965.

Stein, W., (Northrop Nortronics), 'Fundamentals of Performance Testing of Precision Rate Integrating Gyros', presented at the International Symposium Inertial Guidance Testing Technique, Weilheim, Germany, Nov. 1965.

Carter, J.V., 'Some Aspects of Testing Inertial Quality Gyroscopes at the Royal Aircraft Establishment, England' (printed in German), presented at Munich Symposium, Oct. 1963, published by Deutsche Luft-und Raumfaht DLR Mitt 66-09.

Carter, J.V., and Evans, R.H., 'Testing of Gyros for Aircraft Inertial Navigation Application', presented at the Third Inertial Guidance Test Symposium, Holloman AFB, New Mexico, Oct. 1966.

Russell, J., (Capt. USAF), 'Gyroscope Standard Torque-to-Balance Test', MDC-TR-67-79, Central Inertial Guidance Test Facility, Holloman AFB, New Mexico, available through Defense Documentation Center.

9

Diagnostic Testing and Design Shortcomings in Precision Gyroscopes

O.H. WYATT
Royal Aircraft Establishment, Farnborough, UK

Summary

Several tests of precision gyroscopes are discussed which aim to diagnose possible shortcomings in their design; tests used to determine the standard drift rate coefficients are not included.

1. Introduction

Conventional testing of gyroscopes is intended to determine the mean values and stability of various coefficients in equations representing the behaviour of idealized models of the gyroscope. In the simplest model, widely employed, the behaviour is characterized by only three drift rate coefficients; fixed restraint, mass unbalance and anisoelastic term. They are, respectively, independent of gyro acceleration, proportional to acceleration and proportional to (acceleration)^2. Typical tests to determine these parameters are polar axis tumble test, six position servo table test and fixed position closed loop test. In so far as the gyroscope tester is providing data for the system designer, no physical basis for the coefficients is required. However the gyro designer must pursue the relationship between the coefficients and the individual components of the gyroscope. Information of value to both system and design engineers can be obtained from other tests, here called diagnostic testing. These have the triple aims of establishing the source of unsatisfactory values, or stability, of the drift coefficients; of determining the gyro performance in arduous environmental conditions; and of prediciting the likely lifetime during which the coefficients will be maintained.

This chapter will discuss certain critical design features of gyroscopes, particularly of the single-degree-of-freedom floated type, and show how diagnostic testing on complete gyros can be used to establish whether the gyro designer and manufacturer have found satisfactory solutions to the problems.

2. Spin-Axis Ball Bearings

The spin-axis bearings are a major determinant of gyroscope performance, and in most gyroscopes to date a pair of ball bearings, preloaded against each other, has been used. The quality of these bearings has been greatly improved over the last twenty years, in respect of their geometry, surface condition and lubrication control. At the same time several test methods have been developed for assessing the quality of complete bearing assemblies.

(a) Run Down Test. This test measures the time taken for the wheel to slow down after cutting off the motor supply. The time is taken either from full speed

to stop or over selected speed ranges, for example 30-20 cps. The speed can be obtained from the back emf generated in the stator windings, although steps may have to be taken to largely demagnetize the hysteresis ring to prevent eddy current drag introducing an unwanted variable into the RDT (run down time). The supply voltage is reduced to zero over a short time, say 0.5 second, or the stator winding after rapid cut-off is momentarily short-circuited.

The RDT provides a simple quick check on the bearing condition, although the result can be misleading. Two factors affect the RDT in opposite ways, lubrication degradation and pre-load loss due to wear of the bearing surfaces. Thus a stable value of the RDT may be the result of a fortuitous balance. On the other hand, a change of RDT is proof of bearing degradation. In figure 9-1, the RDT has been measured under dead weight loading and the curves show the decrease of RDT with lubricant deterioration. Figure 9-2 shows the RDT of a typical gyro bearing assembly, in which the pre-load is applied with a nearly rigid spring. After an initial fairly rapid increase of RDT, the value usually increases slowly over many thousands of hours. Catastrophic failure, which normally occurs after the pre-load has fallen so far that the gyro performance is no longer satisfactory, causes the RDT to decrease over a few hundred hours to the point at which the motor torque is inadequate to keep the motor in synchronism.

The run down test is also one of the standard methods of setting up the pre-load in the assembly of gyros.

(b) Milliwatt Power Test. In this test the motor power is indicated on a wattmeter but the major part is backed off electrically so that small power changes are recorded on a large scale. One arrangement is shown in figure 9-3. Although the use of a resistive load on the same supply as the motor corrects to some extent for variations in the supply voltage, the correction is only partial, particularly for transients, and a good quality power unit (better than 0.1 percent) is required if the differential power recorded is not to be a recording of the input voltage variations. A simultaneous recording of the supply voltage is desirable to eliminate this possible cause of spurious results.

Typical scales for recording are 0.5 to 1 percent of motor power per cm (i.e. 10-100 mW/cm) and 1-10 cm per minute. Some records are shown in figure 9-4. On the expanded time scale, oscillations are found with frequency of about one cps. These are due to hunting of the hysteresis ring with respect to the magnetic field vector. This has been demonstrated by detecting the wheel position through its mass unbalance by means of an accelerometer and showing this on an oscilloscope against the voltage on one of the phases of the motor supply. The Lissajou's figure was seen to pulsate in time with the milliwatt record. Power fluctuations of this frequency occur in all hysteresis motors and do not appear to be of much value in assessing the bearing condition. For this, the contracted time scale is adequate, and more convenient over the long durations required to get a reliable picture, up to twelve hours.

Analysis of the milliwatt record is difficult. Two particular bearing defects can easily be identified, squeal and oil jags. Squeal causes a high noise level (or hash width) on the milliwatt chart and a rise in the mean power, around 20 percent or more, which is often sufficient to prevent the motor synchronizing. It is caused by violent random movements of the ball retainer, which in turn is due to inadequate lubrication at the bearing land/retainer interface, an effect found especially with 'Nylasint' porous nylon retainers. Closely related is a regular rapid motion of the retainer, with the retainer centre moving on a circular path around the bearing axis. This phenomenon is called retainer whirl and produces an audible note of definite frequency. Squeal can occur intermittently in a bearing and will degrade the gyro performance by a large amount. The second identifiable

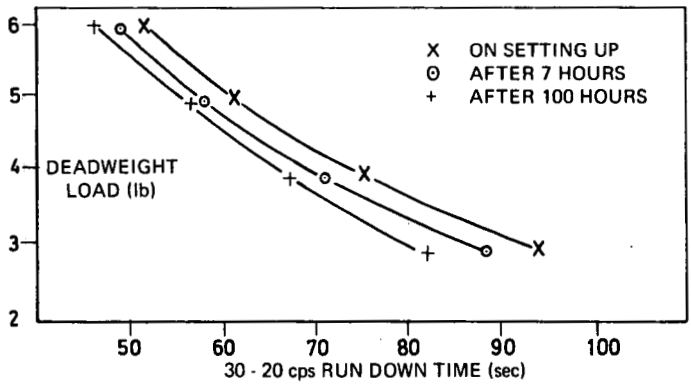

Fig. 9-1 Gyro wheel run down time (30-20 cps) under deadweight loading, at 5 lb preload.

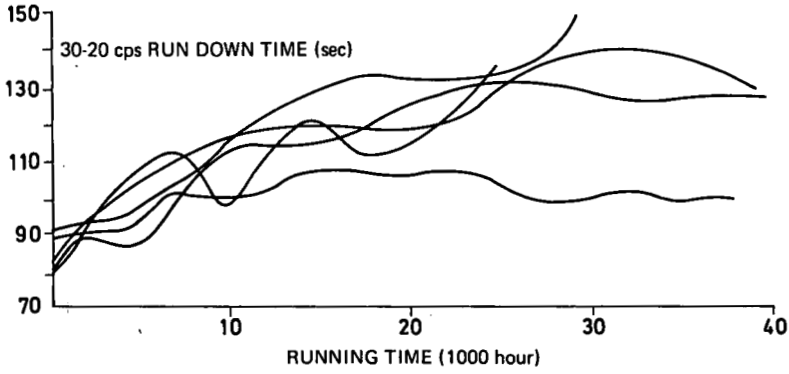

Fig. 9-2 Gyro wheel run down time with hard preload

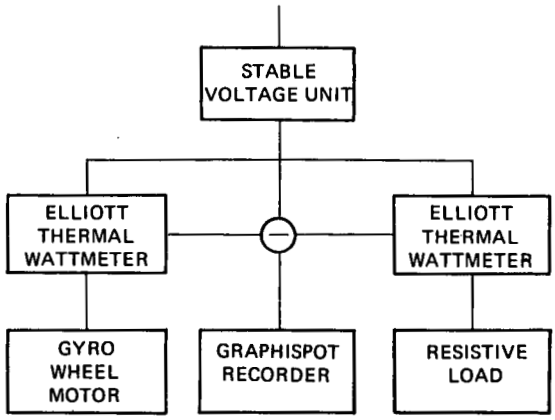

Fig. 9-3 Block diagram for measuring backed off milliwatt power

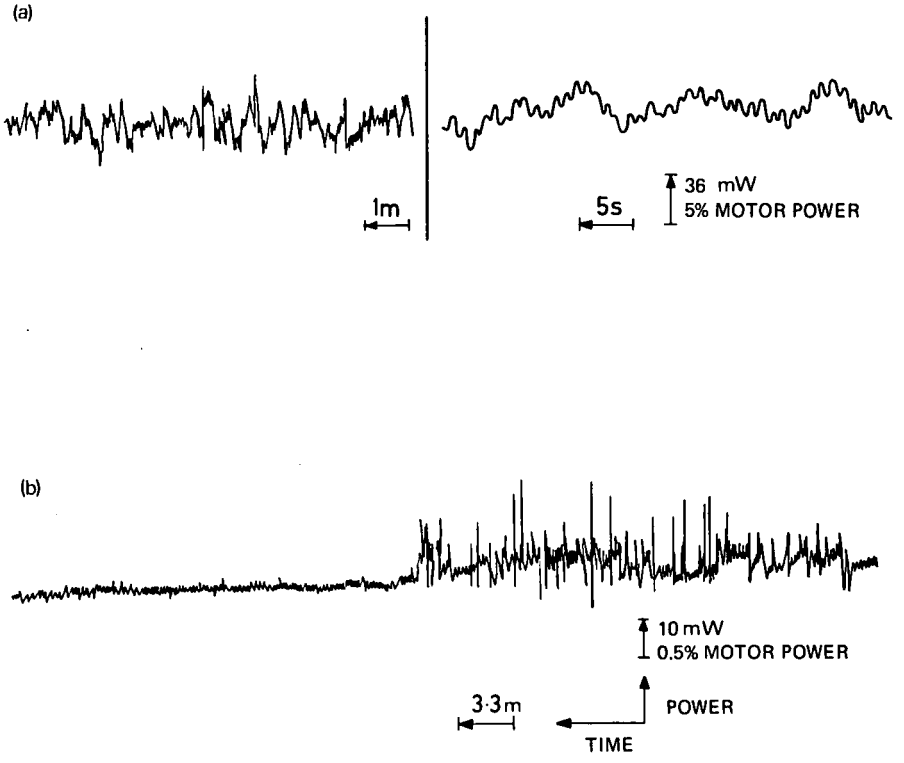

Fig. 9-4 Milliwatt power records from two gyros of different design

pattern consists of a sudden increase in power, of around 10 percent, followed by an exponential decay to the original level over a five minute period (Fig. 9-5). This is called oil jag and is caused by a drop of oil falling on to the ball track (pressure zone). The effect is particularly prevalent in Synthane fabric-resin cages and is related to the ratio of oil present in the retainer to the available porosity.

A good bearing can give a milliwatt power record with a steady noise level around 0.1 percent, but many IN gyros are operating successfully with an order of magnitude higher noise level, in addition to occasional steps in the mean power of similar size. Only individual experience on particular gyroscopes will indicate what levels of behaviour are acceptable.

3. Spin Axis Gas Bearing

Gas lubricated bearings for the spin axis are now beginning to come into service. The attractions are the possibility of indefinite running life and very smooth running. The latter is proving to be the more important factor in the best quality IN gyros and milliwatt records at the 0.1 per cent level or better are obtainable. Some irregularities have nevertheless been observed on occasions, as shown in figure 9-6. Their cause is unknown, but they were related to the motor excitation and could be eliminated by adjusting the voltage.

A serious problem in gyros with gas bearings has been that the wheels have refused to start. The offence is not only that this has happened all too frequently after a short life but also that there is no warning of degradation, the gyro apparently performing very well before shutdown. In this, the behaviour is very different from that of ball bearings which normally degrade in a slow and continuous manner. It can be argued whether gradual or step failure is more desirable to the system operator but any failure after only a few thousand hours is obviously unacceptable. Failure to start may be due to two mechanisms: the first is the result of stop/start which forms wear detritus; the second is the result of continuous running which transfers excess boundary lubricant or other contaminants within the float, such as vapour from the potting compound, into critical regions of the bearing where the wheel sits down on stopping. The latter mechanism is reputed to occur suddenly, over say a ten hour period, and no method of advance diagnosis is known. Luckily it occurs, if at all, in the early life of the gyro.

Failure by wear detritus, leading to failure to start, appears to be a gradual process which can be monitored by measuring the minimum motor voltage required to start the wheel turning. Starting is detected in several ways - for example, by holding the gyro on closed loop (pick-off to torquer) and observing the torque current. The ratio of the normal operating voltage to the minimum starting voltage should be not less than 1.5 and preferably 2.5 at the start of gyro life. Measurements of this parameter during the assessment of a gyro will indicate how soon this mechanism of failure is liable to occur. Measurements of the minimum starting voltage should be done sparingly as the conditions are ideal for producing wear, since there is a long period of rubbing before lift off occurs.

Another parameter of importance to wear damage is the energy to be dissipated at touch down on switching off. Wheels with minimum bearing clearances can be expected to touch down at lower speeds than those built, possibly more cheaply, with large clearances. Evidence on typical values has not been found.

4. Spin Motor Reaction Torque

One source of drift rate is the spin motor reaction torque. Ideally the magnetic

flux generated by the stator current is confined to the stator iron, the hysteresis ring and the intervening air gap. In some gyro designs flux leakage links the sensitive element with the housing, usually a conducting material. Eddy currents are induced and a reaction torque opposes the rotation of the magnetic field. In theory the axis of this torque is the wheel spin axis and thus perpendicular to the output axis. In practice the motor is not perfectly symmetrical and a component of reaction torque develops along the output axis, causing drift. Its value varies with the excitation voltage on the motor and the direction, with respect to the hysteresis ring, in which the magnetic induction vector locks when the motor goes into synchronism.

There are two methods of investigating this effect in a gyro. The drift rate can be measured, say in closed loop, as a function of the motor voltage. The result of varying the voltage above and below the normal operating voltage on one gyro is shown in figure 9-7. The average value of the dependence of the drift rate on the supply voltage was 0.05 degree/hour per volt; which was reduced later by improved shielding of the motor to 0.02 degree/hour per volt.

The second technique is to interrupt the motor supply at regular intervals, typically for 50 ms at 30 s intervals. After each interruption the magnetic induction vector has rotated slightly forward in the hysteresis ring, making a complete revolution in about ten minutes. Due to geometric inaccuracies and material inhomogeneity, the flux leakage and reaction torque vary in a cyclical manner. Peak to peak values of the drift rate for the same gyros as tested above were about 0.06 degree/hour.

The method of motor power interruption can also be used operationally to eliminate the contribution of the spin motor reaction torque to the drift rate.

5. Flotation Fluid

The majority of IN gyroscopes are of the floated variety; that is, the wheel is supported in a can, or sensitive element, which is neutrally buoyant in a dense fluid. The objective is to reduce the loads and friction at the gimbal bearings, which take the form of tungsten carbide pivots (0.040 in diameter) in sapphire olives. In addition, in the single degree of freedom gyro, the fluid is required to be highly viscous and the gap between the sensitive element and housing small (0.010 inch) so as to provide damping and torque integration. The presence of flotation fluid in a gyro is a principle source of trouble and expense, ranking in importance with the spin axis bearings. Various attempts to design gyros without this feature have not so far given the same standard of performance.

Inadequate processing procedures in floated gyros, that is, cleaning degassing and filling, cause friction and mass unbalance due to dirt and gas inclusions. A most powerful test for detecting these faults is the polar axis tumble test. As is fairly well known, in this test the gyro is mounted on a rotating table such that the gyro output axis and the table axis are both parallel to the earth's rotational axis. The gyro input axis is then not sensing any input rate. The table is rotated at about 150 degrees/hour while the gyro is operated in the closed loop mode, with or without the wheel running. The torquer current is recorded. Quantitative analysis can then give the usual gyro parameters, but in addition the test is very useful for qualitative diagnosis.

Figures 9-8 and 9-9 show typical records from tumble tests. Figure 9-8a is from a good gyro with small restraints and mass unbalance, and no friction. The latter is established by injecting a pulse of current to the torquer pulling the float momentarily over to one of the stops. The record shows the subsequent torquer current

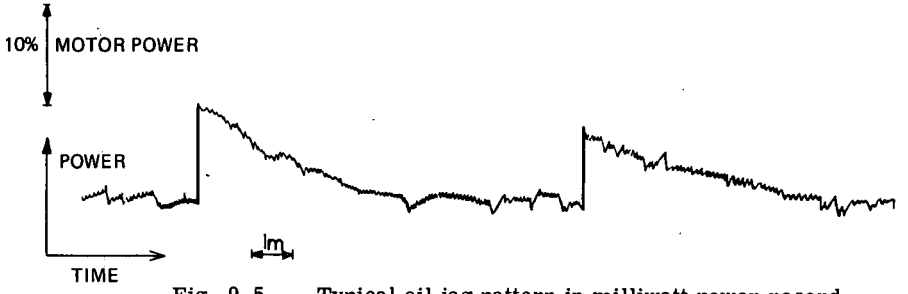

Fig. 9-5 Typical oil jag pattern in milliwatt power record

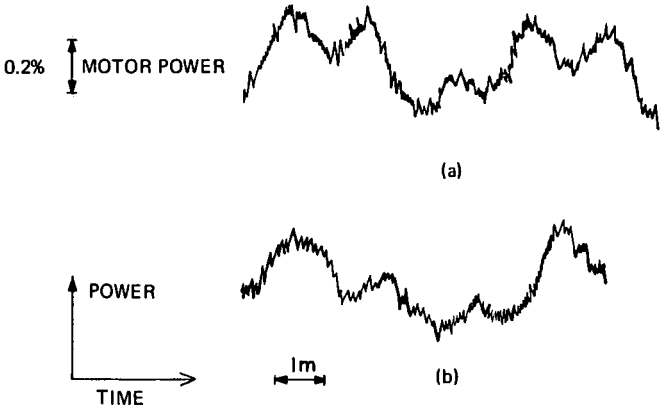

Fig. 9-6 Sample records of milliwatt power from an unstable gas bearing gyro in two separate tests

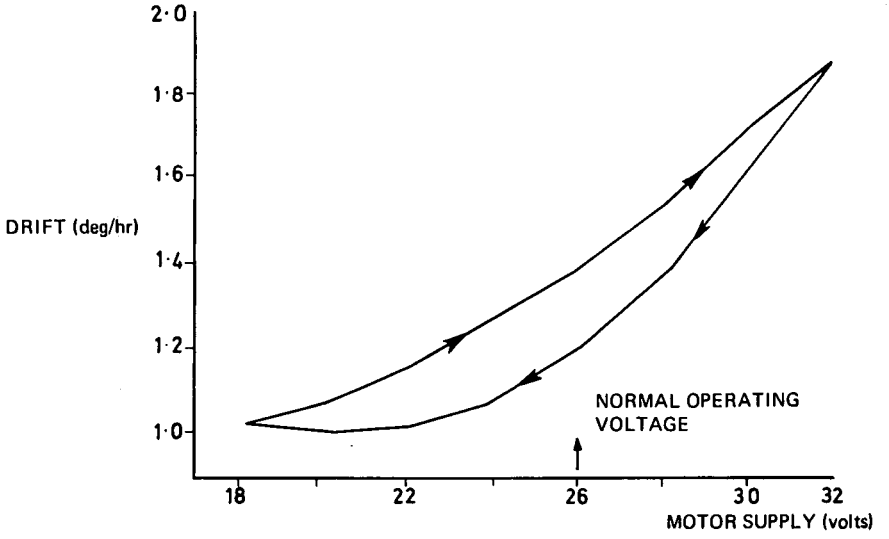

Fig. 9-7 Spin motor reaction torque

as the float is returned to null on closed loop. The trace recovers its original position. In figures 9-8b and 8c failure of the record to return to its original line after pulsing shows the presence of friction - constant and random in nature, respectively. Random friction is probably due to dirt, the source of much trouble. Figure 9-9a shows small disturbances occurring three times a cycle which are due to gas bubbles interacting with the three ligaments. During the test the bubble travels round the gyro keeping at the highest point. Turning the gyro end for end put the bubble amongst the balance screws and four disturbances per cycle were noted. The last record (Figure 9-9b) shows variable mass unbalance due to fluid entering the sensitive element. After several rotations of the gyro the fluid has become uniformly distributed over the walls of the sensitive element.

Flotation fluids are mixtures of various short chain polymers, varying in chain length and composition. One typical fluid consists of polymers of

chlorotrifluoroethylene $\left[\begin{array}{cc} F & F \\ | & | \\ C & - C \\ | & | \\ F & Cl \end{array}\right]_n$ Bromotrifluoroethylene is also used, with slightly higher density. A spread of chain lengths, about n = 2 to n = 10, is required to obtain the high viscosity at the operating temperature (50-70°C) and no solidification during storage, possibly down to -40°C, which would damage the gyro. Some spread of chain lengths is also difficult to avoid in the manufacture of the fluids. Even without solidification, the high viscosity and volumetric contraction on cooling can cause damage, particularly to the ligaments, and draw gas into the gyro past the O-ring rubber seals. In addition the longer chains may separate out from the mixture and fail to dissolve on heating. For these reasons a series of low temperature tests are called for, with alternate periods of temperature cycling and gyro assessment.

For a given fluid, a designer is able to minimize the risk of damage at low temperature by attention to the design of the ligaments and the surrounding volumes and by the location of the bellows to avoid excessive fluid flow during cooling. When there is no low temperature storage requirement, a narrow cut of a single chemical series can be specified.

Besides the risk of low temperature separation, polymer mixtures can separate by means of a process called thermogravitational diffusion. The effect, which is the basis of practical separation methods, is shown schematically in figure 9-10. The heavier long chain molecules diffuse to the colder surface and are carried downwards by convection currents; the lighter short chains diffuse to the hotter surface and are carried upwards by convection. Amongst several factors, the separation rate is a function of the gap width between the hot and cold surfaces, being proportional to the fifth power. If the fluid around the sensitive element separates into layers of differing density, a mass unbalance develops in the direction of the positive density gradient, that is, in the direction of gravity. To produce drift it is then necessary for there to be an acceleration perpendicular to gravity, or for the gyro altitude to be changed. The effect is reputed to have been observed and caused trouble in some precision gyros.

6. *Ligament Creep*

The ligaments or pigtails carrying the current across the suspension to the motor and pick off have been found to cause variable drift in some gyros. The float is held against one of the stops for a period, say overnight, and the gyro is then put into closed loop. If the effect is present, the drift rate shows a transient which

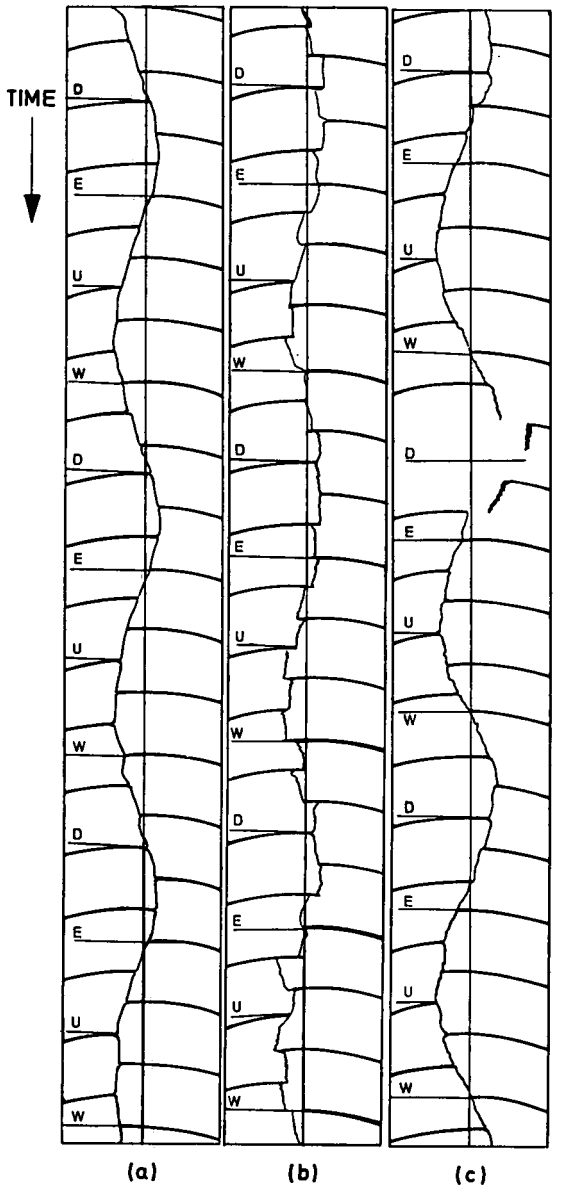

Fig. 9-8 Polar axis tumble test records: (a) good gyro, (b) consistent friction, (c) random friction

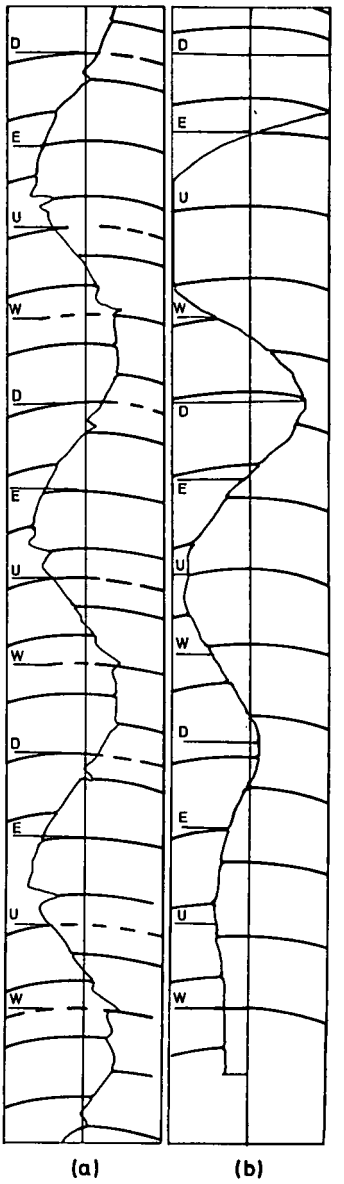

Fig. 9-9 Polar axis tumble test records: (a) bubble interacting with three ligaments, (b) reducing mass unbalance due to fluid in float

may extend several hours. Holding the float on the other stop reverses the direction of the subsequent drift transient. Typical results are given in figure 9-11. The design of this gyro was later modified by limiting the travel of the float to ±0.5 degrees instead of ±3 degrees and changing the ligament material from a silver based alloy to a gold based alloy. The improved creep behaviour is shown in figure 9-12.

Acknowledgements

The author wishes to thank his colleagues in the Royal Aircraft Establishment, the British Aircraft Corporation and Ferranti Ltd., who have developed many of the tests described here.

Note: This chapter expresses the opinions of the author and does not necessarily represent the official views of the Royal Aircraft Establishment.

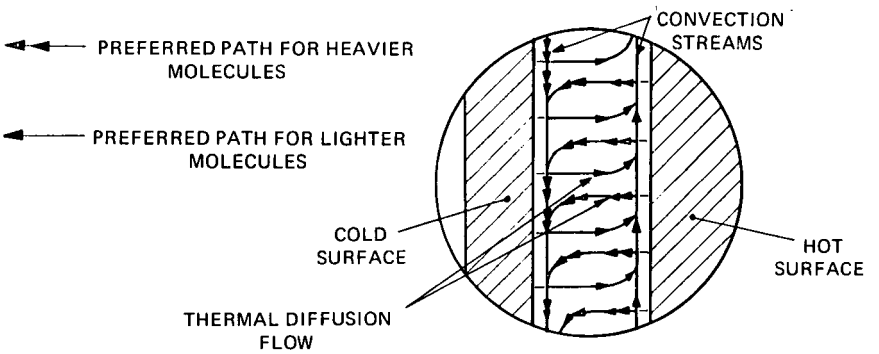

Fig. 9-10 Thermogravitational separation of flotation fluid

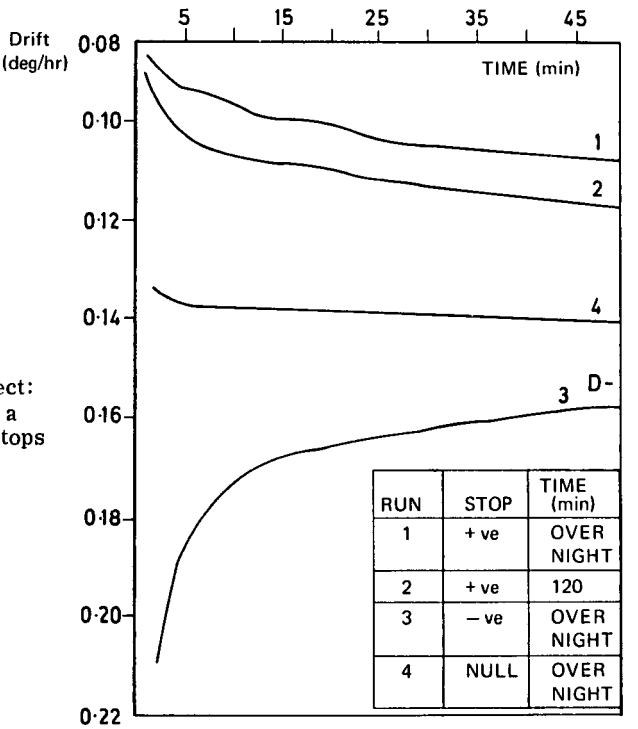

RUN	STOP	TIME (min)
1	+ ve	OVER NIGHT
2	+ ve	120
3	– ve	OVER NIGHT
4	NULL	OVER NIGHT

Fig. 9-11

Ligament creep effect: gyro drift following a period held on the stops

RUN	STOP	TIME (min
1	+ ve	OVER NIGHT
2	+ ve	120
3	– ve	OVER NIGHT

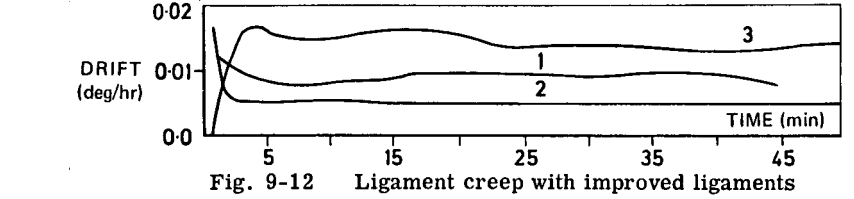

Fig. 9-12 Ligament creep with improved ligaments

10

Mesure du Facteur d'Echelle des Moteurs-couples

D. BERARD
Laboratoire d'Equipements Aéronautiques du Centre d'Essais en Vol,
Brétigny, France

Sommaire

On a cherché à mesurer le facteur d'échelle du moteur couple des gyroscopes à un degré de liberté avec une précision supérieure à 10^{-4}, le gyroscope étant bouclé en asservissement mécanique sur une table à palier à air de grande précision, l'essentiel des moyens étant constitué par la table et un générateur de courant très précis.

Cette recherche a été motivée par la gêne que nous causait une trop grande dispersion des résultats obtenus par différents procédés classiques, en particulier sur des gyroscopes dont la dérive à court terme est supérieure à 0,01 degré par heure.

On a analysé les differentes configurations possibles et utilisé une méthode de mesure et d'exploitation qui permet de s'affranchir partiellement de la dérive du gyroscope.

Les essais et les résultats portent sur la stabilité et la linéarité du facteur d'échelle ainsi que sur l'influence de la température.

Cette expérience pourrait s'appliquer à la détermination précise du facteur d'échelle d'un gyroscope monté sur la plate-forme de son système inertiel en particulier lorsque la commande est digitale.

1. Objet de l'exposé

Généralités

L'étude de la stabilisation d'un système à partir de détecteurs gyroscopiques exclusivement, nécessite toujours la définition d'un trièdre lié au système et en particulier la connaissance de son mouvement par rapport au repère galiléen. Si l'on veut donner à ce trièdre certaines propriétés par rapport à la terre (par exemple un axe du trièdre devant rester vertical) ou par rapport à tout autre système référentiel, il est nécessaire d'imposer aux gyroscopes une certaine précession. Il est commode et souvent même indispensable de se servir pour les calculs d'un trièdre d'entraînement lié à terre et par conséquent d'introduire sur le système à stabiliser une précession globale $\vec{\Omega}$ absolu :

$$\vec{\Omega}\ \text{absolu} = \vec{\Omega}\ \text{terre/absolu} + \vec{\Omega}\ \text{système/terre}$$

Pour les gyroscopes à toupie cette précession est appliquée par l'intermédiaire d'une commande électrique appliquée sur un moteur couple agissant sur l'equipage mobile.

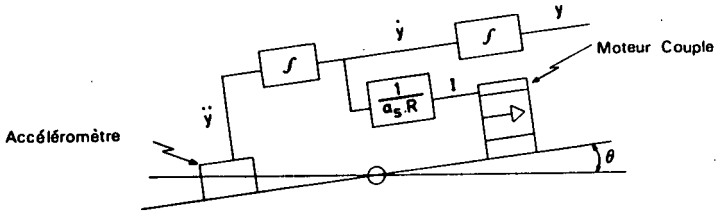

Fig. 10-1 Boucle de Schuler

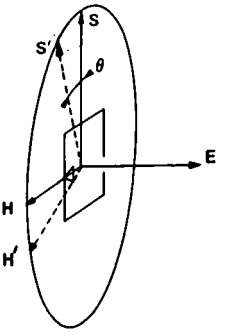

Fig. 10-2 Gyroscope de verticale

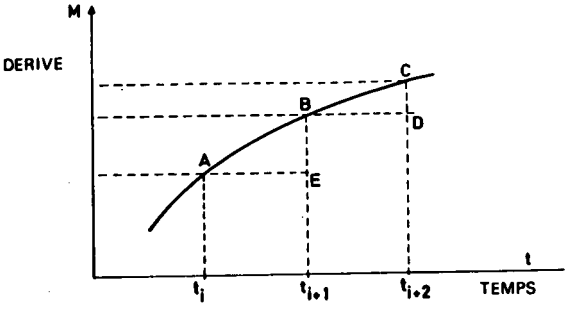

Fig. 10-3 Calcul de la précession

But des essais

Dans un système inertiel, la commande électrique du moteur couple des gyroscopes est élaborée soit à partir du calculateur, soit à partir des détecteurs accélérométriques, soit des deux à la fois. Généralement la commande est digitale et c'est dans cette configuration que doit être qualifié le système de commande de précession, mais il nous est apparu indispensable dans une première étape de pouvoir déterminer avec précision le facteur d'échelle du moteur couple lorsque la précession est imposée par un courant constant, les résultats obtenus par différents procédés classiques nous donnant une trop grande dispersion.

Ainsi cette étude donne les moyens de qualifier le moteur couple par des essais effectués sur le gyroscope seul, essais qui pourraient par la suite être appliqués à la chaîne complète du système inertiel, extraite ou non de la plate-forme, les mêmes moyens et méthodes d'essais étant appliqués alors à l'ensemble complet de la centrale de navigation.

L'exposé ne traite que des essais effectués sur un gyroscope seul.

Précision recherchée et étendue de mesure

Le facteur d'échelle du moteur couple d'un gyroscope est le coefficient de proportionnalité K entre le couple Γ et le courant I

$$K = \frac{\Gamma}{I}$$

La mesure des couples sur l'axe de sortie d'un gyroscope s'exprime en degré par heure (^{o}/h), vitesse angulaire qui appliquée sur l'axe d'entrée du gyroscope provoquerait le même couple :

$$\Gamma = H.\omega = K.I$$

Ceci conduit à définir le facteur d'échelle par le coefficient

$$a_s = \frac{K}{H}$$

exprimé en degré par heure par miliampère; on remarque que la stabilité de a_s est directement liée à celle de H, moment cinétique de la toupie.

Toute erreur sur ce paramètre a_s est équivalente à une dérive du gyroscope (il serait donc aberrant d'avoir un excellent gyroscope si l'on ne disposait pas d'un système de commande de précession de qualité équivalente). Dans cette optique il est bon d'examiner les conditions d'utilisations afin de définir les deux grandeurs: étendue de mesure et précision. Il s'agit ici de gyroscopes flottants à un degré de liberté utilisés sur une plate-forme inertielle. Un des axes du trièdre accélérométrique qui doit coïncider d'ailleurs avec le trièdre gyroscopique est astreint à suivre la verticale, un deuxième axe devant rester dans le plan méridien.

La première condition est obtenue par un bouclage de Schuler, la deuxième par une précession en boucle ouverte commandée par la vitesse est-ouest (appelé également convergence des méridiens). Nous allons estimer dans chaque configuration la dérive équivalente du gyroscope correspondant à une erreur relative

$$\epsilon = \Delta a_s / a_s$$

sur le facteur a_s.

Tableau 10-1

		Précession imposée	Dérive correspondante du gyroscope $\epsilon = 10^{-3}$		Erreur de position Nord	Erreur de position Est
Gyroscope de verticale N-S	Correction de verticale	10°/h	$\epsilon \frac{V}{R}$	0,01°/h		
	Vitesse angulaire d'entraînement	10°/h	$\epsilon \Omega \cos L$	0,01°/h		1550 m
Gyroscope de verticale E-O	Correction de verticale	0				
	Vitesse angulaire d'entraînement	0				
Gyroscope d'azimut	Convergence des méridiens	10°/h	$\epsilon \frac{V}{R} \operatorname{tg} L$	0,01°/h	330 m	0
	Vitesse angulaire d'entraînement	10°/h	$\epsilon \Omega \sin L$	0,01°/h	330 m	0
Total					660 m	3100 m

Tableau 10-2

	$\Delta\theta$	Précision relative sur d	Précision pour un temps de mesure de 5 mn	Dérive max. mesurable avec précision de 0,001°/h	Temps de mesure correspondant
Erreur due à l'inductosyn	1°	$\pm 5,5.10^{-5}$	± 0,00066°/h	18°/h	200 s
	10°	$\pm 0,8.10^{-5}$	± 0,000066°/h	180°/h	
Erreur due à un bruit de ± 0,3"	1°	$\pm 0,8.10^{-5}$	± 0,001°/h	12°/h	300 s
	10°	$\pm 0,8.10^{-5}$	± 0,0001°/h	120°/h	
Total	1°	$\pm 1,3.10^{-4}$	± 0,0016°/h	7°/h	500 s
	10°	$+ 1,3.10^{-5}$	+ 0,00016°/h	70°/h	

Gyroscope de verticale. Dans la boucle de Schuler (Fig.10-1) le signal accélérométrique $\ddot{y}$ intégré est multiplié par $1/a_s$. R (R = rayon terrestre), puis envoyé dans le moteur-couple du gyroscope. La condition à réaliser est

$$a_s . I = \frac{V}{R}$$

V étant la vitesse sur l'axe y du système.

Une erreur relative sur a_s est équivalente à une dérive du gyroscope égale à

$$\frac{\epsilon V}{R}$$

Cette erreur peut être introduite par une non-linéarité du moteur couple, ou par un mauvais réglage de la période de Schuler.

Gyroscope d'azimut. Si l'on désire maintenir un axe de la plate-forme dans le plan méridien, la précession à imposer est égale à

$$\frac{V}{R} \text{ tg } L$$

V étant la vitesse sur un parallèle de latitude L. Cette précession étant imposée par le moteur couple, une erreur relative sur a_s est équivalente à une dérive du gyroscope égale à

$$\epsilon \frac{V}{R} \text{ tg } L$$

Vitesse angulaire d'entraînement. La précession continue imposée au gyroscope par l'intermédiaire du moteur-couple pour compenser la vitesse angulaire d'entraînement de la rotation terrestre est égale à

$$\Omega_T \sin L \quad \text{et} \quad \Omega_T \cos L$$

sur les deux axes horizontal et vertical du plan méridien.

Une erreur ϵ sur a_s est équivalente à une dérive du gyroscope d'azimut de

$$\epsilon \Omega_T \sin L$$

et à une dérive de gyroscope de verticale axe d'entrée Nord-Sud de

$$\epsilon \Omega_T \cos L$$

Récapitulation des erreurs. Le tableau 10-1 récapitule les erreurs de dérive dues à une erreur relative ϵ sur a_s, et donne l'erreur en position correspondante pour un vol à vitesse V = 600 noeuds sur un parallèle de latitude 45°. Les dérives sont calculées pour une erreur relative sur a_s de $\epsilon = 10^{-3}$. L'erreur en position qui en résulte est donnée pour un temps de 84 mn.

On voit qu'une erreur relative de 10^{-3} sur a_s est équivalente dans ces conditions à une dérive de gyroscope de environ 0,02°/h. La précision recherchée sur la détermination de a_s doit être de l'ordre de 10^{-4} ou 0,001°/h sur la précession. La précession à imposer varie de 0 à 25°/h, ce qui limite le domaine de mesure à (-25°/h, +25°/h).

On définira la précision de la précession d que l'on peut commander par le moteur-couple par l'écart quadratique moyen (en °/h) des précessions d par rapport à la meilleure droite : $d = a_s . I$ et ceci dans un domaine que l'on précisera.

d*

2. Principe des Essais

Principe général

De façon à se placer dans les mêmes conditions que sur centrale, un axe de la table Fecker 452 est asservi au gyroscope, que l'on fait précessionner en envoyant dans le moteur couple un courant I connu avec grande précision.

On mesure successivement: (a) le temps t_1 mis pour dériver sur n_1 degrés dans un sens; (b) le temps t_2 mis pour dériver sur n_2 degrés le courant étant inversé ou annulé. Ces deux mesures successives sont répétées N fois.

Par différence entre deux mesures consécutives (t_1 et t_2) on en déduit la précession moyenne $a_s.I$ imposée par le courant I, éliminant ainsi le couple parasite M, et la composante de la rotation terrestre Ω_e sur l'axe d'entrée du gyroscope.

On remarque qu'il existe deux possibilités:

1 ère méthode - inverser le courant: on définit alors une valeur de a_s valeur moyenne pour I positif et I négatif, ce qui revient à supposer la caractéristique du moteur couple symétrique.

2 ème méthode - annuler le courant: ce qui permet de mettre en évidence une éventuelle disymétrie.

Moyens d'essais et précision

La précision sur la mesure de la précession électrique $a_s.I$ est donnée par: (a) la précision sur I; (b) la précision de la mesure de la dérive de la table; (b) l'évolution du couple parasite M entre t_1 et t_2.

Générateur de courant. Les générateurs utilisés du type Julie ou North Hills sont capables de générer des courants de 0 à 1 mA avec une stabilité sur 100 heures de ±2 nA soit pour un facteur d'échelle de 50°/h/mA une stabilité de la dérive du gyroscope de ± 0,0001°/h.

La précision est de l'ordre de 10^{-4} sur 1 mA dans le cas le plus défavorable - il suffit alors de mesurer le courant pour obtenir avec un pont Tinsley une précision de ± 10 nA (soit ± 10 MV sur 1 KΩ) c'est-à-dire ± 0,5. 10^{-3}°/h. La précision relative des différentes valeurs affichées sur le diviseur des sources de grande précision est meilleure généralement que 10^{-5}.

Mesure de la dérive de la table. On détermine la dérive de la table d en mesurant le temps mis pour parcourir un intervalle θ de $n \times 1°$, l'angle minimum étant de 1°.

$$d = \frac{\theta}{t}$$

Le comptage du temps se fait par un compteur dont la stabilité du pilote est de 10^{-6} par 24 heures - l'erreur sur la mesure est négligeable. Le déclenchement du compteur est donné par l'inductosyn de la table Fecker associé à un détecteur de zéro.

L'erreur en position donnée par l'inductosyn à 720 pôles s'écrit

$$Ep = 0,2 \sin 2\theta + 0,1 \sin 66\theta + \text{des harmoniques de pulsation multiple de } 360$$

L'erreur maximum sur un intervalle $\Delta\theta$ autour de θ est obtenue pour

$$\frac{d}{d\theta} \left[E_p (\theta + \Delta\theta) - E_p (\theta) \right] = 0$$

qu'on peut écrire

$$\frac{d^2}{d\theta^2} E_p = 0$$

si θ est faible devant la période de E_p, soit $\theta = 0$

Donc l'erreur maximale sur l'intervalle $\Delta\theta$ autour de $\theta = 0$ aura la même expression que E_p puisqu'on peut l'écrire

$$E_p (0 + \Delta\theta) - E_p(0) = E_p(\Delta\theta)$$

L'erreur sur 1° est de 0,086″ et sur 10° de 0,150″, ce qui explique que les erreurs sur 1° ou 10° sont du même ordre, et majorées à ± 0,2″.

A cette erreur géométrique s'ajoutent les erreurs de répétabilité propres à l'essai, définies par le bruit d'asservissement au niveau de la table (détecteur de zéro). Ce bruit varie de ± 0,1″ à ± 0,3″ (le bruit électrique de l'inductosyn étant inférieur, de l'ordre de ± 0,05″). On améliorera si possible la répétabilité de la mesure en dérivant entre deux positions fixes de la table, éliminant ainsi l'erreur géométrique.

Les erreurs sur la mesure de d sont résumées dans le tableau 10-2.

Evolution du couple parasite. Le principe de la mesure (voir ci-dessus) suppose qu'entre deux mesures successives, la valeur moyenne du couple parasite n'a pas varié. Il est clair que lors d'une mesure de la précession electrique, c'est à dire deux mesures successives de la dérive de la table, l'erreur introduite est égale à la variation de la dérive du gyroscope entre ces deux mesures.

C'est dans la position de gyroscope de verticale que la dérive aléatoire est la plus faible, mais comme on ne peut dériver autour de cette position sans en changer, il est nécessaire de savoir dans quelles conditions ces essais peuvent être effectués.

Différents types d'essais possibles

Gyroscope d'azimut. On ajoute à la précession de la table due à la composante verticale de la rotation terrestré de 10°/h la précession électrique ce qui porte le domaine de mesure à (± 10°/h, ± 35°/h). Les domaines positifs et négatifs sont obtenus par rotation de 180° du gyroscope autour d'un axe horizontal. La précession étant toujours de même signe pendant une série de mesure, la répétabilité des mesures sera égale à la précision, qui peut être très élevée puisque l'angle de mesure n'est pas limité. Le couple parasite $M = C + B_H$, couple indépendant de g et balourd de la toupie peut limiter très rapidement la précision. On constate sur certains gyroscopes des variations discontinues de B_H de plusieurs centièmes de °/h, d'où l'idée de placer le gyroscope en position de verticale.

Gyroscope de verticale (Fig. 10-2). La précession ayant lieu cette fois autour d'un axe horizontal, le développement qui suit a pour but de montrer que la variation du champ de pesanteur g par rapport au gyroscope n'affecte pas la mesure - dans une certaine limite d'angle.

La table dérivant sur n degrés autour de la position de verticale, le couple parasite s'écrit

$$M = C + B_E \sin \theta$$

où θ est la position de la table et B_E est le balourd sur l'axe d'entrée du gyroscope.

Si l'intervalle de dérive $(-\theta o + \theta o)$ est centré sur la position verticale de l'axe de sortie du gyroscope, le couple moyen sur cet axe est égal à

$$\overline{M} = \frac{1}{2\theta o}\int_{-\theta o}^{+\theta o} C \, d\theta + \frac{1}{2\theta o}\int_{-\theta o}^{+\theta o} B_E \sin \theta \, d\theta$$

où θ est une fonction du temps. Le premier terme représente le couple moyen C pendant l'intervalle de temps de la mesure, le second la valeur moyenne de la dérive due à B_E qui est nulle. Théoriquement l'influence de B_E est donc nulle.

En fait la variation de dérive due à un mouvement du gyroscope dans le champ de la pesanteur peut prendre une forme quelconque $f(\theta)$ différente de $B_E \sin \theta$, à l'échelle d'un mouvement de 1 ou 2 degrés (ce que l'on met en évidence couramment dans un essai équatorial). La fonction f peut dépendre également du signe de la précession - le but de l'essai qui est décrit ci-après est de montrer que sur un intervalle de 1 ou 2 degrés la valeur moyenne de $f(\theta)$ peut être représentée par celle de B_E : $\sin \theta \simeq B_E \theta$.

Le principe est le suivant: on fait précessionner la table en envoyant dans le moteur couple un courant de compensation

$$I_o = \frac{\Omega T}{a_s} - \frac{C}{a_s} - \frac{W_e}{a_s}$$

où T est la précession choisie égale à 15°/h et W_e est la composante de la rotation terrestre sur l'axe d'entrée. La dérive de la table est égale à

$$\theta' = a_s I_o + C + f(\theta) + W_e$$

$$\text{c.a.d } \theta' = \Omega T + f(\theta)$$

La sortie de l'inductosyn, de la forme sin et cos de $360.\theta$, est envoyée sur le stator d'un résolver dont le rotor tourne à la vitesse $360 \times \Omega T$ avec une précision de 10^{-4} sur un tour. On enregistre après démodulation la sortie R du rotor.

$$\theta R = \sin 360\,(\Omega T.\ t - \theta)$$

dont la dérive $\theta' R = f(\theta)$. L'essai est répété pour $\pm \Omega T$.

Le dépouillement de $\theta R(\theta)$ permet de tracer $f(\theta)$. L'essai est répétitif, et dans l'intervalle de -1°, +1°on trouve pour la meilleure droite représentative de $f(\theta)$:

$$f_1 : \theta' R_1\ (0,01°/h) = -2,01.\ \theta \ \text{(degré)} - 0,32$$

$$f_2 : \theta' R_2\ (0,01°/h) = -2,07.\ \theta \ \text{(degré)} + 0,57$$

Remarque - le dépouillement n'a de sens que sur un intervalle de degrés entiers si l'on veut s'affranchir de l'erreur géométrique du résolver.

Les équations montrent donc que les pentes sont égales à mieux que 0,001°/h, ce qui rejoint d'ailleurs la précision de la mesure. Cette pente représente un balourd B_E de -1,14°/h, valeur que l'on trouve par les essais classiques. Les

ordonnées à l'origine correspondent à une dérive moyenne non nulle et respectivement égales à +0, 57 et -0, 32 centièmes de degrés/heure. Ceci est dû à l'erreur commise sur l'estimation du facteur d'échelle qui rappelons-le n'est pas encore connu puisque cet essai précède celui qui déterminera a_s avec grande précision. Les corrections de facteur d'échelle étant faites postérieurement (valeur de a_s calculée ici pour une précession de 15°/h), la dérive moyenne est ramenée à 0, 001°/h, ce qui peut s'expliquer soit par une imprécision des mesures soit par une évolution du couple fixe.

Si l'on se contente de définir une valeur de a_s dans le domaine - 25°/h + 25°/h en supposant une symétrie du moteur couple, on peut utiliser la première méthode en plaçant l'axe d'entrée du gyroscope E - O de façon à mesurer les dérives faibles sur 1, 2 ou 3 degrés.

Si on ne suppose pas une symétrie du moteur couple (toujours dans le cas où les performances du gyroscope en azimut sont mauvaises) on placera l'axe d'entrée du gyroscope N - S, la précession électrique s'ajoutant à la composante de la rotation terrestre. La précession de la mesure sera limitée. En effet on pourra espérer 0, 001°/h pour une précession de 14°/h, l'essai étant conduit sur deux degrés (voir analyse de la precision ci-dessous).

3. Méthode de mesure

Méthodes

Comme il a été précisé ci-dessus, la méthode de mesure consiste à envoyer successivement dans le moteur couple des courants + I et - I ou ± I et O.

Equations. Ecrivons les équations des couples sur l'axé de sortie du gyroscope. Ces couples, dus au mouvement de la table, au moteur-couple, aux imperfections du gyroscope et à la rotation terrestre, sont exprimés par convention en degré par heure.

Méthode 1

$$d_1 + a_s.I + M_1 + \Omega_e = 0 \qquad \text{(Eq. 10-1-1)}$$

$$d_2 - a_s.I + M_2 + \Omega_e = 0 \qquad \text{(Eq. 10-1-2)}$$

$$d_3 + a_s.I + M_3 + \Omega_e = 0 \qquad \text{(Eq. 10-1-3)}$$

$$d_i + (-1)^{1+i} a_s.I + M_i + \Omega_e = 0 \qquad \text{(Eq. 10-1-i)}$$

Méthode 2

$$d_1 + a_s.I + M_1 + \Omega_e = 0 \qquad \text{(Eq. 10-2-1)}$$

$$d_2 + 0 + M_2 + \Omega_e = 0 \qquad \text{(Eq. 10-2-2)}$$

$$d_3 + a_s.I + M_3 + \Omega_e = 0 \qquad \text{(Eq. 10-2-3)}$$

$$d_j + (1-(-1)^j) \frac{a_s.I}{2} + M_j + \Omega_e = 0 \qquad \text{(Eq. 10-2-j)}$$

où

d = dérive de la table

a_s = facteur d'echelle du moteur-couple

I = courant du moteur-couple

$a_s.I$ = précession électrique

M = couple parasite

Ω_e = composante de rotation terrestre sur l'axe d'entrée.

Calcul de la précession. On résoud les systèmes non pas avec deux équations mais avec trois. En effet, en raisonnant par exemple pour la méthode 1 on trouve pour l'expression $a_s.I$ de la précession:

Avec deux équations successives: 10-1, i et 10-1, i + 1

$$a_s.I = \frac{1}{2(-1)^{i+1}} [(d_{i+1} - d_i) + (M_{i+1} - M_i)]$$

Avec trois équations: 10-1, i, 10-1, i + 1 et 10-1, i + 2

$$a_s.I = \frac{1}{4(-1)^{i+2}} [(d_{i+2} - 2d_{i+1} + d_i) + (M_{i+2} - M_{i+1}) - (M_{i+} - M_i)]$$

L'erreur introduite par l'évolution inconnue de M (dérive du gyroscope) est beaucoup plus faible évidemment sur l'écart $M_{i+2} - M_{i+1}$ (chiffrée par CD - BE sur la figure 10-3) que sur la variable M (chiffrée par BE).

On trouverait de même en appliquant la méthode 2

$$a_s.I = \frac{1}{2(-1)^{j+1}} [(d_{j+2} - 2d_{j+1} + d_j) + (M_{j+2} - M_{j+1}) - (M_{j+1} - M_j)]$$

Si l'évolution est lente par rapport au temps de mesure, c'est-à-dire si $M_i + M_{i+2} \simeq 2M_{i+1}$, l'erreur commise en négligeant ce terme sera très faible, et il est possible d'en tenir compte. Dans la mesure où cette évolution serait rapide on pourrait néanmoins fournir une valeur a_s qui reflète aussi bien les anomalies du moteur couple que la dérive du gyroscope.

Calcul de la dispersion. Plutôt que d'utiliser les différentes valeurs de a_s données par les calculs précédents, des méthodes 1 et 2, on tire

$$M_i - M_{i+2} = d_{i+2} - d_i$$

On contrôle la dispersion des mesures due à la dérive aléatoire en calculant l'écart quadratique moyen σ sur le terme $(d_{i+2} - d_i)$, sachant que cette dispersion sera évaluée par $\sigma/2$ dans la méthode 1 et par σ dans la méthode 2. Ceci n'est valable évidemment que si l'erreur de mesure sur d est inférieure à σ, c'est-à-dire si on peut admettre que la dispersion sur a_s n'est due qu'à M.

Pour vérifier la validité des hypothèses on peut comparer la valeur du $\sigma(d_{i+2} - d_i)$ avec le σ des dérives trouvées lors d'un essai en dérive intégrée par exemple.

Détermination pratique de la précession. En réalité, comme on n'a pas besoin des différentes valeurs de $a_s.I$ pour calculer la dispersion, on ne les calcule pas, et on prend l'expression générale de la moyenne des différentes valeurs de $a_s.I$ données par les formules du paragraphe 'Calcul de la précession' ci-dessus.

Choix de la méthode et du type d'essai

La configuration à choisir pour mesurer le facteur d'échelle avec le plus de précision possible dépend des paramètres suivants:

(a) la qualité du gyroscope en azimut (stabilité à court terme de la dérive)

(b) l'importance du balourd B_E qui peut également pénaliser la précision que l'on peut attendre d'un essai de verticale

(c) le domaine de mesure

L'essai le plus facile à mettre en oeuvre est l'essai en azimut, et la précision absolue la plus grande sera obtenue dans cette configuration en laissant dériver la table de façon à moyenner les erreurs géométriques de l'inductosyn, c'est à dire en appliquant la méthode 2.

Néanmoins la position de verticale peut permettre de mettre en évidence une sensibilité ou une anomalie éventuelle du moteur-couple car l'essai s'effectuant sur le même intervalle angulaire on peut espérer des conditions de mesure très fidèles. La méthode utilisée quant à elle, sera fonction du but recherché.

Le choix de la position N-S ou E-O du gyroscope de verticale sera défini par le domaine de mesure auquel on s'intéresse.

4. Essais et Résultats

Exploitation des mesures

Quels que soient le type d'essais et la méthode utilisée, pour chaque valeur du courant I dans le moteur couple, on définit la précession électrique $a_s.I$ et la dispersion σ (I) attachée à cette mesure.

Le nombre d'essais n définissant une valeur moyenne de $a_s.I$, c'est à dire le nombre n d'équations 10-1-i ou 10-2-j, a été limité à n = 12, compromis à réaliser entre, d'une part, une bonne estimation de $a_s.I$ et, d'autre part, une durée d'essai convenable (environ une heure pour définir une valeur moyenne de $a_s.I$ pour un courant donné).

Linéarité. Le dépouillement d'un essai de linéarité dans la plage -25, +25 degré/heure est donné en exemple (Tableaux 10-3 et 10-4) pour les gyroscopes no. 2 et no. 301. On a calculé les coefficients A et B de la droite des moindres carrés généralisée associée aux N points $(a_s.I, I)$.

$$a_s.I = A.I + B$$

chaque valeur moyenne de $a_s.I$ étant affectée d'un poids égal au coefficient $\sigma(I)$ écart-type de la variable aléatoire $a_s.I$. On définit ainsi quatres droites:

sur le domaine -I, +I	: $a_s.I = A_1.I + B_1$	(Eq. 10-3)
pour I < 0	: $a_s.I = A_2.I + B_2$	(Eq. 10-4)
pour I > 0	: $a_s.I = A_3.I + B_3$	(Eq. 10-5)
pour B = 0	: $a_s.I = A_4.I$	(Eq. 10-6)

Le facteur d'échelle est par définition A_4. Des différences sur les coefficients A_2 et A_3 mettraient en évidence une disymétrie du moteur-couple. Les coefficients B doivent être négligeables.

On calcule ensuite les écarts E_1, E_2, E_3 et E_4 des différentes valeurs moyennes $a_s.I$ par rapport à la droite représentative associée et on appelle 'linéarité' du moteur couple dans le domaine de mesure le rapport:

$$E \text{ maximum} / | \text{Domaine de mesure} |$$

L'expérience conduit à n = N = 10 pour un domaine de mesure (-25°/h +25°/h).

Dans l'illustration de cet essai (Tableau 10-3), concernant le gyroscope no. 2, figure les variables suivantes:

X : courant du moteur-couple I, en μA

Y : précession moyenne a_s. I, en degré/heure

Sigma : dispersion $\sigma(I)$ attachée à a_s. I, en degré/heure

$A_1, A_2, A_3, A_4, B_1, B_2, B_3$: les coefficients des droits d'équations 10-3 à 10-6 définies précédemment dans ce même paragraphe.

E_1, E_2, E_3 et E_4 : les écarts de chaque valeur moyenne a_s. I par rapport à ces droites.

On voit que les dispersions $\sigma(I)$ varient de 0,002°/h à 0,006°/h, alors que pour le même gyroscope l'écart quadratique moyen de la dérive aléatoire (dans la même position azimutale) varie de 0,010°/h à 0,050°/h et vaut en moyenne 0,026°/h.

L'écart moyen des différentes valeurs de la précession par rapport à la droite $Y = A_1X + B_1$ est de 0,001°/h, ce qui donne un écart moyen relatif au domaine de mesure de 4.10^{-5}. La linéarité calculée sur l'écart maximum qui est de 0,003°/h dans le domaine (-25, +25) °/h est de $1,4.10^{-4}$. Le terme constant B_1 est de 0,0005°/h.

Les pentes des droites pour I positif et I négatif sont égales à mieux que 3.10^{-5}, le moteur-couple est donc parfaitement symétrique.

Influence de la température. Un exemple concernant le gyroscope no. 301 est donné (Tableau 10-5). L'essai est fait en position de gyroscope de verticale dans la gamme 66°C à 76°C.

Supposant dans ce domaine, la variation de a_s linéaire avec la température T, on définit a_s pour une valeur de courant I comme le rapport a_s. I/I et la sensibilité en température K du moteur couple par la pente de la meilleure droite

$$\frac{\Delta a_s}{a_s} = K \frac{\Delta T}{T}$$

On trouve pour le coefficient K (dans une plage de ±5°C autour de la température de fonctionnement)

$$K = -4.10^{-4}/°C$$

le facteur d'échelle variant de 39,384 à 39, 237°/h/mA

Mise en oeuvre

Les seuls essais effectués jusqu'à ce jour concernent des gyromètres intégrateurs flottants à moteur-couple à courant continu et aimant permanent.

Asservissement mécanique. La constante de temps k de ce type de gyroscope, dont la fonction de transfert est de la forme

$$\frac{\theta_s}{\theta_E} = \frac{K}{p(1+kp)}$$

étant généralement faible, de l'ordre de 3 ms, leur asservissement mécanique sur une table à palier à air ne pose aucun problème. La bande passante de l'axe principal de la table se situant vers 10 Hz, le bruit d'asservissement au

Tableau 10-3 Gyroscope no. 2 - linéarité

Essai du 21/22 décembre 1966
Température d'essai : 70°C
Gyroscope d'azimut position 1 et 2
Domaine de mesure : -25, +25 degré/heure

Mesures:

X - courant moteur-couple (microampère)
Y - précession imposée par X (degré/heure)

	X	Y	Sigma	E_1	E_2	E_3	E_4
1	-825, 000	24, 832	0, 003	-0, 001	-0, 001		-0, 000
2	-660, 000	19, 866	0, 002	0, 000	0, 000		0, 000
3	-495, 000	14, 901	0, 006	0, 001	0, 001		0, 001
4	-330, 000	9, 932	0, 003	-0, 000	-0, 000		-0, 000
5	-165, 000	4, 963	0, 002	-0, 003	-0, 002		-0, 003
6	+165, 000	- 4, 965	0, 003	0, 002		0, 001	0, 001
7	+330, 000	- 9, 933	0, 004	0, 000		-0, 000	-0, 000
8	+495, 000	-14, 901	0, 005	-0, 000		-0, 001	-0, 002
9	+660, 000	-19, 868	0, 004	-0, 000		-0, 000	-0, 002
10	+825, 000	-24, 833	0, 004	0, 000		0, 001	-0, 000
			E_{max}	= -0, 003	-0, 002	0, 001	-0, 003

Résultats:

Coefficients de la meilleure droite:

	$Y = A_1 * X + B_1$	A_1 = -0, 030101	B_1 = -0, 00051
X négatif	$Y = A_2 * X + B_2$	A_2 = -0, 030103	B_2 = -0, 00133
X positif	$Y = A_3 * X + B_3$	A_3 = -0, 030103	B_3 = 0, 00054
	$Y = A_4 * X$	A_4 = -0, 030100	

Facteur d'échelle: 30, 100 degré/heure-milliampère

Linéarité: 0, 00014

niveau de la table n'excède pas pour de bon gyroscope 0.3 seconde d'arc et est généralement inférieure à 0,1 seconde d'arc.

Ambiance thermique. Le gyroscope est monté dans un cube dont les faces sont orthogonales aux axes E, S et H du gyroscope. Le cube est lui-même positionné sur une platine finement orientable sur les deux axes du plan de pose de façon à corriger éventuellement une erreur d'axe du gyroscope, l'ensemble étant coiffé par une enceinte isolante et étanche (Figs. 10-4 à 10-6).

Le gyroscope est régulé en température par son enroulement de chauffage sur sa propre sonde de détection. Le régulateur proportionnel est un détecteur synchrone assurant une stabilité au niveau de la sonde meilleure que 0,01°C. L'environnement du gyroscope est assuré par une régulation proportionnelle du cube, l'ensemble étant placé en atmosphère d'hélium. La stabilité thermique jour à jour est assurée par un contrôle du flux thermique du gyroscope vers l'environnement, c'est-à-dire par (a) la puissance fournie au gyroscope (toupie et chauffage d'entretien) et (b) la température de peau du gyroscope.

Comme les essais ont trait au moteur couple, des contrôles de la résistance du moteur couple sont également possibles; en particulier, pour les essais où l'on veut faire varier la température de quelques degrés, le contrôle est indispensable. La constante de temps de la réponse à un échelon provoqué sur le chauffage propre du gyroscope pénalise la durée des essais en température d'au moins 30 mn à chaque palier de température et rend ces essais particulièrement longs.

5. Conclusion

Il apparaît que les essais ainsi définis sont faciles à mettre en oeuvre à partir d'un matériel classique d'essais de gyroscopes, mais généralement assez longs. Aussi, si l'on veut définir la linéarité du moteur-couple d'un gyroscope avec précision, c'est à dire obtenir dans le domaine -25°/h, +25°/h une dizaine de points de la droite $d = a_s.I$, l'essai durera environ 16 heures, soit deux jours. Cela entraîne une immobilisation du matériel sans rapport avec les résultats obtenus.

La stabilité du facteur d'échelle, bien que ce dernier soit défini comme la pente de la droite $d = a_s.I$, se mesurera en conséquence plus rapidement pour une valeur standard du courant I, et ce, sans inconvénient, une fois établi la linéarité du moteur couple. Cet essai est rapide et peut s'incorporer facilement aux essais classiques.

Quant aux essais en température, leur mise en oeuvre avec les moyens classiques de régulation en température est très longue et doivent répondre à un besoin bien précis.

A l'issue de ces essais, on peut remarquer qu'il est possible de donner une dérive aléatoire totale qui serait le reflet des imperfections du moteur-couple, du gyroscope proprement dit et de la commande de précession, et que des essais envisagés dans cette optique ne dissociant pas les différentes imperfections pourraient être menés plus rapidement et qualifieraient la précision globale avec laquelle on peut faire précessionner une plateforme inertielle à détecteurs gyroscopiques, la rentabilité étant accrue du fait du volume du matériel testé.

Tableau 10-4 Gyroscope no. 301 - linéarité

Essai des 9 et 10 Avril 1968
Position azimut 1 et 2
Domaine de mesure +25, -25 degré/heure

Mesures:

X - courant moteur-couple (microampère)
Y - précession imposée par X (degré/heure)

	X	Y	Sigma	E_1	E_2	E_3	E_4
1	+635, 320	25, 002	0, 003	-0, 000		-0, 001	0, 001
2	+381, 190	15, 005	0, 006	0, 002		0, 001	0, 004
3	+127, 060	5, 000	0, 002	-0, 000		-0, 002	0, 000
4	-127, 060	- 5, 003	0, 006	-0, 005	0, 000		-0, 003
5	-635, 320	-24, 996	0, 005	0, 002	0, 000		0, 005
			E_{max} =	-0, 005	0, 000	-0, 002	0, 005

Résultats:

Coefficients de la meilleure droite

	$Y = A_1 * X + B_1$	$A_1 = 0.039351$	$B_1 = 0.00172$
X négatif	$Y = A_2 * X + B_2$	$A_2 = 0.039335$	$B_2 = 0.00536$
X positif	$Y = A_3 * X + B_3$	$A_3 = 0.039351$	$B_3 = 0.00300$
	$Y = A_4 * X$	$A_4 = 0.039352$	

Facteur d'échelle: 39, 352 degré/heure-milliampère

Linéarité: 0. 00020

Tableau 10-5 Gyroscope no. 301 - influence de la température

Essai du 11 Avril 1968
Position verticale P3
Courant moteur-couple: 381, 19 microampère

	Température (degré C)	Précession (degré/h)	Sigma (degré/h)	Ecart (degré/h)	a_s (degré/h-μA)
1	66, 8	-15, 0129	0, 007	0, 0046	39, 3845
2	70, 0	-15, 0032	0, 006	-0, 0061	39, 3606
3	73, 1	-14, 9830	0, 005	-0, 0045	39, 3059
4	76, 0	-14, 9570	0, 008	0, 0035	39, 2377
			E_{max} =	-0, 0061	

Variation rélative du facteur d'échelle = -0, 00041 par degré C

Notations

g	pesanteur, m/s^2
ω	vitesse angulaire, °/h
Ω	rotation terrestre, °/h
R	rayon terrestre, m
V	vitesse linéaire, m/s
Γ	couple, N×m
I	courant, A
H	moment cinétique de la toupie, $g.cm^2/s$
a_s	facteur d'échelle du moteur couple, (°/h)/mA
θ	angle, radian
M	couple parasite sur axe de sortie, °/h
B_E	balourd sur l'axe d'entrée, (°/h)/g
B_H	balourd sur l'axe de spin, (°/h)/g
C	couple indépendant de g, °/h
D	dérive de la table, °/h
σ	écart quadratique moyen
ϵ	erreur relative
Δ	incrément ou erreur
P	variable de Laplace

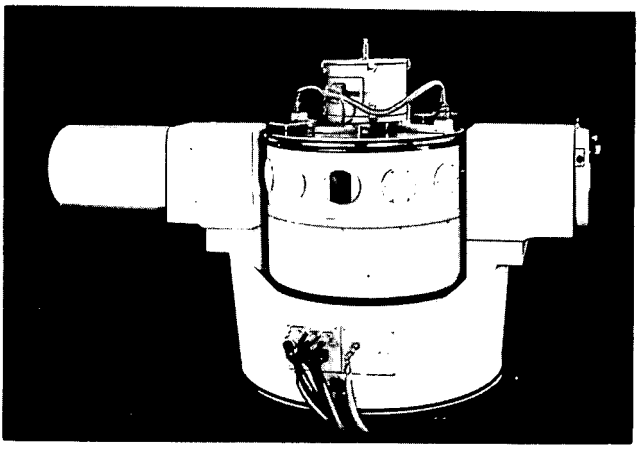

Fig. 10-4 Table à palier à air

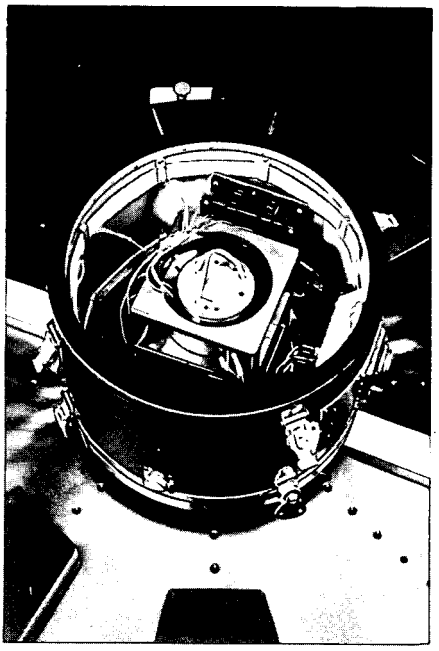

Fig. 10-5 Platine et cube

ee

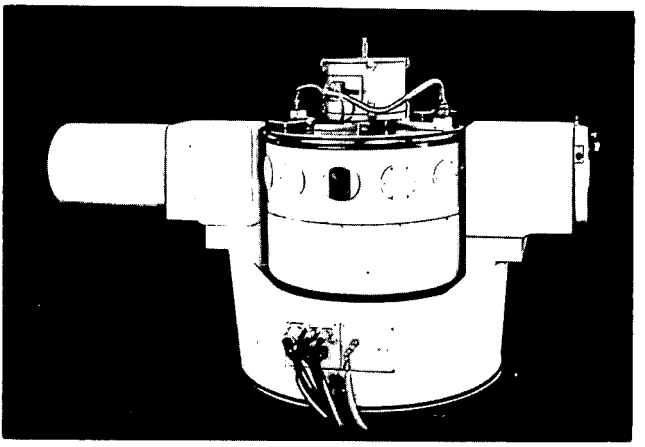

Fig. 10-4 Table à palier à air

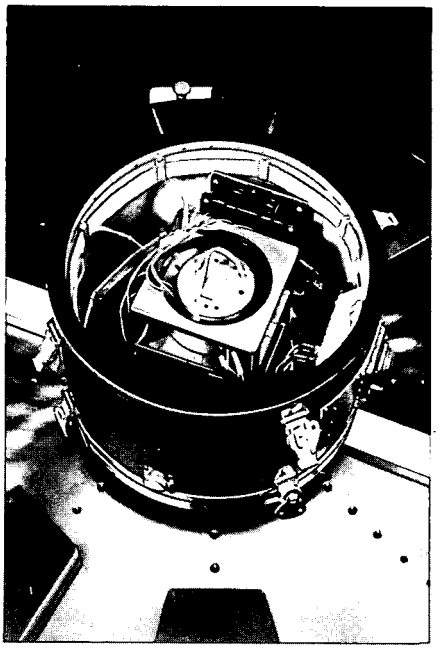

Fig. 10-5 Platine et cube

ee

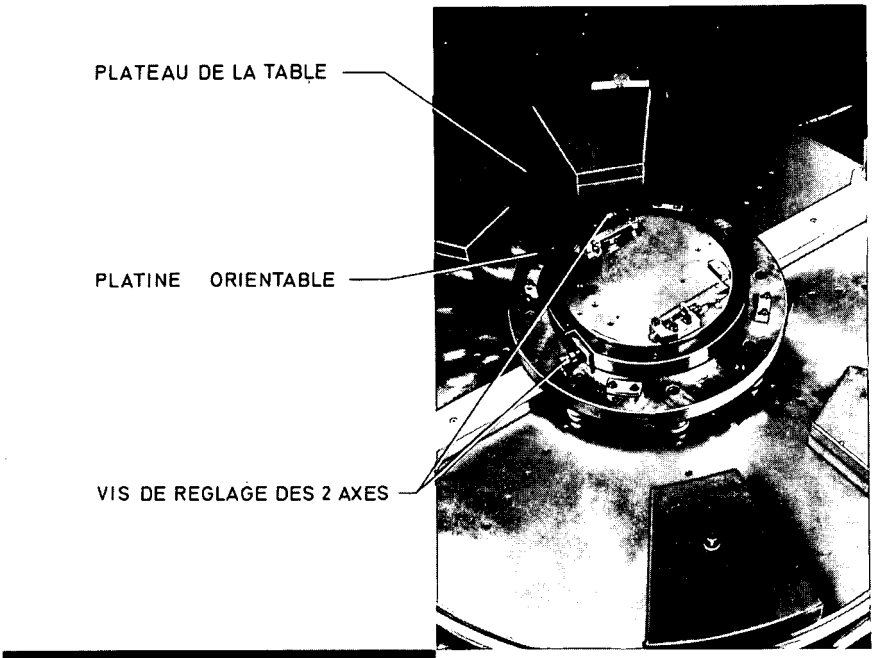

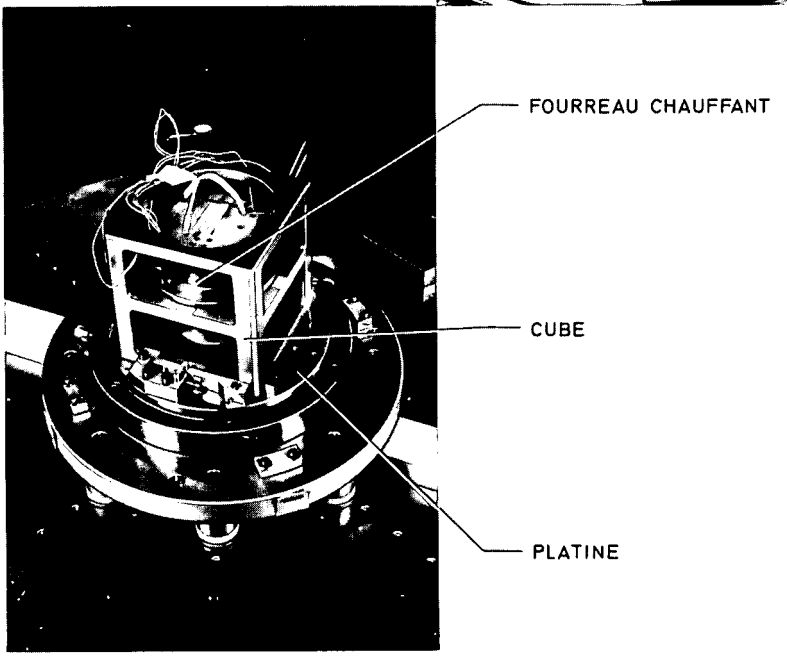

Fig. 10-6 Enceinte

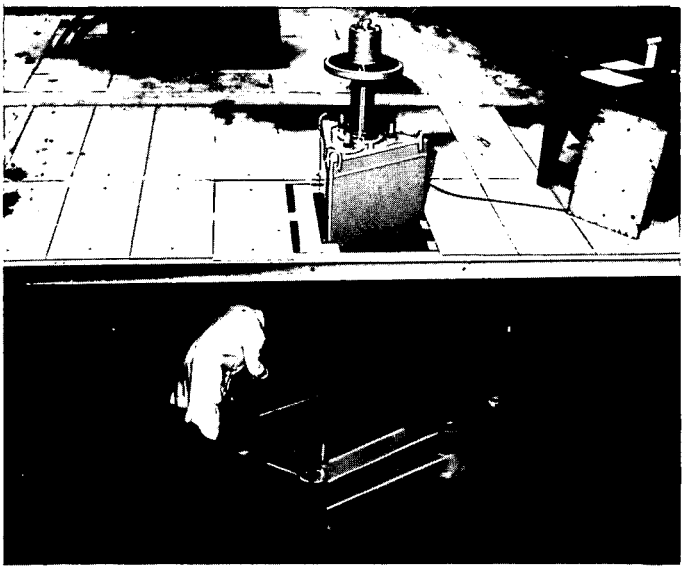

Vue d'ensemble

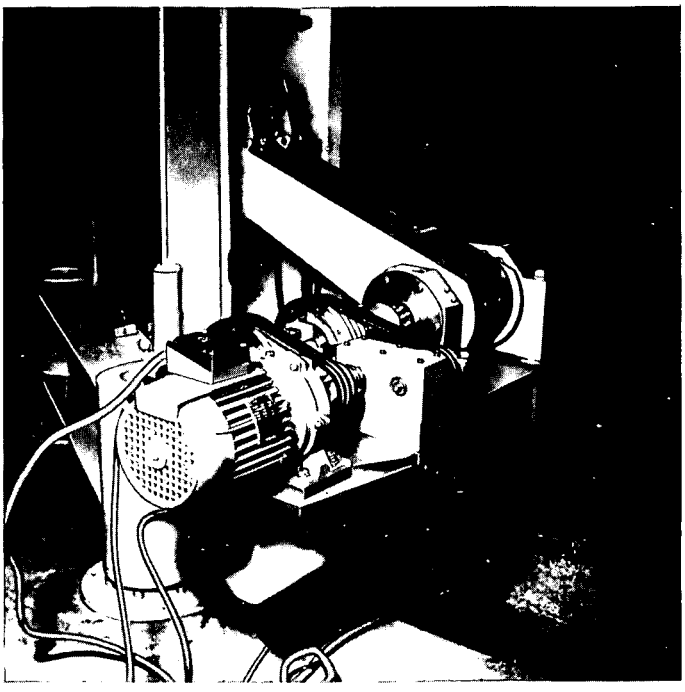

Ensemble électromécanique d'entretien

Fig. 11-1 Table 10g

11

Une Table 10g et le Comportement de Matériels Gyroscopiques sous Accélération

E. OLIVIER
Laboratoire de Recherches Balistiques et Aérodynamiques, Vernon, France

Résumé

Après avoir montré, sur le plan théorique, l'intérêt d'une accélération linéaire sinusoïdale de très basse fréquence, pour l'étude de la dérive des gyroscopes, ce document présente, avec ses performances, un moyen d'essais du laboratoire inertiel du LRBA (Laboratoire de Recherche Balistiques et Aérodynamiques) permettant de produire une telle accélération (10g - 3 Hertz).

Il présente ensuite, à titre d'exemples, les méthodes d'essais et de dépouillement utilisées pour l'évaluation de deux matériels gyroscopiques- gyroscope à deux axes de cardan, et gyromètre.

1. Généralités

L'étude de la dérive des gyroscopes, en fonction des diverses conditions d'utilisation, est l'un des objectifs essentiels de leur évaluation. Les conditions normales d'essai en laboratoire, rotation terrestre et pesanteur, équivalente à une accélération de 1g vers le zénith, conviennent bien pour évaluer les performances des gyroscopes du type avion, car les conditions réelles d'emploi sont voisines; par contre, elles sont nettement insuffisantes pour simuler les conditions d'emploi de gyroscopes du type engin, qui doivent fonctionner sous des accélérations de 10 à 15g et même parfois 60g dans le cas des corps de rentrée.

La pesanteur, en permettant d'évaluer le couple de dérive dû à une accélération de 1g, permet cependant de déduire, par extrapolation, la dérive pour des accélérations plus élevées: c'est le procédé habituel des essais de recette. Mais cette évaluation n'est représentative que dans la mesure où la validité de l'extrapolation a été vérifiée pour le type de gyroscope considéré.

Il est donc nécessaire, pour les essais d'étude et les essais de qualification, de mettre en oeuvre des moyens d'essais spéciaux, capables de communiquer des niveaux d'accélération élevés au matériel testé, tout en ayant des qualités de mouvement telles que les dérives dues à l'accélération puissent être dissociées de celles dues aux mouvements parasites.

C'est cette condition qui rend la réalisation de tels moyens d'essais si difficile.

Plusieurs types de systèmes, fondés sur des principes différents, ont été réalisés:

(a) les rails dynamiques qui fournissent une accélération linéaire, continue, mais limitée dans le temps à quelques secondes.

(b) les centrifugeuses qui fournissent des accélérations, de grandeur fixe et réglable, mais tournantes.

(c) les pots vibrants qui fournissent les accélérations linéaires et alternatives dont la fréquence est limitée inférieurement à 15 ou 20 Hz.

Aucun de ces moyens ne donne entière satisfaction pour des raisons diverses:

(a) les rails dynamiques sont, dans leur principe, techniquement satisfaisants en dépit de leur temps de fonctionnement très court et de la complexité de leur mise en oeuvre, mais ils nécessitent, pour obtenir des performances valables, des investissements très importants et une exploitation onéreuse.

(b) les centrifugeuses de précision, moins onéreuses que les rails dynamiques de qualité, permettent d'essayer des gyroscopes grâce à l'addition d'un plateau en contre-rotation qui annule, en principe, la vitesse de rotation. En pratique, les mouvements parasites résiduels inévitables limitent les possibilités de ce moyen d'essais.

(c) les pots vibrants permettent, outre de vérifier la tenue du matériel aux vibrations, d'étudier les dérives du type anisoélastique, fonction du carré de l'accélération, mais en aucun cas, les dérives du type balourd, leurs fréquences de fonctionnement les plus basses (15 à 20 Hz) étant trop élevées.

Le LRBA - ayant, sous traité à la CFTH (Compagnie Française Thomson Houston), l'étude et la réalisation de la partie mécanique - a mis au point une machine (Fig. 11-1) de conception originale, tout au moins à notre connaissance, destinée à soumettre les matériels gyroscopiques à des accélérations linéaires sinusoïdales de très basse fréquence, et à étudier les dérives qui en résultent: en principe, les dérives du type balourd peuvent être évaluées si la fréquence est suffisamment basse.

Cette fréquence a donc été choisie aussi basse que possible, compte tenu du fait que l'on voulait une accélération maximum de 10g, dans la bande passante habituelle des gyroscopes, tout en ayant des mouvements d'amplitude relativement faible pour des raisons de faisabilité. La machine construite fonctionne à environ 3, 3 Hertz et a donc des débattements de ± 23 cm pour une accélération d'amplitude 10g.

2. Principe d'essai de gyroscopes sous accélération linéaire sinusoïdale

Supposons la table animée d'un mouvement de translation vertical parfait, c'est-à-dire, sans rotation ni accélération parasites. L'accélération, ressentie par le matériel testé, compte tenu de la pesanteur s'écrit:

$$\gamma = g\ (1 + n \sin \omega t) \qquad \text{(Eq. 11-1)}$$

avec g accélération de pesanteur
ω pulsation du mouvement ($\sim$ 20 rad/s)
n nombre de 'g' de l'accélération crête

Le modèle habituel du couple de dérive d'un gyroscope soumis à une accélération linéaire est de la forme:

$$C = C_o + B\gamma + a\gamma^2 \qquad \text{(Eq. 11-2)}$$

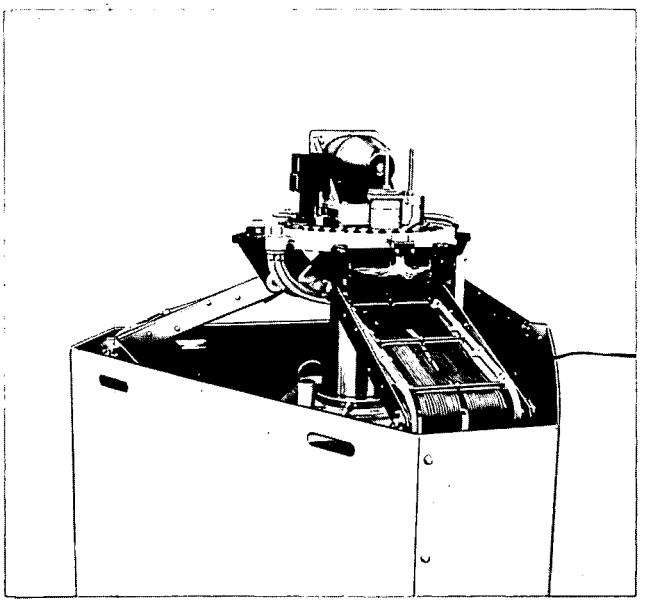

Plateau équipé

Montages d'essais
et de mesures

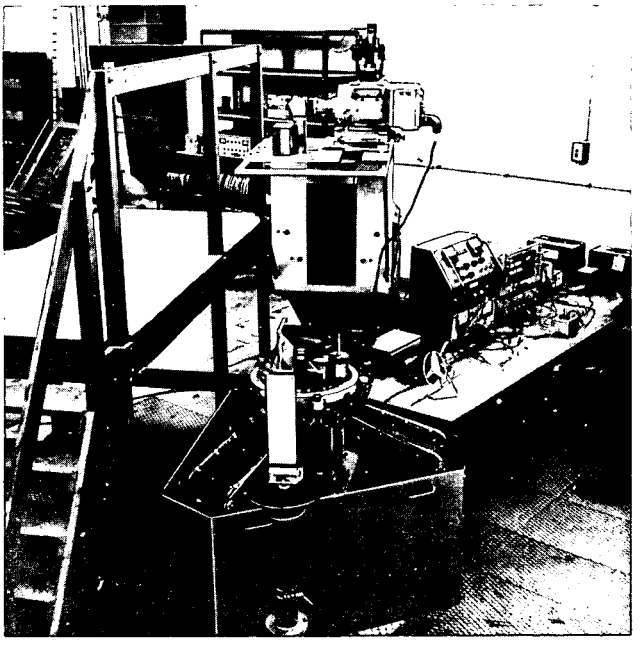

Fig. 11-1 Suivi

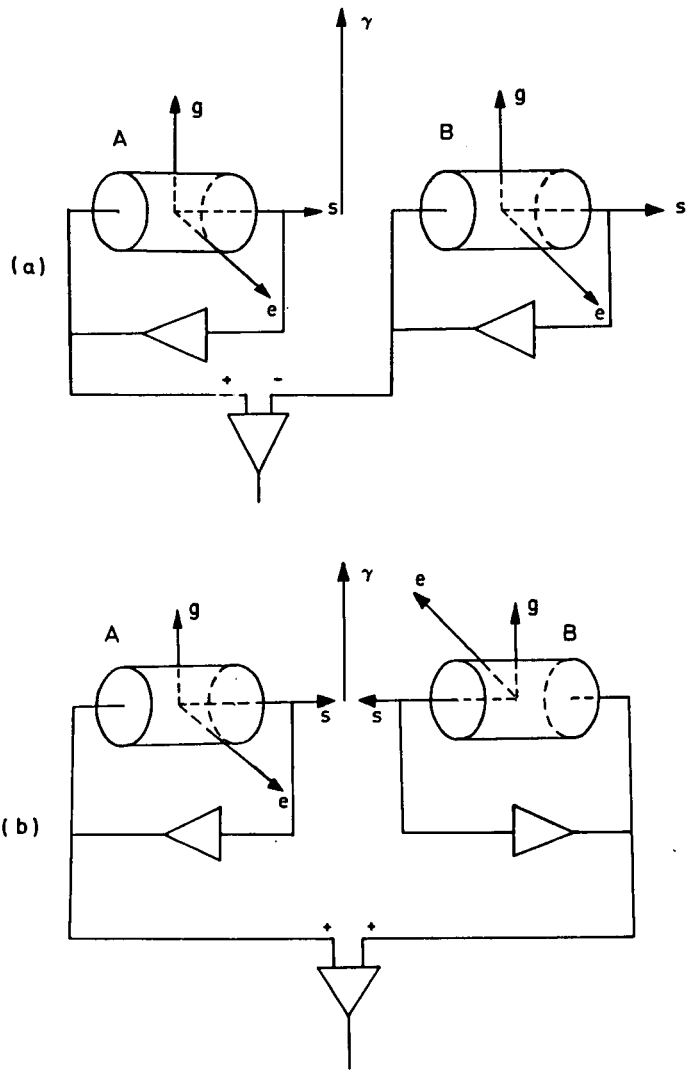

Fig. 11-2 Gyroscopes A et B - deux positions d'essai

avec C_o couple fixe
B coefficient de balourd
a coefficient d'anisoélasticité

Compte tenu de ce modèle et de la relation 11-1, le couple de dérive devient, en fonction du temps:

$$C = C_o + Bg + ag^2 \left(1 + \frac{n^2}{2}\right) + ng\,(B + 2ag)\sin \omega t - \frac{a}{2} n^2 g^2 \cos 2\omega t \qquad \text{(Eq. 11-3)}$$

La mesure de la dérive en fonction de l'accélération et son analyse harmonique permettent donc, théoriquement, d'évaluer pour différents positionnements du gyroscope, couple fixe, balourd et anisoélasticité et de vérifier l'exactitude du modèle employé: la composante continue doit être une fonction parabolique de n; le coefficient en sin ωt doit être une fonction linéaire de n; le coefficient en cos 2 ωt doit être une fonction parabolique de n, dont le terme du second degré est identique à celui de la composante continue.

La mesure de cette dérive peut, *a priori*, être faite de deux façons: ou bien le gyroscope est libre, et la mesure des mouvements angulaires de la toupie, à l'aide, par exemple, de ses détecteurs angulaires, permet d'évaluer les couples de dérive; ou bien le gyroscope est bouclé en gyromètre (toupie asservie en position au boitier) et la mesure du courant du moteur couple fournit directement le couple de dérive.

Une analyse harmonique des signaux permet ensuite d'évaluer les coefficients de la relation 11-3 pour chaque niveau d'accélération et de vérifier ensuite l'exactitude du modèle 11-2.

Mais il suffit de considérer qu'un mouvement sinusoïdal de rotation, d'amplitude 1″ à 3.3 Hertz a une vitesse d'amplitude 20°/h pour s'apercevoir que, si l'on voulait apprécier de l'une des deux façons énoncées, des couples de balourd avec une précision de 1°/h, le moyen d'essais devrait communiquer l'accélération sinusoïdale au boitier du gyroscope testé, avec des rotations parasites inférieures à 0,05″. Ce niveau de performance n'était évidemment pas envisageable avec la machine prévue.

Heureusement une méthode, assez classique (1), qui consiste à soumettre simultanément deux gyroscopes de même type aux mêmes conditions d'ambiance permet de dissocier de leurs signaux, la part due aux mouvements parasites de celle due à leurs défauts propres.

La théorie est simple: considérons à titre d'exemple le cas de deux gyroscopes A et B, à un degré de liberté, fonctionnant en gyromètre et fixés sur le plateau du moyen d'essais de telle sorte que les axes de même nom soient parallèles et de même sens (Fig. 11-2a). (L'application au cas de deux gyroscopes à deux degrés de liberté est immédiate).

Le signal S_A du gyroscope A représente la résultante de la dérive C_A due à accélération et de la composante ω_A de la vitesse de rotation sur l'axe d'entrée de A. De même le signal S_B du gyroscope B représente la résultante de la dérive C_B due à l'accélération et de la composante ω_B de la vitesse de rotation de la table sur l'axe d'entrée de B.

La différence des deux signaux a pour expression:

$$S_A - S_B = C_A - C_B + \omega_A - \omega_B$$

Si les facteurs d'échelle des deux gyroscopes sont identiques et, si les axes d'entrée sont parallèles, $\omega_A = \omega_B$ et par suite $S_A - S_B = C_A - C_B$.

La différence des signaux représente donc une combinaison des défauts des deux gyroscopes; elle n'est pas, en principe, affectée par les mouvements parasites de la table.

Un essai semblable, avec un autre positionnement du gyroscope B (rotation de 180° autour de l'axe toupie - voir figure 11-2b) ne modifie pas C_B et entraîne $\omega_B = -\omega_A$. Par suite

$$S_A + S_B = C_A + C_B + \omega_A + \omega_B = C_A + C_B$$

Ces deux essais permettent donc de dissocier les défauts respectifs de chaque gyroscope.

Remarque: Le cas décrit permet d'étudier la composante de balourd sur l'axe d'entrée - celle sur l'axe toupie ne peut être mise en évidence que par changement du sens de rotation de la toupie.

Mais pour que ces essais soient significatifs, compte tenu des écarts inévitables de réglage et de calage des gyroscopes, il faut que le rapport signal utile / signal global soit supérieur à une certaine valeur minimum: ce minimum peut, *a priori*, être évalué à 5%. Ceci admis, il suffit que le moyen d'essai ait des mouvements de rotation parasites à 3, 3 Hz inférieurs ou égaux à 1″ pour qu'une dérive puisse être mesurée à 1°/h près.

La conception de la machine, décrite ci-après, pouvait permettre une telle performance. C'est pourquoi elle a été fabriquée.

3. Fonctionnement de la Table 10g

Généralités

Pour l'utilisateur, la partie utile de la machine est constituée d'un plateau circulaire horizontal, rainuré, de 40 cm de diamètre, pouvant recevoir des charges d'un poids maximum de 50 kg. Ce plateau peut être animé d'un mouvement vertical linéaire et sinusoïdal à 3, 3 Hz; l'amplitude de l'accélération est réglable de façon continue de 0, 1 à 10g à l'aide d'un asservissement.

Les performances sont caractérisées par les quelques chiffres qui suivent:

(a) distorsion de l'accélération verticale < 1%

(b) accélération transversale < 0, 1g (bruit à 30 Hz)

(c) rotations parasites autour d'axes horizontaux < 2″ crête à crête à 10g

(d) rotations parasites autour de l'axe vertical < 20″ crête à crête à 5g (5″ initialement)

Quelques chiffres complémentaires renseignent sur les conditions d'emploi:

(a) temps de montée à 5g : 17 secondes; à 10g : 70 secondes

(b) temps d'arrêt, table non asservie: 150 secondes

(c) temps d'arrêt avec freinage: 15 secondes.

Un système à trois pantographes permet d'établir toutes les liaisons électriques nécessaires entre le matériel testé, fixé sur le plateau, et le matérial de mise en oeuvre et de mesure.

Une potence, dominant le plateau, et fixée sur un bloc 'isolé' des vibrations, sert de support à divers appareils optiques nécessaires aux mesures d'évaluation ou de contrôle.

Principe de fonctionnement et description

Guidage du plateau. Afin de réduire au minimum les mouvements parasites et les frottements, la technique des paliers à air hydrostatiques a été utilisée.

Le plateau est solidaire d'un arbre de commande vertical, cylindrique qui coulisse dans deux paliers à air hydrostatiques; ces derniers assurent la verticalité de l'axe pendant le mouvement, et empêchent ainsi les rotations parasites autour d'axes horizontaux.

Un système complémentaire de deux paliers à air plans, constitués chacun d'une glissière rectiligne, verticale, solidaire de l'arbre de commande, et d'un patin lié au bâti, contrôle les mouvements de rotation du plateau autour de l'axe vertical.

Mise en mouvement du plateau. Afin de réduire au minimum la puissance à fournir pour la mise en oeuvre, et surtout pour obtenir une loi de mouvement aussi sinusoïdale que possible, l'ensemble plateau, arbre de commande est relié à une barre de torsion de façon à constituer un système masse-ressort, d'amortissement très faible.

La barre de torsion est constituée, en fait, d'un arbre et d'un tube concentriques, long de 6 m, travaillant en série; l'arbre de torsion est lié à un secteur circulaire qui transmet les forces à l'ensemble mobile par l'intermédiaire de sangles métalliques; le tube de torsion est lié au bâti.

Un système d'entretien des mouvements, contrôlé par asservissement, est constitué d'un moteur électrique de faible puissance (1, 5 cv) et de deux embrayages à coupleurs magnétiques, travaillant tour à tour selon le sens du mouvement de la table.

Asservissement (2). Le schéma synoptique (Fig. 11-3) présente les principes de fonctionnement de l'asservissement: il contrôle l'amplitude des oscillations (et non l'amplitude de l'accélération).

Un résolver, monté sur l'axe du secteur circulaire, subit les mouvements angulaires de ce dernier, par rapport au bâti de la machine, et fournit après détection et filtrage une tension continue, représentative de l'amplitude des oscillations. Cette tension est comparée à un tension de référence sert de signal d'erreur à l'asservissement.

D'autre part, un circuit de synchronisation fournit, à partir de la tension résolver, des signaux carrés en phase avec la vitesse de la table; ces signaux permettent,

à l'aide d'un modulateur, de transformer la tension continue d'erreur, en créneaux alternatifs, en phase avec la vitesse de la table, et d'amplitude proportionnelle en grandeur et en signe à cette tension d'erreur.

Chaque coupleur est alimenté, tour à tour, par un courant pratiquement proportionnel à tension d'erreur à l'aide d'un amplificateur à thyratrons solides alimentés en 400 Hz. Cette proportionnalité est obtenue en transformant les variations d'amplitude du signal d'erreur en variations de phase de la tension d'attaque des gachettes des thyratrons solides.

Performances

Nous allons passer rapidement en revue les différentes caractéristiques de cette machine avec les méthodes d'évaluation utilisées, les valeurs obtenues et les possibilités d'amélioration éventuelles.

Accélération verticale. La qualité de cette accélération a été évaluée à l'aide d'un accéléromètre inertiel, pendulaire, de classe 10^{-4}, considéré comme parfait, compte tenu de l'ordre de grandeur des défauts de la machine.

Le principe de fonctionnement de la table: oscillation d'un système masse-ressort à sa fréquence propre et asservissement de l'amplitude des oscillations (et non de l'amplitude de l'accélération) fait que, pour une tension de commande donnée, l'accélération crête dépend de la masse du matériel testé. Elle lui est reliée par une relation de la forme:

$$\gamma_c = A \ \omega_o^2 \ \frac{M}{M + m}$$

avec γ_c amplitude de l'accélération
A amplitude des oscillations
ω_o pulsation propre de la table à vide
m masse de la charge testée
M masse équivalente de la partie mobile de la table (~ 250 kg)

Ainsi, le débattement maximum de la table, qui est de ± 23 cm, correspond à vide avec une fréquence de 3.56 Hz, à une accélération crête théorique de 11, 5g; avec une charge de 50 kg, la fréquence descent à 3, 25 Hz et ce débattement ne correspond plus qu'à 9, 5g.

L'accélération affichée est exacte (à 5.10^{-2} g près) pour une charge de 40 kg. Il est facile, connaissant la masse du matériel testé ou la fréquence des oscillations, de calculer le facteur de correction pour une série d'essais sur un matériel donné.

Pour une charge donnée, la stabilité à court terme de la fréquence des oscillations est de l'ordre de 2.10^{-3}, celle de l'amplitude meilleure que 10^{-2}.

La distorsion de l'accélération a été évaluée en comparant le signal accélérométrique à un signal sinusoïdal de référence, synchrone, et de distorsion inférieure à 5.10^{-4}. Le signal résiduel obtenu par différence entre ces deux signaux, après réglage de la phase et de l'amplitude du signal de référence, a une amplitude de l'ordre de 5 ‰ de celle de l'accélération jusqu'à environ 6g, et de l'ordre de 9 ‰ à 10g; son maximum coincide avec la commutation des coupleurs. Cette distortion est suffisamment faible pour ne pas chercher à la réduire en alimentant les coupleurs avec un courant de forme plus complexe; ceci est heureux car en raison de l'amortissement du système, les coupleurs doivent travailler au couple

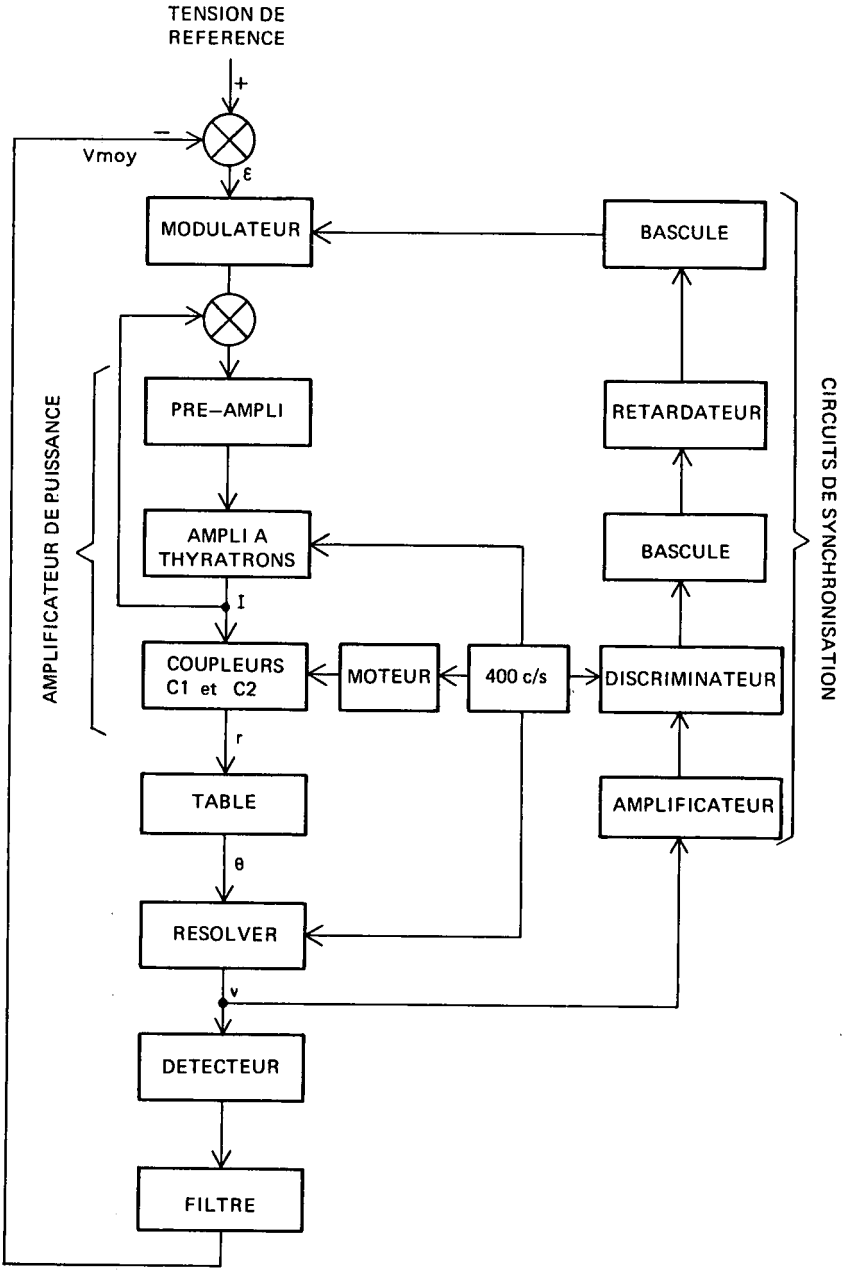

Fig. 11-3 Table 10g - schéma synoptique

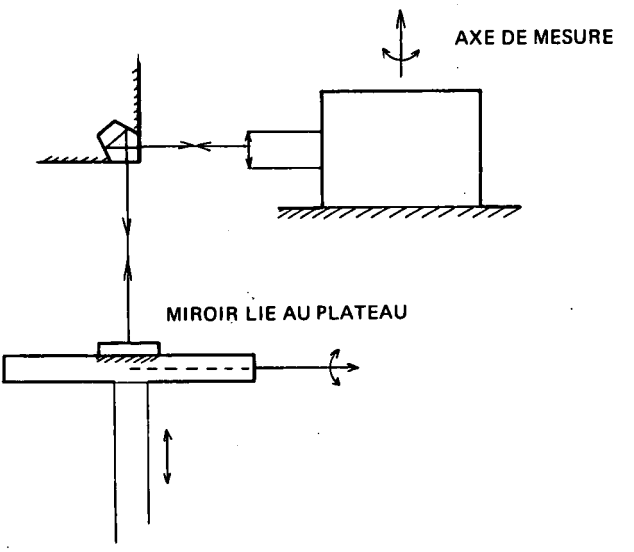

Fig. 11-4 (a) Mesure des mouvements autour d'un axe horizontal

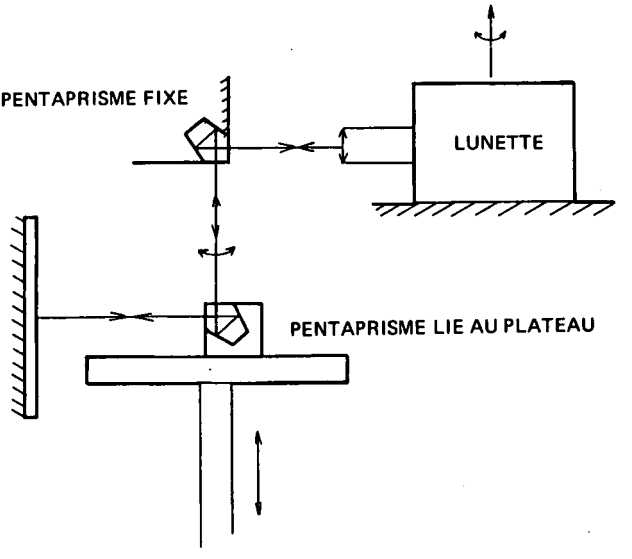

Fig. 11-4 (b) Mesure des mouvements autour de l'axe vertical

maximum (80 Nm) pour faire osciller la table à l'amplitude maximum prévue.

L'étude de l'évolution de l'accélération pour les oscillations non entretenues a en effet montré que le coefficient d'amortissement réduit (en assimilant la machine à un système du second ordre) qui est de 10^{-3} à 3g croit linéairement en fonction de l'accélération pour atteindre $1,6.10^{-3}$ à 10g.

C'est ce phénomène d'amortissement, dû aux pantographes mais aussi à la barre de torsion, qui limite en fait la valeur de l'accélération maximum: cette dernière atteint effectivement 9,5g avec 50 kg mais ne dépasse guère 10,5g à vide.

Les clauses techniques demandaient une distorsion de l'accélération $\leq 10^{-2}$, un niveau maximum de 10g et une fréquence de $3 \pm 0,2$ Hz avec une charge de 50 kg.

Les performances réalisées sont donc dans les tolérances demandées; seule une augmentation de niveau crête de l'accélération maximum, ou une diminution de la fréquence, serait intéressante, mais cela nécessite un dimentionnement supérieur de la machine.

Mouvements parasites. (a) Accélérations transverses - *a priori* la précision du guidage, due à la petitesse de l'entrefer des paliers à air et à leur raideur, est telle que les mouvements transversaux sont de l'ordre de 0,1 mm au maximum ce qui, à la fréquence des oscillations, conduit à une accélération de 4.10^{-3}g.

La mesure de ces accélérations avec le même accéléromètre que précédemment a confirmé cette évaluation mais a révélé en plus l'existence d'un niveau de bruit à 35 Hertz environ, de l'ordre de 0,05 à 0,1g (vibrations qui correspondent à des mouvements de 0,01 à 0,02 mm).

Ce bruit est dû au fait que le guidage par paliers à air est élastique et peu amorti. Le niveau est cependant suffisamment faible pour que les effets soient négligeables.

(b) Rotations parasites autour d'axes horizontaux - les mouvements de rotation, dans le plan du plateau, ont été mesurés à l'aide d'une lunette autocollimatrice à sortie électrique, visant par l'intermédiaire d'un prisme de renvoi à 90°, un miroir fixé horizontalement sur le plateau (Fig.11-4a). La lunette utilisée (Perkin Elmer), à un axe de mesure, a un champ de mesure linéaire de ± 30″; sa résolution est meilleure que 1″.

Ces mouvements dépendent beaucoup du positionnement du centre de gravité de la masse testée. C'est grâce à cette particularité qu'il est possible, à l'aide de masselottes d'équilibrage, de réduire le fondamental de ces rotations à environ 2″ crête à crête à 10g: ce réglage est très facile compte tenu du fait qu'un balourd de 1kg à 20 cm du centre de la table, n'entraîne qu'un mouvement parasite de 5″ crête à crête.

Il subsiste cependant des mouvements de rotation à fréquence plus élevée (35 Hertz environ) de l'ordre de 2 à 3″ à 10g, difficilement évaluables en raison du bruit propre de la lunette. Ils sont dus, comme les accélérations transversales, à l'élasticité peu amortie des paliers à air.

Ces bruits résiduels sont difficilement réductibles car ils sont inhérents au principe de fonctionnement de la machine. Ils ont heureusement une fréquence suffisamment élevée pour avoir une action généralement négligeable sur les matériels testés.

(c) Rotations parasites autour de l'axe vertical - ces rotations, comme les précédentes, ont été mesurées à l'aide d'une lunette autocollimatrice Perkin Elmer.

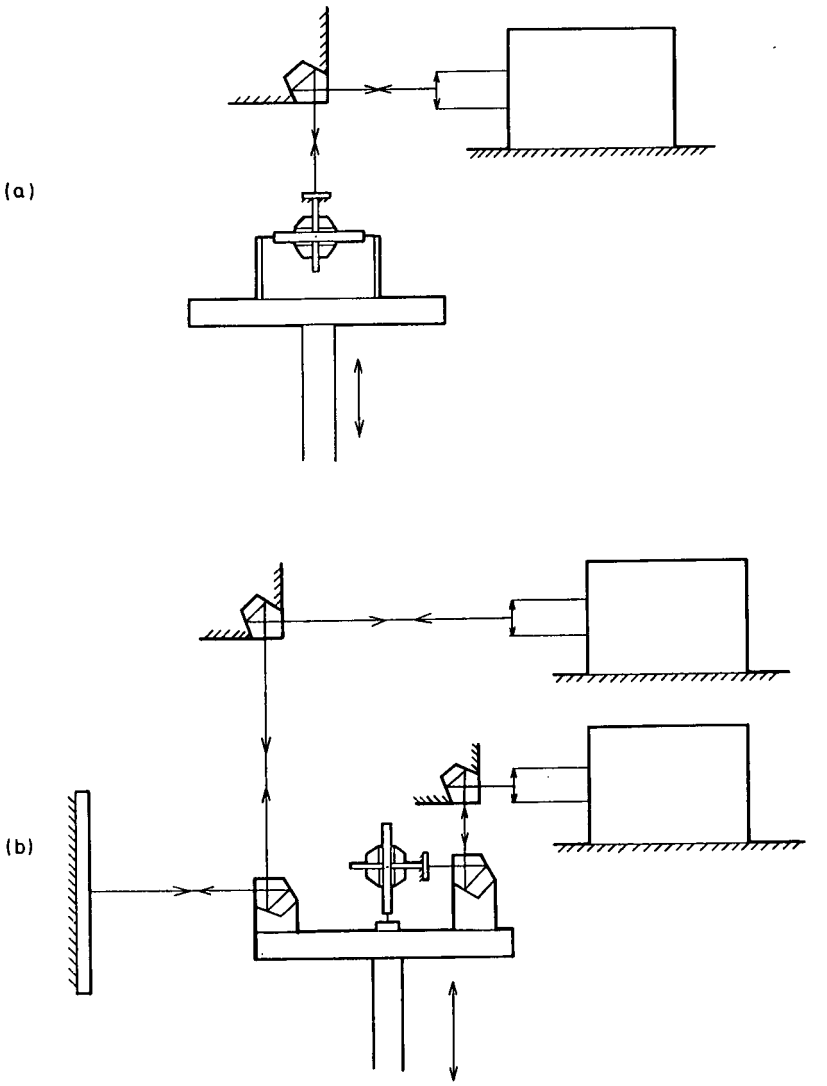

Fig. 11-5 Principes des mesures optiques des mouvements de la toupie sous accélération

Un pentaprisme de renvoi à 90°, fixé sur la table, renvoi le faisceau de la lunette sur un miroir plan vertical de référence dont la grande dimension (35 cm) est parallèle à l'axe de la table (Fig. 11-4b). Le défaut, en torsion, du miroir utilisé, est de 2″.

Afin d'éviter l'influence, parasite pour la mesure, des rotations du plateau autour de l'axe horizontal perpendiculaire à l'arête du pentaprisme, la table est préalablement équilibrée.

Les résultats obtenus sont moins bons que pour les axes horizontaux. Les premières mesures, effectuées sur la machine non équipée de pantographes, ont révélé la présence de mouvements parasites importants: un fondamental d'environ 20″ à 5g avec un bruit de même niveau à 20 Hertz. La mise en place des pantographes a étouffé le bruit et a permis de ramener le fondamental à 5″ à 5g, en jouant sur les couples développés par les déformations des pantographes. Au delà de 6g cependant, le plateau avait, en position haute, un mouvement de rotation important qui atteignait 25″ à 7g.

Actuellement, à la suite d'une détérioration malencontreuse des paliers à air plans, et malgré les soins apportés à réparation, les mouvements parasites sont importants et de forme non sinusoïdale (30″ crête à crête à 6g). Leur régularité implique sans aucun doute, une déformation de la géométrie des glissières.

Ce défaut important, nettement en dehors des performances espérées, limite l'intérêt de la table réalisée: en particulier, le principe des essais décrits au section 2, qui justifiait la construction de la table, ne peut être appliqué (encore que le cas où l'axe toupie est vertical puisse être envisagé, compte tenu du faible niveau des rotations parasites autour des axes horizontaux).

Le principe de la réalisation ne semble cependant pas en cause: les systèmes de guidage, avec les réglages d'appoints décrits, devraient pouvoir empêcher les rotations parasites autour de l'axe vertical à la seconde d'arc près; il faudrait pour cela guider l'arbre de commande avec une précision de 2,5μm à 50cm de l'axe; cette performance est dans le domaine des réalisations possibles de la mécanique de précision.

Des essais instructifs ont pu être effectués jusqu'à présent sur du matériel gyroscopique de qualité moyenne: gyromètre de classe 0,01 °/s et gyroscope à deux degrés de liberté de classe 10 °/h. Les sections suivantes présentent les méthodes d'essai et de dépouillement employées respectivement pour ces deux types d'appareils. Des essais tels que ceux décrits au section 2 n'ont pas encore été réalisés mais sont envisagés.

4. Méthode d'évaluation de la dérive sous accélération d'un gyroscope à deux degrés de liberté

Le LRBA a eu à évaluer la dérive sous accélération d'un gyroscope classique à deux axes de cardan, de classe 10 °/h/g et destiné à fonctionner jusqu'à des accélérations de 10g.

Les essais en ambiance normale de laboratoire permettent théoriquement d'évaluer les couples du type balourd, pour des accélérations de 1g, en combinant les mesures de dérive effectuées dans diverses positions. Mais cette accélération n'est pas suffisante, non seulement pour les raisons de principe déjà évoquées mais aussi pour des raisons pratiques: les instabilités et le manque de répétabilité des dérives ne permettent pas de dissocier la dérive aléatoire due aux fluctuations

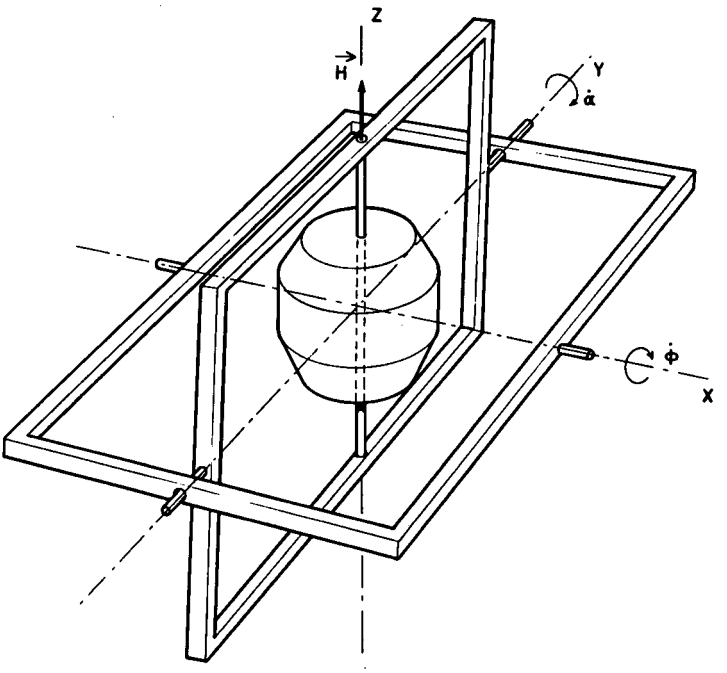

Fig. 11-6 Position canonique des axes

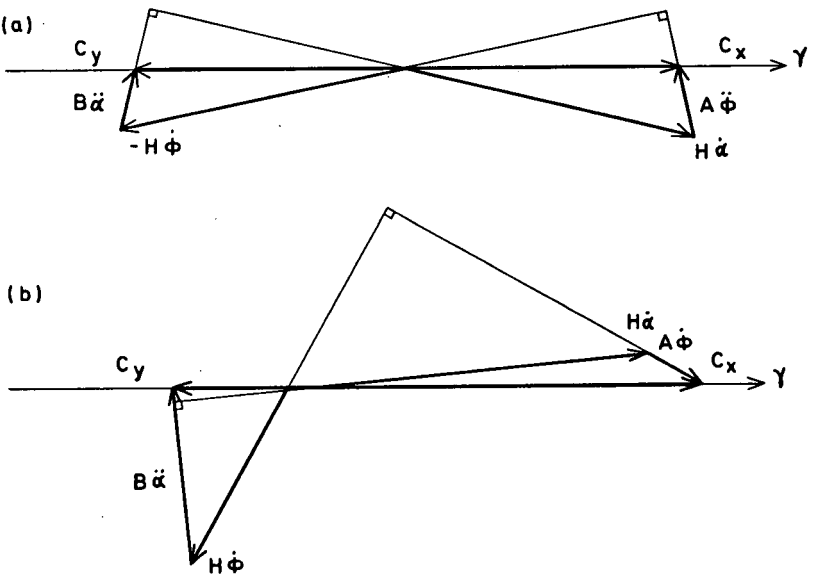

Fig. 11-7 Effets des couples d'inertie à 3, 3 Hz

du balourd de celle due aux fluctuations du couple 'fixe'; il est difficile, dans ce cas, de prévoir la dérive sous ng.

Par contre, des essais sous une accélération linéaire sinusoïdale d'amplitude donnée permettent, avec la mesure de la dérive instantanée, d'attribuer (a) la dérive continue et ses fluctuations au couple 'fixe' et (b) la dérive alternative et ses fluctuations d'amplitude à un couple lié à l'accélération. La méthode décrite ci-après concerne l'évaluation de cette dérive.

Description des méthodes de mesure

Le gyroscope testé, du fait même de sa mission, ne possède que des moteurs-couple grossiers, destinés à faire précessionner rapidement la toupie pour le calage initial, et des détecteurs angulaires dont le niveau de bruit correspond à 10" environ. Mais, heureusement pour l'expérimentateur, le cadre interne possède un miroir plan, dont la normale est parallèle à l'axe de la toupie, visible par un hublot lorsque les cadres sont en position canonique.

Cette particularité permet donc de mesurer optiquement les mouvements de la toupie lorsque le gyroscope est soumis à l'accélération de la table. La figure 11-5 montre les principes de ces mesures optiques, avec les trajets des faisceaux lumineux.

Lorsque le miroir est horizontal (Fig. 11-5a), le trajet optique n'est pas perturbé par les mouvements parasites de la table et la lunette mesure les mouvements angulaires de la toupie par rapport à la terre (successivement suivant chaque axe).

Lorsque le miroir est vertical (Fig. 11-5b), le prisme de renvoi à 90°, situé sur le plateau, subit les mouvements parasites de celui-ci. La mesure des mouvements angulaires du miroir autour de l'axe horizontal n'en est pas affectée: par contre, celle des mouvements autour de l'axe vertical l'est, car les mouvements de la table autour du même axe s'ajoutent; l'utilisation de deux lunettes identiques, l'une visant le miroir de la toupie, l'autre un miroir de référence, permet cependant d'obtenir seulement les mouvements de la toupie par différence de deux signaux. La résolution de ces systèmes de mesure est de l'ordre de 1".

Interprétation des résultats

Equivalence: vitesse de dérive, couple de dérive. Le but des essais est d'essayer d'évaluer la dérive du gyroscope sous une accélération continue: or, dans le cas des essais sur la table 10g, l'accélération est alternative et les mouvements alternatifs des cadres donnent naissance à des couples d'inertie, qui n'existent pas dans les conditions normales d'emploi. Il est nécessaire de vérifier que ces couples ne faussent pas les résultats.

Un calcul simple a montré que, compte tenu de la fréquence de nutation et de l'inertie des cadres, ces couples d'inertie sont pratiquement négligeables pour les mouvements à 3,3 Hertz, sauf cas particuliers où les mesures peuvent cependant être facilement corrigées.

Les équations utilisées ont été les suivantes, valables pour la position canonique des axes (Fig. 11-6).

$$A\ddot{\phi} + H\dot{\alpha} = C_X$$
$$B\ddot{\alpha} - H\dot{\phi} = C_Y$$

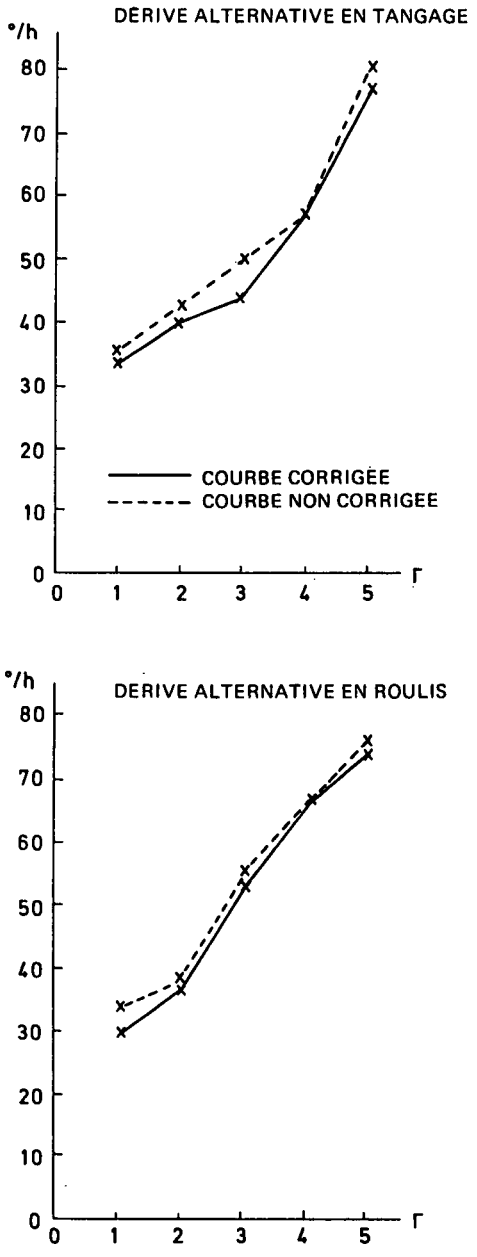

Fig. 11-8 Signaux conformes à la théorie ; axe toupie vertical

avec A inertie autour de l'axe externe

B inertie autour de l'axe interne

ϕ rotation absolue du cadre externe autour de son axe

α rotation absolue du cadre interne autour de son axe

H moment cinétique de la toupie

C_X, C_Y couples de dérive sur les axes X et Y

Les effets des couples d'inertie à 3,3Hz apparaissent sur la figure 11-7 où les termes des équations sont représentés sous forme de vecteurs.

Les caractéristiques du gyroscope (A = 4B, et fréquence de nutation ~ 50Hz) entrainent

$$|A\ddot{\phi}| = 12\% \, |H\dot{\phi}|$$

et $$|B\ddot{\alpha}| = 3\% \, |H\dot{\alpha}|$$

Si $\dot{\alpha}$ et $\dot{\phi}$ ont le même ordre de grandeur (Fig. 11-7a) les vecteurs $A\ddot{\phi}$ et $B\ddot{\alpha}$ ont des modules faibles par rapport aux vecteurs $H\dot{\alpha}$ et $H\dot{\phi}$ et sont presque déphasés de $\pi/2$ par rapport à ceux-ci; par suite

$$\left.\begin{array}{l} |H\dot{\alpha}| \sim |C_X| \\ |H\dot{\phi}| \sim |C_Y| \end{array}\right\} \text{ à mieux que } 1\%$$

et les déphasages sont faibles: quelques degrés.

Si $\dot{\alpha}$ et $\dot{\phi}$ ont des ordres de grandeur différents ($\dot{\phi} << \dot{\alpha}$) (Fig. 11-7b) le vecteur de plus grand module, $H\dot{\alpha}$, est pratiquement confondu avec le vecteur couple de dérive C_X: par contre, $H\dot{\phi}$ diffère notablement de C_Y; on remarque cependant que, $B\ddot{\alpha}$ étant presque perpendiculaire à γ, C_Y est pratiquement la projection orthogonale de $H\dot{\phi}$ sur γ.

La conclusion pratique pour le dépouillement des mesures est que, dans tous les cas, la projection orthogonale des vecteurs vitesse de dérive sur l'axe γ, donc la composante de vitesse, en phase avec l'accélération, représente avec une bonne approximation le couple de dérive cherché.

Dépouillement. Les essais effectués ont fourni, pour certaines configurations du gyroscope, des signaux conformes à la théorie qui vient d'être faite; les couples de balourd concernés ont alors pu être appréciés avec leurs fluctuations (Figs. 11-8 et 11-9).

Par contre, dans d'autres configurations, les signaux ne sont plus sinusoïdaux: ils gardent une allure périodique mais ont des formes diverses (triangulaires ou plus complexes). L'interprétation directe de ces signaux, à l'aide de couples de frottement, peut être faite en égalant vitesse de dérive et couple parasite de dérive. Mais, outre la difficulté pratique de l'application, cette interprétation est fausse dans son principe, à cause des couples d'inertie.

Des dépouillements valables ont cependant pu être effectués grâce à la simulation sur machine analogique d'un modèle mathématique approprié qui a fourni des familles de courbes de référence.

5. Méthode de l'évaluation de l'influence de l'accélération sur les indications d'un gyromètre

Le type de gyromètre, essayé, classique, a une résolution de 0,01 °/s (36 °/h) et l'erreur sous accélération correspond à environ 0,02 °/s/g. Les utilisateurs évaluent l'erreur sous accélération par des essais sur une petite centrifugeuse, toupie arrêtée. Les essais confiés au LRBA et effectués sur table 10g avaient pour but d'évaluer les erreurs sous accélération, toupie tournante et toupie arrêtée, et de comparer les résultats à ceux obtenus sur centrifugeuse afin d'en vérifier la validité.

Au moment des essais, la table 10g n'était pas encore équipée de ses pantographes et les mouvements parasites de rotation autour de l'axe vertical étaient relativement importants, surtout à fréquence élevée (35 Hz), mais cela n'était pas critique, car le gyromètre testé a une fréquence propre de 45 Hz et un amortissement réduit de 10, d'où un affaiblissement de 25 dB environ pour ces bruits; à la fréquence des oscillations de la table, l'affaiblissement est de 4 dB et le déphasage de 55°.

Le principe de base consiste à soumettre le gyromètre à l'accélération de la table, successivement suivant chacun de ses trois axes, toupie arrêtée, puis toupie lancée et à comparer les signaux obtenus.

Mais l'élasticité du guidage de la table peut être utilisée avec profit pour l'évaluation du facteur d'échelle du gyromètre, dans les conditions d'essais: un balourd sur le plateau permet en effet de communiquer au gyromètre en plus de l'accélération linéaire, un mouvement angulaire synchrone, mesurable optiquement.

L'application de ce principe a donné des résultats satisfaisants pour certains gyromètres dont les balourds étaient relativement importants; la figure 11-10 présente, superposés, avec conservation des phases respectives, les enregistrements effectués, toupie arrêtée puis toupie lancée, avec deux gyromètres dont les axes de toupie étaient verticaux; on constate (a) une bonne proportionnalité de l'amplitude des signaux et de celle de l'accélération (environ 0,025 °/s/g) et (b) une bonne superposition des signaux toupie lancée et toupie arrêtée.

Par contre, pour d'autres gyromètres de balourds plus faibles, les essais identiques ont conduit à des enregistrements totalement différents; sur la figure 11-11 on constate que ces signaux n'ont ni la même amplitude, ni la même phase.

L'hypothèse d'une élasticité ou d'un jeu dans la suspension de la partie mobile dans le boitier a alors été émise, de façon à expliquer ce phénomène par des réactions gyroscopiques. Un modèle mathématique a été élaboré (il est présenté en détail en annexe) pour vérifier cette hypothèse et essayer de chiffrer le défaut par un dépouillement approprié des mesures.

Ce modèle d'équations linéaires montre que, dans le cas d'une accélération linéaire sinusoïdale dirigée suivant l'axe toupie (sans autre accélération, ni rotation parasites), le signal sinusoïdal obtenu dépend du signe du moment cinétique de la toupie, si la suspension du corps mobile n'a pas la même raideur aux deux points d'attache; la formule analytique s'écrit:

$$S = \mathcal{P}[B_e - jH\omega \frac{\partial \psi}{\partial \gamma}]\gamma$$

avec S amplitude complexe du signal gyrométrique

B_e balourd sur l'axe d'entrée

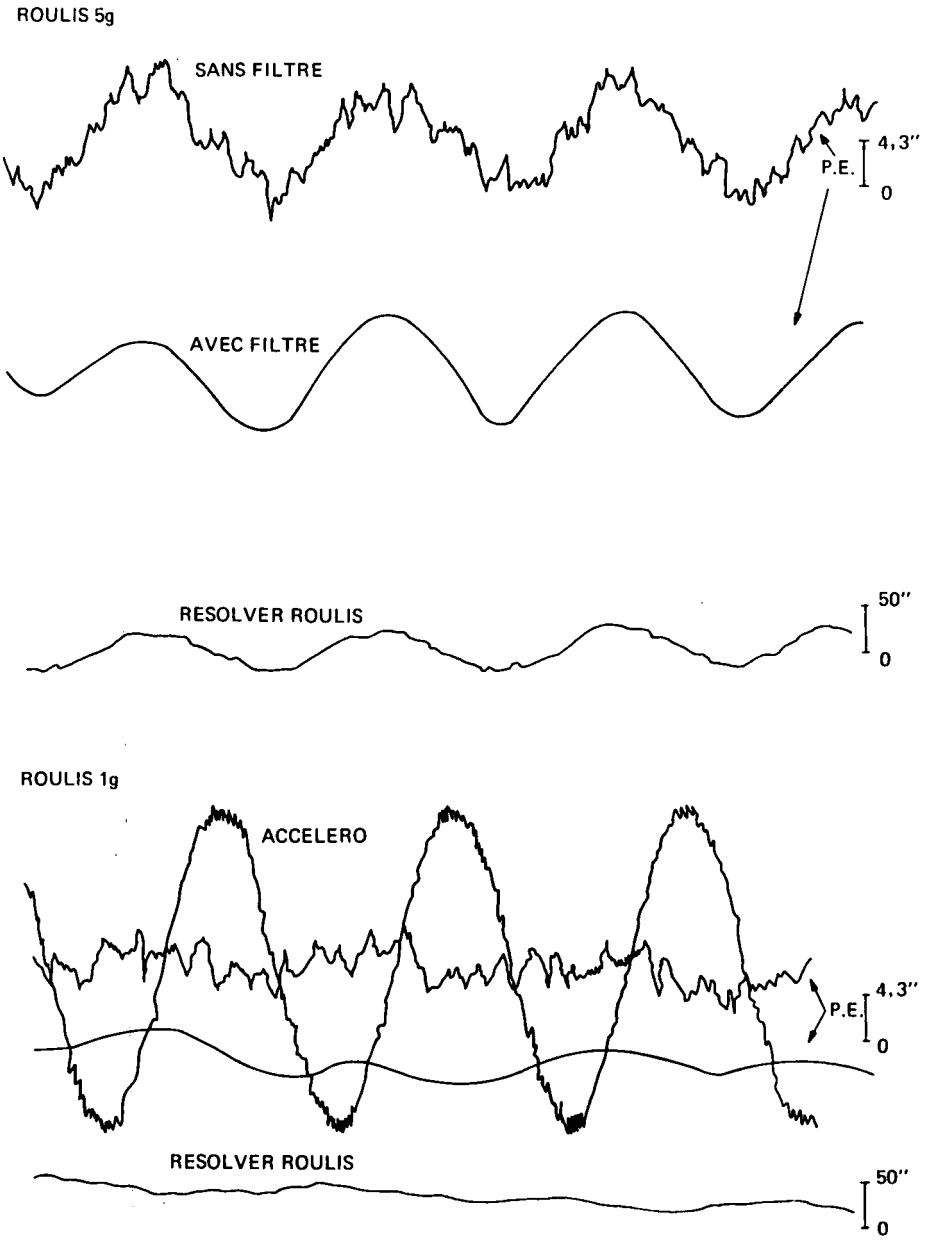

Fig. 11-9 Signaux conformes à la théorie, axe toupie vertical

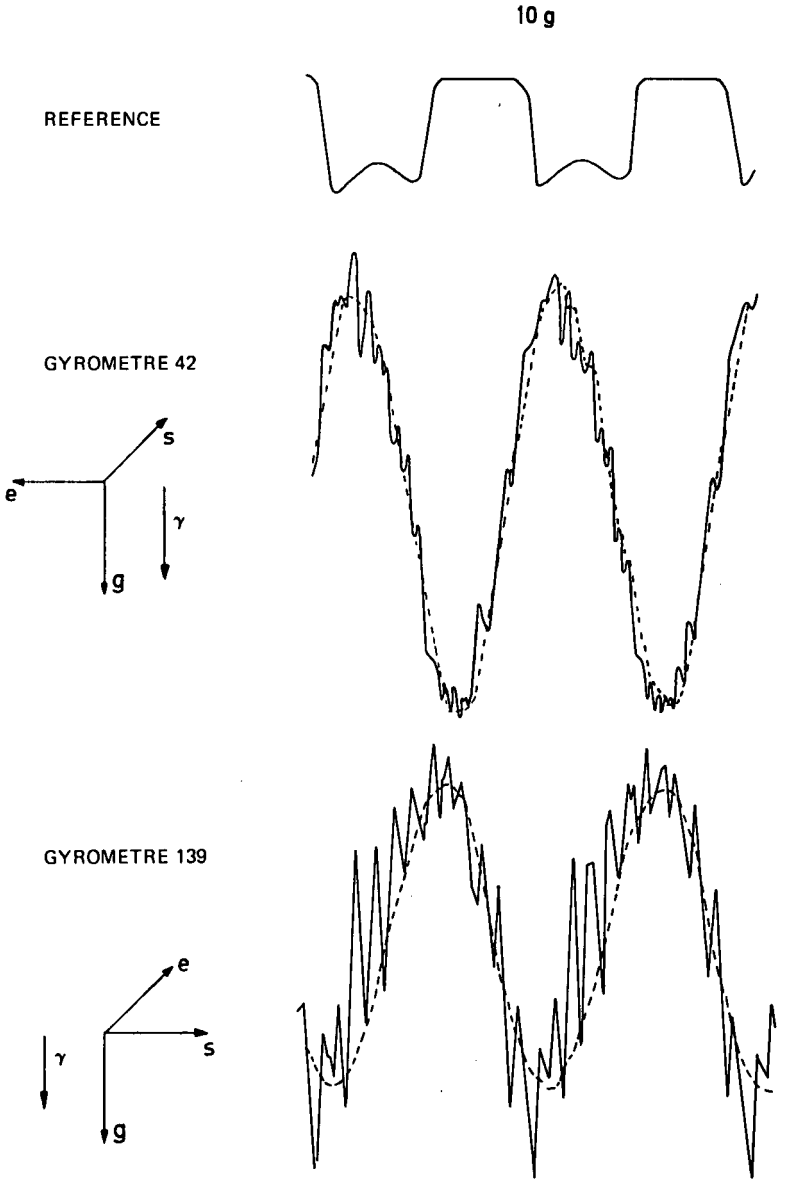

Fig. 11-10 Comparaison de signaux, toupies arrêtées et toupies lancées, des gyromètres de balourds importants

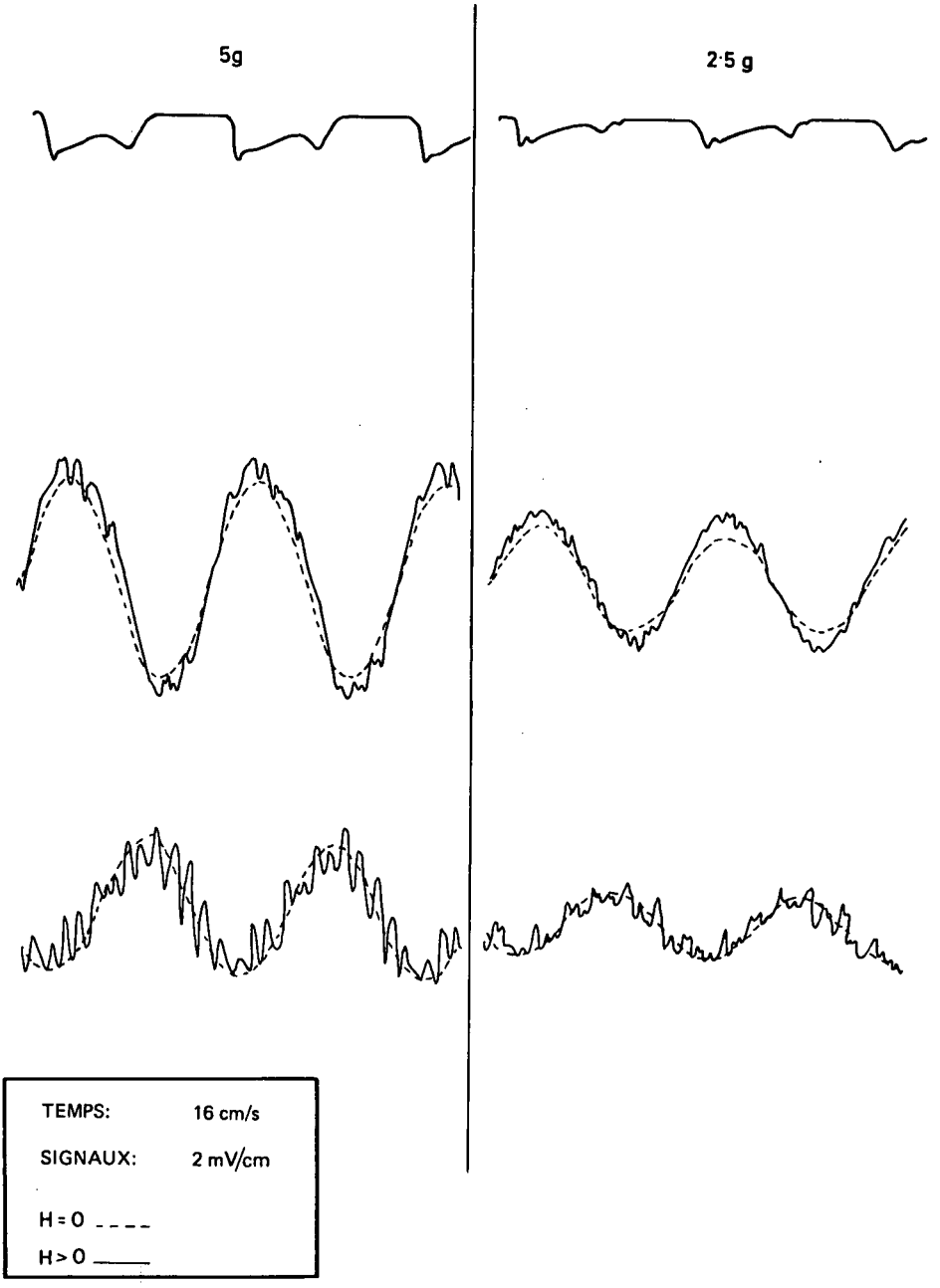

Fig. 11-10 Suivi

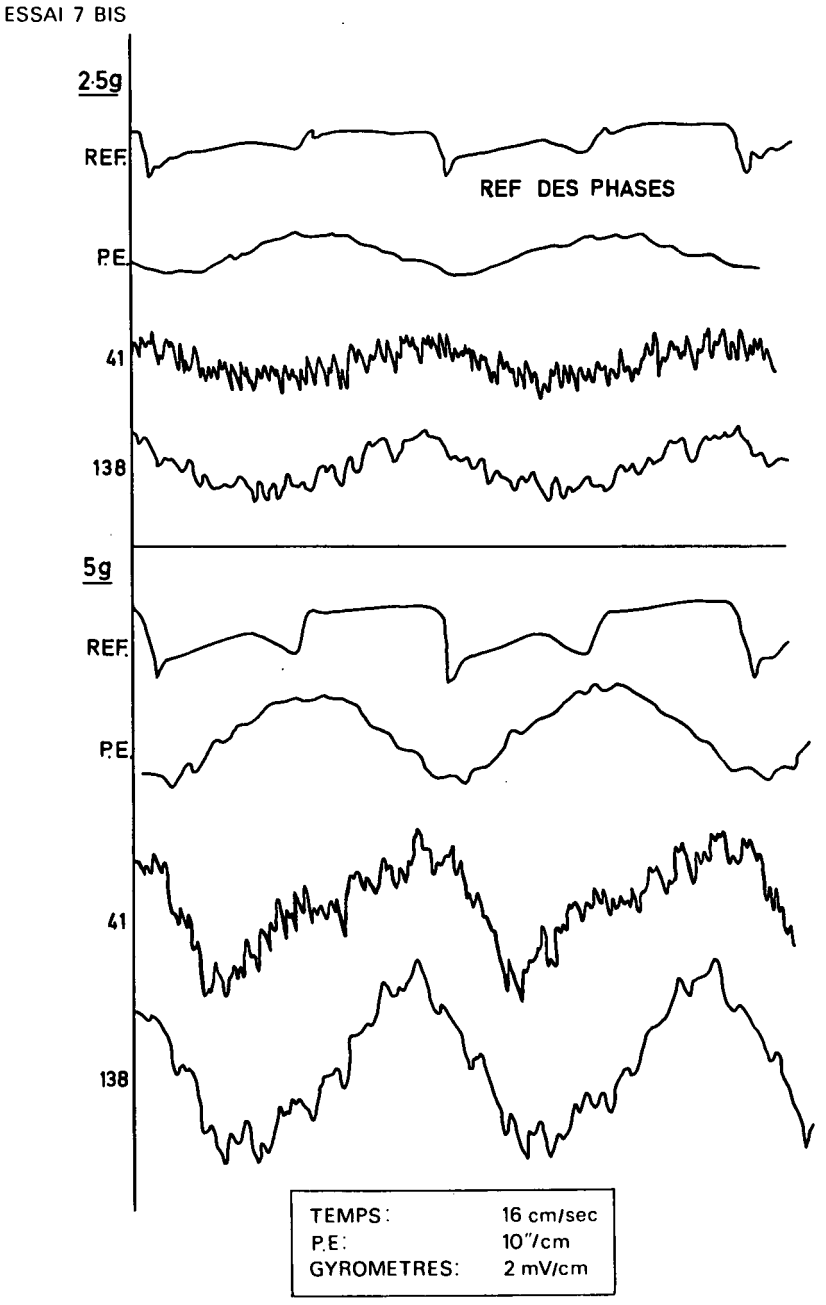

Fig. 11-11 Exemple d'enregistrements des gyromètres de balourds faibles

ESSAIS 9 BIS ET 7

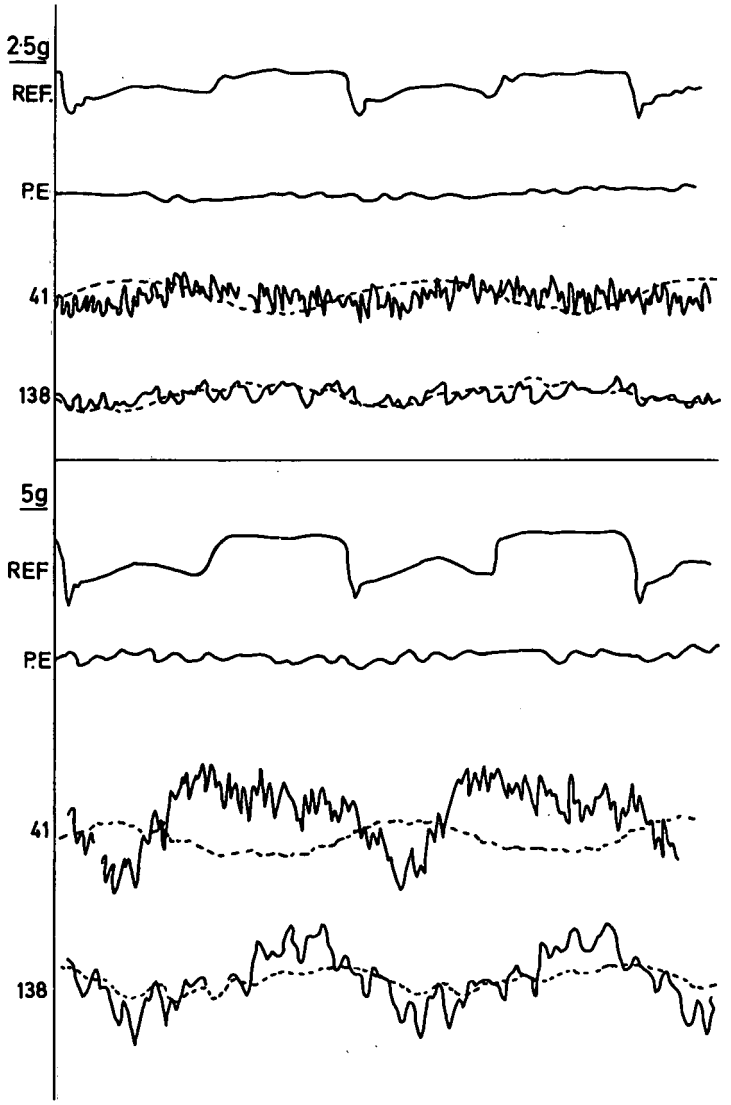

Fig. 11-11 Suivi

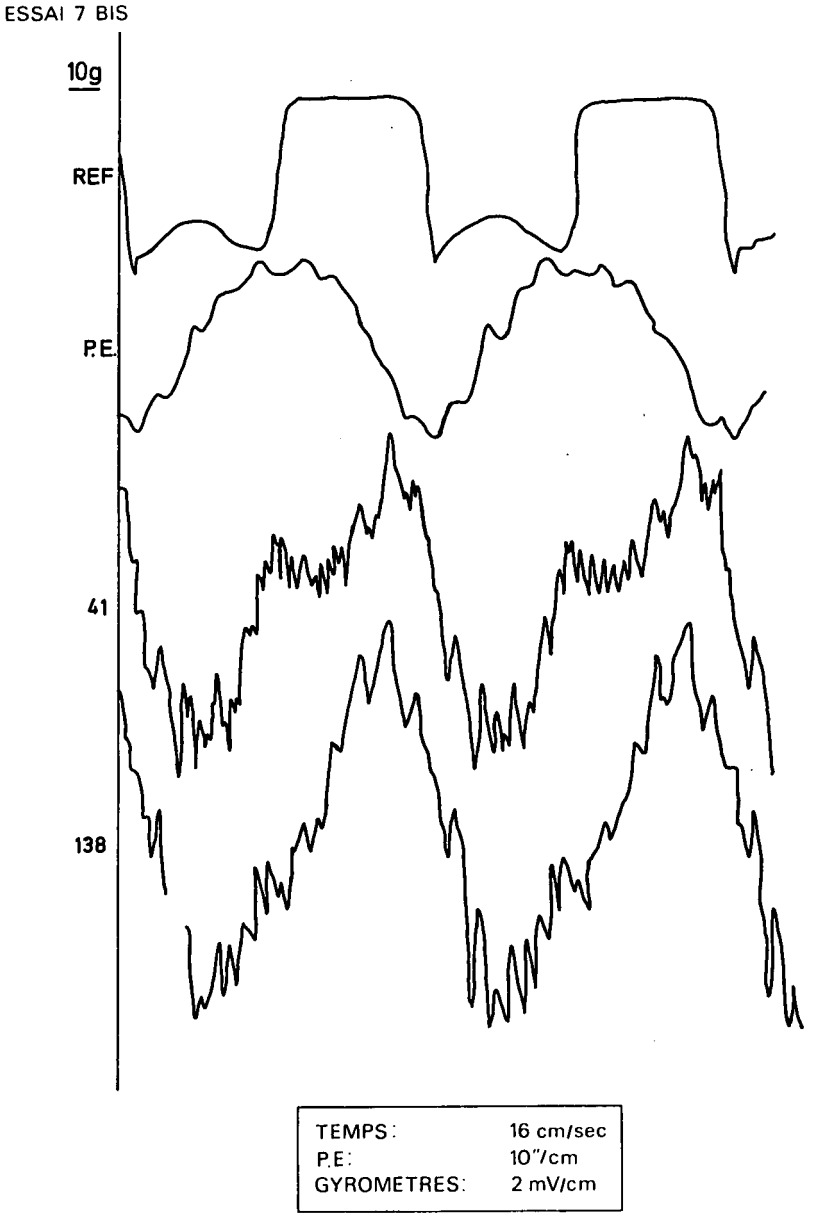

Fig. 11-11 Suivi

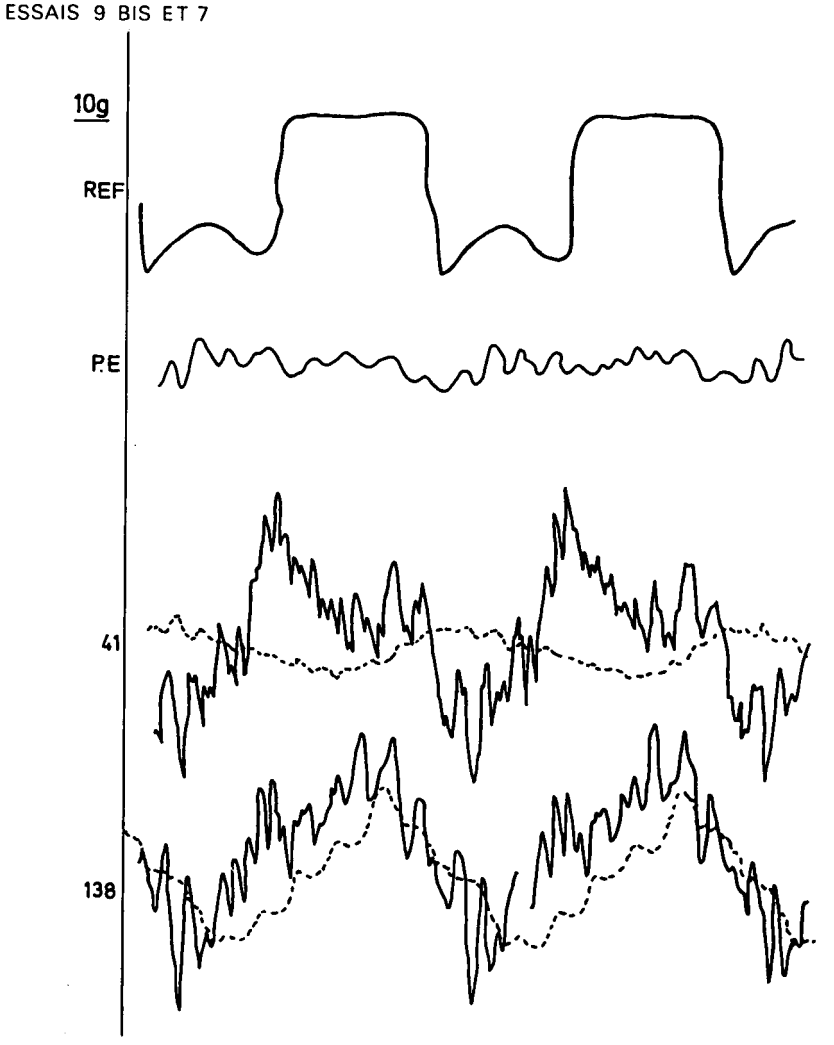

Fig. 11-11 Suivi

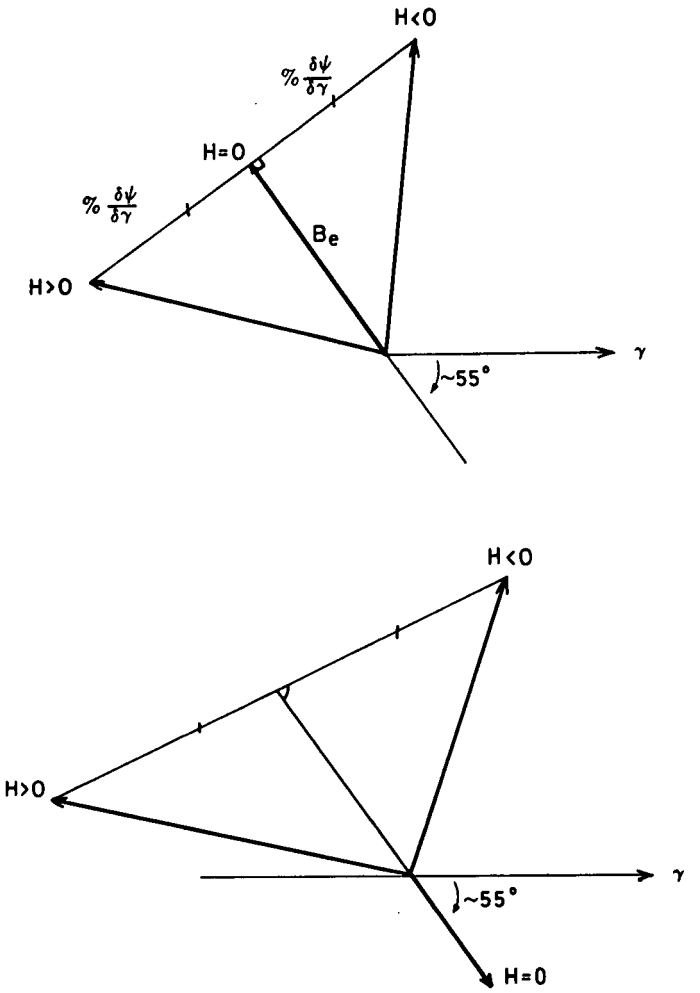

Fig. 11-12 Diagramme (a) théorique et (b) expérimental

H moment cinétique de la toupie

ω pulsation de l'accélération

$\frac{\partial\psi}{\partial\gamma}$ souplesse angulaire du corps suspendu par rapport au boitier autour de l'axe d'entrée, pour une accélération suivant l'axe toupie

γ amplitude de l'accélération

j $\sqrt{-1}$

Le dépouillement des enregistrements a été effectué de la façon suivante:

(a) analyse harmonique des courbes

(b) construction des vecteurs, représentatifs des composantes fondamentales, dans un plan de phase dont le vecteur origine est l'accélération

(c) opération sur ces vecteurs:
correction des signaux de l'influence de la rotation résiduelle du plateau autour de l'axe d'entrée; décomposition des signaux corrigés en composantes représentatives du balourd B_e et de la souplesse $\partial\psi/\partial\gamma$

Théoriquement les diagrammes devraient se présenter sous la forme indiquée dans la figure 11-12, en supposant que B_e a même valeur toupie arrêtée et toupie lancée.

Les diagrammes expérimentataux se sont révélés assez conformes à la théorie mais avec cette différence, que le point H = 0 ne se trouve pas au milieu des points H > 0 et H < 0 mais sur une droite joignant ce point à l'origine. Ceci s'interprête, compte tenu du modêle, comme une variation de la dérive de balourd selon que la toupie tourne ou non; la variation est cependant faible: 0,06 %/s à 10g.

La variation du signal pour H > 0 et H < 0, due à la souplesse de la suspension, est proportionnelle à l'accélération et atteint 0,05 %/s à 10g. Sa faiblesse explique qu'elle n'est visible que lorsque le balourd lui est relativement faible.

Cette souplesse de la suspension est évidemment sans conséquence pour un fonctionnement sous accélération continue, mais elle nécessite de prendre des précautions particulières pour l'interprétation des essais sur table 10g.

Ces essais ont donc permis de vérifier que les coefficients de balourd, toupie arrêtée et toupie lancée, étaient sensiblement les mêmes, compte tenu des tolérances, et que les essais sur centrifugeuse, toupie arrêtée, permettaient une selection valable des appareils.

Conclusion

Cet exposé vous a présenté une machine particulière, prévue pour étudier la dérive sous accélération de systêmes gyroscopiques. Son fonctionnement n'a pas les qualités espérées qui auraient permis l'étude des dérives du type balourd sur des gyroscopes inertiels de classe 1 °/h/g, qualités qu'il semble cependant possible d'obtenir avec la conception adoptée.

Néanmoins les deux exemples d'essais présentés, permettent d'affirmer que cette machine présente un intérêt certain pour les essais d'étude de composants de classe moyenne, en mettant en évidence des phénomênes difficilement accessibles

avec les moyens d'essais classiques; cet intérêt est augmenté par la facilité des conditions d'emploi, la rapidité et le prix de revient négligeable de la mise en oeuvre; l'exploitation des mesures est délicate mais cela est pratiquement systématique pour les essais sous accélération.

Bien entendu, les essais sur ces composants de classe moyenne ne constituent pas les seules applications possibles. D'autres essais ont été effectués ou sont prévus, notamment de centrales complètes, où, en plus des évaluations de dérive anisoélastique des gyroscopes, il est possible d'obtenir des renseignements intéressants sur le fonctionnement sous accélération des asservissements de cardan. Ce moyen d'essais semble également particulièrement bien adapté pour étudier les défauts de linéarité d'un accéléromètre à gyroscope balourdé du type engin, puisque la fréquence des oscillations est dans la bande passante de fonctionnement.

Notre expérience est actuellement limitée, mais nous ne doutons pas de pouvoir la développer et d'obtenir, grâce à ce moyen d'essais, des informations très profitables pour les matériels en essais d'étude.

gg

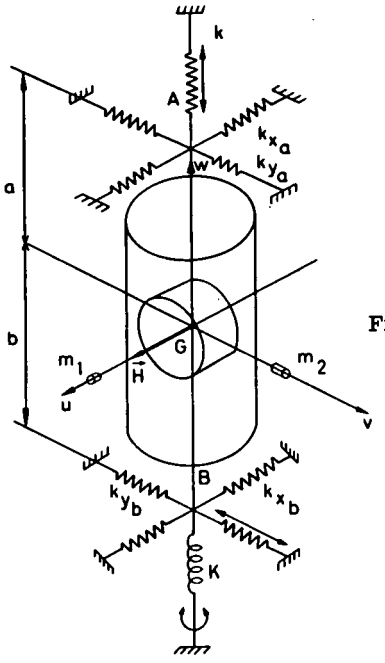

Fig. 11-A1 Liaisons élastiques reliant corps suspendu au boitier

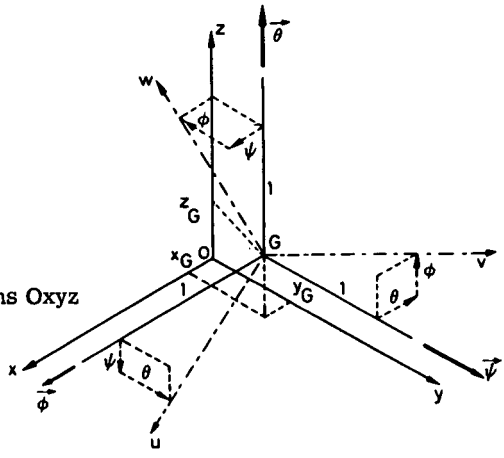

Fig. 11-A2 Repérage de Guvw dans Oxyz

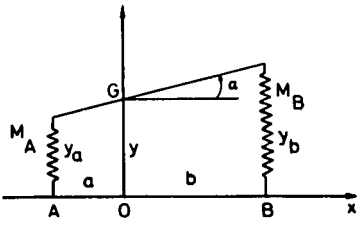

Fig. 11-A3 Solide, centre de gravité G, relié élastiquement á l'axe Ox

Annexe

Modèle mathématique simplifié

Définition

Le modèle suivant, très simplifié, rend compte de certains phénomènes dus à l'élasticité de la liaison: toupie - boitier.

Les hypothèses de départ, forcément assez restrictives, sont les suivantes:

(a) on étudiera les mouvements d'un solide relié au boitier par une suspension élastique et à amortissement visqueux, ce solide étant constitué par la toupie, le rotor du détecteur et leur support commun (la chemise d'amortissement ne fait pas partie de ce solide).

(b) le détecteur est parfait: il détecte uniquement les mouvements de rotation autour de l'axe de sortie et est linéaire.

Par suite, le système peut être représenté comme suit (Fig. 11-A1):

(a) Un trièdre Guvw lié au corps suspendu

avec G le centre de gravité

Gw l'axe de sortie

Gu parallèle à l'axe toupie

Gv l'axe d'entrée.

Ces axes étant donnés, les configurations du système peuvent être considérés comme axes principaux d'inertie avec les moments

I_u, I_v et $I_w = I$

Le fait de mettre le centre de gravité sur l'axe de sortie n'est pas restrictif, les balourds sont introduits fictivement par des masselottes disposées sur les axes Gu et Gv et dont les forces d'inertie seront considérées comme des forces extérieures.

(b) des liaisons élastiques reliant le corps suspendu au boitier (Fig. 11-A1) de raideurs linéaires k_{x_a}, k_{y_a}, k_{x_b}, k_{y_b} agissant perpendiculairement à Gw aux distances a et b de G; de raideur linéaire k agissant suivant Gw; de raideur angulaire K agissant autour de Gw.

(c) des amortissements visqueux, qui seront précisés ultérieurement.

(d) un trièdre Oxyz lié au boitier de gyromètre et coïncidant avec Guvw lorsque les liaisons élastiques sont au repos. Dans le cas général Guvw est

repéré dans Oxyz par (Fig. 11-A2) les coordonnées de G, x_G, y_G, z_G, et les trois angles ϕ, ψ, θ.

Etant donné la petitesse des mouvements (des secondes d'arc) ces angles peuvent être représentés par des vecteurs portés respectivement par les trois axes Gx, Gy, Gz parallèles à Ox, Oy, Oz.

Mise en equation des mouvements

1. Evaluation des forces de liaison (Fig. 11-A2)

Pour un déplacement donné (x_G, y_G, z_G, ϕ, ψ, θ) du corps suspendu, les coordonnées des points d'application A et B des forces de liaison ont pour expressions (au second ordre près)

$$A\begin{cases} x_G + a\psi \\ y_G + a\phi \\ z_G + a \end{cases} \qquad B\begin{cases} x_G - b\psi \\ y_G + b\phi \\ z_G + b \end{cases}$$

Les forces de liaison ont pour composantes (action du boitier sur le corps suspendu)

$$\vec{\Gamma}_R \begin{cases} 0 \\ 0 \\ -K\theta \end{cases}, \quad \vec{F}_A \begin{cases} -k_{x_a}(x_G + a\psi) \\ -k_{y_a}(y_G - a\phi) \\ -k\, z_G \end{cases} \text{ en A}, \quad \vec{F}_B \begin{cases} -k_{x_b}(x_G - b\psi) \\ -k_{y_b}(y_G + b\phi) \end{cases} \text{, en B}$$

En G, elles se réduisent à

$$\vec{F}_G = \vec{F}_A + \vec{F}_B$$

$$\vec{\Gamma}_G = \vec{\Gamma}_R + \vec{GA} \times \vec{F}_A + \vec{GB} \times \vec{F}_B$$

Soit

$$\vec{F}_G \begin{cases} -x_G(k_{x_a} + k_{x_b}) - \psi(a\,k_{x_a} - b\,k_{x_a}) \\ -y_G(k_{y_a} + k_{y_b}) + \phi(a\,k_{y_a} - b\,k_{y_b}) \\ -z_G(2k) \end{cases}$$

$$\vec{\Gamma}_G \begin{cases} a\,k_{y_a}(y_G - a\phi) - b\,k_{y_b}(y_G + b\phi) \\ -a\,k_{x_a}(x_G - a\psi) - b\,k_{x_b}(x_G + b\psi) \\ -K\theta \end{cases}$$

Soit encore, en posant:

$$\begin{cases} k_{x_a} + k_{x_b} = k_x \\ k_{y_a} + k_{y_b} = k_y \\ 2k = k_z \end{cases} \quad \begin{cases} a\,k_{x_a} - b\,k_{x_b} = \lambda_x \\ a\,k_{y_a} - b\,k_{y_b} = \lambda_y \end{cases} \quad \begin{cases} a^2 k_{x_a} + b^2 k_{x_b} = \mu_x \\ a^2 k_{y_a} + b^2 k_{y_b} = \mu_y \end{cases}$$

$$\vec{F}_G \begin{cases} -k_x x_G - \lambda_x \psi \\ -k_y y_G - \lambda_y \phi \\ -k_z z_G \end{cases} \qquad \vec{\Gamma}_G \begin{cases} \lambda_y y_G - \mu_y \phi \\ -\lambda_x x_G - \mu_x \psi \\ -K\theta \end{cases}$$

2. Evaluation des forces d'inertie du corps suspendu

Le boitier du gyromètre est soumis sur la table 10g à un mouvement s'écartant très peu d'un mouvement de translation. Par suite, le trièdre Oxyz peut être repéré dans un trièdre lié à la terre par six quantités X, Y, Z, Φ, Ψ, Θ analogues à x_G, y_G, z_G, ϕ, ψ, θ (mais ici X, Y, Z ne restent pas tous infiniments petits). Ce trièdre lié à la terre: TXYZ coïncide avec Oxyz lorsque la table 10g est au repos.

(a) Le moment cinétique $\bar{\bar{I}}.\vec{\omega}$ du corps suspendu a pour expression sur TXYZ (au second ordre près):

$$\bar{\bar{I}}.\vec{\omega} \begin{cases} I_u [\dot{\Phi} + \dot{\phi}] + H \\ I_v [\dot{\Psi} + \dot{\psi}] \\ I_w [\dot{\Theta} + \dot{\theta}] \end{cases}$$

Par suite, la dérivée du moment cinétique a pour expression (au second ordre près):

$$\bar{\bar{I}} \frac{d\vec{\omega}}{dt} + \vec{\omega} \times \bar{\bar{I}}.\vec{\omega} \quad \begin{cases} I_u [\ddot{\Phi} + \ddot{\phi}] \\ I_v [\ddot{\Psi} + \ddot{\psi}] + H [\dot{\Theta} + \dot{\theta}] \\ I_w [\ddot{\Theta} + \ddot{\theta}] + H [\dot{\Psi} + \dot{\psi}] \end{cases}$$

Les termes en H font apparaitre l'effet gyroscopique.

(b) Les forces d'inertie ont pour résultante en G:

$$-M\vec{\gamma} \begin{cases} - M (\ddot{X} + \ddot{x}_G) \\ - M (\ddot{Y} + \ddot{y}_G) \\ - M (\ddot{Z} + \ddot{z}_G) \end{cases}$$

3. Evaluation des forces de balourd

Soient m_1 et m_2 deux masselottes fixées sur les axes Gu et Gv aux points M_1 et M_2 d'abscisses u_1 et v_2. Ces points ont pour coordonnées dans le trièdre TXYZ:

$$M_1 \begin{cases} X + x_G + u_1 \\ Y + y_G + u_1 [\theta + \Theta] \\ Z + z_G - u_1 [\psi + \Psi] \end{cases} \qquad M_2 \begin{cases} X + x_G - v_2 [\theta + \Theta] \\ Y + y_G + v_2 \\ Z + z_G + v_2 [\phi + \Phi] \end{cases}$$

Les forces d'inertie liées à ces masses et considérées comme actions extérieures sur le corps suspendu ont pour expression:

$$\vec{F}_1 \text{ en } M_1 \begin{cases} - m_1 [\ddot{X} + \ddot{x}_G] \\ - m_1 [\ddot{Y} + \ddot{y}_G + u_1 (\ddot{\theta} + \ddot{\Theta})] \\ - m_1 [\ddot{Z} + \ddot{z}_G - u_1 (\ddot{\psi} + \ddot{\Psi})] \end{cases} \qquad \vec{F}_2 \text{ en } M_2 \begin{cases} - m_2 [\ddot{X} + \ddot{x}_G - v (\ddot{\theta} + \ddot{\Theta})] \\ - m_2 [\ddot{Y} + \ddot{y}_G] \\ - m_2 [\ddot{Z} + \ddot{z}_G + v (\ddot{\phi} + \ddot{\Phi})] \end{cases}$$

Elles ont pour résultantes en G (au second ordre près pour le couple):

$$\vec{F}_B = \vec{F}_1 + \vec{F}_2 \quad \begin{cases} - (m_1+m_2)(\ddot{X} + \ddot{x}_G) + m_2 v_2 (\ddot{\theta} + \ddot{\Theta}) \\ - (m_1+m_2)(\ddot{Y} + \ddot{y}_G) - m_1 u_1 (\ddot{\theta} + \ddot{\Theta}) \\ - (m_1+m_2)(\ddot{Z} + \ddot{z}_G) + m_1 u_1 (\ddot{\psi} + \ddot{\Psi}) - m_2 v_2 (\ddot{\phi} + \ddot{\Phi}) \end{cases}$$

g*

$$\vec{\Gamma}_B = G\vec{M}_1 \times \vec{F}_1 + G\vec{M}_2 \times \vec{F}_2 \begin{cases} (-m_2v_2[\ddot{Z} + \ddot{z}_G + v_2(\ddot{\phi} + \ddot{\Phi})] \\ + m_1u_1[\ddot{Z} + \ddot{z}_G - u_1(\ddot{\psi} + \ddot{\Psi})] \\ - m_1u_1[\ddot{Y} + \ddot{y}_G + u_1(\ddot{\theta} + \ddot{\Theta})] + m_2v_2[\ddot{X} + \ddot{x}_G - v_2(\ddot{\theta} + \ddot{\Theta})] \end{cases}$$

4. Equations des mouvements

Projetons les relations vectorielles suivantes sur les triêdres TXYZ, en séparant les variables d'état: x_G, y_G, z_G, ϕ, ψ, θ et les actions extérieures X, Y, Z, Φ, Ψ, Θ.

$$\vec{F}_G + \vec{F}_B = M\vec{\gamma}$$

$$\vec{\Gamma}_G + \vec{\Gamma}_B = \frac{d}{dt}(\bar{\bar{I}}.\vec{\omega})$$

$\vec{F}_G$ et $\vec{\Gamma}_G$ comportent des termes d'amortissements visqueux, qui peuvent être introduits explicitement au moment de la recherche des solutions en substituant des termes de la forme $k(1 + \tau p)$ aux termes k.

$$\begin{cases} -(M+m_1+m_2)\ddot{x}_G - k_x x_G - \lambda_x\psi + m_2v_2\ddot{\theta} = (M+m_1+m_2)\ddot{X} - m_2v_2\ddot{\Theta} \\ -(M+m_1+m_2)\ddot{y}_G - k_y y_G + \lambda_y\phi - m_1u_1\ddot{\theta} = (M+m_1+m_2)\ddot{Y} + m_1u_1\ddot{\Theta} \\ -(M+m_1+m_2)\ddot{z}_G - k_z z_G - m_2v_2\ddot{\phi} + m_1u_1\ddot{\psi} = (M+m_1+m_2)\ddot{Z} + m_2v_2\ddot{\Phi} - m_1u_1\ddot{\Psi} \end{cases}$$

$$\begin{cases} \lambda_y y_G - m_2v_2\ddot{z}_G - \mu_y\phi - (I_u + m_2v_2^2)\ddot{\phi} = m_2v\ddot{Z} + (I_u + m_2v_2^2)\ddot{\Phi} \\ -\lambda_x x_G + m_1u_1\ddot{z}_G - \mu_x\psi - (I_v + m_1u_1^2)\ddot{\psi} - H\dot{\theta} = -m_1u_1\ddot{Z} + (I_v + m_1u_1^2)\ddot{\Psi} + H\dot{\Theta} \\ m_2v_2\ddot{x}_G - m_1u_1\ddot{y}_G - (I + m_1u_1^2 + m_2v_2^2)\ddot{\theta} - K\theta + H\dot{\psi} = -m_2v_2\ddot{X} + m_1u_1\ddot{Y} \\ \qquad + (I + m_1u_1^2 + m_2v_2^2)\ddot{\Theta} - H\ddot{\Psi} \end{cases}$$

Effectuons les transformations littérales suivantes:

$$\begin{cases} M + m_1 + m_2 \rightarrow M \\ m_1u_1 \rightarrow B_g \\ m_2v_2 \rightarrow B_e \\ x_G, y_G, z_G \rightarrow x, y, z \end{cases} \qquad \begin{cases} I_u + m_2v_2^2 \rightarrow I_u \\ I_v + m_1u_1^2 \rightarrow I_v \\ I + m_1u_1^2 + m_2v_2^2 \rightarrow I \end{cases}$$

Avec l'opérateur p le système s'écrit:

$$\begin{cases} -(Mp^2 + k_x)x - \lambda_x\psi + B_ep^2\theta = Mp^2X - B_ep^2\Theta \\ -(Mp^2 + k_y)y + \lambda_y\phi - B_gp^2\theta = Mp^2Y + B_gp^2\Theta \\ -(Mp^2 + k_z)z - B_ep^2\phi + B_gp^2\psi = Mp^2Z + B_ep^2\Phi - B_gp^2\Psi \end{cases}$$

$$\begin{cases} \lambda_y y - B_ep^2z - (I_up^2 + \mu_y)\phi = B_ep^2Z + I_up^2\Phi \\ -\lambda_x x + B_gp^2z - (I_vp^2 + \mu_x)\psi - Hp\theta = -B_gp^2Z + I_vp^2\Psi + Hp\Theta \\ B_ep^2x - B_gp^2y - (Ip^2 + K)\theta + Hp\psi = -B_ep^2X + B_gp^2Y + Ip^2\Theta - Hp\Psi \end{cases}$$

Etude du système d'équations

1. Généralités et calcul préparatoire

Ce système s'étudie, sans difficulté théorique, par application des règles classiques de résolution des systèmes linéaires. Ici nous nous contentons d'évaluer l'influence

du signe et de la grandeur de H sur les mouvements en θ, provoqués par les différentes actions extérieures (accélérations linéaires et vitesses angulaires).

Dans le calcul des coefficients certains groupements de termes apparaissent systématiquement et peuvent être remplacés par des termes plus parlants 'physiquement'. Le calcul qui suit précise ces groupements.

Considérons un solide de centre de gravité G dont deux de ses points M_A et M_B sont reliés élastiquement à l'axe Ox (Fig. 11-A3). k_A et k_B étant les raideurs de ces deux liaisons, les éléments résultants en G des forces d'action ont pour expressions:

$$F = - (k_A + k_B)\, y - (a\, k_A - b\, k_B)\, \alpha$$

$$C = - (a\, k_A - b\, k_B)\, y - (a^2 k_A + b^2 k_B)\, \alpha$$

Par suite, une action extérieure caractérisée par la force F_e et le couple C_e en G entraînera, en position d'équilibre, un déplacement du solide tel que:

$$y = \frac{(a^2 k_A + b^2 k_B)\, F_e - (a\, k_A - b\, k_B)\, C_e}{(a+b)^2\, k_A\, k_B}$$

$$\alpha = \frac{- (a\, k_A - b\, k_B)\, F_e + (k_A + k_B)\, C_e}{(a+b)^2 k_A\, k_B}$$

Les coefficients de C_e et F_e, qui apparaissent dans le calcul des solutions du système général sont remplacées par des expressions de la forme suivante:

$$\frac{\partial y}{\partial F} = \frac{a^2 k_A + b^2 k_B}{(a+b)^2\, k_A\, k_B} \qquad \frac{\partial y}{\partial C} = - \frac{a k_A - b k_B}{(a+b)^2\, k_A\, k_B}$$

$$\frac{\partial \alpha}{\partial F} = - \frac{a k_A - b k_B}{(a+b)^2\, k_A\, k_B} \qquad \frac{\partial \alpha}{\partial C} = \frac{k_A + k_B}{(a+b)^2\, k_A\, k_B}$$

2. Equation caractéristique du système: $\Delta = 0$

Le calcul du déterminant de ce système linéaire montre que:

(a) H n'apparait dans les coefficients de Δ que par son carré. Par suite, la valeur de Δ ne dépend pas du sens de rotation de la toupie.

(b) les termes en H^2 n'apparaissent qu'à partir du terme en p^2

(c) les premiers coefficients ont pour valeur:

terme constant:

$$C = (a+b)^4\, K\, k\, k_{x_a}\, k_{x_b}\, k_{y_a}\, k_{y_b}$$

terme en p (il provient uniquement des amortissements visqueux en remplaçant les k par $k(1+\tau_p)$), avec $\Sigma\tau_i = T + \tau_z + \tau_{x_a} + \tau_{y_a} + \tau_{x_b} + \tau_{y_b}$:

$$C \sum_1^6 \tau_i$$

terme en p^2, avec $\frac{\partial\theta}{\partial C} = \frac{1}{K}$:

$$C\left[\sum_{\substack{i,j=1\\ i<j}}^{6} \tau_i \tau_j + H^2 \frac{\partial\theta}{\partial C}\frac{\partial\psi}{\partial C} + I_u \frac{\partial\phi}{\partial C} + I_v \frac{\partial\psi}{\partial C} + I \frac{\partial\theta}{\partial C} + M \frac{\partial\theta}{\partial C}\left(\frac{\partial x}{\partial F} + \frac{\partial y}{\partial F} + \frac{\partial z}{\partial F}\right)\right]$$

Si $H^2(\partial\psi/\partial C)$ est faible devant I, c'est à dire si le boitier 'bien' au corps suspendu ses rotations autour de l'axe d'entrée, Δ gardera la même valeur que H soit nul ou non. Par contre si $H^2(\partial\psi/\partial C)$ est important, le coefficient du terme en p^2 sera différent pour $H = 0$ et $H \neq 0$. Mais, même dans ce cas, Δ est peu sensible à cette variation puisque la fréquence propre du gyromètre est éloignée de la fréquence de travail; Δ sera donc considéré comme constant pour les essais effectués.

3. Influence des diverses excitations

(a) accélération suivant l'axe toupie: $\ddot{X}$
Nous avons

$$\frac{\theta}{p^2 \ddot{X}} = \frac{C}{\Delta}\left[\frac{B_e}{K} + \frac{M}{K}\left(-\frac{\partial\psi}{\partial F}\right) Hp + \epsilon p^2\right]$$

- le balourd B_e agit directement sur le signal de sortie;

- une réaction gyroscopique se produit si $\partial\psi/\partial F \neq 0$, c'est-à-dire si les forces de suspension provoquent un basculement du corps suspendu autour de l'axe d'entrée;

- le crochet ne contient pas de termes en H^2.

(b) accélération suivant l'axe d'entrée : $\ddot{Y}$
Nous avons

$$\frac{\theta}{p^2 \ddot{Y}} = \frac{C}{\Delta}\left[-\frac{B_g}{K} + \epsilon p^2\right]$$

- le balourd B_g a une action identique à celle de B_e dans le cas précédent;

- la suite des termes contient un terme en $H\,p^5$ mais de coefficient très faible: $M B_e B_g \frac{\partial\theta}{\partial C}\frac{\partial\psi}{\partial C}\frac{\partial z}{\partial F}\left(-\frac{\partial\phi}{\partial F}\right)$;

- pas de termes en H^2.

(c) accélération suivant l'axe de sortie: $\ddot{Z}$
Nous avons

$$\frac{\theta}{p^2 \ddot{Z}} = \frac{C}{\Delta}\left[\frac{B_g}{K}\left(\frac{\partial\psi}{\partial C}\right) Hp + \frac{B_e B_g}{K}\left(\frac{\partial x}{\partial C} - \frac{\partial y}{\partial C}\right) p^2 + \ldots\right]$$

- si $\partial\psi/\partial C$ n'est pas nul, le balourd B_g fait basculer le corps suspendu d'où réaction gyroscopique;

- le terme en p^2 est faible ; il n'existe que si le basculement du corps suspendu entraîne une translation de G ($\partial y/\partial C$ et $\partial x/\partial C \neq 0$) d'où force d'inertie des balourds qui entraîne un couple autour de Gz:

- pas de termes en H^2.

(d) Mouvement autour de l'axe toupie : Φ
Nous avons

$$\frac{\theta}{p^2\Phi} = \frac{C}{\Delta}\left[\frac{I_x B_g}{K}\left(-\frac{\partial y}{\partial C}\right)p^2 - \frac{B_e B_g}{K} H \left(\frac{\partial z}{\partial F}\right)\left(\frac{\partial \psi}{\partial C}\right)p^3 + \ldots\right]$$

- ce mouvement a peu d'influence sur θ

Le premier terme n'existe que si $\partial y/\partial C \neq 0$, l'accélération de G dans la direction y, produite par le basculement du corps suspendu entraîne une force d'inertie de B_g dirigée suivant Gy d'où couple autour de Gz. Le second terme, faible, a une influence liée au signe de H.

- pas de termes en H^2.

(e) Mouvement autour de l'axe d'entrée: Ψ
Nous avons

$$\frac{\theta}{p\Psi} = \frac{C}{\Delta}\left[\frac{H}{K}\left(1 + \epsilon_1 p^2\right) + \frac{I_y B_e}{K}\left(\frac{\partial x}{\partial C}\right)p^3\left(1 + \epsilon_2 p^2\right)\right]$$

- il n'y a donc pas que des termes en H; le terme en p^3 est dû à une accélération de G suivant Gu ($\partial x/\partial C \neq 0$) lors du basculement du corps suspendu autour de Gv: le balourd B_e produit alors un couple sur l'axe de sortie. Donc si $\partial x/\partial C$ et B_e ne sont pas nuls, un gyromètre, toupie arrêtée, fournira un signal à une vibration angulaire sur l'axe d'entrée.

- pas de termes en H^2.

(f) Mouvement autour de l'axe de sortie:
Nous avons

$$\frac{\theta}{p^2\Theta} = \frac{C}{\Delta}\left[-\frac{I_z}{K} - \frac{H^2}{K}\left(\frac{\partial \psi}{\partial C}\right) + \epsilon\, p^2\right]$$

- le terme I_z/K est inhérent au principe du gyromètre, qui est sensible à une accélération angulaire autour de l'axe de sortie;

- le terme $(H^2/K)(\partial\psi/\partial C)$ est dû à la souplesse de la suspension autour de l'axe d'entrée: une vitesse autour de l'axe de sortie induit un couple gyroscopique dirigé suivant l'axe d'entrée; l'élasticité de la liaison permet un basculement du corps suspendu autour de cet axe, d'où apparition d'un couple gyroscopique porté par l'axe de sortie;

- pas de termes en Hp: le mouvement en θ est indépendant du sens de rotation de la toupie.

Remarques: Les amortissements visqueux, non écrits explicitement, sont inclus dans les termes de la forme $\partial\psi/\partial C$; il suffit en effet de remplacer ces derniers par des expressions de la forme : $(\partial\psi/\partial C)(1 + \tau p + \ldots)$ les coefficients de la parenthèse étant reliés aux τ_{x_a}, τ_{x_b} etc. par l'intermédiaire des relations de la forme:

$$\frac{\partial\psi}{\partial C} = \frac{k_{x_a} + k_{x_b}}{(a+b)^2 k_{x_a} k_{x_b}}$$

Conclusion - améliorations possibles

Ce modèle simplifié et linéaire pour permettre des calculs simples (mais déjà assez longs), permet d'expliquer certains phénomènes liés au sens de rotation de la toupie.

La première hypothèse sur le détecteur (détection des mouvements de rotation autour de l'axe de sortie uniquement) peut être levée; il suffit d'affecter un gain au détecteur pour chacun des déplacements possibles (x, y, z, ϕ, ψ, et θ), de calculer chacun des déplacements en fonction des excitations extérieures et de composer tous ces signaux élémentaires. Ces calculs, identiques à celui qui a été fait pour θ, sont simples mais longs; les solutions indiqueraient sans doute une influence du signe de H, pour chacune des excitations.

Cependant cette méthode d'étude n'est pas très satisfaisante car elle ne rend pas compte de certains phénomènes importants tels que l'anisoélasticité, qui est un phénomène non linéaire. Les équations écrites en permettraient pourtant l'étude à condition d'ajouter aux balourds des termes proportionnels aux accélérations suivant les axes considérés, mais alors les équations ne sont plus linéaires, et les méthodes approchées (méthode des perturbations par exemple) seraient difficiles à appliquer. Dans ce cas, une étude sur machine analogiques est très commode, à condition de pouvoir fixer des valeurs numériques et les ordres de grandeur des paramètres.

Remerciements

L'auteur remercie le LRBA pour l'aide générale apportée à la production de ce document et Messieurs Habermann, Cabillic, Jouannet et Jolivet pour l'aide technique apportée dans la mise au point du moyen d'essais.

Références

(1) **Gates, R. L.**, 'Preliminary Report on Precision Testing of Gyroscopes on a High-g Centrifuge', Second Inertial Guidance Test Symposium.

(2) **Jouannet, F.**, 'Circuits électroniques à thyratrons solides pour l'entretien des oscillations d'une table d'essais mécanique', LRBA, 27 - Vernon, France.

Influences des mouvements du boitier sur le signal gyrométrique

Accélération suivant l'axe toupie:

$$\frac{\theta}{\pi_X} = \frac{C}{\Delta}\frac{\partial\theta}{\partial C}\left[B_e - j M\omega \frac{\partial\psi}{\partial F} + \dots \right]$$

Accélération suivant l'axe d'entrée:

$$\frac{\theta}{\pi_Y} = \frac{C}{\Delta}\frac{\partial\theta}{\partial C}\left[- B_g + \dots \right]$$

Accélération suivant l'axe de sortie:

$$\frac{\theta}{\pi_Z} = \frac{C}{\Delta}\frac{\partial\theta}{\partial C}\left[j H \omega B_g \frac{\partial\psi}{\partial C} - \omega^2 B_e B_g \left(\frac{\partial x}{\partial C} - \frac{\partial y}{\partial C} \right) + \dots \right]$$

Accélération angulaire suivant l'axe toupie:

$$\frac{\theta}{\pi_\Phi} = \frac{C}{\Delta}\frac{\partial\theta}{\partial C}\left[\omega^2 B_g I_x \frac{\partial y}{\partial C} + j \omega^3 H B_e B_g \frac{\partial z}{\partial F}\frac{\partial\psi}{\partial C} + \dots \right]$$

Vitesse angulaire suivant l'axe d'entrée:

$$\frac{\theta}{\dot{\Psi}} = \frac{C}{\Delta}\frac{\partial\theta}{\partial C}\left[H \left(1 + \epsilon \omega^2 + \dots \right) - j \omega^3 I_y B_e \frac{\partial x}{\partial C} \left(1 + \epsilon^1 \omega^2 + \dots \right) \right]$$

Accélération angulaire suivant l'axe de sortie:

$$\frac{\theta}{\pi_\Theta} = \frac{C}{\Delta}\frac{\partial\theta}{\partial C}\left[- I - H^2 \frac{\partial\psi}{\partial C} + \dots \right]$$

avec

$$\frac{\Delta}{C} = 1 + \Sigma\tau_i j \omega - \omega^2 \left[\Sigma \tau_i\tau_j + H^2 \frac{\partial\theta}{\partial C}\frac{\partial\psi}{\partial C} + I_x \frac{\partial\phi}{\partial C} + I_y \frac{\partial\psi}{\partial C} = I_z \frac{\partial\theta}{\partial C} + M \frac{\partial\theta}{\partial C}\left(\frac{\partial x}{\partial F} + \frac{\partial y}{\partial F} + \frac{\partial z}{\partial F} \right) \right] + \dots$$

12

Etude des Ecarts de Linéarité des Accéléromètres sur Centrifugeuse

C. MAUFFRET
Laboratoire de Recherches Balistiques et Aérodynamiques, Vernon, France

Résumé

Ce rapport rappelle d'abord l'intérêt des essais sur centrifugeuse pour déterminer les écarts de linéarité des accéléromètres; il décrit sommairement des méthodes d'essais et d'analyse des résultats courantes; puis il étudie la précision des essais sur centrifugeuse et les spécifications auxquelles doit répondre une centrifugeuse de haute précision.

Enfin, il donne les caractéristiques d'une centrifugeuse mise au point par le Laboratoire de Recherches Balistiques et Aérodynamiques.

1. Intérêt des essais sur centrifugeuse pour déterminer les écarts de linéarité des accéléromètres; méthodes d'essais et d'analyse des résultats

Les essais d'accéleromètres inertiels peuvent avoir deux buts principaux : dans la phase de conception, ils doivent donner au constructeur des informations sur les caractéristiques du matériel lui permettant d'orienter son étude; dans la phase de qualification, ils doivent permettre de vérifier que le matériel a la précision nécessaire pour remplir sa mission, donc répond à des spécifications précises. L'esprit étant différent, les essais ne sont pas effectués ni interprétés de la même façon suivant qu'ils font partie de la première ou de la deuxième catégorie.

Ainsi, en ce qui concerne la linéarité des accéléromètres, dans le premier cas, on mènera les essais en vue d'établir un modèle mathématique de l'appareil; dans le deuxième cas, on étudiera les écarts de linéarité par rapport à des grandeurs accessibles avant tir.

Essais analytiques

Un modèle mathématique de l'accéléromètre a été développé dans un document du Space Technology Laboratories (1).

La sortie de l'appareil : $A_{ind} = A_{out}/K_1$ peut s'écrire :

$$A_{ind} = \frac{A_{out}}{K_1} = K_0 + A_i + K_2 A_i^2 + K_3 A_i^3 + K_o A_o + K_p A_p +$$

$$K_{ip} A_i A_p + K_{io} A_i A_o + K_{op} A_o A_p + K_{p2} A_p^2 + K_{o2} A_o^2 + K_{i2p} A_i^2 A_p +$$

$$K_{ip2} A_i A_p^2 + K_{i2o} A_i^2 A_o + K_{io2} A_i A_o^2 + K_{p3} A_p^3 + K_{o3} A_o^3 + \ldots$$

Ce modèle fait intervenir les accélérations suivant les axes d'entrée, de sortie et de pendule : A_i, A_o, A_p et les caractéristiques suivantes de l'appareil :

(a) le facteur d'échelle K_1

(b) l'erreur de zéro K_0

(c) les non-linéarités $K_2 A_i^2$, $K_3 A_i^3$

(d) les sensibilités aux accélérations transverses $K_o A_o$, $K_p A_p$, $K_{p2} A_p^2$

(e) les couplages d'axe $K_{ip} A_i A_p$

Il suppose l'appareil stable et dépourvu d'hystérésis.

Les documents cités en références (1) et (2) montrent que les essais statiques sont bien adaptés à la mesure de K_0, K_1, K_{ip}, K_{io}, K_{op} ; ces coefficients peuvent être déterminés par des essais dans le champ de la pesanteur ou certains essais spéciaux quand la cause des écarts de linéarité est bien connue. Par contre, ils ne permettent pas une détermination précise des coefficients K_2, K_3, ... : pour un accéléromètre de bonne qualité, on peut avoir $K_2 < 5\,\mu g/g^2$, ce qui impose une précision de mesure et de positionnement compatibles avec une précision globale de 5.10^{-6}. Il est cependant possible d'apprécier K_2 à quelques $\mu g/g^2$ près; par contre, la détermination de K_3 est impossible.

Le document en référence (1) montre que les essais sur centrifugeuse de précision permettent de compléter les renseignements obtenus lors des essais statiques en donnant une évaluation précise des termes K_2, K_3 ...

L'exploitation d'une série de six essais effectués dans diverses configurations permet de déterminer la plupart des coefficients K. Cependant, par suite des incertitudes sur le rayon et le positionnement pour la majorité des centrifugeuses, les déterminations de K_0, K_1, K_o, K_p sont imprécises. En négligeant les termes d'ordre supérieur au troisième, on arrive à un système d'équations relativement simple pour déterminer les coefficients. Pour déterminer les coefficients K_2 et K_3, il suffit d'exploiter les deux essais effectués en dirigeant l'axe sensible successivement suivant l'accélération centripète et en opposition avec cette accélération.

Les résultats des essais sont ainsi exploités : on détermine pour chaque essai le polynome $C_0 + C_1 A_{CF} + C_2 A_{CF}^2$ qui représente le mieux les résultats (méthode des moindres carrés).

$$A_{ind} = C_0^+ + C_1^+ A_{CF} + C_2^+ A_{CF}^2$$

et

$$A_{ind} = C_0^- + C_1^- A_{CF} + C_2^- A_{CF}^2$$

pour chaque essai, on calcule les écarts de linéarité :

$$Y_{i+} = A_{ind_i} - C_0^+ + C_1^+ A_{CF_i} \quad \text{(i point de mesure)}$$

$$Y_{i-} = A_{ind_i} - C_0^- - C_1^- A_{CF_i}$$

ensuite, on détermine le polynome $Y = C_0 + C_1 A_{CF} + C_2 A_{CF}^2 + C_3 A_{CF}^3$ qui représente le mieux $Y_i (A_{CF_i})$ (méthode des moindres carrés).

Ceci permet de déterminer $K_2 = C_2$ et $K_3 = C_3$.

Cette méthode permet de déterminer K_2 et K_3 avec précision, sans qu'il soit nécessaire de connaître la valeur absolue du rayon R de la centrifugeuse à l'arrêt, ni le défaut de verticalité du plan de pose de l'accéléromètre. Combinée avec une série d'essais statiques, elle permet donc de déterminer les termes d'erreurs principaux des appareils.

L'intérêt de cet essai vient de ce qu'on a constaté que les coefficients K_2, K_3 sont en général très stables dans le temps: le coefficient K_2 caractérise particulièrement bien les accéléromètres pendulaires et ne dépend pas de la durée de l'essai, ce qui est heureux, car celle-ci est sans commune mesure avec la durée d'un tir.

Essais de qualification

Les seules caractéristiques des accéléromètres généralement accessibles avant tir sont le biais et le facteur d'échelle mesurés à partir d'essais à ± 1g. Le facteur d'échelle S ainsi mesuré est introduit dans le calculateur : les erreurs de mesure de l'accélération sont donc égales à $\gamma_{ind} - \gamma_{reel} = (A_{out}/S) - \gamma_{reel}$. Les écarts de linéarité doivent donc être mesurés en se référant à l'accélération mesurée à 1g. Ceci conduit à une exploitation des résultats d'essais différente de la précédente.

La sortie de l'appareil est mesurée, centrifugeuse à l'arrêt, ce qui donne I_o ; elle est ensuite mesurée pour diverses valeurs de γ, dont γ = 1g. On calcule le facteur d'échelle pour chaque accélération, défini par $S_\gamma = (I_\gamma - I_o)/\gamma$, et les variations relatives de ce facteur d'échelle par rapport à la valeur obtenue pour γ = 1g :

$$\left(\frac{\Delta S}{S}\right)_\gamma = \frac{S_\gamma - S_{1g}}{S_{1g}}$$

Ces variations relatives représentent bien les écarts relatifs de linéarité : on obtient deux demi courbes (Fig. 12-1) correspondant respectivement aux accélérations positives et négatives (axe sensible parallèle ou opposé à l'accélération centripète).

On peut remarquer que cette méthode est voisine de la précédente, mais moins précise, car elle n'utilise pas l'ensemble des résultats, mais attribue une importance particulière aux résultats de mesure obtenus à l'arrêt et pour γ = 1g.

En reprenant les termes ci-dessus, on a approximativement

$$I_o = C_0^+, \quad A_{ind} = I_\gamma, \quad \gamma = A_{CF}$$

d'où

$$\frac{I_{+\gamma} - I_o}{\gamma} = C_1^+ + C_2\gamma + C_3\gamma^2$$

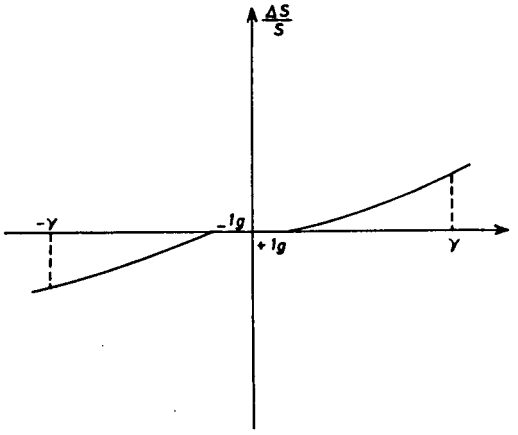

Fig. 12-1 Demi courbes correspondant aux accélérations positives et négatives

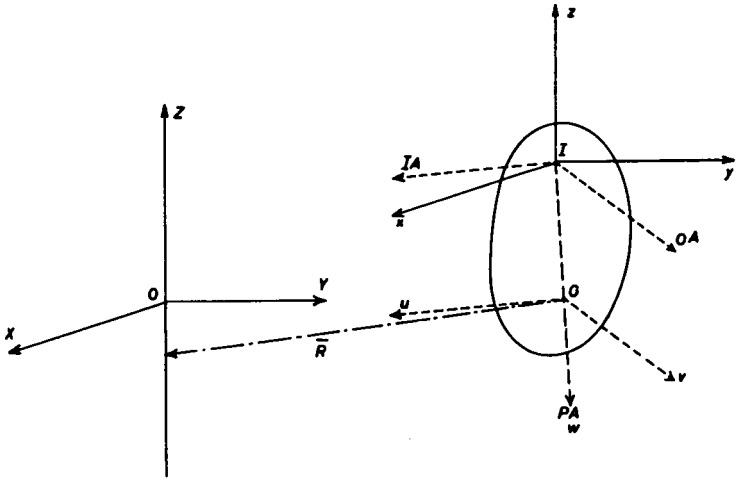

Fig. 12-2 Diagramme de l'accéléromètre sur centrifugeuse

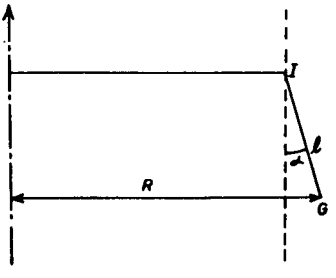

Fig. 12-3 Détermination du rayon R

$$I_{+1g} - I_o = C_1^+ + C_2 + C_3$$

$$\left(\frac{\Delta S}{S}\right)_{\gamma} = \frac{C_2}{C_1^+}(\gamma - 1) + \frac{C_3}{C_1^+}(\gamma^2 - 1)$$

de même pour $\gamma < 0$:

$$\left(\frac{\Delta S}{S}\right)_{-\gamma} = \frac{C_2}{C_1^-}(-\gamma + 1) + \frac{C_3}{C_1^-}(\gamma^2 - 1)$$

L'étude des ces courbes permet donc d'obtenir une valeur approximative de C_2/C_1 et C_3/C_1.

Si les courbes sont regulières, on peut se borner à utiliser les points de mesure correspondants aux accélérations extrêmes :

$$A = \left(\frac{\Delta S}{S}\right)_{+\gamma} \qquad \text{et} \qquad B = \left(\frac{\Delta S}{S}\right)_{-\gamma}$$

d'ou l'on tire, C_1^+ étant peu différent de C_1^-:

$$\frac{C_3}{C_1} = \frac{A + B}{2(\gamma^2 - 1)} \qquad \text{et} \qquad \frac{C_2}{C_1} = \frac{A - B}{2(\gamma - 1)}$$

Cette méthode permet donc d'évaluer simplement C_2 et C_3. Elle présente un autre avantage : certains accéléromètres présentent de l'hystérésis; il devient alors difficile d'appliquer la première méthode sans la compliquer notablement, tandis que la deuxième, plus descriptive, met en évidence le comportement des appareils.

2. Précision des essais sur centrifugeuse; spécifications auxquelles doit répondre une centrifugeuse de précision

On se bornera à étudier la précision des essais effectués axe sensible de l'accéléromètre parallèle ou opposé à l'accélération centripète, qui permettent de déterminer K_2 et K_3 comme cela a été vu ci-dessus.

En général, on admet que le système des quantités d'accélération se réduit à une force $M\vec{\gamma}_G = M\omega^2 \vec{R}$ appliquée au centre d'inertie de la masse sensible.

En fait, ce n'est qu'une approximation. Nous allons étudier, en faisant quelques hypothèses simplificatrices, les principales causes d'erreur.

Soient (Fig. 12-2):

OXYZ un trièdre lié à la terre, OZ étant l'axe de rotation de la centrifugeuse

$\vec{\omega}$ vitesse de rotation de la centrifugeuse, considérée comme constante

G le centre d'inertie de la masse sensible (IG = ℓ)

hh

$\overline{IA}, \overline{PA}, \overline{OA}$ les axes d'entrée, de pendule, de sortie de l'accéléromètre, axes liés à la masse sensible

Ixyz le trièdre équipollent au trièdre OXYZ issu de I.

On supposera que le trièdre $\overline{IA}, \overline{PA}, \overline{OA}$ est équipollent au trièdre principal d'inertie Guvw.

La matrice de changement de coordonnées est la suivante :

	x	y	z
IA	$\sin\omega t$	$-\cos\omega t$	α
PA	$\alpha \sin\omega t + \beta\cos\omega t$	$\beta\sin\omega t - \alpha\cos\omega t$	-1
OA	$\cos\omega t$	$\sin\omega t$	β

α et β définissent les défauts d'orientation des axes.

Soient : I_{IA}, I_{PA}, I_{OA} les moments d'inertie principaux de la mass sensible;
δ le défaut d'orthogonalité de $\overline{OA}$ avec le rayon de la centrifugeuse passant par G.

Le problème consiste à étudier l'équilibre des couples autour de $\overline{OA}$:

Prenons OXYZ comme repère de mouvement. Si $\bar{\gamma}$ et $\bar{v}$ sont les accélérations et vitesses angulaires relatives à ce trièdre, la loi fondamentale de la mécanique se traduit par

$$\text{sys } m\bar{\gamma} \sim \text{sys } \bar{F}_e + M\bar{g} - \text{sys } (2\bar{\Omega} \times m\bar{v})$$

$M\bar{g}$ appliqué en G comprend l'accélération d'entraînement due au mouvement de la Terre. sys $(2\bar{\Omega} \times m\bar{v})$ correspond à l'accélération de Coriolis due à la rotation terrestre $\bar{\Omega}$.

Les éléments de réduction du système $(m\bar{\gamma})$ en G sont les suivants :

$\bar{D}$ résultante dynamique: $\bar{D} = M\bar{\gamma}_G$

Si $\bar{K}_G$ et $\bar{H}_G$ sont les moments dynamiques et cinétiques par rapport à G:

$$\bar{K}_G = \frac{d\bar{H}_G}{dt} = \bar{\omega} \times \bar{H}_G$$

sys $(2\bar{\Omega} \times m\bar{v})$ peut être simplifié :

Si $\bar{\Omega}_H$ et $\bar{\Omega}_V$ sont les composantes suivant OZ et suivant OX de la rotation terrestre, située dans le plan XOZ, $2\bar{\Omega} = 2\bar{\Omega}_H + 2\bar{\Omega}_V$.

sys $(2\bar{\Omega}_V \times m\bar{v})$ se déduit de sys $(m\bar{\gamma})$ = sys $(\bar{\omega} \times m\bar{v})$ en multipliant chaque vecteur par $2\Omega_V/\omega$; il cause donc une erreur relative $2\Omega_V/\omega$.

$$\text{sys } (2\bar{\Omega}_H \times m\bar{v}) = \text{sys } [2\bar{\Omega}_H \times (\bar{\omega} \times m\,\overline{OM})] = \text{sys } \bar{\omega}\ (m\,\overline{OM}.2\bar{\Omega}_H) -$$

$$\text{sys } m\,\overline{OM}\ (\bar{\omega}.2\bar{\Omega}_H) = \text{sys } \bar{\omega}\ (m\,\overline{OM}.2\bar{\Omega}_H) = \bar{\omega}\,(M\,\overline{OG}.2\Omega_H) +$$

$$\text{sys } \bar{\omega}\ (m\,\overline{GM}.2\bar{\Omega}_H)$$

Ce système de force a donc été réduit en une force $\bar{\omega}\ (M\,\overline{OG}.2\bar{\Omega}_H)$ appliquée en G et en un couple sys $\bar{\omega}\ (m\,\overline{GM}.2\bar{\Omega}_H)$.

Il est maintenant possible d'écrire l'équation d'équilibre des couples en I:

$$\frac{\omega + 2\Omega v}{\omega}\quad (\overline{IG} \times M\bar{\gamma}_G + \bar{\omega} \times \bar{H}_G) = \mathcal{M}_I \text{ sys } \bar{F}_e + \overline{IG} \times M\bar{g}$$

$$-\overline{IG} \times \bar{\omega}\ (M\,\overline{OG}.2\bar{\Omega}_H) \quad + \text{ sys } \bar{\omega}\ (m\,\overline{GM}.2\bar{\Omega}_H)$$

L'équation d'équilibre des couples autour de OA s'obtient en prenant comme trièdre de calcul $(\overline{IA}, \overline{PA}, \overline{OA})$ et en ne s'intéressant qu'à la composante des vecteurs sur OA:

$$\overline{IG} \left|\begin{matrix} 0 \\ \ell \\ 0 \end{matrix}\right. , M\bar{\gamma}_G \left|\begin{matrix} \omega^2\ R \\ \omega^2\ R\,\alpha \\ \omega^2\ R\,\delta \end{matrix}\right. , \bar{\omega} \left|\begin{matrix} \alpha\omega \\ -\omega \\ \beta\omega \end{matrix}\right. , \bar{H}_G \left|\begin{matrix} I_{IA}\ \alpha\omega \\ I_{PA}\ \omega \\ I_{OA}\ \beta\omega \end{matrix}\right. , \bar{g} \left|\begin{matrix} -g\alpha \\ +g \\ -g\beta \end{matrix}\right.$$

Les différents vecteurs ont les projections suivantes sur $\overline{OA}$:

$\overline{IG} \times M\bar{\gamma}_G$: $\quad -M\ell\omega^2 R$

$\bar{\omega} \times \bar{H}_G$: $\quad \alpha\omega^2\ (I_{IA} - I_{PA})$

$\mathcal{M}_I$ sys $\bar{F}_e$: $\quad C_e$

$\overline{IG} \times M\bar{g}$: $\quad M\ell\, g\alpha$

$\overline{IG} \times \bar{\omega}\ (M\,\overline{OG}.2\bar{\Omega}_H)$: $\quad -2\,M\ell\,\omega\Omega_H R\,\alpha \sin\omega t$

sys $\bar{\omega}\ (m\,\overline{GM}.\ 2\bar{\Omega}_H)$: $\quad -2\omega\Omega_H \sin\omega t\ I_{(PA,\ OA)}$ en négligeant les termes en α^2 et $\alpha\,\beta$, et en appelant $I_{(PA,\ OA)}$ le moment d'inertie par rapport au plan $(\overline{PA}, \overline{OA})$

D'ou l'équation d'équilibre:

$$\frac{\omega + 2\Omega v}{\omega}\ [-M\ell\omega^2 R + \alpha\omega^2\ (I_{IA} - I_{PA})] = C_E + M\ell\, g\alpha$$

$$-2M\ell\,\omega\Omega_H R\alpha \sin\omega t - 2\omega\Omega_H \sin\omega t\ I_{PA,\,OA}$$

Importance relative des divers termes : étude des erreurs quand on fait l'approximation $-M\ell\omega^2 R = C_E$

Influence de la rotation terrestre. La composante verticale de la rotation terrestre conduit à une erreur relative $2\Omega_v/\omega$: $\Omega_v \sim 5,5.10^{-5}$ rad/s. Si à 1g $\omega = 2,5$ rad/s

$$\frac{2\Omega_V}{\omega} = 2,2.10^{-5}$$

Si l'on désire faire des mesures précises, il faut donc tenir compte de Ω_V, ou prendre la moyenne des résultats obtenus en inversant le sens de ω.

La composante horizontale de la rotation terrestre entraîne des couples sinusoïdaux, variant à la fréquence de rotation de la centrifugeuse. Si on fait les rapports de leurs valeurs maximales au couple principal $M\ell\omega^2R$, on obtient $(2\Omega_H/\omega)\alpha$ et $(2\Omega_H/\omega)$. $(I_{PA,OA}/M\ell R)$. Ces couples sont donc tout à fait négligeables.

Influence du terme $\alpha\omega^2 (I_{IA}-I_{PA})$. Pour fixer les idées, prenons un accéléromètre pendulaire pour lequel M = 2g, ℓ = 2 cm, $I_{IA} = 0,6\ gcm^2$, $I_{PA} = 0,4\ gcm^2$.

Le terme $\alpha\omega^2 (I_{IA} - I_{PA})$ crée une erreur relative $\epsilon = \alpha(I_{IA} - I_{PA})/M\ell R$, qui est inversement proportionnelle à R.

Pour l'accéléromètre défini ci-dessus, et une centrifugeuse de rayon supérieur à 1 m, $\epsilon < 5.10^{-4}\ \alpha$.

Cette erreur reste inférieure a 10^{-6} tant que $\alpha < 7'$.

On voit donc qu'il faut s'assurer lors de l'essai d'un accéléromètre que ce terme est négligeable : il dépend de la géométrie de l'appareil par le terme $(I_{IA}-I_{PA})/M\ell$ et du défaut de parallélisme de l'axe $\overline{PA}$ et de l'axe de rotation : ce défaut est dû, d'une part à un mauvais positionnement initial, qui doit donc être réduit, d'autre part à la déflexion du pendule sous accélération, de la forme $\alpha = k\gamma$, qui peut conduire à une mauvaise évaluation du terme K_2.

Influence du terme $M\ell g\alpha$. Ce terme crée une erreur $M\ell g\alpha$. Si l'angle α est constant, l'effet de ce terme, qui subsiste quand $\omega = 0$, est éliminé quand on fait la différence $I_\gamma - I_o$.

Si α varie en accélération, une erreur subsiste : si à 20g, $\alpha = 10''$, l'erreur relative est égale à

$$\frac{g}{\omega^2 R}\alpha = \frac{1}{20}.\ 5.10^{-5} = 2,5.10^{-6}$$

La déflexion du pendule dans le boitier de l'appareil crée une déflexion α proportionnelle à l'accélération $\alpha = k\gamma$; l'erreur relative correspondante $\frac{Mg\ell}{M\ell\gamma} k\gamma = kg$ est constante. Cette erreur conduit donc uniquement à une mauvaise appréciation du facteur d'échelle de l'appareil.

Influence des fluctuations de la vitesse $\overline{\omega}$. Dans les calculs précédents, la grandeur de $\overline{\omega}$ a été considérée comme constante. En fait, il y a toujours des fluctuations de vitesse :

$$\omega = \omega_o\ (1 + \epsilon\ \sin \omega_1 t)$$

Dans ce cas, le calcul du moment dynamique $\overline{K}_G$ est un peu plus compliqué, la

formule $\bar{K}_G = \bar{\omega} \times \bar{H}_G$ ne s'appliquant plus. On voit aisément qu'il faut alors ajouter à $\alpha\omega^2 (I_{IA} - I_{PA})$ un terme de la forme $I_{OA}\, \beta\, \omega'$, tout à fait négligeable.

$\bar{\gamma}_G$ n'est pas égal dans ce cas à $\omega^2\bar{R}$, mais se décompose en $\bar{\gamma}_N = \omega^2\bar{R}$ et $\bar{\gamma}_T$, perpendiculaire à $\bar{\omega}$ et $\bar{R}$, de grandeur $R(d\omega/dt)$. Cette accélération tangentielle, faible et presque parallèle à OA, crée un couple $\overline{IG} \times M\bar{\gamma}_T$, absolument négligeable.

Influence d'un défaut de verticalité ϵ' de l'axe de rotation. Le terme $M\ell g\alpha$ devient $M\ell g\epsilon' \cos\omega t$ et crée donc un couple modulé à la période de rotation de la machine. Ceci n'a pas d'importance pour les accéléromètres intégrateurs, mais peut nuire à la précision des mesures des accéléromètres analogiques.

Pour avoir $\Delta S/S < 10^{-6}$, il est bon d'avoir $\Delta\gamma/\gamma < 10^{-5}$, soit $g\epsilon'/ng < 10^{-5}$.

On doit donc avoir dans la mesure du possible $\epsilon' < 2n$ (secondes d'arc).

Mesure de l'accélération $\gamma_N = \omega^2 R$

Le probleme se ramène à la détermination de ω et de R.

(a) Détermination de ω. Quand la centrifugeuse est stabilisée, s'il n'y a pas de dérive moyenne, par suite des fluctuations de vitesse, ω peut s'écrire :

$$\omega = \omega_o (1 + \epsilon \sin\omega_1 t)$$

ω_o peut être évalué en mesurant le temps mis pour faire un nombre de tours suffisamment élevé pour avoir la précision nécessaire. Un accéléromètre inertiel analogique permet d'évaluer les fluctuations de vitesse.

γ_N est déduit de ω_o par la formule $\gamma_N = \omega_o^2 R$. On effectue ainsi une erreur $\Delta\gamma = \omega_o^2 R(1 + \epsilon \sin\omega_1 t)^2 - \omega_o^2 R$ dont la valeur moyenne est $(\epsilon^2/2)\, \omega_o^2 R$. Pour avoir $\Delta\gamma/\gamma < 10^{-7}$, il suffit que $\epsilon < 4,5.10^{-4}$, ce qui est relativement facile à réaliser. Les fluctuations de vitesse n'ont pas d'autre effet sur les accéléromètres integrateurs, mais elles peuvent nuire considérablement à la précision des mesures des accéléromètres à sortie analogique : les fluctuations de vitesse de fréquence inférieure à 1 Hz rendent particulièrement difficile les mesures de tension au pont potentiométrique, par suite des oscillations du spot du galvanomètre de zéro. Si l'on désire une précision de $\pm 1.10^{-6}$, il est nécessaire d'avoir une stabilité de vitesse de $\pm 5.10^{-6}$.

Si ω dérive à une vitesse β, $\omega = \omega_o + \beta t$; si le temps de mesure est T, on prend pour le calcul $\omega = \omega_o$; donc $\gamma = \omega_o^2 R$.

Ceci introduit certaines erreurs lors des essais d'accéléromètres intégrateurs:

On prend $\gamma = \omega_o^2 R$, donc $\Delta v = \omega_o^2 RT$. En fait

$$\Delta v = \int_{-\frac{T}{2}}^{+\frac{T}{2}} (\omega_o + \beta t)^2 R\, dt = \omega_o^2 RT + \frac{\beta^2}{3} R \cdot \frac{T^3}{4}$$

d'où l'erreur $\frac{\delta \Delta v}{\Delta v} = \frac{\beta^2}{12\omega_o^2} T^2$.

Pour que $\delta \Delta v/\Delta v < 10^{-7}$, avec un temps de mesure T = 5 mn, il faut que $\beta < 0,013\ \omega_o$ par heure; il est évidemment facile d'avoir une stabilité de vitesse meilleure que 1.3 %par heure.

(b) Détermination de R. R est la distance de l'axe de rotation au centre de gravité G. Il est très difficile de connaitre la valeur absolue de R, par suite des difficultés de localisation du centre de gravité G et de l'axe de rotation.

Si R = 1430 mm, pour avoir une erreur $\Delta R/R < 1.10^{-6}$, il faut connaitre R avec une erreur $\Delta R < 1.4\mu$, ce qui semble impossible. La centrifugeuse Genisco G 460 possède cependant un dispositif permettant de mesurer R avec une précision voisine de 1.10^{-5}.

En fait, pour l'étude des écarts de linéarité, il n'est pas nécessaire de connaitre la valeur exacte de R. En effet, si pour γ = 1g, $\omega = \omega_1$ et $R = R_1$ et si, pour γ = ng, $\omega = \sqrt{n}.\ \omega_1$ et $R = R_1 + \Delta R$,

$$S_{ng} = \frac{I_{ng} - I_o}{n\omega_1^2(R+\Delta R)} \qquad S_{1g} = \frac{I_{1g} - I_o}{\omega_1^2 R}$$

$$\left(\frac{\Delta S}{S}\right)_{ng} = \frac{S_{ng} - S_{1g}}{S_{1g}} = \frac{I_{ng} - I_o}{n(I_{1g}-I_o)} \cdot \frac{1}{1 + \frac{\Delta R}{R}} - 1$$

L'expression ne fait pas intervenir R, mais ses variations relatives $\Delta R/R$, qui créent une erreur en l'absence de correction: $\delta(\Delta S/S)_{ng} \sim \Delta R/R$. Le problème essentiel est donc de mesurer les variations relatives de rayon en cours d'essai.

Le rayon est la somme de deux longueurs (Fig. 12-3): la distance entre l'axe de rotation et le plan de pose de l'accéléromètre et la distance entre le plan de pose et le centre de gravité de l'appareil. Les variations de cette dernière distance, qui dépendent du comportement de l'appareil, peuvent conduire à des non-linéarités: la déflexion du pendule $\alpha = k\gamma$ entraine une variation de rayon $\Delta R - k\ell\gamma$ d'où une erreur relative

$$\frac{\Delta\gamma}{\gamma} = \frac{k\ell}{R}\gamma.$$

Avec ℓ = 2 cm, R = 143 cm, $k = 15.10^{-6}$ rad/g, a 20g $\Delta\gamma/\gamma = 4,3.10^{-6}$.

L'erreur sur C_2 est égale à $0,2/\mu g/g^2$. Si k est plus élevé, l'erreur sur C_2 peut atteindre des valeurs non négligeables.

Les variations de la distance entre l'axe de rotation et le plan de pose doivent être mesurées. La méthode consiste en général à mesurer les allongements à partir de références extérieures. Si on est parfaitement sûr de la stabilité de l'axe de rotation, il suffit d'une référence; sinon, il en faut deux diamétralement opposées.

Si R = 1430 mm et si l'on veut $\Delta R/R < 5.10^{-6}$, il est nécessaire de disposer d'un appareil permettant de mesurer 7μ.

Conclusion : spécifications d'une centrifugeuse de précision

Pour mesurer avec une précision voisine de 5.10^{-6} les ecarts de linéarité des accéléromètres, il faut disposer d'une centrifugeuse ayant les caractéristiques suivantes:

(a) la vitesse angulaire moyenne doit être connue à 1.10^{-6} près; les fluctuations doivent être inférieures en valeur relative à $\pm 5.10^{-4}$; cependant, si les appareils essayés sont analogiques, les fluctuations ne doivent guère dépasser $\pm 5.10^{-6}$;

(b) les variations relatives de rayon doivent être connues avec une précision de 2 à 3.10^{-6};

(c) l'inclinaison du plan de pose doit être proportionnelle à l'accélération, ou, si elle est quelconque, inférieure à 10" d'arc à 20g (accéléromètre de gamme $\pm$ 20g);

(d) si l'accéléromètre a une sortie analogique, la verticalité de l'axe de rotation doit être exacte à quelques secondes d'arc près. Ceci est imposé également par la méthode de mesure de $\Delta R/R$ avec une seule référence.

Le Laboratoire de Recherches Balistiques et Aérodynamiques de Vernon a été amené pour équiper son laboratoire inertiel, à s'intéresser au problème des centrifugeuses de précision: il a été décidé d'acheter une centrifugeuse Genisco G 460 et simultanément de lancer l'étude d'une centrifugeuse originale. Une première version était operationnelle à la fin de 1963. Les bons résultats obtenus ont conduit à la réalisation d'un deuxième exemplaire amélioré dont voici la description.

Caractéristiques de la centrifugeuse de précision du LRBA

Caractéristiques générales

Cette centrifugeuse est capable de soumettre les appareils en essais à 41 valeurs d'accélération comprises entre 0, 25 et 60g. Elle peut porter une charge maximale de 40 kg sur deux plateux de mesure symétriques de 40 x 40 cm^2. Quatre surfaces horizontales de 34 cm x 40 cm disposées près de l'axe permettent de placer du matériel électronique. Les liaisons électriques avec l'extérieur sont assurées par 25 collecteurs à mercure.

Les idées directrices ayant conduit la réalisation sont les suivantes:

(a) Une grande précision et une grande stabilité de la vitesse ont été assurées grâce à un asservissement par quartz et en évitant les fluctuations des couples résistants par un carénage en forme de toupie, l'utilisation de paliers hydrauliques, l'emploi de collecteurs à mercure, et grâce à une grande inertie de la partie tournante.

(b) Une réalisation simple et robuste du bras et du bâti doit permettre d'assurer une bonne stabilité géométrique.

(c) Deux appareillages spéciaux permettent de mesurer les variations de rayon et l'inclinaison du plateau de mesure en rotation.

(d) Enfin, un dispositif de réglage fin de la verticalité de l'axe de rotation a été prevu.

(e) La centrifugeuse est placée dans un local climatisé en dessous de la salle de mesure.

Description de la centrifugeuse

Partie mécanique. La centrifugeuse est supportée par un bâti en tôles d'acier soudées, stabilisées thermiquement, constitué d'un socle à trois branches reposant sur le sol en trois points et portant en son centre le palier hydraulique inférieur et le stator du moteur, et de trois bras dont les extrémités portent le palier supérieur (Fig. 12-4).

L'appui sur le sol en trois points se fait par un système point-trait-plan, qui supprime toute contrainte dans le bâti. Deux verins hydrauliques permettent de régler finement la verticalité de l'axe de rotation, à mieux que la seconde d'arc près. Un dispositif de blocage est utilisé après réglage.

Le rotor est constitué de la façon suivante : sur un axe en acier traité, stabilisé thermiquement, est monté une poutre caisson en acier, symétrique, au moyen d'un assemblage par cônes. La section décroissante de la poutre permet de limiter les déformations sous l'effet du poids et de la charge. L'usinage des deux plateaux de mesure est terminé par grattage après montage de la machine; le défaut de parallélisme de l'axe de rotation et de ces plateaux est inférieur à 5 secondes d'arc.

La liaison bâti-rotor se fait par deux paliers hydrauliques: un palier cylindrique à la partie supérieure, un palier hydraulique combiné à une butée hydraulique à la partie inférieure. Le palier hydraulique supérieur, alimenté en trois points à 120° centre l'arbre automatiquement; la butée inférieure équilibre automatiquement le poids du rotor. La pression des paliers est de 60 bars, l'entrefer de 0, 2 mm; la raideur des paliers est supérieure à celle du bâti.

Un dispositif de sécurité coupe l'alimentation du moteur de la centrifugeuse et actionne le dispositif de freinage dès que la pression descend en dessous de 40 bars. Le freinage se fait par trois freins à mâchoire actionés hydrauliquement agissant sur un disque unique. Ce dispositif de freinage, relativement brutal, n'est pas utilisé normalement.

L'equilibrage dynamique se fait au moyen de huit masses placées dans deux plans distants de 550 mm au bout de bras très rigides de longueur 1 m. Pour faire l'équilibrage, on utilise la souplesse transversale du bâti. Celle-ci est faible, mais peut être aisément détectée grâce à un microcapacimètre monté à l'angle supérieur d'un des trois montants du bâti. La partie fixe du microcapacimètre est montée sur une poutre solidaire du mur du local (Fig. 12-6).

En cas de déséquilibre dynamique, le détecteur délivre un signal sinusoidal à la fréquence de rotation de la machine. Ce signal est enregistré ainsi que le top délivré par une cellule photoélectrique à chaque tour, ce qui permet de situer le balourd. L'équilibrage à vide est effectué par tatonnement. Ensuite, il suffit de compenser la charge utile placée sur un plateau par une charge identique sur le plateau opposé. L'équilibrage peut être tel que le déplacement sur un tour soit inférieur à 1 μ.

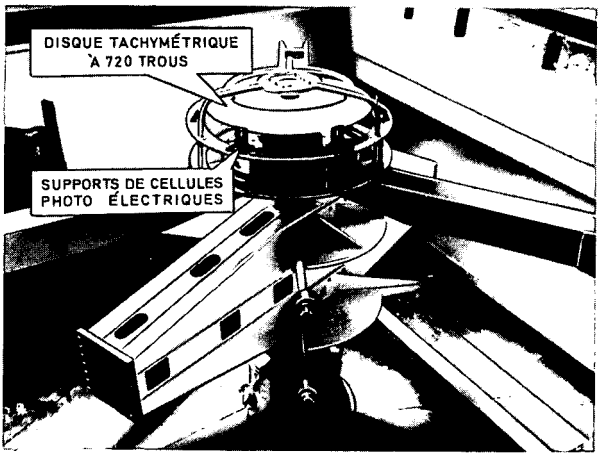

Fig. 12-4 Centrifugeuse en cours de montage

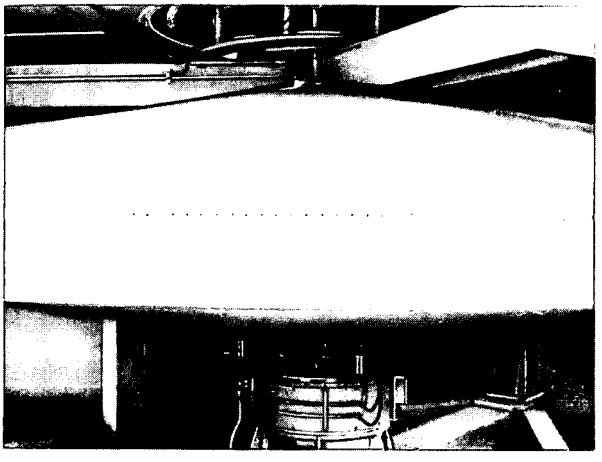

Fig. 12-5 Centrifugeuse en fin de montage

Pour assurer la constance des couples aérodynamiques, un capotage de révolution en tôles enveloppe la partie tournante (Fig. 12-5).

Le moteur, placé sous le rotor au dessus du palier hydraulique inférieur, est un moteur diphasé à double cage d'écureuil, spécialement conçu pour donner un couple constant sur un tour. Le rotor est lié à l'axe de la centrifugeuse. Il est alimenté en 45, 3Hz; il délivre une puissance maximale de 6 kW, correspondant à un couple de 80 mN. Le refroidissement est assuré par une circulation d'eau dans un tube enroulé en hélice autour du stator.

Le collecteur à mercure est visible sur la Figure 12-7: chacun des 25 contacts est constitué d'une cloche en cuivre plongeant dans une réserve annulaire de mercure. Ce type de contact n'amène qu'un bruit négligeable (inférieur à 50 μV).

Electronique, Asservissement. Le but de l'asservissement de la centrifugeuse est d'assurer la constance de la vitesse de rotation.

Le détecteur de rotation (Fig. 12-7) est constitué de la façon suivante: le rotor de la machine porte à sa partie supérieure un détecteur de vitesse constitué par un disque percé de 720 trous qui permettent un éclairage modulé de cellules photo-électriques. Afin d'obtenir le détecteur de vitesse le plus précis possible, les précautions suivantes ont été prises: la précision angulaire sur le positionnement des trous est de 5 secondes d'arc (précision relative 3.10^{-3}); pour éliminer au maximum les erreurs dues aux imperfections du disque, six cellules photoélectriques sont utilisées au lieu d'une, de façon à limiter l'amplitude des fluctuations aléatoires de fréquence, à éliminer la fréquence fondamentale et les six premiers harmoniques. Les six informations sont additionnées dans un ampli sommateur, qui délivre un signal périodique dont la fréquence est la valeur moyenne des six fréquences délivrées par les six cellules.

Un discriminateur de phase compare ce signal à celui délivré par un quartz: il y a 13 pilotes à quartz, qui fournissent $13 \times 5 = 65$ fréquences étalons; grâce à une série de bascules la stabilité des quartz est telle que leur dérive est inférieure à $\pm 2,5.10^{-7}$ par jour, $\pm 1.10^{-6}$ par mois, $\pm 5.10^{-6}$ par an. Le discriminateur de phase fournit un signal proportionnel au decalage angulaire du signal quartz et du signal détecteur. L'asservissement est un asservissement de position du rotor par rapport à un trièdre tournant à la vitesse correspondant à la fréquence du quartz. La figure 12-8 montre un schéma de la chaine d'asservissement.

Le principe est le suivant : Lorsque la centrifugeuse tourne, elle est soumise à des couples de frottement à peu près proportionnels au carré de la vitesse de rotation. Pour entretenir la rotation, il est nécessaire de fournir à la centrifugeuse un couple d'entretien qui est donc aussi proportionnel au carré de la vitesse de rotation. Il est indispensable que ce couple moyen d'entretien soit parfaitement constant de façon à éviter les fluctuations de vitesse. Il a donc été nécessaire d'alimenter le moteur par une tension moyenne issue des amplificateurs d'asservissement et non par un transformateur alimenté par le secteur, insuffisamment stable.

On dispose de huit amplificateurs pour chaque phase : il est possible de faire varier par paliers la tension de commande et de prélever une fraction variable de la tension de sortie. La sélection, faite automatiquement quand on appuie sur le bouton correspondant à l'accélération désirée sur le pupitre de commande (Fig. 12-9) permet de fournir le couple moteur nécessaire pour combattre le couple de frottement moyen. La chaine d'asservissement prend en charge le couple résiduel:

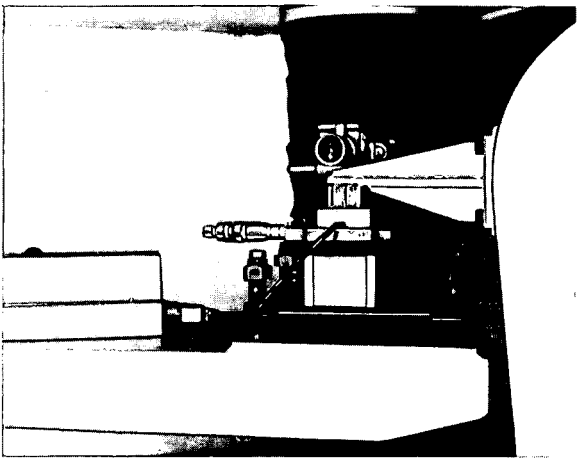

Fig. 12-6 Microcapacimètre servant à l'équilibrage dynamique

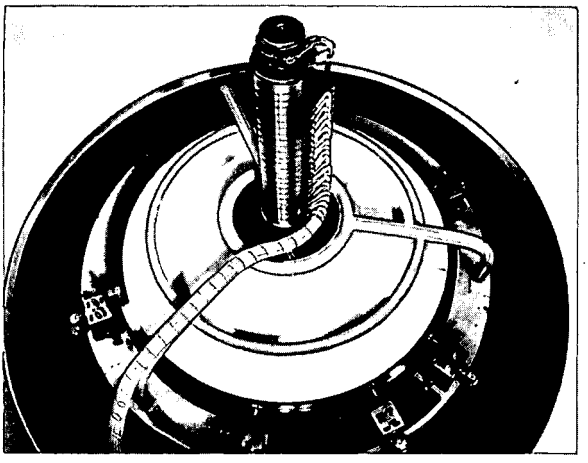

Fig. 12-7 Vue de dessus de la centrifugeuse

un réseau correcteur qui est une simple avance de phase rend l'asservissement stable. L'affaiblissement élevé à partir de la fréquence 6Ω évite de suivre les erreurs du disque.

Chaque amplificateur, de 400 W, comprend 14 transistors de puissance refroidis par eau.

Un groupe tournant fournit les tensions ± 24 V, 30 V nécessaires aux préamplificateurs et amplificateurs.

Implantation, Moyens de contrôle. La centrifugeuse est posée sur un massif de béton isolé, de 1 mètre de profondeur et située dans un local climatisé à ± 1°C près, en sous-sol. Un massif isolé porte les appareils de contrôle. Les contrôles possibles sont les suivants:

(a) Mesure de la vitesse de rotation - une cellule photoélectrique, éclairée à chaque tour, donne un signal qui peut être exploité pour contrôler la vitesse moyenne; les essais ont montré que cette mesure n'était pas nécessaire lors de l'utilisation normale, par suite de la qualité de l'asservissement en vitesse à la fréquence des quartz.

(b) Mesure de la distance du plateau à l'axe de rotation - une barre en invar de 2800 mm permet de mesurer la distance du plateau de mesure à l'axe de rotation à l'arrêt avec une précision de ± 3μ. Cette mesure n'a d'intérêt que si la distance du plateau au centre de gravité de l'accéléromètre a pu être mesurée préalablement.

(c) Mesure de l'allongement en rotation - cette mesure se fait à l'aide d'un microcapacimètre visible sur la figure 12-10. L'armature fixe est liée au plateau de contrôle; l'armature mobile est liée au bras de la centrifugeuse. Les capacités formées quand les armatures fixe et mobile sont en regard font partie d'un pont qui est équilibré pour la position médiane de la pièce mobile et qui se déséquilibre dans un sens ou dans l'autre suivant le sens de déplacement de celle-ci. Le pont, alimenté en 500 kHz, délivre 16 mV/μ avec un faux zéro et un bruit résiduel qui n'excèdent pas 1 mV à 25°C. En rotation, le signal délivré lors du passage de l'armature mobile est visualisé sur un oscilloscope. L'erreur de mesure ne dépasse pas ± 2,5μ.

(d) Mesure de l'inclinaison du plateau en rotation - l'inclinaison du plateau, autour de l'horizontale de son plan lors de la rotation, est mesurée à l'aide du dispositif visible sur la figure 12-11.

Une lunette autocollimatrice Wild (sensibilité 1″) est placée sur le plateau de contrôle. Un miroir, placé sur le plateau de mesure, permet de faire l'autocollimation lors du passage du bras en face du plateau de contrôle. Un appareil photographique, placé au dessus de la lunette, photographie la croix lumineuse réfléchie; l'énergie lumineuse est fournie par un générateur d'éclair, déclenché lors du passage du bras. Ce dispositif donne une précision de ± 2″.

Performances de la centrifugeuse

La qualification de la machine a conduit aux résultats suivants:

(a) la verticalité de l'axe de rotation peut être réglée à 1″ d'arc près, mais elle évolue de 4 à 5 secondes d'arc en trois mois, elle doit donc être réglée périodiquement.

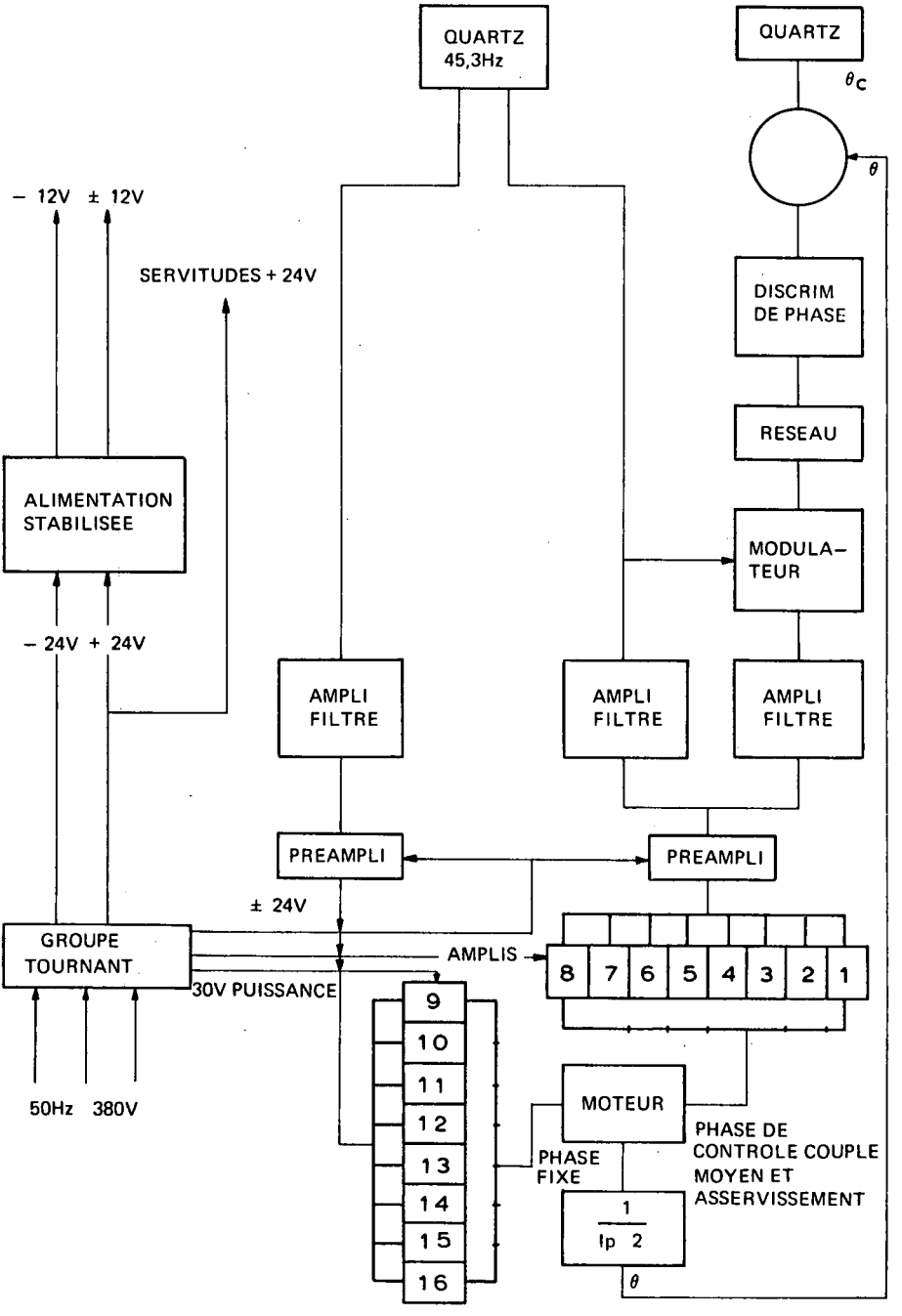

Fig. 12-8 Schéma synoptique de l'asservissement

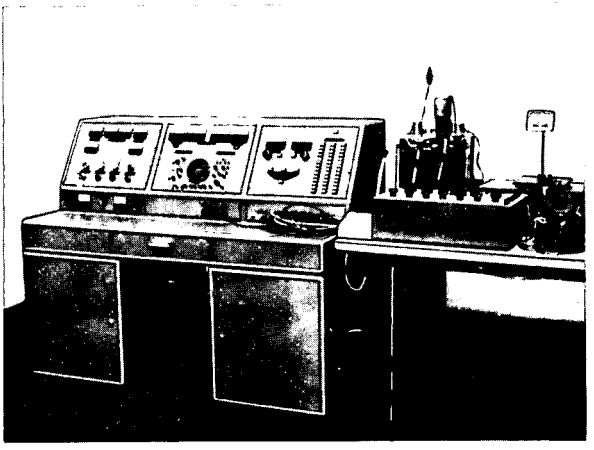

Fig. 12-9 Pupitre de commande

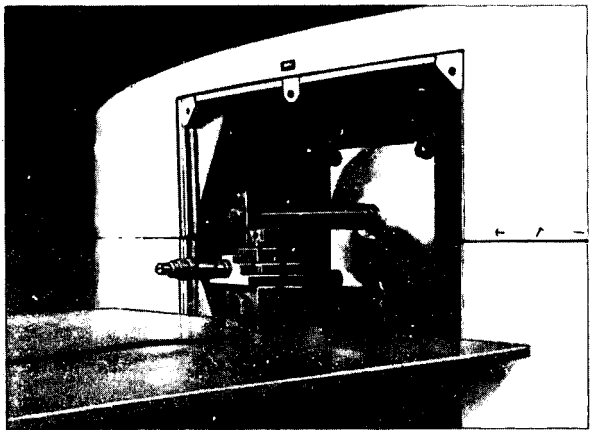

Fig. 12-10 Microcapacimètre

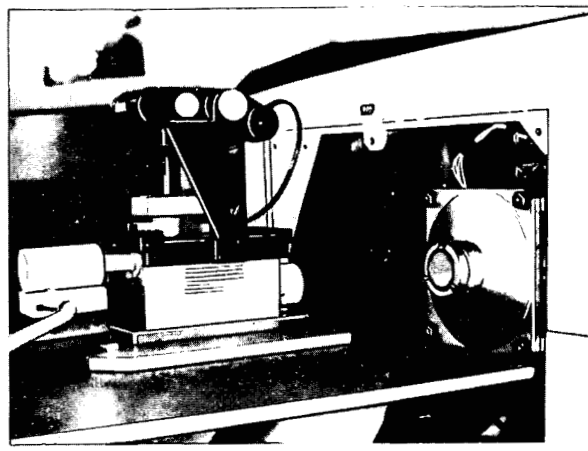

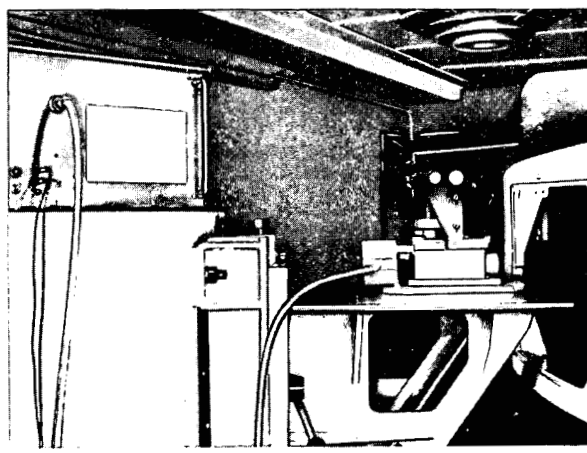

Fig. 12-11 Appareillage de mesure de l'inclinaison du plateau en rotation

(b) il est possible de mesurer la distance entre le plateau de mesure et l'axe de rotation à l'arrêt à mieux que ± 3 μ près (R = 1430, 131 + 0,003 mm à 20°C).

(c) par suite d'une réalisation trop sommaire de la climatisation, l'axe de rotation de la centrifugeuse se déplace en cours d'essai : en effet, les bouches de soufflage, mal réparties, causent des gradients thermiques qui se modifient quand la centrifugeuse tourne, le rotor créant un brassage d'air. Les variations de température du bâti créent des déplacements de l'axe qui peuvent atteindre 20 μ à la hauteur du bras au cours d'un essai, ce qui correspond à une erreur sur l'appréciation de ΔR : $\Delta R/R = 1,4.10^{-5}$. Dans les conditions actuelles, il est donc impossible d'utiliser dans de bonnes conditions les dispositifs de mesure d'allongement et d'inclinaison. La climatisation sera revue et un deuxième massif sera disposé symétriquement au premier.

Des essais variés ont cependant permis de vérifier les points suivants:

(a) l'allongement du bras en fonction de la température moyenne est de $12.10^{-6}/°C$. En relevant cette température en cours d'essai et en corrigeant des variations de rayon correspondantes, l'erreur résiduelle $\Delta R/R$ est inférieure à 3.10^{-6} ($\Delta\theta$ reste $\leq 1°C$);

(b) l'allongement du bras en fonction de γ est proportionnel à γ et voisin de $1,1.10^{-6}/g$. En faisant cette correction, l'erreur résiduelle $\Delta\gamma/\gamma$ est inférieure à 4.10^{-6} pour $\gamma \leq 20$ g.

(c) la vitesse moyenne ω est connue à 1.10^{-6} près, à condition de vérifier les quartz périodiquement. Les fluctuations de vitesse instantanées $\Delta\omega/\omega$ atteignent 4.10^{-6} a 1g et deviennent inférieures à 1.10^{-6} dès 3g. Cette excellente stabilité de vitesse permet l'utilisation de ponts potentiométriques de résolution au moins égale à 1 μV.

Précision de mesure des écarts de linéarité des accéléromètres

$$\frac{\Delta\gamma}{\gamma} \leq \left| 2\frac{\Delta\omega}{\omega} \right| + \left| \frac{\Delta R}{R} \right|$$

en prenant la somme quadratique des diverses erreurs évaluées ci-dessus, on obtient $\Delta\gamma/\gamma \leq 6.10^{-6}$.

Donc, actuellement, moyennant une correction d'allongement du bras en fonction de sa température et une correction systématique $1,1.10^{-6}/g$, cette centrifugeuse permet de déterminer les écarts de linéarité des accéléromètres avec une précision supérieure à 6.10^{-6}; la faible inclinaison de l'axe en rotation et la grande stabilité de la vitesse permettent d'étudier sans difficultés de mesure les accéléromètres à sortie analogique. Le fonctionnement très automatisé réduit au maximum la durée des essais (1 h 30 pour 21 points de mesure).

Afin de montrer la bonne qualité des essais effectués, on a reproduit sur le tableau 12-1 les résultats de calculs de C_2/C_1 et C_3/C_1 effectués à partir de divers essais:

(a) essais de linéarité sur la centrifugeuse qui vient d'être décrite;

(b) essais de linéarité sur une centrifugeuse basée sur le même principe, mais un peu moins élaborée;

(c) essais statiques aux points cardinaux.

Pour cinq accéléromètres essayés, C_2/C_1 se recoupent à $0,7\ \mu g/g^2$ près, C_3/C_1 à $0,11\ \mu g/g^3$ près; la corrélation avec les essais statiques est compatible avec les incertitudes de mesure.

Tableau 12-1

Accéléromètre	Centrifugeuse LRBA		Ancienne centrifugeuse		Essais statiques
	$\frac{C_2}{C_1}$	$\frac{C_3}{C_1}$	$\frac{C_2}{C_1}$	$\frac{C_3}{C_1}$	$\frac{C_2}{C_1}$
	$\mu g/_{g^2}$	$\mu g/_{g^3}$	$\mu g/_{g^2}$	$\mu g/_{g^3}$	$\mu g/_{g^2}$
No 1	+ 3,8	+ 0,15	+ 3,4	+ 0,17	+ 3 ± 3
No 2	+ 0,8	+ 0,07	+ 0,4	+ 0,11	0 ± 2
No 3	- 6,9	- 0,01	- 6,6	+ 0,01	- 6 ± 3
No 4	+ 1,4	- 0,41	+ 0,7	- 0,47	
No 5	+ 0,3	- 0,20	+ 0,5	- 0,09	

Remerciements

L'auteur remercie MM. Habermann, Cabillic, Joly, du Laboratoire de Recherches Balistiques et Aérodynamiques, chargés de l'étude de la centrifugeuse, qui lui ont donné toutes les informations nécessaires pour la rédaction de ce rapport.

Références

(1) **Evans, B.H., Fuhran, T.**, 'Determination of Accelerometer Non-linearities from Precision Centrifuge Testing', Second Inertial Guidance Test Symposium.

(2) **Grimme, B.H.**, 'Centrifuge Linearity Verification of Analog and Digital Accelerometers', Second Inertial Guidance Test Symposium.

(3) **Ebbinghaus, J.**, 'Precision Indexing of an Accelerometer to Facilitate the Measurement of Higher-order Non-linearities',

(4) **Cabillic et Joly**, 'Centrifugeuse 60g de haute précision', note technique no 29/67/EG, LRBA, Vernon.

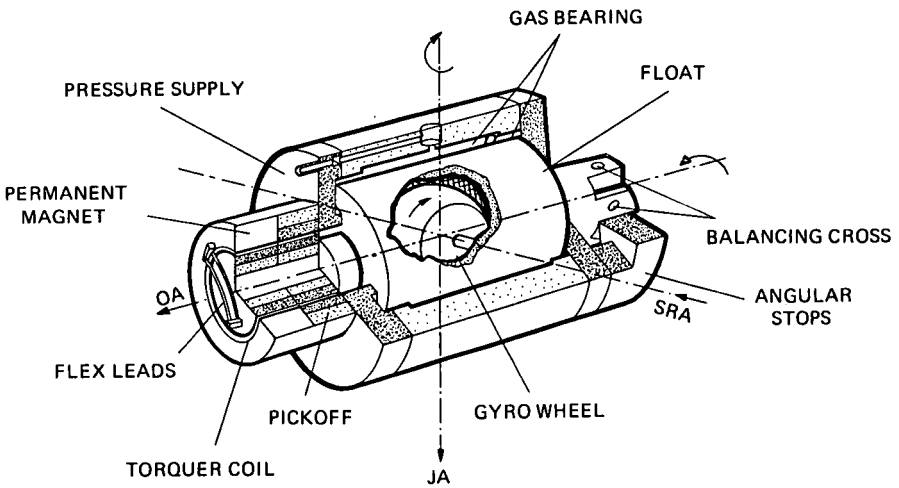

Fig. 13-1 Double integrating rate gyro GWK 38 (schematic)

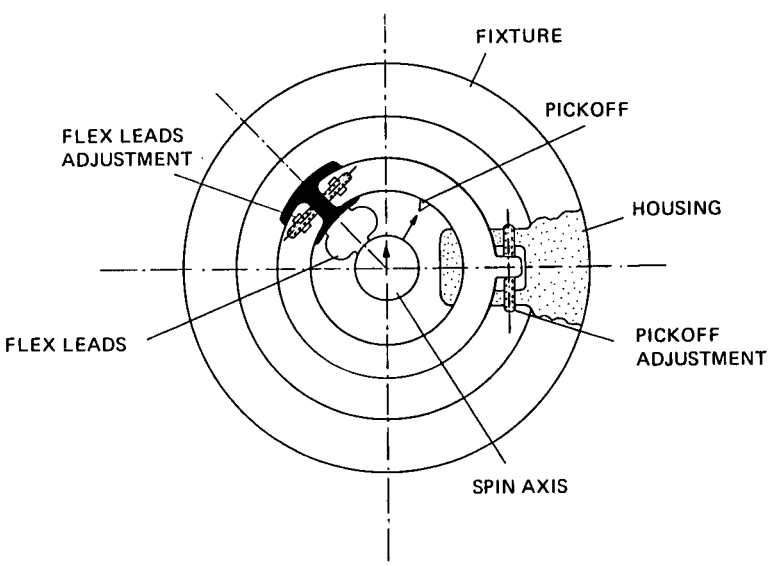

Fig. 13-2 Calibrating principle

13

Testing of Gyros and Accelerometers with Hydrostatic Gas Bearings

W. AUER, W. FEHSE and A. WAND
TELDIX Luftfahrt-Ausrüstungs GmbH
Heidelberg, Germany

Summary

This chapter gives some information on the testing of gyros and accelerometers using hydrostatic gas bearings for the sensitive axis.

These inertial sensors are briefly described. The development of the gas bearing rate gyro GWK 38 (Gasgelagerter Wende-Kreisel) was started in 1965, that of the gas bearing accelerometer GBM 531 (Gasgelagerter Beschleunigungs-Messer) in 1966. Parallel to this an adequate testing philosophy was gained. For the gyros it represents the procedures suited for development and production of small quantities; for the accelerometer so far only developmental points of view are of interest.

To get comparable data wherever possible, known testing principles were adopted. Some of the test results are given.

1. Gyro Testing

Design of the Gas Bearing Gyro

The double integrating rate gyro GWK 38 is a high precision angular rate sensor which is utilized for the stabilization of inertial platforms and similar applications. Its special feature is the hydrostatic gas bearing of the precession axis. Hydrostatic bearings provide the advantage of a complete lack of any solid friction, unlike most other bearings.

Compared to the gyro with fluid flotation, the gyro with hydrostatic bearings offers the following advantages: the float need not necessarily be restricted to a certain density, thus permitting heavier materials to be used for the gyro rotor and making possible at the same time a greater angular momentum at the same diameter. Furthermore, the hydrostatic bearing, and in particular the hydrostatic gas bearing, is not bound to a certain temperature. Thanks to this advantage, an optimum temperature can be chosen which is most suitable with respect to the total system and the environmental conditions, and in addition temperature control need not be precise as with the other type of gyro. Another great merit is that all measuring and adjustment elements are freely accessible. Contrary to the hermetic sealing required in gyros with fluid flotation, in gas bearing gyros only a cover as protection against dust particles and against external electric and magnetic fields is necessary.

A drawback of the hydrostatic bearing on the other hand is the necessity of compressed gas supply. In addition, the associated servo loop is somewhat more

complex on account of the absence of a mechanical damping feature. This disadvantage, however, will be of hardly any importance once the relevant development work is completed. The additional constructional demands for the electronic damping are insignificant.

Due to these considerations and on account of the experience with hydrostatic gas bearings dating back to the development work on the North-seeking gyro NSK, the decision was taken right from the outset of the inertial grade gyro development at the turn of 1964/1965 in favor of gas bearings as the precession axis bearings.

In determining the dimensions of the unit, the diameter of the gyro rotor was taken as criterion; after weighing up the various points of consideration it was fixed at 38mm. At first, ball bearings were envisaged for the gyro rotors; at the same time, however, development work was set under way on a hydrodynamically gas suspended gyro motor, which shortly is to be installed for the first time.

The design concept of the GWK 38 is shown in principle in figure 13-1. The unit consists essentially of two main assemblies: the float with the attached pickoff and torquer rotor elements and the air feeding sleeve with the stator and the required means for adjustment.

The gyro motor mounted in a fork is accomodated inside the float, while outside at one end the rotor windings of both the pickoff and the torquer are provided and at the other end the balancing cross is incorporated.

The gap between the float and the air feeding sleeve provides the gas bearing. The bearing type applied in our gyro - i.e. the combined one-row step bearing - is a novel development of TELDIX which is intended to achieve a minimum of turbine torques and flow rates (power) at minimum manufacturing cost. The air feeding sleeve comprises, besides the sleeve with the nozzles, the two thrust plates: the one on the balancing cross side carries the stops, while the other one carries the stator windings of the pickoff, the permanent magnet ring of the torquer and the adjustment means - for adjusting both the pickoff null to a housing reference direction and the flex-lead null to the pickoff null.

Figure 13-3 gives a clear view of the adjustment features of the rotor and stator elements of the pickoff and the torquer as well as of the flex-leads. Figure 13-2 demonstrates in principle the function of the adjustment parts.

The underlying design philosophy of the adjustment devices is based on the objective of assuring that time-consuming alignment procedures of the gyro during its installation into the platform will no longer be necessary and that the gyro can be oriented instead by means of fixed mating surfaces on the stable element of the platform, so that it can be easily replaced. This requires, of course, that the mating surfaces of both the stable element and the gyro be machined with extremely high accuracy to insure the orthogonality and the parallelism of the axes. A further condition, as far as the gyro is concerned, is that the spin axis be very accurately aligned either parallel or perpendicular to the mounting plane. To assure this, the two above mentioned adjustment devices are required. Mounting is accomplished by means of clamps and four pads on the gyro housing, i.e. the air-feeding sleeve. The mating surface which is formed by the bottom side of the four pads must be lapped parallel to the output axis to within 4 μm with an evenness of 1 μm. To bring the gyro axes into a definite position within the platform, a further mating surface is required: it is obtained in the GWK simply by utilizing one of the front surfaces of the air-feeding sleeve which must in any case be even and square with respect to the output axis within 0.25 μm, since the thrust plates of the hydrostatic gas bearing are mounted on to these surfaces. This mounting procedure is illustrated in principle in figure 13-4.

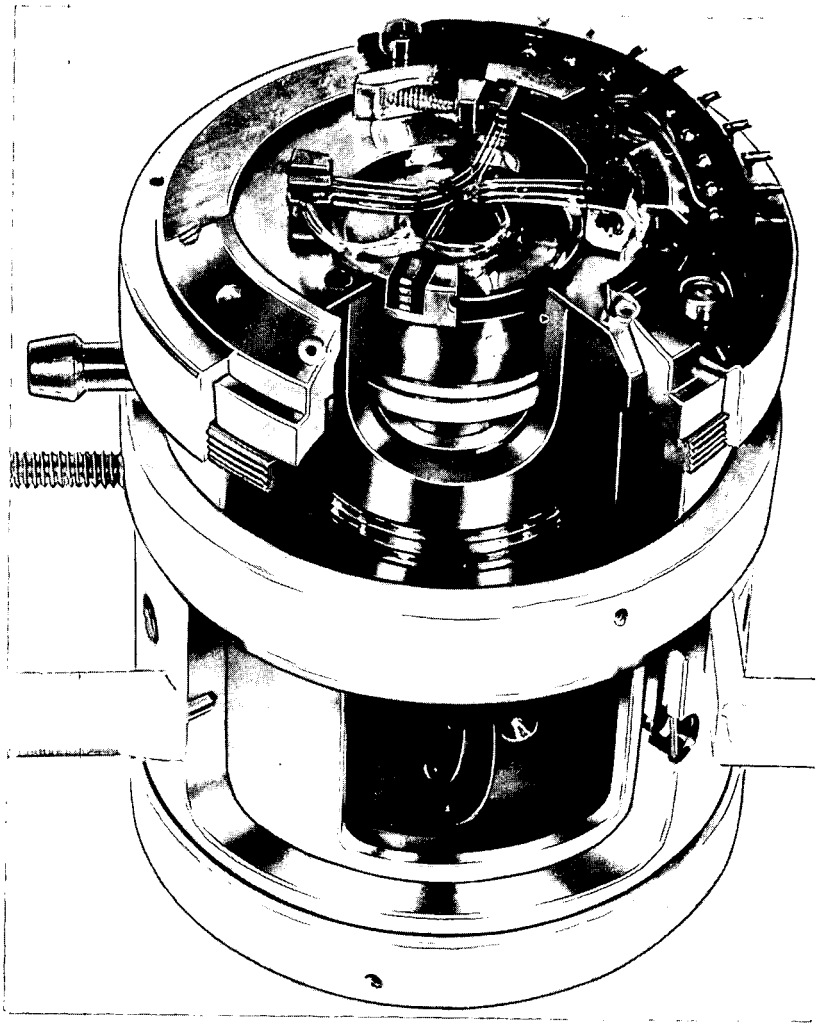

Fig. 13-3 Cut-away model of gyro GWK 38

Preliminary Measurements and Adjustments

Preliminary measurements and adjustments comprise all operations for reducing disturbing torques, aligning the gyro axis and calibrating the electromechanical transducer, the pickoff and the torquer.

Measurement of Turbine Torques: The first step in this series is the measurement of the torques of the gas bearing (Fig 13-5) as a function of the acceleration direction. During the turbine torque measurement, both the flex-leads and the stops are not yet attached to enable the float to move freely within the sleeve. With the gas bearing axis (output axis) in a horizontal position, the float is first of all accurately balanced and then restrained to the vertical by means of a small definite seismic mass. Following this, the outer cylinder is rotated about its own axis and every 30°the seismic mass displacement from the vertical is measured using a mirror attached to the float and an autocollimator: from the measurement obtained the turbine torque is computed.

In the vertical position, the turbine torque is computed from the speed. Owing to the fact that the viscous friction torque is proportional to the speed, a steady state will be reached after a short period, at which the turbine torque is equivalent to the viscous friction torque and therefore to the speed.

A typical turbine torque curve at horizontal output axis is shown in figure 13-6. The curve is essentially composed of a linear portion (independent of g) and a sine portion (proportional to g).

The occurrence of higher harmonics is insignificant. While the linear portion and the portion of the turbine torque proportional to g can be precisely compensated by flex-lead unbalance torques, harmonics of higher order cannot be compensated.

The g-dependent turbine torque approximates normally 1 dyne-cm at 1 g, while the constant portion and the portions of the higher harmonics range approximately one to two orders below. Air-feeding sleeves with considerably higher turbine torques are rejected and probably reworked.

Adjustment of Flex Lead Null and Pickoff Null. The adjustments succeeding the preceding measurements comprise the adjustment of the flex lead null to the pickoff null and the adjustment of the pickoff null to the housing reference direction.

The setting of the mechanical zero position might be done by observation of decreasing oscillations of the float when the motor is switched off, if there did not exist the undefined residual magnetism of the motor. With the motor running, on the other hand, problems arise which are due to the earth rotation speed component. The simplest method of evading this would be to align the output axis to the axis of the earth. This is the position which is used for the tumble test to balance the float about the output axis. Errors are measured in this test by means of the gyro servo loop procedure which is described in closer detail in the section 'Drift Measurements' below.

Unfortunately, the null position of the flex lead torques is also dependent upon the respective position; i.e. when the output axis is in a vertical position then the corresponding null position is different from that in the tumble test. Although the difference is only very slight, it is desirable in certain applications to achieve an accurate null position adjustment in the vertical position, as for instance with gyros for north-seeking missions. In such a case, the spin axis is coarsely aligned to north, and subsequently the flex lead null is adjusted to the pickoff null using the iteration method differentiating the north-drifting gyro torques from the flex lead torques by varying the angular momentum. This iteration method can also be used

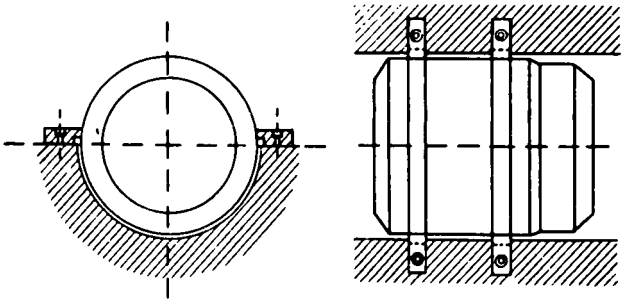

Fig. 13-4 Mounting of the gyro

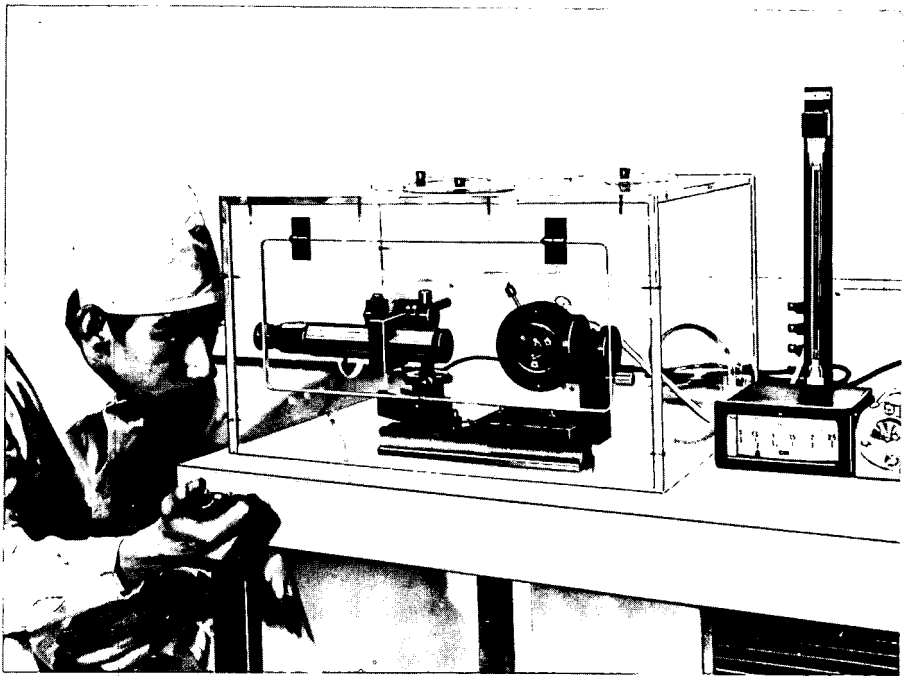

Fig. 13-5 Measurement of turbine torques

for a simultaneous adjustment of the electrical null position.

A simpler means of adjusting the pickoff null to the reference direction of the housing offers the following procedure: the gyro is mounted in a fixture with accurately machined parallel faces and clamped on to a sidereal turntable. At a sufficiently high speed of rotation of the table all other torques are negligibly small as compared to the gyro torque which forces the spin axis to align to the table axis of rotation. Then the pickoff is adjusted until the pickoff signal is zero.

Calibration of the Torquer. Finally, the scale factor of the torquer is tested. For this purpose, the gyro is mounted with its input axis in a vertical position on the sidereal turn table whose axis is in the vertical. Then the table is slaved to the gyro (Fig 13-7), whereby the gyro is allowed to drift freely and the drift rate is measured. Following this, accurately defined currents of varying levels are fed into the torquer, and the drift rate is measured again. The difference from the original drift value permits the computation of both the scale factor and the linearity of the torquer.

With regard to the adjustment operations, the hydrostatic gas bearing offers a great advantage when used as the bearing of the precession axis, in as much as all adjustment devices are freely accessible. Furthermore, the balancing of the float has to be accomplished only statically on a balancing cross owing to the good stiffness of the bearing with respect to angular torques. As opposed to this, with a bearing of fluid flotation careful attention has to be paid that the center of gravity coincides with the center of buoyancy of the float and that, in addition, a certain density is maintained.

Drift Measurements

Two measurement procedures have proved especially expedient for measurements on inertial grade single-degree-of-freedom gyros. In both procedures, the gyro pickoff signal is retained at zero to ensure that both the position and the orthogonality of the gyro axes are maintained.

The advantages of the first method, the table servoloop test (Fig. 13-7), are, first, that the conditions are similar to the actual performance of a single-degree-of-freedom gyro used in a platform, and, second, that it provides a high accuracy in long-term measurements.

In the second method, the gyro caging procedure (Fig. 13-8), the pickoff signal is demodulated, amplified and subsequently fed back to the gyro torquer. The inherent advantages of this method are: first, that no servo table is required; second, that the measurements can be carried through rapidly and easily; third, that the drift measurements can be continuously recorded; and, fourth, that the gyro retains its position during the measuring time. The gyro caging method is particularly suited for short-term measurements. The only drawback is that measurement accuracies better than 0.01 deg/hr can be obtained only with great effort.

Both measuring methods have long been known to be suitable for drift measurements on single-degree-of-freedom gyros, and especially for rate integrating gyros, and have been often described in the relevant literature. In their application to gas-suspended double integrating rate gyros provision has to be made, however, that in both methods – the servo table as well as the gyro caging procedure – a stabilization network (electronic damping) is incorporated into the servo loops, since these gyros are undamped.

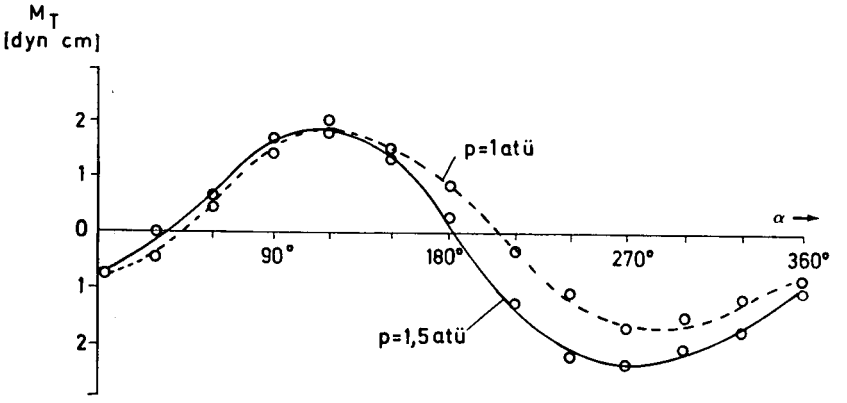

Fig. 13-6 Turbine torque function

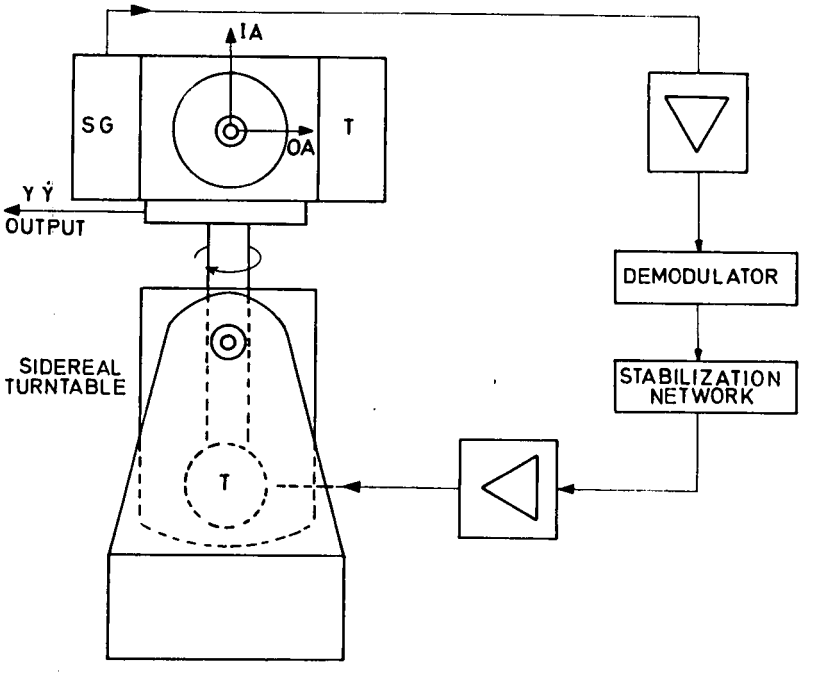

Fig. 13-7 Servo test; input axis vertical

While the preliminary measurement and adjustment serve the purpose of correcting errors in the performance of the individual gyros as far as possible, the drift measurements described in the following paragraphs are a final test to establish the characteristics and the magnitude of the residual errors.

There are various criteria for a classification of gyro drifts, the measuring of which is an important part of the test program. For one thing, the drifts occurring can be categorized as systematic – i.e. those depending upon deterministic principles – or random – i.e. those which can only be evaluated using statistical means. On the other hand, drifts can be differentiated according to their dependence upon outside-influence parameters, such as acceleration, temperature, pressure, humidity, vibration etc. If each of these parameters were varied with the others, an infinite number of drift components would result. Making allowance for the fact that all these influences, with the exception of acceleration, can be eliminated by appropriate provisions, the systematic drifts in particular are subdivided, according to their respective dependence upon the acceleration only, into drifts which are:

(a) non-g-sensitive
(b) g-proportional
(c) g-square-sensitive

The effect of the other environmental parameters is established in environmental tests for certain confined ranges of specific interest(see pp. 560 - 9) and is then expressed as environmental change of the three above defined systematic drifts.

Final Tests on Systematic Drifts. The approved six-position rate test utilizing the gyro caging method is carried out as a final test of the systematic drifts (Fig. 13-9). Particularly in application to the six-position test, the gyro caging procedure provides a great advantage in that the gyro axes do not change their position with respect to the gravitational field and the earth's rate component.

Continuous drift recording for a period of five minutes is performed in each of the six positions.

In accordance with the envisaged application of the gyro, both the adjustments and the final drift measurements are executed at either room temperature or platform operation temperature. Since the gyro itself is not equipped with a heater, a thermostatically controlled heater box is mounted on the turntable, providing for a control of any chosen temperature ranging from room temperature up to +85°C which can be kept constant to 1°C.

The six-position-rate test is repeated five times with intermediate shutdowns and cooling down of the gyro to room temperature level. From the results of the five measurements, the respective average values of the non-g-sensitive and the g-proportional components of the systematic drift are computed. In addition, the maximum differences established in the five test runs yield the drift changes from one switch-on to the next (see below). The g-square sensitive component of the systematic drift is obtained on the basis of the Fourier analysis in the concluding tumble test.

Final Test on Random Drifts. The measuring program and the purpose of the test evaluation of the random drift, as opposed to the systematic drift, components is largely dependent upon the intended gyro application. Depending upon the respective causes, the corresponding frequencies of the statistically evaluated drift variations may range from a few milliseconds (ball bearing noise) up to months and years (creep of the structure, life). Hence data of general validity on the random drifts as a measure of the performance of the gyro cannot be stated. According to the individual application, the respectively applicable part of the whole spectrum must

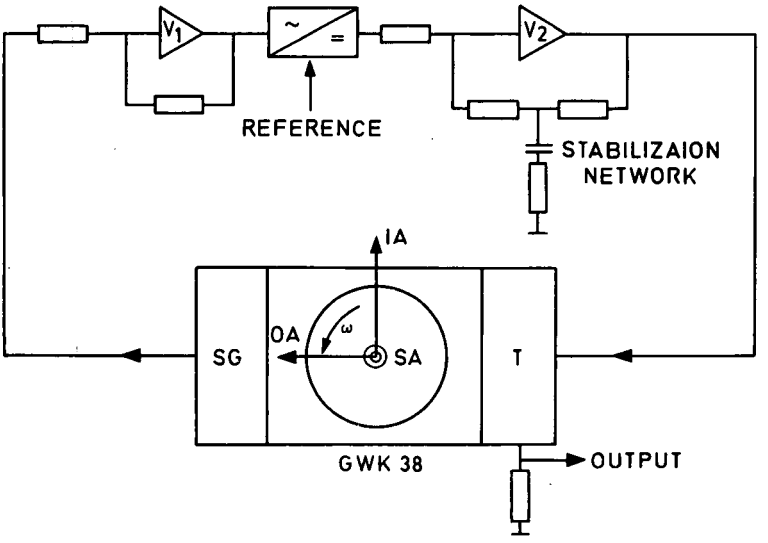

Fig. 13-8 Caging loop

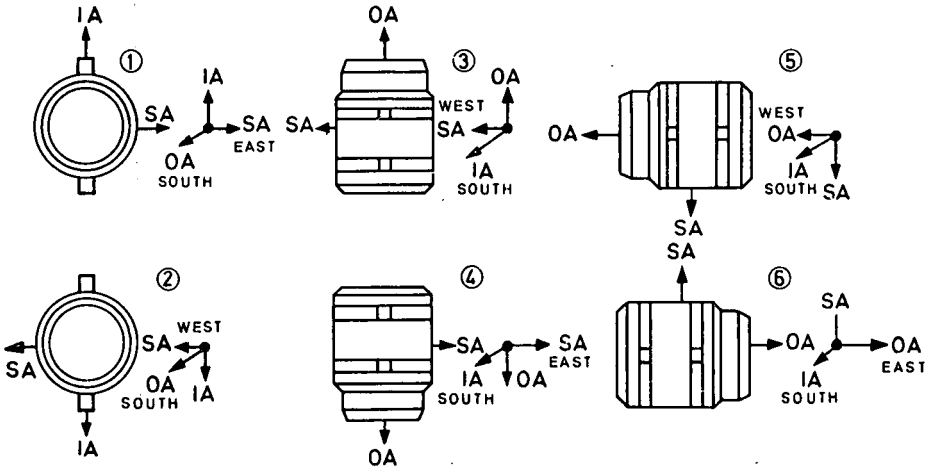

Fig. 13-9 Six-position test

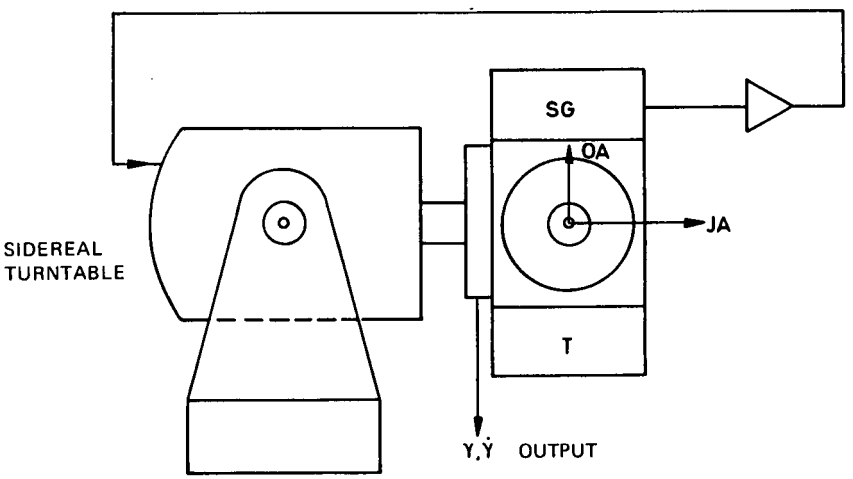

Fig. 13-10 Short term random drift servo test; output axis vertical

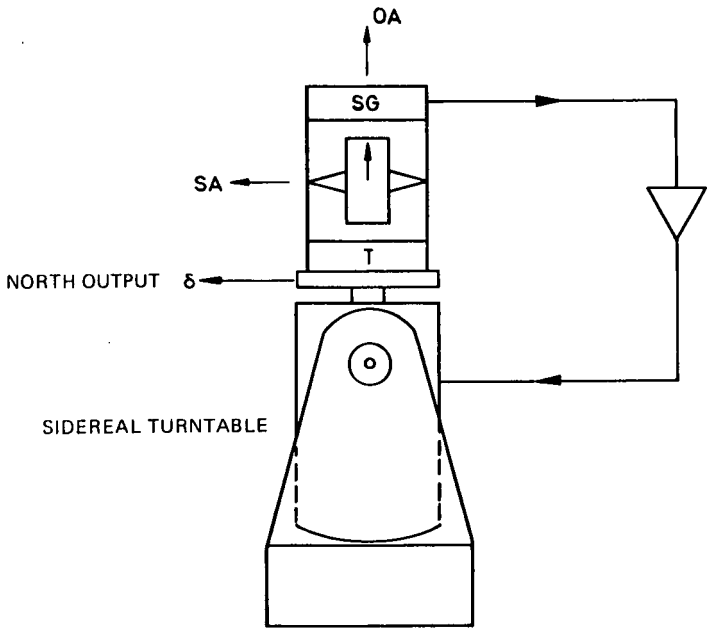

Fig. 13-11 North-seeking mode

be taken into consideration. Rapid fluctuations, for instance, will be uncritical for long-terms missions, provided that they are averaged over the time. In the case of short term missions, however, long-term drift variations will be uncritical, particularly so if the gyros are checked for their drift behaviour prior to the start.

Two different measurement procedures for the evaluation of random drifts are for this reason being carried out at TELDIX, a short-term and a long-term random drift test, according to the envisaged application of the gyros. Both tests are conducted by the servo table test procedure, which permits the best stimulation of platform conditions.

Short-term Random Drift – to separate the g-sensitive from the non-g-sensitive drift, a short-term random drift test in two positions is carried out. The greatest gravity effect is obtained with both the spin axis and the output axis in horizontal position, while both the input axis and the table axis are vertical. The time for a one degree turn of the table is measured by means of a crystal controlled counter and subsequently printed out by a connected printer. For twenty readings from which the standard deviation is computed, the measurement carried out in the above described manner takes, in Heidelberg with a vertical earth's rate component of 11.43 deg/hr, approximately $1^{3}/_{4}$ hours.

The measurement of the non-g-sensitive drift in the servo test raises several problems, in so far as no gyro or table position satisfies the two requirements demanding the elimination of unbalance torques and the retaining of the earth's rate component at a constant level. Hence a compromise has to be found if the non-g-sensitive portion of the random drift is also to be measured in the servo test.

In our laboratories, the test is carried through in the following way. The table axis is tilted to a horizontal level and the gyro is mounted in a manner insuring that the output axis is vertical while the input axis is in a horizontal position coincident with the table axis (Fig. 13-10). The measurement starts with the output axis deviating from the precise vertical position by 5 degrees. At -5 degrees from the vertical, the measurement is interrupted and subsequently repeated. Since the systematic unbalance drift component along the input axis is known from the preceding measurements, the tumble test and the six-position test, the corresponding sine component can be deducted from each measurement value. Following this, the standard deviation is computed in the usual manner on the basis of the obtained values. Owing to the fact that the cos component of the earth's rate in Heidelberg is only 9.7 deg/hr, the test run through 10 degrees takes slightly more than one hour.

The test on the long-term random drift is conducted in the same way as the short-term drift, but in only one position, i.e. with the input axis and the table axis in the vertical. Since long-term systems are employed mainly in craft navigating relative to the earth only, it is in the final analysis only the azimuth gyro of which a particularly high accuracy is demanded. As with short-term random drift measurements, the time is expressed in terms of the time required for a one degree turn. But only every fifth measurement value is used for the computation of the standard deviation. The total measuring time required for long-term random drift measurements amounts to eight hours.

The standard deviation is computed for all random drifts on the basis of the equation:

$$G = \sqrt{\frac{1}{n-1} \sum_{i=1}^{n} (x_i - x_m)^2}$$

Table 13-1 Measured drift values

Systematic drifts		
non-g-sensitive	0.1 - 0.5	deg/hr
g-sensitive	0.1 - 0.5	deg/hr/g
g^2-proportional	0.2	deg/hr/g^2
Random drifts		
(a) Day-to-day drift changes		
non-g-sensitive OA ⊥	0.05 - 0.1	deg/hr
g-sensitive → SA	0.05	deg/hr/g
g-sensitive → IA	0.03	deg/hr/g
(b) Short-term random drift (table slaved to gyro)		
non-g-sensitive OA ⊥	0.002-0.005	deg/hr
g-sensitive IA ⊥	0.008-0.02	deg/hr
(c) Long-term random drift (table slaved to gyro)		
g-sensitive IA ⊥	estimated 0.02 - 0.05	deg/hr
Sufficient representative measurements not yet available		

Fig. 13-12 Sidereal test stand

where

$$x_i = \frac{1^\circ}{\text{elapsed time}}$$

and

$$x_m = \frac{1}{n} \sum_{i=1}^{n} x_i$$

The measurement of day-to-day drift rate changes, which are included in the category of random drifts, has already been described in connection with the six-position test. The measurement results are to provide information on the long-term stability of the systematic drift. Proceeding from the maximum spread of the five measurement values obtained during a total elapsed time of a few days, conclusions are drawn with regard to a considerably longer mission period. This, of course, poses some problems, since long-term changes, resulting for instance from creeps of the material, are not being taken into consideration in the measurement. As a consequence, it may happen that, although in a renewed day-to-day drift test after the elapse of some months the distribution of the measurements is the same, the systematic drift level has changed. The validity of the drift change values obtained on this basis is therefore limited with respect to the time factor.

Gyros which are envisaged for missions including north-seeking operations are subjected to still another long-term test. The gyro is mounted on a table in the north-seeking position, i.e. with the output axis and the table axis in the vertical and the table being slaved to the gyro (Fig. 13-11). The gyro will then align to north with its spin axis. In this position the gyro is very sensitive to any disturbing torques or, to be more precise, to any disturbing torque changes about its output axis. The objective of these measurements is the recording, first, of the north value readings at specific intervals on a test run extending over several hours and, second, of the differences between the north readings achieved in north alignment operations on different days. The data obtained in this manner are particularly conclusive with regard to the torque stability of the flex-leads and the related means for adjustment.

The hitherto obtained measurement values for systematic and random drift components are listed in table 13-1.

Gyro Test –for testing and measurements on components and systems, a test laboratory is available at TELDIX for development programs; it comprises four test stands for inertial grade gyros and accelerometers, north-seeking gyro platforms and conventional gyros (directional and vertical gyros). All test stands are installed on an 80 tons concrete base covering an area of 4m × 6m. This concrete block is supported on the soil and is isolated from the rest of the building to a depth of 2.5m. Apart from the openings for the bases of the test stands, the concrete base is fully bridged, covered and accessible. The test room is air-conditioned; its temperature is kept at a constant level of $22^\circ \pm \frac{1}{2}\,^\circ$C and its relative humidity is controlled so as not to exceed 40 per cent ± 3 per cent.

The inertial grade gyro test stand consists essentially of an air bearing sidereal turntable type American Optical, Fecker Model 201, the associated electronics including counter and printer, the feedback electronics with recorder and oscillograph for the gyro caging procedure and the required power supply for both the motor and the pickoff. Figure 13-12 shows the sidereal turntable and part of the electronics. In the illustration, the gyro is being subjected to the tumble test.

Environmental Tests

Unlike drift measurements, which are carried out on each single gyro, environmental tests are type tests performed on a few representative samples only.

Environmental tests can be executed to serve various purposes. First, the test may be carried out to establish drift rate changes during the impact of a specific environmental parameter (acceleration, temperature, pressure, vibration); second, after the impact, for instance of extreme environmental parameters (temperature extremes, heating up and cooling down, maximum vibration, shock); and, third, to test the load capacity of the gyro structure to the point of functional incapability or even destruction.

The second category of environmental tests, the measurement of drift rate changes subsequent to the impact of a specific environmental parameter, is the easiest test to perform. This series includes in some respect also the measurement of drift rate changes from switch-on to switch-on. Any drift rate changes measured in this way are irreversible and are included therefore among the random drifts.

The results of the first test category yield essentially the reversible changes of the systematic drifts as a function of the various environmental parameters. With regard to some parameters, as for instance the increase of the external temperature, this test can be performed with relative ease in both the table servo test and the gyro caging test method. Other tests, however, as for instance with respect to vibrations or extremely low temperatures, can be accomplished in the gyro caging procedure only. The effect of higher linear accelerations (exceeding 1g), on the other hand, can practically not be tested at all, since centrifuges, the only devices suitable for the measurement of linear acceleration of constant magnitude over the longer periods required for measurements of this kind, entail very high speeds of rotation which render a drift measurement impossible. Hence the effect of higher linear accelerations can be evaluated only in the second and third test categories – i.e. the measurement of irreversible drift rate changes and of maximum loading capability.

The third category, testing the maximum loading capability under the influence of various parameters, raises problems with regard to the hazard of destruction. Anyway, only very few parameters is it of real interest to test. In general, tests will be confined to those in which it is likely that at a certain magnitude of the parameter under consideration parts of the gyro will fail to operate without entailing a total destruction.

Even with such limitations, the total number of tests which can reasonably be carried through is so large that a confinement to the tests which are indispensable for the envisaged mission of the gyro is expedient, not only for temporary but also for financial reasons, and especially in the case of a development project at such an early stage as the TELDIX GWK 38 is at present. The environmental tests performed on the GWK 38 which are described in the following paragraph are for this reason sequenced not according to the three above defined testing categories but on the basis of the influencing parameters, thus providing a clearer survey. It is four parameters in particular that are of significance for the hydrostatic gas - suspended gyro GWK 38:

(a) temperature
(b) ambient pressure, and difference between supply pressure and ambient pressure
(c) linear acceleration
(d) vibration

This sequence of the parameters does not necessarily reflect their importance; it can be said, however, that temperature and heat problems are likely to be the most significant factors among the environmental influences.

Temperature Effects. Since the GWK 38 is not equipped with an incorporated heater and thus lacks its own inherent temperature control, drift rate changes due to temperature effects play a significant role with respect to the whole system design concept. The amount of the reversible drift rate changes resulting from the temperature is for instance a measure of the accuracy of the required platform temperature control.

The reversible drift rate changes with horizontal and vertical output axis and temperature variations ranging from room temperature level to 75°C have been measured on the gyro during operation (Fig. 13-13). The established temperature dependence with the output axis in a vertical position was 0.003 deg/hr/°C, which is not yet satisfactory for the envisaged application. In both positions, on the other hand, the temperature dependence was linear over the whole range.

In addition, tests on irreversible drift rate changes at extremely high temperature loads have been performed which yielded, above all, changes in the center of gravity along the spin axis- i.e. g-proportional drift rate changes along the spin axis. These measurements have so far been carried out only on two samples which displayed a different behaviour, so that general conclusions on the GWK in this respect are not yet possible. The same applies for the tests at extremely low temperatures according to category two.

Systematic testing in accordance with category three has not yet been performed with respect to temperature effects. On the basis of the constructional design and also from accidental measurement values it is possible, however, to assume that the upper limit of the storage temperature capability ranges from 100°C to 120°C.

Besides the drift rate change tests, temperature tests were simultaneously utilized to establish in addition the warm-up time constant. Caused by the bad heat conductivity properties of both the titanium and the gas bearing air films, the respective level is somewhat higher than that of aluminium or beryllium structures. This factor comes to bear, however, only with regard to the dependence of reversible drifts upon temperature. If this influence is insignificant, the warm-up time constant carries no weight with regard to the time required for making the whole system ready for operation.

Ambient Pressure and Supply Pressure. The GWK 38 was originally developed for use in the inertial platforms of launch vehicles. In this case, the necessary gas supply for gyros on the platform was to be provided by means of a high-pressure bottle. With a comparatively coarse control of the internal platform pressure, the supply pressure difference would also change with the decrease of the ambient pressure, provided that the supply pressure were kept constant. Changes of the supply pressure difference would likewise occur in a closed system with a circulation of the gas by means of a compressor, as a result of temperature and acceleration changes. The evaluation of the pressure dependence of the gyro drift thus permits at the same time the determination of the accuracy required for effective pressure control.

Pressure changes affect not only the g-proportional but also the non-g-sensitive turbine torques. Therefore, tests on drift rate changes have been performed with horizontal and vertical output axis and with supply pressures of 0.5, 1.0 and 1.5 kg/cm^2 (atü). While in the gas bearings of the first development models of the GWK the turbine torque changes still amounted to several dyn cm per 1 atü supply

pressure change (1 dyn cm = 0.4 deg/hr with the GWK 38), the turbine torque changes per 1 atü still occurring at present are reduced to fractions of dyn cm. The maximum drift rate changes measured on the present GWK model were 0.1 deg/hr/atü.

Effect of Linear Accelerations. The effect of linear accelerations up to 1g is very closely examined on each individual gyro in the various drift measurement tests.

As mentioned before, drift measurements under the impact of high linear accelerations can virtually not be realized with reasonable technical efforts. Although centrifuges with counter-rotating turntables have already been built it is nevertheless questionable whether the interference in such a system with attitude stability, turning stability, counter-rotation stability etc. can be kept at such a low level as to render them suitable for testing inertial grade gyros. The same applies to sled tests.

Hence environmental tests with higher linear accelerations than 1g have been conducted at TELDIX in categories two and three only. Under these conditions, the tests which we considered most important with respect to the maximum load capacity were those to evaluate the supporting capacity of both the output axis and the rotor bearing.

The supporting capacity of the hydrostatic gas bearing of the output axis had already been examined on an experimental gas bearing, where the acceleration load was simulated by corresponding weights. To evaluate the real conditions on the gyro itself, the GWK was accelerated in a centrifuge with switched-off motor, and the supply pressure was measured for each acceleration level while the float was just slightly touching the air-feeding sleeve. In addition the electrical resistance between float and air-feeding sleeve, which decreases to zero when the two parts are in contact, was measured.

As far as the gyro rotor bearing is concerned, it is essentially irreversible drift rate change – i.e. displacement of the center of gravity along the spin axis – that is of primary interest. Shifts of the gravity center of the motor are attributable mainly to excessive loads on the bearing due to the imposed acceleration. Since the gyro motor consists of several parts, other component parts besides the bearing can also be responsible for shifts of the gravity center. For this reason, the measurement results are by no means as clear and unambiguous as are those regarding the supporting capacity of the gas bearing. In any case, too few measurements have so far been conducted on the GWK in this respect to make definite statements at this stage. Generally it can be said, however, that under the impact of an acceleration of 10g the irreversible drift rate changes were not greater than the day-to-day drifts.

It is not possible, however, to measure with greater accuracy, since the gyro rotor is standing still during the acceleration impact upon the centrifuge. Subsequently it has to be re-mounted on the sidereal turntable, and only then can it be started.

Vibration Tests. Vibration tests have so far been performed to ascertain three different phenomena. First, individual components, for instance the motor and the associated fork, then the whole gyro were tested to ascertain resonance peaks.

These checks were indispensable for a correct interpretation of later drift measurements under vibration. The second test served to evaluate the effect on the load capacity of the gas bearing (Fig. 13-14) of vibration as well as linear acceleration. Finally, as already mentioned, drift rate changes occurring under the impact of vibration were measured in various directions.

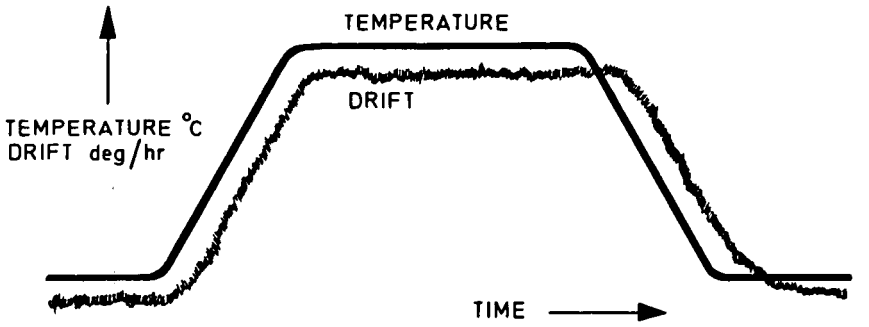

Fig. 13-13 Temperature gradient of drift

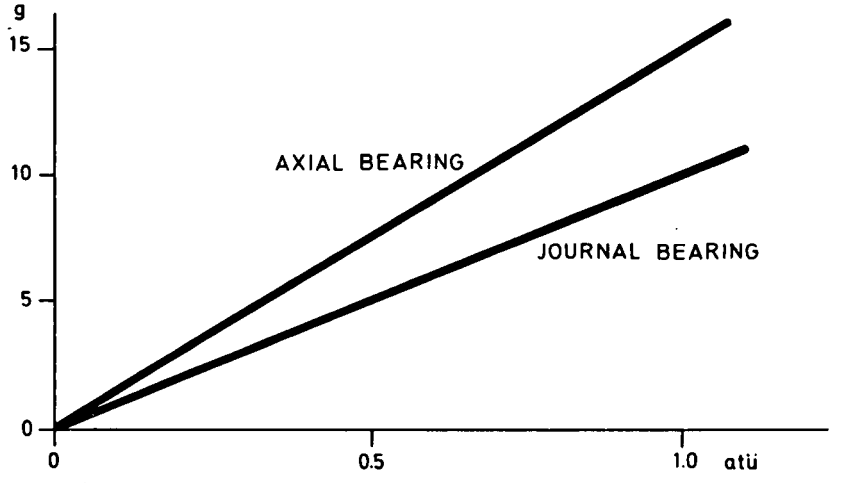

Fig. 13-14 Load capacity of the pressurized gas bearing

The resonance tests were conducted at an acceleration of 2g in a frequency range between 10 and 2000 Hz. The first test series concerned the motor and the associated fork. The resonance of the motor at standstill with excitation in the axial direction averaged 1500 Hz and in the radial direction 1700 Hz, and the resonances of the fork with the motor running with excitation in the axial direction were 830 Hz, in the radial direction 1000 Hz and 1200 Hz (Fig. 13-15 and 13-16). The results reflect a comparatively large anisoelasticity, as had already been established in the tumble test. This error was considerably reduced in the latest version of the GWK by providing for a greater stiffness of the fork.

The gas bearing frequencies were measured by the same procedure. The tests yielded a natural frequency of the radial bearing of between 500 and 700 Hz; this, however, does not result in a great resonance rise and is relatively independent of the supply pressure. The resonance of the axial bearing, on the other hand, shows a large rise at a supply pressure of 1.5 atü approximating 580 Hz. When the supply pressure is reduced to 0.5 atü, the resonance curve pattern becomes much flatter with a maximum, similar to that of the radial bearing, extending from 200 to 300 Hz.

In measuring the effect of vibration on the load capacity of the gas bearing, behaviour corresponding to these results could be observed (Fig. 13-17 and 13-18). In these tests a voltage was applied between float and air-feeding sleeve. The vibration accelerations were increased until contact occurred.

Drift rate changes under constant vibration impacts of 2g were evaluated in the gyro caging procedure. In all, twelve different positions were tested to vary the orientation of the gyro axis in relation to the earth's rate vector, the gravity vector, and the direction of vibration. The resultant measurement values are so numerous that their thorough discussion would go beyond the scope of this chapter. Therefore, attention will be drawn only to some particularly characteristic drift patterns and, beyond this, only a brief description will be given of frequency characteristics in general.

All major drift rate changes occur within the range of the gas bearing and fork resonance points. In two distinct positions, the drift rate changes amounted to a maximum of about 2 deg/hr. Outside the resonance ranges of both the gas bearing and the fork, the drift rate changes in general did not exceed 0.2 deg/hr, with the measuring accuracy amounting to no more than ± 0.05 deg/hr due to environmental influences.

The effect of anisoelasticity is clearly visible in figure 13-19. Here again the maximum drift rate change occurs in the gas bearing resonance range, with a further peak in the natural frequency range of the fork.

Figure 13-20 represents the drift changes with excitation in both directions of the input axis. Up to a frequency of 500 Hz, there are practically no changes at all; above this level drift rate changes up to 0.4 deg/hr are evidenced at gas bearing resonance, and at the natural frequency of the flex-leads and of the fork.

Especially at the resonance peaks of the gas bearing – in the axial bearing approximating 500 Hz, in the radial bearing 700 Hz – drift rate changes occurred in various positions, the causes of which theoretically cannot be fully explained. In any position, however, it was possible to establish drift rate changes only from 150 to 200 Hz upward. At this level, however, the damping provided in the platform by the shockmounts and the gimbals is already sufficiently large to insure that at an input vibration of 10g the acceleration exerting its influence upon the gyro is reduced to only 1/10g and, as far as the natural frequency of the gas bearing is concerned, to 1/100g.

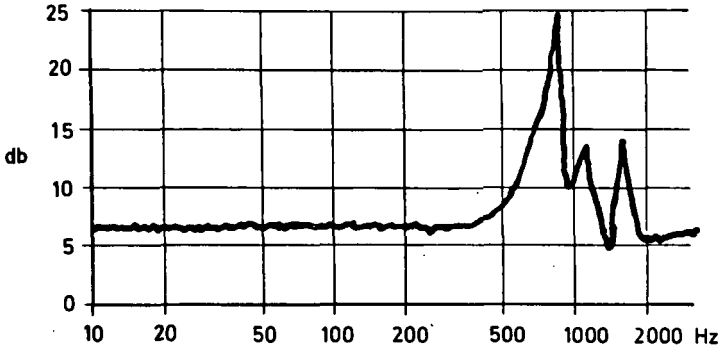

Fig. 13-15 Frequency response; axial excitation

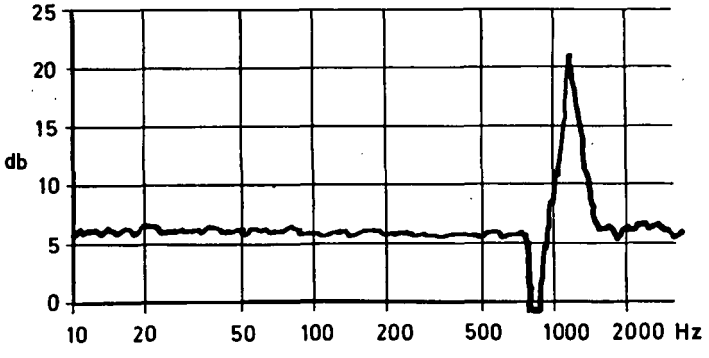

Fig. 13-16 Frequency response; radial excitation

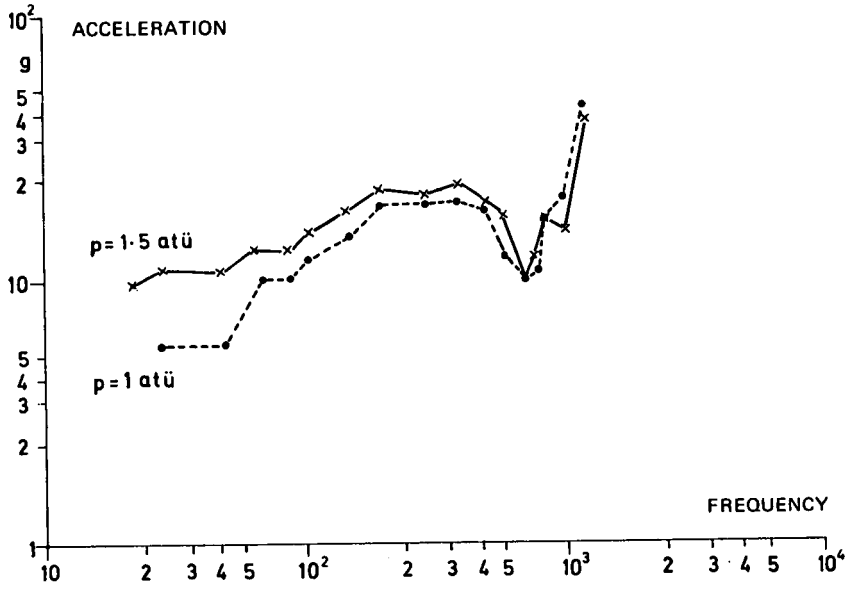

Fig. 13-17 Load capacity of the journal bearing: radial vibration

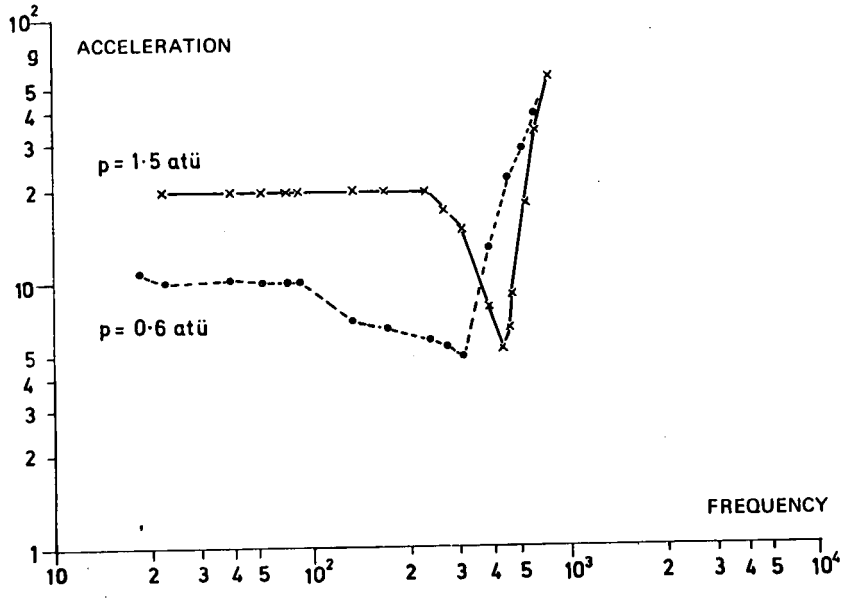

Fig. 13-18 Load capacity of the thrust bearing: axial vibration

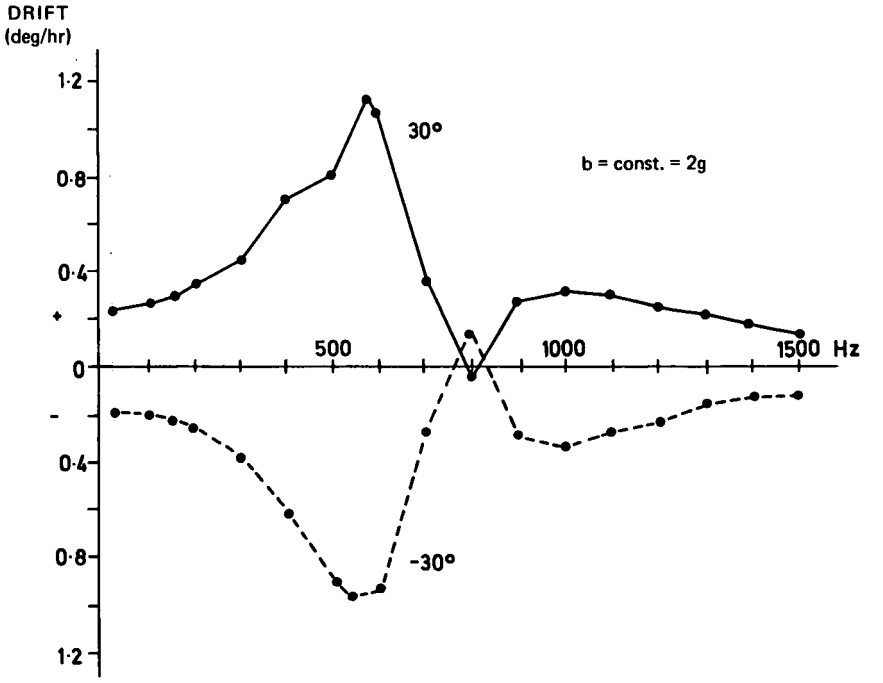

Fig. 13-19 Drift due to anisoelasticity

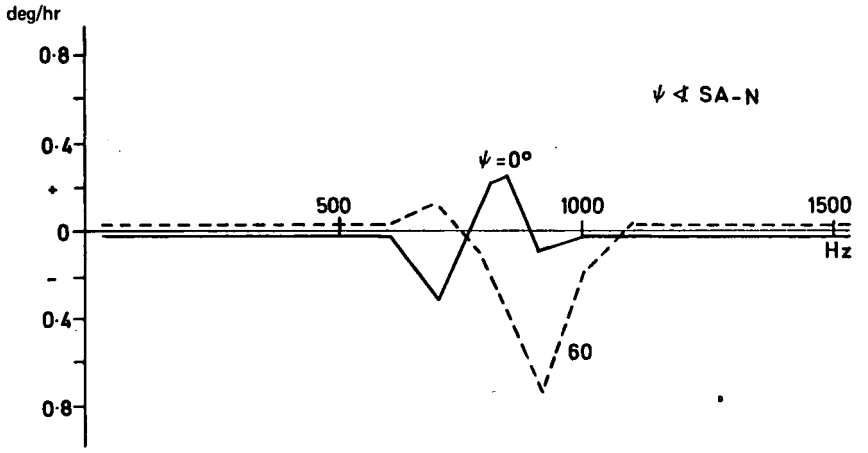

Fig. 13-20 Drift due to vibration; excitation in input axis

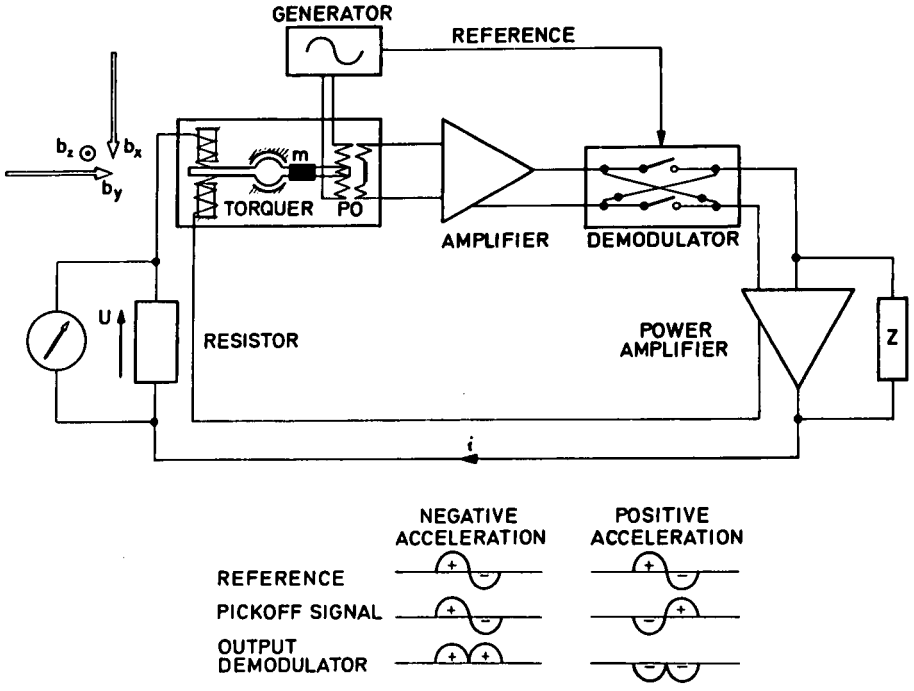

Fig. 13-21 Servo loop of the gas bearing accelerometer

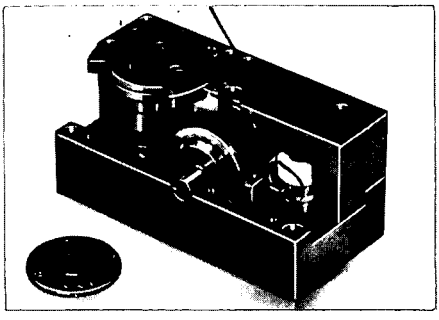

Fig. 13-22

Cut-away model of the GBM 531

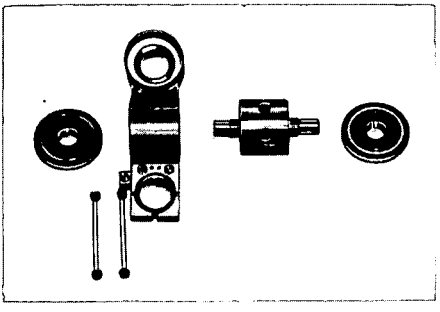

Fig. 13-23

Gas bearing parts of the GBM 531

The vibration tests were conducted on shakers type C10 with vibraplane and C30 of the MB-Electronics company. The environmental laboratory in which these tests were carried out is accomodated outside the TELDIX manufacturing and development buildings and is largely isolated against vibrations.

2. Accelerometer Testing

Design Philosophy of the Accelerometer Type GBM 531

The accelerometer type GBM 531 operates on the force balance principle. Figure 13-21 shows the servo loop. The constructional design of the accelerometer type GBM 531 is represented in figures 13-22 and 13-23.

The measuring axis – the axis along which accelerations are measured – is normal to the mounting surface. This approach was chosen for the intended application to insure easy installation and replacement, saving additional tedious and expensive adjustment operations during the installation into the platform.

The accelerometer type GBM 531 utilizes as acceleration-sensitive element a gas-suspended pendulum (Fig. 13-23) which carries on one end the secondary coil of the electromagnetic differential pickoff, while the two magnetic force balance restoring ring coils of the force generator producing the force necessary to return the displaced mass to null are mounted on the other end. In addition, the pendulum carries the clamps for the flex-leads.

The excitation of the pickoff is accomplished by two coils fixed to the case. These coils are embedded in the grooves of a ceramic bar. The pickoff frequency is 12.8 kHz. The two force balance restoring coils each enter a pot-type magnet. An integrated preamplifier increasing the output signal by 35 dB is firmly mounted in the case of the accelerometer, insuring a more effective suppression of interference with the transmission of the acceleration signals via the slip rings of the platform. External accommodation provision has been made for the components of the electronic servo loop.

Force Generator. The force generator consists of two opposed coils each moving in the air gap of a pot-type magnet. Both the polarity and the direction of the windings of the two magnets are opposite, thus assuring a higher linearity (for further details refer to page 578.

Sensing Element Suspension. The suspension of the force balance pendulum as sensing element should provide low friction, since hysteresis and threshold should be kept to a minimum.

This requirement would be insufficiently met by a pivot bearing, despite a certain weight reduction by the surrounding liquid. The inherent difficulties of liquid damping with respect to the buoyancy force would add to this problem.

Another alternative would be a spring suspension. It is quite evident, however, that a spring, when providing a stable support of the pendulum in two directions, cannot possibly be indefinitely flexible in the sensitive direction. Zero errors of the pickoff and the electronic system as well as amplification variations result in errors which are proportional to the ratio

$$\frac{\text{spring stiffness}}{\text{feedback loop stiffness}}$$

Hence a very high electrical amplification factor would have to be chosen. With a

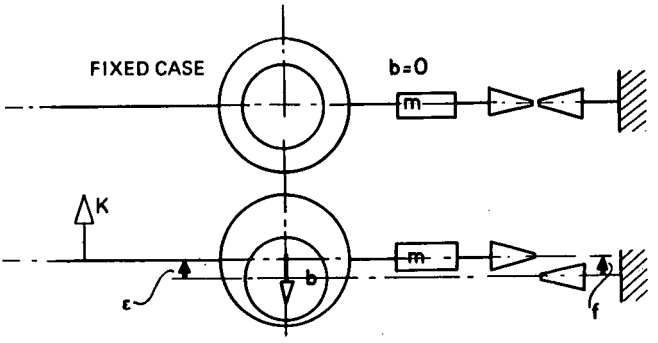

Fig. 13-24 Bearing displacement

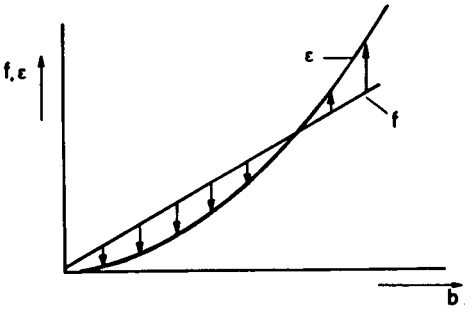

Fig. 13-25 Cross coupling

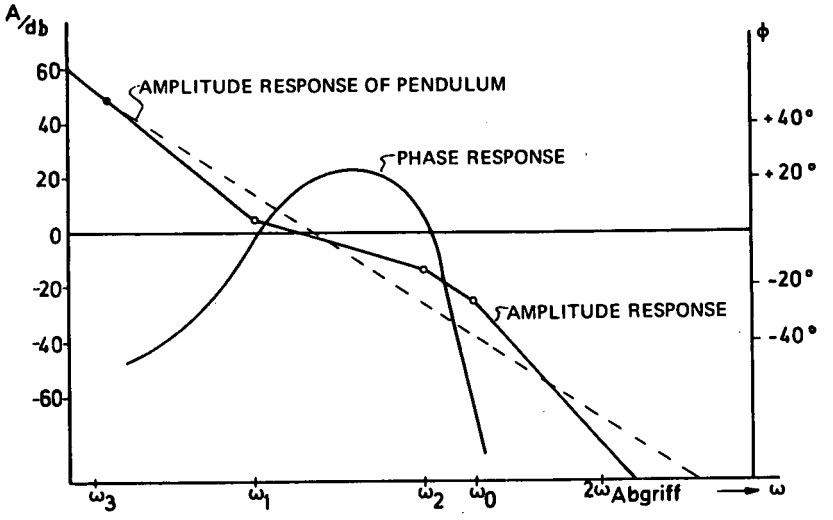

Fig. 13-26 Bode diagram

high amplification and a pickoff frequency which for system design reasons would have to be low, electronic damping would be difficult to realize. Apart from that, the machining and the thermal treatment of the springs would require much effort to assure a high zero stability.

Gas Bearing - Advantages and Requirements: in developing the GBM 531 the final choice was taken in favor of a gas bearing. This type of bearing rules out any solid friction and in addition renders both the threshold and the hysteresis immeasurably small. In addition, flex-leads-torques are sufficiently small and an excessively stiff capture of the servo loop is not necessary. As a consequence, electronic damping can be realized even with low pickoff frequencies.

Asymmetries due to the manufacture of the bearing may cause turbine torques within the bearing. The effect of these torques on the measuring accuracy must be sufficiently small.

The turbine torque has the following components with the corresponding consequences:

(a) The constant portion contributes to the bias and is taken into account in the navigation computer.

(b) The turbine torque proportional to the input acceleration, superimposed upon the torque generated by the mass unbalance, thus entails no error.

(c) The turbine torque proportional to the two lateral accelerations is compensated for by the adjustment of the input axis.

Pressure variations of the gas supply may have an impact upon the turbine torques. Appropriate manufacturing procedures make it possible, however, to reduce bearing asymmetries, and thus also the turbine torques, to such a low level (0.1 dyn cm) that changes due to pressure variations become negligible; such manufacturing methods are succesfully being applied in the TELDIX workshop.

Further advantages offered by the gas bearing include the following:

(a) Gas bearings operate over a broad temperature range, whereas liquid floated bearings necessitate a precise temperature control to insure constant damping and buoyancy values.

(b) Gas bearings are inert to cosmic radiation.

(c) Hardly any zero variations due to aging occur within the gas bearing itself.

Resulting Design Considerations: the incorporation of a gas bearing entails some considerations with respect to the servo loop design which include the following.

(a) Unlike a pivot or spring bearing, a gas bearing retains a reproducible displacement under acceleration even after excessive load impacts and aging. This effect can be utilized to obtain an extremely small cross coupling.

The relation between bearing displacement ϵ and the acceleration forces is represented in figure 13-24. The diagram in figure 13-25 illustrates the determination of the tilt of the force balance pendulum and the influence on cross coupling. The deflection f measured at the pickoff is a linear function of the acceleration. By adjusting the two factors to each other (by appropriate choice of the amplification factor and the supply pressure) it is possible to realize a minimum tilt and thus low cross coupling.

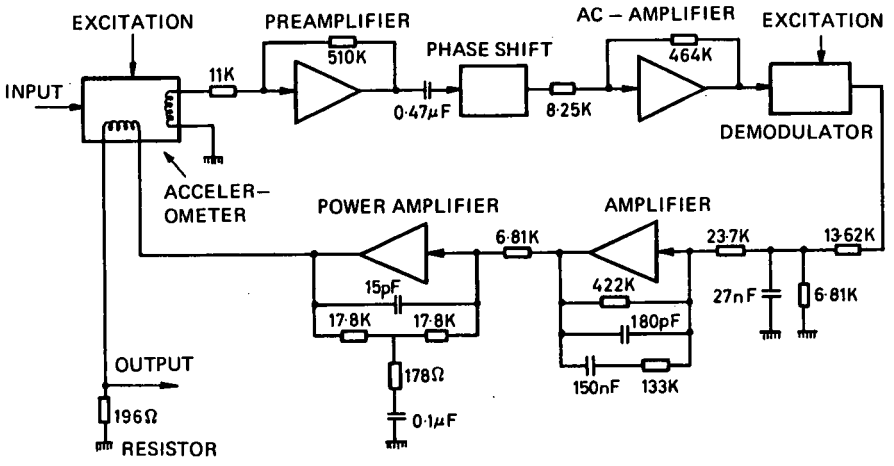

Fig. 13-27 Servo loop - electronics

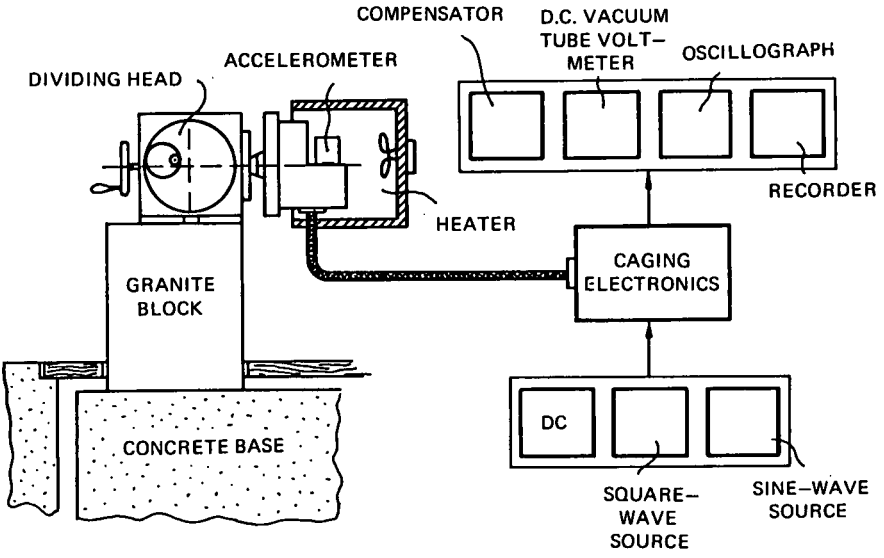

Fig. 13-28 Setup for testing accelerometers

(b) When a gas bearing is incorporated fluid damping is not possible. The existing eddy-current damping in the metallic core of the force balance restoring coils is not sufficient to stabilize the servo loop. Damping is introduced therefore by the incorporation of an electronic network in the servo loop.

(c) The transfer function of the force balance pendulum was also tested. The force balance pendulum was excited to oscillate by the sinusoidal excitation of the force generator. The response shows the envelope of the pickoff voltage. In the ideal case, the pendulum characteristics should be like those of a double integrator. The phase angle between input and output signal should be 180 degrees. However, the gas bearing does not constitute an ideal, rigid center of rotation – a pivot. This explains why the phase angle in the Bode diagram exhibits a decreasing tendency at higher frequencies (from 300 Hz). This behaviour had to be taken into account in the design of the stabilization networks.

Control Engineering Design of the Servo Loop. In selecting the most suitable stabilization networks attention had to be given to the requirement that, on the one hand, a sufficiently high stability of the servo loop be insured and, on the other hand, the ripple voltage of the double pickoff frequency remaining after demodulation be adequately suppressed.

This requirement could not be satisfied by incorporating a simple lead-lag element of the type

$$\frac{1 + T_1 s}{1 + T_2 s} \qquad \text{(where } T_1 > T_2\text{)}$$

since the difference between the pickoff frequency and the natural frequency of the servo loop is not sufficiently large and the required high amplification for avoiding cross coupling could not be achieved. Therefore, an additional lag-lead feature (ω_1, ω_2) has been inserted in the loop performing below the natural frequency.

Within the natural frequency range, the lead-lag effect prevails (ω_1, ω_2) while at high frequencies a couple of complex poles effects (ω_o) an intensified decrease in the amplitude response. The Bode Diagram is represented in figure 13-26.

Description of the Servo Electronics. The servo loop is represented in figure 13-27. The servo electronics are a part of the servo loop. The comparatively weak a.c. signal of the inductive pickoff in the accelerometer is transformed into a d.c. current, causing the displaced mass to return to a level near zero.

The individual assemblies are designed in the form of soldered modules: each electronic component is placed between two etched plates and soldered on the outer surfaces. The individual modules are mounted on a plug-in card by soldering their connecting leads. One plug-in card accommodates the components for three servo loops; for an inertial platform only one card is needed.

Test and Adjustment on the Accelerometer

Tests of the dynamic behaviour of accelerometers as well as the determination of the scale error, temperature coefficient, bias error and axes errors as well as their time and temperature-caused variations require test equipment satisfying extremely high accuracy requirements. The test setup is presented in block notation in figure 13-28.

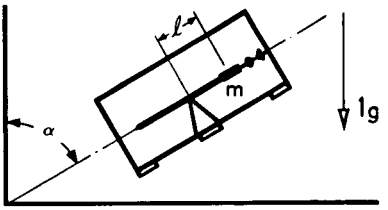

$$M = m \cdot g \cdot l \cdot \sin \alpha$$

Fig. 13-29 Accelerations < 1g

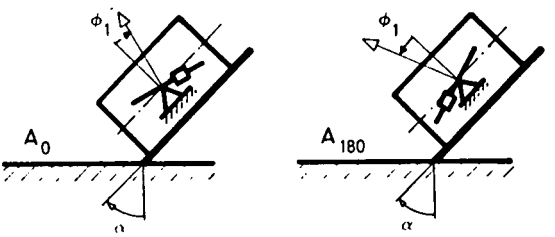

$$A_0 = k[g \cdot \sin(\alpha + \phi_1) + G]$$
$$A_{180} = k[g \cdot \sin(\alpha - \phi_1) + G]$$
$$A_0 - A_{180} = k \cdot g \cdot 2\phi_1$$

Fig. 13-30 Measurement of the input axis misalignment

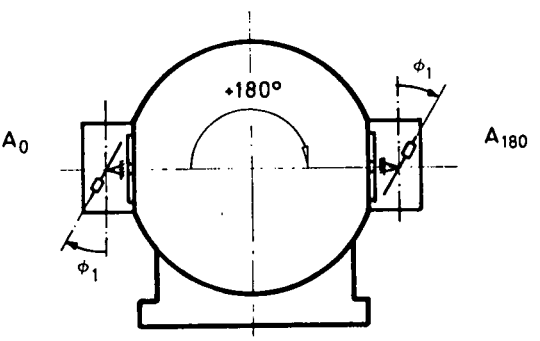

Fig. 13-31 Bias measurement

Test Equipment. A concrete base 4×6×2m isolated from the building is available at TELDIX to provide a fixed gravity vertical reference plane. This concrete base carries a granite block which supports an optical dividing head. Using this test setup, a drift of only some seconds of arc was established over a period of several weeks using as a measure an electronic level. The dividing head enables the accelerometer to be adjusted to a chosen angle with reference to the earth's vertical. The set angle can be read from the scale to an accuracy of 2″. Due to this adjustment, the portion of the acceleration vector acting upon the accelerometer can be determined. As can be seen from figure 13-29, the corresponding equation is

$$M = m \cdot g \cdot \ell \cdot \sin \alpha$$

The adjustment accuracy of 2″ is equivalent to an acceleration component of 10^{-5}g. The output voltage can be measured to an accuracy of 10^{-5}V using a compensator eliminating thermo-voltages. This accuracy corresponds to approximately 10^{-5}g even at a scale factor of about 1 V/g.

Furthermore a sensitive vacuum tube voltmeter and a recorder are available for long-term bias stability and axis error measurements. A sine-wave generator permits the examination of the frequency response of the individual servo loop elements. A square-wave generator produces step functions which can be additionally fed into the force generator simulating acceleration steps. Oscillograph curves reflect the transients at individual points of the servo loop.

When a d.c. voltage is fed into the force generator the force balance pendulum can be warmed up, allowing the influence of accelerations of longer duration upon zero stability to be investigated.

An incorporated heating device facilitates the measurement of the temperature coefficient of the scale factor and the adjustments of the accelerometer at the envisaged operating temperature.

Test of the Dynamic Behaviour. Upon the completion of the layout of the individual stabilization networks and amplifications a test of both the phase and amplitude response, first of the individual elements and subsequently of the whole open servo loop, is carried out.

Unlike that in fluid damped accelerometers, damping is not provided with the GBM 531 on the pendulum itself. It is rather obtained by incorporation of lead-lag elements in the servo loop. As a consequence, the overshoot of the force balance pendulum excursion and the individual servo loop signals are not identical. The advantage of an aperiodic response of the force balance pendulum to a step function for instance would be accompanied, on the other hand, by high overshoot of the restoring current and thus a reduction of the output range. The optimum solution was a design in which the overshoot of both the force balance pendulum and the restoring current was about 30 per cent.

Measurements of Axis Errors, Bias and Scale Factor. The axis error is the deviation between the normal to the mounting plane and the measuring axis, which is normal to both the bearing axis and the line from the center of gravity to the bearing central point at pickoff zero. The axis error is represented in two components parallel to the housing surfaces. Bias is the output signal when no acceleration is present. These two errors can be separated by the following measurement procedures:

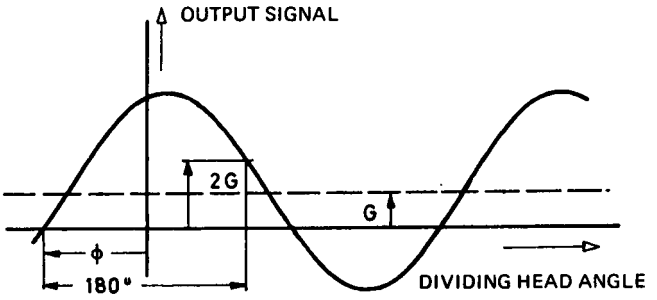

Fig. 13-32 Determination of the bias

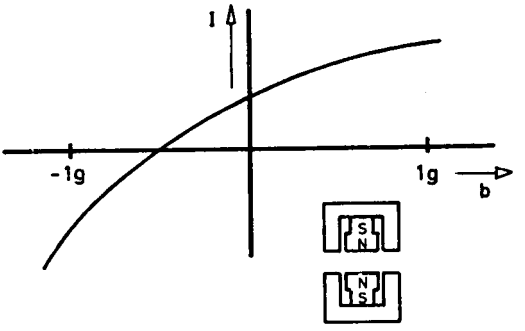

Fig. 13-33 Characteristic of the force generator

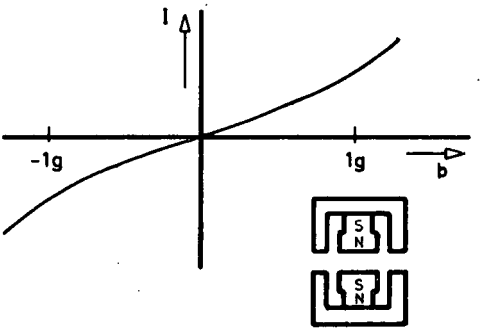

Fig. 13-34 Characteristic of the force generator

Axis errors (input axis misalignment) - as shown in figure 13-30, the accelerometer is placed on an approximately vertical plane and subsequently rotated on this plane by 180 degrees. From the difference between the two signals it is possible to determine the axis error with respect to the longitudinal axis.

The advantage of this method is that no absolutely vertical mounting plane is required. Remounting, however, has proven disadvantageous, since slight mounting inaccuracies cannot be avoided. The measurement of the axis error component in the direction of the bearing axis is carried out in a corresponding manner.

The coarse alignment of the measuring axis with respect to the longitudinal axis is accomplished by adjusting the fixed pickoff part and cementing it. The fine setting is performed subsequently by means of vernier screws on the force balance pendulum which allow one to shift the seismic mass center.

When the accelerometer has been aged by subjection to varying temperature conditions and when the measurement results at the operating temperature have been obtained, it is possible to correct both axis errors simultaneously by a corresponding lapping of the supporting pads. For this purpose, a precise lapping of all three supporting pads by fractions of 1 μm is required. This work demands great practical experience. Owing to the high stability of a gas bearing, this procedure makes it possible to attain accuracies in the axis alignment of some few seconds of arc.

Bias – for the determination of the bias, the accelerometer is adjusted on the optical dividing head so as to insure that the output signal is zero. Then the dividing head is rotated by 180 degrees. The measurement procedure can be seen in figures 13-31 and 13-32.

The signals are

$$A_{0\,3} = 0 = k\,[\,G + g \sin \phi\,]$$

$$A_{180\,3} = k\,[\,G + g \sin (\phi + 180)\,]$$

The bias can be calculated from the sum of both signals as follows:

$$A_{0\,3} + A_{180\,3} = 2kG$$

The bias which is a result of the turbine torque and the torque of the flex-leads is in the order of 10^{-4} g. It is inexpedient to provide for an adjustment of this order, since such adjustments do not afford sufficient stability. The constant bias can be taken into account in the navigation computer.

Scale factor – the measurement of the scale factor is carried out under varying operating temperatures. To eliminate errors arising from a temperature-caused deformation of the dividing head or a bias change, two measurements have to be made at each temperature level.

The dividing head is rotated into a position where the output signal of the accelerometer is zero. Subsequently, a rotation of 90 degrees is performed. The obtained measurement is

$$A_{90\,4} = k\,[\,G + g\,]$$

Upon a further rotation through 180 degrees, the output signal is

$$A_{270\ 4} = k\,[\,G - g\,]$$

The scale factor calculated from the differences of the two values is then

$$k = \frac{A_{90\ 4} - A_{270\ 4}}{2g}$$

The temperature coefficient of the scale factor can be obtained from the measurements at varying temperature levels.

Nonlinearity of the Output Signal as a Function of Acceleration. When only one force generator, or two force generators working in push-push operation, are used, the force of the force generator magnet will increase at positive accelerations, and thus at positive restoring currents, whereas the force of the magnet will decrease with negative accelerations. Due to this effect, less restoring current will be required at positive accelerations than at negative accelerations. This is shown in principle in figure 13-33. It can be seen that the sum of the two maximum values at ± 1g contains the bias G and the nonlinearity factor N.

The corresponding equations are:

$$A_{90\ 4} + A_{270\ 4} = k\,(2G + 2N)$$

$$A_{0\ 3} + A_{180\ 3} = 2kG$$

$$N = \frac{A_{90\ 4} + A_{270\ 4} - (A_{0\ 3} - A_{180\ 3})}{2k}$$

To eliminate this error, the present accelerometer design provides for two force generators performing in push-pull operation. The magnets are designed with opposite polarity. An identical force direction can be obtained by a reversal of the current flow in the two coils, so that one magnet is being remagnetized by the restoring current, while the magnet with opposite polarity is simultaneously being demagnetized. The remaining nonpolarity is represented in figure 13-34.

This remaining nonlinearity is attributable to the magnetization characteristics. In evaluating this nonlinearity, the scale factor k, the bias G and the axis error ϕ were first determined in the above specified manner. Following this, the output signal was measured as function of the dividing head angle α. The corresponding equation is

$$A = f\,(\alpha + \phi)$$

This function is a slightly distorted sine function which is in addition displaced along both axes, as can be seen in figure 13-32. The measurements of the output signals A were corrected by subtraction of the bias G, and the values of α by subtraction of the axis error ϕ. The resultant function values were then compared with the exact sine values. The differences between the measured and the exact values were without exception within the obtainable measurement accuracy of 10^{-5}.

Effect of Accelerations larger than 1g on the Accuracy. For simulations of accelerations exceeding 1g, for instance 15g, the accelerometer could be loaded with a mass fifteen times that of the seismic mass normally used. This would, however, necessitate modifications, so that, after all, no definite conclusion can be made.

A further approach is the use of a centrifuge. According to the specifications, nonlinearity shall be below 3×10^{-5} g/g^2. This however, would put high demands

on the accuracy of the centrifuge. Unfortunately, a centrifuge of the required accuracy is at present not available in Germany.

Furthermore, the influence of thermal conditions at high acceleration upon the accuracy of the accelerometer was tested. For this purpose, a current of 60 mA was fed through the force generator coils over a period of 30 to 60 seconds. This current is equivalent to an acceleration of 15g. Thereby not only the force generator coils and the force balance pendulum but also the flexleads were warmed up. After this period, the current was switched off and the servo loop was closed again.

The bias measured immediately after heating up amounted at early development stages to approximately 10 mV, corresponding to 10^{-2}g. The damping out of this bias proceeds in a curve similar to an exponential function with a time constant of approximately 20 minutes.

It can be assumed that the force generator coils act as a heat reservoir in combination with the force balance pendulum, in that the heat is transferred to the housing via the surrounding air and the flex-leads. This is the only reasonable explanation for the high time constant. Tests with pre-bent springs confirm this assumption that the large zero displacements are attributable to temperature-dependent bias variations in the pairs of flex-leads. By using pre-bent flex-leads this effect could not be sufficiently reduced, since no success could be obtained in installing both spring pairs without preload. The tests were continued with new materials for the flex-leads and finally brought the desired success.

As a result of the above described heating-up, zero displacements of only 10^{-5}g take place. Tedious tests were necessary to ascertain the most adequate treatment for the thin flex-leads.

Environmental Tests

An environmental test program has been prepared. Preliminary tests, in which the vibrational inputs were simulated by introducing voltages into the servo loop, have had good results. The set up for the tests on a shaker has been made; results are not yet available.

Conclusion

By using hydrostatic gas bearings it was possible to design and build inertial sensors of relatively good quality in a short time. To get these results the main efforts were directed to testing work and philosophy.

To our knowledge, TELDIX is the only manufacturer in Europe of gas bearing gyros and accelerometers. This chapter should be a contribution to stimulating the discussion on the bearing principle used.

Concluding this chapter we want to express our thanks to the German Ministry of Scientific Research (BMwF), the German Ministry of Defence (BMVtdg) for the financial support of these developments and our colleagues who by their enthusiastic cooperation made these achievements possible.

Bibliography

Thomaier, D., 'Aufbau und Wirkungsweise des Gaslager-Wendekreisels GWK 381', TELDIX-Report, Nov. 1966.

Reithmüller, H., 'Weiterentwicklung des Gaslager - Wendekreisels GWK 381', TELDIX-Report, June 1967.

Reithmüller, H., 'Justage und Vermessung der Gaslager-Wendekreisel auf dem sid. Drehtisch', TELDIX-Report, June 1967.

Reithmüller, H., 'Weiterentwicklung des GWK 381 mit kugel-gelagertem Kreiselmotor Typ KKM 38', TELDIX-Report, Feb. 1968.

Auer, W., 'Gasgelagerte Kreisel und deren Anwendung in der Raumfahrt', Raumfahrtforschung, July 1967.

Kearfott Co., 'Technical Information for the Engineer No. 4. Testing and Test Equipment', Firmenschrift der Firma General Precision, Kearfott Division, Little Falls, New Jersey, USA, 1964.

Fehse, W., 'Driften bei Wendekreiseln mit hydrostatisch gasgelagerter Präzessionsachse', TELDIX-Report, Dec. 1967.

Fehse, W., 'Theoretische und experimentelle Untersuchungen zur Tragkraft des einreihigen hydrostatischen Radiallagers mit Staukammering', BMwF Forschungsbericht W67-09, June 1967.

Savet, P.H., 'Gyroscopes: Theory and Design', McGraw-Hill Book Company Inc. New York, Toronto, London, 1961.

Auer, W., 'Kreisel und Beschleunigungsmesser mit hydrostatischen Gaslagern', AGARD Symposium, Braunschweig, May 1968.

Fischer, H., 'Systemanalyse für den magnetischen, luftgelagerten Beschleunigungsmesser mit analogem Rückführkreis', TELDIX-Report, Jan. 1967.

Wand, A., 'Abgleicharbeiten am GBM 531', TELDIX-Report, Oct. 1967.

Wand, A., Weinert, J., 'Untersuchungen an elastischen Stromzuführungen', TELDIX-Report, Feb. 1968.

14

General Discussion

W. G. Denhard: I said I would try to take one particular question first; it is addressed to me. There are two questions inferred, both of which are rather difficult to answer. I would ask that the rest of the panel offer comments also. I will state the question and see if we can evolve anything that resembles a direct answer. There is some comment first and then the question:

> 'It seems that, in spite of all the excellent work done during the past two decades or so, one still has to do a considerable amount of testing of inertial gyros before one knows that one has made a good gyro. There are those individuals who would say that you test the life out of them. Has not the state of the gyro art yet got to the point when one can write a prescription to the manufacturing department such that, after a period of gestation, out come gyros which meet specifications with an adequate quality and predictable life?'

I will answer in part, and I am afraid there will be no answer in full.

There have been comments by at least two of us, and one comment also from the floor, relative to this. Mr. Fertig spoke about a fully adequate interface specification, and that gyros must really be delivered to such a specification. The comment from the floor was:

> 'Could not the requirement wait until the instruments caught up?'

In my comments on cost, I tried to introduce the thought not only of specifications closely defined as to failure, but also of specifications and tests which provided an incentive to the manufacturer to achieve a higher percentage of acceptable instruments. I said that the poorer they were, the more he had to test them in order to make sure that every possible reject had been determined.

I believe that there cannot be a prescription specification which does not involve honor as well. I believe that in obtaining instruments or materials or anything which you must purchase of the highest quality, it must be furnished with honor as an ingredient. If we work only with what is in the written specification, we will never be satisfied. It is more important for us at home not only to know the company that will furnish the product, but also to know the man in charge and know what he represents. No amount of words will replace what that man represents - knowledge, and honor, and experience. I personally do not know how to put these things into a specification, or how to obtain what I want without these things. Some might say I was waving the flag, and so on - being naive, perhaps - I don't know how to do it on paper. I would like to defer to some of the others.

P. J. Palmer: It seems that unless we can rely on some of the vendors to produce, for example, the bearings, as Mr. Denhard said, we can't take the time to find out that we have a manufacturer who is a loser. We can't afford to wait long enough to find out that we're dealing with a manufacturer who is doing things behind our back, so to speak. We do usually follow this procedure back in our own country, of trying

to reach the people who are doing the work, get to know them, and try to indicate to them what our problems are with their product. In a great many cases this has worked very well.

W. G. Denhard: You could put within the specifications what the penalties are for failure to accomplish the necessary results to save costs on the contract, but you can't save the time that it takes to find that out.

M. S. Sapuppo: I still feel that one of the problems we have today is not so much the specification, but the fact that test people and designers are not spending enough time with the people who build the instruments. I've had the opportunity to do this myself more recently, and the vendors don't want to produce poor equipment but they do want to make a profit. They would be very happy to have defined to them those techniques, methods, specifications, that give them 100 percent yield.

What I find at this point in time is that they have had to deduce or infer what is really wanted in the device somewhat on their own. There has been this split between design, engineering test, and production. Too much compartmentalization. The more successful manufacturers in the United States have broken down this wall between these groups of people. They have integrated them and they are getting surprisingly good results. I commented to one of the gentlemen at lunch yesterday, and he was surprised to hear it, that we as a design agency were writing specifications and procedures that would be used directly in production by relatively unskilled labor. This has turned out to be quite a challenge, and is also turning out to be quite successful. We permit ourselves to define this documentation and the specific test methods; to see the results we must really and truly understand their problems. If we define the system in such a fashion that we become responsible for it, they will come to us and tell us what their problems are, and we must jointly provide a solution.

I don't say that this will result in more testing or less testing. I don't know that yet. I do know that this is the path we must follow. It appears to be reasonably successful so far. It is probably the most effective one that we can perform at this time.

Dr. O. H. Wyatt: Perhaps I could just point out the use of incentive schemes, penalizing one manufacturer and greasing up another. Our American friends are in a very fortunate position in having competitive sources. Most other countries are lucky to have one firm or perhaps two. Talking about all these economic incentives and knocking one over the head if they do not toe the specification line is not very easy in most places.

W. G. Denhard: Very quickly, another question, addressed to the panel in its entirety:

> 'There is need for a gyro which would cost on the order of $2500 in quantities of a few hundred per annum. Would any of the speakers comment as to whether they feel this could be realized? The thought is that unless such a goal can be achieved, higher costs will restrict the application of inertial navigation for both military and civilian purposes.

We haven't within the question defined either performance or life in terms of their influence on cost. If I may build on this at the expense of the question, all too often at home the effort is defined by the amount of money to be put into the program rather than by the required life and performance. There are people I know who will answer 'yes' to your question; commercial people in the States. I guess you'd like the accelerometer for the same cost, would you?

I would venture to say that in the States you can buy an instrument for any price you want to pay, starting at near $100. What that instrument will do, how long it will run, bears some relation to cost, but that relation is not a true relation. You can pay a lot of money for an inadequate instrument, so paying more is not a solution to the problem. The solution would appear to be more adequate testing, which has been the theme of this whole meeting.

Dr. Wyatt, can we take you up on some of your questions here?

Dr. O.H. Wyatt: Yes, I have five questions here. I'll take the most difficult first. The first question asked is:

> 'When you have an azimuth gyro with the output axis horizontal, the drift rate is a function of the temperature. Why?'

Well, there are two aspects to this which one can think of at the spur of the moment. One is the temperature distribution being generated by the motor. I would say that there is potentially quite a lot of mass shift if you suddenly alter the power into the motor and thereby the temperature distribution. If on the other hand you are altering the environmental temperature, I would think the gyro is not so sensitive, though the following point certainly is to be considered. If your center of gravity and your center of buoyancy are not well matched, then in this case in altering the temperature of the environment you expect some sensitivity. On the other hand, if the centers of gravity and buoyancy are fairly well matched, the probability is that the gyro won't be so sensitive to temperature.

Question two is:

> 'If you are comparing the azimuth gyro with its output axis horizontal and the leveling gyro with its output axis vertical, what is the relation between their drift rates?'

While rather dependent on the instrument, a round figure shows the fellow with the mass unbalance coming in the azimuth gyro likely to be five or ten to one worse on the stability figure.

The third question is:

> 'What happens if you compare two gyros, both with matched unbalances on spin and input axes, one of which you have the input axis vertical, spin-axis horizontal, one of which you have the input axis horizontal and therefore the spin-axis vertical?'

Well, the first of those with the spin-axis horizontal would, I think, turn out quite a bit worse than the one with the spin-axis vertical. You get a lot more mass movements along the spin-axis, I think, than along the input axis, probably throwing another five to one factor there.

The fourth question is:

> 'Do you have more information on the use of milliwattmeter traces on spin-axis gas bearings?'

Information I am afraid is very limited, and I think I gave in my paper the more important points I knew on that one.

The fifth question is:

'As mentioned in Dr. Wyatt's paper, power fluctuations at about one cps occur due to the rotor hunting about the magnetic vector. Does some prominent English firm use this as a method of detecting that the wheel is in sync?'

I've consulted Mr. Carter on this, who also is in touch with the majority of prominent English firms, and we don't either of us know of anyone who is doing this.

M.S. Sapuppo: The question is:

'In testing the PIGA on the centrifuge, do you have to reduce the angular momentum of the PIG?'

The answer is: yes, at the very high centrifuge rates equivalent to 100 g's or so. We have tested the PIGA up to rates as high as 50 g's (equivalent) in some configurations without having to reduce the speed of the wheel.

One could overcome this by increasing the power to the wheel, but in doing that it would disturb the thermal symmetry. In other words, we could design the instrument for the centrifuge, but that wouldn't be equivalent to the instrument that would fly in the system. So we do have this problem.

I have one other question here:

'What is the maximum payload of the air bearing table you described?'

The larger one can support as much as 300 or 400 pounds; the smaller one a good deal less. You might be interested in the stiffness of the small one. We have not been able to detect any deflections with the normal full load on.

W.G. Denhard: Here is a question addressed to me. The question is quite appropriate. You gentlemen may have noticed Dr. Draper had to leave to return to the States, but this morning he put essentially the same question to me because I had not expressed myself very well. This question is:

'I still cannot understand why your presentation shows that operating life increases with testing time. If your term 'operating life' is a statistical figure, isn't it so that gyroscopes of a specific type have a certain mean life, depending on design, workmanship, etc. ? Of course it is useful to extend the testing time till the early failure period is past, but after this period the mean life is constant. There is no sense to increasing testing time beyond this.'

I am afraid I did a very poor job in putting across my message. This question is quite appropriate. If the testing is too simple and the manufacturer is allowed at his own discretion to repeat any test he wishes until he has one set of data that makes the instrument acceptable, the manufacturer has only to take any instrument he makes and, without improving on it a bit, do as much or as little testing as he desires until he gets some data which passes. Then he delivers the instrument, and the customer must accept it.

My point was that testing of itself will not improve on an instrument. But testing with very firm specifications as to what the test will be, what the failure criteria will be, and what allowances will be made for retesting, could force a manufacturer of an inferior quality instrument to have such a high reject rate that his only salvation would be to make a better instrument. Increased testing as I define it (not as the manufacturer defines it) would in the end force the manufacturer to produce an instrument of higher reliability and higher quality. Those instruments

made to these higher standards would have longer life. The only way you can force the manufacturer into that position is to put upon him a set of specifications in testing which gives him an unacceptable reject rate for poor quality instruments. Most of the money that gets associated with the higher cost gyro would go into the quality of the instrument and not into the testing. It would, however, have been the greater amount of testing and the specifications which accomplished the result. Once the character of the instrument has been identified and the quality has been raised, then there is no need of further extended 'penalty' testing.

The need for correcting my message was the very strong request I got from Dr. Draper this morning, and he is absolutely right, and your question is absolutely right.

I mentioned the point of honor before. If the manufacturer has only to produce some data which is acceptable, no matter how many tries it took him, he's living up fully to the terms of the contract, and having lived up to the terms of the contract, he's entitled to be paid and you're obliged to accept the instrument. So I guess I'm taking some of the honor out of his jurisdiction and trying to put some of it into the contract, although I do not consider that totally self-sufficient.

J. V. Carter: I've been asked two questions - I think you had one, Mr. Denhard, and I believe I remember it. It says:

> 'Please compare tumble testing taken at a continuous rate as against tumble testing taken in steps.'

I think you will remember that in my paper I did indicate we were testing in these two modes. Very simply, in fact, I'd like to think about continuous rate tumble testing purely in a qualitative sense. In this way I can pick out the gyros with the lumps of solder, for example, that Mr. Fertig commented on a little earlier this afternoon. This test finds the ones that have gross manufacturing faults, the ones possibly out of specification from friction, bubbles, and so on. In continuous tumble testing, a possible major source of error is the table rate itself. When rotating at a rate of 150 degrees per hour, if we have our input axis misaligned by a minute of arc, we are going to pick up an appreciable component of this table rate.

The justification for doing a step tumble test is partly to remove any possibility of the table rate being seen by the gyro's sensitive axis. But it also does give us the opportunity to get the numbers out from an equivalent tumble test in a much shorter period of time. If I give a continuous tumble, I am obviously not going to go at a rate much faster than 150 degrees per hour. But if I am happy with acquiring 12 bits of data from one cycle of tumbling, then I can go quite quickly from one 30 degree position to another and just sit perfectly still in each of these positions for a few minutes of time. This enables my integrating digital milliampmeter or whatever instrument I'm using to take out the gyro data. I believe I am getting my estimate of gyro coefficients in a much shorter period of time and I am not confusing my calibration of gyro coefficients with gyro stability as such.

Now obviously we have a point of difference here. I think Mr. Fertig pointed this out. I am sure that if one takes several looks at gyro drift rate - in absolute terms, in switch-on to switch-on terms, and in testability terms - then if your immediate object in life is to calibrate gyro coefficients, you want to do this as quickly as you possibly can.

The second question had to do with tests to establish a gyro's magnetic sensitivity. I think the comment stated that if a quantitative test of this nature were desired,

one could put the gyro in the uniform field generated by a Helmholtz coil arrangement. The questioner has suggested that it would be a good thing if we had a standard field in which we could do this test; or have some international agreement, I think Mr. Denhard said, for a field strength in which to do a calibration of this sort. I can't see the reason for this, and it may be because I haven't had long enough to think about it. I don't consider magnetic sensitivity as too important, though I must admit all our system designers are not as conscientious as Mr. Fertig has shown he can be. There has been a tremendous amount of trouble caused in platforms by having magnetic materials near to gyros when the system is working. As a result, this has caused drift changes. I think it is satisfactory to have a calibration of gyro drift in terms of the field which you expect to apply to the gyro - in oersteds, e.g. degree per hour per oersted for change of a particular gyro coefficient or drift rate in a particular attitude.

Having said that, I think this is something Mr. Fertig is asking for - this is one of the variables he would like to know: degree per hour per oersted. I don't think we have to say any particular field arrangement as an international standard.

G. J. Dalton: I had a small question to put to Mr. Denhard. I said that his paper on the economics of gyro testing appears to concentrate on the relation between testing and the cost per running hour of system gyros. As far as I remember, he made no mention of the matter of shelf life testing, although in some operational equipment this can be economically at least as important as running life testing. The equipments I am thinking of are those in which the stated shelf life of gyros may possibly be used up long before the operational running hours approach the limits laid down by the gyro developers.

I have in mind a particular case where we in the United Kingdom have taken pains to call back a number of the older gyros from service each year in a particular system. We made performance and fluid gas contents tests on these gyros, and as a result we were able to extend the stated shelf life very steadily. We are in fact currently recommending that in-service gyros need not be replaced on shelf life grounds until they have completed eight years from the date at which they were filled by Ferranti. Initially, this period had been three years. The direct saving in cost of gyro refurbishing has been very appreciable and the saving of cost of stripping down and regyroing platforms has been very much greater than this. I wondered if Mr. Denhard could comment on this aspect of gyro testing, and whether he could say if he has any knowledge of any other systems where it has been an important economic factor?

W. G. Denhard: I asked that Mr. Dalton present this for I think he is presenting some information on a viewpoint we haven't discussed here. It was worthwhile presenting it as his own.

I truly cannot speak for everything that goes on in the States because I truly do not know. I do know of a case for an operational system where there was a known wearout situation which is not truly shelf life as Mr. Dalton described it. At a specified period of time in the life of these instruments, they were pulled out. This was a wearout definition: the bathtub failure curve was going up and it was known that with further time there would be trouble. It was better to take an opportune time before that than have a field failure. For our own particular instruments at MIT, we have never defined any limit on shelf life and have not considered shelf life in the sense of being a limitation. That is not a universal statement, that's the MIT gyro. I don't truly know of limitations imposed by shelf life time. Our experience goes back to 1954 and earlier, and the gyros are still going. They've been on the shelf and out and back and forth with no problem. We just haven't had to weigh the question.

M.S. Sapuppo: You might say that in some instances we found that the gyros, or in this particular case accelerometers, seemed to be like good wine - the longer they age, the better they get. I've seen the reliability go up with time and the performance improve with time. The reliability, depending on how you calculate it, can improve with time in a batch of instruments, depending on how you add to that number of units in the field. That number can improve with time as the instruments do age in the systems.

K. Fertig: One of the peculiar aspects of shelf life, one which involves the interface specification between an instrument and a system, is the aspect of instruments that are bought to meet an interface specification, but then are stored without further testing and then will not work in the system platform. I personally do know of companies which had the interface specifications set at a level at which they got a reasonable instrument production rate and then did not use their own instruments in their own platforms. They could sell them off to the stockpiling agency and get them in the pipeline to place on the 'shelf'. That is possibly the worst aspect of shelf life. You've got something in the pipeline, think it's available, and then when you have to use it, you can't. That's the interface spec problem, and that's one of the reasons why I attempted to say, make it work and perform and pay off at its ultimate destination - the system. What doesn't work in the system is no good in the stockpile.

I've got one simple question from Mr. Dalstein of Mattra.

> 'You mentioned the problem of starting up air bearing gyros. Have you used this type of gyro in an orbital environment, and is the starting up easier in a no-gravity environment? Is it better to have the spinner rotating during vibration?'

The problem I spoke of had to do with insufficient wheel power for initial turnon. Gas bearings want to get up on that step quickly. They usually require an overvoltage condition to do this. The problem I spoke about had to do with that element of overvoltage being left out of an initial specification. An electrical motor voltage implies a potential speed that the motor can go at and current supplies the torque it can deliver at that speed. Voltage, of course, determines the current, particularly at starting.

One can get a gas bearing started with sufficient torque either by applying overvoltage to get higher current and torque, or alternatively by starting it using a lower frequency supply so that the wheel has less impedance and therefore, for the same voltage, will draw more current. Once started, you switch over to your standard running frequency. Either of these two methods works, but one must be built into the system. If left out of the specification, the delivered instrument will not start. That was the problem I was addressing.

I personally have not tried or known of gyros with gas bearings in orbiting environments - I just don't know. I can't imagine that it is significantly easier to start it in a no-gravity environment, but again, I do not know.

'Is it better to have the spinner rotating during vibration?' I would imagine by several orders of magnitude, but the designers here could state it. You'd better have that thing spinning; otherwise it has no stiffness, and you can have the thing flapping from side to side.

I have another question here:

> 'What information do you derive from a platform test on a centrifuging

machine? Overall operation or evaluation of component errors under acceleration?'

Section 10 of my paper does describe some aspects of centrifuge testing and of instruments in a system. In fact, I have at least twice in my career been involved in centrifuging a system with instruments in it where centrifuging the system was the prime factor. Certain restrictions prevent me from going into the equations and data reduction processes. In fact, the testing is rather like a higher-than-one-g tumbling test, and that's about all there is to it. There are some trickier things involved.

Question from the floor (paraphrased and inferred because of poor recorded quality):

'I think in reality it is too complicated, in particular to derive from the platform data alone all information about the gyro.'

K. Fertig: I did speak of an instrument model equation for a floated instrument. In an instrument model, you can have a term which would describe the motion of the float to case along the output axis under acceleration. In fact, I was proposing that that precise signal be monitored. If there is a measure of the g environment, cyclical or whatever, on the instrument, you will be measuring the actual motion of your float-to-case within the gyro as a function of acceleration. You can then derive a torque factor for it.

The thing we typically are looking for in a system on the centrifuge is to verify our instrument compliance model. That is something we can do.

We use theodolites for before-and-after measurements for the system platform orientation. If one has a large enough mirror on the platform, one can even (in a sense, like a strobe motion picture camera) make measurements of the orientation of the platform as the centrifuge goes around. So there are a great many things you can do, and I would insist that it is very much like tumbling tests, only more sophisticated - but not that much more sophisticated.

We have used counter-rotating tables to carry a system. If you have a stabilized system platform, the platform itself will provide counter-rotation. The main reason for having a counter-rotating table is so that the platform servos are not stressed more than they would be in a normal flight.

If one does provide counter-rotation, either in platform servo or counter-rotating table, or use the two of them together, there is still one thing about centrifuge testing, in particular at high g's, which is strange and which is perhaps a little unfair to the instruments. This is what it does to the PIGA's.

You build up a PIGA model which, among other things, is based on acceleration rate of change, the so-called 'jerk term' - when you put an accelerometer on a stabilized platform on a centrifuge, you rather quickly will build up a very high jerk term caused by the rotating specific force (g vector) and imperfect (nonsmooth) counter-rotation. The requirements in your thermal model of the accelerometer may become more stringent because you try to learn, as you put more and more power into the PIGA servo motor, how this power affects the thermal environment of the PIGA. That is why you should have an instrument model. More importantly, you may have designed the correct servo for your system application, but it may not be the correct servo for your centrifuge application. That's something else to take into account. I know in my own work with the centrifuge, the environment was at least a factor of three more stringent than for the ultimate application, in terms of the jerk term. This affected the voltage, and the servo requirements, and so on.

Another aspect of centrifuge testing with a complete system is that there can be a cyclic torque on the system servos from imperfect mass balancing of the system platform. As we described before, the centrifuge looks just like a large amplitude low-frequency shaker. One should be careful how these torques are in effect added up, because now the platform stabilization servos have to fight off those torques as well as others.

The centrifuge test does in many ways look like a tumble test. You've got a larger-than-one-g vector rotating through your platform.

W. G. Denhard: There is a question addressed to Dr. Draper. I can't answer it as well as he, but I'll try. The question I'm trying to answer is this:

> 'Can one imagine, or are there actually, inertial navigation or inertial guidance systems with only accelerometers on the assumption that an accelerometer can detect rotation by any translation? If so, would the electronics for these accelerometers be complicated to make?'

I can more readily picture an instrument physically, an instrument that detects both rotation and acceleration. Unfortunately, in a sense, all the gyroscopes we've been talking about today will do this because they all have mass. Now that's a facetious answer, but not my complete answer. The basic problem we have in testing occurs because the instruments do detect acceleration. One can conceive, as an answer to your question, of a mass, perhaps a ball, suspended by a field. This field can be electric, magnetic or fluid, although for what I'm going to say a magnetic or electric field is better, as the ball must be spinning about a preferred axis. Since it is spinning, it is a gyroscope, and its load upon the field can be used to detect acceleration, since the ball has mass. I believe this is actually something one can accomplish. However, if you try to accomplish both factors, acceleration and rotation sensitivity, with great precision, then the details that were secondary because it was only a gyro are now primary because it is now an accelerometer also, and vice versa. The instrument probably requires, if it is to have any considerable accuracy, orders of magnitude of improvement in things that were once secondary when it had only one purpose. The alignment of the supporting field is now critical because it is a direction to measure acceleration.

I would think that the problem might more likely be in the instrument rather than in the electronics. If you wish to consider the supporting field and the definition of an axis in it as part of the electronics, then, yes, it's in the electronics. But truthfully, the element of our instruments that we speak of as a ducosyn can measure on those instruments acceleration if we do not perfectly float the instrument. That is the best answer I can give you. I believe it is a feasible thing. I can picture it; the complications you enter into to do it will depend upon the accuracy you demand.

Editor's Note: It later developed that this was not a direct answer to the question. The question posed was more nearly meant to query the use of an accelerometer at each wing tip of an aircraft such that, by manipulation of sums and differences of output, rotation could be identified as well as acceleration. The answer to this could very well be that it is theoretically feasible and like a system platform itself would require a computer to translate information into useful terms and coordinates. The practicability is not known. Instinctively (not necessarily correctly) it is not recommended.

K. Fertig: I was asked what, in my opinion, was the best method of in-orbit calculation of an inertial reference for a high stability satellite. I have no opinion. I have not thought about the problem.

Part two of the question, which I also cannot answer, is whether the available stellar calculation of an inertial reference must be maintained always during satellite stabilization periods, or could an extrapolation procedure be foreseen?

Some sort of periodic thing - I presume the questioner is thinking in terms of Kahlman filter update. All I can say is, yes; I haven't thought about it in enough detail to know what periods could exist between calibrations.

W. G. Denhard: There are programs in the States associated with this. The Laboratory is working on one, and it becomes dependent entirely on the drift of the gyros. In the gyroscope, particularly what we call the bias term, which is independent of acceleration, causes drift even in space. We know people who would like to calibrate once a year. It remains to be seen what will be accomplished.

I will read this question from the floor. It is a comment on Mr. Fertig's paper, and is:

> 'When one does in-depth testing, one may also receive early indications which are perhaps undetected with a strict reject accept limit, when anything is (incipiently) going wrong or only on the verge of going wrong in the production process. My own experience once showed this in randomly executed lifetime tests on a vibrating component. Mr. Fertig has presented us with a figure which says that when there is normal production, there is a bell curve relating to the density of different performance capability levels. When there is faulty production, the bell curve is distorted with an indent due to faulty production.'

Do you wish to comment on this, Mr. Fertig?

K. Fertig: I think what you're saying is, you can keep track of successive production lots this way and find out if the value engineers have sneaked something in on you. Yes, you can't trust them. All done inadvertently, all done honorably - some parameter which is the equivalent of profit, extra week's vacation, promotion, and so on.

W. G. Denhard: I would hope that, as I make these closing remarks, the people who are interpreting for us will continue to do so. I wish to thank them most sincerely for their help which has been indispensible to our communicating with each other, and I for one, when I return, will study French some more. My instructions from my wife this time were to speak English!

R. A. Willaume: I would very much like to thank Mr. Denhard and all the others for all the work they have done in preparing their papers. It is thanks to them that we have this exchange of information these last three days. This is part of our operation, and I hope that you have benefited from the exchange of views. I must say that Mr. Denhard did a tremendous job in first selecting these excellent speakers. I'm very thankful to him and to all of the speakers for the work they have done, probably after the normal hours of work every day. So for all of you gentlemen, I would like to express my very sincere thanks to them.

Index